

University of Alberta

**TIGHT GAS RESERVOIR CHARACTERIZATION IN
MONTNEY FORMATION, NORTHEASTERN BRITISH
COLUMBIA, WESTERN CANADA**

By

Edwin Ikhuoria Egbobawaye

A thesis submitted to the Faculty of Graduate Studies and Research
in partial fulfillment of the requirements for the degree of

Doctor of Philosophy

Department of Earth and Atmospheric Sciences

©Edwin Ikhuoria Egbobawaye

Fall, 2013

Edmonton, Alberta

Permission is hereby granted to the University of Alberta Libraries to reproduce single copies of this thesis and to lend or sell such copies for private, scholarly or scientific research purposes only. Where the thesis is converted to, or otherwise made available in digital form, the University of Alberta will advise potential users of the thesis of these terms.

The author reserves all other publication and other rights in association with the copyright in the thesis and, except as herein before provided, neither the thesis nor any substantial portion thereof may be printed or otherwise reproduced in any material form whatsoever without the author's prior written permission.

DEDICATION

This thesis is dedicated to my father and mother, to my beloved children (Ogbemudia Josiah and Ogbewi Emmanuel), and to everyone that has contributed in one way and another to my overall educational achievement from elementary school to Ph.D. level.

ABSTRACT

The Montney Formation is a primary focus of unconventional gas reservoir in northeastern British Columbia, Western Canada. This study presents the sedimentology and ichnology, Rock-Eval geochemistry and reservoir potential, C¹³ and O¹⁸ isotopic composition, and magnetostratigraphy correlation of the Montney Formation in the Fort St. John area (T86N, R23W and T74N, R13W), northeastern British Columbia.

The Montney Formation consists of siltstone with subordinate interlaminated very fine-grained sandstone. Five lithofacies association were identified in the study interval: Lithofacies F-1 (organic rich, wavy to parallel laminated, black coloured siltstone); Lithofacies F-2 (very fine-grained sandstone interbedded with siltstone); Lithofacies F-3A (bioturbated silty-sandstone attributed to the *Skolithos* ichnofacies); Lithofacies F-3B (bioturbated siltstone attributed to *Cruziana* ichnofacies); Lithofacies F-4 (dolomitic, very fine-grained sandstone); and Lithofacies F-5 (massive siltstone). The depositional environments interpreted for the Montney Formation in the study area is lower shoreface through proximal offshore to distal offshore settings.

Rock-Eval data (hydrogen Index and Oxygen Index) shows that Montney sediments contains mostly gas prone Type III/IV with subordinate Type II kerogen, TOC ranges from 0.39 – 3.54 wt% with a rare spike of >10.9 wt% along the Montney / Doig boundary. The vitrinite reflectance data and T_{max} shows that thermal maturity of the Montney Formation is in the realm of 'peak gas' generation window.

Magnetostratigraphy analyses from this study shows that the Montney Formation in the study area exhibits normal and reverse polarity intervals across the Upper Montney and Lower Doig formations boundary. The geomagnetic polarity correlation matched

known intervals of the Triassic GPTS at 245 Ma. The results suggest that Lowermost Doig phosphatic zone (Montney / Doig boundary) occur within a single magnetostratigraphic interval characterized by a coplanar *Trypanites* – *Glossifungites* demarcated discontinuity surface, interpreted herein as a regionally correlatable surface.

ACKNOWLEDGEMENT

First and foremost, I thank the Almighty God for keeping me alive, and for making it possible for me to complete this dissertation, despite many obstacles that would have hindered my successful completion of this program.

I'm indeed grateful to my supervisor, Dr. Murray Gingras for his exceptional leadership, and how he has mentored me throughout the entire period of my doctoral residence here at the University of Alberta. I'm very thankful to Dr. Murray Gingras for his supervision of my research, corrections of my thesis, his patience, and polite correspondences. His genius and exceptional ability to communicate in the most effective demeanor is a personality quality that I enjoyed, admired, and appreciated during my day-to-day dealings with Dr. Gingras, which I have emulated, and considered as an additional gain to the degree I earned at the University of Alberta. Dr. Murray Gingras, for all that you did to polish me and constructively guarded me through the tempestuously turbulent times during the entire period of the graduate program is greatly appreciated. Murray, I sincerely thank you immensely from my heart.

Dr. S. George Pemberton is thank and will forever be applauded by me in my geological career because of his persistent, fatherly, pedagogic persuasiveness on me and our research team (IRG) through sharing his unmatched intellectual experiences, providing support, propping and luring me and our research team (IRG) into becoming academic journal publishers, by exemplifying his experiences in his early days in academic journals publications. These and many more of Dr. Pemberton's stimulating pedagogy has tremendously illuminate and broadened my horizon, expanded my knowledge, and has equipped me enormously beyond the sphere of a traditional sedimentologist to a paradigm who combines the schools of the dynamic interplay of sedimentology and ichnology to sedimentary depositional systems. With these acquired endowments by virtue of my interactions with Dr. Pemberton and Dr. Murray Gingras during my academic pursuit at the University of Alberta has fully prepared me for my geological career.

Dr. Vadim Kravchinsky is thanked for his corrections on the Magnetostratigraphy Chapter. Dr. Vadim Kravchinsky will be best remembered in my mind and in my geological career as the professor who introduced me to the field of paleomagnetism and magnetostratigraphy. His avid dedication and teaching of paleomagnetic studies to me led to the utilization of paleomagnetic technique in my research, which subsequently resulted in a co-authored paper with Dr. Vadim,

et al. (2010). Dr. Vadim's kind words, and mutual respect in his communication is highly appreciated. Dr. Vadim was always available to shed his thoughts on many of my paleomagnetic questions.

I thank Dr. Karlis Muehlenbachs for making his isotope geochemistry laboratory available to me to analyze my samples. Throughout the period of my analyses in his lab, Dr. Karlis was very cooperative, given me supportive advice, publication suggestions, and insightful and stimulating discussions on interpretation of carbonates using isotopic compositions.

I sincerely thank the Graduate Chair, Dr. Tom Chacko of the department of Earth and Atmospheric Sciences here at the University of Alberta for his brave, unbiased, and moral oriented leadership.

I thank Dr. Andrew Cullen and Doug Bellis for linking me with Chesapeake Energy Corporation, Oklahoma, USA; and as our discussions on the Montney Formation tight gas reservoir continued at a time, Andrew and Doug Bellis made it possible for me to get free laboratory analyses (tight rock, Rock-Eval, porosity, permeability and quantitative X-ray diffraction analyses) for my samples. This relationship further paves way for me to do internship with Chesapeake Energy in the summer of 2011. Without you Andrew, these would not have been possible; for all of the above, I thank you.

My profound appreciation goes to the Faculty of Graduate Studies and Research for the four years scholarship awarded to me during my doctorate degree program here at the University of Alberta. Similarly, I would like to express my appreciation to Geoscience B.C for awarding me a scholarship in 2010. Chesapeake Energy Corporation in Oklahoma City is thanked for performing tight rock analyses for me in their shale gas laboratory.

Igor Jakab is appreciated and thanked for the tremendous help he constantly rendered to me with issues relating to digitizing, formatting of my thesis in 'in-design' to meet FGSR thesis specification, and his usual cooperation for last minute requests to print posters for conferences. For my entire four years of my study at the U of A, Igor Jakab was consistently my solution and tutor for software related problems. Thank you so much, Igor.

Chris Lough is appreciated for always helping me to enhance, repair, maintain, and update my computer and backing-up of my data. Without Chris, I would have suffered the loss of too many hours of work.

Valery Companytsev was very helpful in showing me how to use GIS in the plotting of my well data, map digitizing, online data searching, retrieval and data

manipulations to meet my desired GIS needs.

I thank Mark Labbe for promptly making available materials that were needed during the time I spent in the rock-crushing house when I was using the Pulverizing shatter box machine to crush my samples.

Diane Caird is thanked for the timely analysis of my samples using XRD and for helping to adjust mineral picks in the XRD data output.

I'm truly thankful to laboratory technician Olga Levner in Prof. Karlis Isotope Lab for practically teaching me how to operate the isotope geochemistry flow line in the lab, helping to take my extracted CO₂ to mass spectrometer for analyses. Similarly, I thank paleomagnetic laboratory technician L.P. Koukhar (Department of Physics) in the paleomagnetic lab for the cooperation and for working with me during the measurement and analyses of my samples for magnetostratigraphy.

My friend, Dr. Chima Nzewunwah deserves the record of my appreciation. He has been an avid supporter of my endeavors; sharing the good times, the bad times, and challenging time with me without showing frustration towards me when I'm weak and incapable. Chima has been and continue to be a true friend that I cherish and grateful to God for making it possible for us to be friends through attending the same undergraduate geology degree program as classmates at the Enugu State University of Science and Technology, Nigeria. I thank Chima and his wife, Carla for housing me in in their home free of charge during my summer internship at Chesapeake Energy Corporation, Oklahoma, U.S.A.

To my fellow grad student, Greg Baniak, Andrew Lawfield, Ryan King, Chelsea Fefchak, and Rares Bistran of Ichnology Research Group (IRG), University of Alberta are thanked for the various scientific fights, stimulating discussions and the cooperation we shared and enjoyed during my study at the University of Alberta.

I'm very grateful to my parents (William Enarunan Egbobawaye and Felicia Egbobawaye) for giving me a solid foundation in my upbringing that made me very courageous in the pursuit of the good things of life. Dad and mum, you showed to me countless times the meaning of true love through the dedication and sacrifices of your lives to make my own life better than yours. Many times, you both gave me **all** your earnings, and a few times you both borrowed with 'interests from moneylenders just to make me have a university degree. Your reservoir of love is my reality everyday, and when times I tough, I fetch from that buoyant well – a reservoir of love, spirit of optimism, and hope in adversity. These qualities that mum and dad bestowed on me in my upbringing makes me resilient, keep me replenished, and reminded of your parable: “no matter how dark the night is, it must

break into day light". My beloved mother, I thank you for coming to Canada to help me and my wife to be the caregiver to our son: Ogbewi Emmanuel, who was born a few months before my doctoral candidacy examination. I would not have been able to juggle baby-sitting with preparing for my candidacy exam without the selfless help from you, mum. Thank you very much, my dear mother.

My acknowledgement and expression of appreciation to my brother, Odion Collins Egbobawaye is crucial. In remembrance of his life and the hardwork he contributed to my mother's petty trading business that partly paid for my undergraduate degree in Nigeria, I sincerely thank my late younger brother, Odion Collins Egbobawaye who passed away in the summer of 2011. Odion was just three weeks away from his graduation with a Bachelor's degree in Banking and Finance at the University of Benin, Nigeria. Odion, I miss you and all that you would have become; I wish you were alive for us to see together how our humble beginnings turn out great!!!

This acknowledgement will be incomplete without appreciation to my wife, Natalie Egbobawaye, for enduring among other things, tight income from Graduate Teaching Assistantship, and many nights of a absent husband from home due to staying late in school upto 0500 hours just to be able to complete my thesis and defend the thesis within the four years of my scholarship. Thank you very much my friend, my wife and my lover. Now you can see that all the tough times we went through because of this doctorate degree is worthwhile.

Table of Contents

CHAPTER 1: INTRODUCTION.....	1
GENERAL OVERVIEW AND OBJECTIVES	1
PREVIOUS WORK.....	7
Tectonic Setting.....	7
Reservoir History and Development.....	12
Sedimentology.....	12
METHOD OF STUDY	13
Software.....	14
PROJECT OBJECTIVES	15
REFERENCES.....	17
CHAPTER 2: SEDIMENTOLOGY AND ICHNOLOGY OF THE UPPER MONTNEY FORMATION (LOWER TRIASSIC) TIGHT GAS RESERVOIR, NORTHEASTERN BRITISH COLUMBIA, WESTERN CANADA.....	24
INTRODUCTION	24
GEOLOGICAL SETTING	30
METHOD OF STUDY AND SCOPE.....	34
FACIES ANALYSIS CONCEPT	41
Ichnofacies	41
RESULT OF FACIES ANALYSIS	42
Lithofacies F-1 Description: Organic rich siltstone.....	44
F-1 Interpretation.....	46
Lithofacies F-2 description: Very fine-grained sandstone and siltstone	53
F-2 Interpretation.....	57
Lithofacies: F-3 Description	67
Lithofacies F-3A Description: <i>Skolithos</i> ichnofacies.....	70
F-3A Interpretation.....	70
Lithofacies F-3B Description: <i>Cruziana</i> ichnofacies	76
F-3B Interpretation	76
Lithofacies F-4 Description: Dolomitic very fine-grained sandstone.....	79
F-4 Interpretation	79
Lithofacies F-5 Description: Massive siltstone	81
F-5 Interpretation.....	83
DISCUSSION.....	89
Sedimentology and Depositional Environment	89

Trace Fossils.....	92
Mineralogy.....	93
Hydrocarbon Potential of the Montney Formation	95
CONCLUSIONS.....	97
CHAPTER 3: SOURCE-ROCK GEOCHEMISTRY AND RESERVOIR	
POTENTIAL OF THE UPPER MONTNEY FORMATION (LOWER	
TRIASSIC) NORTHEASERN BRITISH COLUMBIA, WESTERN CANADA... 130	
INTRODUCTION	130
GEOLOGICAL SETTING	134
METHOD OF STUDY	138
RESULTS	143
Rock-Eval Geochemistry	143
Description: Montney Formation Total Organic Carbon (TOC)	143
Interpretation.....	145
Description: Montney Formation Hydrogen Index and Oxygen Index	147
Interpretation	149
Type II Kerogen	150
Type III Kerogen	151
Type IV Kerogen	151
Thermal Maturity.....	152
Description: The Montney Formation Thermal Maturity – T_{max}	153
Interpretation	154
Description: The Montney Formation Thermal Maturity – Vitrinite	
Reflectance	159
Interpretation	162
Description: Thermal maturity – Production Index (PI)	164
Interpretation.....	165
Reservoir Characteristics of the Montney Formation.....	166
Porosity Data – Description	166
Interpretation	168
Permeability Data Description.....	171
Interpretation	172
Fluid Saturation – Data Description	173
Interpretation	174
DISCUSSION.....	175
Source-rock quality.....	175

Thermal Maturity.....	177
Future Exploration Prospect	178
CONCLUSIONS.....	182
REFERENCES.....	184
CHAPTER 4: ISOTOPE GEOCHEMISTRY OF THE MONTNEY FORMATION (LOWER TRIASSIC), NORTHEASTERN BRITISH COLUMBIA, WESTERN CANADA	193
INTRODUCTION	193
GEOLOGICAL SETTING	195
METHOD OF STUDY	200
Stable Isotope Geochemistry – Description of Data	203
Interpretation of Isotopic Signature	205
DISCUSSIONS	207
Carbon and Oxygen Isotope Geochemistry	207
Dolomitization of the Montney Formation.....	211
CONCLUSIONS.....	217
CHAPTER 5: MAGNETOSTRATIGRAPHY DATING AND CORRELATION OF THE UPPER MONTNEY AND LOWER DOIG FORMATIONS, NORTHEASTERN BRITISH COLUMBIA, WESTERN CANADA SEDIMENTARY BASIN.....	227
INTRODUCTION	227
STUDY OBJECTIVES	229
LABORATORY METHODS AND PROCEDURES	231
RESULTS	238
DISCUSSIONS	239
CONCLUSIONS	241
REFERENCES.....	242
CHAPTER 6: SUMMARY AND CONCLUSIONS	245
REFERENCES.....	251

Appendix

APPENDIX – 1: Table below is showing compilation of all the wells in the study area that penetrated the Montney Formation in the subsurface of northeastern British Columbia. The Montney Formation tops and base were picked in all wells generate the isopach and structure maps of the Montney Formation..... 256

APPENDIX – 1 B: Letter of authorization to publish core analysis data from British Columbia Ministry of Energy, B.C. Oil and Gas Commission..... 264

APPENDIX – 2A: Logged core showing facies of the Montney Formation, northeastern British Columbia, Western Canada.....265

Appendix – 2B. List of thin-sections analyzed in this study.....274

APPENDIX – 3A: Complete Rock-Eval data set used in this study for evaluation of hydrocarbon potential of the Montney Formation in northeastern British Columbia and part of Alberta. These data were also used to make TOC and Tmax maps presented in this study. Additional Rock-Eval data comes from Faraj, et al. (2002) and B.C. Oil and Gas Commission, Ministry of Energy and Mines, British Columbia..... 276

APPENDIX – 3B: Graphs showing Rock-Eval polysis for samples analyzed and used in this study..... 292

APPENDIX – 4A: Calculation of the temperature of fractionation using isotopic data from the Montney Formation, northeastern British Columbia, Western Canada..... 415

APPENDIX – 4B: X-ray Diffraction Analyses (XRD) results of the Montney Formation, showing mineralogical composition of each sample from the study area, northeastern British Columbia, Western Canada..... 418

List of Tables

Table 2.1. Summary of the lithology, characteristics, and description of facies associations (F-1 through F-5) and interpretation of depositional environments.	39
Table 2.1. Continues.....	40
Table 2.2. Trace fossils description reported from the studied cores in the Upper Montney Formation, northeastern British Columbia.	43
Table 3.1. Criteria for ranking source rock and richness (Peters, 1986) and Cassa (1994).	145
Table 3.2. Hydrocarbon generation and maturity measurement using vitrinite reflectance (After Dow, 1977; Senftle and Landis, 1991).	146
Table 3.3. Interpretation of Hydrogen Index (HI) and Oxygen Index (OI) Values to determine Kerogen types (Modified After Peters, 1986; Dembicki, 2009).	149
Table 3.4. Vitrinite reflectance measured from the Montney Formation sediments in British Columbia.	160
Table 3.4. Continued.	161
Table 3.5. Geochemical parameters describing the level of thermal maturation (Peters and Cassa, 1994).	166
Table 3.6. Petrophysical characterization of the Montney Formation in well 16-17-82-25W6 (Data source: B.C Oil and Gas Commission).	170
Table 4.1. Carbon and oxygen isotope data for bulk calcite cement and bulk dolomite of the Montney Formation, northeastern British Columbia.....	202
Table 4.3. X-ray diffraction (XRD) analyses showing mineralogy of the Montney Formation, well: 16-17-83-25 W6, northeastern British Columbia, Western Canada Sedimentary Basin. Data source: B.C. Oil and Gas Commission.	215
Table 5.1. Data showing well location, sample depth and analyses from Cryogenic machine.	234

List of Figures

Figure 1.1. Location map of study area, showing the various gas fields where core and well data were collected for analysis in northeastern British Columbia, Western Canada Sedimentary Basin.	3
Figure 1.2. Classification scheme for unconventional reservoirs based on Total Organic Carbon (TOC) content (Modified from Integrated Reservoirs Solutions Divisions of Core Lab Reservoir Optimization, 2009).....	4
Figure 1.3. Type Log of the Montney Formation from the subsurface of northeastern British Columbia showing Gamma-ray log signature of Triassic [Montney, Doig and Halfwayformations] (Armitage, 1962).....	6
Figure 1.4. Liard Basin, Bovie Lake seismic section (two-way travel time), showing fault displacement of Middle Devonian to Triassic time. Line courtesy of Mobil Oil Canada, 1971 Vintage; 1200% fold; migrated. Adapted from Atlas of Western Canada Sedimentary Basin (Wright et. al., 1994).....	8
Figure 1.5. Stratigraphic chart showing Triassic nomenclature in British Columbia and Alberta portion of Western Canada Sedimentary Basin, Front Ranges, and the Foothills through the Interior Plains.....	9
Figure 1.6. Well log correlation showing the Triassic succession thinning eastwards (Modified from Edwards, et al., 1994). The variation thickness from British Columbia to Alberta may be related to the progradation of sediments from the east (sediment provenance) into the depocentre.	11
Figure 2.1. (A) Shows tectonic deformation and structure in Western Canada (Modified from Porter et al., 1982). Tectonic Provinces (After Douglas, 1960; Kanasevich, et al., 1969; Fraser et al., 1972). (B) Shows location of study area in northeastern British Columbia, Western Canada Sedimentary Basin.....	26
Figure 2.2. Gamma-ray log correlated with logged core (well d-39-F/93-P-9) showing lithofacies of the Montney Formation, and the overlying erosional contact of Glossifungites – Trypanites surface demarcating the overlying Doig Formation from the Montney Formation in the subsurface of northeastern British Columbia.	28
Figure 2.3. (A) Erosional lag deposit showing pebble clast along the Montney / Doig Formation boundary. (B) Shows the Montney Formation and the overlying Doig Formation seperated by erosional surface. (C) Lag, clast of the Lower Doig Formation along the Doig / Montney boundary. (D) Discontinuity surface along the Montney /Doig boundary.	29
Figure 2.4. Stratigraphic chart showing Lower and Middle Triassic deposits and a corrrrelation of outcrop with coeval subsurface strata in the western Canada Sedimentary Basin (Modified from Orchard and Zonneveld, 2009).....	32

Figure 2.5. Isopach map of the Montney Formation showing the trends of thickness in northeastern British Columbia and northwestern Alberta. The Montney Formation fairway and play segments distinctively show up in the map, displaying three major exploration prospects along the contours > 300 metres in the isopach.	33
Figure. 2.6. Structure contour map of the Montney Formation in northeastern British Columbia and northwestern Alberta.....	34
Figure 2.7. Gamma-ray log correlated with logged core (well: 2-29-79-14W6) showing lithofacies of the Montney Formation, northeastern British Columbia..	36
Figure 2.8. Gamma-ray log correlated with logged core (well: 11-04-79-14W6) showing lithofacies of the Montney Formation, northeastern British Columbia.	37
Figure 2.9. Gamma-ray log correlated with logged core (well: 2-19-79-14W6) showing lithofacies of the Montney Formation, northeastern British Columbia..	38
Figure 2.10. Shows core photo, scanning electron microscopy (SEM) images and petrographic microphotographs of Lithofacies association (F-1) from the Montney Formation. (A) Core photo of Lithofacies F-1, organic rich siltstone with wavy laminae (Well: 1-10-82-23-W6, depth 1996m), Monias gas field, northeastern British Columbia. (B) Shows the mineralogy of Lithofacies association F-1 composed of dolomite and mica (Well: 7-13-79-15W6, depth 2084m). (C) Shows clay mineral associated with the organic component of Lithofacies association F-1, with distinctive layering characteristic of kaolinite clay (Well: 7-13-79-15W6, depth 2084). (D) Detrital dolomite admixed quartz-grained siltstone (Well: J-54-K/93-I-8, depth 1384.2m). (E through G) Shows very fine-grained, well sorted siltstone of Lithofacies association F-1 (Well: b-32-G/93-P-9).....	46
Figure 2.11. Schematic representation of the relationship between processes affecting transport and deposition of fine-grained sediments into distal offshore/and deep-water (Stow, 1985).....	47
Figure 2.12. Depositional environment profile showing dominant energy in the sub-environments from lagoonal – backbarrier area to deepwater setting. Ichnofacies associated with the Montney Formation in the study cores are those attributed to the Skolithos and Cruziana ichnofacies, which typically occur in the shoreface through offshore to slope environment as shown in blue and red bar above.	52

Figure 2.13. Core photographs showing depositional characteristics of Lithofacies F-2. (A) Shows interbedded sandy siltstone (well: 9-29-79-14W6; depth: 1970m). The percentage of sand proportion decreases upward from base of A to top of A (B) Laminated siltstone interbedded with very fine-grained sandstone (well: 11-04-79-14W6; depth: 2052.5m). (C) Shows interlaminated silty-sandstone with fracture along sandstone bedding plane (well: 11-04-79-14W6; depth: 2051m). (D) Very fine-grained sandstone with soft sediment deformation structure overlying coarse-grained siltstone (well: 11-04-79-14W6; depth: 2053.4 m). (E) Plane laminated silty-sandstone. Interbedded silty-sandstone (well: 11-04-79-14W6; depth: 2055 m). (F) The proportion of sand increases towards the top of Plate – F (well: 9-29-79-14W6; depth: 1973.5 m). 54

Figure 2.14. Microphotograph of core samples showing sedimentary structures in Lithofacies association F-2. (A) Laminated, very fine-grained silty-sandstone (well: 11-04-79-14W6; depth: 2070m). (B) Coarse-grained siltstone and very fine-grained sandstone with poorly formed bedding planes (well: 11-04-79-14W6; depth: 2077m). (C) Shows soft sediment deformation structure (well: 11-04-79-14W6; depth: 2071m)..... 55

Figure 2.15. Core photographs showing depositional characteristics of Lithofacies F-2. (A) Laminated very fine-grained, silty-sandstone with current ripple (well: d-39-F/93-P-9; depth: 2655.5m). (B) Siltstone with fractured along bedding planes (well: 8-22-82-20W; depth: 1818.7m). (C) Shows interbedded silty-sandstone and very fine-grained sandstone (well: 9-29-79-14W6; depth: 1946.9 m). (D) Shows siltstone, current ripple and bedding plane fracture (well: 11-04-79-14W6; depth: 2076.2m). 56

Figure 2.16. Microphotographs analyzed using scanning electron microscopy (SEM) and thin-section petrography. (A) Shows potassium feldspar [k-spar], calcium rich feldspar [ca-spar], pyrite cast (white arrow), which forms as a result of diagenesis (well: 1-10-82-23W6; depth: 1996m). (B) Pyritic dolomitic sandstone, sub-rounded grains, and moderately poorly sorted (well: d-21-G/93-P-9, depth 2527m). (C) Shows dolomite with perfect cleavage. The crystal faces exemplified brittleness of lithology due to tensile stress (well: 1-10-82-23-W6, depth 1996m, Monias field). (D) very fine-grained sandstone and siltstone (well: d-21-G/93-P-9, depth 2537m). (E) A mixture of massive, fractured dolomite and quartz exhibiting conchoidal fracture. (F) Shows vuggy porosity associated with intergranular and grained moldic, formed by partial leaching to complete dissolution of feldspar grains and other unstable minerals (well: b-57-G/93-P-9; depth: 2707m). (G) Shows authigenic quartz overgrowth due to diagenesis (well: b-57-G/93-P-9; depth: 2707m). (H) Shows parallel, interlaminated, interstratified very fine-grained sandy-siltstone and argillaceous siltstone due to grain size difference (well: J-54-K/93-I-8; depth: 1386.6m). (I) Shows quartz overgrowth (insect for Plate G), illite clay and micro void spaces (interparticle porosity) (well: b-57-G/93-P-9; depth: 2707m). 60

Figure 2.17. Photomicrographs in thin-sections showing mineralogy for lithofacies F-2. [red arrow = Quartz; yellow arrow = Dolomite; white arrow = Mica (A) Crossed polarized light showing pyrite mineral admixed dolomite mineral, quartz, mica and detrital grains. Pyrite is an indication of diagenesis in the Montney Formation. (B) Dolomitic silty-sandstone. The detrital dolomite forms ripple. (C) Detrital dolomite admixed silty-sandstone. (D) Shows mica, quartz, dolomite, and detrital grains. 61

Figure 2.18. Core photographs showing depositional characteristics of Lithofacies F-2. (A) Shows lamination and current ripple (well: d-39-F/93-P-9; depth: 2660.6m). (B) Shows sediment deformation structure and parallel lamination of very fine-grained silty-sandstone (well: d-39-F/93-P-9; depth: 2659.8m). (C) Shows convolute bedding / sediment deformation (well: d-21-G/93-P-9; depth: 2526.5m)..... 66

Figure 2.19. Core photographs showing various types of sediment deformation in Lithofacies F-2. (A) Shows convolute lamination / bedding (well: d-21-G/93-P-9; depth: 2526.5m). (B) Shows micro-fault that resulted in discontinuity of parallel lamination due to sediment deformation (well: d-21-G/93-P-9; depth: 2540.5m). (C) Shows fugichnia resulting from sediment deformation caused by escape trace during high or episodic sedimentation (well: 9-29-79-14W6; depth: 1985.2m). (D) Shows soft sediment deformation structure caused by sediment loading and dewatering (well: d-21-G/93-P-9; depth: 2541m). (E) Shows soft sediment deformation / convolute lamination (well: 9-29-79-14W6; depth: 1965.5m). (E) Shows lamination and sediment deformation (well: 11-04-79-14W6; depth: 2097m)..... 68

Figure 2.20. Archetypal expression of the Skolithos ichnofacies and Cruziana ichnofacies. The diversity and abundances of trace fossils suite represented in this model is far fetched from the reality of the trace fossils observed in the study core interval of the Montney Formation (see Table 2.2 for trace fossils recorded in the Montney Formation in this study). This model serves the generality of the typical Skolithos ichnofacies and the Cruziana ichnofacies that may exist in any locality. However, a departure from this may occur when dealing with mixed Skolithos and Cruziana ichnofacies, in which cut crossing ichnofacies of opportunistic association dominates. The Skolithos ichnofacies interpretation of abbreviation in Figure A: Ophiomorpha (O), Conichnus (C), Skolithos (Sk), Diplocraterion habichi

(Dh), Roselia (R), Lingulichnus (Li), Arenicolites (Ar), Rhizocorrallium (Rh), Schaucylindrichnus (Sc), Fugichnia (Fu), Cylindrichnus (Cy), Bergaueria (Be), Gyrolithes (Gy), and Palaeophycus tubularis (Pt). For the Cruziana ichnofacies, the interpretation of abbreviations for Figure B are: Arenicolites (Ar), Skolithos (Sk), Diplocraterion habichi (Dh), Rhizocorrallium (Rh), Ophiomorpha (O), Phycosiphon (Ph), Siphonichnus (Si), Planolites (P), Psammichnites (Ps), Thalassinoides (Th), Rhizocorrallium (Rh), Zoophycos (Z), Palaeophycus heberti (Pa), Rusophycus (Ru), Teichichnus (Te), Rosselia socialis (Rs), Conichnus (C), Cruziana (Cr), Phoebichnus (Pb), Lockeia (Lo), Helminthopsis (H), Fugichnia (Fu), Chondrites (Ch), and Cylindrichnus (Cy)... 69

Figure 2.21. (A) Laminated very fine-grained sandstone and coarse siltstone with Planolites (Pl). (B) The lower part of the core is cryptically bioturbated with poor preservation of biogenic structures. The upper part of the core is bioturbated with trace fossils such as Palaeophycus (P), Phycosiphon (Ph), Planolites (P), and Chondrites (Ch). (C) Laminated siltstone interbedded with very fine-grained sandstone. (D) Laminated siltstone interbedded with very fine-grained sandstone. Fugichnia (fu) is present. Trace fossil present: Planolites (P). (E) Cryptically bioturbated silty-sandstone with Phycosiphon (Ph)..... 71

Figure 2.22. Shows Lithofacies F-3A trace fossils. (A) Laminated very fine-grained sandstone and coarse siltstone with Planolites (Pl) (well: A-20-H/93-P-9; depth: 2465.2m). (B) Bioturbated, very fine-grained sandstone showing trace fossils such as Planolites (P), Chondrites (Ch), and Palaeophycus (Pa) (well: d-21-G/93-P-9; depth: 2528.5m). (C) Shows lamination and mono-specific traces of Planolites (P), (well: d-21-G/93-P-9; depth: 2541m). (D) Shows poorly preserved trace fossil record. Fugichnia is present with indiscernible Thalassinoides? (Th) (well: d-21-G/93-P-9; depth: 2527.3m). 72

Figure 2.23. Shows depositional characteristics of Lithofacies F-3. (A) Shows bioturbated Lithofacies F-3 by Planolites and Chondrites (well: d-21-G/93-P-9; depth: 2534m). (B) Shows wave ripple, lamination and fugichnia (well: 9-29-79-14W6; depth: 1967m). (C) Shows fugichnia, 'escape trace' formed as a result of infauna attempt to escape burial during high, episodic sedimentation (well: 9-29-79-14W6; depth: 1984m). 73

Figure 2.24. Microphotographs showing textural and mineralogical characteristics of Lithofacies F-3 of the Montney Formation in the Fort St. John study area, eastern British Columbia. (A and B) Dolomitic silty-sandstone, bioturbated by Phycosiphon and Chondrites trace fossils. (C and E) Shows pyritized detrital dolomite in a silty-sandstone matrix. (D) Shows vuggy porosity associated with bioturbation. Skolithos (Sk) trace fossil is identified in thin-section in Plate D [shown in red arrow], and pyrite [shown in yellow arrow]. (F) Shows very fine-grained siltstone with preserved wood/plant material indicating continental provenance. 75

Figure 2.25. Core photographs showing depositional characteristics and trace fossils in Lithofacies F-3B. (A) Shows fugichnia and lamination (well: 9-29-79-14W6; depth: 1983.7). (B) Shows fugichnia (well: 9-29-79-14W6; depth: 1985.2m). (C) Shows sediment deformation (well: d-39/G93-P-9; depth: 2683m). (D) Shows *Thalassinoides* (Th) (well: 9-29-79-14W6; depth: 1980.5m). (E) Shows increased sand proportion in a siltstone matrix. Fugichnia is also present. (F) Shows poorly preserved traces – *Thalassinoides* (Th)? 78

Figure 2.26. Core log showing Lithofacies associations (F-1 through F-5). 80

Figure 2.27. Shows massive siltstone of Lithofacies F-5. (A) Shows inset for plate C. Illustration shows the sharp facies contact between F-5 and F2 (well: 8-22-82-20-W6; depth: 1817.5). (B) Massive siltstone with pyrite lamina (well: a-39-F/93-P-9; depth: 2455m). (C) Shows magnification of plate A. Illustration shows massive siltstone (well: 8-22-82-20-W6; depth: 1817.5m). (D) Shows massive siltstone and erosional lag deposit, and facies contact along the Montney Fm. / Doig Fm. boundary (well: d-39-F/93-P-9; depth: 2652.5m). 82

Figure 2.28. Shows microphotographs of scanning electron microscopy (SEM) and petrography of lithofacies association F-2 of the Montney Formation. The textural characteristics are exemplified. (A) Angular to sub-angular grains, quartz rich, well sorted. (B) Pyritic sandstone, sub-rounded grains, and moderately well sorted. (B) Shows magnification of plate D. Illustration shows dolomite, and pyritized, organic carbon rich siltstone. Pyrite replaces organic matter during diagenesis. (C) Shows siltstone and some pyrite. (D) Shows inset for plate B. Illustration shows dolomitic siltstone that have been pyritized due to diagenesis. (E) Shows magnification of plate F. Illustration shows very well formed palygorskite clay, a form of clay mineral growth, derived from the transformation of illite to dickite, and further transformation of dickite to palygorskite due to diagenesis (severe temperature and pressure). (F) Shows inset for plate E. Illustration shows dolomite, quartz, illite, dickite and palygorskite clay. 86

Figure 2.29. Shows X-ray diffraction analysis of mineral spectrum present in the Montney Formation. 89

Figure 2.30. Total Organic carbon (TOC) vs. vitrinite reflectance (Ro) showing the thermal maturity of the Montney Formation source rock, and hydrocarbon generating phases in the Montney Formation sediments from study area, northeastern British Columbia. 96

Figure 2.31. Thermal maturity of the Montney Formation determined with Tmax and vitrinite reflectance (Ro). The dotted line (Ro) is vitrinite reflectance calibrated with Tmax. This shows that the Montney Formation in northeastern British Columbia is extensively matured. 96

Figure 3.1. (A) Map of Canada showing provinces. (B) Shows tectonic deformation and structure in Western Canada Sedimentary Basin (Modified from Porter et al., 1982). (C) Shows location map of study area in northeastern British Columbia. The black dots represent drilled wells. 132

Figure 3.2. Stratigraphic chart showing Lower and Middle Triassic deposits and a correlation of outcrop with coeval subsurface strata in the western Canada Sedimentary Basin (Modified from Orchard and Zonneveld, 2009). 137

Figure 3.3. Structure contour map of the Montney Formation in the study area, northeastern British Columbia. Dash contour lines indicate no data point for well control. The structure map decreases in elevation westward, which indicates that sediment source area was from east, and prograded westward. 138

Figure 3.4. The Montney Formation core description showing lithofacies, tracefossils, and depositional sedimentary features. Gamma-ray log and core are from well 11-04-79-14W6, northeastern British Columbia. 140

Figure 3.5. Shows the lithofacies of the Montney Formation. (A) Plane lamination [well: 11-04-79-14W6, 2051m]. (B) Fractured siltstone along bedding plane [well: 11-04-79-14W6, 2065.5m]. (C) Silty-sandstone with current ripple sedimentary structure [well: 11-04-79-14W6]. (D) Shows sediment deformation structure [well: d-21-G/93-P-9]. (E) Bioturbation by Phycosyphon [well: 11-04-79-14W6, 2092m]. (F) interbedded silty-sandstone [well: 11-04-79-14W6, 2055.5m]. (G) Escape structure (fugichnia?) in a silty-sandstone. 141

Figure 3.6. Rock-Eval pyrolysis for Montney Formation sample (well 2-19-79-14W6, depth: 2085 m). (A) illustrates the effect of pyrolysis temperature with Rock-Eval. The S1 peak is the free hydrocarbon liberated during thermal decomposition at less than 3000C. The S2 peak is derived from the conversion of total organic matter to kerogen during pyrolysis (pyrolyzed fraction). The S2 corresponds to the maximum temperature (Tmax). (B) shows the S3 peak (CO₂) corresponding to 4000C, which represents the oxidation of CO₂. It also shows the difference in organic matter. (C) illustrates the pyrolysis carbon monoxide (CO). (D) shows the oxygen indices. The determination of oxygen index (OI) is based on using CO₂ and CO; the $CO = S3CO \times 100/TOC$ Total oxygen index (OI) = CO₂ + OI (CO). (E) shows the S4 peak, the oxidation carbon monoxide (CO), the peak shows the present of siderite mineral (400 - 6000C). (F) Oxidation of CO and CO₂. The red line is the temperature trace in 25 minutes from 3000C to 6500C. Distinctly bi-modal curve is due to pyrobitumen. See complete pyrolysis graphs for analyzed samples in Appendix 3-B 142

Figure 3. 7. The Montney Formation average TOC (wt%) map within the study area, northeastern British Columbia and northwestern Alberta. The red dots represent wells with Rock-Eval data. 144

Figure 3.8. Shows a plot of Oxygen index (OI) vs. Hydrogen index (HI). The low OI and HI indicate that the Montney Formation in the study area is primarily a Type III/IV kerogen, with a mixed Type II/III kerogen.....	148
Figure 3.9. Pseudo Van Krevelen diagram showing kerogen types and TOC richness in the Montney Formation.	150
Figure 3.10. Shows the remaining hydrocarbon generating capacity (S ₂) in the Montney Formation, plotted with total organic carbon (TOC). Hydrogen index (HI) line indicates the kerogen type.....	152
Figure 3.11. Shows S ₂ peak (remaining hydrocarbon generating capacity) for the Montney Formation, which corresponds to the T _{max} . The S ₁ peak is the liberated hydrocarbon during rapid artificial thermal cracking of kerogen during pyrolysis. Sample location: well 2-19-79-14W6 (depth: 2085 m).	154
Figure 3.12. Thermal maturity of the Montney Formation determined with T _{max} and vitrinite reflectance (R _o). The dotted line (R _o) is vitrinite reflectance calibrated with T _{max} . This shows that the Montney Formation in northeastern British Columbia is extensively matured.	155
Figure 3.13. The Montney Formation average T _{max} (°C) map. T _{max} values are posted over TOC map to show geographical distribution of source rock quality (TOC), and thermal maturity of source rock. The red dots represent wells with Rock-Eval data. Evidently, the Montney Formation kerogen is thermally matured, and it is within the 'peak gas' generation window in the study area, northeastern British Columbia, and northwestern Alberta as shown by the average T _{max} values.	158
Figure 3.14. Total Organic carbon (TOC) vs. vitrinite reflectance (R _o) showing the thermal maturity of the Montney Formation source rock, and hydrocarbon generating phases in in the Montney Formation sediments from study area, northeastern British Columbia.	163
Figure 3.15. Shows that the Montney Formation kerogen is thermally matured, and extensively charged with gas.....	164
Figure 3.16. Shows porosity and gas filled porosity of the Montney Formation (well 16-17-82-25W6). The graph shows very excellent correlation between porosity and gas filled porosity. (Data source: B.C. Oil and Gas Commission).....	167
Figure 3.17. Porosity vs. permeability crossplot for the montney Formation, well: 2-19-79-14W6 (depth 2037.40 - 2091.90 m). Data source: B.C. Oil and Gas Commission.	168
Figure 3.18. Microphotograph showing dolomitic siltstone facies and the associated vuggy porosity resulting from dissolution of material. Yellow arrow labeled 'P' is pointing to vuggy porosity.....	169
Figure 3.19. Graph showing permeability vs. depth of the Montney	

Formation from well 16-17-82-25W6, northeastern British Columbia (Data source: B.C. Oil and Gas Commission).....	171
Figure 3.20. Illustrates fluid saturation (gas, oil, and water) of the Montney Formation from well 16-17-82-25W6, northeastern British Columbia (Data source: B.C. Oil and Gas Commission).....	174
Figure 3.21. A cross plot showing total organic carbon (TOC wt%) values and S ₂ values (the amount of hydrocarbon formed during thermal decomposition of the kerogen). The higher S ₂ values indicate greater hydrocarbon generating potential. In general, the S ₂ and TOC values show that the Montney Formation in the study area, northeastern British Columbia has good source rock quality.....	177
Figure 3.22. Isopach map of the Montney Formation showing the trends of thickness in the study area, northeastern British Columbia.....	179
Figure 3.23. The Montney Formation gas in-place estimates (Walsh, et al., 2006).....	181
Figure 4.1. (A) Map of Canada showing provinces. (B) Shows tectonic deformation and structure in Western Canada Sedimentary Basin (Modified from Porter et al., 1982). (C) Shows location map of study area in northeastern British Columbia. The black dots represent drilled wells.	194
Figure 4.2. Stratigraphic chart showing Lower and Middle Triassic deposits and a correlation of outcrop with coeval subsurface strata in the western Canada Sedimentary Basin (Modified from Orchard and Zonneveld, 2009).....	196
Figure 4.3. Shows the isopach of Triassic succession in the Western Canada Sedimentary Basin. The Succession thickened to the west from Alberta to British Columbia, towards the Cordilleran deformation front (Edwards and Gibson, 1994).....	198
Figure 4.4. Isopach map of the Montney Formation showing the trends of thickness in the study area, northeastern British Columbia.....	199
Figure 4.5. Structure contour map of the Montney Formation in the study area, northeastern British Columbia. Dash contour lines indicate no data point for well control. The structure map decreases in elevation westward, which indicates that sediment source area was from east, and prograded westward.	200
Figure 4.6. Isotopic data plot for the Montney Formation. (A) Bar graph showing calculated $\delta^{13}\text{C}$, and $\delta^{18}\text{O}$ and SMOW. (B) Displays the $\delta^{13}\text{C}$ and $\delta^{18}\text{O}$ (PDB) fields. (C) Crossplot of bulk calcite and bulk dolomite. (D) Shows linear graph of oxygen and carbon isotopes showing the bulk dolomite and bulk calcite (SMOW) of the isotopic composition. The lower linear graph shows the PDB of bulk calcite and bulk dolomite isotopic composition.....	204
Figure 4.7. Shows the variation pattern of concentration of trace elements. (A) Illustrates the composition of dolomite, in which there is higher	

concentration of magnesium (Mg) relative to the calcite (Ca) component. The graph pattern shows good correlation between Mg and Ca. (B) Shows major elements, potassium (K) and aluminum (Al). The concentration of K is very high because of the clay mineral and the organic richness of the Montney Formation sediments. The A concentration is related to the clay mineralogy and partly has affinity to organic matter. The graph pattern of K and Al correlates very well. (C) Shows alkaline earth metals – Strontium (Sr) and Rubidium (Rb) concentration. (D) Illustrates the concentration of Iron (Fe) and Manganese (Mn). Fe and Mn are both related to diagenesis. The concentration of Fe is very high compared to the concentration of Mn. This indicates that Fe has more dominating diagenetic influence in the Montney Formation. Evidence from thin-section petrography (Fig. 4.15-D) shows replacement of organic matter by pyrite. (E) Shows the relationship between radioactive elements – Uranium (U) and Thorium (Th). These elements are particularly related to the clay mineralogy and organic components of the Montney Formation sediments. (F) Shows the relationship between calcite (Ca) and Potassium (K). Evidently, Ca has enormously high concentration due to the stoichiometric co-existence with dolomite..... 211

Figure 4.8. Microphotographs showing SEM and thin-section petrography of the Montney Formation illustrating the mineralogical composition. (A) Dolomite and quartz matrix. The quartz exhibits conchoidal fracture. (B) Shows magnification of plate C. Authigenic quartz overgrowth is illustrated in plate-B as evidence of grain dissolution due to diagenesis, and subsequent mineral precipitation (calcite) in the form of calcite cement that welded the grains together. (C) Shows quartz and illite with the authigenic quartz overgrowth. (D) Illustrates pyritized, dolomitized, organic carbon rich siltstone. Pyrite replaces organic matter in plate-D during decomposition of organic matter due to diagenesis. (E) Illustration of a very well formed palygorskite clay; a form of clay mineral growth, formed from the transformation of dickite to illite, and further transformation of illite to palygorskite due to severe temperature and pressure in a diagenetic regime. 213

Table 4.3. X-ray diffraction (XRD) analyses showing mineralogy of the Montney Formation, well: 16-17-83-25 W6, northeastern British Columbia, Western Canada Sedimentary Basin. Data source: B.C. Oil and Gas Commission. 215

Figure 4.9. Photomicrographs showing Dolomitic silty-sandstone. (A) Shows detrital dolomite resembles ripple. (B) shows detrital dolomite admixed siltstone. (C) Crossed polarized light showing detrital dolomite (yellow – arrow), quartz (red – arrow), and mica (white – arrow). 216

Figure 5.1. (A) Map of Canada showing provinces. (B) Shows tectonic deformation and structure in Western Canada Sedimentary Basin (Modified from Porter et al., 1982). (C) Shows location map of study area in northeastern British Columbia. The black dots represent drilled wells. 230

Figure 5.2. Synthetic example of magnetostratigraphic dating in the drilled

core where alternating polarity intervals are registered. Normal polarity (black color intervals), coincides with present day geomagnetic field direction and is observed in the studied Montney and Lower Doig formations cores. Reverse polarity (white color intervals) corresponds to the geomagnetic field direction which is opposite to the present day geomagnetic field and is observed in the Montney Formation..... 232

Figure 5.3. (A) Shows sample preparation for demagnetization measurement. Samples size and precise orientation indicating magnetic north is crucial. The top (magnetic north) of samples are distinguished from the bottom (south orientation) by marking an arrow on samples to indicate top. (B) Shows the cryogenic machine and samples were being loaded into the machine for demagnetization experiment. (C) Illustrates sample measurement in progress and rendering of samples in incremental steps to demagnetize remnant magnetization in the Paleomagnetic Lab, Department of Physics, University of Alberta..... 233

Figure 5.4. Shows normal and reverse polarity of measured samples from well: 12-35-14W6. The expected normal polarity inclination for the Early-Middle Triassic deposits range from 30 to 60 degrees. The expected reverse polarity inclination for the Early-Middle Triassic deposits range from -60 to -30 degrees. The observed inclination match the expected inclination for the Early-Middle Triassic..... 235

Figure 5.5. Shows normal and reverse polarity of measured samples from well: 9-29-79-14W6. The expected normal polarity inclination for the Early – Middle Triassic deposits range from 30 to 60 degrees. The expected reverse polarity inclination for the Early – Middle Triassic deposits range from -30 to -60 degrees. The observed inclination presented in this figure match the expected inclination for the Early – Middle Triassic..... 236

Figure 5.6. Results of alternating field demagnetization for the reverse and normal polarity for samples obtained from core (well: 12-35-79-17-W6). (A and B) Illustrates typical equal-area projections showing demagnetization paths during experiments. (C and D) Shows demagnetization orthogonal vector plots indicating strong normal remnant magnetization. (E and F) Illustrates normalized intensity of magnetization versus applied laboratory field in mT. Closed (open) symbols in orthogonal plots: projections onto the horizontal (vertical) plane. The core was not oriented azimuthally therefore declination is arbitrary..... 237

Figure 5.7. Paleomagnetic correlation of Lower Triassic (Lower Doig and Upper Montney formations) with known Triassic paleomagnetic data for Triassic. Ellesmere Island composite is from the Smith Creek and Creek of Embry sections of Ogg and Steiner (1991) and Orchard (2008). Upper Silesia composite (Nawrocki 1997; Nawrocki and Szulc, 2000); Spitsbergen composite (Hounslow et al., 2008a, b; Galfetti, et al., 2007b). The base Anisian used is the first occurrence of *Cs. timorensis* in the De ħli Cairra section (Gra ħdinaru et al. 2007)..... 240

CHAPTER 1: INTRODUCTION

GENERAL OVERVIEW AND OBJECTIVES

The Western Canada Sedimentary Basin (WCSB) is well known for the prolific hydrocarbon resources associated with the thick sedimentary rocks (more than 6,000 metres thick) in the subsurface (Porter, et al., 1982). This research in the Fort St. John area of northeastern British Columbia (Fig. 1.1) is undertaken because hydrocarbon exploration and production in WCSB has attained maturity and attention is shifting to alternative reservoir types, such as shale gas and tight gas reservoir systems.

Tight gas reservoirs are characteristically composed of heterogeneous lithologies, varying from a mixture of argillaceous, siliceous, calcareous to end members matrix compositions with variability in mineralogy both in vertical or lateral extent, and characteristically exhibiting low porosity ($\leq 10\%$), low permeability ($\leq 0.1\text{mD}$), and low total organic carbon (TOC) content (0.01 – 0.8wt.%) (Fig. 1.2).

The Montney Formation is a primary focus of tight gas reservoir exploration in WCSB. Despite strong economic interest in unconventional silt-hosted hydrocarbon reservoir in this unit, the geology, geochemistry, mineralogy, petrophysics and characterization of the succession remain poorly understood and have not been adequately characterized.

A type log of the Montney Formation (Fig. 1.3) from the subsurface of northeastern British Columbia in the discovery well Texaco NFA Buick Creek 6-26-87-21W6 (1715 to 1981 m), which is ~40km northwest of Fort St. John was originally and formerly assigned by Armitage (1962) as the type section of the Montney Formation. The Montney Formation is characteristically a complex and enigmatic deposit of siliciclastics, in part dolomitic, and phosphatic (along the

Montney/Doig boundary); the lithofacies comprises siltstone, very fine-grained sandstone, organic rich mudstone, and bioclastic packstone/grainstone (coquina) (Zonneveld, et al., 2010). Core from the type section shows that the lower Montney Formation consists of interbedded dolomitic siltstone and shale, whereas the upper Montney Formation consists of siltstone with interbedded very fine-grained to fine-grained sandstone (Zonneveld, 2010). The Montney Formation in the subsurface of northeastern British Columbia is the lateral equivalent to outcrop of the Grayling and Toad formations and the Vega and Phroso members of the Sulphur Mountain Formation, respectively, in the northern and southern Rocky Mountain Foothills and Front Ranges (Gibson, 1971; Gibson and Barclay, 1989; Gibson and Edwards, 1990; Zonneveld et al., 1997; 2010). Davies et al. (1997) and Dixon (2000) have proposed two informal subdivisions of the Montney Formation. This subdivision is not generally accepted by workers of the Montney Formation.

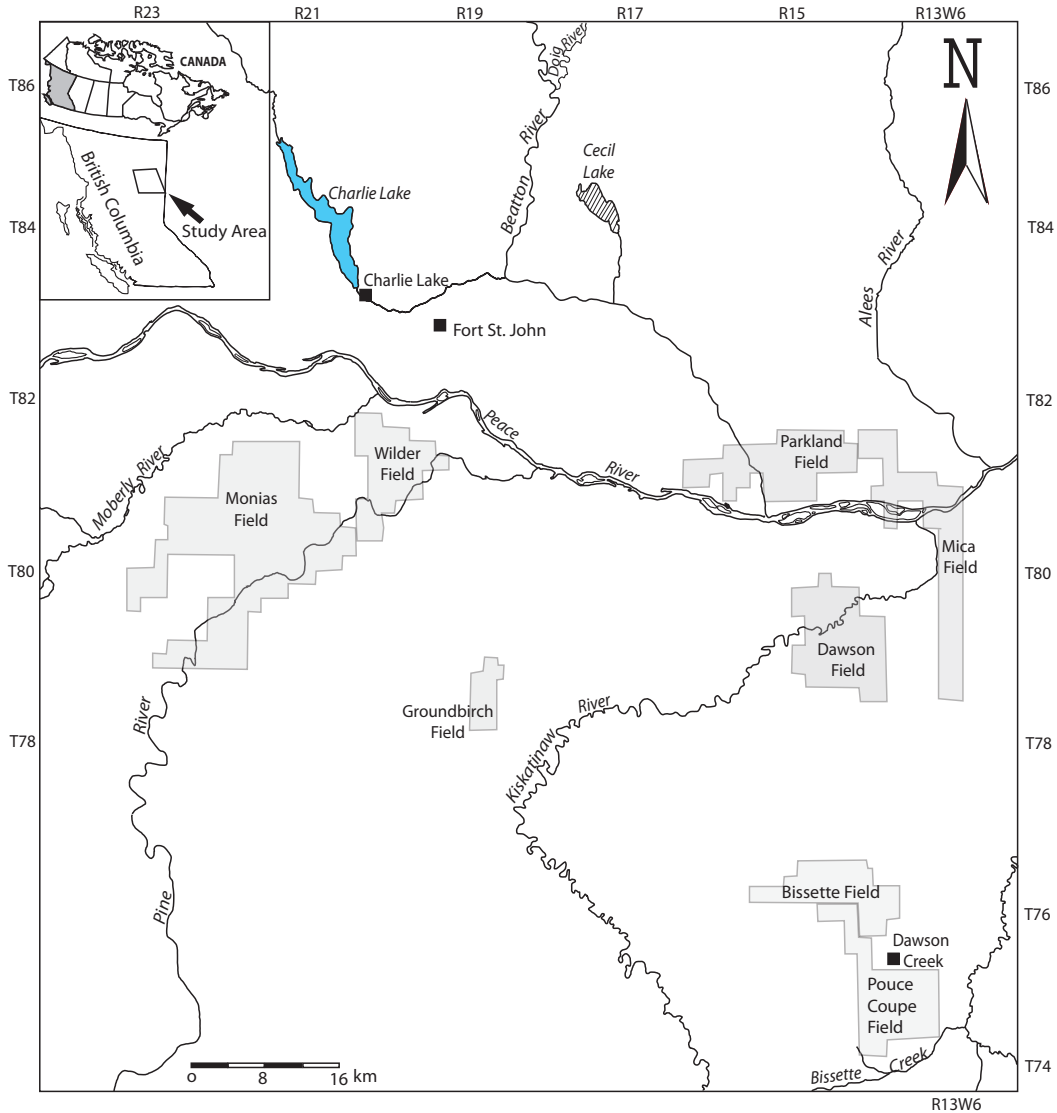


Figure 1.1. Location map of study area, showing the various gas fields where core and well data were collected for analysis in northeastern British Columbia, Western Canada Sedimentary Basin.

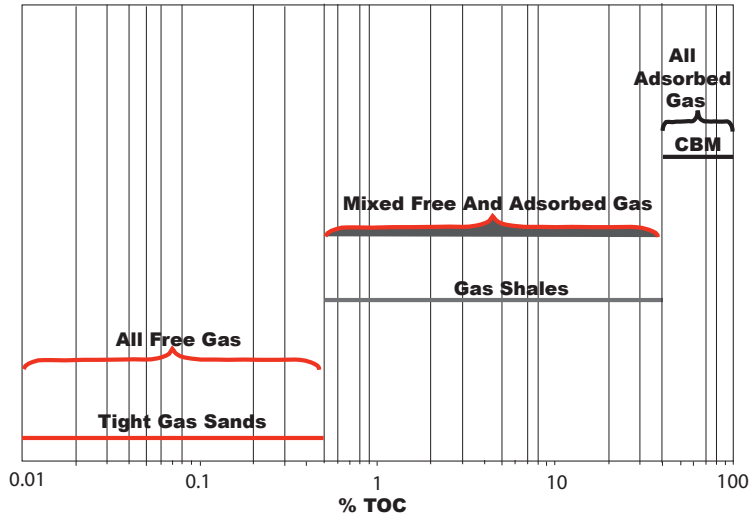


Figure 1.2. Classification scheme for unconventional reservoirs based on Total Organic Carbon (TOC) content (Modified from Integrated Reservoirs Solutions Divisions of Core Lab Reservoir Optimization, 2009).

The Montney Formation is separated by unconformity from the underlying Permian Belloy Formation (Gibson and Barclay, 1989; Tozer 1994). It is separated from the overlying Doig Formation by a strongly radioactive, phosphate-rich interval known informally as the “Doig Phosphate Zone” (Armitage, 1962; Gibson and Edwards, 1990; Tozar, 1997). The Montney/Doig boundary has the same paleomagnetic record of normal polarity, which corresponds to the normal polarity interval MT2 in the bottom of the Anisian age that starts at ~ 245 Ma (Eggbowaye et al., 2011). The trace fossil record show that the Montney / Doig boundary is a coplanar *Trypanites–Glossifungites* demarcated discontinuity surface and it is a regionally correlatable surface (Eggbowaye, et al., 2011). The outcrop coeval of the Montney Formation is the Grayling and Toad formations in Alberta and British Columbia (Armitage, 1962; Dixon, 2007; Orchard and Tozar, 1997; Zonneveld et al., 2001; Zonneveld, 1999).

The Montney Formation occurs at the Permian-Triassic boundary. It is the basal stratigraphic unit of Triassic deposits in the subsurface of WCSB. It rests,

unconformably in most areas, upon carbonate strata of Carboniferous to Permian age (Edward et al., 1994; Pudruski et al., 1988; Riediger et al., 1990; Gibson and Edwards, 1990). The succession was deposited in a west-facing, arcuate extensional basin in the western margin of Supercontinent Pangaea (Davies et al., 1997; Orchard and Tozar, 1997; Zonneveld, 1999; Zonneveld et al., 2001). The Montney Formation has the highest thickness in the center of the Peace River Embayment, but gradually thin eastwards, where the outcrop limit is truncated by Jurassic strata (Davies et al., 1997; Davies et al., 1994; Gibson and Edwards, 1990; Gibson and Barclay, 1989).

Montney Formation Discovery Well: Texaco N.F.A Buike Creek No. 7
6-26-87-21-W6

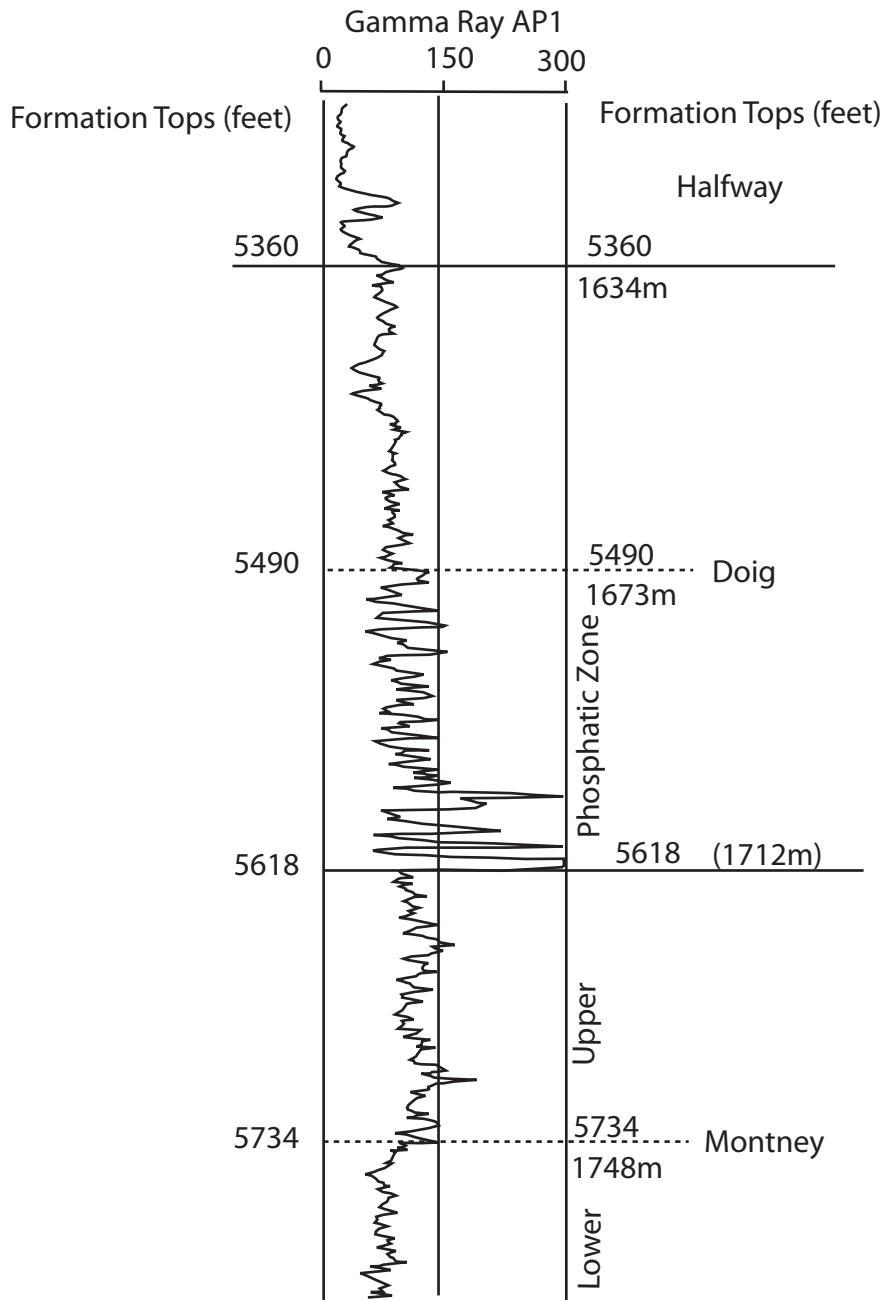


Figure 1.3. Type Log of the Montney Formation from the subsurface of northeastern British Columbia showing Gamma-ray log signature of Triassic [Montney, Doig and Halfway formations] (Armitage, 1962).

PREVIOUS WORK

Previous work on the WCSB has dealt with the tectonics, sedimentology, regional stratigraphy, and ichnology. However, no detailed work is available in published literature on tight gas reservoir of the Montney Formation. Some of the relevant previous work in the Triassic succession are discussed below.

Tectonic Setting

The WCSB developed during early Carboniferous and Permian time, coinciding with the area occupied by the Devonian Peace River Arch (Edwards, et al., 1994). The formation of the WCSB is attributed to the subsidence of a Carboniferous – Permian embayment as a result of a broad downwarp with large central half-graben complex along the axis of the arch, with subsidence accompanied by intense block faulting (Richards, 1989; Henderson, 1989; Barclay et al., 1990; O’Connell et al., 1990). As the embayment persisted and subsided during the Triassic period, minor fault block movement associated with a broad downwarp resulted in the rejuvenation of structural collapse within the Monias areas of southwest Fort St. John, which subsequently influenced sedimentation pattern in the basin (Edwards, et al., 1994). Evidence of structural deformation in the WCSB is exemplified in the seismic profile shown in Figure 1.4.

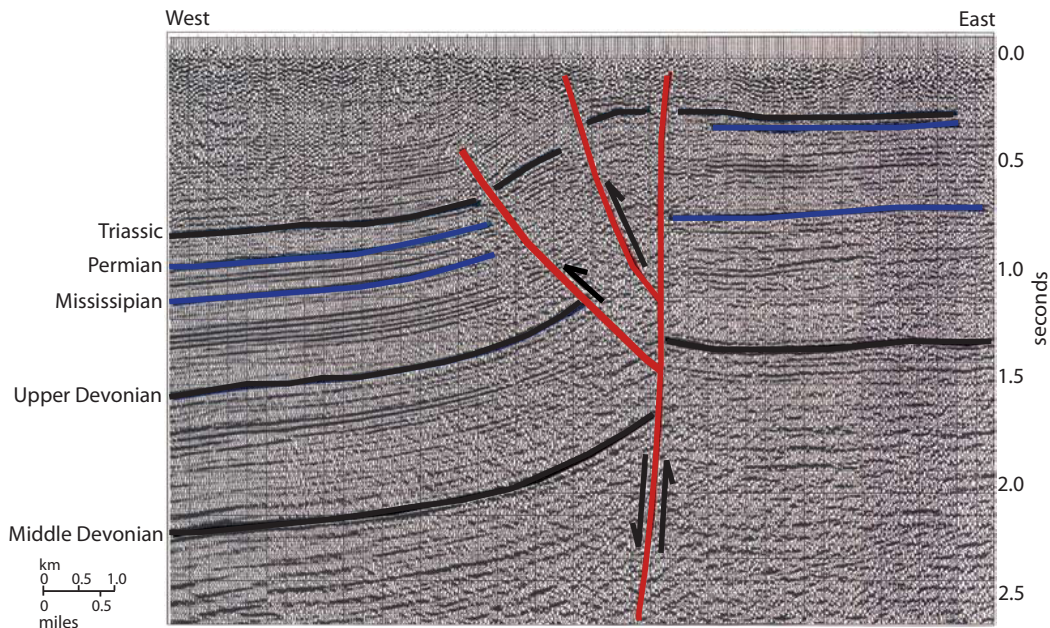


Figure 1.4. Liard Basin, Bovie Lake seismic section (two-way travel time), showing fault displacement of Middle Devonian to Triassic time. Line courtesy of Mobil Oil Canada, 1971 Vintage; 1200% fold; migrated. Adapted from Atlas of Western Canada Sedimentary Basin (Wright et. al., 1994).

Regional Stratigraphy

The age of the Montney Formation in WCSB is Lower Triassic (Fig. 1.5). In Western Canada, Triassic deposits thicken westwards reaching about 1200 metres thick in the western-most outcrop in the Rocky Mountain Foothills (Willis, 1992). The Triassic strata are divided into Early, Middle and Late stages (Orchard and Tozer, 1997). In chronostratigraphic order, the formations in outcrop range in age from Griesbachian to Norian, namely: Grayling Formation, Toad Formation, Liard Formation, Charlie Lake Formation, Baldonnel Formation, Pardonet Formation and Bocoock Formation(Orchard and Tozer, 1997; Edwards, et al.,

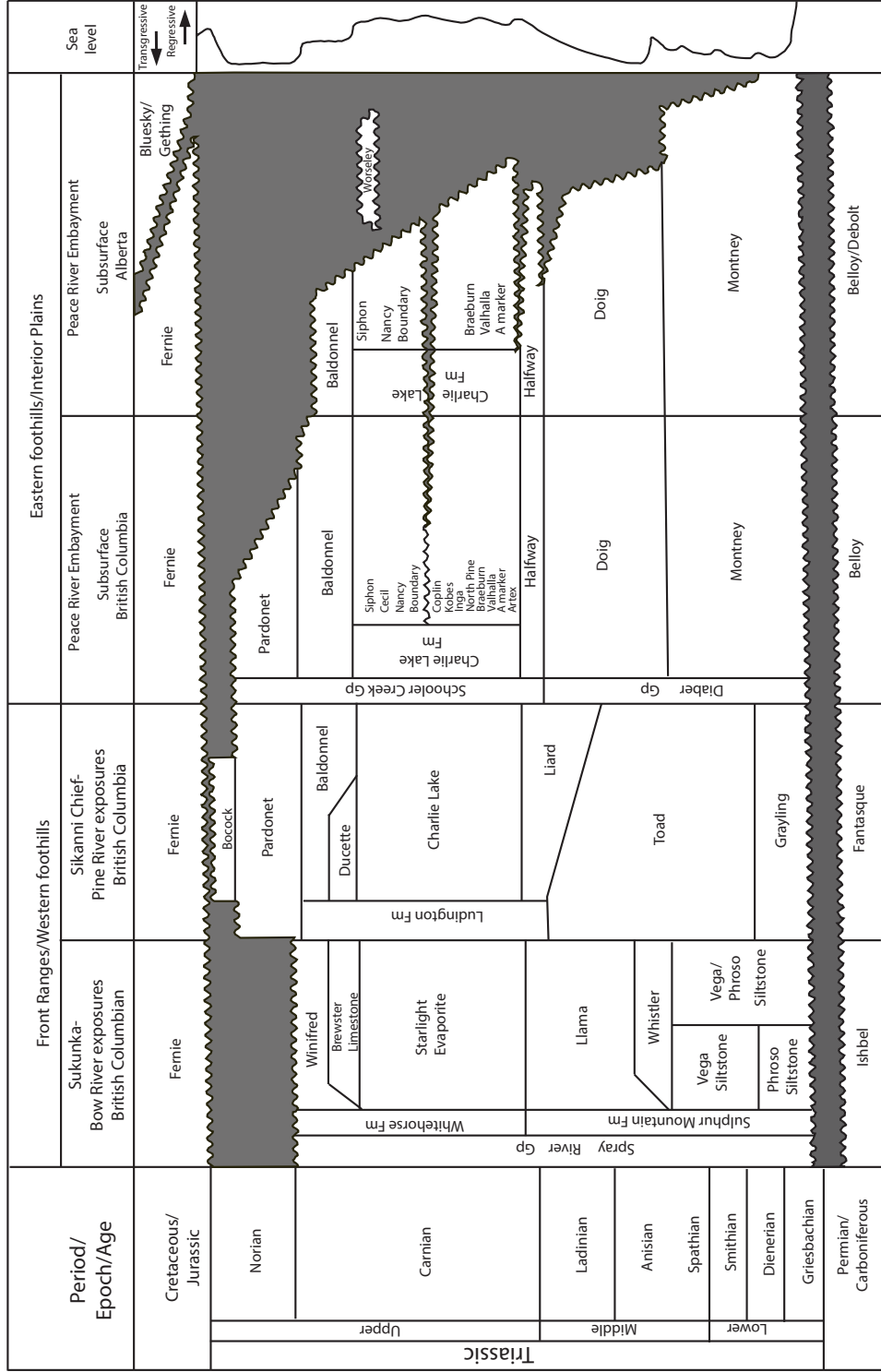


Figure 1.5. Stratigraphic chart showing Triassic nomenclature in British Columbia and Alberta portion of Western Canada Sedimentary Basin, Front Ranges, and the Foothills through the Interior Plains.

1994). In the subsurface of Western Canada, the Grayling-Toad Formation is the equivalent of the Montney Formation; the Toad-Liard Formation corresponds to the Doig Formation in the subsurface; and the upper Liard Formation is the equivalent of the Halfway Formation in the subsurface (Edwards, et al., 1994). The Triassic succession thins eastwards (Fig. 1.6), rests unconformably in most areas, upon Permian carbonate strata of Belloy Formation (Edwards, et al., 1994).

Davies et al. (1997) attributes the deposition of the Montney Formation to the influence of arid climatic conditions. Panek (2000) reported the presence of cyanobacterial mats in the Montney Formation as an indication of aridity. Cyanobacterial mats have been interpreted to be associated with typically warm, arid, low energy intertidal to supratidal environments (Pratt, et al., 1992), which supports the arid climate in Davies et al. (1997). However, downslope gravity movement enhancing the deposition of the Montney Formation has been argued (Davies et al., 1997). Such evidence is based on paleostructure of topographic highs over underlying Upper Devonian Leduc reefs associated with graben trends in the Peace River Embayment, which is suggested to have triggered slope failure that lead to the deposition of the Montney Formation (Davies et al., 1997).

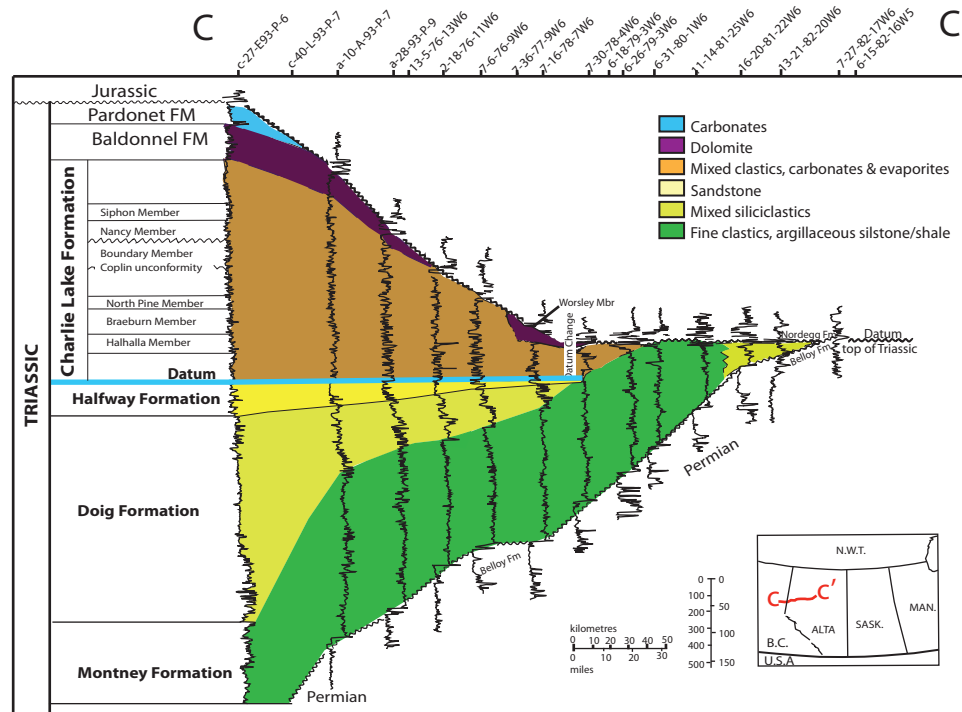


Figure 1.6. Well log correlation showing the Triassic succession thinning eastwards (Modified from Edwards, et al., 1994). The variation thickness from British Columbia to Alberta may be related to the progradation of sediments from the east (sediment provenance) into the depocentre.

In west-central Alberta, the Lower Triassic Montney Formation has been divided into two major third-order sequences distinguished by a sequence boundary that correlates to an Early Triassic global eustatic sea level fall during the Dienerian and Smithian Stages, which caused mass-wasting processes that deposited turbidite channel and lobe complex within the lowstand systems tract of the upper Montney sequence (Moslow and Davies, 1997). The depositional environments for the Montney facies range from mid to upper shoreface sandstones; middle to lower shoreface sandstones and coarse siltstones; finely laminated lower shoreface sand and offshore siltstones; and turbidites (Davies et al., 1997; Panek, 2000; Zonneveld, 2002). Bioclastic sandstones are locally common in Montney Formation in north-western Alberta (Markhasin, 1997).

Reservoir History and Development

The WCSB has attracted numerous workers since 1918, particularly oil and gas companies, owing to the abundant petroleum resources in Alberta and British Columbia with proven reserve of approximately 1,781 million barrels of oil and 53.2 TCF of gas (CAPP, 2007).

Podruski et al. (1988) assessed the conventional oil potential of the WCSB. Most of the hydrocarbon production from the Montney has been by conventional reservoir development in fine-grained sandstone and coquina (bioclastic grainstone) units deposited in a variety of shallow marine (e.g. barrier island shoreface, tidal inlet channel, etc.) and deep marine (e.g. turbidite fan) depositional settings (Podruski et al., 1988; Walsh et al., 2006; Zonneveld, 2008).

Reported in-place gas potential for the Montney and Doig formations in Alberta and British Columbia are estimated to be 187 TCF for the Montney Formation and 139.7 TCF for Doig formation (Faraj et al., 2002). In British Columbia where the present study is located (Fig. 1.1), 41 percent of its natural gas reserve and 80 percent of the conventional oil reserve were discovered within the Triassic succession (Bird et al., 1994).

Sedimentology

McLearn (1918) began the study of Triassic rocks in relation to sedimentology and stratigraphy in WCSB in the Rocky Mountain Foothills region, which is summarized by McLearn and Kindle (1950). A notable study of outcrops in British Columbia was done by Hunt and Ratcliffe (1959), who first subdivided the Triassic of northwestern Alberta into the Toad-Grayling, Halfway and Charlie Lake formations. Subsequent work (e.g. Armitage, 1962) conducted a subsurface study

in British Columbia and divided the subsurface equivalents of the Toad-Grayling formations into the Montney and Doig formations.

The sedimentology and stratigraphy of the Montney Formation have been worked on by Gibson and Barclay (1989, 1990); and Moslow and Davies (1992). Edwards et al. (1994) summarized the Triassic succession of WCSB in the Atlas of Western Canada Sedimentary Basin.

Biostratigraphic and paleontological studies were done by Henderson (1997); Orchard and Tozer (1997); and Paull, et al. (1997). Orchard and Tozar (1997) used ammonoid and conodont derived from WCSB to set standard North America conodont zones.

The sedimentology and sequence biostratigraphic framework of a mixed siliciclastic-carbonate depositional system in the Middle Triassic of northeastern British Columbia was investigated by Zonneveld (1999). Zonneveld and Pember-ton (2001) used ichnospecies to interpret the lower Montney Formation as tempestites based on the preserved trace fossils record, such as *Planolites*, *Treptichnus* and *Chondrites* in shale and silty intervals of the lower Montney Formation.

METHOD OF STUDY

This study is divided into seven chapters to elucidate unconventional the tight gas reservoir of the Montney Formation. Data were gathered from eight gas fields within the study area, namely: Wilder field, Groundbirch field, Dawson field, Parkland field, Sunset field, Bissette field, Pouce Coupe field, and Monias field. The datasets for this study consists of 275 well logs and 20 cored wells (Appendix 1-A). All cores were logged and described (Appendix 2-A).

Laboratory methods used in this research comprises core logging, pulverizing rock samples into powdered form with the shatter-box machine, X-Ray

Diffraction (XRD), Scanning Electron Microscopy (SEM), Inductively Coupled Plasma Mass Spectrometry (ICP-MS) for whole-rock geochemistry, Stable isotope geochemistry, thin-section petrography, Tight Rock Analysis (TRA), and A 2G Enterprises Superconducting Horizontal Magnetometer, and Bartington Susceptibility Meter System were used for paleomagnetic analyses by measuring remnant magnetization, which involves a demagnetization procedure using the alternating field (AF) in incremental steps up to 100 mT to show polarity inclination or declination (Normal or Reverse polarity) in the Montney Formation studied cores.

Core analyses were collected from the Government of British Columbia: B.C. Oil and Gas Commission. The Commission generously gave authorization to EDWIN I. EGBOBAYE to use all data from the B.C. Oil and Gas Commission in publication in a journal (Appendix 1-B).

The AccuMap well log database was used extensively for querying and retrieving well data from the database, well production history and drilling activities in northeastern British Columbia. All of the cores used in this research were accessed at the Core Storage Facility of the British Columbia Ministry of Energy and Mines, located at Charlie-Lake, near the town of Fort St. John, B.C., Canada. A total of twenty core of the Montney Formation in the study area were logged (Appendix 2–A).

Software

Geographix software was used at Chesapeake Energy Corporation, Oklahoma City, USA to make maps (isopach and subsea structure maps). The ArcGIS (Aeronautical Reconnaissance Coverage Geographic Information Systems) software was used to plot well locations on the map of the study area, and also to plot TOC and T_{\max} maps.

PROJECT OBJECTIVES

This thesis is divided into six chapters for the purpose of meeting the overall research objectives stated below:

- 1) To provide detailed lithofacies characteristics, sedimentological and ichnological analyses of the Montney Formation.
- 2) To determine the geochemistry, source-rock potential, and reservoir characteristics of the Montney Formation.
- 3) To apply these results within the context of unconventional gas reservoir characterization and to better understand in particular the newly evolving tight gas reservoir play within the Montney Formation.

In reference to the above objectives, chapter one provides the general overview and framework of this thesis, literature review of previous work, objectives of research, and the methodology employed in this study.

In chapter two, the Sedimentology and Ichnology of the Montney Formation tight gas reservoir is discussed in detail, particularly with emphasis on the identified five recurring lithofacies associations in this study, which are based on sedimentological and ichnological criteria. Description of the lithofacies and interpretation, including depositional environments, are presented in this chapter.

Chapter three deals with the Source-rock Geochemistry of the Montney Formation. Rock-Eval pyrolysis analytical method was utilized, and the data derived helped to establish hydrocarbon potential of the Montney Formation tight gas reservoir by determining the total organic carbon (TOC) richness, thermal maturity, and their geographical distribution in the subsurface of the study area. The plotted TOC and T_{\max} data shows the geographical distribution of TOC and T_{\max} in the study area.

Chapter four discusses Stable Isotope Geochemistry of the Montney Formation. Isotope geochemistry is an established method used in the study of dolomite, dolomitization and diagenesis by utilizing $\delta^{18}\text{O}$ and $\delta^{13}\text{C}$ isotopic composition (Kasting, et al., 2006). Because the Montney Formation is dolomitized, stable isotope analysis is a unique method to understand and interpret the occurrence of dolomite and paleotemperature of dolomitization in the Montney Formation.

Chapter five deals with Magnetostratigraphy of the Montney Formation. Paleomagnetism is employed in this study to augment well log correlation because paleomagnetic record is a useful chronostratigraphic tool that is based upon geomagnetic polarity change, which is a global phenomenon that provides an independent means of correlation that is not reliant upon well-log correlation and interpretations.

Chapter six summarizes the thesis and gives concise conclusions of the research findings.

REFERENCES

- Armitage, J.H. 1962. Triassic oil and gas occurrences in northeastern British Columbia, Canada. *Journal of the Alberta Society of Petroleum Geologists*, vol. 10, p. 35–56.
- Aukes, P.G., and Webb, T.K., 1986, Triassic Spirit River Pool, northwestern Alberta. In: *Canadian Society of Petroleum Geologists, 1986 Core conference*, Calgary, Alberta, Canada. N.C. Meijer Drees (ed.), p. 3.1-3.34.
- Barclay, J.E., Krause, F.F., Campbell, R.I., and Utting, J., 1990, Dynamic casting and growth faulting: Dawson Creek Graben Complex, Carboniferous-Permian Peace River Embayment, Western Canada, In: *Geology of the Peace River Arch*, S.C.
- O’Connell and J.S. Bell (eds.), *Bulletin of Canadian Petroleum Geology*, vol. 38A, p.115-145.
- Bird, T.D., Barclay, J.E., Cambell, R.I., Lee, P.J., Waghmere, R.R., Dallaure, S.M., and Conn, R.F., 1994, Triassic gas resources of Western Canada Sedimentary Basin, Interior Plains. *Geological Survey of Canada Bulletin* vol.483, p. 66.
- CAPP - Canadian Association of Petroleum producers, 2007, Technical Report, *Statistic handbook for Canada’s Upstream Petroleum Industry*. Charpentier, R.R., and J.W.
- Schmoker, 1982, Volume of organic-rich Devonian shale in Appalachian Basin relating “Black” to organic-matter content, *Bulleting of American Assoc. of Petroleum Geologists*, vol. 62, p. 98-120.
- Kasting, J.F., M.T. Howard, K. Wallman, J.Veizer, G. Shieds, J. Jafres, 2006, Paleoclimate, ocean depth, and the oxygen isotope composition of seawater. *Earth and Planetary Science Letters*, vol. 252, p. 82 – 93.
- Core Lab, 2009, *Reservoir characterization and production properties of gas*

- shales. American Association of petroleum Geologists Bulletin, Short Course no. 10, Denver, Colorado.
- Davies, G.R. 1997, The Triassic of the Western Canada Sedimentary Basin: tectonic and stratigraphic framework, paleogeography, paleoclimate and biota. Bulletin of Canadian Petroleum Geology, v. 45, p. 434–460.
- Davies, G.R., Moslow, T.F., and Sherwin, M.D, 1997, The Lower Triassic Montney Formation, west-central Alberta. Bulletin of Canadian Petroleum Geology, vol. 45, 474 – 505p.
- Edwards, D.E., Barclay, J.E., Gibson, D.W., Kvill, G.E., and Halton, E. 1994, Triassic strata of the Western Canada Sedimentary Basin. In: Geological Atlas of the Western Canada Sedimentary Basin. G.D. Mossop and I. Shetson (compilers). Canadian Society of Petroleum Geologists, p. 257–275.
- Egbobawaye, E.I., J.P., Zonneveld, and M.K., Gingras, 2010, Tight gas reservoir evaluation in Montney and Lower Doig formations, northeastern British Columbia, western Canada. AAPG Abstract, vol. 19, p. 66-67.
- Egbobawaye, E.I., Kravchinsky, V.A, Zonneveld, J-P, and Gingras, M.K., 2011, Magnetostratigraphy Dating and Correlation of the Lower Doig and Upper Montney Formations (Lower Triassic), Northeastern British Columbia, Western Canada. Canadian society of Petroleum Geologists, CSPG, CSEG, CWLS Convention Abstract, Calgary, Alberta, Canada, 5p. Accessed online on June 20, 2011: <http://www.geoconvention.com/conference/technicalprogram/tuesday/pm-2/montney-i.html>
- Evoy, R.W., and Moslow, T.F., 1995, Lithofacies associations and depositional environments in the Middle Triassic Doig Formation, Buick Creek Field, northeastern British Columbia. Bulletin of Canadian Petroleum Geologists, vol. 43, p. 461–475.
- Envoy, R.W, 1997, Lowstand shoreface in the Middle Triassic Doig Formation:

Implications for hydrocarbon exploration in the Fort St. John area, north-eastern British Columbia. *Bulletin of Canadian Petroleum Geology*, vol. 45, 525-537p.

Faraj, B., H. Williams, G. Addison, B. McKinstry, R. Donaleshen, G. Sloan, J. Lee, T. Anderson, R. Leal, C. Anderson, C. Lafleur, and J Ahlstrom, 2002, Shale potential of selected upper Cretaceous, Jurassic, Triassic and Devonian shale formations, in the WCSB of Western Canada: Implications for shale gas production. A report for Gas Technology Institute (GTI), Des Plaines, Illinois, USA.

Gibson, D.W and Barclay, J.E. 1989, Middle Absaroka Sequence, the Triassic stable craton. In: *Western Canada Sedimentary Basin: A Case History*. B.D. Ricketts (ed.). Canadian Society of Petroleum Geologists, p. 219–231. Gibson, D.W and Edwards, D.E. 1990, An overview of Triassic stratigraphy and depositional environments in the Rocky Mountain Foothills and Western Interior Plains, Peace River Arch area. *Bulletin of Canadian Petroleum Geology*, vol. 38A, p. 146–158.

Haines, L., N. Darbonne, M. A. Barbee, P. Williams, G. Clouser, D. Wagman, M. Conly, and J. Grant, 2006, Tight gas. A supplement to *Oil and Gas Investor*. Hart Energy Publishing, Houston, Texas, 14p.

Henderson, C.M., 1997, Uppermost Permian conodont and Permian-Triassic boundary in the western Canada Sedimentary Basin, *Bulletin of Canadian Petroleum Geology*, vol. 45, no. 4, p.693-707.

Hunt, A.D., and Ratcliffe, J.D., 1959, Triassic stratigraphy, Peace River area, Alberta and British Columbia, Canada, *American Assoc. of Petroleum Geol. Bulletin*, vol. 43, no. 3, p.563-589.

Hunt, J.M., 1996, *Petroleum Geochemistry and Geology*, (2nd Ed.). Freeman and Company, New York, 741p.

- Kasting, J.F., M. T. Howard, K. Wallman, J. Veizer, G. Shields, J. Jafres, 2006, Paleoclimates, ocean depth, and the oxygen isotopic composition of sea-water. *Earth and Planetary Science Letters*, vol. 252, p. 82 – 93.
- McLearn, F.H., and Kindle, E.D., 1950, *Geology of northeast British Columbia*, Geological Survey of Canada, Memoir 259.
- Markhasin, B., 1997, *Sedimentology and Stratigraphy of the Lower Triassic Montney Formation, subsurface of Northwestern Alberta*: Unpublished M.Sc. Thesis, University of Calgary, Calgary, Alberta, 212p.
- Moslow, T.F., and Davies, G.R., 1992, *Triassic Reservoirs Facies and Exploration Trends: western Canada Sedimentary Basin*, Canadian Society of Petroleum Geologists-American Assoc. of Petroleum Geologists, (Short Course), Calgary, Alberta, 166p.
- Moslow, T.F., and Davies, G.R., 1997, *Turbidite Reservoir Facies in the Lower Triassic Montney Formation, west-central Alberta*, *Bulletin of Canadian Petroleum Geology*, vol. 45, no. 4, p. 507-536.
- O'Connell, S.C., Dix, G.R., and Barclay, J.E., 1990, *Origin, history, and regional structural development of the Peace River Arch, Western Canada*, *Bulletin of Canadian Petroleum Geology*, Vol. 38A, P. 4-24.
- Orchard, M.J. and Tozer, E.T., 1997, *Triassic conodont biochronology, its calibration with the ammonoid standard, and a biostratigraphic summary for Western Canada Sedimentary Basin*. *Bulletin of Canadian Petroleum Geology*, vol. 45, 675-692p.
- Orchard, M.J. and J-P Zonneveld, 2009, *The Lower Triassic Sulphur Mountain Formation in the Wapiti Lake area: Lithostratigraphy, conodont biostratigraphy, and a new biozonation for the lower Olenekian (Smithian)*: *Canadian Journal of Earth Sciences*, v. 46, p. 757–790.
- Panek, R., 2000, *The sedimentology and stratigraphy of the Lower Triassic*

- Montney Formation in the subsurface of the Peace River area, northwestern Alberta: Unpublished M. Sc. Thesis, University of Calgary, Calgary, Alberta, 275 p.
- Paull, R.K., R.A Paull, and Laudon, T.S., 1997, Conodont biostratigraphy of the Lower Triassic Mackenzie Dolomite Lenticle, Sulphur Mountain Formation in the Cadomin area, Alberta, *Bulletin of Canadian Petroleum Geology*, vol. 45, no. 4, p.708-714.
- Porter, J. W., R. A. Price and R. G. McCrossan, 1982, The Western Canada Sedimentary Basin. *Phil. Trans. R. Soc. Lond.* 305, 169-192
- Podruski, J.A., Barclay, J.E., Hamblin, A.P., Lee, P.J., Osadetz, K.G., Procter, R.M., and Taylor, G.C., 1988, Conventional Oil Resources of Western Canada. Geological Survey of Canada Paper, 149p.
- Pratt, B.R., James, N.P., and Cowan, C.A., 1992, Peritidal carbonates. In: R.G.Walker and N.P. James (eds.), *Facies Models: Response to sea level change*, Geological Assoc. of Canada, St. John's Nfld. p. 303-322.
- Reidiger, C.L., Fowler, M.G., Brooks, P.W. and Snowdon, L.R. 1990a, Triassic oils and potential Mesozoic source rocks, Peace River Arch area, Western Canada Basin. *Organic Geochemistry*, v. 16, p. 295–305.
- Richards, B.C. 1989. Upper Kaskaskia Sequence: Uppermost Devonian and Lower Carboniferous. In: *Western Canada Sedimentary Basin - A Case History*. B.D. Ricketts (ed.). Canadian Society of Petroleum Geologists, Special Publication No. 30, Calgary, Alberta, p. 165-201.
- Tozer, E.T. 1982a. Marine Triassic faunas of North America: Their significance for assessing plate and terrane movements. *Geologische Rundschau*, v. 71, p. 1077- 1104.
- Tozer, E.T. 1994, Canadian Triassic ammonoid faunas. Geological Survey of Canada. *Bulletin* 467, 663p.

- Tozer, E.T. 1967, A standard for Triassic time, Geological Survey of Canada, Department of Energy, Mines and Resources, Paper 12, 14p.
- Walsh, W., Adams, A., Kerr, B. and Korol, J, 2006, "Regional Shale Gas" Potential of the Triassic Doig and Montney Formations, Northeastern British Columbia. Ministry of Energy, Mines and Petroleum Resources, Oil and Gas Division, Resource Development and Geoscience Branch, British Columbia, Petroleum geology open file 2006-02, 19p.
- Willis, A. J, 1992, Sedimentology and Stratigraphic Framework of the Middle Triassic Halfway Formation, Wembly Oil field, Alberta. Unpublished master's degree thesis, University of Alberta, 412p.
- Wright, G.N., McMechan, M.E., and Potter, D.E.G, 1994, Structure and architecture of the Western Canada Sedimentary Basin. In: G.D. Mossop and I. Shetson (comps). Geological Atlas of the Western Canada Sedimentary Basin. Calgary, Canadian Society of Petroleum Geologists and Alberta Research Council, Chapter 3.
- Zonneveld, J.P., Moslow, T.F., and Henderson, C.M. 1997, Lithofacies associations and depositional environments in a mixed siliciclastic-carbonate coastal depositional system, upper Liard Formation, Triassic, northeastern British Columbia. Bulletin of Canadian Petroleum Geology, vol. 45, p. 553–576.
- Zonneveld, J.P., 1999, Sedimentology and sequence biostratigraphic framework of mixed siliciclastic-carbonate depositional system, Middle Triassic, northeastern British Columbia. Unpublished Ph.D. Dissertation, University of Alberta, 287p.
- Zonneveld, J.P., Gingras, M.K., and Pemberton, S.G., 2001, Trace fossils assemblages in a Middle Triassic mixed siliciclastic-carbonate marginal marine depositional system, British Columbia. Palaeogeography, Palaeoclimatol-

ogy, *Palaeoecology*, vol. 166 (3-4), p.249-276.

Zonneveld, J.P., Pemberton, S.G., Saunders, T.D.A., and Pickerill, R.K., 2002, Large robust *Cruziana* from the Middle Triassic of northeastern British Columbia: ethologic, biostratigraphic and paleobiologic significance. *Palaios*, vol. 17. p. 435-448.

Zonneveld, J.P, 2008, Triassic Sedimentary Framework and Sequence Stratigraphy, Williston Lake, British Columbia, CSPG, CSEG, CWLS Convention, P. 1-9.

Zonneveld, J.P., MacNaughton, R.B, Utting, J, Beatty, T.W, Pemberton, S.G, and Henderson, C.M., 2010, Sedimentology and ichnology of the Lower Triassic Montney Formation in the Pedigree-Ring/Border-Kahntah River area, northwestern northwestern Alberta and northeastern British Columbia. *Bulletin of Canadian Society of Petroleum Geology*, vol. 57, No. 2, p. 115-140.

Zonneveld, J.P., MacNaughton, R.B, Utting, J, Beatty, T.W, Pemberton, S.G, and Henderson, C.M., 2010, Sedimentology and ichnology of the Lower Triassic Montney Formation in the Pedigree-Ring/Border-Kahntah River area, northwestern Alberta and northeastern British Columbia. *Bulletin of Canadian Society of Petroleum Geology*, vol. 57, No. 2, p. 115-140.

CHAPTER 2: SEDIMENTOLOGY AND ICHNOLOGY OF THE UPPER MONTNEY FORMATION (LOWER TRIASSIC) TIGHT GAS RESERVOIR, NORTHEASTERN BRITISH COLUMBIA, WESTERN CANADA

INTRODUCTION

The Montney Formation is the basal stratigraphic unit of the Triassic succession in the subsurface of western Canada. It rests, unconformably in most areas, upon carbonate or mixed siliciclastic-carbonate strata of Carboniferous to Permian age (Edward et al., 1994; Pudruski, et al., 1988; Gibson and Edwards, 1990; Zonneveld, et al., 2010b). The succession was deposited in a west-facing, arcuate extensional basin on the western margin of Pangaea (Davies et al., 1997; Orchard and Tozar, 1997; Zonneveld, 1999; Zonneveld, et al., 2001).

The Montney Formation is a primary focus of tight gas exploration in Western Canada because: 1) it is a source rock rich in organic matter (Riediger, et al., 1990) that lies within the gas generating window, and contains gas prone Type II/III kerogen (Riediger, et al., 1990); 2) the present study shows that the kerogen of the Montney Formation in the study area also comprises composed of Type III/IV kerogen (TOC range from 0.34 – 4wt%; and upto 8.2 wt. % TOC are rare, but present); 3) it has a reservoir thickness up to 320 meters in northeastern British Columbia; 4) it hosts substantial volumes of unconventional gas, estimated to be 187 TCF (Walsh, et al., 2006); and 5) porosity range from 2 – 10%, and sporadically >10% in some intervals where ichnological modification of facies heterogeneities or dolomite dissolution have resulted in the formation of secondary porosity. These criteria make the Montney Formation an unconventional resource play with high potential within the Fort St. John study area (T86N, R23W and T74N, R13W), northeastern British Columbia (Fig. 2.1). However, despite the strong

economic interest in unconventional silt-hosted hydrocarbon reservoirs within this stratigraphic interval (Eggbowaye, et al., 2010), the geology, geochemistry, mineralogy and sedimentology have not been adequately characterized.

The Montney Formation consists of siltstone, very fine-grained sandstone, and bioclastic packstone/grainstone (coquina) (Davies, et al., 1997; Zonneveld, et al., 2010). The Lower Triassic Montney Formation is separated by an unconformity from the underlying Permian Belloy Formation (Gibson and Barclay, 1989; Tozer 1994). The unconformity along the Permian-Triassic boundary has been interpreted by Henderson (1997); Edward, et al. (1994); Davies, et al. (1997) to be related to a global eustatic sea level fall. The global eustatic fall was related to the amalgamation of Pangaea Supercontinent, and was followed by a protracted Late Permian transgression that continued into the Triassic period (Henderson, 1997). The transgression was accompanied by anoxic conditions that induced profound environmental change (Zonneveld, 2011), and may have severe increased levels of greenhouse gases (Payne et al., 2004; Kump et al., 2005; Luo et al., 2011). These were the primary factors that contributed to the Late Permian – Triassic extinction crises, the largest extinction episode in geologic history (Henderson, 1997). Conodonts were only marginally affected by this extinction, thus, they provide valuable indices for high-resolution sequence biostratigraphic correlation within the Permian – Triassic boundary of Western Canada Sedimentary Basin (Henderson, 1997).

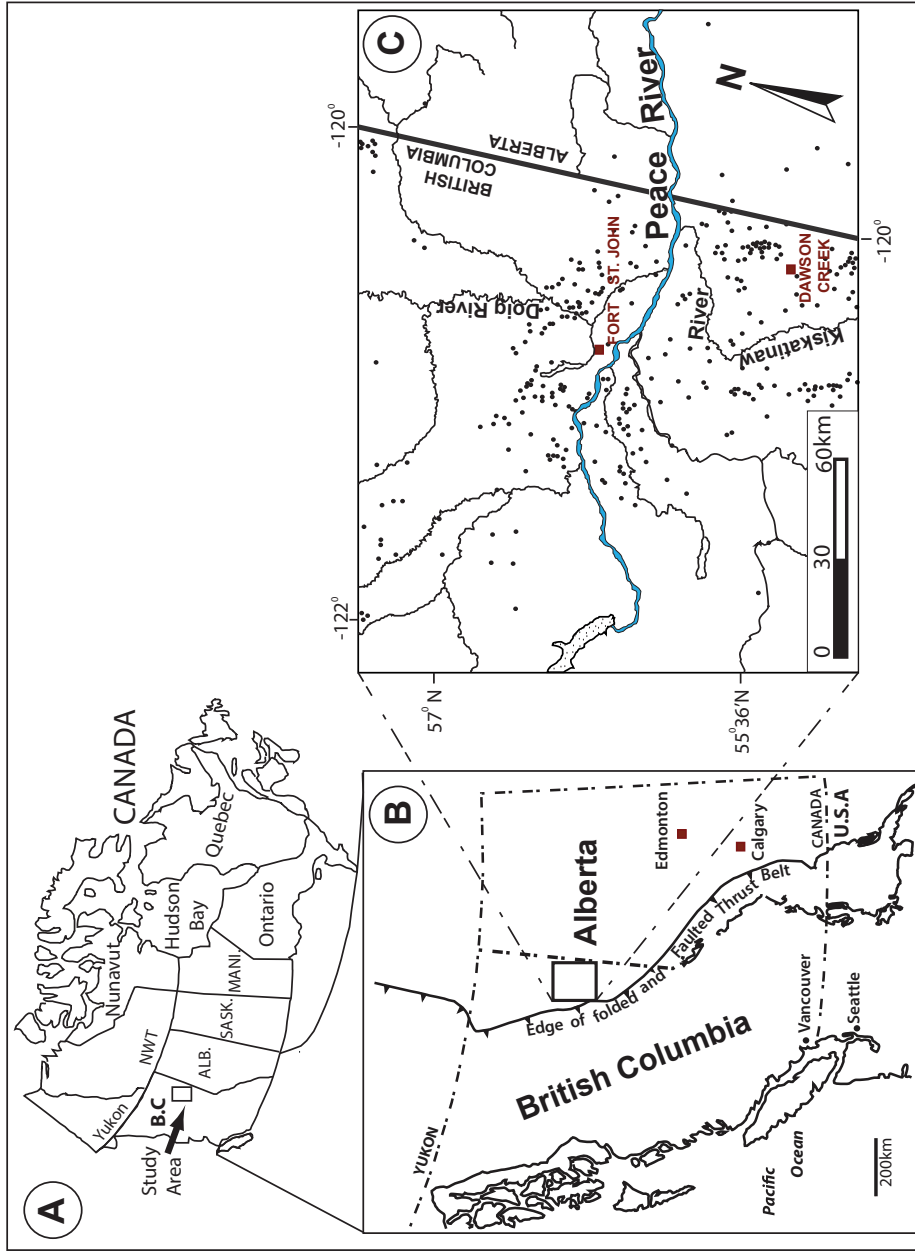


Figure 2.1. (A) Shows tectonic deformation and structure in Western Canada (Modified from Porter et al., 1982). Tectonic Provinces (After Douglas, 1960; Kanasevich, et al., 1969; Fraser et al., 1972). (B) Shows location of study area in northeastern British Columbia, Western Canada Sedimentary Basin.

The Montney Formation is separated from the overlying Doig Formation by a strongly radioactive, phosphate-rich interval known informally as the “Doig Phosphate Zone” (Armitage, 1962; Gibson and Edwards, 1990). This boundary is an erosional surface, and has the same paleomagnetic record of normal polarity, which likely corresponds to the normal polarity interval MT2 in the bottom of the Anisian age that starts at ~ 245 Ma (Eggbowaye, et al., 2011). The Montney / Doig boundary is locally represented by a coplanar *Trypanites* – *Glossifungites* demarcated discontinuity surface (Fig. 2.2 and Fig. 2.3), which is correlatable on a regional scale (Eggbowaye, et al., 2011; Wilson and Zonneveld, 2011).

The outcrop equivalent of the Montney Formation is the Grayling and Toad formations in northern British Columbia; Sulphur Mountain Formation in British Columbia, the and Grayling and Toad formations south of the Peace River area in Alberta (Armitage 1962; Orchard and Tozar, 1997; Zonneveld et al., 2001; Zonneveld, 1999). In west-central Alberta, the Montney Formation has been reported by Moslow and Davies (1997) to include turbidite channel lobe complexes interpretive of mass wasting processes caused by Early Triassic (Smithian / Dienerian) global eustatic sea level fall. Within the study area in northeastern British Columbia, there is no evidence of turbidites channel lobe complexes associated with the (Smithian / Dienerian) global eaustatic sea level fall. Within the study area in northeastern British Columbia, there is no evidence of turbidites channel lobe complexes in the Montney Formation.

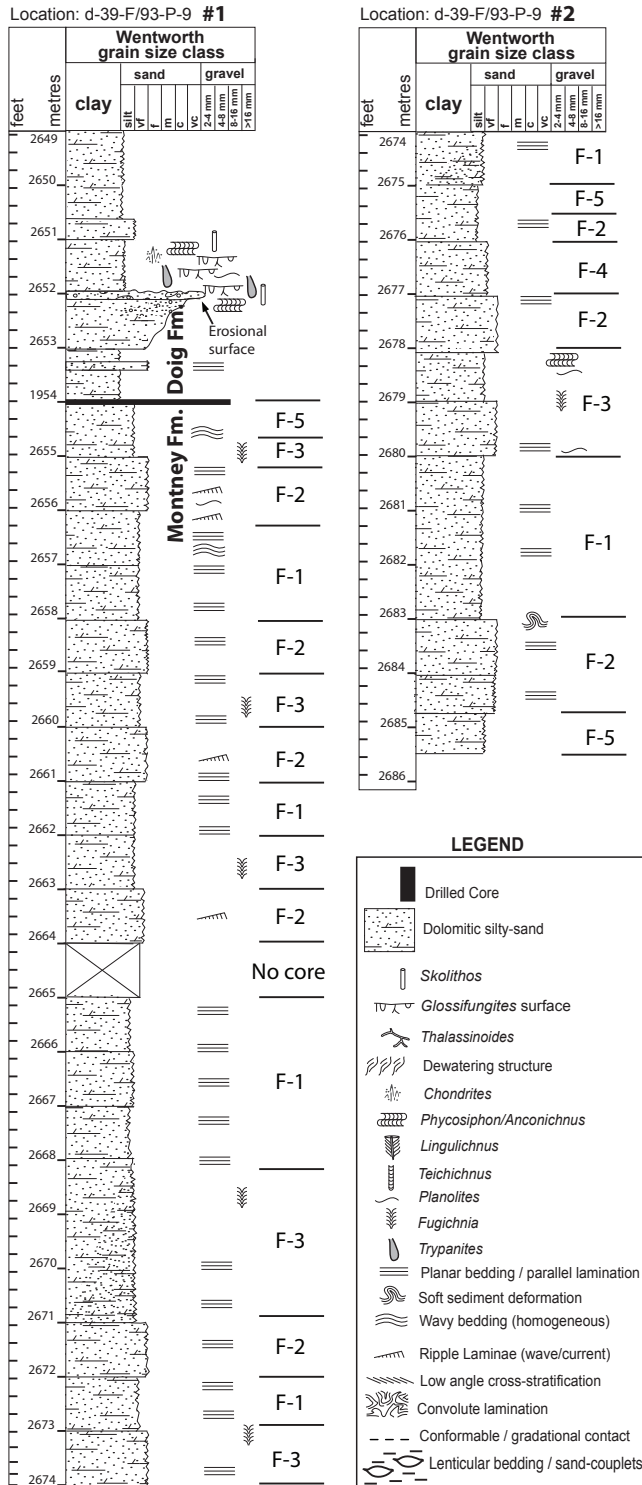


Figure 2.2. Gamma-ray log correlated with logged core (well d-39-F/93-P-9) showing lithofacies of the Montney Formation, and the overlying erosional contact of *Glossifungites* – *Trypanites* surface demarcating the overlying Doig Formation from the Montney Formation in the subsurface of northeastern British Columbia.

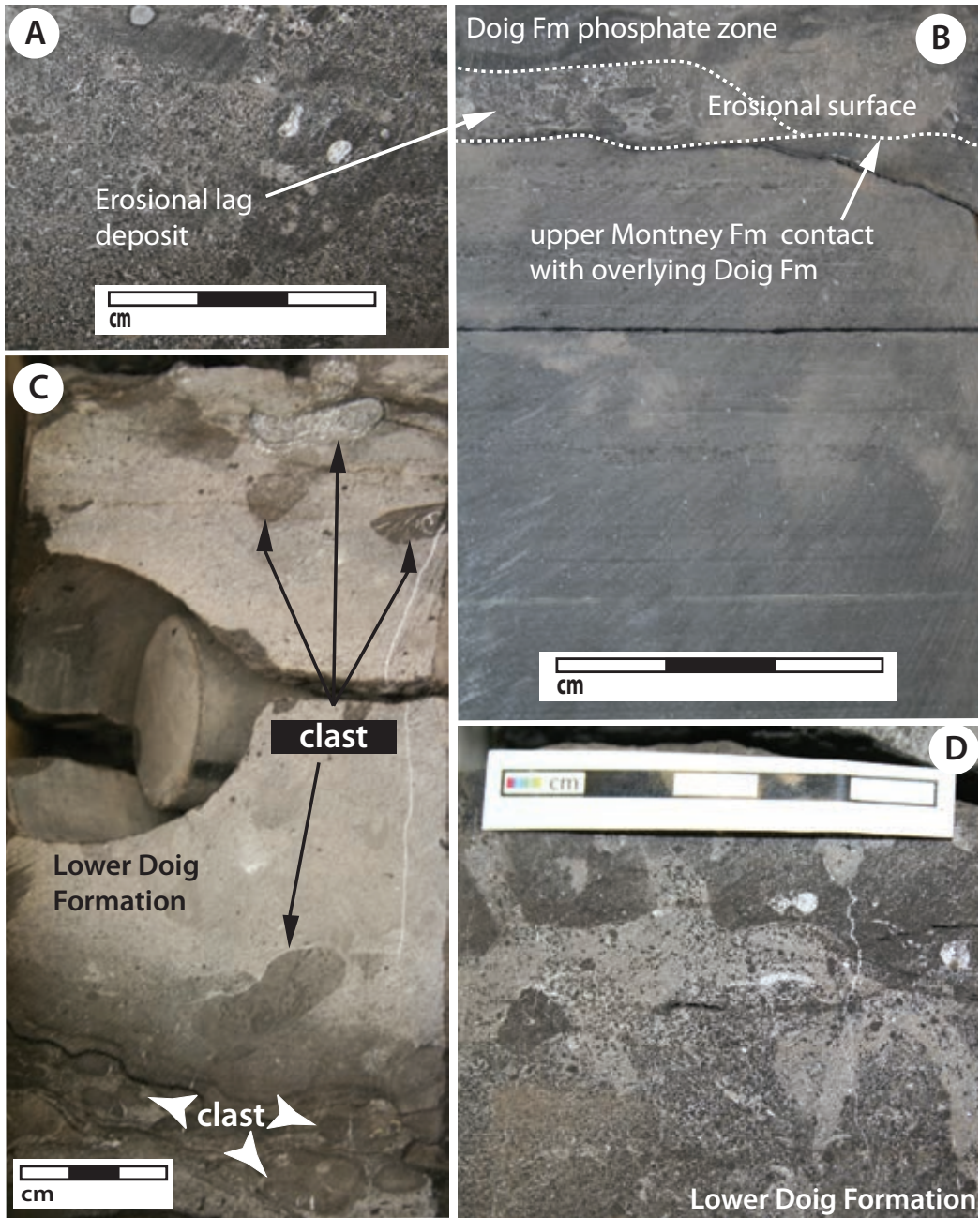


Figure 2.3. (A) Erosional lag deposit showing pebble clast along the Montney / Doig Formation boundary. (B) Shows the Montney Formation and the overlying Doig Formation separated by erosional surface. (C) Lag, clast of the Lower Doig Formation along the Doig / Montney boundary. (D) Discontinuity surface along the Montney /Doig boundary.

This paper synthesizes the sedimentology and ichnology of the Montney Formation in Fort St. John area (T86N, R23W and T74N, R13W) of northeastern British Columbia (Fig. 2.1), Western Canada.

GEOLOGICAL SETTING

Based on analyses of paleomagnetic data, paleolatitude and paleoclimatic zonation (Habicht, 1979), and fauna record (Tozer, 1982), the Western Canada Sedimentary Basin (WCSB) during the Triassic time was situated at approximately 30° N paleolatitude. The paleoclimate reconstruction suggests that the paleoclimate may have ranged from sub-tropical to temperate (Habicht, 1979; Tozer, 1982; Gibson and Barclay, 1989; Barclay, et al., 1990). The region has been interpreted to be arid during the Triassic, and was dominated by westerly winds from the west (Habicht, 1979; Arnold, 1994; Edwards, et al., 1994).

The WCSB forms a northeast thinning wedge of sedimentary rocks with thickness of more than 6,000 meters, which extends southwest from the Canadian Shield into the Cordilleran foreland thrust belt (Porter et al., 1982; Gibson and Barclay, 1989). The Cordilleran of the WCSB provides the evidence that the origin and development of the basin was associated with tectonic activity attributed to episodes of epeirogenic subsidence (Porter, et al., 1982; Gibson and Barclay, 1989; Price, 1994; Monger and Price, 1979); this is interpreted to be post Triassic, especially due to mountain influences (Gibson and Barclay, 1989). Wittenberg and Moslow (1991) and Cant (1994; 1986) interpreted sediment loading, evidenced by deformed beds, slump structures and small-scale faults as indicators of tectonic influences on the deposition of Triassic successions. Within the Foothills and Rocky Mountain Front Ranges, Triassic rocks were subjected to Jurassic – Cretaceous Columbian and Upper Cretaceous – Lower Tertiary Laramide orogenies, which caused a series of imbricate thrust faults and folds in the region (Edwards et al.,

1994; Berger, et al., 2009).

In Alberta and British Columbia, Triassic sediments were deposited in a central sub-basin known as the Peace River Embayment, which extended eastward from the Panthalassa western ocean onto the North American craton (Edwards et al., 1994). During the Triassic period, the Peace River Embayment was a low mini basin associated with minor fault block movement associated with a broad downwarp resulted in the rejuvenation of structural deformation within the Monias areas of southwest Fort St. John, British Columbia (Edwards et al., 1994; Berger, et al., 2009).

Stratigraphically (Fig. 2.4), the Triassic Montney Formation is Griesbachian to Spathian in age (Orchard and Zonneveld, 2009). The Triassic succession thicken westward (Edwards, et al., 1994), and rests unconformably in most areas, upon the Belloy Formation in outcrop of northeastern British Columbia; Carboniferous in parts of northeastern British Columbia and Alberta; and Fantasque Formation in outcrop at Williston (Orchard and Zonneveld, 2009). The thickness of Triassic deposits is about 1200 meters in the western-most outcrop in the Rocky Mountain Foothills (Willis, 1992). The thickness of the Montney Formation within the Fort St. John study area, varies in the east along British Columbia / Alberta boarder boundary and to the western portion of British Columbia (Fig. 2.5). The Montney Formation structure map (Fig. 2.6) indicates higher paleostructure in the east and low in the western portion of the study area. The structural tilt shows a depositional thinning to the east and north due to erosional removal (Edwards, et al., 1994). Isopach map of the Montney Formation indicates a maximum thickness of approximately 320 meters in the study area of northeastern British Columbia.

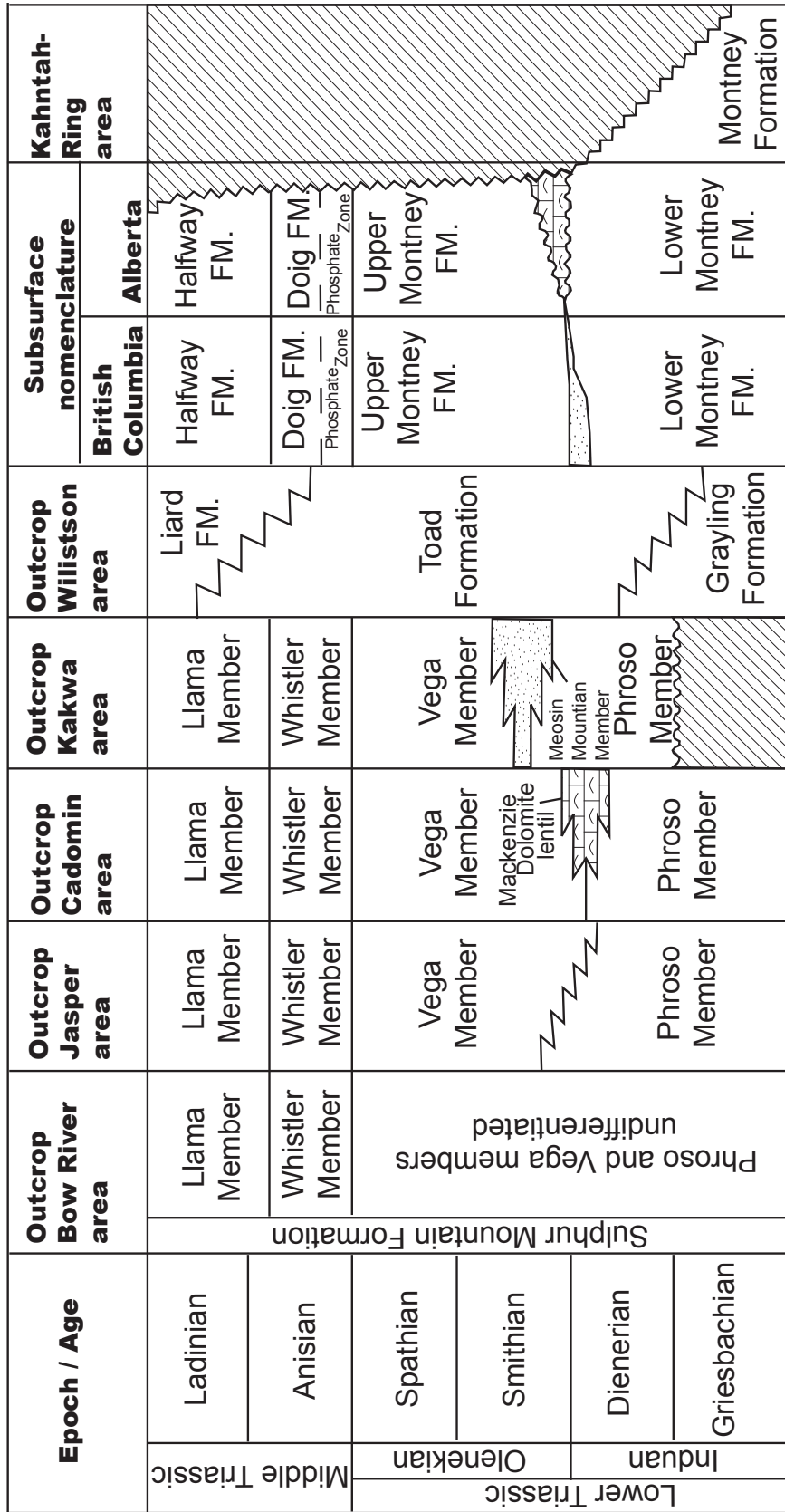


Figure 2.4. Stratigraphic chart showing Lower and Middle Triassic deposits and a correlation of outcrop with coeval subsurface strata in the western Canada Sedimentary Basin (Modified from Orchard and Zonneveld, 2009).

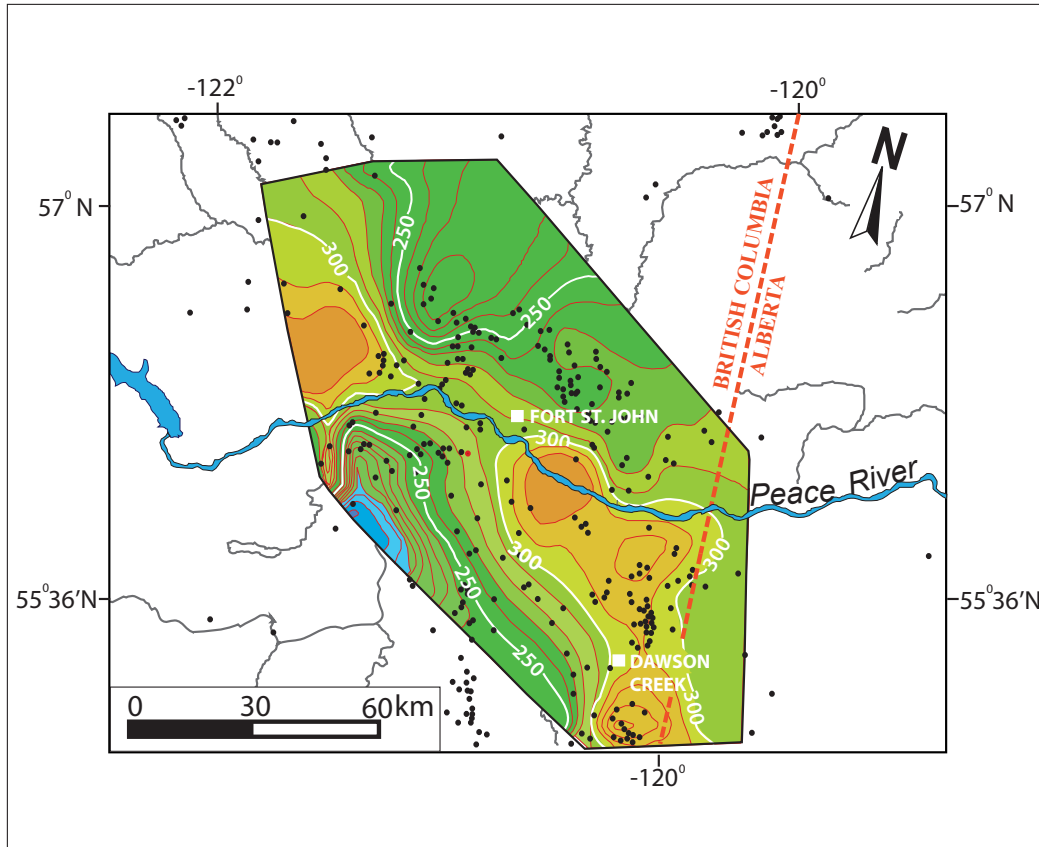


Figure 2.5. Isopach map of the Montney Formation showing the trends of thickness in northeastern British Columbia and northwestern Alberta. The Montney Formation fairway and play segments distinctively show up in the map, displaying three major exploration prospects along the contours > 300 metres in the isopach.

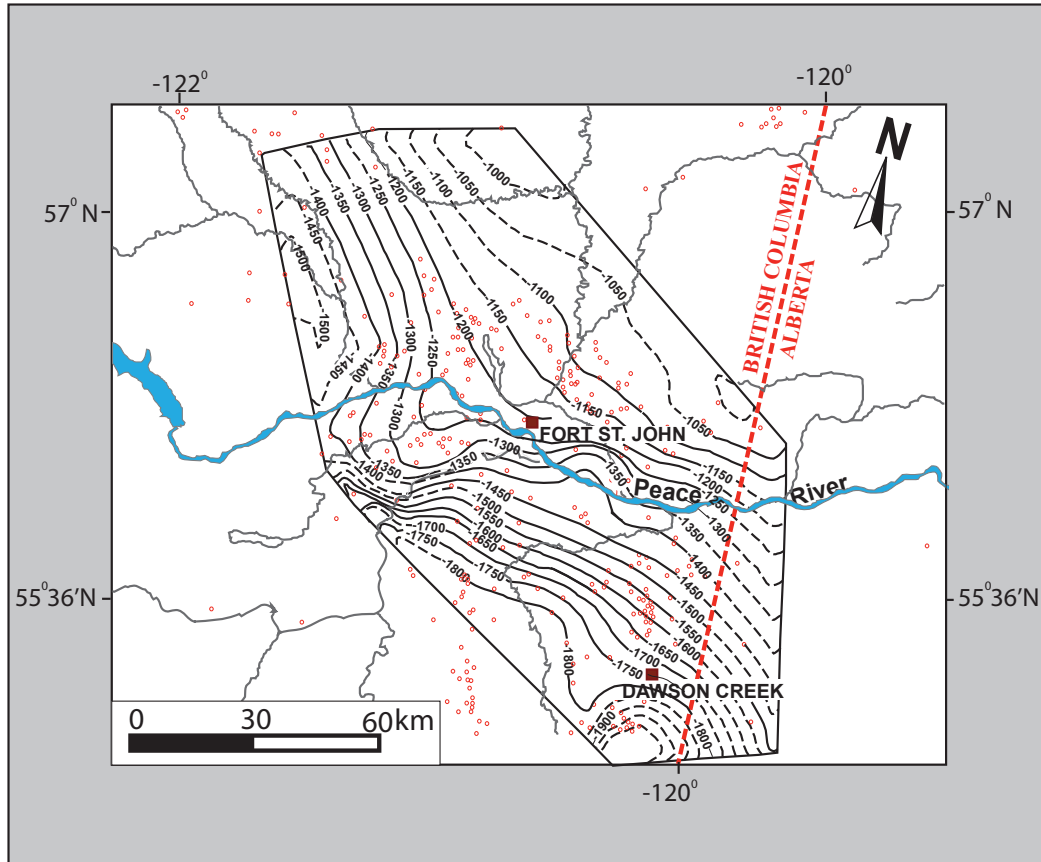


Figure. 2.6. Structure contour map of the Montney Formation in northeastern British Columbia and northwestern Alberta.

METHOD OF STUDY AND SCOPE

Drill core of the Montney Formation from northeastern British Columbia were logged to assess sedimentological, ichnological and facies characteristics. The lithologic features and accessories, sedimentary texture, sedimentary structure, the nature of bedding contacts, and lithofacies were compiled in detail (Figures 2.7 through 2.9).

Samples were collected from cores for thin-section petrography, X-ray diffraction (XRD) analysis, scanning electron microscopy (SEM) analysis, and Rock-Eval geochemistry. XRD is essential in fine-grained sediments, and it allows moderately accurate determination of the amount of magnesium substitution in

calcite or dolomite lattices (Tucker, 1988). Thin-sections were prepared with blue-dye epoxy to highlight porosity and examined with petrographic microscope in accordance with the method of thin-section petrography originally developed by Henry Sorby (1858), and were examined petrographically for textural characteristics, mineralogical composition, and porosity analyses. Thin-section petrography was used to determine grain sizes and sorting. Zones showing distinct features were photographed.

Samples were crushed into powder using a pulverized shatter-box machine. Samples were sent to Geological Survey of Canada and Chesapeake Energy Corporation, Oklahoma, USA, for Rock-Eval analyses with additional geochemistry data from B.C Oil and Gas Commission (Table 2.1, and Appendix 3-A). Ichnological study of the core samples involves recording and identification of ichnogenera, ichnofossil assemblages, distribution and paucity. Ichnofossils, lithofacies and depositional characteristics were integrated and used to interpret the paleoenvironments within the studied interval.

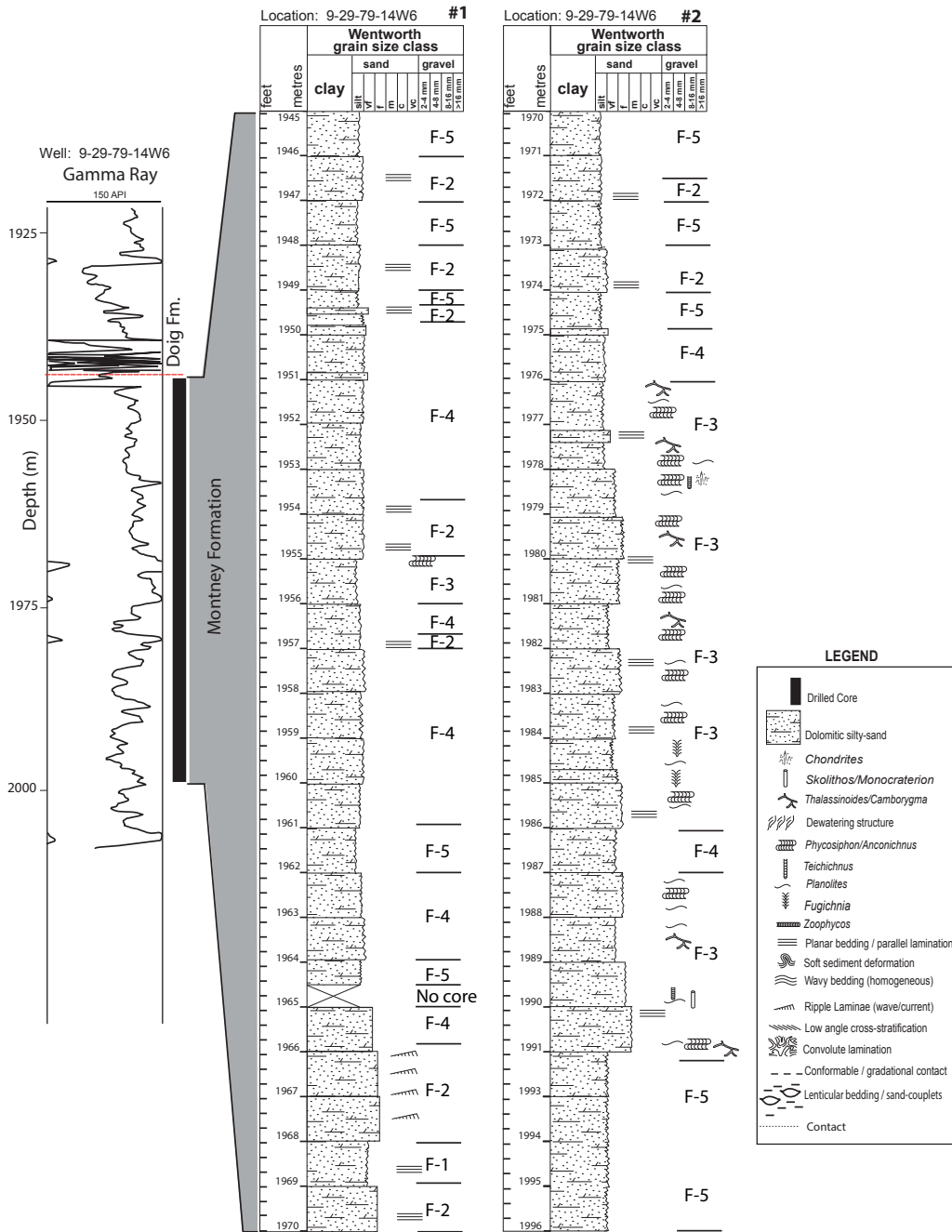


Figure 2.7. Gamma-ray log correlated with logged core (well: 2-29-79-14W6) showing lithofacies of the Montney Formation, northeastern British Columbia.

Table 2.1. Summary of the lithology, characteristics, and description of facies associations (F-1 through F-5) and interpretation of depositional environments.

Facies	Lithologic description	Sedimentary structures	Ichnology/Fossil content	Interpretation
F-1: Organic rich siltstone	<ul style="list-style-type: none"> Dark to black coloured organic-rich, dolomitic siltstone. The grains are subangular to subrounded, and well sorted. Mineralogy comprises quartz, dolomite, mica, and clay. 	<ul style="list-style-type: none"> Preserved sedimentary structures appears as horizontal to wavy lamination. The thickness of individual fine-silt lamina within F-1 is approximately 2 to 3mm. The basal contact between lithofacies F-1 and lithofacies F-2 is abrupt. 	<ul style="list-style-type: none"> Trace fossils and bioturbation are not present in lithofacies F-1. There are no body fossils preserved in F-1. 	<ul style="list-style-type: none"> The dark coloured organic rich content of lithofacies F-1 is related to high nutrient rich sediment source and rapid sedimentation, which enhanced the preservation of organic matter in oxygen-depleted depositional environment. The organic carbon richness of F-1 makes it a potential source rock. Mechanism of deposition of silt and very fine-grained sediment of F-1 is related to mobilization of fines across-shelf or transported through processes, which may include sediments deposition from suspension or hyper-pycnal plumes. suspended silty-clay sediments are transported primarily as flocculated material. Conclusion: Distal offshore (outershell) depositional environment.
F-2: Very fine-grained sandstone and siltstone	<ul style="list-style-type: none"> F-2 is composed of interbedded, laminated, very fine-grained silty-sandstone. The ratio of sand to silt in F-2 is ~3:1 in some successions and ~2:1 ratio in some beds. Petrographic examination of F-2 further shows that the grains sorting are variable, from moderately well sorted to poorly sorted, and texturally matured, but mineralogically submature as evidenced by the present of feldspar and clay. 	<ul style="list-style-type: none"> F-2 has well-preserved plane parallel laminae. The sand laminae exhibit fractures along sandstone bedding planes F-2 has well preserved de-waxing structures, soft sediment deformation structures, convolute bedding / lamination, and small-scale current ripples. The current ripples are dominantly straight-crested, and rarely bifurcating. The basal contact of lithofacies F-2 with lithofacies F-3 is sharp, and abruptly ungradational. 	<ul style="list-style-type: none"> Trace fossils and bioturbation are not present in lithofacies F-2. There are no body fossils preserved in F-2. Fugichnia are present as evidence of episodic, event or rapid deposition in F-2 	<ul style="list-style-type: none"> The present of preserved interbedded sandy-siltstone, and thinly laminated layers (< 10mm) in F-2 reflect variation in sediment texture. Laminae form due to transcurrent migration of grains due to low relief in topography, and bed waves. The absence of sedimentary structures characteristic of upper shoreface environment, such as hummocky cross stratification, wave or oscillatory ripples, finer quietset depositional mechanism. The present of current ripples in F-2 probably correspond to waning flow conditions. Soft sediment deformation structures in F-2 are due to a deformational event at or near the contemporary surface of unconsolidated sediments either before, or soon after burial. The silty grains in F-2, in part suggest input from aeolian sediment source Pyrite in F-2 is interpreted as post-depositional emplacement due to diagenesis. Conclusion: Lower shoreface through proximal offshore depositional environment.
F-3A: Bioturbated very fine-grained sandy-siltstone composed of <i>Skolithos</i> ichnofacies	<ul style="list-style-type: none"> Very fine-grained sandy-siltstone. Thin-section shows that the grain sizes are moderately well sorted, and vuggy porosity resulting from bioturbation are present. 	<ul style="list-style-type: none"> F-3A has preserved wavy to parallel lamination (~10mm to 15mm in thickness), wave ripples, and escape structures such as fugichnia indicates rapid, episodic, or even deposition. 	<ul style="list-style-type: none"> The trace fossils in F-3A comprises <i>Pianolites</i>, <i>Phycosiphon</i>, <i>Cruziana</i>, <i>Skolithos</i>, <i>Teichichnus</i>, and <i>Palaephycus</i>. There are no body fossils preserved in F-2. 	<ul style="list-style-type: none"> F-3A is characteristic of a diverse but low abundance of ichnological assemblage, typical of the <i>Skolithos</i> ichnofacies. The <i>Skolithos</i> ichnofacies is indicative of relatively high energy environment such as the shoreface, and they are associated with wave, current energy and typically developed in slightly muddy to clean, moderately sorted sediments.

Table 2.1. Continuues.

Facies	Lithologic description	Sedimentary structures	Ichnology/Fossil content	Interpretation
F-3A: Bioturbated very fine-grained sandy-siltstone composed of <i>Skolithos</i> ichnofacies	<ul style="list-style-type: none"> Very fine-grained sandy-siltstone. Thin-section shows that the grain sizes are moderately well sorted, and vuggy porosity resulting from bioturbation are present. 	<ul style="list-style-type: none"> F-3A has preserved wavy to parallel lamination (~10mm to 15mm in thickness), wave ripples, and escape structures such as fugichmia indicates rapid, episodic, or even deposition. 	<ul style="list-style-type: none"> Fugichmia are present as evidence of episodic, event or rapid deposition in F-2 	<ul style="list-style-type: none"> The <i>Skolithos</i> ichnofacies can also develop in a loose or shifting particulate (sand-prone) substrates in marine environments. The present of escape traces in F-3A correspond to disturbances made by organisms entrained in, or buried by, the event bed during sedimentation. Conclusion: Lower shoreface depositional environment.
F-3B: Bioturbated siltstone composed of <i>Cruziana</i> ichno facies.	<ul style="list-style-type: none"> F-3B is composed of siltstone dominated by <i>Cruziana</i> ichnofacies. F-3B is moderately well sorted. 	<ul style="list-style-type: none"> No sedimentary structures 	<ul style="list-style-type: none"> The trace fossils recorded in F-3B are rare <i>Zoophycos</i>?, <i>Planolites</i>, <i>Phycosiphon</i>, <i>Chondrites</i>, <i>Thalassinoides</i>, <i>Cruziana</i>, <i>Skolithos</i>, <i>Teichichnus</i>, and <i>Palaeophycos</i>. In cores, these traces are not well preserved. F-3B fugichmia – escape structures are present. 	<ul style="list-style-type: none"> Trace fossils such as <i>Planolites</i>, <i>Thalassinoides</i>, <i>Cruziana</i>, and <i>Palaeophycus</i> are ichnocoenosis of the <i>Cruziana</i> ichnofacies. The <i>Cruziana</i> ichnofacies is commonly characterized by a high diversity of trace fossils associated with a variety of ichnofauna The present of these trace fossils in F-3B are indicative of distal offshore setting. Conclusion: Distal offshore depositional environment
F-4: Dolomitic very fine-grained sandstone	<ul style="list-style-type: none"> F-4 consist of dolomitic, thin beds (≤ 1 meter) of very fine-grained sandstone. Thin-section petrography confirms that F-4 is quartz rich, moderately well sorted and dolomitic. F-4 succession shows a coarsening upward trend. 	<ul style="list-style-type: none"> The basal contact of F-4 with lithofacies F-5 is sharp and grades into coarse siltstone grade. No sedimentary structures 	<ul style="list-style-type: none"> Trace fossils and bioturbation are not present in lithofacies F-4. There are no body fossils preserved in F-4. 	<ul style="list-style-type: none"> The coarsening-upward trend in lithofacies F-4 is interpreted as basinward shoreline shift, which often characterizes a progradational trend. The coarsening upward succession of F-4 is likely to have accumulated in deepening water, particularly in areas that are not adjacent to the shoreline and are characteristic of facies that prograded basinward during a falling stage of regression. Conclusion: Proximal offshore depositional environment.
F-5: Massive siltstone.	<ul style="list-style-type: none"> Dark grey to black colored, organic rich, pyritized, massive siltstone. Petrographic examination of F-5 confirmed the that grains are sub-angular to sub-rounded. The texture of pyrite in F-5 under reflected light microscopy appears as irregularly rounded 'clots' that partly coalesce with one another and partly separated by non-reflective dolomite 	<ul style="list-style-type: none"> No sedimentary structures The upper contact of F-5 of with the overlying Doig Formation is reminiscent of erosional lag deposit characterized by a <i>Glossifungites</i> – <i>Trypanites</i> surface. 	<ul style="list-style-type: none"> Trace fossils and bioturbation are not present in lithofacies F-5. There are no body fossils preserved in F-5. 	<ul style="list-style-type: none"> The dark grey to black colored, organic carbon content F-5 is a result of high nutrient rich sediment source and rapid sedimentation, which enhanced the preservation of organic matter. The composition of detrital dolomite in F-5 is interpreted as post-depositional in origin, rather than in-situ. Pyrite in F-5 is related to post-depositional emplacement caused by the dissolution of organic matter due to diagenesis. The deposition of massive siltstone of F-5 may be related to transport and deposition from suspension, principally enhanced by the influence of waves mobilization of sediment by hyperpycnal mechanisms. Conclusion: Distal offshore (outer shelf) depositional environment to ramp setting.

FACIES ANALYSIS CONCEPT

Gressly (1838) first introduced the term *facies* into the geological literature to describe a body of rock with specified biological and geological characteristics in the Jura Mountains of Europe. Although the original definition of a *facies* was very concise from its inception, several ideologies of what constitute a *facies* have been proposed (Reading, 1996; Miall, 1999), and the usage of the term *facies* has been a subject of debate for several decades (Reading, 1996; Miall, 1999).

The core meaning of a *facies* with respect to a distinctive rock unit that forms under certain conditions of sedimentation, depicting a particular depositional process or specific depositional characteristics (Cross and Homewood, 1997) remain central to the the term *facies*. The *facies* concept is the building block of modern stratigraphy (Cross and Homewood, 1997), and sequence stratigraphy. This paradigm led to descriptive rock attributes independent of time connotation to signify observable physical, chemical, and biological characteristics of rocks that aid objective description and differentiation of *facies* (Cross and Homewood, 1997). As a result, different *facies* schemes are used depending on the particular characteristics under consideration, or the scale of analysis (Reading, 1996; Miall, 1999). For example, a consideration of trace fossil assemblage in the rock record will be *ichnofacies*; whereas a consideration of the physical, petrological, and chemical characteristics of the rock will be *lithofacies*.

Ichnofacies

Trace fossils (animal tracks, trails, burrows, excavation, etc.) represents the vestiges of animal behavior in responds to stimuli within their environments, such as net sedimentation rates, salinity, oxygenation, temperatures, turbidity and a host of other environmental parameters (Gingras et al., 2005). The fundamental utility and strengths of the *ichnofacies* concept lies in its ease of interpretation with

classical physical sedimentological facies analysis and its adherence to Walther's Law (MacEachern, et al., 2005).

The overall behavior and coping strategies of animals are controlled by the prevailing physio-chemical conditions of the environment (Gingras, et al., 2005). Trace fossil morphology, resulting from the interaction of animals with sedimentary substrates, and subsequently preserved in the rock record become interpretive tool when integrated with physical sedimentary structure, and are invaluable in the delineation of depositional environments (Gingras et al., 2005; MacEachern, et al., 2005).

RESULT OF FACIES ANALYSIS

Based on sedimentological and ichnological criteria from examination of Montney Formation core in the study area, five lithofacies were identified: Lithofacies F-1, Lithofacies F-2, Lithofacies F-3, Lithofacies F-4, and Lithofacie F-5. Detailed description and interpretation are presented below. Sedimentological and ichnological parameters were integrated into the interpretation of depositional environments for the Upper Montney Formation based on subsurface cores. The trace fossils recorded in this study from cores is described in detail in Table 2.2. The small-scale lithofacies scheme developed herein (F1 through F5) help to associate genetically related facies, which were interpreted cogenetically. A summary of the sedimentary facies scheme used in this study is shown on Table 2.2. Specific interpretations for the depositional environments for the facies were based on consideration of facies associations (Zonneveld, et al., 2004), and detailed description and interpretation of the facies are discussed below following the classification scheme and analyses of Reading and Collison (1996).

Table 2.2. Trace fossils description reported from the studied cores in the Upper Montney Formation, northeastern British Columbia.

1. *Chondrites* isp erected by Sternberg, 1833. It is a dendritically complex burrow system, consisting of asymmetrical and branching smooth – walled tunnels. The *Chondrites* tunnels have a circular cross-sectional view.

2. *Cruziana*. Erected by Alcide D’Orbigny, 1842. The burrow consists of elongate, and bilaterally symmetrical morphology. The burrow is preserved along bedding planes, with a sculpture of repeated striations that are mostly oblique to the long dimension.

3. *Fugichnia*. Erected by Simpson, 1975. The burrow is an escape structure, which has the shape of chevron pattern showing the upward direction the organism tunneled through in responds to sudden, episodic, or high sedimentation events.

4. *Planolites montanus* isp. Erected by Nicholson, 1873. The burrows are horizontal to sub-horizontal, unlined, unbranched, and small diameter ~ 2mm. The shape of the burrow is sinuous, to tortuous, and circular to elliptical in cross-section. Burrow filled are structureless, and differ from the host rock / sediment. Walls are mostly smooth.

5. *Skolithos linearis*. Erected by Haldeman, 1840. Burrows are straight, cylindrical to curve, distinctly smoothed walled, rarely branched, and vertical to steeply inclined. Unornamented simple shafts are mostly retrusive and merge upward at various angles with bedding planes.

6. *Thalassinoides suevicus*. Erected by Reith, 1932. Burrow system is pre-dominantly horizontal and regularly branched. They form bedding-parallel mazes. Branches ramify at acute angles. The Y-shaped dichotomous bifurcations dominate T-shaped branches. The branches are cylindrical in shape and circular to oval shape in transverse section.

7. *Teichichnus rectus*. Erected by Seilacher, 1955. Vertical and unbranched spreite consist of tightly packed, straight to broadly U-shaped laminae. Burrows have variable dimensions. Longitudinal sections show nested burrows of simple, long, straight to sinous, upward migrated, horizontal to sub-horizontal tunnels. These tunnels are mostly retrusive and merge upward at various angles with bedding planes.

8. *Phycosiphon*. Erected by Von Fisher-Ooster, 1858. The structure is irregularly meandering, black-colour burrows with a pale halo of coarse silt. In cross-section, the burrows are elliptical to sub-circular, U-shaped in the longitudinal profile. Burrow structure is normally erratic, vermicularly tanged. In core, it commonly appears as tiny dark pin-head sized spots. In longitudinal cross-section, it shows discontinuous and surrounded by a pale silt halo.

9. *Palaeophycus*. Erected by Hall, 1847. The structure is straight, slightly curved, slightly undulose or flexuous, smooth or ornamented, typically lined, essentially cylindrical, predominantly horizontal structures are interpreted as open burrows; burrow-fill typically massive, similar to host rock, although substantial fill may be absent; where present, bifurcation is not systematic, nor does it result in swelling at the sites of branching. The structures is characterised by passively filled, typically lined, burrows (Pemberton and

Frey, 1982).

10. *Zoophycos*. Erected by Massalongo, 1855. Burrow is a circular to lobate sheet-like spreite; either flat, curved, inclined or wound in screw fashion around a central vertical axis. The spreite is a horizontal or sub-horizontal web of closely juxtaposed parallel burrow tunnels. Burrow tunnels system show the path of feeding apparatus during a single probing of the sediment. Successive probing side-by-side in the same direction or plane produces a horizontal spreite.

Lithofacies F-1 Description: Organic rich siltstone

Lithofacies association F-1 is a dark to black coloured organic-rich, dolomitic siltstone. The grain-size is primarily composed of coarse-silt with thin laminae of fine-silt. The fine-silt laminae are preserved as horizontal to wavy lamination (Fig. 2.10-A). The thickness of individual fine-silt lamina within Lithofacies F-1 is approximately 2 to 3mm. Thin-section petrography of samples obtained from Lithofacies association F-1 confirm the nature of silt composition and further show that the grains are subangular to subrounded, and well sorted. SEM analysis shows that the organic rich siltstone of Lithofacies F-1 is composed of dolomite, mica, and clay minerals (Fig. 2.10 –B and C). Trace fossils are not present in Lithofacies F-1. The basal contact between lithofacies F-1 and lithofacies F-2 is abrupt. Grain sorting and textural characteristics have implications for porosity and permeability in terms of interconnectivity of void spaces that enhance effective porosity for subsurface fluid migration into reservoirs.

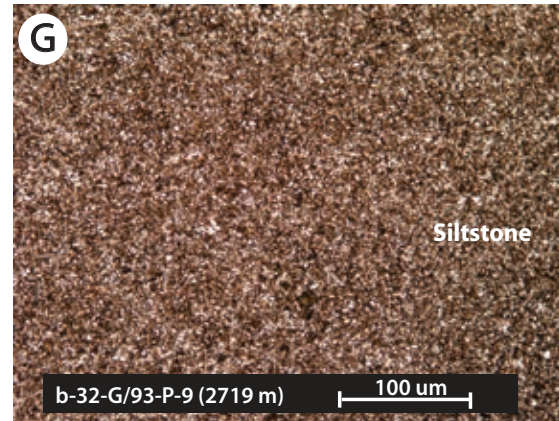
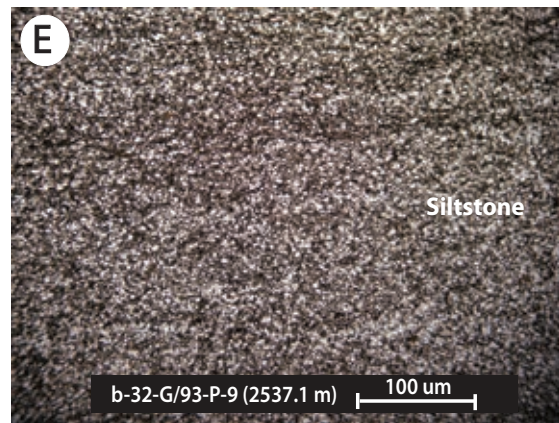
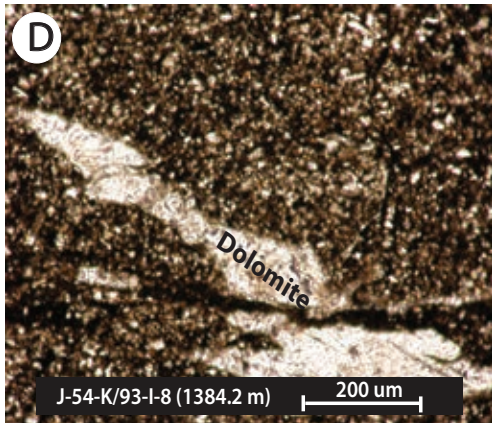
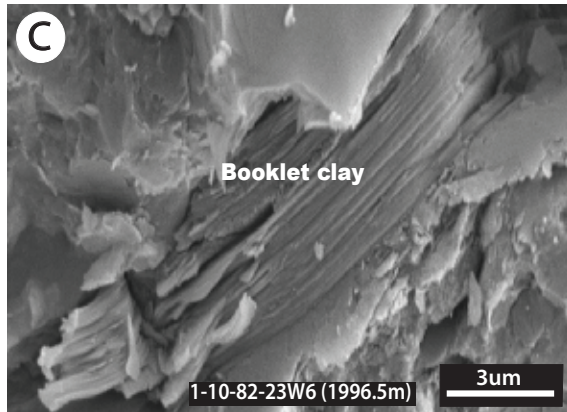
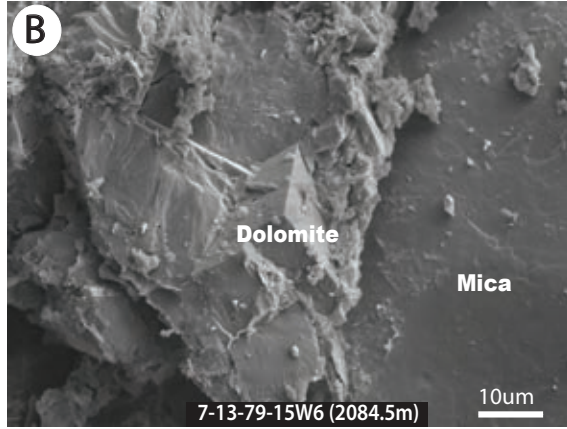
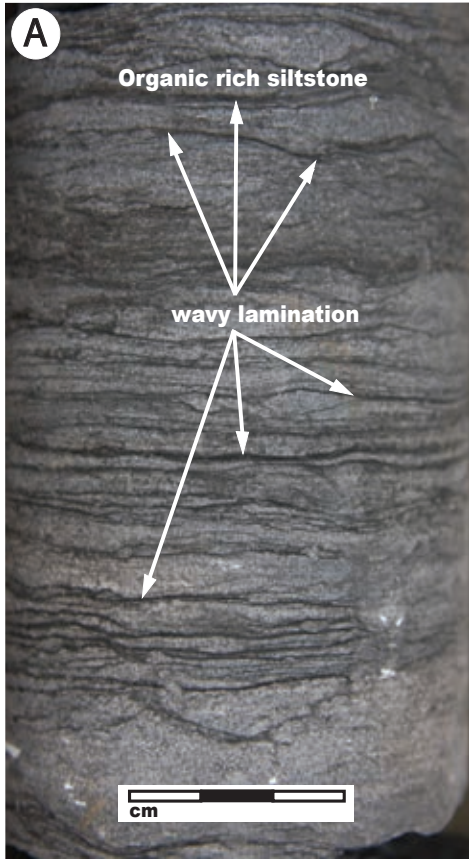


Figure 2.10. Shows core photo, scanning electron microscopy (SEM) images and petrographic microphotographs of Lithofacies association (F-1) from the Montney Formation. (A) Core photo of Lithofacies F-1, organic rich siltstone with wavy laminae (Well: 1-10-82-23-W6, depth 1996m), Monias gas field, northeastern British Columbia. (B) Shows the mineralogy of Lithofacies association F-1 composed of dolomite and mica (Well: 7-13-79-15W6, depth 2084m). (C) Shows clay mineral associated with the organic component of Lithofacies association F-1, with distinctive layering characteristic of kaolinite clay (Well: 7-13-79-15W6, depth 2084). (D) Detrital dolomite admixed quartz-grained siltstone (Well: J-54-K/93-I-8, depth 1384.2m). (E through G) Shows very fine-grained, well sorted siltstone of Lithofacies association F-1 (Well: b-32-G/93-P-9).

F-1 Interpretation

The dark colour organic rich content (~3 wt% TOC) of Lithofacies F-1 is related to high nutrient rich sediment source and rapid sedimentation, which enhanced the preservation of organic matter (Muller and Suess, 1979) in oxygen-poor depositional environment (Demaison and Moore, 1980; Ekdale and Mason, 1988; Wishner, et al., 1990; Tyson and Pearson, 1991; Wignall and Hallam, 1991; Bentley and Nittrouer, 1999), where density or temperature stratified water column form, typically below wave-base (Demaison and Moore, 1980). Oxygen poor environments can be characteristic of a distal offshore setting (Ekdale and Mason, 1988; Wignall and Hallam, 1991; Houseknecht and Schenk, 2004). The high TOC content of Lithofacies F-1 makes it a potential source rock.

Lithofacies F-1 is mainly composed of coarse silt-sized grains. Silt and very fine-grained sediment is the product of weathering, and transported by fluvial or aeolian mechanisms. Stow (1985) used depositional model to show sediment source. Particularly, Stow (1985) shows that the deposition silt and very finegrained sediments are related to mobilization of fines across-shelf (Fig. 2.11), or transported through processes, which may include sediments deposition from hyperpycnal plumes (Milliman and Meade, 1983; Stow, 1985; Wright, et al., 1986; Wiseman,

et al., 1986). As hyperpycnal flow gradually loses part of its suspended load progressively seaward, the finer-grained silt-sized particles are deposited in distal offshore environments (Pedersen, 1985), where changes in bottom-water anoxia and sediments settling from suspension mostly dominate (Ghadeer and Macquaker, 2011).

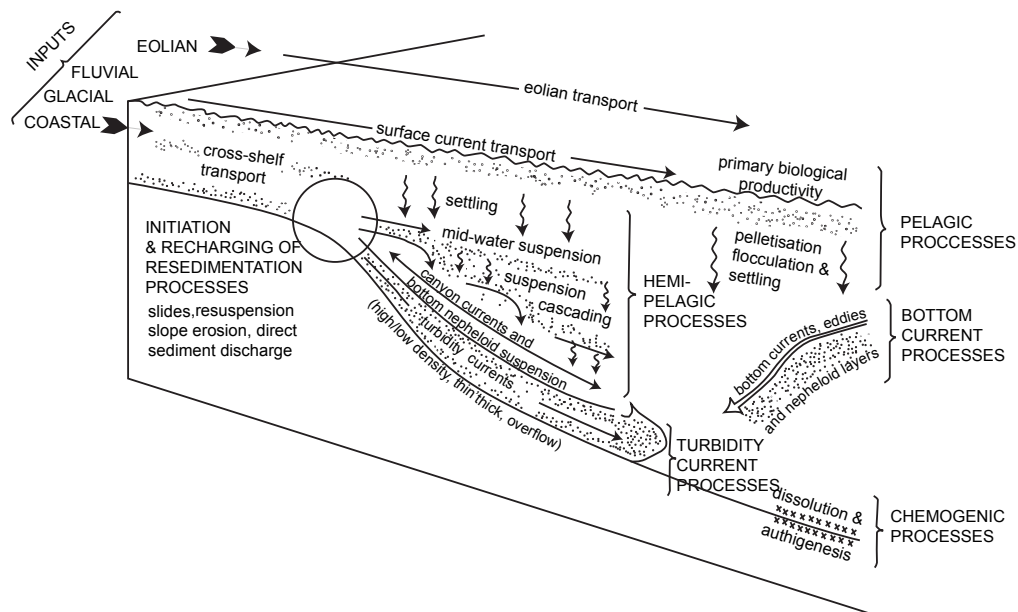


Figure 2.11. Schematic representation of the relationship between processes affecting transport and deposition of fine-grained sediments into distal offshore/and deep-water (Stow, 1985).

Preserved horizontal to wavy lamination in Lithofacies F-1 developed during sedimentation when finer-grains settle from suspension under gravity influence in a decelerating flow regime as experimented by Berthault (1988). The outershelf (distal offshore setting) environment is a locus for such decelerated bottom flow regime (Pedersen, 1985). The sluggish flow regime enhances the development of lamination, characterized by very distinct, abrupt laminae surfaces of less than 1mm thick, which contains finer-grained particles than the surrounding deposit (Thomas,

et al., 2007). The absence of soft-sediment deformation structures and convolute bedding in lithofacies F-1 imply that wave loading, episodic, or seismically triggered deposition were not at play in the depositional process of Lithofacies F-1.

The subangular to subrounded grains (Wadell, 1935; Russell and Taylor, 1937; Krumbein, 1941; Pettijohn, 1949) of Lithofacies F-1 have implications for the sediment source, transport mechanism and duration of entrainment (Bridge, 1981; Middleton, 1976). Generally, grain roundness is a fundamental physical property of sediment particles, affecting their entrainment, transport, deposition, and, therefore provides clues about the sediment provenance, transport history and depositional conditions (Folk and Ward, 1957; Blott and Pye, 2011). Subangular to subrounded grain-sizes of Lithofacies F-1 infers relatively short distance of transport from sediment source-rock prior to initial entrainment into suspension (Bagnold, 1956; Visher, 1969). The well sorted textural characteristics of Lithofacies F-1 imply the evenness of the mass of particles with the total amount of material that are within the same grain-size distribution (Sharp and Fan, 1963) as seen under microscopy.

Mineralogical composition of Lithofacies F-1 includes silt-sized quartz, dolomite, mica, and clay. The silt size grains in Lithofacies F-1 derived its origin from the mechanical and chemical breakdown of quartz (Kuenen, 1959; 1969; Riezebos and van der Waals, 1974; Moss and Green, 1975; Blatt, 1970; 1987). In support of weathering as a mechanism of disintegration of quartz into silt sized particles, an account of structural defects in quartz crystals was experimentally presented by Moss and Green (1975); Blatt (1970); Riezebos and van der Waals (1974), and their findings suggest that silts may be released directly from bedrock during weathering (Moss and Green, 1975; Blatt, 1970; 1975; Riezebos and van der Waals, 1974). Furthermore, production of silt is associated with fracturing of coarser quartz grains during weathering and pedogenesis (Blatt, 1987).

The deposition of silty sediments into distal settings is significantly related to

flocculation of fines due to the affinity of mica as a major component of siliciclastic sediments (Tucker, 1988). Suspended sediments are well known to be transported primarily as flocculated material (Droppo, 2001). Floccs are composed of a complex matrix of organic particles, inorganic particles (e.g. clays and silts) and substantial interfloc spaces (pores) that allows for the retention, sustenance and flow through the water (Droppo, 2001). The profound plume experimental work of Schieber and Southard (2009) shows bedload transport of mud by floccule. Therein, Schieber, et al. (2007); Schieber and Southard (2009) show that floccule is associated with bedload transport in a thin layer of floccule-carrying clay in suspension within boundary layer of higher concentration and interpreted the phenomenon as a direct analogue to the heavy fluid layer in sand transport. Flocculation can significantly alter particles in a hydrodynamic flow by modifying grain-size and shape, thereby enhancing effective transport of sediment (Droppo, 2001).

Thin-section petrography shows that the dolomite in Lithofacies F-1 is detrital. The detrital nature of the dolomite in some thin-sections show sigmoidal morphorlogy resembling ripple lamination, suggesting that the dolomite fragments may have been sheld from carbonate apron as debris. The scattered, detrital dolomite nature seen in thin-section petrography could be interpreted as postdepositional in origin, rather than in situ (Bone, et al., 1992). The clay mineral is associated with the organic matter in Lithofacies F-1. Kennedy, et al. (2002) studied the relationship between organic matter and shale in modern sediments and found that adsorption of carbon compounds onto clay mineral surfaces played a fundamental role in the burial and preservation of total organic carbon in the sediment. Organic matter is an economically important source of hydrocarbons, minerals, and metals (Sethi and Schieber, 1998; Schieber, 2009). Organic carbon is derived mostly from photosynthesis by plants and algae, which are atoms of carbon buried in sediments

implies a molecule of oxygen added to the atmosphere (Schieber, 2003). The absence of bioturbation in Lithofacies F-1 imply stressed and disaerobic conditions (Rhoads and Morse, 1971; Byers, 1977; Savrda, et al., 1984; Ekdale, 1988; Stow, et al., 2002). Thus, Lithofacies F-1 deposition may be related to pelagic processes (Bodungen, et al., 1995; Billet, et al., 1983; Walsh, 1983).

Pelagic depositional process is supported by the absence of depositional features characteristic of shoreface, such as storm or wave generated primary sedimentary structures (cross bedding or hummocky cross stratification). The absence of trace fossils in Lithofacies F-1 may be due to dysaerobic or oxygenation stress (Ekdale, 1985; Gingras, et al., 2005; MacEachern, et al., 2005; Burnnet, 1977; Bentor, 1980). Dysoxic conditions prevailed for most of the Permian-Triassic (P-T) boundary that caused mass extinction, which ravaged biotic communities, the most severe in Earth's history (Raup, 1979; Erwin, 1993; Twitchett, et al., 2004; Zonneveld, 2011), due to unequalled decline in the amount of dissolved oxygen in the world's oceans (Isozaki, 1994, 1997; Grice et al., 2005; Berner et al., 2007).

The anoxic conditions extended intermittently into shallow marine (proximal shelf) depositional settings (Hallam, 1991; Wignall and Hallam, 1992; Zonneveld, et al., 2010), which have been reported to be associated with global anoxic conditions that subsequently caused a prolonged faunal recovery in the aftermath of Permian-Triassic biota crises (Erwin, 1993; Erwin, et al., 2002). The protracted fauna recovery continued into the Lower and Middle Triassic time (Zonneveld, et al., 2010), thereby delaying fauna revitalization for several millions of years following the fauna mass extinction (Wignall and Hallam, 1992; Hallam, 1995; Wignall and Twitchett, 2002a, 2002b; Twitchett and Wignall, 1996; Twitchett, et al., 2004). The harsh environmental conditions post P-T fauna environmental crises have implications for the non-fossiliferous, or the non-evidence of fauna traces in

Lithofacies association F-1.

Based on the above sedimentological characteristics of Lithofacies association F-1 (organic rich siltstone), it is interpreted herein as a deposition in a distal offshore (outershelf) to ramp setting (Fig. 2.12). A shelfal environment has been interpreted for similar siltstone facies (Pedersen, 1985; Thomas, et al., 2007), or outershelf to continental slope bathymetry (Eyles, et al., 1998; Ghadeer and Macquaker, 2011). This interpretation is in line with previously reported depositional environment for the Lower Triassic Montney Formation by Moslow and Davies (1997); Davies et al. (1997); and Zonneveld, et al. (2010).

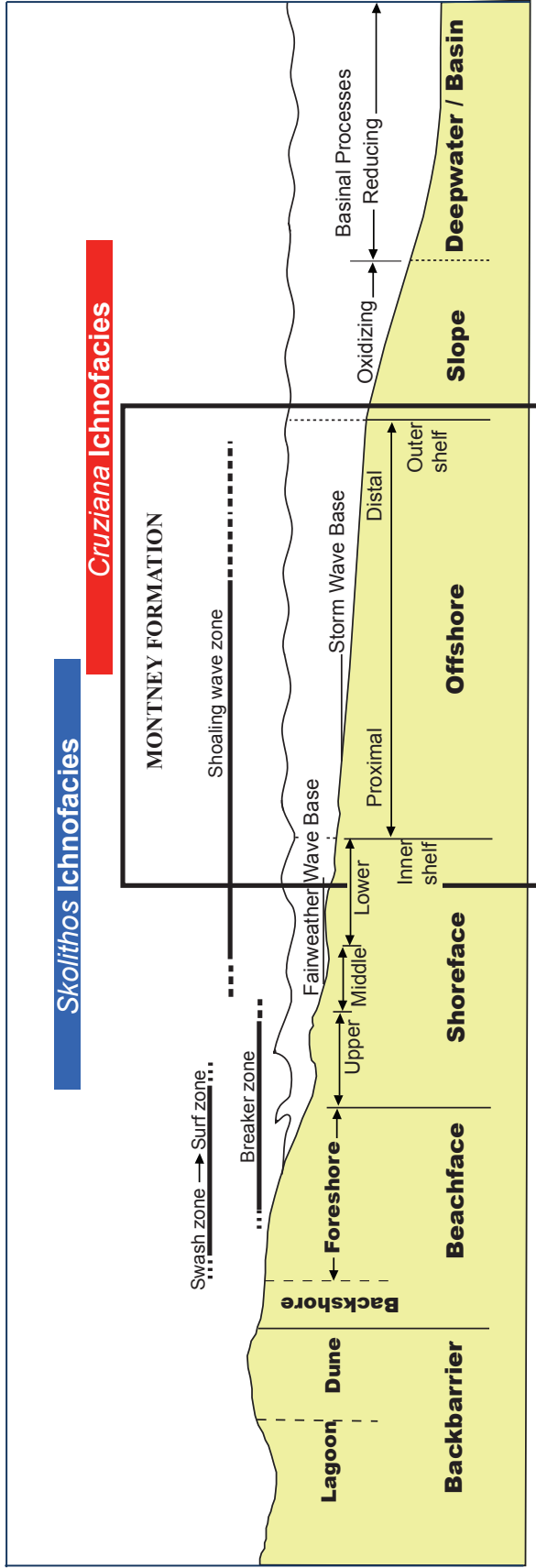


Figure 2.12. Depositional environment profile showing dominant energy in the sub-environments from lagoonal – backbarrier area to deepwater setting. Ichnofacies associated with the Montney Formation in the study cores are those attributed to the *Skolithos* and *Cruziana* ichnofacies, which typically occur in the shoreface through offshore to slope environment as shown in blue and red bar above.

Lithofacies F-2 description: Very fine-grained sandstone and siltstone

Lithofacies association F-2 is composed of interbedded, laminated, very fine-grained sandstone and siltstone (Figs. 2.13-A, 2.14, and 2.15-C). The ratio of sand to silt in Lithofacies F-2 is approximately 3:1 (Fig. 2.15-C) in some successions and ~2:1 ratio in some beds (Fig. 2.13-B, C, and D). Thin-section analysis of Lithofacies association F-2 confirms that the lithology is siliceous, and the grain-size ranges from very fine-grained sandstone to coarse siltstone grade (Fig. 2.16-B and D). Petrographic examination of Lithofacies F-2 further shows that the grains sorting are variable, from moderately well sorted to poorly sorted (Fig. 2.16-B and D), and texturally matured, but mineralogically submature as evidenced by the present of feldspar and clay (Fig. 2.16-A). In addition, thin-section petrography shows that the mineral composition of Lithofacies F-2 comprises quartz, mica, pyrite, and detrital dolomite (Fig. 2.16). SEM analysis further shows that some of the quartz in Lithofacies F-2 has developed authigenic quartz overgrowth (Fig. 2.16-G).

Lithofacies F-2 has well-preserved plane parallel laminae (Figs. 2.14, 2.16-H, 2.18, and 2.19). The sand laminae exhibit fractures along sandstone bedding planes (Fig. 2.13-B, C and Fig. 2.15-B). Depositional features in Lithofacies F-2 comprise dewatering sedimentary structures, soft sediment deformation structures, convolute bedding / lamination (Fig. 2.14-C), and small-scale current ripples (Figs. 2.14-C, 2.18-B and C; 2.19, 2.13-D). The current ripples are dominantly straight-crested, and rarely bifurcating (Fig. 2.15-A, D). Body fossils are not present in Lithofacies F-2. The basal contact of Lithofacies F-2 with Lithofacies F-3 is sharp, and abruptly ungradational.

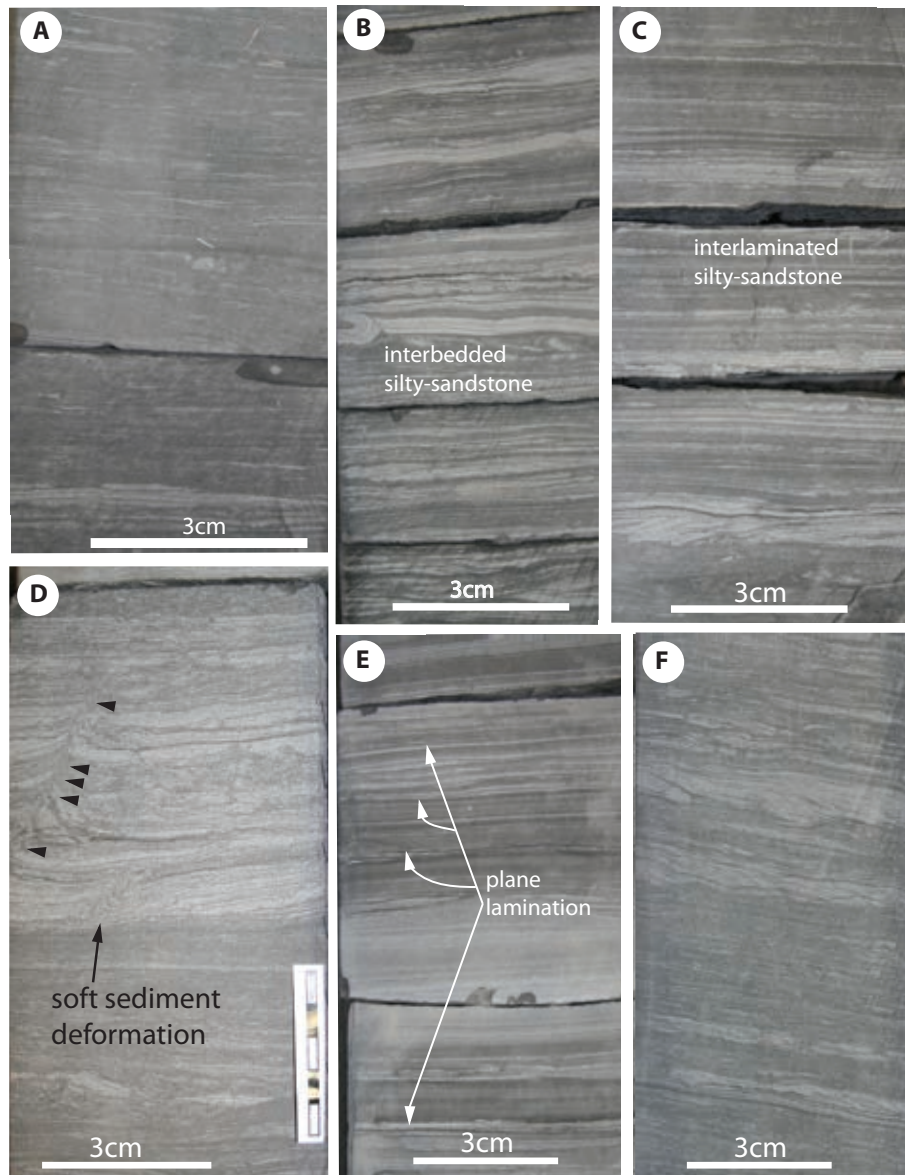


Figure 2.13. Core photographs showing depositional characteristics of Lithofacies F-2. **(A)** Shows interbedded sandy siltstone (well: 9-29-79-14W6; depth: 1970m). The percentage of sand proportion decreases upward from base of A to top of A **(B)** Laminated siltstone interbedded with very fine-grained sandstone (well: 11-04-79-14W6; depth: 2052.5m). **(C)** Shows interlaminated silty-sandstone with fracture along sandstone bedding plane (well: 11-04-79-14W6; depth: 2051m). **(D)** Very fine-grained sandstone with soft sediment deformation structure overlying coarse-grained siltstone (well: 11-04-79-14W6; depth: 2053.4 m). **(E)** Plane laminated silty-sandstone. Interbedded silty-sandstone (well: 11-04-79-14W6; depth: 2055 m). **(F)** The proportion of sand increases towards the top of **Plate - F** (well: 9-29-79-14W6; depth: 1973.5 m).



Figure 2.14. Microphotograph of core samples showing sedimentary structures in Lithofacies association F-2. **(A)** Laminated, very fine-grained silty-sandstone (well: 11-04-79-14W6; depth: 2070m). **(B)** Coarse-grained siltstone and very fine-grained sandstone with poorly formed bedding planes (well: 11-04-79-14W6; depth: 2077m). **(C)** Shows soft sediment deformation structure (well: 11-04-79-14W6; depth: 2071m).

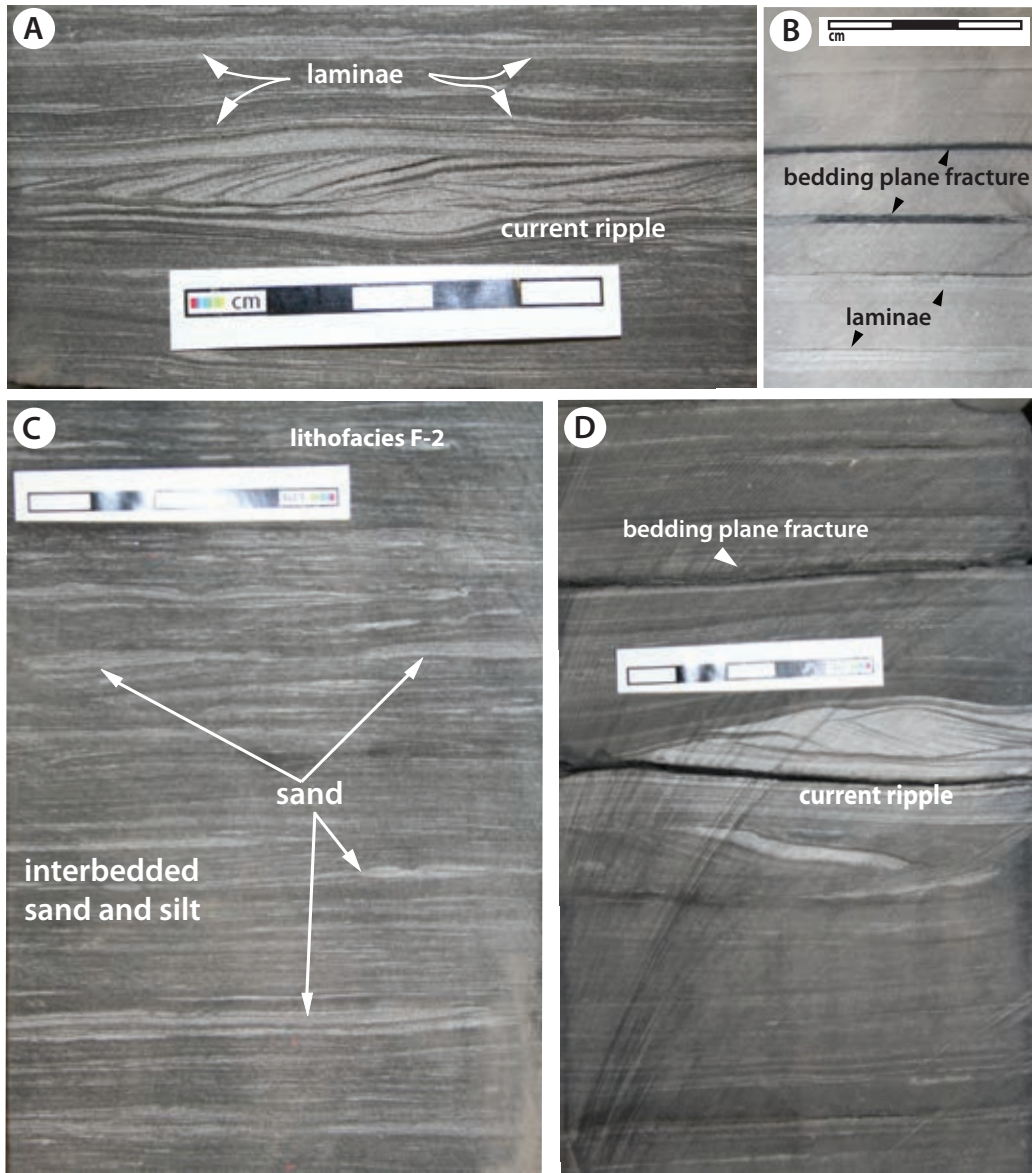


Figure 2.15. Core photographs showing depositional characteristics of Lithofacies F-2. **(A)** Laminated very fine-grained, silty-sandstone with current ripple (well: d-39-F/93-P-9; depth: 2655.5m). **(B)** Siltstone with fractured along bedding planes (well: 8-22-82-20W; depth: 1818.7m). **(C)** Shows interbedded silty-sandstone and very fine-grained sandstone (well: 9-29-79-14W6; depth: 1946.9 m). **(D)** Shows siltstone, current ripple and bedding plane fracture (well: 11-04-79-14W6; depth: 2076.2m).

F-2 Interpretation

Lithofacies association F-2 is composed of interbedded, laminated, and very fine-grained sandy-siltstone. McKee and Weir (1953) originally defined laminae (Fig. 2-14-A) as sedimentary strata that are less than 10mm thick. The present of preserved interbedded sandy-siltstone, and thinly laminated layers (approximately < 10mm) in Lithofacies association F-2 reflect variation in sediment texture between grain-size during sedimentation (Best and Bridge, 1992). The formation of laminae involves transcurrent migration of grains due to low relief in topography, and bed waves (Cheel and Middleton, 1986; Poala, et al., 1989). Low relief and bed waves migration of sediments (Allen, 1982) are characteristic of the lower shoreface through proximal offshore environment (Cheel and Middleton, 1986; Poala, et al., 1989). Thinly laminated silt and very fine-grained sand in lithofacies F-2 may be related to deposition resulting from gravity influenced sedimentation (Reineck and Singh, 1972) in a lower shoreface environment, where fair weather processes are dominant (Reineck, 1984.).

The silty and very fine-grained textural characteristics of Lithofacies F-2 suggests that the sediments may have been initially deposited on the shelf as fine-grained sediments, and subsequently transported either via suspension or near-bed migration to lower shoreface – proximal offshore settings (Johnson and Baldwin, 2002). This interpretation is supported by the absence of sedimentary structures characteristic of upper shoreface environment, where higher energy dominate (Weise 1980), such as hummocky cross stratification, wave or oscillatory ripples, which are primarily a response to high-energy currents and waves (Harms et al., 1982). Thus, quiescent sedimentation processes may have dominated during the deposition of very fine-grained sandstone interbedded with siltstone of Lithofacies F-2.

The very fine-grained sand and silt in Lithofacies F-2, in part suggest the possibility of input from aeolian sediment source. Evidence supporting aridity in Western Canada Sedimentary Basin (WCSB) during the Triassic time was reported by Habicht (1979) in the study of paleogeographic, paleolatitude and paleomagnetic analyses. Fauna record (Tozer, 1982) and paleolatitude (Habicht, 1979) study shows that paleoclimate may have ranged from sub-tropical to temperate (Habicht, 1979; Tozer, 1982; Gibson and Barclay, 1989) during the Triassic period of WCSB, and has been interpreted to be arid, and was dominated by winds from the west (Habicht, 1979; Arnold, 1994; Wilson, et al., 1994). Paleoclimate of 30° N as the location of the WCSB in Triassic time is consistent with arid climate and desert conditions, in which aeolian depositional processes can thrive. Evidence that supported seasonal aridity during the Triassic was established by Arnold (1994) through the measurement of paleocurrent on aeolian sandstone beds, which indicated a wind flow direction from northeast in a southwest direction. The southwest directional wind transport of sediments is believed to have released seasonal offshore silt and very fine-grained sands into marine surface water (Moslow and Davies, 1997). The north to south longshore sediment transport affected Montney sedimentation (Moslow and Davies, 1997). The siliceous characteristics of Lithofacies F-2 imply quartz dominant amongst the sandstone mineralogical composition. The variable grain sorting (moderately well sorted to poorly sorted), of Lithofacies F-2 is related to the interbedded sandy-siltstone (Fig. 2.16-A and D), and is interpreted as texturally matured, but mineralogically submature.

The sedimentological manifest of small-scale current ripples (Figs. 2.15-D; 2.18-A) form a continuum of Lithofacies F-2 interpretation. Current ripple probably correspond to waning flow conditions (MacEachern, 1994). Current ripples readily form in shallow water, but can also form in deepwater setting due to ocean-bottom currents (Collinson, et al., 2006). However, the current ripple reported in Lithofacies

F-2 may have formed in lower shoreface or proximal offshore environment. The proximal offshore setting has relatively low topographic gradient, which provides an excellent platform for the formation of ripples under deceleration of currents, as sand and silt fall from suspension during low energy coupled with dominance of sand that are reworked on the beds into ripples (Collinson, et al., 2006).

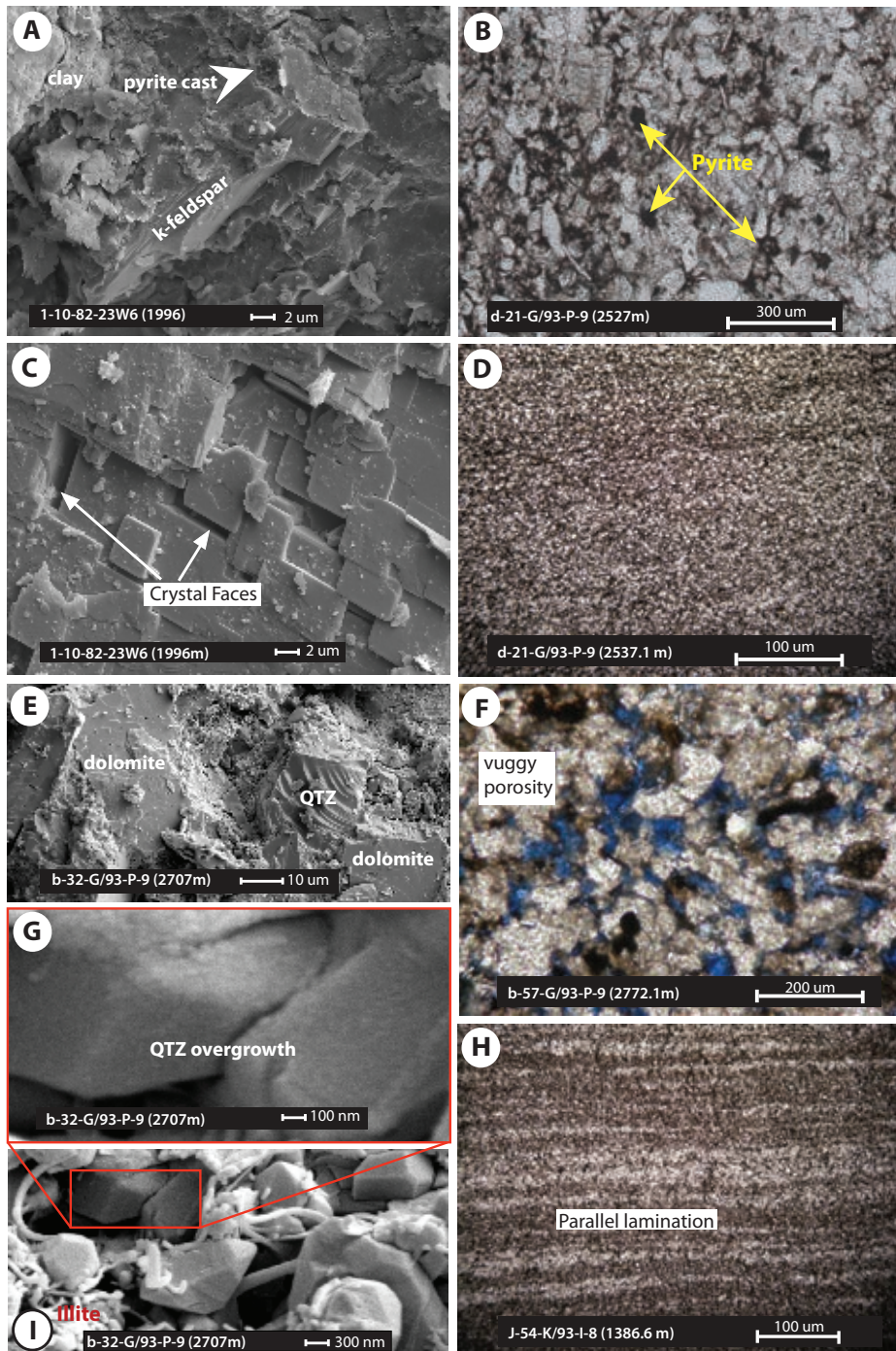


Figure 2.16. Microphotographs analyzed using scanning electron microscopy (SEM) and thin-section petrography. (A) Shows potassium feldspar [k-spar], calcium rich feldspar [ca-spar], pyrite cast (white arrow), which forms as a result of diagenesis (well: 1-10-82-23W6; depth: 1996m). (B) Pyritic dolomitic sandstone, sub-rounded grains, and moderately poorly sorted (well: d-21-G/93-P-9, depth 2527m). (C) Shows dolomite with perfect cleavage. The crystal faces exemplified brittleness of lithology due to tensile stress (well: 1-10-82-23-W6, depth 1996m, Monias field). (D) very fine-grained sandstone and siltstone (well: d-21-G/93-P-9, depth 2537m). (E) A mixture of massive, fractured dolomite and quartz exhibiting conchoidal fracture. (F) Shows vuggy porosity associated with intergranular and grained moldic, formed by partial leaching to complete dissolution of feldspar grains and other unstable minerals (well: b-57-G/93-P-9; depth: 2707m). (G) Shows authigenic quartz overgrowth due to diagenesis (well: b-57-G/93-P-9; depth: 2707m). (H) Shows parallel, interlaminated, interstratified very fine-grained sandy-siltstone and argillaceous siltstone due to grain size difference (well: J-54-K/93-I-8; depth: 1386.6m). (I) Shows quartz overgrowth (insect for **Plate G**), illite clay and micro void spaces (interparticle porosity) (well: b-57-G/93-P-9; depth: 2707m).

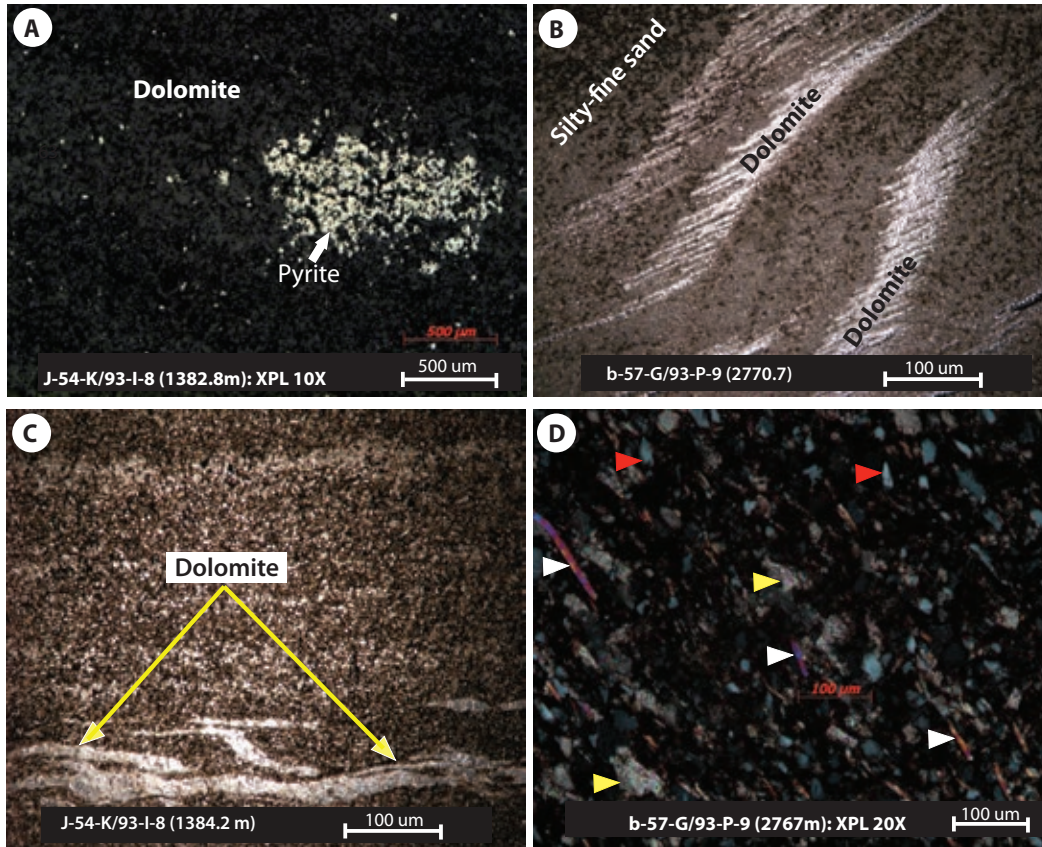


Figure 2.17. Photomicrographs in thin-sections showing mineralogy for lithofacies F-2. [red arrow = Quartz; yellow arrow = Dolomite; white arrow = Mica (A) Crossed polarized light showing pyrite mineral admixed dolomite mineral, quartz, mica and detrital grains. Pyrite is an indication of diagenesis in the Montney Formation. (B) Dolomitic silty-sandstone. The detrital dolomite forms ripple. (C) Detrital dolomite admixed silty-sandstone. (D) Shows mica, quartz, dolomite, and detrital grains.

Deformation structures in Lithofacies F-2 (Figs. 2.13-D; 2.14-C; 2.18-B and C; 2.19) is a result of wave loading commonly due to storm or high-energy deposit (Pemberton and MacEachern, 2001; Zonneveld et al., 2010). Soft sediment deformation structures in Lithofacies association F-2 are formed due to processes occurring during a deformational event at or near the contemporary surface of unconsolidated sediments either before, or soon after burial (Bhattacharya and Bandyopadhyay, 1998). Deformation structure are produced due to mechanical

forces causing plasticity, commonly related to gravity acting upon weak sediment, usually silts or sands, prior to or soon after, or at deposition along the sediment surface (Collinson, et al 2006). Soft sediment deformation structures can develop only in the presence of susceptible sediments, with appropriate forces that can trigger deformation mechanism (Allen, 1982; 1986). Liquefaction or fluidization is the most important agent for the development of sediment deformation structures in water-saturated and cohesionless sediments (Allen, 1982). Liquefaction or fluidization in unconsolidated sediments may be triggered by several processes such as seismic shocks, or after shocks, wave loading or overloading, groundwater movements, and effect of storm waves (Moretti, 2000). The contrasting grain-size (very fine-grained sand and silt) of Lithofacies F-2 characterized by alternating grain-sizes, overlying homogeneous sediments makes deformation structure possible (Moretti, 2000).

The analysis of soft-sediment deformation structures can unravel the driving force, deformation mechanism, timing of deformation relative to sedimentation, and the triggering agent (Owen 1987). Sediment deformation structures in Lithofacies F-2 may be related to the Triassic tectonic activity. Wittenberg and Moslow (1991) and Cant (1994; 1986) interpreted sediments loading, deformed beddings, slumping structures and small-scale faults as indicators of tectonically driven factors that influenced the deposition of Triassic succession. Other workers (e.g. Beranek and Mortensen, 2006; 2007; Ferri and Zonnveld, 2008) have interpreted some of the deformation structures in the Montney Formation to be related to initial terrane collision in the British Columbia/Yukon as part of a regional tectonism of Early to Middle Triassic. Other possibilities for the formation of deformation structures in lithofacies F-2 include seismicity, current turbulence associated with the onset of sediment-laden hypopycnal plumes could trigger deformation of laminae (Stewart, 1963; Selley 1969, 1970), and hydrostatic pressure effects associated with upwelling

groundwater (Williams 1966, 1969, 1970).

Convolute bedding (McKee, 1953), and convolute lamination (Ten Haaf, 1956; Sanders, 1960) in Lithofacies F-2 are associated with fluid escape, and their formation is related to grain-size and deformation mechanism. The convolute lamination/bedding structures involve folding of lamination into cusped upright form with a sharp anticline and a relatively gentle syncline (Fig. 2.14-C), and they are formed as a result of plastic deformation of partially liquefied sediment usually occurring shortly after deposition (Collinson, et al., 2006). Convolute lamination may also be the product of seismically triggered event that results in rapid deposition. The presence of soft sediment deformation, convolute lamination, and fugichnia in lithofacies F-2 (Fig. 2.14-C) are evidence of penecontemporaneous event, or small-scale episodic deposition. This is interpreted as small-scale local episodic deposition that resulted in escape structures.

The observed bedding plane fractures in Lithofacies association F-2 formed as a result of grain-size gradations and internal layering of parallel lamination and depositional fabric (Wall, 2006). Natural fractures are important and can help deliver hydrocarbons from the tight matrix of a Formation to the wellbore (Reid and McIntyre, 2001). The natural bedding plane fractures in Lithofacies F-2 have the potential to serve as both initial and hydraulically enhanced permeability conduits for hydrocarbon flow from tight matrix (MacKinnon, 1989; Reid and McIntyre, 2001).

Mineralogical composition of Lithofacies F-2 comprises quartz, dolomite, feldspar, mica, illite clay and pyrite. Quartz is the most abundant mineral in sandstone and serves as an indicator of textural and compositional maturity (Folks, 1959; Folks and Ward, 1957).

Quartz rich sediments have implication for porosity, particularly, effective porosity – the result of interconnectivity of pores in a siliciclastic matrix. Based

on SEM analysis, the quartz shows evidence of quartz overgrowth. Although quartz overgrowth within a dolomitic fabric insinuates complex relationships between quartz and carbonate, however, textural evidence from SEM (Fig. 2.16–G) suggests that at least two different phases of cementation may have taken place during authigenic modification of quartz. The dolomitic nature of the Montney Formation siltstone within the study area implies that carbonate cements may have been precipitated subsequent to, or post-dated an early quartz cement, and may have peripherally replaced the cement of overgrowth and detrital grain surfaces (Burley and Kantorowicz, 1986).

The present of feldspar in Lithofacies F-2 is a diagnostic mineral useful in the determination of provenance (Pittman, 1970), and estimation of paleoclimatological conditions can be derived from unstable minerals (Todd, 1968), particularly, the present of feldspar group in a siliciclastic deposit (Krynine, 1941; Folk, 1959). Plagioclase feldspar tends to be unstable during weathering, which limits its use to rocks that were deposited under tectonic conditions and favorable for rapid deposition (Pittman, 1970). The instability of plagioclase feldspar is useful in the interpretation of provenance and sediment history because any sandstone containing appreciable amounts of plagioclase feldspar would probably be first-cycle, and therefore, do not lead to erroneous interpretation on multi-cycle material (Pittman, 1970). Second-cycle feldspar grains are not common, because feldspar is not resistant to weathering. In general, most plagioclase feldspar in sedimentary rocks are sourced from igneous or gneiss (Kuenen, 1959, Folk, 1959). The interpretation for the present of feldspar in Lithofacies association F-2 indicate that the sediments are compositionally immature and have not undergone multiple cycles of sedimentation and redeposition (Pittman, 1970).

Pyrite in Lithofacies F-2 (Figs. 2.16-B; 2.17-A) is interpreted as post-depositional emplacement due to diagenesis (Hudson, 1982; England, et al., 2002).

The pyrite in Lithofacies F-2 (Fig. 2.17-A) appears as detrital pyrite aggregate within a dolomitic, very fine-grained, siltstone. Aggregated pyrite has been defined by Hudson (1982) as “a texture seen under the microscope, under reflected light microscopy appearing as small pyrite crystals that are aggregated into irregularly rounded ‘clots’ that are partly coalescent with one another and partly separated by non-reflective clay and carbonate”.. Aggregate pyrite in Lithofacies F-2 is interpreted to have formed *in situ* during diagenesis (England, et al., 2002; Hudson, 1982). Pyrite is an important diagenetic mineral and can help define the diagenetic history of sediments (Hudson, 1982). Thus, the present of pyrite in Lithofacies F-2 is an indication of diagenesis in the Montney Formation.

Detrital dolomite in Lithofacies F-2 appears to have been shed-off from carbonate apron as debris (Fig. 2.17-B). The present of detrital dolomite has been interpreted by Bone, et al. (1992) as post-depositional in origin. Based on the aforementioned lithological description, petrographic examination, scanning electron microscopy, and depositional characteristics of Lithofacies association F-2, it is interpreted herein as a deposition in the lower shoreface through proximal offshore depositional environment, occurring just below fair-weather wavebase (Fig. 2.12).

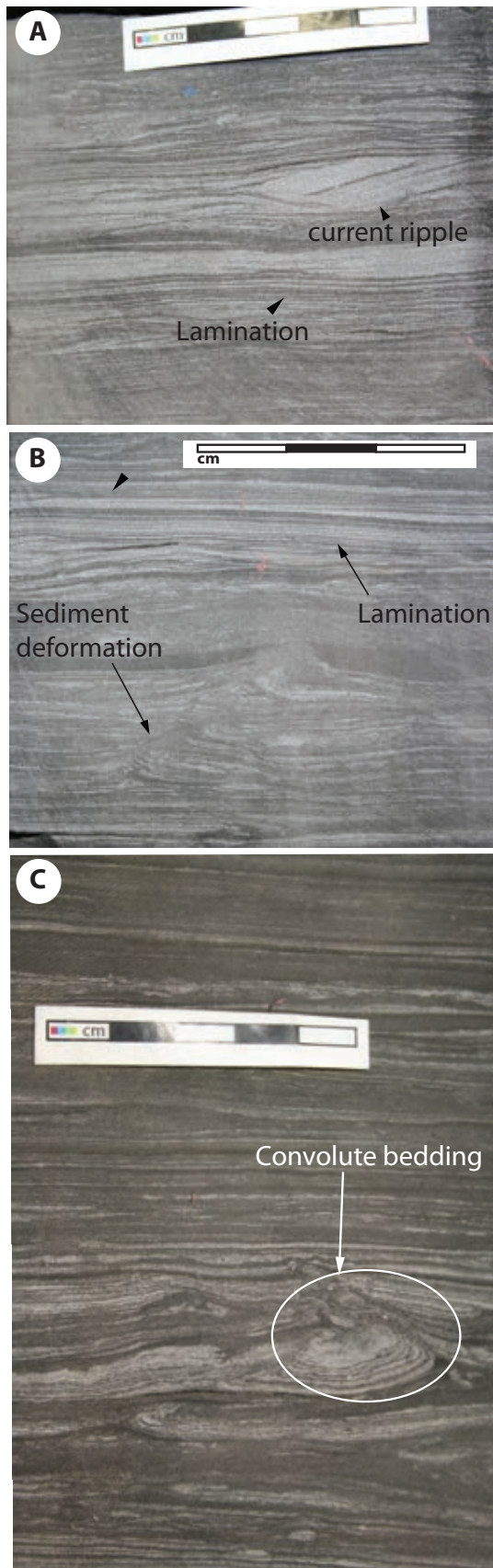


Figure 2.18. Core photographs showing depositional characteristics of Lithofacies F-2. (A) Shows lamination and current ripple (well: d-39-F/93-P-9; depth: 2660.6m). (B) Shows sediment deformation structure and parallel lamination of very fine-grained silty-sandstone (well: d-39-F/93-P-9; depth: 2659.8m). (C) Shows convolute bedding / sediment deformation (well: d-21-G/93-P-9; depth: 2526.5m).

Lithofacies: F-3 Description

Lithofacies F-3 is primarily composed of very fine-grained sandstone and coarse siltstone grade. Based on trace fossil assemblage, Lithofacies F-3 is subdivided into: Lithofacies F-3A (*Skolithos* ichnofacies) and Lithofacies F-3B (*Cruziana* ichnofacies). The typical assemblage of the *Skolithos* ichnofacies and *Cruziana* ichnofacies is presented as a model in Fig. 2.20. Although the model show ichnofauna diversity and abundance, the recorded trace fossils within the study interval of the Montney Formation in British Columbia does not have abundance and diversity of either the *Skolithos* ichnofacies, or the *Cruziana* ichnofacies. The description of Lithofacies association F-3A and F-3B are discussed below. The recorded infauna traces in cores in the study area are defined morphologically in Table 2.2.

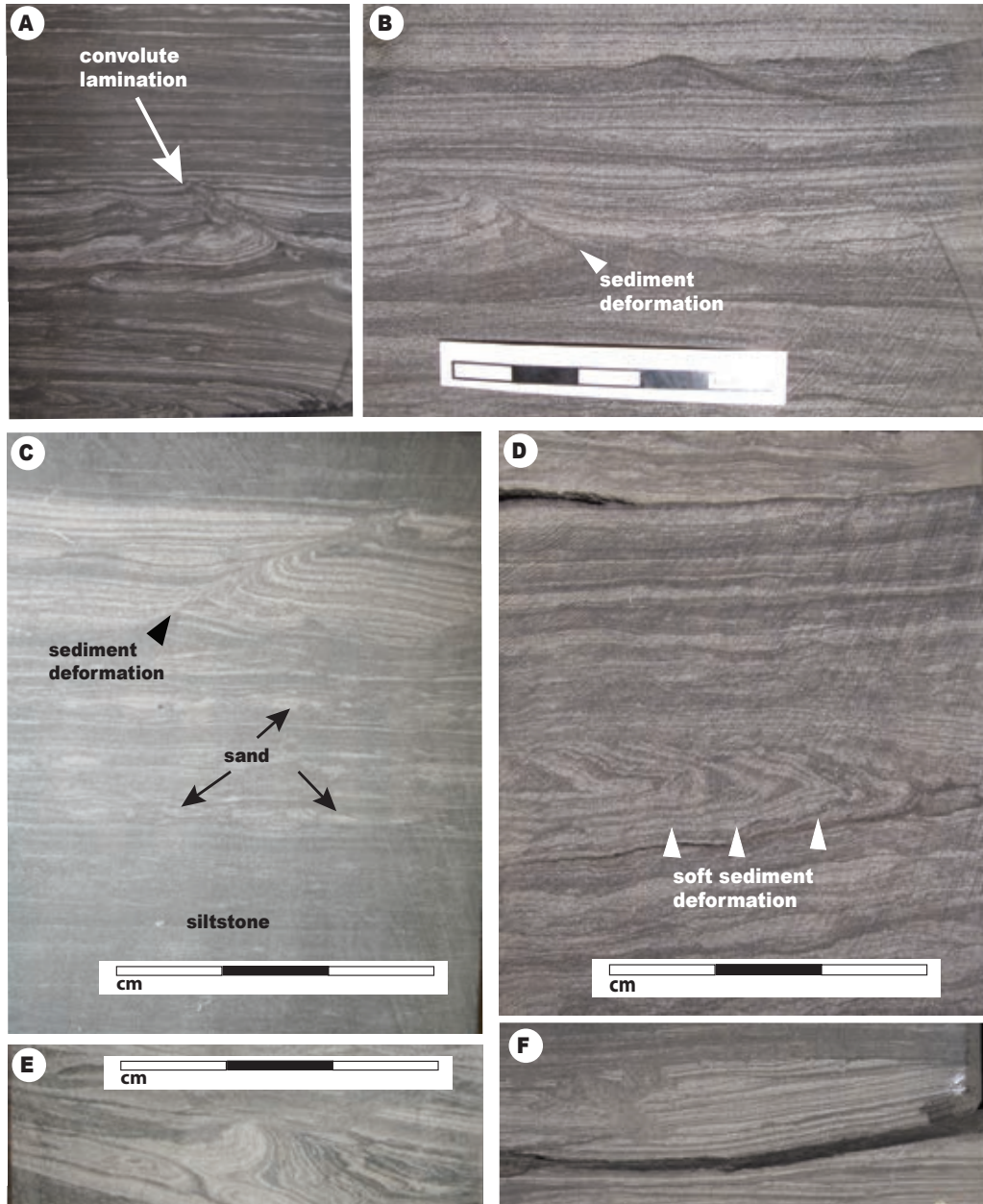


Figure 2.19. Core photographs showing various types of sediment deformation in Lithofacies F-2. **(A)** Shows convolute lamination / bedding (well: d-21-G/93-P-9; depth: 2526.5m). **(B)** Shows micro-fault that resulted in discontinuity of parallel lamination due to sediment deformation (well: d-21-G/93-P-9; depth: 2540.5m). **(C)** Shows fugichnia resulting from sediment deformation caused by escape trace during high or episodic sedimentation (well: 9-29-79-14W6; depth: 1985.2m). **(D)** Shows soft sediment deformation structure caused by sediment loading and dewatering (well: d-21-G/93-P-9; depth: 2541m). **(E)** Shows soft sediment deformation / convolute lamination (well: 9-29-79-14W6; depth: 1965.5m). **(F)** Shows lamination and sediment deformation (well: 11-04-79-14W6; depth: 2097m).

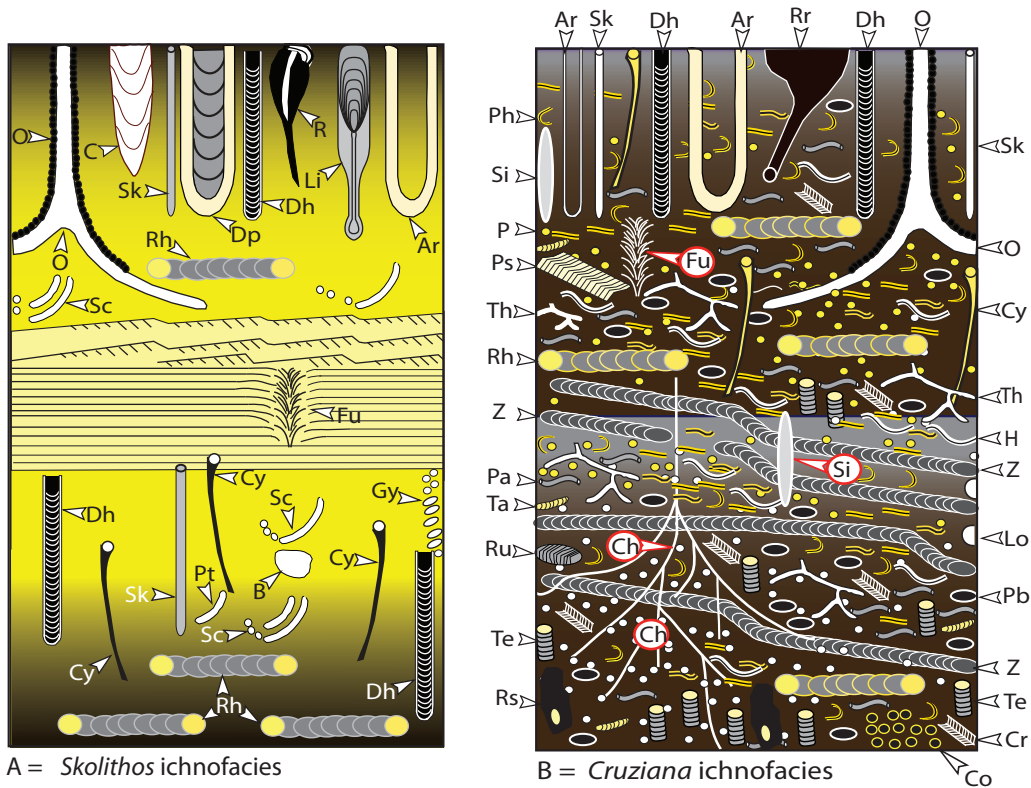


Figure 2.20. Archetypal expression of the *Skolithos* ichnofacies and *Cruziana* ichnofacies. The diversity and abundances of trace fossils suite represented in this model is far fetched from the reality of the trace fossils observed in the study core interval of the Montney Formation (see Table 2.2 for trace fossils recorded in the Montney Formation in this study). This model serves the generality of the typical *Skolithos* ichnofacies and the *Cruziana* ichnofacies that may exist in any locality. However, a departure from this may occur when dealing with mixed *Skolithos* and *Cruziana* ichnofacies, in which cut crossing ichnofacies of opportunistic association dominates. The *Skolithos* ichnofacies interpretation of abbreviation in Figure A: *Ophiomorpha* (O), *Conichnus* (C), *Skolithos* (Sk), *Diplocraterion habichi* (Dh), *Roselia* (R), *Lingulichnus* (Li), *Arenicolites* (Ar), *Rhizocorrallium* (Rh), *Schaucylindrichnus* (Sc), *Fugichnia* (Fu), *Cylindrichnus* (Cy), *Bergaueria* (Be), *Gyrolithes* (Gy), and *Palaeophycus tubularis* (Pt). For the *Cruziana* ichnofacies, the interpretation of abbreviations for Figure B are: *Arenicolites* (Ar), *Skolithos* (Sk), *Diplocraterion habichi* (Dh), *Rhizocorrallium* (Rh), *Ophiomorpha* (O), *Phycosiphon* (Ph), *Siphonichnus* (Si), *Planolites* (P), *Psammichnites* (Ps), *Thalassinoides* (Th), *Rhizocorrallium* (Rh), *Zoophycos* (Z), *Palaeophycus heberti* (Pa), *Rusophycus* (Ru), *Teichichnus* (Te), *Rosselia socialis* (Rs), *Conichnus* (C), *Cruziana* (Cr), *Phoebichnus* (Pb), *Lockeia* (Lo), *Helminthopsis* (H), *Fugichnia* (Fu), *Chondrites* (Ch), and *Cylindrichnus* (Cy).

Lithofacies F-3A Description: *Skolithos* ichnofacies

Lithofacies F-3-A is composed of bioturbated, very fine-grained sandy-siltstone (Fig. 2.21). The trace fossils in lithofacies F-3A comprises *Planolites*, *Phycosiphon*, *Cruziana*, *Skolithos*, *Teichichnus*, and *Palaephycus*. Lithofacies F-3A has preserved wavy to parallel lamination (~10mm to 15mm in thickness), wave ripples, sediment deformation, and escape structures such as fugichnia (Figs. 2.22 and 2.23). Thin-section analysis of Lithofacies F-3A shows *phycosiphon* trace fossil (Fig. 2.23-A and B), and vuggy porosity resulting from bioturbation (Fig. 2.24). Thin-section examination of Lithofacies F-3A shows that the grain-sizes are moderately well sorted (Fig. 2.24-C).

F-3A Interpretation

Lithofacies F-3A comprises trace fossils characteristic of a diverse ichnological assemblage, which is typical of the *Skolithos* ichnofacies. Such trace fossils suite characterizes fine-grained siltstones and mudstones with diverse suites (Pemberton and MacEachern, 2001). The trace fossils within Lithofacies F-3A are *Skolithos*, *Planolites*, *Phycosiphon*, *Cruziana*, *Teichichnus*, and *Paleaeophycos*. The *Skolithos* ichnofacies is indicative of relatively high-energy environment (MacEachern, et al., 2005) such as the shoreface. They are associated with wave, current energy and typically developed in slightly muddy to clean, moderately sorted sediments (MacEachern, et al., 2005). The *Skolithos* ichnofacies can also develop in a loose or shifting particulate (sand-prone) substrates in marine environments (MacEachern, et al., 2005; Pemberton and MacEachern, 2001).

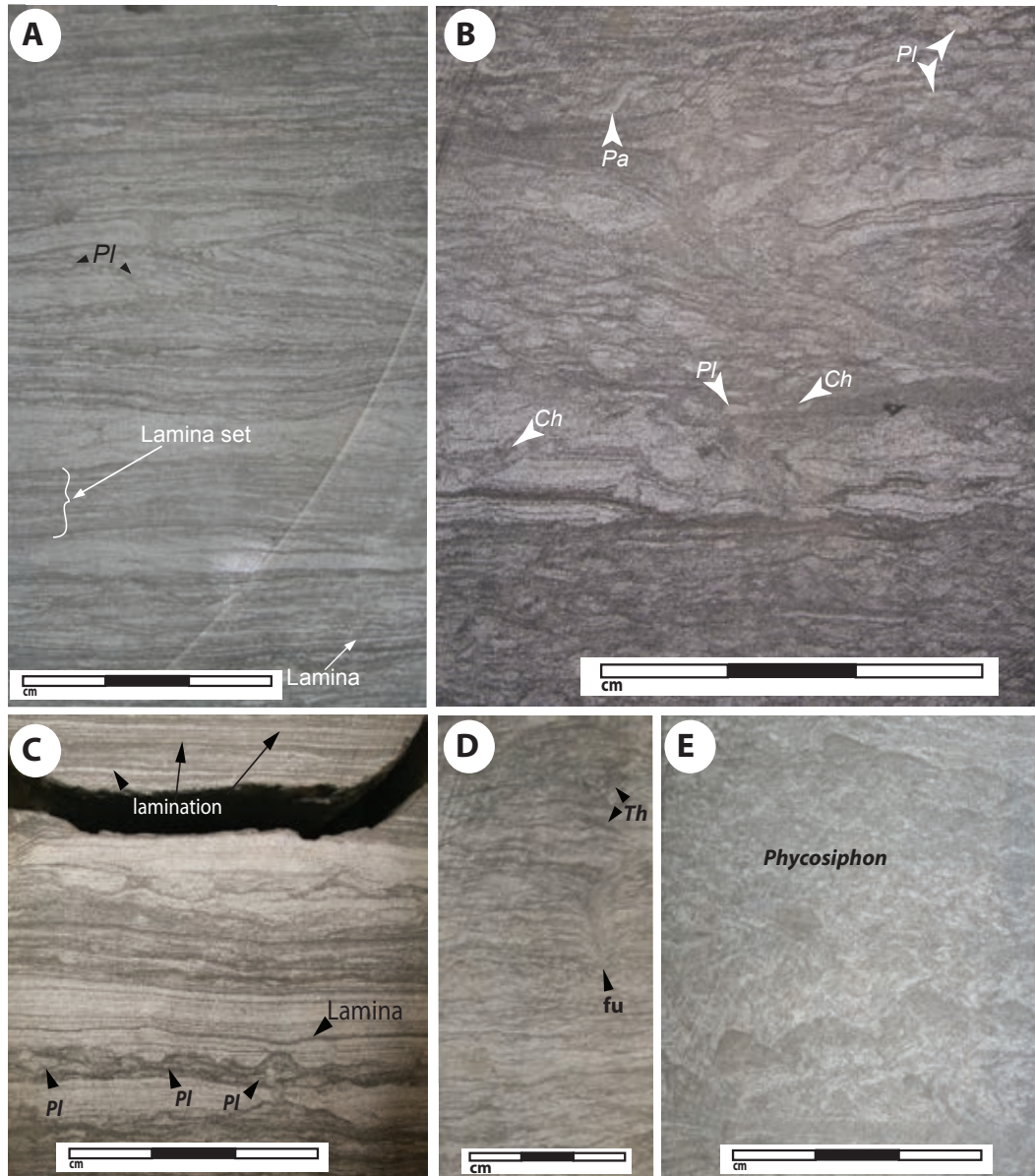


Figure 2.21. (A) Laminated very fine-grained sandstone and coarse siltstone with *Planolites* (*Pl*). **(B)** The lower part of the core is cryptically bioturbated with poor preservation of biogenic structures. The upper part of the core is bioturbated with trace fossils such as *Palaeophycus* (*P*), *Phycosiphon* (*Ph*), *Planolites* (*P*), and *Chondrites* (*Ch*). **(C)** Laminated siltstone interbedded with very fine-grained sandstone. **(D)** Laminated siltstone interbedded with very fine-grained sandstone. Fugichnia (*fu*) is present. Trace fossil present: *Palaeophycus* (*P*). **(E)** Cryptically bioturbated silty-sandstone with *Phycosiphon* (*Ph*).

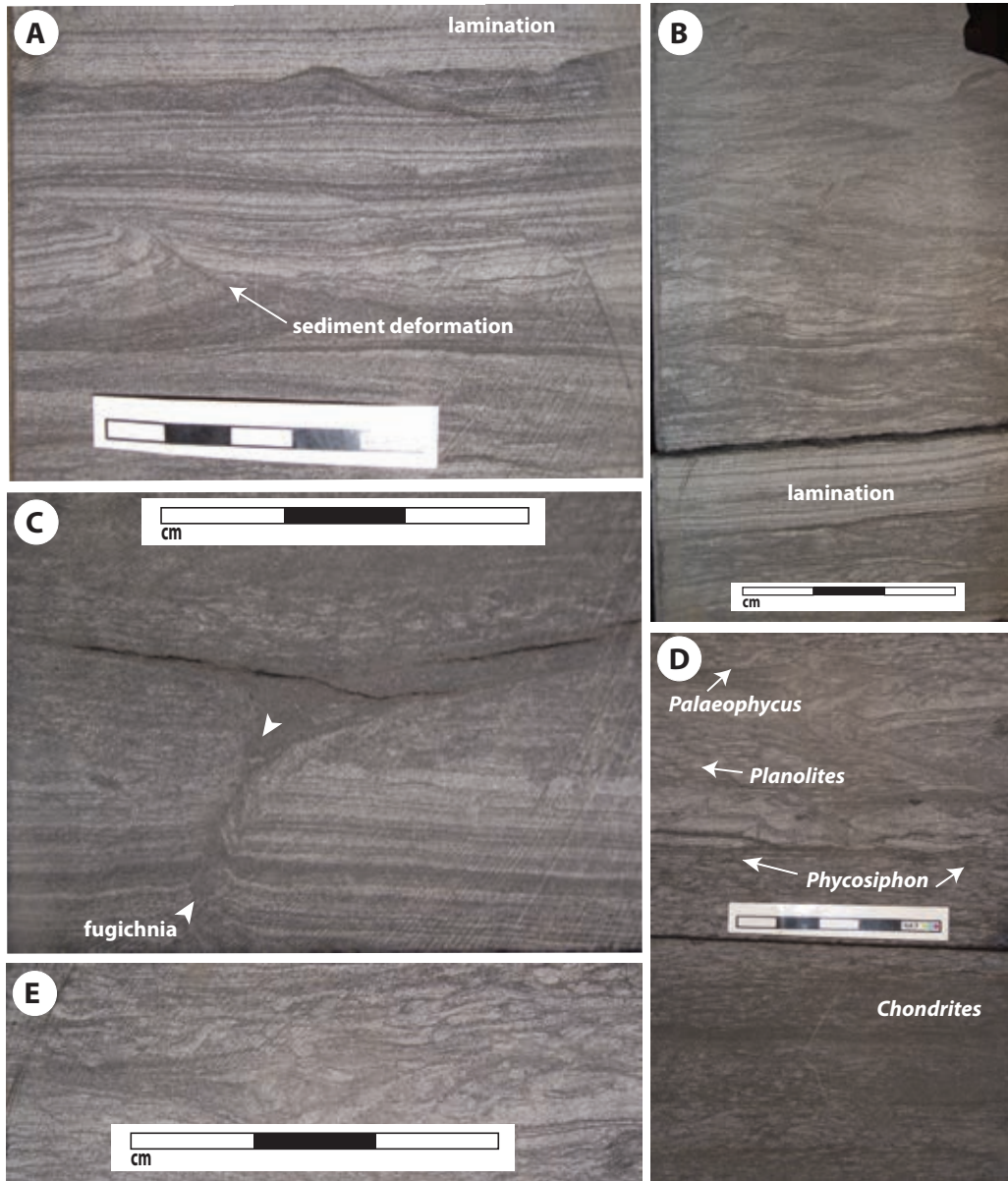


Figure 2.22. Shows Lithofacies F-3A trace fossils. **(A)** Laminated very fine-grained sandstone and coarse siltstone with *Planolites* (*Pl*) (well: A-20-H/93-P-9; depth: 2465.2m). **(B)** Bioturbated, very fine-grained sandstone showing trace fossils such as *Planolites* (*P*), *Chondrites* (*Ch*), and *Palaeophycus* (*Pa*) (well: d-21-G/93-P-9; depth: 2528.5m). **(C)** Shows lamination and mono-specific traces of *Planolites* (*P*), (well: d-21-G/93-P-9; depth: 2541m). **(D)** Shows poorly preserved trace fossil record. Fugichnia is present with indiscernible *Thalassinoides?* (*Th*) (well: d-21-G/93-P-9; depth: 2527.3m).

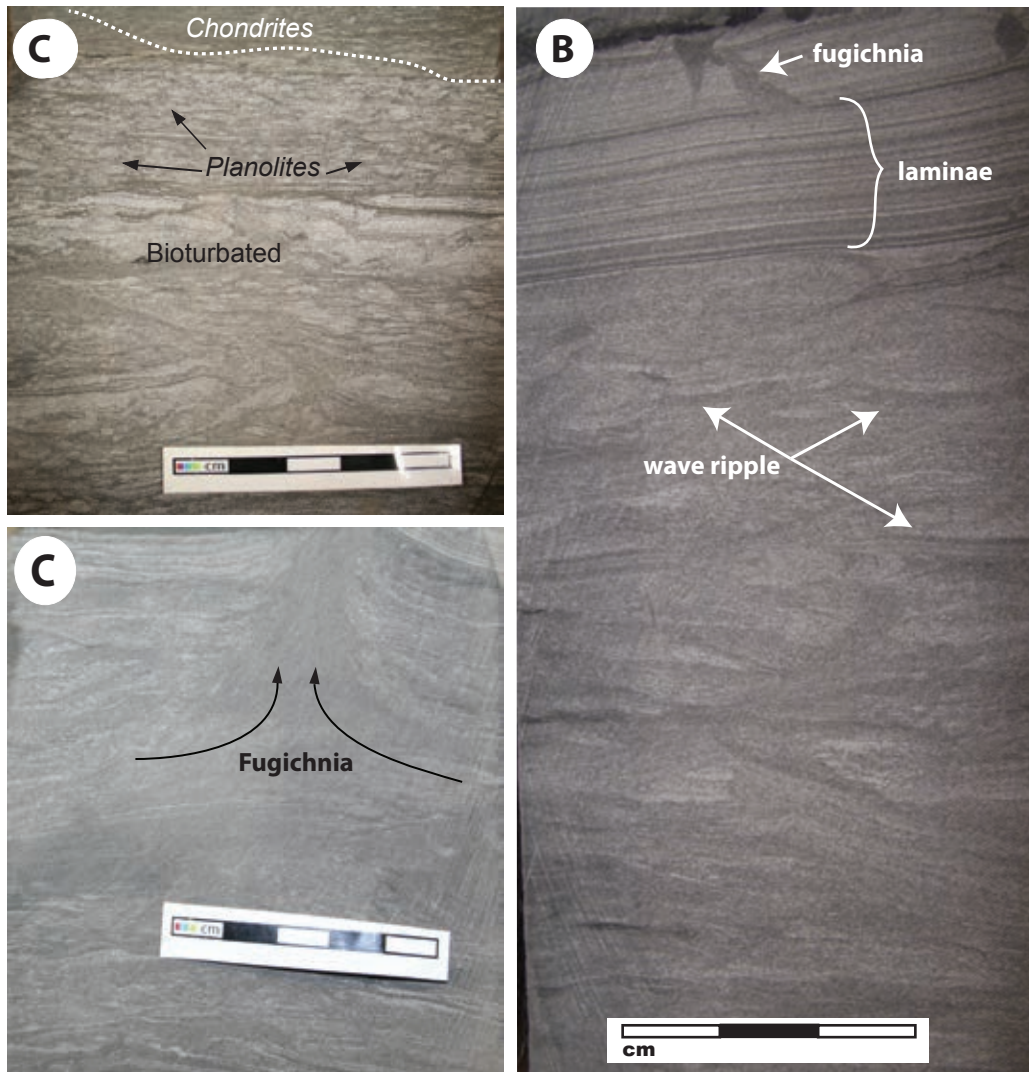


Figure 2.23. Shows depositional characteristics of Lithofacies F-3. **(A)** Shows bioturbated Lithofacies F-3 by *Planolites* and *Chondrites* (well: d-21-G/93-P-9; depth: 2534m). **(B)** Shows wave ripple, lamination and fugichnia (well: 9-29-79-14W6; depth: 1967m). **(C)** Shows fugichnia, 'escape trace' formed as a result of infauna attempt to escape burial during high, episodic sedimentation (well: 9-29-79-14W6; depth: 1984m).

The present of escape traces in Lithofacies F-3A correspond to disturbances made by organisms entrained in, or buried by, the event bed during sedimentation (MacEachern, 1994).

The porosity observed in Lithofacies F-3A is associated with biogenic

modification or reorganization of sediment fabric due to burrows by organisms, coupled with heterogeneous distribution of cements (Fig. 2.24). Such observation signifies that petrography should not be overlooked as a useful technique in assessing reservoir quality in sediments. Although, due to over reliance on wire-line log analysis and other large-scale methods of reservoir evaluation, petrography seems to be overlooked. Evidently, petrography offers a microscopic opportunity to assess reservoir characteristics, albeit, not possible by large-scale assessment methods (Gordon, et al., 2010).

Based on the present of *Skolithos* ichnofacies in Lithofacies F-3A, the depositional characteristics corresponds to the lower shoreface depositional environment (MacEachern, et al., 2005). Thus, the bioturbated very fine-grained sandy-siltstone of Lithofacies F-3A is assigned to the *Skolithos* ichnofacies and interpreted herein as a deposit in a lower shoreface environment.

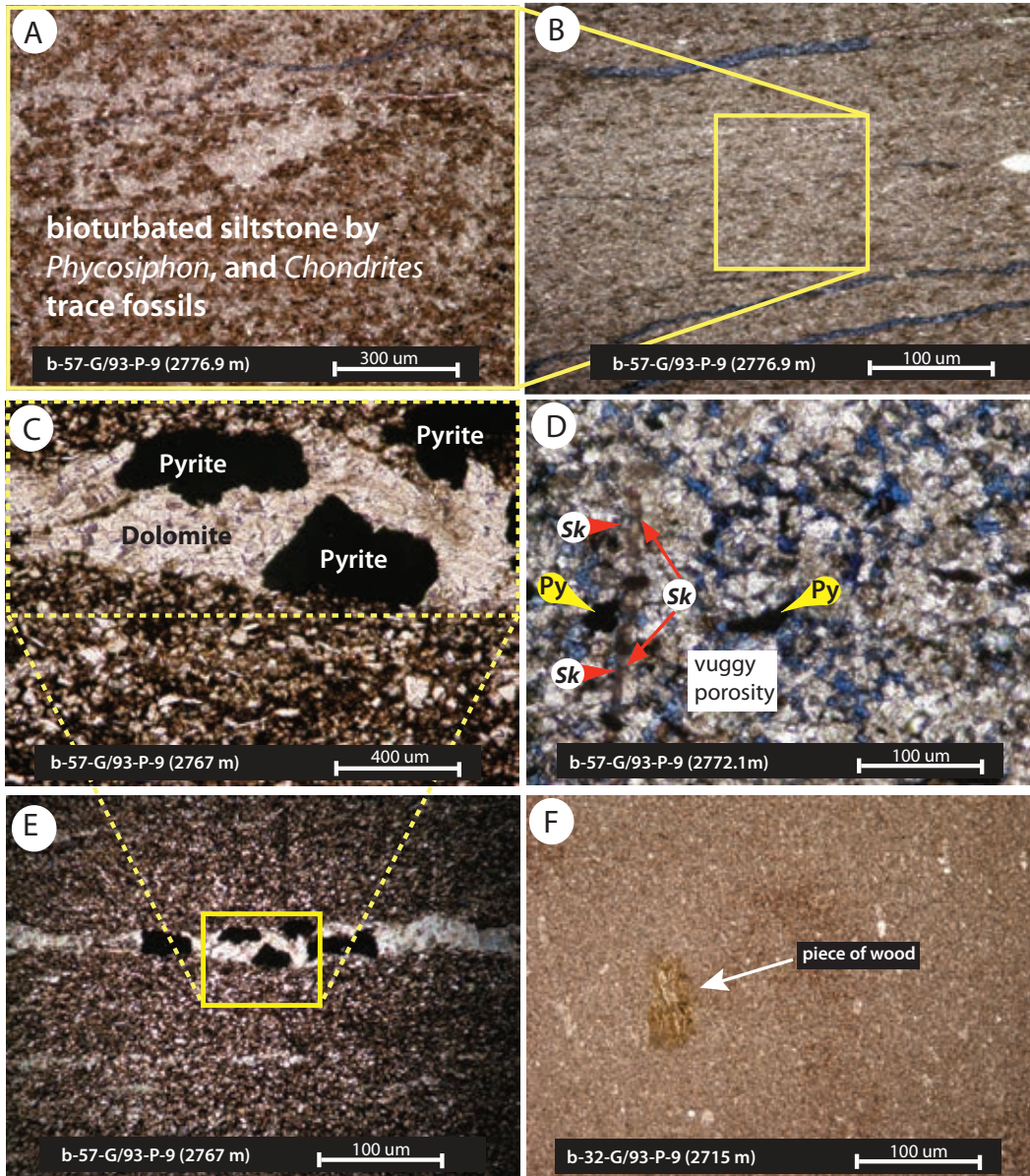


Figure 2.24. Microphotographs showing textural and mineralogical characteristics of Lithofacies F-3 of the Montney Formation in the Fort St. John study area, eastern British Columbia. **(A and B)** Dolomitic silty-sandstone, bioturbated by *Phycosiphon* and *Chondrites* trace fossils. **(C and E)** Shows pyritized detrital dolomite in a silty-sandstone matrix. **(D)** Shows vuggy porosity associated with bioturbation. *Skolithos* (*Sk*) trace fossil is identified in thin-section in **Plate D** [shown in red arrow], and pyrite [shown in yellow arrow]. **(F)** Shows very fine-grained siltstone with preserved wood/plant material indicating continental provenance.

Lithofacies F-3B Description: *Cruziana* ichnofacies

Lithofacies F-3B is composed of bioturbated siltstone dominated by *Cruziana* ichnofacies. The trace fossils recorded in Lithofacies F-3B are rare *Zoophycos?*, *Planolites*, *Phycosiphon*, *Chondrites*, *Thalassinoides*, *Cruziana*, *Skolithos*, *Teichichnus*, and *Palaephycos* (Fig. 2.25). In some cores, these traces are not well preserved, but appeared as cryptic bioturbation. The grain-size of Lithofacies F-3B is moderately well sorted. Sedimentary structures in Lithofacies F-3B include fugichnia – escape structures (Fig. 2.25–A,B,C).

F-3B Interpretation

Trace fossils such as *Planolites*, *Thalassinoides*, *Cruziana*, and *Palaephycos* are ichnocoenosis of the *Cruziana* ichnofacies (MacEachern, et al., 2005). The generalized ichnogenera attributed to the *Cruziana* ichnofacies is shown in Fig. 2.20. The *Cruziana* ichnofacies is commonly characterized by a high diversity of trace fossils (Fig. 2.20) associated with a variety of ichnofauna (Pemberton and Frey, 1984; Frey et al., 1990). *Cruziana* expressions of distal proximal offshore environment are transitional between distal expression of the *Skolithos* ichnofacies and the archetypal *Cruziana* ichnofacies (MacEachern, et al., 2005). Distal expressions of the *Cruziana* ichnofacies are associated with muddy siltstone, silty mudstone, reflecting a soft, cohesive substrate under persistent quiescent fully marine condition (Frey and Pemberton, 1985), which is the case in Lithofacies F-3B. Lithofacies F-3B shows an increased proportion of *Phycosiphon*, *Planolites*,

Thalassinoides, *Helminthopsis*; *Chondrites* and rare *Zoophycos*?, which reflects a basinward ichnofacies. Thus, the present of these trace fossils in Lithofacies F-3B are indicative of distal offshore setting.

Facies associated with rapid deposition rates are usually characterized by reduction in bioturbation intensity (MacEachern, et al., 2005; Howard 1975). Ichnofauna associated with such deposits are those showing escape behavior structure such as fugichnia (Fig. 2.25–A, B, E), and simple feeding structures, persistently high rate of deposition or event sedimentation results in low biodiversity and sparse ichnological imprint. Indications of rapid, episodic, or seismically generated tempestites (small scale = cm) in Lithofacies F-3B are suggested by the presence of finer-grained sand overlying siltstone, fluid escape structures, and soft sediment deformation (Fig. 2.25–C). Such episodic or event deposition typically results in reduced or non-bioturbation due to insufficient time for endobenthic fauna to recolonize the tempestite substrate (MacEachern, et al., 2005).

Commonly known *Cruziana* ichnofacies are those with deeply penetrating dwelling structures (e.g. *Thalassinoides*, *Ophiomorpha*) and rapidly adjusting structures (e.g. *Diplocraterion*, *Teichichnus*), intrabasinal feeding structures (e.g. *Planolites*, *Macaronichnus*) and escape structures tend to be the most common elements in the suites characteristic to rapid sedimentation (MacEachern, et al., 2005). The dwelling structures trace fossils, feeding structures traces, and rapidly adjusting structures occur as mono-specific ichnogenera with poor diversity in Lithofacies F-3B. Based on the above sedimentological and ichnofacies characteristics of Lithofacies F-3B, it is interpreted as a deposition in a distal offshore setting (Fig. 2.12).

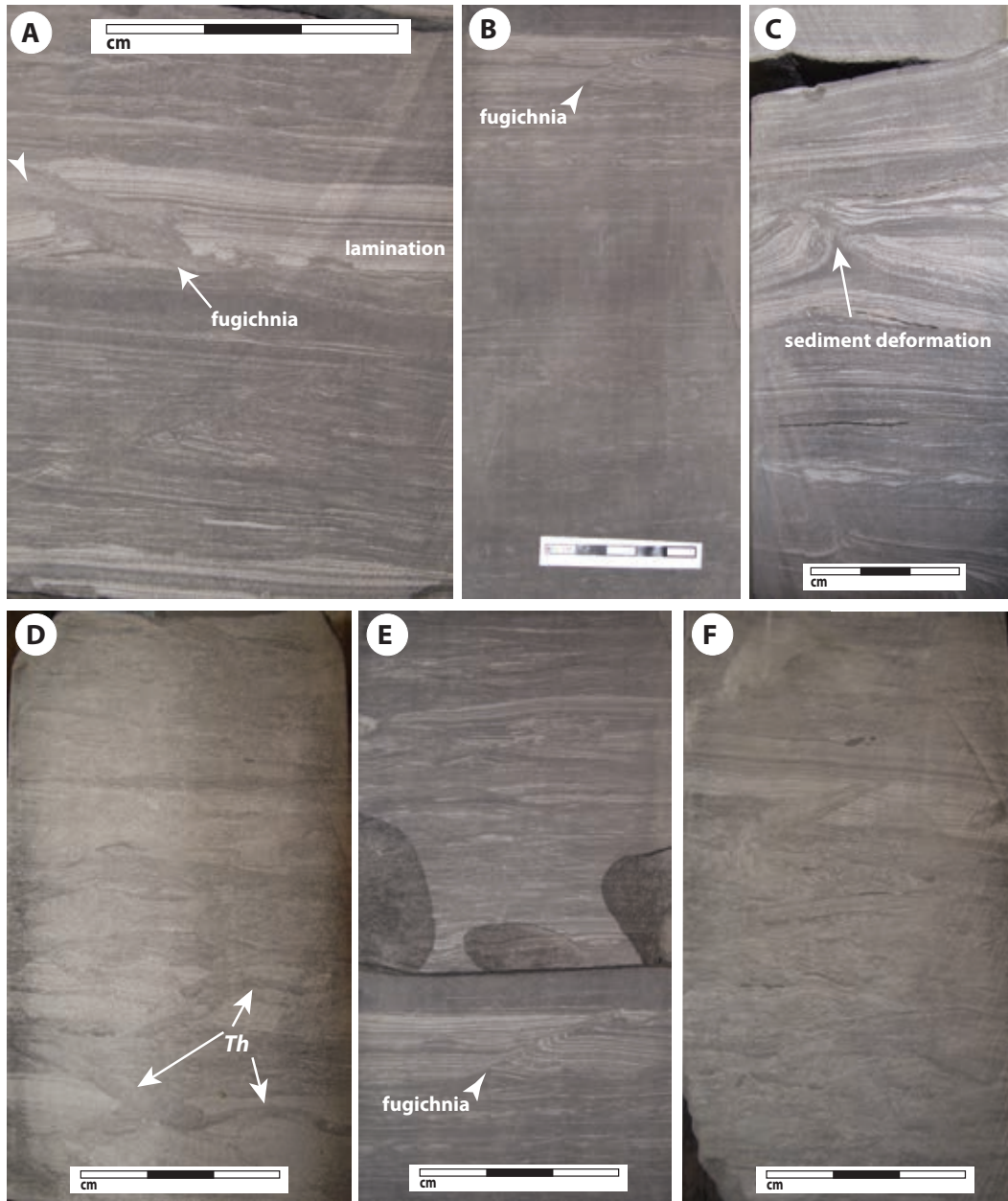


Figure 2.25. Core photographs showing depositional characteristics and trace fossils in Lithofacies F-3B. **(A)** Shows fugichnia and lamination (well: 9-29-79-14W6; depth: 1983.7). **(B)** Shows fugichnia (well: 9-29-79-14W6; depth: 1985.2m). **(C)** Shows sediment deformation (well: d-39/G93-P-9; depth: 2683m). **(D)** Shows *Thalassinoides* (*Th*) (well: 9-29-79-14W6; depth: 1980.5m). **(E)** Shows increased sand proportion in a siltstone matrix. Fugichnia is also present. **(F)** Shows poorly preserved traces – *Thalassinoides* (*Th*)?

Lithofacies F-4 Description: Dolomitic very fine-grained sandstone

Lithofacies F-4 consists of dolomitic, thin beds (≤ 1 metre) of very fine-grained sandstone reoccurring as facies association throughout the entire successions in the logged cores (Fig. 2.26). Thin-section petrography confirms that Lithofacies F-4 is quartz rich, moderately well sorted and dolomitic. Bioturbation and sedimentary structures are not present in lithofacies association F-4. In general, Lithofacies F-4 succession shows a coarsening upward trend. The basal contact of lithofacies F-4 with lithofacies F-5 is sharp and grades into coarse siltstone grade.

F-4 Interpretation

The coarsening-upward trend in Lithofacies F-4 is interpreted as basinward shoreline shift, which often characterizes a progradational trend (Catuneanu, 2006). The coarsening upward succession of Lithofacies F-4 is likely to have accumulated in deepening water, particularly in areas that are not adjacent to the shoreline (Naish and Kamp, 1997; Catuneanu, et al., 1998), and are characteristic of facies that prograded basinward during a falling stage of regression (Catuneanu, 2006). Based on depositional characteristics of Lithofacies F-4, it is interpreted herein as a deposition in proximal offshore depositional environment (Fig. 13). The proximal offshore is characterized by storm wave base, immediately seaward of the lower limit of minimum fairweather wave base, where offshore processes operate continually (Reinson, 1994).

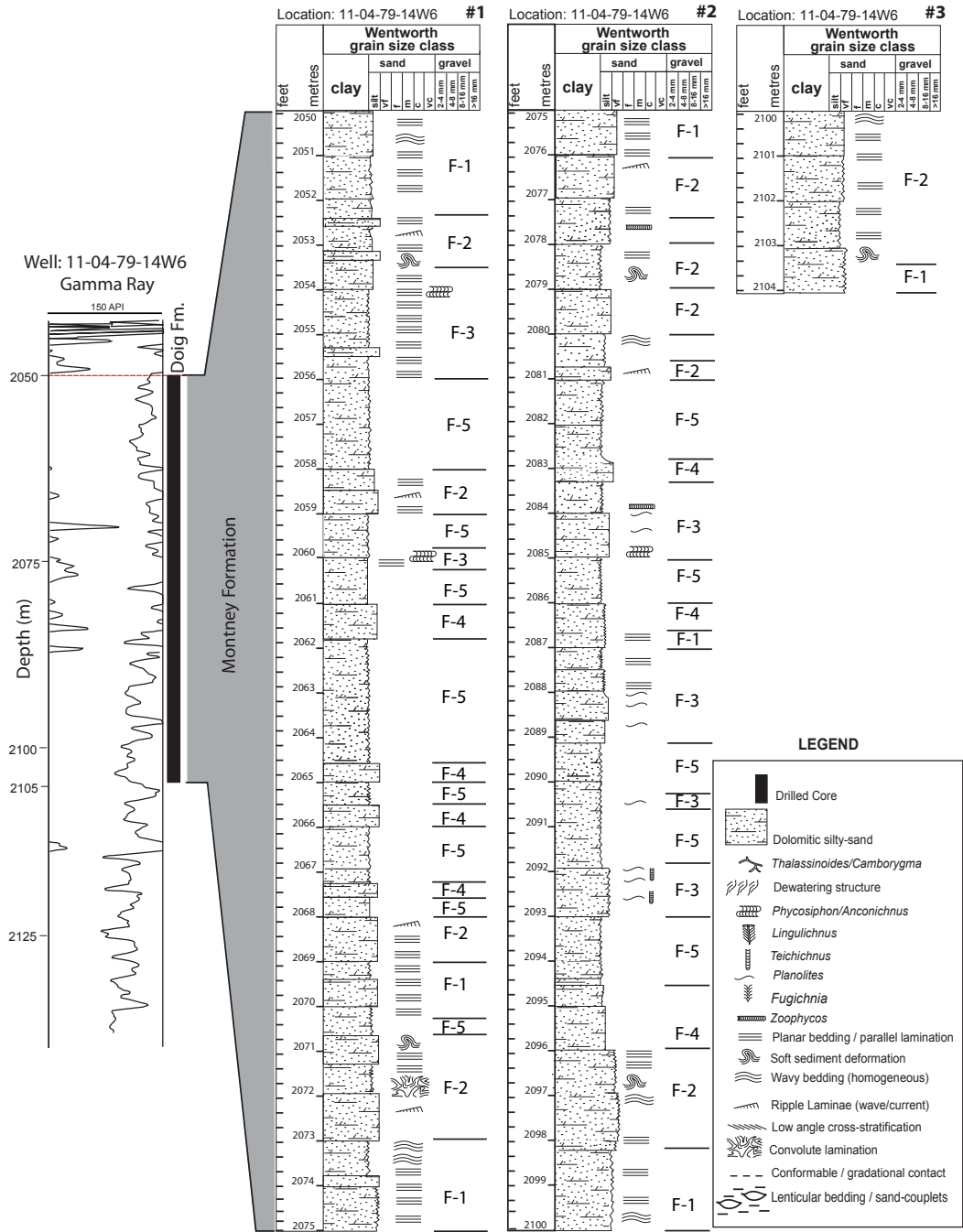


Figure 2.26. Core log showing Lithofacies associations (F-1 through F-5).

Lithofacies F-5 Description: Massive siltstone

Lithofacies F-5 is composed of dolomitic dark grey to black colored, organic rich, pyritized, massive siltstone (Fig. 2. 27). Petrographic examination of Lithofacies F-5 confirmed the present of dolomite, quartz grains that are sub-angular to sub-rounded, and pyrite (Fig. 2.28 – A through D). The texture of pyrite in Lithofacies F-5 under reflected light microscopy appears as irregularly rounded ‘clots’ that partly coalesce with one another and partly separated by non-reflective dolomite (Fig. 2.28–B). SEM analysis of Lithofacies F-5 further shows that mineralogy comprises clay (smectite, illite, dickite, and polygorskite), and detrital dolomite (Fig. 2.28–E and F). X-ray diffraction (XRD) analysis shows a spectrum and arrays of major and accessory minerals in Lithofacies F-5, which further confirmed the present of dolomite, pyrite, and in addition, shows mica, and Albite (Fig. 2. 29). Stable isotope geochemistry indicates that calcite is not present with dolomite in Lithofacies F-5. Bioturbation are not present in Lithofacies F-5. The basal contact of lithofacies F-5 with lithofacies F-4 is sharp. The upper contact of Lithofacies F-5 in some succession is sharp and erosionally demarcated from the overlying Doig Formation by an erosional lag deposit (Fig. 2.27 – D).

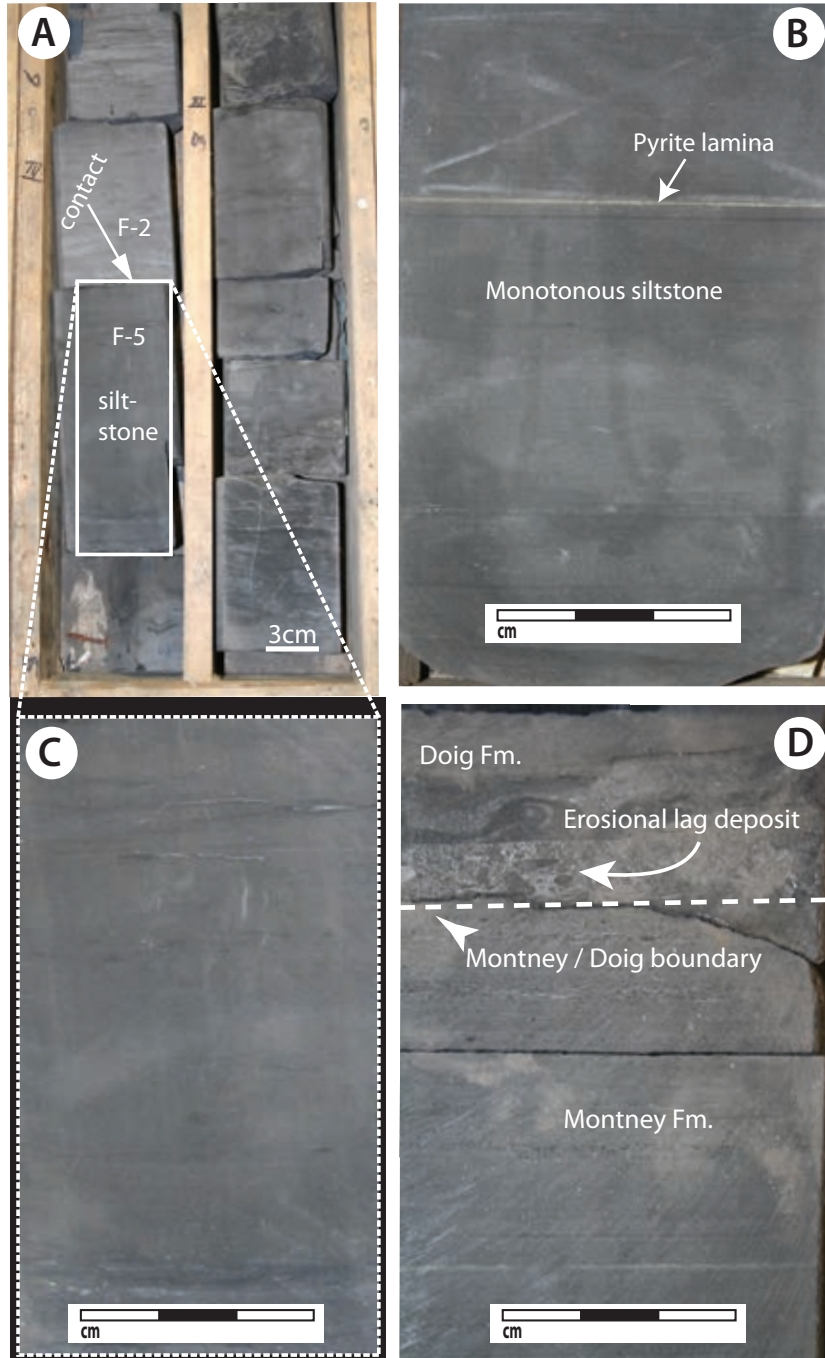


Figure 2.27. Shows massive siltstone of Lithofacies F-5. **(A)** Shows inset for plate C. Illustration shows the sharp facies contact between F-5 and F2 (well: 8-22-82-20-W6; depth: 1817.5). **(B)** Massive siltstone with pyrite lamina (well: a-39-F/93-P-9; depth: 2455m). **(C)** Shows magnification of plate A. Illustration shows massive siltstone (well: 8-22-82-20-W6; depth: 1817.5m). **(D)** Shows massive siltstone and erosional lag deposit, and facies contact along the Montney Fm. / Doig Fm. boundary (well: d-39-F/93-P-9; depth: 2652.5m).

F-5 Interpretation

The dark grey to black colored, organic carbon content of Lithofacies F-5 is a result of high nutrient rich sediment source and rapid sedimentation, which enhanced the preservation of organic matter (Muller and Suess, 1979) in oxygen-depleted depositional environment (Demaison and Moore, 1980; Ekdale and Mason, 1988; Wishner, et al., 1990; Tyson and Pearson, 1991; Wignall and Hallam, 1991; Bentley and Nittrouer, 1999), where density or temperature stratified water column form, typically below wave-base (Demaison and Moore, 1980). Oxygen-depleted environment is characteristic of a distal offshore setting (Ekdale and Mason, 1988; Wignall and Hallam, 1991; Houseknecht and Schenk, 2004). The organic carbon richness of Lithofacies F-5 implies that F-5 is a potential hydrocarbon source rock.

The present of detrital dolomite in Lithofacies F-5 is interpreted as post-depositional in origin, rather than in-situ (Bone, et al., 1992). The extraction of CO₂ during isotopic analysis for bulk calcite and bulk dolomite reveals that although Lithofacies F-5 is dolomitized, however, analyzed samples show no evidence of calcite. This observation was confirmed with XRD analysis (Fig. 2.29). Interpretation for the absent of calcite in lithofacies association F-5 can be attributed to the mode of substitution of magnesium (Mg) and calcite (Ca) in carbonate rocks (Goldsmith and Graf, 1958; Carpenter, 1980). Thermodynamically, dolomite is stable in most natural solutions at earth surface conditions, and a thermodynamic drive exists for the conversion of calcite to dolomite (Morrow, 1990). Thus, most natural dolomite exhibits some degree of mixing of calcium and magnesium between cation layers (Goldsmith and Graf, 1958; Carpenter, 1980). The phenomenon of the present/absent of calcite/dolomite in Lithofacies F-5 proves that dolomites commonly depart from stoichiometric composition of an excess of calcium, which is accommodated in the magnesium layers (Goldsmith and Graf, 1958; Lumsden and Chimahusky,

1980). Further interpretation of the absent of calcite in lithofacies F-5 may be due to the fact that several cations, principally, Fe, Sr, Na, and Mn, substitute for calcite in many dolomites (Veizer, et al., 1978).

Pyrite in Lithofacies F-5 is related to post-depositional emplacement (England, et al., 2002) caused by the dissolution of organic matter due to diagenesis (Figs. 2.28–D). Pyrite is an important diagenetic mineral and their present in a sample can help define the diagenetic history of sediments (Hudson, 1982). Therefore, the occurrence of pyrite in Lithofacies F-5 is a strong evidence of post depositional changes, and interpreted herein to have formed *in-situ* during diagenesis (England, et al., 2002).

The clay mineral in Lithofacies F-5 is associated with the organic carbon richness. Kennedy, et al. (2002) studied the relationship between organic matter and shale in modern sediments and found that adsorption of carbon compounds onto clay mineral surfaces played a fundamental role in the burial and preservation of total organic carbon in the sediment. This evidence proved that organic matter are within the smectite interlayers of clay, which implies that hydrocarbon prone source rock may be closely related to clay mineralogy (Kennedy, et al., 2002). The depositional mechanism of the silt-sized grains and clay in Lithofacies F-5 may be related to flocculation of fines due to the affinity of mica mineral as a major component of siliciclastics sediments, which is particularly more associated with silts and very fine-grained sediments (Tucker, 1988).

Raitzsch, et al. (2007) observed that the distance of transport of clay rich sediments affects clay mineral composition, thus they differ from one depositional environment to another (e.g., coastal clay mineral differs from continental slope clay mineral). The observation of Raitzsch, et al. (2007) shows that chlorite proportion of clay mineral increase from the lower slope to upper slope, corresponding with a decrease in the proportion of smectite. The illite component of the clay reaches its

maximum on the middle slope (Raitzsch, et al., 2007). Differential proportion of clay in the different depositional environment may be due to different mineral grain-sizes that characterize different depositional settings, and the different affinities to flocculation effects associated with deposition of hemipelagic (Raitzsch, et al., 2007). The illitic / palygorskite clay in Lithofacies F-5 (Fig. 2.28–E and F) has significant interpretation in relation to petrogenesis of the Montney Formation. Einsele (2000) stated that kaolinite tends to flocculate near the river mouths, whereas illite (Fig. 2.28–E and F) and montmorillonite (smectite) are transported further offshore, thus, supporting a distal depositional environment interpretation for Lithofacies F-5. Carson and Arcaro (1983); Gibbs (1985); and Lamy et al. (1998) have reported similar depositional environment based on clay mineralogy.

The X-ray diffraction response of illite (clay mineral) coupled with SEM image is an indication of the diagenesis, and low-grade metamorphic history of a sedimentary rock (Weaver, 1960; Frey, 1970; Gill, et al., 1977; Stalder, 1970). Kaolinite is transformed to illite during diagenesis, typically at temperatures of 212 – 230°F (100 – 110°C), which lies within the oil-generating window (Burst, 1969). The transformation of illite clay to dickite, and further transformation to polygorskite clay (Fig. 2.28–E and F), supports the interpretation of diagenesis in Lithofacies F-5. The clay associated with Lithofacies F-5 is interpreted as post depositional in origin based on the diagenetic transformation of illite clay to polygorskite clay (Fig. 2.28–E and F). Hardy and Tucker (1988) have reported that post-depositional origin is one of the ways clay minerals in sediments are derived, or by diagenetic modification.

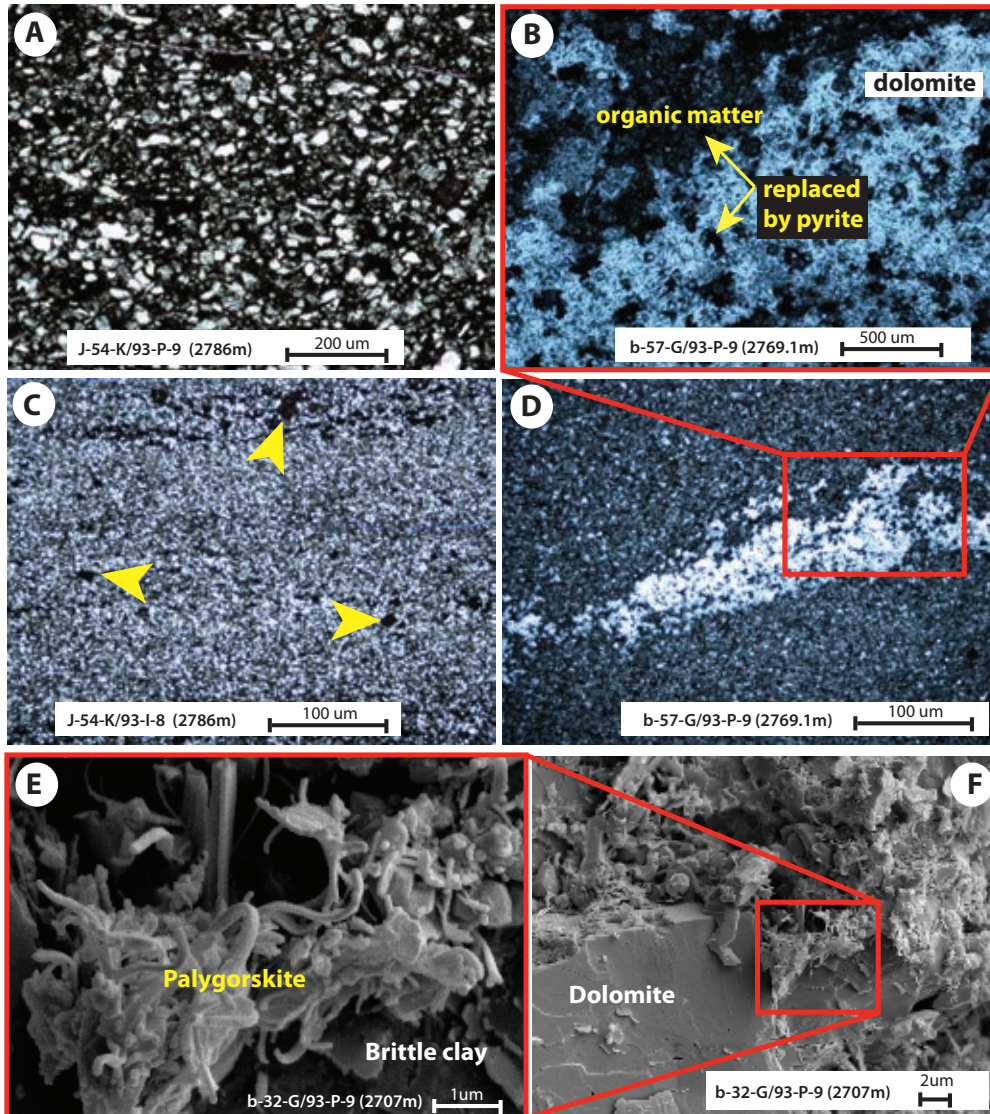


Figure 2.28. Shows microphotographs of scanning electron microscopy (SEM) and petrography of lithofacies association F-2 of the Montney Formation. The textural characteristics are exemplified. **(A)** Angular to sub-angular grains, quartz rich, well sorted. **(B)** Pyritic sandstone, sub-rounded grains, and moderately well sorted. **(B)** Shows magnification of **plate D**. Illustration shows dolomite, and pyritized, organic carbon rich siltstone. Pyrite replaces organic matter during diagenesis. **(C)** Shows siltstone and some pyrite. **(D)** Shows inset for **plate B**. Illustration shows dolomitic siltstone that have been pyritized due to diagenesis. **(E)** Shows magnification of plate F. Illustration shows very well formed palygorskite clay, a form of clay mineral growth, derived from the transformation of illite to dickite, and further transformation of dickite to palygorskite due to diagenesis (severe temperature and pressure). **(F)** Shows inset for **plate E**. Illustration shows dolomite, quartz, illite, dickite and palygorskite clay.

The absence of bioturbation in Lithofacies F-5 implies stressed and anaerobic conditions in restricted or oxygen-poor environments (Rhoads and Morse, 1971; Byers, 1977; Savrda, et al., 1984; Ekdale, 1988; Stow, et al., 2002). Thus, lithofacies F-5 deposition may be related to pelagic processes (Bodungen, et al., 1995; Billet, et al., 1983; Walsh, 1983). Pelagic depositional processes are supported by the absence of depositional features characteristic of shoreface environments, such as storm or wave-generated primary sedimentary structures (cross bedding, or hummocky cross stratification). The absence of trace fossils in lithofacies F-5 may be due to dysaerobic or oxygenation stress (Ekdale, 1985; Gingras, et al., 2005; MacEachern, et al., 2005; Burnnet, 1977; Bentor, 1980).

The upper contact of Lithofacies F-5 of the Montney Formation with the overlying Doig Formation is reminiscent of an erosional lag deposit characterized by a *Glossifungites – Trypanites* surface (Wilson and Zonneveld, 2011; Egbobawaye, et al., 2011). The mechanics of the deposition of a rip-up clast of pebble-sized to very coarse-grained sandstone, an erosional disconformity that marks the boundary between the Montney and Lower Doig formations, is interpreted to be akin to an upper flow regime (Miall 1980, 1992; Schomacker, et al., 2010).

The deposition of massive siltstone of Lithofacies F-5 may be related to transport and deposition from suspension, principally enhanced by the influence of waves mobilizing sediment by hyperpycnal mechanisms (Milliman and Meade, 1983; Nielsen, 1984; Stow, 1985; Wright, et al., 1986; Wiseman, et al., 1986; Shibayama et al., 1986). As hyperpycnal flow gradually loses competence, part of its suspended load progressively settles from suspension seaward, the finer-grained silt-sized particles are deposited in distal offshore environments (Pedersen, 1985), where changes in bottom-water anoxia and suspension sediments settling from buoyant plumes mostly dominate (Ghadeer and Macquaker, 2011). The initial

entrainment of sediments into suspension in the surf zone is due to turbulence, convection and eddy currents (Smith and Mocke, 2002). As sediments go beyond shoreface environment, energy starts to dwindle and coarser grain-size begins to fall off from suspension and are deposited, while finer grains (silt-size) particles continue in suspension basinward.

Aagaard and Greenwood (1994) reported that gravity waves contribute significantly to the entrainment and transport of sediment, by enhancing near-bed velocities. Kana (1978) proved with field measurement that turbulence is significantly responsible for sediment suspension in hydrodynamic flows.

Siltstone deposit commonly occurs in a variety of depositional settings where energy and hydrodynamic processes are subtle and quiescent. Lithofacies F-5 massive siltstone was deposited by quiescent hydrodynamic processes, in which settling of silt size particles through the water column. The organic rich nature of Lithofacies F-5 suggests pelagic or hemipelagic processes commonly associated with distal settings (Stow, 1985). Based on the sedimentological and mineralogical characteristics of Lithofacies F-5 as described above, it is interpreted herein, as a deposition in a distal offshore (outer shelf) depositional environment to ramp setting.

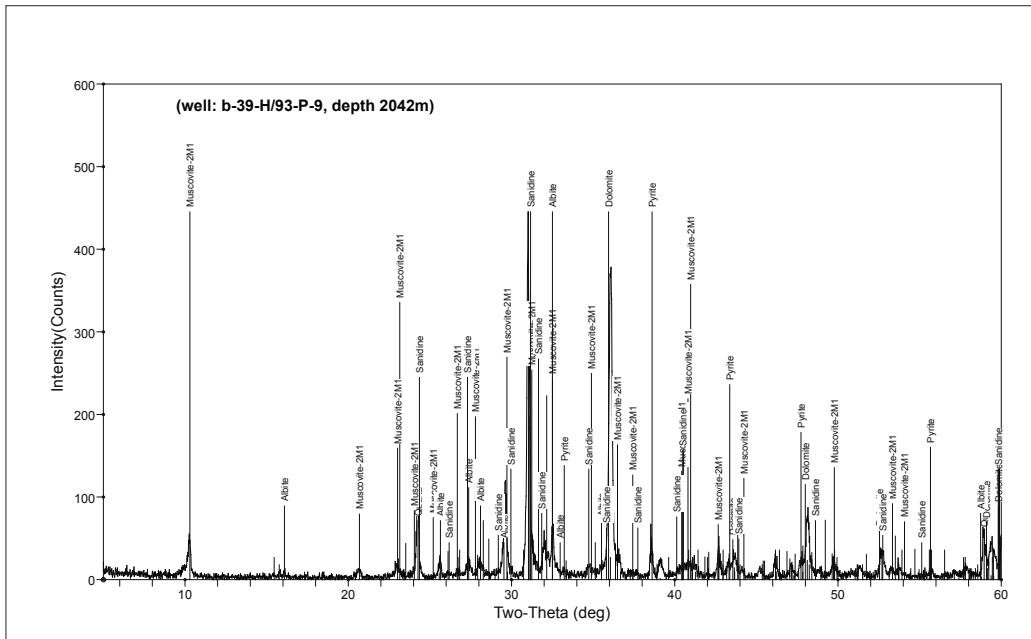


Figure 2.29. Shows X-ray diffraction analysis of mineral spectrum present in the Montney Formation.

DISCUSSION

Sedimentology and Depositional Environment

The Montney Formation in in the Fort St. John study area (T86N, R23W and T74N, R13W), northeastern British Columbia is composed of dolomitic siltstone, interbedded with very fine-grained sandstone. The sedimentary facies described in this study were named Lithofacies F-1 through F-5; and they provide sedimentological evidence as to the prevailing mechanism of sediment transport to the environment of deposition, including post-depositional modifications. The silty and very fine-grained size of the Montney Formation facies suggest strongly that sediment source for the Montney Formation was of continental origin derived

due to various denudational processes associated with fluvial, and possibly, aeolian mechanisms due to longshore drift from the north resulted in aeolian input from the land (Zonneveld et al., 1997a; 1997b; 2001; Davies; 1997b; Zonneveld, 1999).

Soon after initial deposition of the sediments in the foreshore zone (Fig. 2.12), sediments were reworked, and subsequently remobilized across shelf into shoreface through distal/deepwater setting. The depositional environment interpreted for the Montney Formation in in the Fort St. John study area (T86N, R23W and T74N, R13W) in northeastern British Columbia range from lower shoreface through proximal offshore to distal offshore settings. In west-central Alberta area, the Montney Formation has been reported by the work of Moslow and Davies (1997) as turbidite channel lobe complex resulting from mass wasting processes caused by Early Triassic (Smithian / Dienerian) global eustatic sea level fall.

Habicht, 1979; Davies, et al., 1997; Gibson and Barclay, 1989 have reported that the location of the Western Canada Sedimentary Basin (WCSB) that lies approximately at 30°N during Triassic time and the paleoclimate reconstruction suggests that paleoclimate may have ranged from sub-tropical to mid-temperate (Gibson and Barclay, 1989), thus, the region was arid and dominated by winds from the west (Habicht, 1979), which implies that aeolian processes delivered seasonal longshore sediment transport to offshore environment affected the Montney Formation sedimentation (Davies, et al., 1997). Evidence that supported seasonal aridity during the Triassic was established by Arnold (1994) through the measurement of paleocurrent on aeolian sandstone beds, which indicated a wind flow direction from northeast in a southwest direction.

The sedimentary structures in the Montney Formation recorded from cores in the study area includes parallel to wavy lamination on very fine-grained sandstone and siltstone, soft sediment deformation, current ripples, convolute lamination / bedding, and infaunal escape traces (fugichnia) These structures were interpreted

on the basis of the hydrodynamic processes prevalent during the formation of such sedimentary structures.

Deformation structures are a result of wave loading commonly due to storm or high-energy deposit (Pemberton and MacEachern, 2001; Zonneveld et al., 2010). Soft sediment deformation structures are formed due to processes occurring during a deformational event at or near the contemporary surface of unconsolidated sediments prior to, or soon after burial (Bhattacharya and Bandyopadhyay, 1998). Deformation structures are produced due to mechanical forces causing plasticity, commonly related to gravity acting upon weak sediment, usually silts or sands, soon after or at deposition along the sediment surface (Collinson, et al 2006). The occurrence of soft sediment deformation and convolute lamination in the Montney Formation lithofacies are evidence of penecontemporaneous event, or episodic deposition. Beranek and Mortensen, 2006; 2007; Ferri and Zonneveld, 2008 have interpreted some of the deformation structures in the Montney Formation to be related to initial terrane collision in the British Columbia/Yukon as part of a regional tectonism of Early to Middle Triassic. Wittenberg and Moslow (1991) and Cant (1994; 1986) interpreted sediments loading, deformed beddings, slumping structures and small-scale faults as indicators of tectonically driven factors that influenced the deposition of Triassic succession.

Convolute lamination structures in the Montney Formation lithofacies are associated with fluid escape structures and their formation is related to grain-size, and deformational mechanism. The convolute lamination/bedding structure involves folding of lamination into cusped upright form with a sharp anticline and a relatively gentle syncline, and they are formed as a result of plastic deformation of partially liquefied sediment usually occurring shortly after deposition (Collinson, et al., 2006).

Escape structures were common in the logged cores in northeastern

British Columbia. Fugichnia escape traces tend to be the most common elements in deposits characteristic to rapid sedimentation (MacEachern, et al., 2005). These structures in the Montney Formation are interpreted as evidence of rapidly deposited sediments. Because of the episodic depositional nature, infauna typically responds by burrowing their way out of the sediments thereby creating fugichnia trace. Episodic or event deposition typically results in reduced or non-bioturbation due to insufficient time for endobenthic fauna to recolonize the tempestite substrate (MacEachern, et al., 2005).

Trace Fossils

The ichnofauna records in the study area are mostly associated with Lithofacies F-3, which is divided into Lithofacies F-3A and F-3B as the *Skolithos* ichnofacies and *Cruziana* ichnofacies respectively. The basis of this subdivision was to differentiate the *Skolithos* ichnofacies from the archetypal *Cruziana* ichnofacies. There was considerable diversity of ichnofauna traces in Lithofacies F-3, except for mono-specific genera, and similarly, abundance of ichnogenera was low. The recorded trace fossils are *Chondrites*, *Planolites montanous*, *Skolithos linearis*, *Thalassinoides*, *Teichichnus*, *Phycosiphon*, *Palaeophucus*, and very rare *Zoophycos?*. The escape traces (fugichnia) were very common in most cores logged in the study area. The morphology of fugichnia is akin to the shape of chevron pattern, typically showing an upward direction the organism tunneled through in responds to sudden, episodic, or high sedimentation events. *Planolites* was the most pervasive and abundant in the cores from the study area.

The impoverished trace fossils in lithofacies in the Montney Formation may be due to dysaerobic or oxygenation stress (Ekdale, 1985; Gingras, et

al., 2005; MacEachern, et al., 2005; Burnnet, 1977; Bentor, 1980). Dysoxic conditions prevailed for most of the Permian-Triassic (P-T) boundary that caused mass extinction, which ravaged biotic communities, the most severe in Earth's history (Raup, 1979; Erwin, 1993; Twitchett, et al., 2004; Zonneveld, 2011), due to unequalled decline in the amount of dissolved oxygen in the world's oceans (Isozaki, 1994, 1997; Grice et al., 2005; Berner et al., 2007). The anoxic conditions extended intermittently into shallow marine (proximal shelf) depositional settings (Hallam, 1991; Wignall and Hallam, 1992; Zonneveld, et al., 2010), which have been reported to be associated with global anoxic conditions that subsequently caused a prolonged faunal recovery in the aftermath of Permian-Triassic biota crises (Erwin, 1993; Erwin, et al., 2002). The protracted fauna recovery continued into the Lower and Middle Triassic time (Zonneveld, et al., 2010), thereby delaying fauna revitalization for several millions of years following the fauna mass extinction (Wignall and Hallam, 1992; Hallam, 1995; Wignall and Twitchett, 1996, 2002a, 2002b; Twitchett, et al., 2004). The harsh environmental conditions post P-T fauna environmental crises have implications for the non-fossiliferous, or the non-evidence of fauna traces in Lithofacies association F-1. The delayed recovery of biota communities obstructed diversification of species as well as prolonged elevated extinction levels that continued into the earliest Triassic (Zonneveld, et al., 2010), causing a depressed biota habitat for much of the Lower Triassic (Batten, 1973; Stanley, 1990; Twitchett, 1999). The harsh environmental conditions have implications for the non-fossiliferous, or the impoverished nature of facies from the Montney Formation.

Mineralogy

Pyrite in Lithofacies F-5 is related to post-depositional emplacement (England, et al., 2002) caused by the dissolution of organic matter due to diagenesis

(Figs. 2.28–D). Pyrite is an important diagenetic mineral and their present in a sample can help define the diagenetic history of sediments (Hudson, 1982). Therefore, the occurrence of pyrite in Lithofacies F-5 is a strong evidence of post depositional changes, and interpreted herein to have formed *in-situ* during diagenesis (England, et al., 2002).

The clay mineral in Lithofacies F-5 is associated with the organic carbon richness. Kennedy, et al. (2002) studied the relationship between organic matter and shale in modern sediments and found that adsorption of carbon compounds onto clay mineral surfaces played a fundamental role in the burial and preservation of total organic carbon in the sediment. This evidence proved that organic matter are within the smectite interlayers of clay, which implies that hydrocarbon prone source rock may be closely related to clay mineralogy (Kennedy, et al., 2002). The depositional mechanism of the silt-sized grains and clay in lithofacies F-5 may be related to flocculation of fines due to the affinity of mica mineral as a major component of siliciclastics sediments, which is particularly more associated with silts and very fine-grained sediments (Turker, 1988).

Detrital dolomite in Lithofacies F-2 appears to have been shed-off from carbonate apron as debris (Fig. 2.17–B). The present of detrital dolomite has been interpreted by Bone, et al. (1992) as post-depositional in origin. The extraction of CO₂ during isotopic analysis for bulk calcite and bulk dolomite reveals that although Lithofacies F-5 is dolomitized, however, analyzed samples show no evidence of calcite. This observation was confirmed with XRD analysis (Fig. 2.29). Interpretation for the absent of calcite in Lithofacies association F-5 can be attributed to the mode of substitution of magnesium (Mg) and calcite (Ca) in carbonate rocks (Goldsmith and Graf, 1958; Carpenter, 1980). Thermodynamically, dolomite is stable in most natural solutions at earth surface conditions, and a thermodynamic drive exists for the conversion of calcite to dolomite (Morrow, 1990). Thus, most natural dolomite

exhibits some degree of mixing of calcium and magnesium between cation layers (Goldsmith and Graf, 1958; Carpenter, 1980). The phenomenon of the present/absent of calcite/dolomite in Lithofacies F-5 proves that dolomites commonly depart from stoichiometric composition of an excess of calcium, which is accommodated in the magnesium layers (Goldsmith and Graf, 1958; Lumsden and Chimahusky, 1980). Further interpretation of the absent of calcite in Lithofacies F-5 may be due to the fact that several cations, principally, Fe, Sr, Na, and Mn, substitute for calcite in many dolomites (Veizer, et al., 1978).

Hydrocarbon Potential of the Montney Formation

Analyses of the Total Organic Carbon (TOC), S₂, OI, HI and T_{max} shows variably source rock richness, hydrocarbon generating potential with a kerogen Type II / Type III/IV. These parameters altogether indicate that the Triassic Montney Formation has good source rock richness (Fig. 2.30) and thermal maturity is within the gas generating window base on T_{max} and vitrinite reflectance data (Fig. 31). Rock Eval result coupled to porosity observed in this study has significant implication for reservoir quality and hydrocarbon production in the Montney Formation in northeastern British Columbia where isopach map and stratigraphic thickness is in the range of 200m to 350m.

The observed porosity on a thin-section (micron scale), shows that the porosity is associated with: 1) dissolution of organic matter, or dolomitic material during diagenesis; 2) bioturbation-enhanced porosity resulting from burrows by organisms; and 3) fracture porosity along bedding planes. Pemberton and Gingras (2005) and Gordon, et al. (2010) have shown that reservoir enhancement in unconventional thinly bedded, silty to muddy lithologies that often characterizes permeability of unconventional reservoir can be enhanced by the activity of burrows.

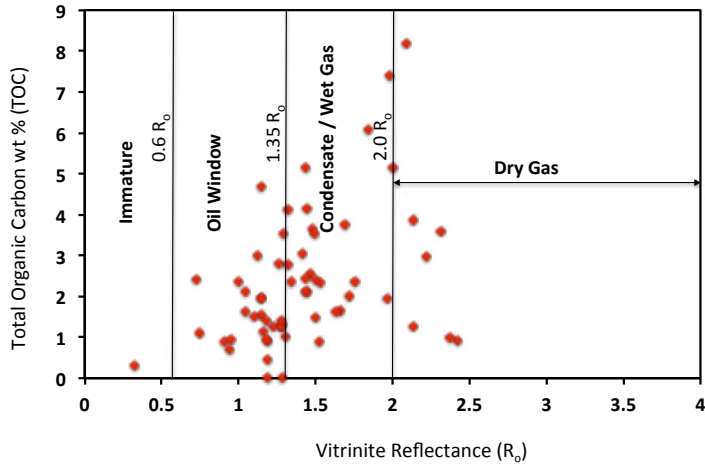


Figure 2.30. Total Organic carbon (TOC) vs. vitrinite reflectance (R_o) showing the thermal maturity of the Montney Formation source rock, and hydrocarbon generating phases in in the Montney Formation sediments from study area, northeastern British Columbia.

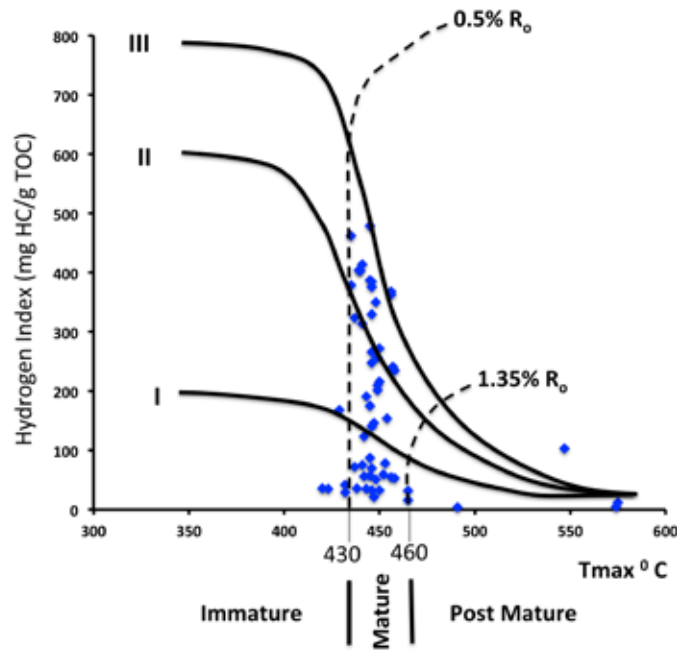


Figure 2.31. Thermal maturity of the Montney Formation determined with T_{max} and vitrinite reflectance (R_o). The dotted line (R_o) is vitrinite reflectance calibrated with T_{max} . This shows that the Montney Formation in northeastern British Columbia is extensively matured.

CONCLUSIONS

The Montney Formation in northeastern British Columbia is a thick succession of siltstone and very fine-grained sandstone. The facies of the Montney Formation is characterized by sedimentary structures such as lamination, soft sediment deformation, convolute lamination/bedding, current ripples, and infauna escape. The Montney Formation lithology is primarily composed of interbedded siltstone and very fine-grained, and interlaminated silty-sandstone. The Montney Formation in the study area is interpreted as deposit in the lower shoreface through proximal offshore to distal offshore settings.

Although trace fossils were not in abundance in the study area, however, infauna / biodiversity was relatively high and represent ichnocoenoses attributed to the *Skolithos* and the *Cruziana* ichofacies. The low diversity of indigenous infauna, support the hypothesis of dysoxic depositional conditions in the lower Montney Formation during the Griesbachian time (Zonneveld, 2010). The traces recorded in this study from the Montney Formation cores in northeastern British Columbia are *Chondrites*, *Cruziana*, *Fugichnia*, *Planolites*, *Skolithos*, *Thalassinoides*, *Teichichnus*, *Phycosiphon*, and *Zoophycos*.

Hydrocarbon potential in the Montney Formation assessed from Rock-Eval data shows that the source rock is rich in organic matter, has thermal maturity that lies within gas generating window, and primarily a gas prone Type III / Type IV kerogen. Mineralogical composition of the Montney Formation consists of dolomite, quartz, calcite, plagioclase, Illite/mica, K-feldspar, pyrite, and illite/smectite.

REFERENCES

- Aagaard, T. and B. Greenwood, 1994. Sediment transport by wind waves, long waves and mean currents: an experiment on nearshore morphodynamics, Lake Huron, Canada. *Coastal Dynamics*, p. 14 – 28.
- Allen, J. R. L., 1986, Earthquake magnitude-frequency, epicentral distance and soft sediment deformation in sedimentary basins. *Sedimentary Geology*, vol.46, p. 67 – 75.
- Allen, J. R. L., 1982, *Sedimentary Structures: Their Character and Physical Basis*. Elsevier, New York, vol. 2, p. 663.
- Archie, G. E., 1950, Introduction to Petrophysics of Reservoir Rocks. *American Association of Petroleum Geologists Bulletin*, vol. 34, no. 5, p. 943-961.
- Armitage, J.H., 1962. Triassic oil and gas occurrences in northeastern British Columbia, Canada. *Journal of the Alberta Society of Petroleum Geologists*, vol. 10, p. 35–56.
- Arnold, K.J., 1994, Origin and distribution of eolian sandstones in the Triassic Charlie Lake Formation, northeastern British Columbia. Unpublished M.Sc. thesis, University of Alberta, Edmonton, 320p.
- Aukes, P.G., and Webb, T.K, 1986, Triassic Spirit River Pool, northwestern Alberta. In: *Canadian Society of Petroleum Geologists, 1986 Core conference*, Calgary, Alberta, Canada. N.C. Meijer Drees (ed.), p. 3.1-3.34.
- Bagnold, R.A., 1956, The flow of cohesionless grains in fluids. *Transaction Royal Society of London*, vol. 249, p. 235 – 297.
- Barclay, J.E., Krause, F.F., Campbell, R.I., and Utting, J., 1990, Dynamic casting and growth faulting: Dawson Creek Graben Complex, Carboniferous-Permian Peace River Embayment, Western Canada, In: *Geology of the Peace River Arch*, S.C. O’Connell and J.S. Bell (eds.), *Bulletin of Canadian Petroleum Geology*, vol. 38A, p.115-145.

- Beranek, L.P. and Mortensen, J.K. 2006. A Triassic link between Yukon-Tanana and North America; new detrital zircon age, geochemical, and biostratigraphic data. Geological Society of America, Cordilleran Section, Abstracts with Program, vol. 38, p. 5–6.
- Best, J.L and L.S Bridge, 1992, The morphology and dynamics of low amplitude bedwaves upon upper stage plane beds and the preservation of planar laminae. *Sedimentology*, vol. 39, p. 737 – 752.
- Behar, F., Beaumont, V., and Penteadó, H. L. De B., 2001, Rock-Eval 6 Technology: performances and Developments. *Oil and gas Science and Technology - Revue de l'Institut Francais du Petrole*, vol. 56, p. 111-134.
- Bhattacharya, H. N. and Bandyopadhyay, S., 1998, Seismites in a Proterozoic tidal succession, Singhbhum, Bihar, India. *Sedimentary Geology*, vol. 119, p. 239 – 252.
- Beard, D.C, and Weyl, P.K, 1974, Influence of texture on porosity and permeability of unconsolidated sand. *Association of Petroleum Geologists Bulletin*, vol. 57, p. 349 – 369.
- Bentor, Y.K., 1980, Phosphorites – the unsolved problems. In: *Marine phosphates* (Ed.by Y.K, Bentor), Special Publication of Society of Economic Paleontology and Mineralogy, Tulsa, vol. 29, p. 3-18.
- Bentley, S.J. and Nitouer, C.A., 1999, Physical and biological influences on the formation of sedimentary fabric in an oxygen-restricted depositional environment: Eckernförde bay, southwestern Baltic Sea. *Palaios*, vol. 14, p. 585 – 600.
- Berger, Z., M. Boast, and M. Mushayandebvu, 2009, The contribution of Integrated HRAM studies to exploration and Exploitation of unconventional plays in North America. Part 2: Basement structures control on the development of the Peace River Arch's Montney / Doig resource plays.

- Reservoir, vol. 36, Issue 2, p. 40 – 44.
- Behar, F., Beaumont, V., and Penteadó, H. L. De B., 2001, Rock-Eval 6 Technology: performances and Developments. Oil and gas Science and Technology – Revue de l'Institut Français du Pétrole, vol. 56, p. 111-134.
- Cant, D.J., 1984, Possible syn-sedimentary tectonic controls on Triassic reservoirs, Halfway and Doig, Charlie Lake formations, west-central, Canadian Society of Petroleum Geologists, Calgary, p.45.
- Berner, R.A., Vandenbrooks, J. M., and Ward, P.D., 2007, Oxygen and Evolution. Science, vol. 316, P. 557 – 558.
- Berthault, G., 1988, Experiments on lamination of sediments. EN Tech. Journal, vol. 3, p. 25 – 29.
- Billet D.S.M., Lampitt, R.S, Rice, A.L, Mantoura, R.F.C., 1983, Seasonal sedimentation of phytoplankton to the deep-sea benthos. Nature, vol. 302, 520 – 522.
- Blatt, H., 1970. Determination of mean sediment thickness in the crust: a sedimentologic method. Geological Society of America, vol. 81, p. 255 – 262.
- Blatt, H., 1987, Oxygen isotopes and the origin of quartz. Journal of Sedimentary Petrology, vol. 57, p. 373 – 377.
- Blott, S.J., and Pye, K., 2001, Gradistat: a grain size distribution and statistics package for the analysis of unconsolidated sediments. Earth Surface Processes and Landforms, vol. 26, p. 1237 – 1248.
- Bridge, J.S., 1981, Hydraulic interpretation of grain-size distributions using a physical model for bedload transport. Journal of sedimentary petrology, vol. 51, no. 4, p. 1109 – 1124.
- Bird, T.D., Barclay, J.E., Cambell, R.I., Lee, P.J., Waghmere, R.R., Dallaure, S.M., and Conn, R.F., 1994, Triassic gas resources of Western Canada

- Sedimentary Basin, Interior Plains. Geological Survey of Canada Bulletin vol.483, p. 66.
- Bone, Y., N.P. James, and Kyser, T.K., 1992, Synsedimentary detrital dolomite in Quaternary cool-water carbonate sediments, Lacepede shelf, South Australia. *Geology*, vol. 20, no. 2, p. 109 – 112.
- Bodungen, B.V., Antia, A., Bauerfeind, E., Haupt, O., Koeve, W., Machado, E., Peeken, I., Peinert, R., Reitmeier, S., Thomsen, C., Voss, M. Wunsch, M., Zeller, U., and Zeitzschel, B., 1995, Pelagic processes and vertical flux of particles: an overview of a long-term comparative study in the Norwegian Sea and Greenland Sea. *Geol Rundsch*, vol. 84, p. 11 – 27.
- Bone, Y., James, N.P., and Kyser, T.K., 1992, Synsedimentary detrital dolomite in Quaternary cool-water carbonate sediments, Lacepede shelf, South Australia. *Geology*, vol. 20, p. 109 – 112.
- Bowker, K. A., 2003a, Recent development of the Barnett Shale play, Fort Worth Basin: *West Texas Geological Society Bulletin*, vol. 42, No. 6, p. 1–11.
- Burnett, C.W., 1977, Geochemistry and origin of phosphorite deposits from off Peru and Chile. *Bulletin of Geological Society of America*, vol. 88, p. 813-823.
- Burst, J. F., 1969, Diagenesis of Gulf Coast clayey sediments and its possible relation to petroleum migration. *American Association of Petroleum Geologists Bulletin*, vol. 53, p. 73–93.
- Burley, S.D., and Kantorowicz, J.D., 1986, Thin section and S.E.M. textural criteria for the recognition of cement-dissolution porosity in sandstones. *Sedimentology*, vol. 33, p. 587 – 604.
- Byers, C.W., 1977, Biofacies patterns in euxinic basins: A general model, in Cook, H.E, and Enos, P.E., eds., *Deep-water carbonate environments*. Society of Economic Paleontologists and Mineralogists Special

Publication 25, p. 5 – 17.

- Cambell, C.V., and Horne, J.C., 1986, Depositional facies of the Middle Triassic Halfway Formation, Western Canada Basin. In: Modern and Ancient Shelf Clastics: a Core Workshop, T.F. Moslow and E.G. Rhodes, (eds.), Society of Economic Paleontologists and Mineralogists, Core Workshop, no. 3, p. 33-64.
- Cant, D.J., 1984, Possible syn-sedimentary tectonic controls on Triassic reservoirs, Halfway and Doig, Charlie Lake formations, west-central, Canadian Society of Petroleum Geologists, Calgary, p.45.
- Cant, D.J., 1986, Hydrocarbon trapping in the Halfway Formation (Triassic), Wembly Field, Alberta, Bulletin of Canadian Petroleum Geology, vol. 34, p. 329-338.
- Carpenter, A.B., 1980, The chemistry of dolomite formation 1: the stability of dolomite. *In*: Zenger, D.H., Dunham, J.B. and Ethington, R.L., Eds., Concepts and Models of Dolomitization. Society of Economic Paleontologists and Mineralogists, Special Publication 28, p. 111 – 121.
- Carson, B., Arcaro, N.P., 1983. Control of clay mineral stratigraphy by selective transport in Late Pleistocene–Holocene sediments of northern Cascadia basin–Juan de Fuca abyssal plain: implication for studies of clay mineral provenance. *Journal of Sedimentary Petrography*, vol. 53, p. 395–406.
- CAPP - Canadian Association of Petroleum producers, 2007, Technical Report, Statistic handbook for Canada's Upstream Petroleum Industry.
- Charpenter, R.R., and J.W. Schmoker, 1982, Volume of organic-rich Devonian shale in Appalachian Basin relating "Black" to organic-matter content, *Bulleting of American Assoc. of Petroleum Geologists*, vol. 62, p. 98-120.
- Cheel, R.J., and G.V. Middleton, Horizontal lamination formed under upper flow regime plane bed conditions. *Journal of Geology*, vol. 94, p. 489 – 504.

- Catuneanu, O., 2006, Principles of sequence stratigraphy, (ed.), Oxford, p. 255.
- Catuneanu, O., Willis, A.J., Miall, A.D., 1998. Temporal significance of sequence boundaries. *Sedimentary Geology* 121, 157–178.
- Collinson, J., N. Mounney, and D. Thompson, 2006, *Sedimentary structures* (3rd Ed.). Terra publishing, England, 292p.
- Crimes, T.R., J.F. G. Hidalgo, and D.G. Poire, 1992, Trace fossils from Arenig flysch sediments of Eire and their bearing on the early colonisation of the deep seas. *Ichnos*, vol. 2, p. 61 – 77.
- Crimes, T.P., 1975, The production and preservation of trilobite resting and burrowing traces. *Lethaia*, vol. 8, p. 35–48.
- Cox, P.A., 1997. *The Elements on Earth. Inorganic Chemistry in the Environment*. Oxford University Press, Oxford, UK, 284p.
- Cross, T. A., and Homewood, P. W., 1997, Amant Gressly's role in founding modern stratigraphy. *Geological Society of America Bulletin*, vol. 109, no.12, p. 1617 – 1630.
- Davies, G.R., Moslow, T.F., and Sherwin, M.D, 1997, The Lower Triassic Montney Formation, west-central Alberta. *Bulletin of Canadian Petroleum Geology*, vol. 45, 474 – 505p.
- Davies, G.R., 1997, The Triassic of the Western Canada Sedimentary Basin: tectonic and stratigraphic framework, paleogeography, paleoclimate and biota. *Bulletin of Canadian Petroleum Geology*, vol. 45, p. 434–460.
- Davies, G.R., 1997b, Aeolian sedimentation and bypass, Triassic of Western Canada. In: *Triassic of the Western Canada Sedimentary Basin*. T.F. Moslow and J. Wittenberg (eds.). *Bulletin of Canadian Petroleum Geology*, vol. 45, p. 624 – 642.
- Dembicki, Jr. H., 2009, Three common source rock evaluation errors made by geologists during prospect or play appraisals. *American Association of*

- Petroleum Geologists Bulletin, vol. 93, No. 3, p. 341–356.
- Demaison, G.J., and G.T. Moor, 1980, Anoxic environments and oil source rock bed genesis. American Association of Petroleum Geologists Bulletin, vol. 64, p. 1179 – 1209.
- Dow, W., 1977, Kerogen studies and geological interpretations: Journal of Geochemical Exploration, vol. 7, p. 79–99.
- Edwards, D.E., Barclay, J.E., Gibson, D.W., Kvill, G.E., and Halton, E. 1994, Triassic strata of the Western Canada Sedimentary Basin. In: Geological Atlas of the Western Canada Sedimentary Basin. G.D. Mossop and I. Shetson (compilers). Canadian Society of Petroleum Geologists, p. 257–275.
- Edwards, D.E., Barclay, J.E., Gibson, D.W., Kvill, G.E., and Halton, E. 1994, Triassic strata of the Western Canada Sedimentary Basin. In: Geological Atlas of the Western Canada Sedimentary Basin. G.D. Mossop and I. Shetson (compilers). Canadian Society of Petroleum Geologists, p. 257–275.
- Eggbowawaye, E.I., M.K. Gingras, and J-P., Zonneveld, 2011, The geochemistry of the Montney and Lower Doig tight gas reservoir, northeastern British Columbia. American Association of Petroleum Geologists Abstract, no. 90124. Accessed online on March 16, 2012: <http://www.searchanddiscovery.com/abstracts/html/2011/annual/abstracts/Eggbowawaye.html?q=%2BtextStrip%3Aeggbowawaye>
- Eggbowawaye, E.I., J-P. Zonneveld, and M.K., Gingras, 2010, Tight gas reservoir evaluation in Montney and Lower Doig formations, northeastern British Columbia, western Canada. American Association of Petroleum Geologists Abstract, vol. 19, p. 66-67.
- Eggbowawaye, E.I., Kravchinsky, V.A, Zonneveld, J-P, and Gingras, M.K, Magnetostratigraphy Dating and Correlation of the Lower Doig and Upper

Montney Formations (Lower Triassic), Northeastern British Columbia, Western Canada. Canadian society of Petroleum Geologists, CSPG, CSEG, CWLS Convention Abstract, Calgary, Alberta, Canada, p. 1 – 5. Accessed online on February 22, 2012: <http://www.geoconvention.com/conference/technicalprogram/tuesday/pm-2/montney-i.html>

- Erwin, D.H., 1993, The great Paleozoic crisis: Life and death in the Permian: Columbia University Press, New York, 327 p.
- Erwin, D.H., Bowring, S.A., Jin, Y.G., 2002. End-Permian mass extinctions: a review. In: Koeberl, C., MacLeod, K.G. (Eds), Catastrophic Events and Mass Extinction: Impacts and Beyond. Geological Society of America Special Paper., vol. 356, p. 363 – 383.
- Ekdale, A.A., and Mason, T.R., 1988, Characteristic trace-fossil associations in oxygen-poor sedimentary environments. *Geology*, vol. 16, p. 720 – 723.
- Ekdale, A. A, 1985. Trace fossils and mid-Cretaceous anoxic events in the Atlantic Ocean. In: Biogenic Structures: Their Use in Interpreting Depositional Environments. H.A. Curran (ed.), p. 333–342.
- Eyles, C.H., N. Eyles, and V.A Gostin, 1998, Facies and allostratigraphy of high-latitude, glacially influenced marine strata of the Early Permian southern Sydney Basin, Australia. *Sedimentology*, vol. 45, p. 121 – 161.
- Ekdale, A. A., 1985. Trace fossils and mid-Cretaceous anoxic events in the Atlantic Ocean. In: Biogenic Structures: Their Use in Interpreting Depositional Environments. H.A. Curran (ed.), p. 333–342.
- England, G.L., B. Rasmussen, B. Krapez, and D.I. Groves, 2002, Palaeoenvironmental significance of rounded pyrite in siliciclastic sequences of the Late Archean Witwatersrand Basin: oxygen-deficient atmosphere or hydrothermal alteration?. International Association of Sedimentologists,

- vol. 49, p. 1133 – 1156.
- Einsele, G., 2000, Sedimentary basins: evolution, facies, and sediment budget. Springer-Verlag, Berlin, Heidelberg, 791p.
- Evoy, R.W., and Moslow, T.F., 1995, Lithofacies associations and depositional environments in the Middle Triassic Doig Formation, Buick Creek Field, northeastern British Columbia. Bulletin of Canadian Petroleum Geologists, vol. 43, p. 461–475.
- Evoy, R.W., 1997, Lowstand shoreface in the Middle Triassic Doig Formation: Implications for hydrocarbon exploration in the Fort St. John area, northeastern British Columbia. Bulletin of Canadian Petroleum Geology, Vol. 45, 525-537p.
- Espitalie, J., Deroo, G. and Marquis, F., 1985, Rock Eval Pyrolysis and Its Applications. Preprint; Institut Francais du Petrole, Geologie, no. 27299, 72 p. English translation of, La pyrolyse Rock-Eval et ses applications, Premiere, Deuxieme et Troisieme Parties, in Revue de l'Institut Francais du Petrole, vol. 40, p. 563-579 and 755-784; vol. 41, p. 73-89.
- Espitalie, J., J. L. Laporte, M. Madec, F. Marquis, P. LePlat, J. Paulet, and A. Boutefeu, 1977a, Methode rapide de caracterisation des roches meres de leur potentiel petrolier et de leur degre d'evolution: Revue l'Institute Franc,ais du Pe'trole, v. 32, p. 23–42.
- Espitalie, J., M. Madec, B. Tissot, J. J. Mennig, and P. Leplat, 1977b, Source rock characterization method for petroleum exploration: Proceedings of the 9th Annual Offshore Technology Conference, v. 3, p. 439–448.
- Ferri, F. and J-P. Zonneveld, 2008. Were Triassic rocks of the Western Canada Sedimentary Basin deposited in a foreland? Canadian Society of Petroleum Geologists Reservoir, vol. 35, p. 12–14.
- Frey, M., 1970, The step from diagenesis to metamorphism in pelitic rocks during

- Alpine orogenesis. *Sedimentology*, vol. 15, p.261-279.
- Frey, R.W. and S.G. Pemberton, 1985, Biogenic structures in outcrop and cores. *Approaches to Ichnology. Bulletin of Canadian Petroleum Geology*, vol. 33, p. 72 – 115.
- Frey, R.W., Pemberton, S.G., and Saunders, T.D.A., 1990, Ichnofacies and bathymetry: a passive relationship. *Journal of Paleontology*, vol. 64, p.155 – 157.
- Folk, R. L., 1955, Note on the significance of “Turbid” feldspars: *American Mineralogist*, vol. 40, p. 344-359.
- Folk, R.L, Ward, W.C., 1957. Brazos River bar: a study in the significance of grain size parameters. *Journal of Sedimentary Petrology*, vol. 27, p. 3 – 26.
- Folk, R. L., 1959, *Petrology of sedimentary rocks*. Hemphill’s, Austin, Texas, 150p
- Folk, R.L, 1954, The distinction between grain size and mineral composition in sedimentary-rock nomenclature. *Journal of Geology*, vol. 62, p. 344 – 359.
- Gehman, H. M. Jr., 1962, Organic matter in limestones; *Geochimica et Cosmochimica Acta*, vol. 26, p. 885-897.
- Ghadeer, S.G., and Macquaker, J.H.S., 2011, Sediment transport processes in an ancient mud-dominated succession: a comparison of processes operating in marine offshore settings and anoxic basinal environments. *Journal of Geological Society of London*, vol. 168, p. 1121 – 1132.
- Gill, W.D., F.E. Khalaf, and Massoud, M.S, 1977, Clay minerals as an index of the degree of metamorphism of the carbonate and terrigenous rocks in the South Wales coalfield. *Sedimentology*, vol. 39, p. 330-332.
- Gibson, D.W. 1975, Triassic rocks of the Rocky Mountain Foothills and Front Ranges of northeastern British Columbia and west-central Alberta, Geological Survey of Canada, Bulletin 247, 61p.

- Gibson, D.W. 1993, Triassic. In: Sedimentary Cover in the Craton of Canada. D.F. Stott and J.D. Aitken (eds.). Geological Survey of Canada, Geology of Canada no. 5, p. 294–320.
- Gibson, D.W and Barclay, J.E. 1989, Middle Absaroka Sequence, the Triassic stable craton. In: Western Canada Sedimentary Basin: A Case History. B.D. Ricketts (ed.). Canadian Society of Petroleum Geologists, p. 219–231.
- Gibson, D.W and Edwards, D.E. 1990, An overview of Triassic stratigraphy and depositional environments in the Rocky Mountain Foothills and Western Interior Plains, Peace River Arch area. Bulletin of Canadian Petroleum Geology, vol. 38A, p. 146–158.
- Gibbs, R.J., 1985, Settling velocity, diameter, and density for flocs of illite, kaolinite and montmorillonite. Journal of Sedimentary Petrography, vol. 55, p. 65 – 68.
- Gingras, M.K., K.B. Barn, J.A., MacEachern, S.G., Pemberton, 2005, Conceptual framework for the application of Trace Fossils. AAPG and SEPM short course note, no. 52, p. 1-26., no. 52, p. 1-26.
- Gingras, M.K., S.G., Pemberton, F., Henk, J.A., MacEachern, C. Mendoza, B. Rostron, R. O'hare, M. Spila, and K. Konhauser, 2005, Application of Ichnology to fluid and gas production in hydrocarbon reservoirs. AAPG and SEPM short course note, no. 52, p. 129-142.
- Grice, K., Cao, C., Love, G.D., Böttcher, M.E., Twitchett, R.J., Grosjean, E., Summons, R.E., Turgeon, S.C., Dunning, W., and Yügan, J., 2005, Photic Zone Euxinia During The Permian–Triassic Superanoxic Event: Science, vol. 307, P. 706 – 709.
- Gosh, S.K., Shyam S.S., Y. Ray, and S. Sinha, 2010, Soft-sedimentary deformational structures: seismites or penecontemporaneous, a study from the Palaeoproterozoic Lesser Himalayan succession, India. Research

- Communications, *Current Science*, vol. 98, No. 2, p.248-252
- Gordon, J.B., S.G. Pemberton, and M.K. Gingras, 2010, Biogenically enhanced permeability: A petrographic analysis of *Macaronichnus segregatus* in the Lower Cretaceous Bluesky Formation, Alberta, Canada. *American Association of Petroleum Geologists Bulletin*, vol. 94, no. 11, p. 1779 - 1795.
- Goldhaber, M.B., and I.R. Kaplan, 1974, The sulfur cycle. In: *The Sea*, vol. 5, Marine Chemistry (Ed. by E.D. Goldhaber), Wiley (Inter-science), London, p.569 – 655.
- Goldsmith, J.R. and Graf, D.G., 1958, Structural and compositional variations in some natural dolomites. *Journal of Geology*, vol. 66, p. 678 – 693.
- Gressly, A., 1838, *Observations géologiques sur le Jura soleurois: Nouveaux mémoires de la Société Helvétique des Sciences Naturelles*, Neuchâtel, v. 2, 349 p., 14 pl.
- Grice, K., Cao, C., Love, G.D., Böttcher, M.E., Twitchett, R.J., Grosjean, E., Summons, R.E., Turgeon, S.C., Dunning, W., and Yügan, J., 2005, Photic zone euxinia during the Permian–Triassic superanoxic event: *Science*, vol. 307, p. 706–709.
- Habicht, J.K.A. 1979. Paleoclimate, paleomagnetism, and continental drift. AAPG Studies in Geology No. 9, American Association of Petroleum Geologists, Tulsa, Oklahoma, U.S.A., 31 p.
- Hall, J., 1847, *Palaeontology of New York. Volume 1: Containing descriptions of the organic remains of the Lower Division of the New York System (equivalent to the Lower Silurian rocks of Europe)*. In: C. van Benthuyzen, Albany, State of New York. 338 p.
- Hardy, R.G, and M.E, Turcker, 1988, X-ray power diffraction of sediments, in *Techniques in sedimentology*, Blackwell Scientific Publication, Oxford, p.191-228.

- Hallam, A., 1991, Why was there a delayed radiation after the end-Paleozoic extinction?. *Historical Biology*, vol. 5, p. 257 – 262.
- Hallam, A., 1995, The Earliest Triassic as an anoxic event, and its relationship to the end-Paleozoic mass extinction. *Canadian Society of Petroleum Geologists Memoir*, vol. 17, p. 797–804.
- Henderson, C.M., 1997, Uppermost Permian conodont and Permian-Triassic boundary in the western Canada Sedimentary Basin, *Bulletin of Canadian Petroleum Geology*, vol. 45, no. 4, p.693-707.
- Henderson, C.M. 1989. Absaroka Sequence - The Lower Absaroka Sequence: Upper Carboniferous and Permian. In: *Western Canada Sedimentary Basin - A Case History*. B.D. Ricketts (ed.). Canadian Society of Petroleum Geologists, Special Publication No. 30, Calgary, Alberta, p. 203-217.
- Henderson, C.M., and Baud, A., 1997, Correlation of the Permian-Triassic boundary in Arctic Canada and comparison with Meishan, China, *Proc. 30th Int'l Geol. Congr.*, vol. 11, p.143-152.
- Houseknecht, D.W. and Schenk, C.J., 2004, Sedimentology and sequence stratigraphy of the Cretaceous Nanushuk, Seabee, And Tuluvak formations exposed on Umiat Mountain, North-Central Alaska. U.S Geological Survey Professional Paper 1709-B, p. 1 – 18.
- Howard, J.D., 1975, The sedimentological significance of tracefossils. In: R.W. Frey, ed., *The Study of Trace Fossils*. New York Springer – Verlag, p.131-146.
- Hudson, J.D., 1982, Pyrite in ammonite-bearing shales from the Jurassic of England and Germany. *International Association of Sedimentologists*, vol. 37, p. 639 – 667.
- Hunt, A.D., and Ratcliffe, J.D., 1959, Triassic stratigraphy, Peace River area, Alberta and British Columbia, Canada, *American Assoc. of Petroleum Geol.*

- Bulletin, vol. 43, no. 3, p.563-589.
- Hunt, J.M., 1996, *Petroleum Geochemistry and Geology*, (2nd Ed.). Freeman and Company, New York, 741p.
- Henk, F., 2005, Lithofacies of the Barnett Shale Formation from outcrop to subsurface Abstract, Barnett Shale Symposium III, Ellison Miles Geotechnology Institute: Texas Petroleum Technology Transfer Council, Texas Region, CD-ROM.
- Henk, F., J. T. Breyer, and D. M. Jarvie, 2000, Lithofacies, petrography, and geochemistry of the Barnett Shale in conventional core and Barnett Shale outcrop geochemistry (abs.), in L. Brogdon, ed., Barnett Shale Symposium, Fort Worth, Texas: Oil Information Library of Fort Worth, Texas, p. 7.
- Isozaki, Y., 1994, Superanoxia across the Permo–Triassic boundary: Record in accreted deep-sea pelagic chert in Japan, in Embry, A.F., Beauchamp, B., and Glass, D.J., eds., *Pangea: Global Environments and Resources: Memoir*, Canadian Society of Petroleum Geologists, vol. 17, p. 805–812.
- Isozaki, Y., 1997, Permo–Triassic boundary superanoxia and stratified superocean: Records from lost deep sea: *Science*, vol. 276, p. 235 – 238.
- Jarvie, D. M., R. J. Hill, T. E. Ruble, and R. M. Pollastro, 2007, Unconventional shale-gas systems: The Mississippian Barnett Shale of north-central Texas as one model for thermogenic shale-gas assessment: *AAPG Bulletin*, vol. 91, p. 475–499.
- Johnson, H.D and C.T. Baldwin, 2002, Shallow clastic seas. In: *Sedimentary environments: Processes, Facies, and Stratigraphy* (Ed by Reading, H.G), Blackwell Science, Oxford, p. 232 – 279.
- Kana, T., 1978. Surf zone measurements of suspended sediment. *Proc. 16th Int. Conference on Coastal Eng., ASCE*, p. 1725 – 1741.

- Killops, S. and V. Killops, 2005, *Introduction to Organic Geochemistry* (ed.). Blackwell Science, Oxford, UK, 393p.
- Kindle, E.D., 1994, Geological reconnaissance along Fort Nelson, Liard and Beaver Rivers, northeastern British Columbia and southeastern Yukon, Geological Survey of Canada, Paper 44-16, 19p.
- Kump, L.R., Pavlov, A., and Arthur, M.A., 2005, Massive release of hydrogen sulfide to the surface ocean and atmosphere during intervals of oceanic anoxia: *Geology*, vol. 33, p. 397–400.
- Kennedy, M.J., Pevear, D.R., and Hills, R.J., 2002, Mineral surface control of organic carbon in black shale. *Science*, vol. 295, p. 657 – 660.
- Krumbein, W. C., 1941, Measurement and geological significance of shape and roundness of sedimentary particles. *Journal of Sedimentary Petrology*, vol. 11, p. 64 – 72.
- Krynine, P. D., 1941, Triassic sediments of Connecticut: *Geological Society of America Bulletin.*, vol. 52, p. 1919.
- Kuenen, P.H.H., 1959. Experimental abrasion: Fluvial action on sand. *American Journal of Science*, vol. 257, p. 172 – 190.
- Kuenen, P.H.H., 1969, Origin of quartz silt. *Journal of Sedimentary Petrology*, vol. 39, p. 1631 – 1633.
- Kvill, G.E. 1994, *Geological Atlas of Western Canada Sedimentary Basin*, 259-275p. Moslow, T.F and Davies, G.R., 1997, Turbidite reservoir facies in the Lower Triassic Montney Formation, west-central Alberta. *Bulletin of Canadian Petroleum Geology*, vol. 45, No. 4, p. 507-536.
- Loucks, R. G., and S. C. Ruppel, 2007, Mississippian Barnett Shale: Lithofacies and depositional setting of a deep-water shale-gas succession in the Fort Worth Basin, Texas. *American Association of Petroleum Geologists Bulletin*, vol. 91, No. 4, p. 579–601.

- Lamy, F., Hebbeln, D., Wefer, G., 1998, Terrigenous sediment supply along the Chilean continental slope: modern latitudinal trends of texture and composition. *Geology Rundsch.* No. 87, p. 477 – 494.
- Livingstone, I., Warren, A., 1996. *Aeolian Geomorphology*. Longman, Harlow, 211p.
- Luo, G., Wang, Y., Yang, H., Algeo, T.J., Kump, L.R., Huang, J., and Xie, S., 2011, Stepwise and large-magnitude negative shift in $d^{13}C_{carb}$ preceded the main marine mass extinction of the Permian–Triassic crisis interval: *Palaeogeography, Palaeoclimatology, Palaeoecology*, vol. 299, p. 70–82.
- Lumsden, D.N. and Chimahusky, J.S., 1980, Relationship between dolomite nonstoichiometry and carbonate facies parameters. *In: Zenger, D.H., Dunham, J.B. and Ethington, R.L., Eds., Concepts and Models of Dolomitization*. Society of Economic Paleontologists and Mineralogists, Special Publication 28, p. 123 – 137.
- MacEachern, J.A., 1984, *Ichnology of Viking and Peace River formations*, Alberta. Unpublished Ph.D Thesis, University of Alberta, Edmonton, 617p.
- MacEachern, J.A., Pemberton, S.G., Bann, K.L., and M.K. Gingras, 2005, Departure from the Archetypal Ichnofacies: Effective recognition of physico-chemical stresses in the rock record. *Applied Ichnology, Short Course Note No. 52*, SEPM and CSPG, 2005. American Association of Petroleum Geologists Bulletin and SEPM short course note, no. 52, p. 66-88.
- MacEachern, J.A., K.B. Barn, S.G., Pemberton, and M.K. Gingras, The Ichnofacies paradigm: high-resolution paleoenvironmental interpretation of the rock record. AAPG and SEPM short course note, no. 52, p. 27-57.
- MacKinnon, T. C., 1989, *Petroleum geology of the Monterey Formation in the Santa Maria and Santa Barbara coastal and offshore areas*, in T.

- MacKinnon, ed., Oil in the California Monterey Formation: Washington, D.C., American Geophysical Union, Field Trip Guidebook T311, p. 11–27.
- McCave, I.N., 1984, Erosional, transport and deposition of fine-grained marine sediments. In: Fine Grained Sediments: Deepwater Processes and Facies (Ed. by D.A.V. Stow and D.J.W. Piper). Special Publication of Geological Society of London, Vol. 7, No. 6, p. 35-69.
- McKee, E.D., and G.W. Weir, 1953, Terminology for stratification and cross-stratification in sedimentary rocks. Bulletin of the Geological Society of America, vol. 64, p. 381 – 390.
- McLearn, F.H., 1930, A preliminary study of the faunas of the upper Triassic Schooler Creek Formation, western Peace River, British Columbia. Transactions of the Royal Society of Canada, ser.3, sec. 4, vol. 24, p. 13-19.
- Moretti, M., 2000, Soft-sediment deformation structures interpreted as seismites in Middle–Late Pleistocene aeolian deposits (Apulian foreland, southern Italy). Sedimentary Geology, vol. 135, p. 167–179.
- McLearn, F.H., 1940, Preliminary study of Triassic pelecypods and ammonoids from the Peace River Foothills, British Columbia, The Canadian Field Naturalist, vol. LIV., p. 111-116.
- McLearn, F.H., 1941, Triassic stratigraphy of Brown Hills, Peace River Foothills, British Columbia, The Canadian Field Naturalist, vol. LV., p. 31-33.
- McLearn, F.H., and Kindle, E.D., 1950, Geology of northeast British Columbia, Geological Survey of Canada, Memoir 259.
- McKee, E.D., and Weir, G.W., 1953, Terminology for stratification and cross-stratification in sedimentary rocks. Bulletin of the geological society of America, vol. 64. p. 381 – 390.
- Monger, J.W.H. and Price, R.A., 1979. Geodynamic evolution of the Canadian Cordillera- progress and problems. Canadian Journal of Earth Sciences, vol.

16, p. 770-791.

- Moss, A.J., and Green, P., 1975, Sand and silt grains: predetermination of their Formation and properties by microfractures in quartz. *Journal of the Geological Society of Australia* 22, 485– 495.
- Moslow, T.F., and Davies, G.R., 1997, Turbidite Reservoir Facies in the Lower Triassic Montney Formation, west-central Alberta, *Bulletin of Canadian Petroleum Geology*, vol. 45, no. 4, p. 507-536.
- Moslow, T.F., and Davies, G.R., 1992, Triassic Reservoirs Facies and Exploration Trends: western Canada Sedimentary Basin, *Canadian Society of Petroleum Geologists-American Assoc. of Petroleum Geologists, (Short Course)*, Calgary, Alberta, 166p.
- Morrow, D.W., 1990, Dolomite part 1: The geochemistry of Dolomitization and Dolomite Precipitation. In: McIlreath, I.A and Morrow, D.W, 1990, *Diagenesis. Geoscience Canada Reprint 4*, p. 113 – 121.
- Miall, A.D., 1980, Cyclicality and the facies model concept in geology. *Bulletin of Canadian Society of Petroleum Geologists*, vol. 28, p. 59 – 80.
- Miall, A.D., 1980, Alluvial deposits. In: *Facies Models: Response to Sea-level Change* (Eds. R.G. Walker and N.P. James), Geological Association of Canada, p.119 –142.
- Miall, A.D., 1999, *Principles of Sedimentary Basin Analysis* (third edition), Springer-Verlag, Berlin Heidelberg, Germany.
- Middleton, G. V., 1976, Hydraulic interpretation of sand size distributions: *Jour. Geology*, vol. 84, p. 405 – 426.
- Milliman, J.D., and Meade, R.H., 1983, World-wide delivery of river sediment to the oceans. *Journal of Geology*, vol. 91, p. 1 – 21.
- Moss, A.J., and Green, P., 1975, Sand and silt grains: predetermination of their formation and properties by microfractures in quartz. *Journal of the*

- Geological Society of Australia 22, 485– 495.
- Muller, P.J. and Suess, E., 1979, Productivity, sedimentation rate and sedimentary organic matter in the oceans – 1. Organic carbon preservation. Deep-Sea Research, pergamon Press Ltd, vol. 26A, p. 1347 – 1362.
- Naish, T. and Kamp, P.J.J., 1997, Foraminiferal depth palaeoecology of Late Pliocene shelf sequences and systems tracts, Wanganui Basin, New Zealand. Sedimentary Geology 110, 237–255.
- O’Connell, S.C., Dixon, G.R., and Barclay, J.E., 1990, Origin, history, and regional structural development of the Peace River Arch, Western Canada, Bulletin of Canadian Petroleum Geology, vol. 38A, P. 4-24.
- Orchard, M.J. and Tozer, E.T., 1997, Triassic conodont biochronology, its calibration with the ammonoid standard, and a biostratigraphic summary for Western Canada Sedimentary Basin. Bulletin of Canadian Petroleum Geology, vol. 45, 675-692p.
- Orchard, M.J., Zonneveld, J-P., Johns, M.J., McRoberts, C.A., Sandy, M.R., Tozer, E.T., and Carrelli, G.G, 2001, Fossil succession and sequence stratigraphy of the Upper Triassic of Black Bear Ridge, northeast British Columbia. Albertiana, vol. 25, 10-22p.
- Orchard, M.J. and J-P Zonneveld, 2009, The Lower Triassic Sulphur Mountain Formation in the Wapiti Lake area: Lithostratigraphy, conodont biostratigraphy, and a new biozonation for the lower Olenekian (Smithian): Canadian Journal of Earth Sciences, v. 46, p. 757–790.
- Owen, G., 1987, Soft-Sediment Deformation in Upper Proterozoic Torridonian Sandstones (Applecross Formation) at Torridon, Northwest Scotland. Journal of Sedimentary Research, vol. A. 65, No. 3. P. 495 – 504.
- Packard, J.J, Al-Aasm, I., and Samson, I., Berger, Z, and Davies, J., 2001, A Devonian hydrothermal chert reservoir: the 225 bcf Parkland field, British

- Pemberton, S.G. and Frey, R.W. 1982. Trace fossil nomenclature and the *Planolites Palaeophycus* dilemma. *Journal of Paleontology*, vol. 56, p. 843 – 881.
- Pedersen, G.K., 1985, Thin, fine-grained storm layers in a muddy shelf sequence: an example from the Lower Jurassic in the Stenlille 1 well, Denmark. *Journal of Geological Society of London*, vol. 142, p. 357 – 374.
- Pelletier, B.R., 1961, Triassic stratigraphy of the Rocky Mountains Foothills, northeastern British Columbia, Geological Survey of Canada, Paper 61-8.
- Pelletier, B.R., 1963, Triassic stratigraphy of the Rocky Mountain Foothills, Peace River District, British Columbia, Geological Survey of Canada, Paper 62-26.
- Pelletier, B.R., 1964, Triassic stratigraphy of the Rocky Mountains and Foothills, between Peace and Muskwa rivers, northeastern British Columbia, Geological Survey of Canada, Paper 63-33.
- Peters, K. E., 1986, Guidelines for evaluating petroleum source rock using programmed pyrolysis. *American Association of Petroleum Geologists Bulletin*, vol. 70, No. 3, p. 318-329.
- Peters, K. E., 1986, Guidelines for evaluating petroleum source rock using programmed pyrolysis: *American Association of Petroleum Geologists Bulletin*, vol. 70, p. 318 – 329.
- Pettijohn, F. J., 1949, *Sedimentary Rocks*, Harper and Brothers, New York.
- Powers, M.C., 1953, A new roundness scale for sedimentary particles. *Journal of Sedimentary petrology.*, vol. 23, no. 2, p. 117 – 119.
- Podruski, J.A., Barclay, J.E., Hamblin, A.P., Lee, P.J., Osadetz, K.G., Procter, R.M., and Taylor, G.C., 1988, *Conventional Oil Resources of Western Canada*. Geological Survey of Canada Paper, 149p.
- Porter, J.W., Price, R.A., and McCrossan, R.G. 1982. *The Western Canada*

- Sedimentary Basin. *Philosophical Transactions of the Royal Society of London*, v. A305, p. 169-182.
- Pitman, E.D., 1970, Plagioclase feldspar as an indicator of provenance in sedimentary rocks. *Journal of Sedimentary Petrology*, vol. 40, no. 2, p. 591-598.
- Pratt, B.R., James, N.P., And Cowan, C.A., 1992, Peritidal carbonates. In: R.G. Walker and N.P. James (eds.), *Facies Models: Response to sea level change*, Geological Assoc. of Canada, St. John's NFld. p. 303-322.
- Price, R.A. 1973, Large-scale gravitational flow of supracrustal rocks, southern Canadian Rockies. In: *Gravity and Tectonics*. K.A. De Jong and R. Scholten (eds.). New York, Wiley and Sons, p. 491-502.
- Price, R.A. 1979, Intracontinental ductile crustal spreading linking the Fraser River and northern Rocky Mountain Trench transform fault zones. *Geological Society of America, Programs with Abstracts*, vol. 11, p. 499.
- Price, R.A., 1994, Cordilleran Tectonics and the Evolution of the Western Canada Sedimentary Basin. *In: Geological Atlas of the Western Canada Sedimentary Basin*. G.D. Mossop and I. Shetson (compilers). Canadian Society of Petroleum Geologists, p. 257-275.
- Raup, D.M., 1979, Size of the Permo-Triassic bottleneck and its evolutionary implications: *Science*, v. 206, p. 217-218.
- Reading, H.G., 1996, *Sedimentary Environments and Facies* (third edition), Blackwell Scientific Publications, Boston, 615p.
- Rhoads, D.C., and Morse, J.W., 1971, Evolutionary and environmental significance of oxygen-deficient marine basins: *Lethaia*, vol. 4, p. 413 - 428.
- Raitzsch, M., D. Völker, and C. Heubeck, 2007, Neogene sedimentary and mass wasting processes on the continental margin off south-central Chile inferred

- from dredging samples. *Marine Geology*, vol. 244, p. 166 – 183.
- Reinson, G.E., 1994, Barrier-island and associated strand-plain systems. In: R.G Walker (Ed) *Facies Models*, 2nd Edition, Geoscience Canada, Reprinted Series 1, Geological Association of Canada, *Geotext* 1, p. 179-194.
- Reineck, H.E., and I.B. Singh, 1972, Genesis of laminated sand and graded rhythmites in storm-sand layers of shelf mud: *Sedimentology*, vol. 18, p. 123 – 128.
- Reid S. A., and J. L. McIntyre, 2001, Monterey Formation porcelanite reservoirs of the Elk Hills field, Kern County, California. *American Association of Petroleum Geologists Bulletin*, vol. 85, no. 1, p. 169 – 189.
- Richards, B.C. 1989. Upper Kaskaskia Sequence: Uppermost Devonian and Lower Carboniferous. In: *Western Canada Sedimentary Basin - A Case History*. B.D. Ricketts (ed.). Canadian Society of Petroleum Geologists, Special Publication No. 30, Calgary, Alberta, p. 165-201.
- Reidiger, C.L., Fowler, M.G., Brooks, P.W. and Snowdon, L.R. 1990. Lower and Middle Triassic source rocks, thermal maturation and source rock correlations in the Peace River Embayment area, Alberta and British Columbia. *Bulletin of Canadian Petroleum Geology*, v. 38A, p. 218-235.
- Reidiger, C.L., Fowler, M.G., Brooks, P.W. and Snowdon, L.R. 1990a, Triassic oils and potential Mesozoic source rocks, Peace River Arch area, Western Canada Basin. *Organic Geochemistry*, v. 16, p. 295–305.
- Riezebos, P.A., and van der Waals, I., 1974, Silt-sized quartz particles: a proposed source. *Sedimentary Geology*, vol. 12, p. 279 – 285.
- Richards, B.C., Barclay, J.E., Bryan, D., Hartling, A., Henderson, C.M., and Hinds, R.C., 1994, Carboniferous strata of the Western Canada Sedimentary Basin, In: *Geological Atlas of the Western Canada Sedimentary Basin*, G.D. Mossop and I. Shetsen, (comps.), Calgary, Canadian Society of Petroleum

- Geologists and Alberta Research Council, p. 221-250.
- Russell, R. D. and Taylor, R. E., 1937, Roundness and shape of Mississippi River sands. *Journal of Geology*, vol. 45, pp. 225-267.
- Sanders, J. E., 1960, Origin of convoluted laminae: *Geology Magazine*, vol. 97, p. 409 – 421.
- Seilacher, A. 1955. Spuren und Fazies im Unterkambrium, p. 11-143. *In*: O.H. Schindewolf and A. Seilacher, Beiträge zur Kenntnis des Kambriums in der Salt Range (Pakistan), Akademie der Wissenschaften und der Literatur zu Mainz, Mathematisch-naturwissenschaftliche Klasse, Abhandlungen, No. 10.
- Seilacher, A., 1970, *Cruziana* stratigraphy of “non-fossiliferous” Palaeozoic sandstone. *In*: Trace Fossils. T.P. Crimes and J.C. Harper (eds.). *Geological Journal*, Special Issue 3, p. 447–476.
- Stow, D.A.V., H.G. Reading, and Collison, J.D, 2002, Deep seas. *In*: Sedimentary environments: Processes, Facies, and Stratigraphy (Ed by Reading, H.G), Blackwell Science, Oxford, p. 395-453.
- Smith, G.G., and G.P. Mocke, 2002, Interaction between breaking/broken waves and infragravity-scale phenomena to control sediment suspension transport in the surf zone. *Marine Geology*, vol. 187, p. 329 – 345.
- Shibayama, T., 1986, Higuchi, A., Horikawa, K., 1986, Sediment transport due to breaking waves. Proc. 20th Coastal Engineering Conference, ASCE, p. 1509 – 1522.
- Simpson, S., 1975, Classification of trace fossils. *In*: Frey, R.W. (ed.): *The Study of Trace Fossils*, Springer-Verlag, New York, p. 39 – 54.
- Senftle, J. T., and C. R. Landis, 1991, Vitrinite reflectance as a tool to assess thermal maturity, in R. K. Merrill, ed., *Source and migration processes and evaluation techniques: AAPG Treatise of Petroleum Geology, Handbook of*

- Petroleum Geology, p. 119–125.
- Selley, R.C., 1969, Torridonian alluvium and quicksands: *Scottish Journal of Geology*, vol. 5, p. 328 – 346.
- Selley, R.C., 1970, Origin of disturbed bedding in Torridon Group sandstones: *Scottish Journal of Geology*, vol. 6, p. 411.
- Stow, D.A.V, 1985, Deep-sea clastics: where are we and where are we going?
In: *Sedimentology; Recent developments and applied aspects* (Ed. By P.J. Brenchley and B.J.P. Williams), p. 67-93
- Sternberg, K.V., 1833, Versuch einer geognostisch-botanischen Darstellung der Flora der Vorwelt. Leipzig and Prague. *In: on the Trace-Fossil Chondrites*.
In: (S. Simpson, 1956), vol. 22, part 4, p. 475 – 499.
- Stalder, P.J., 1970, Organic and inorganic metamorphism in the Taveyyannaz sandstone of Swiss Alps and equivalent sandstones in France and Italy. *Journal of Sed. Petrol.*, vol. 49, p.463-482.
- Savrda, C.E., Bottjer, D.J., and Gorsline, D.S., 1984, Development of a comprehensive oxygen-deficiency marine biofacies model: Evidence from Santa Monica, San Pedro, and Santa Barbara basins, California continental borderland. *American Association of Petroleum Geologists Bulletin*, vol. 68, p. 1179 – 1192.
- Schomacker, E.R., Kjemperud, A.V., Nystuen, J.P., and Jahren, J.S, 2010, Recognition and significance of sharp-based mouth-bar deposits in the Eocene Green River Formation, Uinta Basin, Utah. *Sedimentology*, vol. 57, p. 1069 – 1087.
- Sharp, W.E., and Fan, P.F., 1963, A sorting index. *Journal of Geology*, vol. 71, no. 1, p. 76 – 84.
- Staplin, F. L., 1969, Sedimentary organic matter, organic metamorphism and oil and gas occurrence: *Bulletin of Canadian Petroleum Geology*, v. 17, p. 47–

66.

- Stamatiakis, M.G., 2003, Phosphate deposits of Neogene age in Greece. Mineralogy, geochemistry and genetic implications. *Chemistry*, vol. 64, p. 329 – 357.
- Stewart, A.D., 1963, On certain slump structures in the Torridonian sandstones of Applocross: *Geological Magazine*, vol. 100, p. 205-218.
- Sorby, H.C., 1858, On the microscopic structure of crystals, indicating the origin of minerals and rocks. *Quarterly Journal of the Geological Society of London*, vol. 14, p. 453 – 500.
- Ten Haaf, E., 1956, Significance of convolute lamination: *Geology en Mijnbouw.*, vol. 18, p. 188 – 194.
- Todd, T.W., Paleoclimatology and the relative stability of feldspar minerals under atmospheric conditions. *Journal of Sedimentary Petrology*, vol. 38, no. 3, p. 832 – 844.
- Tozer, E.T. 1982a, Marine Triassic faunas of North America: Their significance for assessing plate and terrane movements. *Geologische Rundschau*, v. 71, p. 1077-1104.
- Tissot, B. P., and Welte, D. H., 1978, *Petroleum formation and occurrence*; Springer-Verlag, Berlin, 538 p.
- Tissot, B. P., Pelet, R., and Ungerer, P., 1987, Thermal history of sedimentary basins, maturation indices, and kinetics of oil and gas generation. *American Association of Petroleum Geologists, Bulletin*, vol. 71, No. 12, p. 1445-1446.
- Tozer, E.T. 1961, The sequence of marine Triassic faunas in Western Canada, Geological Survey of Canada, Department of Energy, Mines and Resources, Bulletin 156, 135p.
- Tozer, E.T. 1967, A standard for Triassic time, Geological Survey of Canada,

- Department of Energy, Mines and Resources, Paper 12, 14p.
- Tozer, E.T., 1982, Marine Triassic faunas of North America: their significance for assessing plate and terrane movements. *Geologische Rundschau* 71, 1077–1104.
- Tozer, E.T. 1994, Canadian Triassic ammonoid faunas. Geological Survey of Canada. Bulletin 467, 663p.
- Thomas, S.G., C.R. Fielding and T.D. Frank, 2007, Lithostratigraphy of the late Early Permian (Kungurian) Wandrawandian Siltstone, New South Wales: record of glaciation?. *Australian Journal of Earth Sciences*, vol 54, p.1057 – 1071.
- Turcker, M., 1988, *Techniques in sedimentology* (ed.). Blackwell scientific publication, 393 p.
- Twitchett, R.J., 2001. Incompleteness of the Permian–Triassic fossil record: a consequence of productivity decline? *Geol. J.* 36, 341–353.
- Twitchett, R.J., Krystyn, L., Baud, A., Wheeley, J.R., Richoz, S., 2004. Rapid marine recovery after the end- Permian mass-extinction event in the absence of marine anoxia. *Geology* 32, 805–808.
- Tyson, R.V., and Pearson, T.H., 1991, Modern and ancient continental shelf anoxia: An overview: in Tyson, R.V., and Pearson T.H., eds., *Modern and Ancient Continental Shelf Anoxia: Geological Society of London Special Publication* 58, p. 1 – 24.
- Veizer, J., Lemieux, J., Jones, B., Gilling, J.R., and Savelle, J., 1978, Paleosalinity and dolomitization of a Lower Paleozoic carbonate sequence, Somerset and Prince of Wales Island, Arctic Canada. *Canadian Journal of Earth Sciences*, vol. 15, p. 1448 – 1461.
- Visher, G.S., 1969, Grain size distributions and depositional processes. *Journal of Sedimentary Petrology*, vol. 39, p. 1074 – 1106.

- Walsh, W., Adams, A., Kerr, B. and Korol, J, 2006, "Regional Shale Gas"
Potential of the Triassic Doig and Montney Formations, Northeastern
British Columbia. Ministry of Energy, Mines and Petroleum Resources, Oil
and Gas Division, Resource Development and Geoscience Branch, British
Columbia, Petroleum geology open file 2006-02, 19p.
- Waples, W. Douglas, 1945, *Geochemistry in Petroleum Exploration*. International
Human Resources Development Corporation, Boston, 232p.
- Waples, D.W., 1985, *Geochemistry in Petroleum Exploration*. International
Human Resources Development Corporation, Boston, 332p.
- Weaver, C.E., 1960, Possible uses of clay minerals in the search for oil. *AAPG
bulletin*, vol. 44, p.1505-1518.
- Weise, B.R., 1980, *Wave-dominated Delta Systems of the Upper Cretaceous
San Miguel Formation, Maverick Basin, South Texas*. Bureau of Economic
Geology, Report of investigations, 107, Austin, Texas, 33p.
- Wittenberg, J. 1992, *Origin and stratigraphic significance of anomalously thick
sandstone trends in the Middle Triassic Doig Formation of west-central
Alberta*. Unpublished M.Sc. thesis, University of Alberta, Edmonton,
Alberta, p. 600.
- Wittenberg, J., and Moslow, T.F., 1991, *Origin and variability of overthickened
sandstone in the Doig Formation, west-central Alberta*, Canadian Society of
Petroleum Geologists, Calgary, p. 146.
- Willis, A. J, 1992, *Sedimentology and Stratigraphic Framework of the Middle
Triassic Halfway Formation, Wembly Oil field, Alberta*. Unpublished
master's degree thesis, University of Alberta, 412p.
- Willis, A.J., and Moslow, T.F., 1994, *Sedimentology and stratigraphy of tidal
inlet reservoirs in the Triassic Halfway Formation, Wembley Field, Alberta,
Canada*, *Bulletin of Petroleum Geology*, vol. 42, p. 245-262.

- Wadell, H., (1935) Volume, shape and roundness of quartz particles: *Journal of Geology* vol. 43, pp. 250-280.
- Wall, B. R., Girbacea, G., R., Mesonjesi, A., and Aydin, A., 2006, Evolution of fracture and fault-controlled fluid pathways in carbonates of the Albanides fold-thrust belt. *American association of Petroleum Geologists Bulletin*, vol. 90, no. 8, p. 1227 – p. 1249.
- Walsh, J.J., 1983, Death in the sea: enigmatic phytoplankton losses. *Prog. Oceanogr* vol. 12, p. 1 – 86.
- Wishner, K., Levin, L., Gowing, M., And Mullineaux, L., 1990, Involvement of the oxygen minimum in benthic zonation on a deep seamount. *Nature*, vol. 346, p. 57–58.
- Wiseman, W.J. Jr., Fan, Y-B., Bornhold, B.D., Keller, G.H., Su, Z-Q, Prior, D.B., Yu, Z-X, Wright, L.D, Wang, F-Q, Qian, Q-Y., 1986, Suspended sediment advection by tidal currents off the Huanghe (Yellow River) Delta. *Geo-Marine Letters*, vol. 6, p.107 – 113.
- Wignall, P.B., and Hallam, A., 1991, Biofacies, stratigraphic distribution, and depositional models of British onshore Jurassic black shales: in Tyson, R.V., and Pearson, T.H., eds., *Modern and Ancient Continental Shelf Anoxia: Geological Society of London Special Publication 58*, p. 291–309.
- Wignall, P.B., and Hallam, A., 1992, Anoxia as a cause of the Permian/Triassic mass extinction: Facies evidence from northern Italy and the western United States. *Palaeogeography, Palaeoclimatology, Palaeoecology*, vol. 93, p. 21 – 46.
- Wignall, P.B., and Twitchett, R.J., 2002a, Oceanic anoxia and the end Permian mass extinction: *Science*, v. 272, p. 1155–1158.
- Wignall, P.B., and Twitchett, R.J., 2002b, Extent, duration, and nature of the

- Permian-Triassic superanoxic event, in Koeberl, C., and MacLeod, K.C., eds., *Catastrophic Events and Mass Extinctions: Impacts and Beyond*: Geological Society of America Special Paper 356, p. 393–413.
- William, G.E., G.E., 1966, Palaeogeography of the Torridonian Applecross Group: *Nature*, vol. 209, p. 1303 –1306.
- William, G.E., G.E., 1969, Characteristics and origin of a Preamble pediment: *Journal of Geology*, vol. 77, p. 183 – 207.
- William, G.E., G.E., 1970, Origin of disturbed bedding in Torridon Group sandstones: *Scottish Journal of Geology*, vol. 6, p. 409 – 411.
- Wilson, N. and Zonneveld, J-P., 2011, Transition of the Montney to Doig Formations; subsurface to outcrop correlations, Northeastern British Columbia Unconventional Gas Forum Presentation, April 2011.
- Wright, L.D., Yang, Z.-S., Bornhold, B.D., Keller, G.H., Prior, D.B, and Wiseman Jr., W.J., 1986, Hyperpycner plumes and plume fronts over the Huanghe (Yellow River) delta front. *Geo-marine Letters*, vol. 6, p. 97 – 105.
- Zonneveld, J.P, 2008, Triassic Sedimentary Framework and Sequence Stratigraphy, Wiliston Lake, British Columbia, CSPG, CSEG, CWLS Convention, P. 1-9.
- Zonneveld, J.P, 2001, Middle Triassic biostromes from the Liard Formation, British Columbia, Canada: oldest examples from Mesozoic of NW Pangea. *Sedimentary geology*, vol. 145, p.217-341.
- Zonneveld, J.P., MacNaughton, R.B, Utting, J, Beatty, T.W, Pemberton, S.G, and Henderson, C.M., 2010, Sedimentology and ichnology of the Lower Triassic Montney Formation in the Pedigree-Ring/Border-Kahntah River area, northwestern Alberta and northeastern British Columbia. *Bulletin of Canadian Society of Petroleum Geology*, vol. 57, No. 2, p. 115-140.

- Zonneveld, J.P., Gingras, M.K., and Pemberton, S.G., 2001, Trace fossils assemblages in a Middle Triassic mixed siliciclastic-carbonate marginal marine depositional system, British Columbia. *Palaeogeography, Palaeoclimatology, Palaeoecology*, vol. 166 (3-4), p.249-276.
- Zonneveld, J.P., 1999, Sedimentology and sequence biostratigraphic framework of mixed siliciclastic-carbonate depositional system, Middle Triassic, northeastern British Columbia. Unpublished Ph.D. Dissertation, University of Alberta, 287p.
- Zonneveld, J.P., 1999b, Paleocological succession of Middle Triassic (Ladinian) brachiopod-echinoderm biostromes, Liard Formation, northeastern British Columbia, Canada. Geological Society of America Annual Meeting, October, 1999, Denver, Colorado, Abstracts with Programs 31, A242.
- Zonneveld, J.P., Moslow, T.F., Gingras, M.K., 1997a, Sequence Stratigraphy and Sedimentary Facies of the Lower and Middle Triassic of Northeastern British Columbia: Progradational shoreface associations in a mixed carbonate siliciclastic system. Field trip guide, Sedimentary Events-Hydrocarbon Systems, 1997, Canadian Society of Petroleum Geologists-Society for Sedimentary Geology (SEPM) joint convention, Calgary, 118 p.
- Zonneveld, J.P., Moslow, T.F., and Henderson, C.M. 1997, Lithofacies associations and depositional environments in a mixed siliciclastic-carbonate coastal depositional system, upper Liard Formation, Triassic, northeastern British Columbia. *Bulletin of Canadian Petroleum Geology*, v. 45, p. 553–576.
- Zonneveld, J.P., Pemberton, S.G., Saunders, T.D.A., and Pickerill, R.K., 2002, Large robust *Cruziana* from the Middle Triassic of northeastern British Columbia: ethologic, biostratigraphic and paleobiologic significance. *Palaios*, vol. 17. P. 435-448.

Zonneveld, J-P., 2011, Suspending the rules: Unraveling the ichnological signature of the Lower Triassic post-extinction recovery interval. *Palaios*, vol. 26, p. 677 – 681.

Zonneveld, J-P., Gingras, M.K., and Beatty, T.W., 2010b, Diverse Ichnofossil Assemblages Following The P-T mass extinction, Lower Triassic, Alberta and British Columbia, Canada: Evidence For Shallow Marine Refugia on the northwestern coast of Pangaea. *Palaios*, vol. 25, no. 6, p. 368 – 392.

CHAPTER 3: SOURCE-ROCK GEOCHEMISTRY AND RESERVOIR POTENTIAL OF THE UPPER MONTNEY FORMATION (LOWER TRIASSIC) NORTHEASERN BRITISH COLUMBIA, WESTERN CANADA

INTRODUCTION

Source-rocks are the precursors for hydrocarbon accumulation and reservoir potential. In general, source rocks are organic rich sediments that have, or may generate hydrocarbons (Tissot and Welte, 1984), and are a primary element in any petroleum system. Successful exploration for petroleum depends largely upon the quality of source-rock. To determine source rock quantity (TOC) and quality, Rock-Eval technique is used. Rock-Eval pyrolysis methods have been used worldwide for more than three decades as an aid to determining source-rock parameters: T_{max} , TOC richness, Hydrogen Index (HI), Oxygen Index (OI), Production Index (PI), the remaining hydrocarbon generating potential (S2), and a host of other products (Barker, 1974; Claypool and Reed, 1976; Espitalié et al., 1977 and 1984; Clementz et al., 1979; Larter and Douglas, 1982; Horsfield, 1985; Peters and Simoneit, 1982; Peters, 1986).

Rock-Eval pyrolysis is used to rapidly evaluate and depict the petroleum generating potentials of prospective source rocks (Peter, 1986) by providing information about their: 1) kerogen type and organic matter quality; 2) type of organic matter and characteristics; and 3) thermal maturity of the organic matter; and 4) hydrocarbon type (oil, gas or both).

The geographical distribution of source-rocks parameters within a particular acreage of exploration objective constitutes part of the assessment mechanics of hydrocarbon exploration (Peters, 1986). Source-rock evaluation involves assessing

the hydrocarbon generating potential of sediments by examining the sediment's capacity for hydrocarbon generation, type of organic matter present and what hydrocarbons might be generated, including sediment's thermal maturity and how it has influenced generation (Dembicki, 2009).

The Triassic Montney Formation in the Forth St. John study area (T86N, R23W and T74N, R13W), northeastern British Columbia (Fig. 3.1) is classified as unconventional hydrocarbon reservoir (Faraj, et al., 2002, Walsh, et al., 2006; Berger, et al., 2009; Core Lab, 2009; Zonneveld, 2009; Egbobawaye, et al., 2010, 2011). In general, unconventional hydrocarbon reservoirs comprises tight gas, shale gas and coalbed methane (Haines, 2006). Until recently, these reservoirs were previously considered non-economical, unproductive, and non-exploitable geological formations owing to poor understanding of lithological heterogeneity and variability in mineralogy coupled with lesser advancement in technology. The inherent petrophysical properties of unconventional reservoirs are low matrix porosity of $\leq 10\%$ and permeability of $\leq 0.1\text{mD}$ millidarcy, exclusive of fracture permeability (Haines, 2006). Typically, these reservoirs depend on stimulation for production, and in general, contain large amounts of hydrocarbons; although, gas recovery factors may be low (Schmoker, 1995).

The Montney Formation in the study area is a primary focus of tight gas reservoir exploration in Western Canada Sedimentary Basin (WCSB) because: 1) it is a source rock rich in organic matter (Riediger, et al., 1990); 2) it has a thermal maturity that lies within the gas generating window, and it is primarily a gas prone mixed Type II/III kerogen (Riediger, et al., 1990); 3) the present study shows that the kerogen of the Montney Formation in the study area is mainly composed of Type III/IV and some mixed Type II/III kerogen with average TOC of 0.5 – 4%; and are upto 8.2% TOC (rare), but present); 4) it has a reservoir thickness upto 320 metres in the study area;

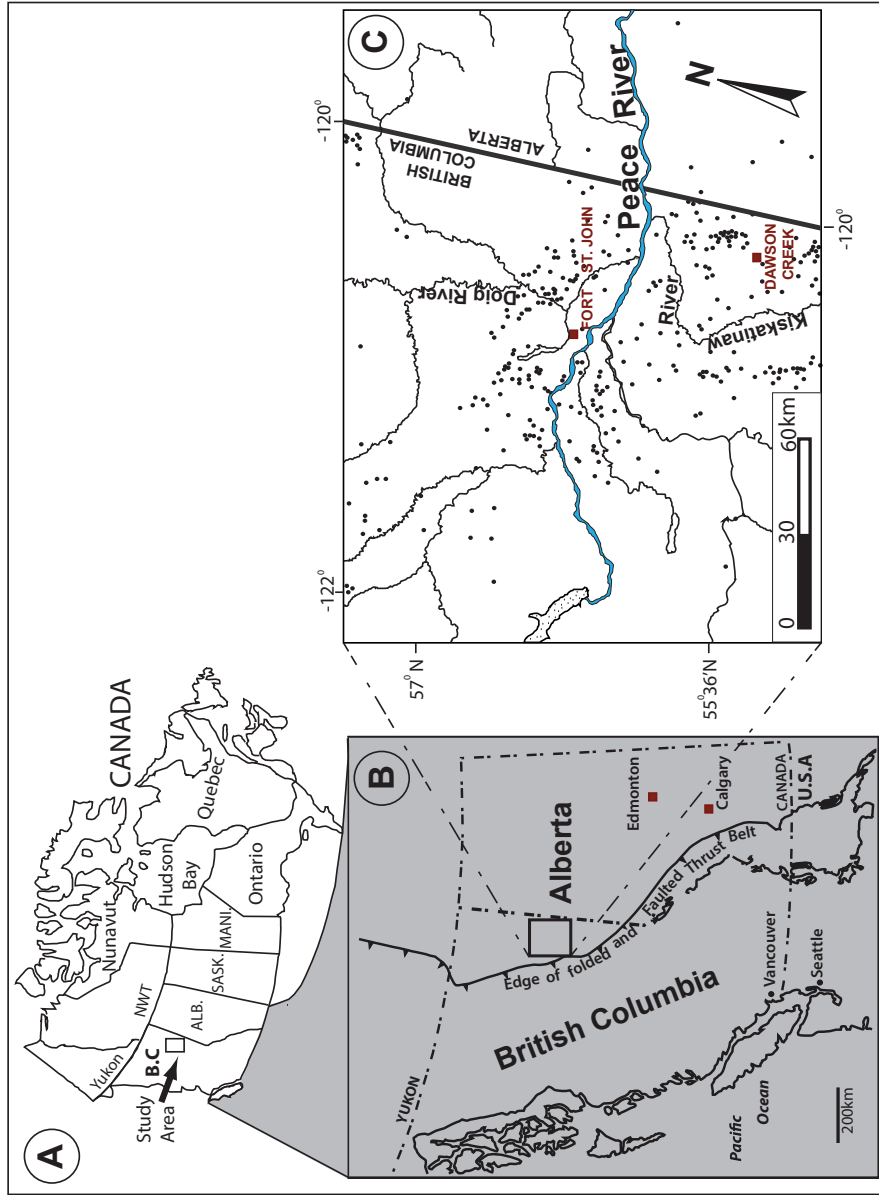


Figure 3.1. (A) Map of Canada showing provinces. (B) Shows tectonic deformation and structure in Western Canada Sedimentary Basin (Modified from Porter et al., 1982). (C) Shows location map of study area in northeastern British Columbia. The black dots represent drilled wells.

5) it hosts substantial volumes of unconventional gas, estimated to be 187 TCF (Walsh, et al., 2006); and 6) porosity range from 2 – 10%, and sporadically >10% in some intervals where ichnofabric or dolomite dissolution have resulted in the formation of secondary porosity. These criteria make the Montney Formation an unconventional resource play with high potential within the Fort St. John study area, northeastern British Columbia (Fig. 3.1). However, despite the strong economic significance of this hydrocarbon resource hosted in finer-grained lithologies ‘siltstone/very fine-grained sandstone’ interval, the location and predictability of the best reservoir units remains conjectural: in large part because the geochemistry, lithologic variability, and mineralogy of the Montney tight-rocks hosting thermogenic gas in the subsurface of Western Canada has not been adequately characterized (Eggboway, et al., 2010; 2011).

The Montney Formation in the study area consists of siltstone with subordinate interlaminated very fine-grained sandstone. Five lithofacies were identified in the study area: Lithofacies F-1 (organic rich, wavy laminated black siltstone); Lithofacies F-2 (very fine-grained sandstone interbedded with siltstone); Lithofacies F-3A (bioturbated silty-sandstone attributed to the *Skolithos* ichnofacies); Lithofacies F-3B (bioturbated siltstone composed of *Cruziana* ichnofacies); Lithofacies F-4 (dolomitic siltstone interbedded with very fine-grained sandstone); and Lithofacies F-5 (massive siltstone).

The depositional environments interpreted for the Montney Formation in the study area is characteristic of lower shoreface through proximal offshore to distal offshore settings. The lower shoreface environment record trace fossils attributed to the *Skolithos* ichnofacies (MacEachern, et al., 2005). The proximal offshore environment have sedimentary structures formed under quiescent depositional conditions typically found below the fair weather wave base (Reineck and Singh, 1972); such as lamination and current ripples (Reinson, 1994). The distal offshore

environment has trace fossils attributed to distal expression of the *Cruziana* ichnofacies (MacEachern, et al., 2005). The observed sedimentary structure that was recorded in the logged Montney Formation core are current ripples, deformation structures, convolute lamination / bedding. The sediment deformation structures, convolute lamination / bedding formed due to mechanical forces causing plasticity, commonly related to gravity acting upon weak sediments usually silt or sands, prior to or soon after, or at deposition along the sediment surface (Allen, 1986; Collison et al., 2006); and escape traces (Fugichnia?), which are evidence of small scale episodic deposition due to local transport from the lower shoreface or proximal offshore, to distal setting.

This study in the Fort St. John area (T86N, R23W and T74N, R13W), northeastern British Columbia (Fig. 3.1) is focused on source-rock geochemistry and reservoir potential of the Montney Formation. This paper concerns itself with: 1) evaluation of the Montney Formation source rock richness; 2) thermal maturity and hydrocarbon generation; 3) geographical distribution of Rock-Eval (TOC and T_{max}) parameters; and 4) reservoir quality within the Montney Formation in the Fort St. John area, northeastern British Columbia.

GEOLOGICAL SETTING

The paleogeographic location of the Western Canada Sedimentary Basin (WCSB) during the Triassic time was situated at approximately 30° N paleolatitude based on analyses of paleomagnetic data, paleolatitude and paleoclimatic zonation (Habicht, 1979), and fauna record (Tozer, 1982). The paleoclimate reconstruction suggests that the paleoclimate may have ranged from sub-tropical to temperate (Habicht, 1979; Tozer, 1982; Gibson and Barclay, 1989). The region has been interpreted to be arid during the Triassic, and was dominated by winds from the

west (Habicht, 1979; Arnold, 1994; Wilson, et al., 1994).

The WCSB forms a northeasterly tapering wedge of sedimentary rocks with thickness of more than 6,000 meters, which extends southwest from the Canadian Shield into the Cordilleran foreland thrust belt (Porter et al., 1982; Gibson and Barclay, 1989). The Cordilleran of the WCSB provides the evidence that the origin and development of the basin was associated with tectonic activity (Price, 1994; Gibson and Barclay, 1989). Later epeirogenic episodes resulted in subsidence that created the basin for sediment accumulation, which were attributed to the effects of contemporaneous episodes of orogenic deformation in the Cordillera (Porter, et al., 1982; Monger and Price, 1979). This is interpreted to be post Triassic, especially due to mountain influences (Gibson and Barclay, 1989). Wittenberg and Moslow (1991) and Cant (1994; 1986) interpreted sediment loading, evidenced by the deformed bed, slump structures and small-scale faults as indicators of tectonic influences on the deposition of Triassic successions. Within the Foothills and Rocky Mountain Front Ranges, Triassic rocks were subjected to Jurassic – Cretaceous Columbian and Upper Cretaceous – Lower Tertiary Laramide orogenies, which caused a series of imbricate thrust faults and folds in the region (Edwards et al., 1994).

In Alberta and British Columbia, Triassic sediments were deposited in a central sub-basin known as the Peace River Embayment, which extended eastward from the Panthalassa western ocean onto the North American craton (Edwards et al., 1994). During the Triassic period, the Peace River Embayment was a low mini basin associated with minor fault block movement associated with a broad downwarp resulted in the rejuvenation of structural deformation within the Monias areas of southwest Fort St. John, British Columbia (Edwards et al., 1994).

Stratigraphically (Fig. 3.2), the Triassic Montney Formation is Griesbachian to Spathian in age (Zonneveld and Orchard, 2009). The Triassic succession thickened westward (Edwards, et al., 1994), and rests unconformably in most areas, upon

the Belloy Formation in outcrop of northeastern British Columbia; Carboniferous in parts of northeastern British Columbia and Alberta; and Fantasque in outcrop at Williston (Orchard and Zonneveld, 2009). The thickness of Triassic deposits is about 1200 meters in the western-most outcrop in the Rocky Mountain Foothills (Willis, 1992). The Montney Formation structure map (Fig. 3.3) indicates higher paleostructure in the east and low in the western portion of the study area. This structural tilt shows a depositional thinning to the east and north due to erosional removal (Edwards, et al., 1994).

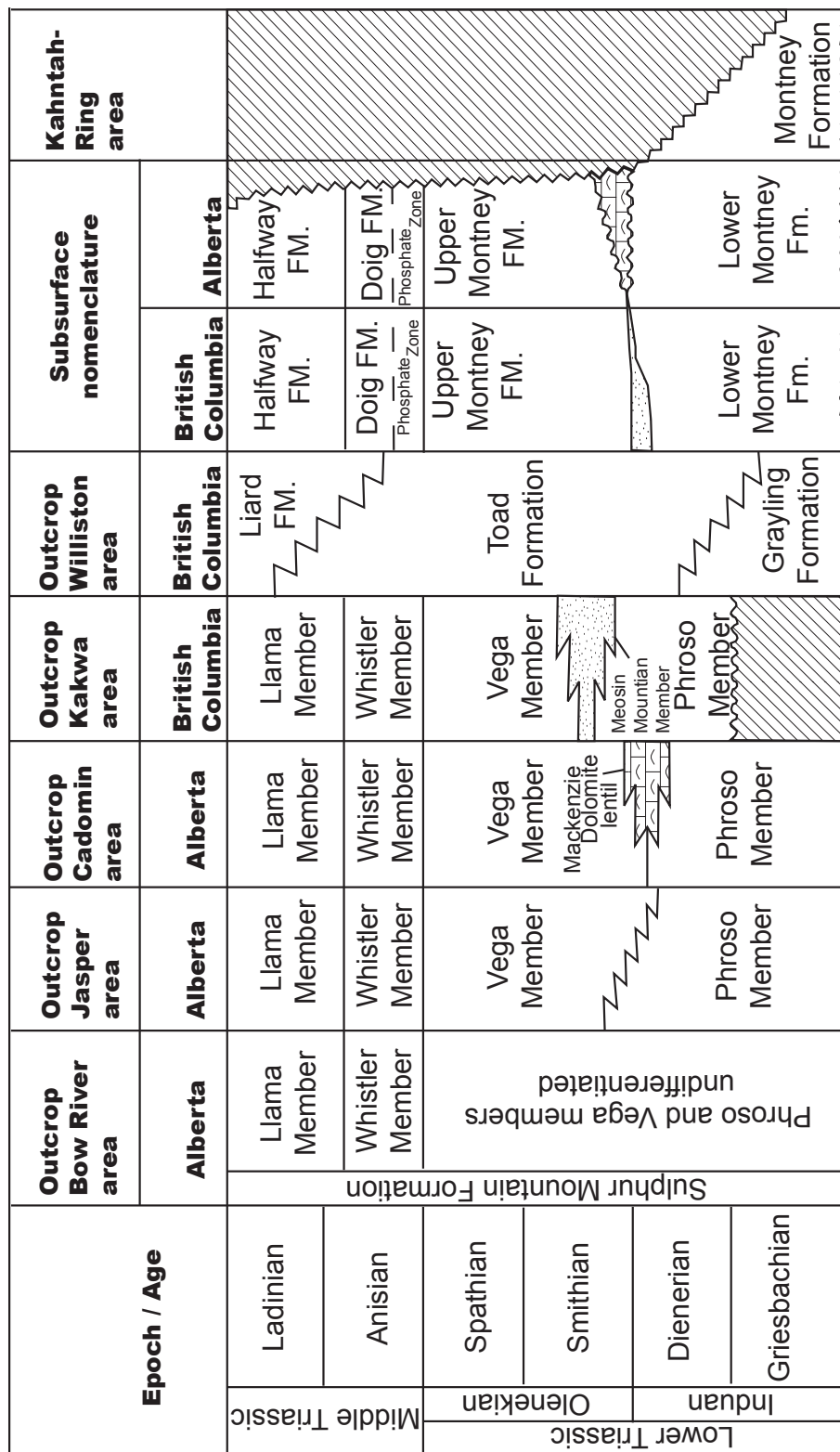


Figure 3.2. Stratigraphic chart showing Lower and Middle Triassic deposits and a correlation of outcrop with coeval subsurface strata in the western Canada Sedimentary Basin (Modified from Orchard and Zonneveld, 2009).

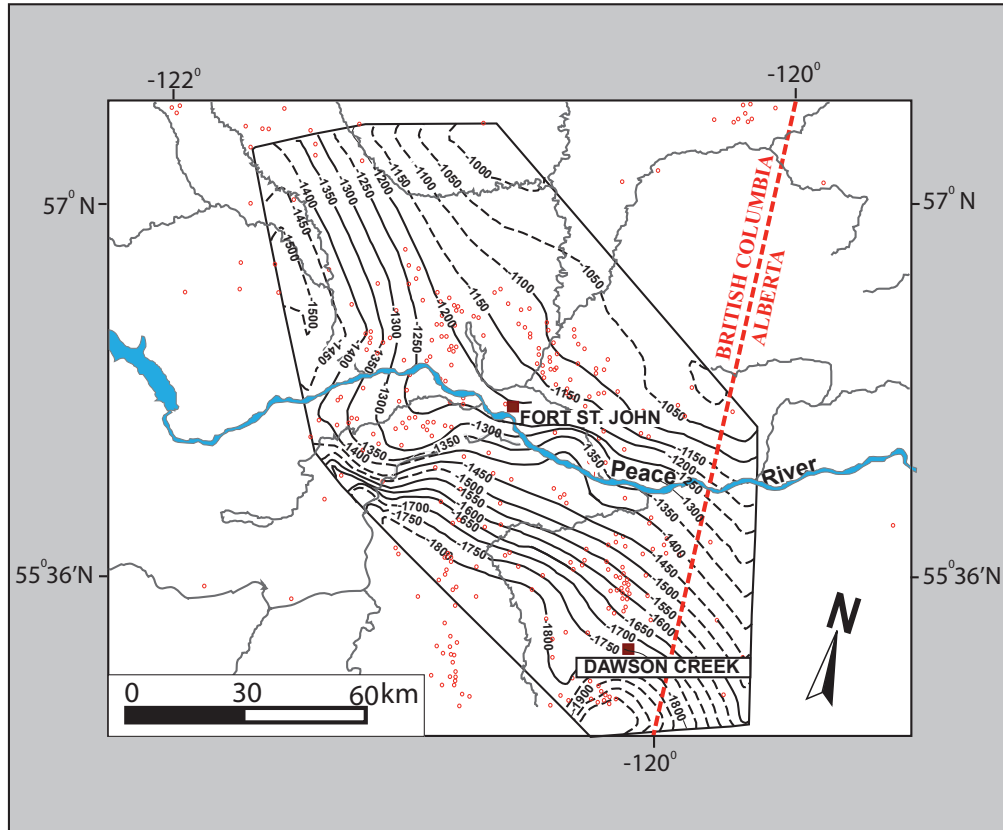


Figure 3.3. Structure contour map of the Montney Formation in the study area, northeastern British Columbia. Dash contour lines indicate no data point for well control. The structure map decreases in elevation westward, which indicates that sediment source area was from east, and prograded westward.

METHOD OF STUDY

Drilled cores of the Montney Formation from the study area in the Fort St. John vicinity, northeastern British Columbia were logged to assess sedimentological, ichnological and facies characteristics. The lithologic features and accessories, sedimentary texture, sedimentary structure, the nature of bedding contacts, and lithofacies were compiled in detail (Fig. 3.4 and Fig. 3.5).

Samples were crushed into powder using the pulverized shatter-box machine. Samples were sent to Geological Survey of Canada and Chesapeake Energy Corporation, Oklahoma, USA, for Rock-Eval analyses (Appendix 3-A).

Additional Rock-Eval data included in Appendix 3-A comes from Faraj, et al. (2002) and Oil and Gas Commission, Ministry of Energy, British Columbia.

The anhydrous pyrolysis technique used in this study evaluates oil and gas shows, oil and gas generation potential, thermal maturity and identifies organic matter type (Behar et al., 2001; Espitalie', et al., 1985; Peters, 1986; Tissot and Welte, 1978). The Montney Formation rock samples were pyrolyzed using Rock-Eval 6. Lafargue, et al. (1998) described the Rock-Eval technique as an apparatus, which consists of a programmed temperature heating of a small amount of rock sample (100mg) in an inert atmosphere (Helium or Nitrogen) to determine the amount of free hydrocarbons present in a sample (usually denoted by the S1 peak). The amount of hydrocarbons and oxygen containing compounds (CO_2) that are produced during the thermal cracking of the insoluble organic matter (kerogen) in the rock is represented by the S2 peak, which indicates the oil not yet released from the rock by natural processes and represents the residual petroleum potential (Fig. 3.6).

Rock-Eval pyrolysis is a standard analytical method used to determine the petroleum potential and the thermal maturity of the kerogen occurring in a rock, as proposed by Espitalie'et al. (1977, 1985). The procedure consists of progressive heating the whole rock from initial temperature of 25°C by using the Rock-Eval 6 analyzer to measure the hydrocarbons released during the increased artificial thermal heating to 650°C (Lafargue, et al., 1998) as shown in Figure 3.6. The key parameters from Rock-Eval analyses are: 1) the total organic carbon (TOC); 2) T_{max} ; 3) Hydrogen Index (HI); 4) Oxygen Index (OI); 5) Production Index (PI); and 6) S2 peak.

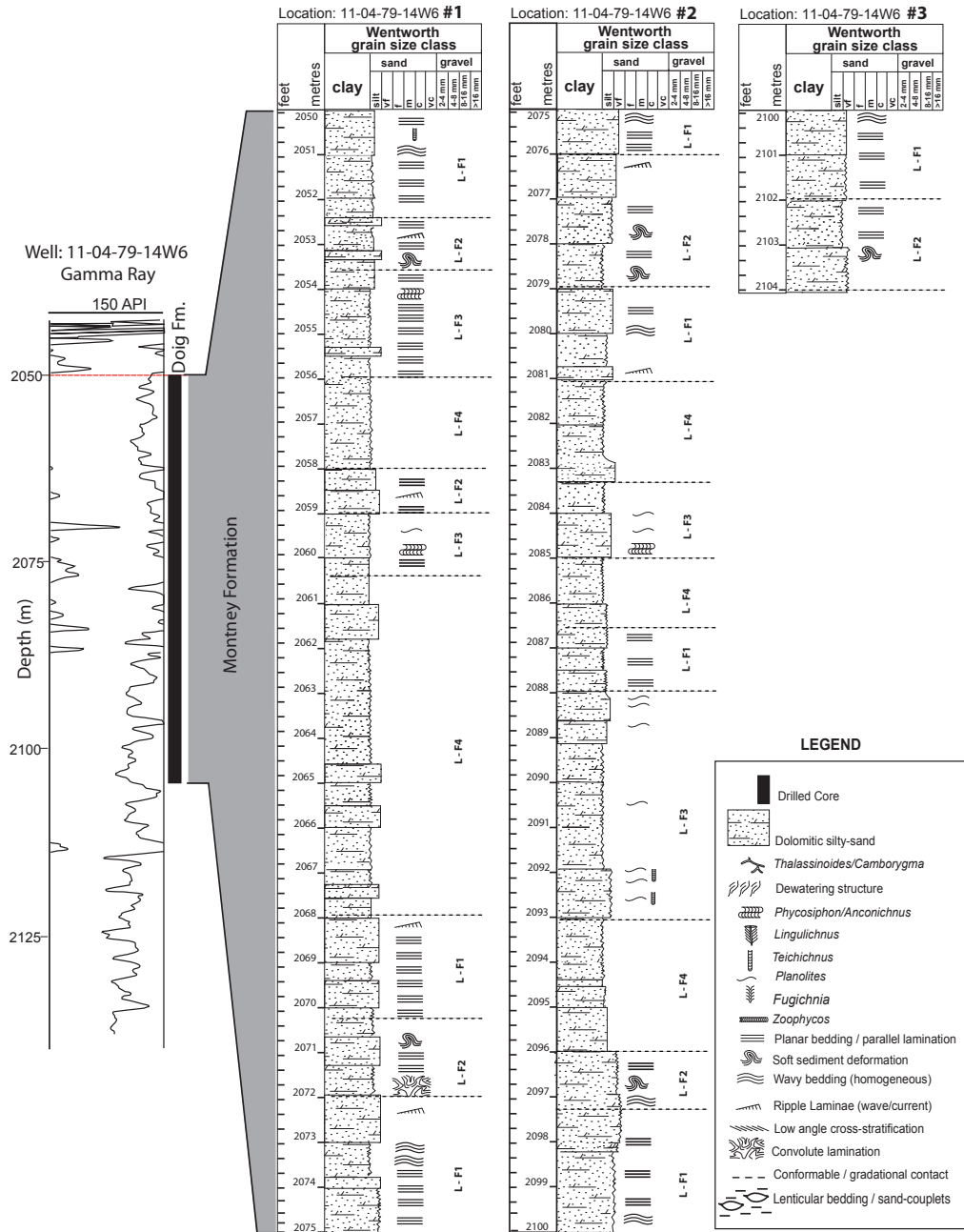


Figure 3.4. The Montney Formation core description showing lithofacies, tracefossils, and depositional sedimentary features. Gamma-ray log and core are from well 11-04-79-14W6, northeastern British Columbia.

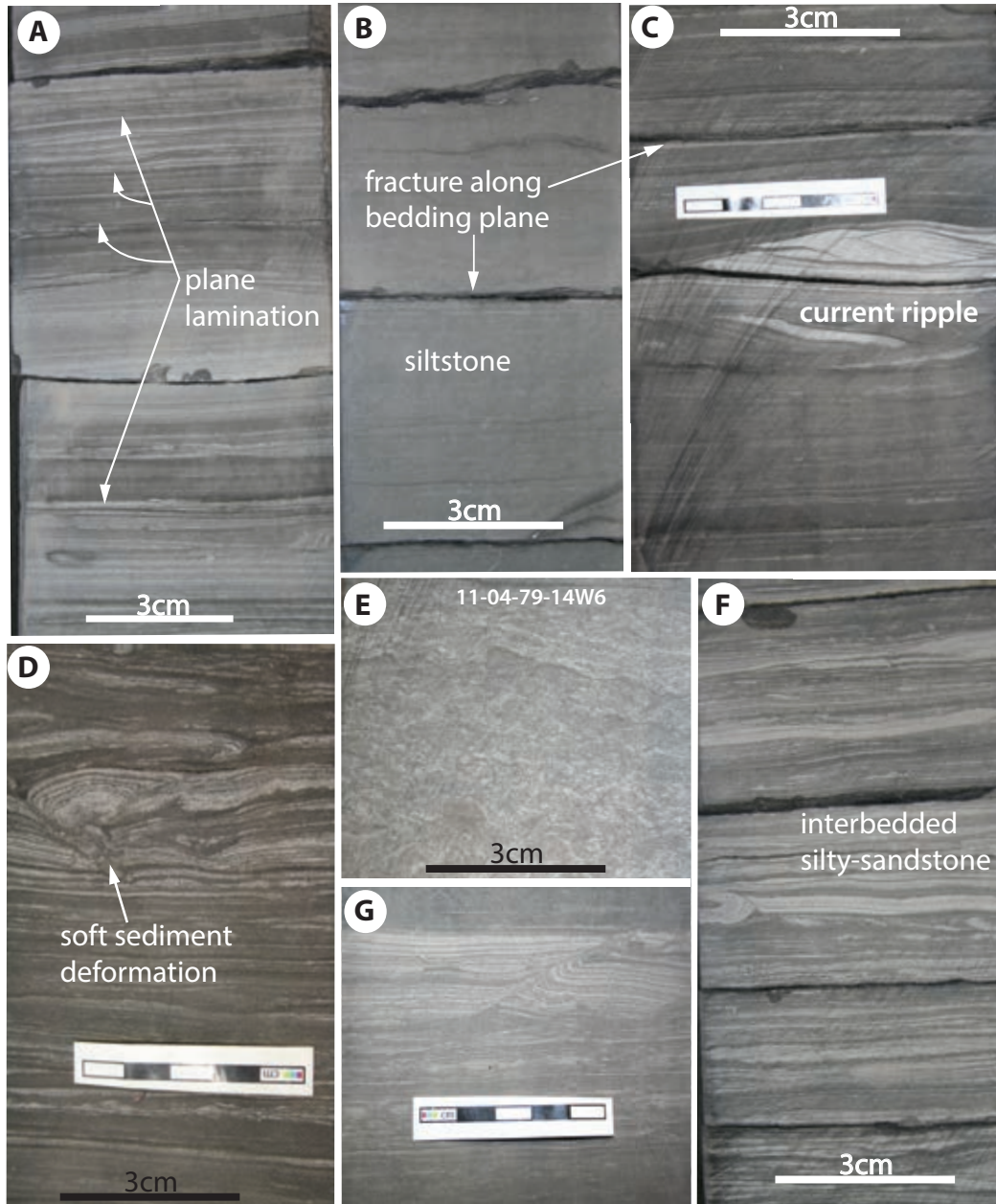


Figure 3.5. Shows the lithofacies of the Montney Formation. **(A)** Plane lamination [well: 11-04-79-14W6, 2051m]. **(B)** Fractured siltstone along bedding plane [well: 11-04-79-14W6, 2065.5m]. **(C)** Silty-sandstone with current ripple sedimentary structure [well: 11-04-79-14W6]. **(D)** Shows sediment deformation structure [well: d-21-G/93-P-9]. **(E)** Bioturbation by *Phycosyphon* [well: 11-04-79-14W6, 2092m]. **(F)** interbedded silty-sandstone [well: 11-04-79-14W6, 2055.5m]. **(G)** Escape structure (fugichnia?) in a silty-sandstone.

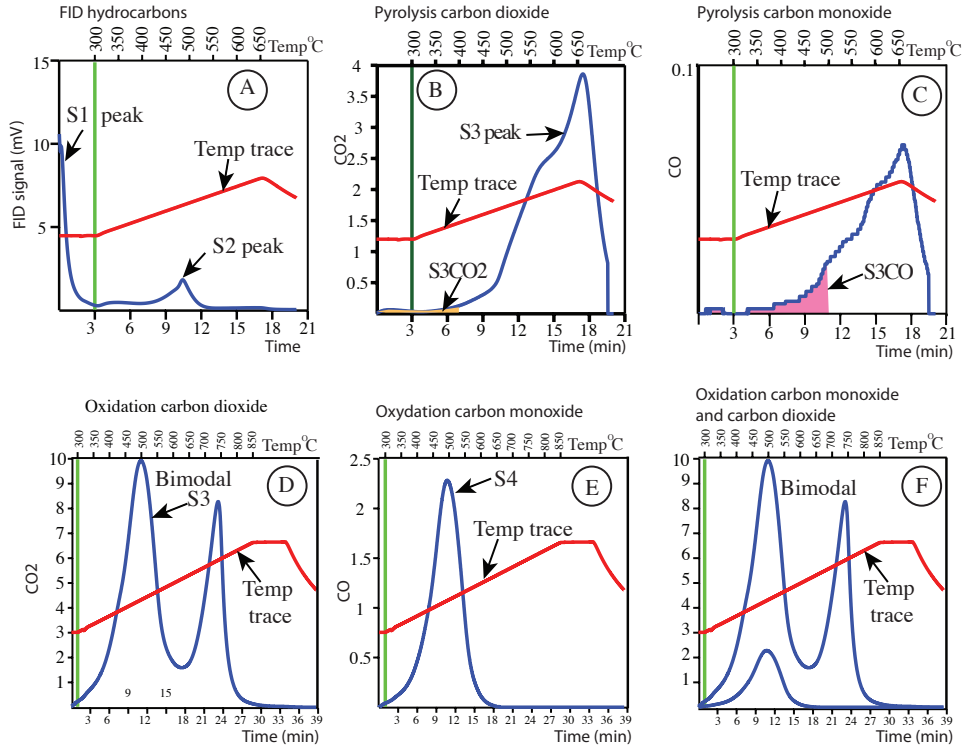


Figure 3.6. Rock-Eval pyrolysis for Montney Formation sample (well 2-19-79-14W6, depth: 2085 m). **(A)** illustrates the effect of pyrolysis temperature with Rock-Eval. The S1 peak is the free hydrocarbon liberated during thermal decomposition at less than 300°C. The S2 peak is derived from the conversion of total organic matter to kerogen during pyrolysis (pyrolyzed fraction). The S2 corresponds to the maximum temperature (Tmax). **(B)** shows the S3 peak (CO₂) corresponding to 400°C, which represents the oxidation of CO₂. It also shows the difference in organic matter. **(C)** illustrates the pyrolysis carbon monoxide (CO). **(D)** shows the oxygen indices. The determination of oxygen index (OI) is based on using CO₂ and CO; the CO = S3CO X 100/TOC Total oxygen index (OI) = CO₂ + OI (CO). **(E)** shows the S4 peak, the oxidation carbon monoxide (CO), the peak shows the present of siderite mineral (400 - 600°C). **(F)** Oxidation of CO and CO₂. The red line is the temperature trace in 25 minutes from 300°C to 650°C. Distinctly bimodal curve is due to pyrobitumen. See complete pyrolysis graphs for analyzed samples in Appendix 3-B

RESULTS

Rock-Eval Geochemistry

Rock-Eval was originally designed for measuring the maturity of coal mackerel (Waples, 1945; Espitalie et al. 1977). It is a useful screening technique for recognizing source rock and kerogen quality, and has become a major oil and gas exploration tool that give insights to the exploration geologist in terms of source rock characteristics, and reservoir potential. The key parameters of Rock-Eval (TOC, T_{max} , HI, OI, PI and S2 values) are fundamental to determining source rock richness, kerogen type, and maturation, which altogether form critical elements in the assessment of a petroleum system, risks segments and high grading resource plays.

Description: Montney Formation Total Organic Carbon (TOC)

The TOC content of a rock is determined by oxidation under air, in an oven from the organic carbon residue after pyrolysis (Lafargue, et al., 1998). The measured TOC values for the Montney Formation are shown in Appendix 3-A. The geographical distribution of TOC in the study area in Figure 3.7. The general trend of TOC is low in the western part of study area, and TOC value increases eastwards into Alberta Province (Fig. 3.7). TOC in the Montney Formation is variably and statistically distributed in the order of highest percentile into low TOC (<1.5wt%), medium (1.5 – 3.5wt%), and high (>3.5wt%).

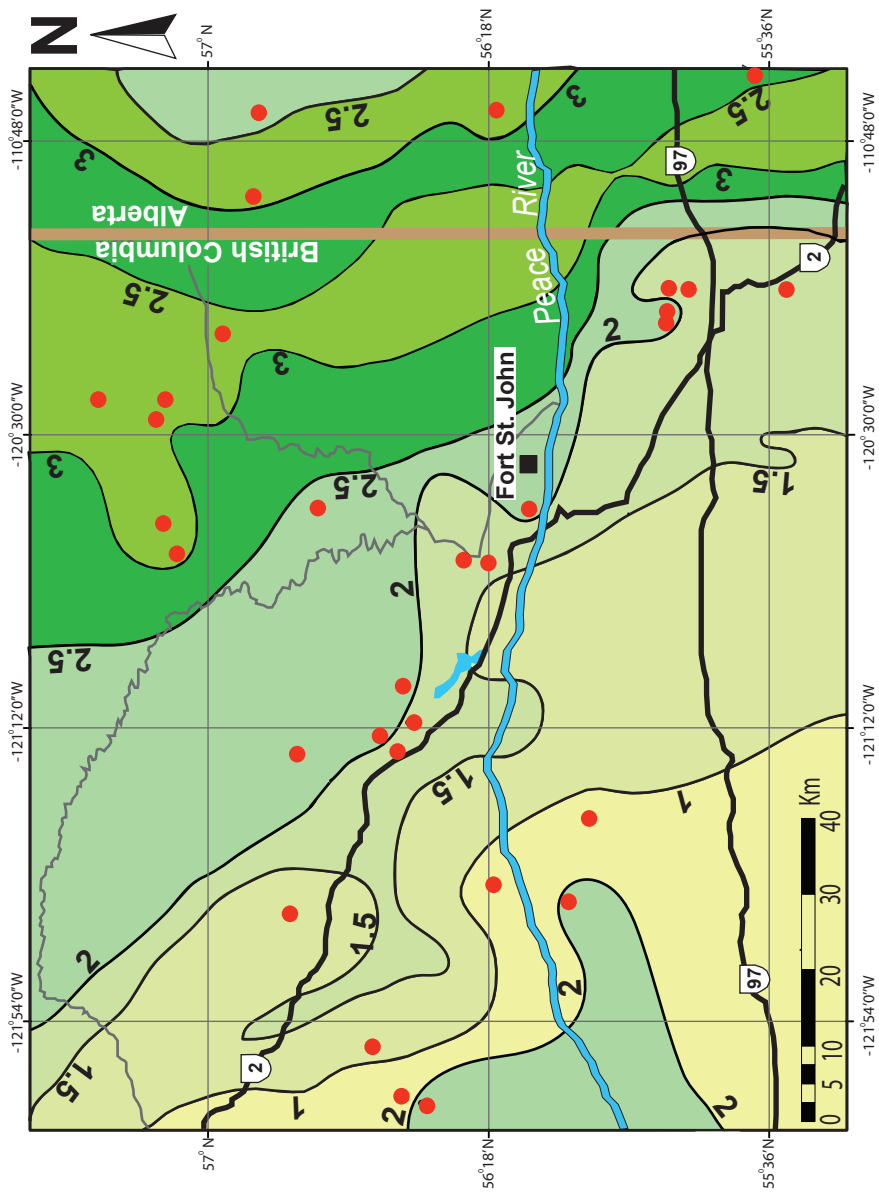


Figure 3. 7. The Montney Formation average TOC (wt%) map within the study area, northeastern British Columbia and northwestern Alberta. The red dots represent wells with Rock-Eval data.

Interpretation

TOC is an indicator of the total amount of organic matter present in the sediment (Ronov, 1958). The standard criteria for ranking source-rock richness (Table 3.1) was proposed by Peters and Cassa (1994). The hydrocarbon generating potential is commonly interpreted using a semi quantitative scale (Table 3.2) according to Senthle and Landis (1991) and (Jarvie, 1991). The Montney Formation TOC richness and distribution within the study area may be related to factors such as: 1) depositional condition of organic matter, its concentration and preservation, including oxygen content of the water column and sediment type, i.e. oxic versus anoxic as proposed by Demaison and Moor (1980); Jacobson, (1991); Peters and Cassa (1994); 2) biological productivity influence and availability of nutrient and replenishment (Peters and Cassa, 1994; Jacobson, 1991), controlled by sunlight, temperature, pH and Eh of waters (Jacobson, 1991). Within the study area, the depositional environment interpreted for the Montney Formation is generally an offshore setting (inner shelf – proximal offshore to distal environment). The environment of deposition affects organic matter productivity and preservation (Demaison and Moor, 1980; Peters and Cassa, 1994; Jacobson, 1991; Killops and

Table 3.1. Criteria for ranking source rock and richness (Peters, 1986) and Cassa (1994).

Source rock richness	Organic Matter			
	TOC (wt) Shale	TOC (wt%) Carbonate	Rock-Eval Pyrolysis S ₁	Pyrolysis S ₂
Poor	0.0–0.5	0.00–0.12	0–0.5	0–2.5
Fair	0.5–1.0	0.12–0.25	0.5–1.0	2.5–5
Good	1.0–2.0	0.25–0.50	1.0–2.0	5–10
Very Good	2.0–4.0	0.50–1.00	2.0–4.0	10–20
Excellent	>2.0	>1.00	>20	-----

Table 3.2. Hydrocarbon generation and maturity measurement using vitrinite reflectance (After Dow, 1977; Senftle and Landis, 1991).

Oil Prone Generation		Gas Prone Generation	
Generation Stage	R _o (%)	Generation Stage	R _o (%)
Immature	<0.6	Immature	<0.8
Early oil	0.6 – 0.8	Early gas	0.8 – 1.2
Peak oil	0.8 – 1.0	Peak gas	1.2 – 2.0
Late oil	1.0 – 1.35	Late gas	>2.0
Wet gas	1.35 – 2.0		
Dry gas	>2.0		

Killops, 2005). Organic matter is preserved in oxygen-restricted environment at depths below wave base in waters where density or temperature stratified water columns form, or in locations where oxygen replenishment is low (Demaison and Moor, 1980).

We hypothesize herein that the TOC distribution in the study area (Fig. 3.7) may be related to depositional environment's proximity to organic matter source and preservation conditions. Where TOC values are greater than 2.4 wt% around Fort St. John (in a NNW – SEE transverse trending contour value 2) and east of that contour boundary (Fig. 3.7), TOC values increases eastwards into Alberta where Faraj, et al. (2002) have reported TOC for the Montney Formation > 4 wt%. TOC data from well 16-17-83-25W6, provided by Oil and Gas Commission, Ministry of Energy, British Columbia, which is located outside of this study area also shows TOC upto 8.2wt % in the Montney Formation. In the western portion of study area (west of the boundary contour value 2 in Figure 3.7), the TOC values are generally lower. In the eastern portion where there is higher TOC value, the area lies within the region that has been interpreted as outer shelf depositional setting. Relatively

higher TOC value in this geographical region (eastwards) is probably due to increase oxidation, while reducing condition may have dominated the western portion in the study area where TOC is low in a distal / deep basinal setting. Several workers (e.g. Hunt, 1979; Peters and Cassa, 1994; Demaison and Moor, 1980; Peters, 1986; Peters and Cassa, 1994; Jacobson, 1991; Killops and Killops, 2005) have reported that the high TOC content or richness in sediments are related to the depositional environment, transport of organic matter and preservation. The abundant supply of nutrient and upwelling condition may have dominated the region with higher TOC values in the NE – SW portion of the study area (Fig. 3.7)

Determination of the original total organic carbon (TOC) of a source rock provides a quantitative means to estimate the total volume of hydrocarbons that it can generate depending on kerogen type (Jarvie, et al., 2007). However, it is common practice to rate carbonate rocks with lower TOC comparable with richer clastic rocks (Waples, 1945). Extractable Hydrocarbon yields from leaner carbonate rocks are comparable to richer clastic rocks (Tissot and Welte, 1978; Gehman, 1962). The organic matter associated with carbonate rocks are often more hydrogen-rich and thermally labile than that in fine-grained clastic rocks (Tissot and Welte, 1978; Behar et al., 2001; Espitalie et al. 1985). The Montney Formation is partly dolomitic and has variable TOC contents ranging from poor to excellent using the standard TOC richness metrics (Table 3.1) of Peters (1986). The low TOC content of the Montney Formation in the study area may be related to the mixed siliciclastic-dolomite composition.

Description: Montney Formation Hydrogen Index and Oxygen Index

The Oxygen Index (OI) measure in mgCO₂/gTOC is calculated from the amount of CO₂ released and trapped at temperature ranging from 300°C to 390°C (Fig. 3.6) during pyrolysis (Lafargue, et al., 1998). The Oxygen Index

corresponds to the quantity of carbon dioxide from S3 peak (Fig. 3.6) relative to the TOC ($\text{mgCO}_2/\text{gTOC}$); while Hydrogen Index (HI) corresponds to the quantity of pyrolyzable organic compounds or ‘hydrocarbons’ (HC) from S2 peak relative to the total organic carbon (TOC) according to Peters (1986). The hydrogen index (HI) was calculated from the ratio of S2/TOC using the method of Espitalie’ et al., 1985a.

In the Montney Formation samples analyzed in this study shows that the HI is statistically distributed into four categories in the order of highest percentile: low HI values (0 – 150); medium values (150 – 300); and high values (300 – 900). Of these categories, ~ 88% of the values are within the low HI values, while about 10% falls into the category of medium values; 1% are of the very high values bracket. The OI values are very low (Fig. 3.8), mostly less than 160 and a couple have exceptionally high HI and OI data point were evident as well (Fig. 3.8).

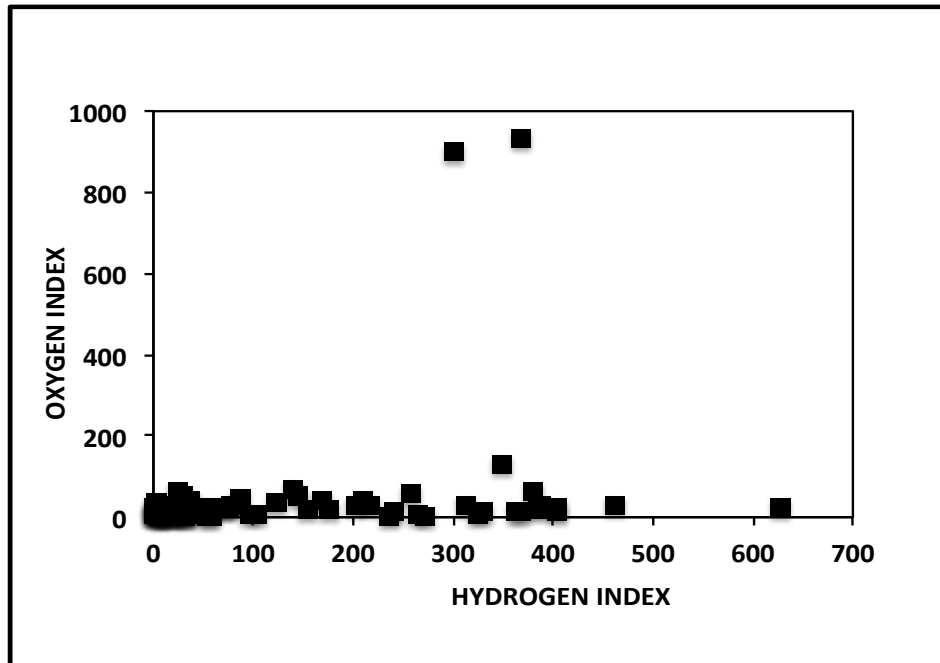


Figure 3.8. Shows a plot of Oxygen index (OI) vs. Hydrogen index (HI). The low OI and HI indicate that the Montney Formation in the study area is primarily a Type III/IV kerogen, with a mixed Type II/III kerogen.

Interpretation

The Hydrogen (HI) and Oxygen (OI) indices are used to determine the type of kerogen (Table 3.3) present in a source-rock (Espitalie' et al., 1977; Espitalie' et al., 1985; Lafargue, et al., 1998; Peters, 1986). Based on the data plot of HI and TOC on the pseudo Van Kravellen diagram, it shows that the Montney Formation in the study area is primarily a Type III/IV kerogen with some mixed Type II/III kerogen (Fig. 3.9 and 3.10). For organic matter to generate hydrocarbons, the carbon has to be associated with hydrogen (Dembicki, 2009). Waples (1947); Tissot and Welt (1984) define kerogen as a polymeric organic material from which hydrocarbons are produced with increasing burial and temperature. Kerogen is composed of the remains of algae, spores, pollen, and vegetative tissues and they are the same groups of maceral found in coals: liptinite, vitrinite, and inertinite (Waples, 1945; Tissot and Welt, 1984; Peters and Cassa, 1994; Peters, 1986; Killops and Killops; 2005).

Table 3.3. Interpretation of Hydrogen Index (HI) and Oxygen Index (OI) Values to determine Kerogen types (Modified After Peters, 1986; Dembicki, 2009).

Kerogen	HI (mg HC/g TOC)	OI	S ₂ / S ₃	Main Expelled Product at peak maturity
Type I	>600	15	>15	Oil
Type II	300–600	40	1.2–1.5	Oil
Type II/III	200–300	40–115	1.0–1.2	Mixed oil and gas
Type III	50–200	115	0.7–1.0	Gas
Type IV	<50	100	<0.7	Gas

Kerogen is mainly classified into three types: Type I, Type II, Type III, (Tissot, et al., 1974; Tissot and Welte, 1984) and Type IV (Demaison et al., 1983). Kerogen types are defined on the basis of hydrogen/carbon (H/C) and oxygen/carbon (O/C) values, i.e. Hydrogen Index (HI) and Oxygen Index (OI) according to Van Krevelen

(1961); Stach et al. (1982); Jacobson (1991). The use of the van Krevelen diagram was extended by Tissot et al. (1974) from coals to include kerogen dispersed in sedimentary rocks.

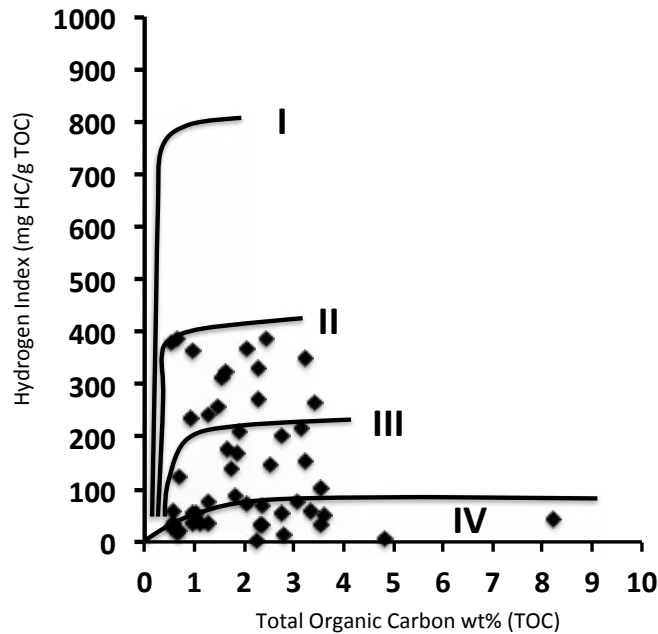


Figure 3.9. Pseudo Van Krevelen diagram showing kerogen types and TOC richness in the Montney Formation.

Type II Kerogen

The analyzed Montney Formation sediments in the study area show that Type II kerogen is present in the Montney Formation (Fig. 3.9). Type II kerogen is oil prone (Peters, 1986), relatively rich in hydrogen and characterized by its pure (monomaceral) form of exinite (Jacobson, 1991). Examples of materials from which type II kerogen are derived are spores and pollen grains of lands plants, marine phytoplankton cysts, some leaf and stem cuticles (Waples, 1945; Jacobson, 1991). The occurrence of type II kerogen depends on high biological productivity due to nutrient supply, low mineralogical dilution, and restricted oxygenation (Jacobson, 1991).

Type III Kerogen

Type III kerogen interpreted herein for the Montney Formation sediments in the study area is approximately ratio 2:1 in relation to type IV kerogen using the HI and TOC graph (Fig. 3.9), but using the S₂ values (remaining hydrocarbon generating potential) versus TOC, the ratio of Type III kerogen to Type IV kerogen is approximately 3:1 (Fig. 3.10). Peters (1986) described Type III kerogen as primarily a gas prone kerogen, which contains dominantly vitrinite, and it is identical to macerel of humic coal (Waples, 1945) formed from land plant, or largely woody and cellulosic debris (Waples, 1945). However, various macerel mixtures or degradational processes can contribute to the type III kerogen formation (Jacobson, 1991). Type III kerogen is the most reliable kerogen to estimate in terms of the degree of maturation using T_{max} (Espitalie' et al., 1986).

Type IV Kerogen

Analyzed data in this study shows that Type IV kerogen constitutes the highest percentile. Waples (1945); Demaison et al., 1983; Peters and Cassa (1986); Jacobson (1991) defined Type IV kerogen as inertinite (gas prone), composed of hydrogen poor (HI ≤ 50) constituent, difficult to distinguish from type III kerogen by using only Rock-Eval pyrolysis (Jacobson, 1991). A graphical plot of S₂ versus TOC with pseudo HI indicates that Type IV kerogen constitutes about 80% of the kerogen based on Rock-Eval dataset (Fig. 3.10, and Supplement 1). Type IV kerogen is formed from materials of various origin, and has undergone extensive oxidation, or may in some cases represent detrital organic matter oxidized directly by thermal maturation, sedimentological recycling of materials (Jacobson, 1991), or organic facies that has been reworked from a previous depositional cycle (Waples, 1945; Demaison et al., 1983; Peters and Cassa 1986; Jacobson (1991).

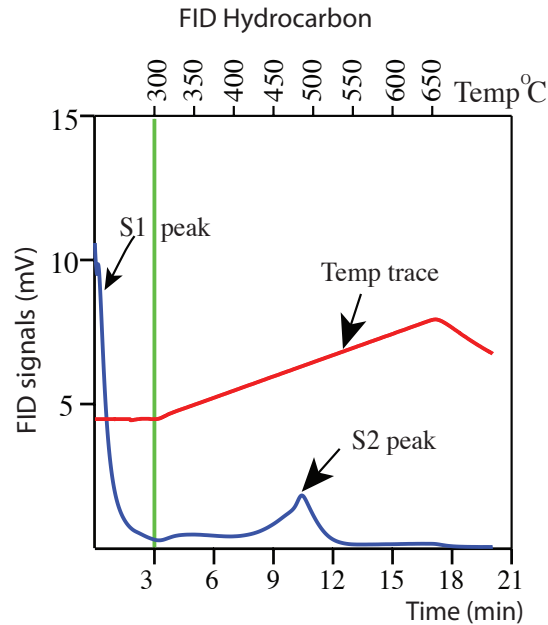


Figure 3.10. Shows the remaining hydrocarbon generating capacity (S2) in the Montney Formation, plotted with total organic carbon (TOC). Hydrogen index (HI) line indicates the kerogen type.

Thermal Maturity

Thermal maturity of organic rich sediment is the resultant effect of temperature driven reactions dependent upon time duration that convert sedimentary organic matter (source-rock) to oil, wet gas, and finally to dry gas and pyrobitumen (Peters and Cassa, 1994). Thermal maturity is conventionally classified into three categories: 1) immature; 2) mature; and 3) post-mature sources rocks (Waples, 1945; Peters and Cassa, 1994). Knowing a rock's remaining source capacity solves only one part of the source rock evaluation puzzle. It is also necessary to know what level of thermal maturity is represented by the source rock (Dembicki, 2009). Maturity can be estimated by several techniques (Waples, 1945; Tissot and Welte, 1978; Espitalie et al. 1985; Peters, 1986; Lafargue, et al. (1998). In this study, T_{max} and vitrinite reflectance (R_o) measurement were used in the determination of the thermal maturity of the Montney Formation in the study area. The key to using

maturity parameters effectively lies in evaluating the measured data carefully (and sometimes with skepticism), and whenever possible, it is better to obtain more than one maturity parameter (Waples, 1945). Thus, T_{\max} , vitrinite reflectance (R_o) and Production index (PI) were interpreted separately in this study, and then, a comparison between the three maturity parameters were synchronized to verify similarity or dichotomy between the three data.

The amount and composition of hydrocarbons generated from a particular kerogen vary progressively with increasing maturity (Killops and Killops, 2005). Thermal maturity of kerogen is commonly measured using T_{\max} and vitrinite reflectance (Héroux, et al., 1979; Barker, 1988,1991; Dembicki, 1984, Corcoran and Clayton, 2001; Dembicki, 2009), however, there are other parameters that are used as indicators of thermal maturity (Waple, 1945; Senfle and Landis, 1991). T_{\max} and transformation ratio for organic matter (OM) Type 1, II and Type III/IV, shows that the maximum paleotemperatures and vitrinite reflectance indicates the level of kerogen maturity (Tissot, et al., 1987).

Description: The Montney Formation Thermal Maturity – T_{\max}

T_{\max} is defined as the maximum pyrolysis temperature at which the maximum amount of hydrocarbon is released by kerogen (Espitalié et al., 1977). It is the maximum S2 peak in Rock-Eval pyrolysis (Fig. 3.11), the point at which the abundance of artificially generated hydrocarbons are at the greatest as a result of ramping up of temperature upto 550°C (Lafargue, et al., 1998; Lafargue, et al., 1998). The macromolecular kerogen network is cracked during pyrolysis to give an estimate of the thermal maturity of a source rock (Barker, 1974; Espitalié et al., 1977; Alixant et al., 1998).

T_{\max} values in analyzed core samples from the Montney Formation in the study area range from 347 _{T_{\max}} to 521 _{T_{\max}} (Appendix 3-A). The average T_{\max} values

range from $423_{T_{max}}$ to $567_{T_{max}}$ from each well and were plotted as T_{max} contour map to show the geographical distribution of thermal maturity within the study area in Fort St. John, northeastern British Columbia. Statistical distribution of the analyzed T_{max} values for the Montney Formation in the study area shows that > 90% of the reported T_{max} values are within $450_{T_{max}}$ and $528_{T_{max}}$.

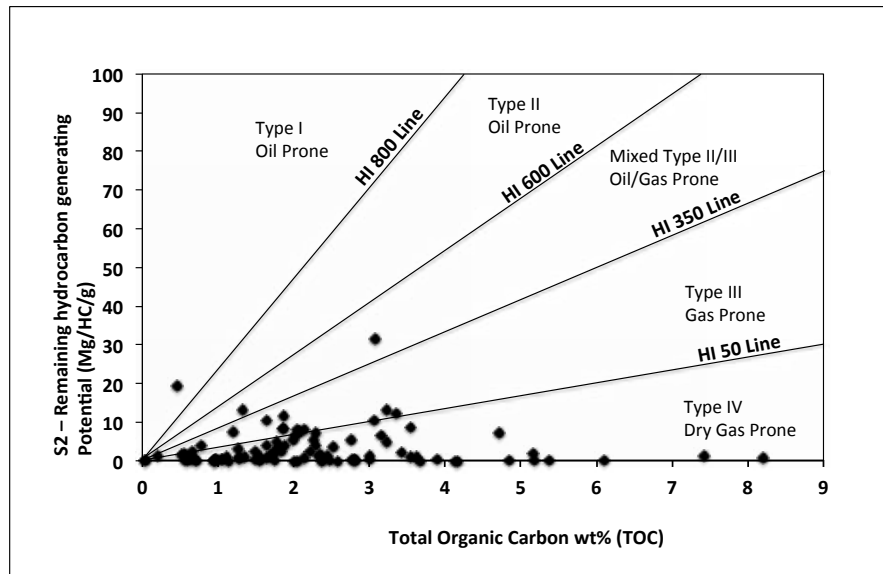


Figure 3.11. Shows S2 peak (remaining hydrocarbon generating capacity) for the Montney Formation, which corresponds to the T_{max} . The S1 peak is the liberated hydrocarbon during rapid artificial thermal cracking of kerogen during pyrolysis. Sample location: well 2-19-79-14W6 (depth: 2085 m).

Interpretation

The interpretation of thermal maturity using T_{max} criteria of Senfle and Landis (1991) indicates that more than 90% of the Montney Formation samples reported in this study are thermally matured (Fig. 3.12). The geographical distribution of T_{max} values in the study area prompted a consideration of what might be the controlling factors on thermal maturity and the relationships with geothermal gradient in the study area (Fig. 3.13). The understanding of the geothermal regime in sedimentary basin is important for the studies of the evolution of a sedimentary basin as well

as accumulation of hydrocarbons and other energy resources (Bachu, 1992). The generation of hydrocarbons (oil and gas) from any basin is dependent on the temperature reached by the organic-rich source rocks during their burial history (Bachu, 1991, 1993). Several workers (e.g. Gerland and Lennox, 1962; Angling and Beck, 1965; Ribach, 1981; Hitchon, 1984; Bachu, 1985; 1988; 1990; 1992; Bachu and Burwarsh, 1991; Majorowicz and Jessop, 1981; Majorowicz et al., 1984; 1985; 1986; Jones et al., 1985a,b) have reported the heat transfer processes (convection and conduction), observed geothermal pattern, thermal and hydraulic conductivities, heat generated internally in the crust by the decay of radioactive elements, regional scale distribution of geothermal gradient, hydrogeological effects in establishing geothermal pattern, and statistical distribution of geothermal

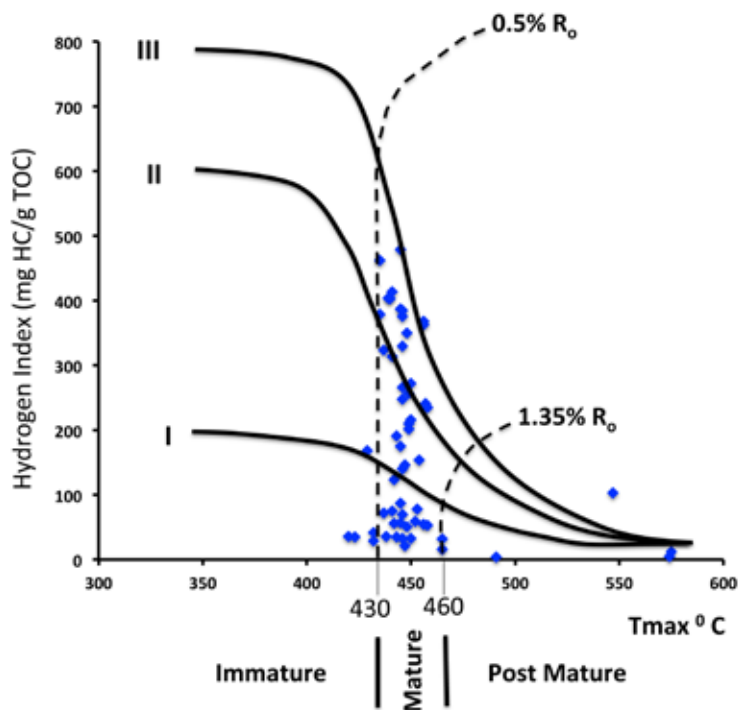


Figure 3.12. Thermal maturity of the Montney Formation determined with Tmax and vitrinite reflectance (R_0). The dotted line (R_0) is vitrinite reflectance calibrated with Tmax. This shows that the Montney Formation in northeastern British Columbia is extensively matured.

values in Western Canada Sedimentary Basin. Using geothermal calculations of Angling and Beck (1965); Bachu and Burwash (1991); Bachu (1991; 1992; 1993) in Western Canada Sedimentary Basin, a comparison of the distribution of T_{\max} in the study area shows no particular striking relationship with the distribution of geothermal gradient owing to the small size of the study area, but there appears to be somewhat higher values of T_{\max} along the NNW – SE direction in the vicinity around Fort St. John (Fig. 3.13), but T_{\max} progressively decreases in values eastwards into Alberta. Bachu (1992) shows a regional-scale (basin-wide) distribution of the internal geothermal gradient across the entire Western Canada Sedimentary Basin, which shows a NW – SE increase in geothermal gradients. Angling and Beck (1965) reported a northerly trending increase in heat flow, which was interpreted to be caused by crustal thinning. The controlling mechanisms of heat transfer in the Western Canada Sedimentary Basin are conduction and convection by moving fluids or flow of formation water (Bachu, 1992), and hydrogeological effects (Majorowicz and Jessop, 1981; Hitchon, 1984; Majorowicz et al., 1984; 1985; 1986; Jones et al., 1985a,b; Bachu, 1985; 1988; 1992; Bachu, and Burwash, 1991; Bachu and Cao, 1992). This interpretation of geothermal distribution provides the underlying factors responsible for T_{\max} values in the study area. The geothermal gradient provides the answer to thermal maturity differences evident by the T_{\max} values in the Montney Formation within the study area in northeastern British Columbia (where the Montney Formation is mainly a gas prone reservoir) and in Alberta (the Montney Formation is mostly oil prone). The type of hydrocarbons produced (oil vs. gas) in the two Provinces (British Columbia and Alberta) from the Montney Formation is interpreted herein to be related to geothermal gradient that differentially affected the thermal maturity in British Columbia and Alberta (Bachu, 1992; Angling and Beck, 1965). The differential heating of the Montney Formation Kerogen at different temperatures (higher) in British Columbia than in

Alberta (lower) as shown by Angling and Beck (1965) is responsible for the type of hydrocarbon that have been generated in Montney Formation in British Columbia and in Alberta.

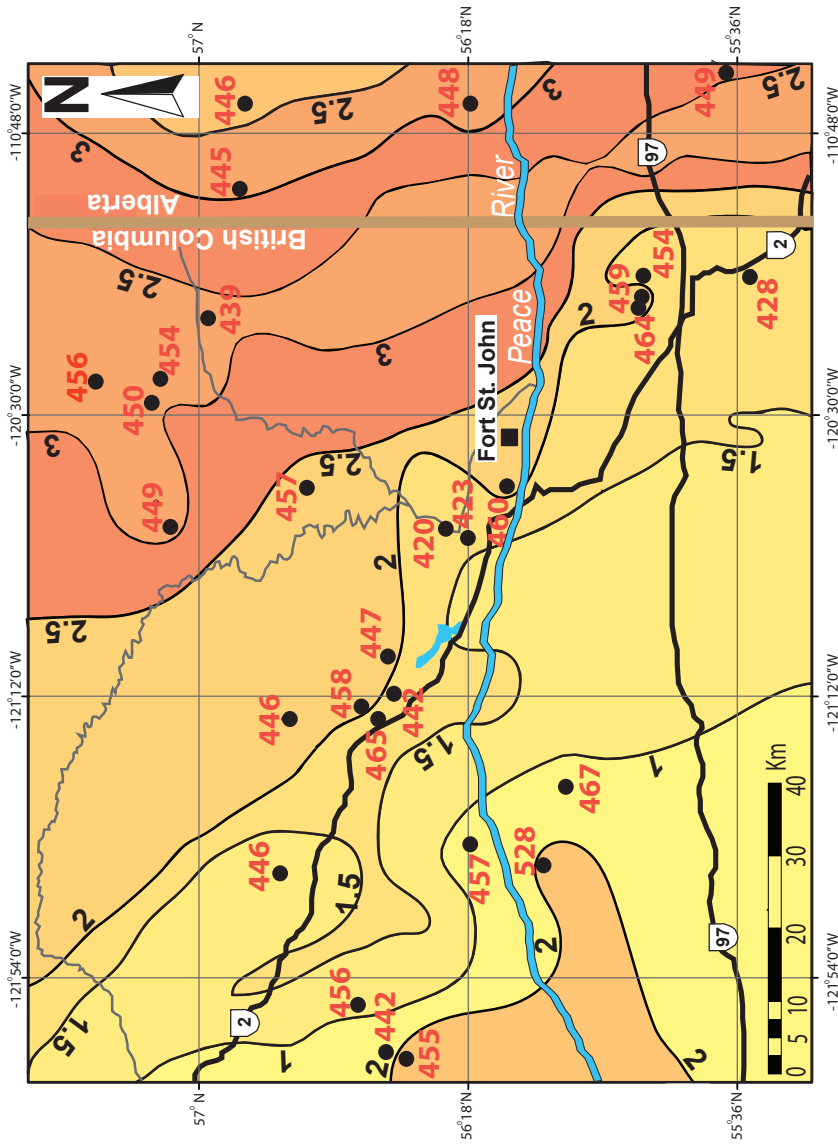


Figure 3.13. The Montney Formation average Tmax (°C) map. Tmax values are posted over TOC map to show geographical distribution of source rock quality (TOC), and thermal maturity of source rock. The red dots represent wells with Rock-Eval data. Evidently, the Montney Formation kerogen is thermally matured, and it is within the ‘peak gas’ generation window in the study area, northeastern British Columbia, and northwestern Alberta as shown by the average Tmax values.

Description: The Montney Formation Thermal Maturity – Vitrinite Reflectance

The vitrinite data analyzed from the Montney Formation in this study is shown in Table 3.4). The available organic matter for each samples analyzed varies from 0 – 6 (Table 3.4). The vitrinite particles available for analysis in the analyzed samples range from 0 – 4. The measurement of vitrinite particles involves the recording of the percentage of incident light, usually at a wave length of 546 nm, reflected from vitrinite particles under oil immersion (Stach et al., 1982). The none availability (zero values in Table 5) of vitrinite particles, and very low vitrinite particles in the organic matter resulted in the low level of confidence as shown in Table 3.4 (using a ranking scale 0 – 9). The level of thermal maturation of the Montney Formation kerogen as revealed by vitrinite reflectance (R_o) analysis shows that data values range from (R_o 0.74 to 2.09%). Samples that have no vitrinite particles to measure are designated null (zero values) of vitrinite in Table 3.4.

Table 3.4. Vitrinite reflectance measured from the Montney Formation sediments in British Columbia.

Sample No.	Well Location	Depth (m)	Primary vitrinite pop statistics			Polish	Organic matter available	vitrinite available	Confidence in measurement (rated on 0 – 9) bases	TOC wt (%)
			Mean	SD	n					
C-492838	A-20-H-93-P-9	2455.00	1.50	0.035	2	7	2	1	3	2.42
C-492839	A-20-H-93-P-9	2457.00	--	--	0	7	2	0	2	0.72
C-492837	A-20-H-93-P-9	2460.57	1.81	0.000	1	7	1	1	2	0.94
C-492841	d-39-F-93-P-9	2668.88	--	--	0	7	1	0	2	1.00
C-492840	d-39-F-93-P-9	2685.40	1.34	0.134	2	8	1	1	2	2.37
C-492844	7-13-79-15-w6	2055.22	1.49	0.152	6	8	6	5	6	3.54
C-492843	7-13-79-15-w6	2078.50	1.52	0.064	2	8	1	1	2	0.90
C-492842	7-13-79-15-w6	2084.50	1.27	0.084	3	8	1	1	3	1.29
C-492846	2-19-79-14-w6	2048.00	1.18	0.151	3	8	1	1	3	1.43
C-492847	2-19-79-14-w6	2069.50	1.22	0.150	4	7	1	1	3	1.27
C-492845	2-19-79-14-w6	2085.00	1.04	0.000	1	7	1	1	2	2.13
C-492848	11-04-79-14-w6	2064.10	--	--	-	--	--	--	--	1.66
C-492849	11-04-79-14-w6	2073.20	1.18	0.113	4	7	1	1	2	0.95
C-492850	9-29-79-14-w6	1999.00	1.14	0.120	6	7	1	1	3	1.96
C-492852	13-16-79-14-w6	2015.00	1.04	0.032	3	7	1	1	2	1.63

Table 3.4. Continued.

Sample No.	Well Location	Depth (m)	Primary vitrinite pop statistics			Polish	Organic matter available	vitrinite available	Confidence in measurement (rated on 0 – 9) bases	TOC wt (%)
			Mean	SD	n					
C-492853	b-39-HI-93-P-9	2042	--	--	0	7	0	0	2	0.32
C-492854	b-32-G-93-P-9	2707	--	--	0	7	0	0	2	1.16

Interpretation

Vitrinite is a type of kerogen particle formed from humic gels thought to be derived from the lignin-cellulose cell walls of higher plants (Teichmüller, 1989). Vitrinite is a common component of coals, and the reflectance of vitrinite particles was first observed to increase with increasing time and temperature in a predictable manner in coals (Teichmüller, 1982).

Based on the vitrinite reflectance data of the Montney Formation in the study area, the results indicate that vitrinite reflectance (R_o) range from 0.74% – 2.09%, which is interpreted herein as primarily a gas prone kerogen (Fig 3.14) using standard vitrinite interpretation criteria (Table 3.2) of Senfle and Landis (1991) and Dow (1977). This interpretation has credibility because it corresponds to the same indication of gas window maturity using T_{max} interpretive standard of Senfle and Landis, (1991) as shown in Figure 3.12. However, it is common, or not unusual to encounter low availability of vitrinite particles during laboratory analysis as seen in some of the samples shown in Table 3.4.

The low, or none availability of vitrinite particles can result to difficulty in differentiation of primary vitrinite coupled with insufficient grains to make a reliable determination of the reflectance of the samples constitute factors that affect the quality of vitrinite reflectance (Corcoran and Clayton, 2001). Similarly, inconsistencies or error can result from the measurements of vitrinite reflectance (Dembicki, 1984; 2009), and variation in chemical composition of vitrinite may lead to invalid comparison of vitrinite gradient (Corcoran and Clayton, 2001). Although the aforementioned analytical mechanics makes vitrinite reflectance results to be viewed with skepticism (Waples, 1945), the method remains useful and conventionally implored in thermal maturity determination (Héroux, et al., 1979).

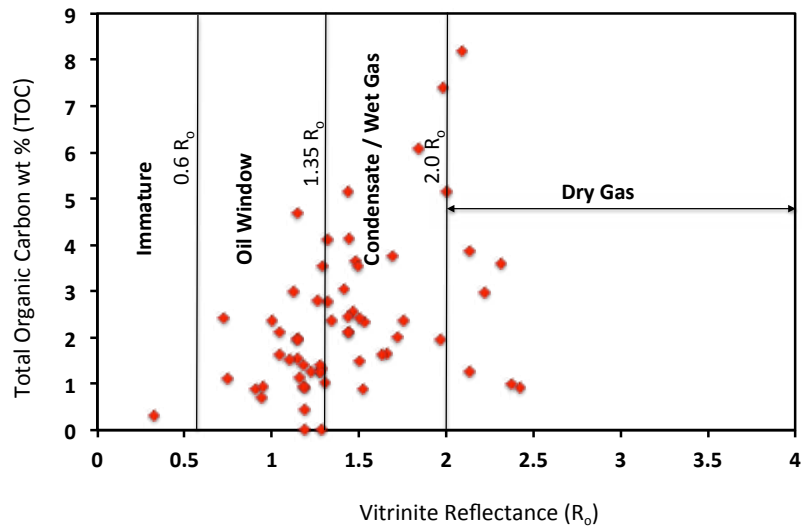


Figure 3.14. Total Organic carbon (TOC) vs. vitrinite reflectance (R_o) showing the thermal maturity of the Montney Formation source rock, and hydrocarbon generating phases in in the Montney Formation sediments from study area, northeastern British Columbia.

Vitrinite reflectance in source-rock kerogen is related to the hydrocarbon generation history of sediments (Corcoran and Clayton, 2001). Vitrinite reflectance has been successfully used to demonstrate the reliability of the technique as indicator of organic maturation in source-rock, indicating potential areas of oil and gas generation within a prospect (Peter and Cassa, 1994). Vitrinite reflectance (R_o) is one of the methods used in evaluation of thermal transformation of organic-rich sedimentary rocks (H eroux, et al., 1979) in hydrocarbon exploration (Hunt, 1979; Waples, 1981; Tissot and Welte, 1984; Tissot et al., 1987). Vitrinite increases during thermal maturation due to complex, irreversible aromatization reactions (Peters and Cassa, 1994). It has been established that vitrinite reflectance correlates well with coal rank, which is primarily a function of time and temperature (Van Krevelen, 1961; Tschamler and De Ruiter, 1963).

The thermal transformation of vitrinite can be related to geothermal and paleotemperature (Corcoran and Clayton, 2001), which proceeds by a series of

irreversible chemical reactions that cause organic matter alteration due to thermal cracking (Hood et al. 1975; Heroux, et al., 1979). Thus, vitrinite reflectance is used as thermal maturation indicator that provides a means of determining the maximum temperature exposure of sedimentary rocks (Hood et al. 1975; Heroux, et al., 1979).

Description: Thermal maturity – Production Index (PI)

The production index (PI) data of the Montney Formation from the Rock-Eval analysis shows that the PI has very low values (range from 0.11 to 2.6). More than 90% of PI values from the study area are less than 1. The relationship between production index (PI) and T_{max} is shown in Figure 3.15).

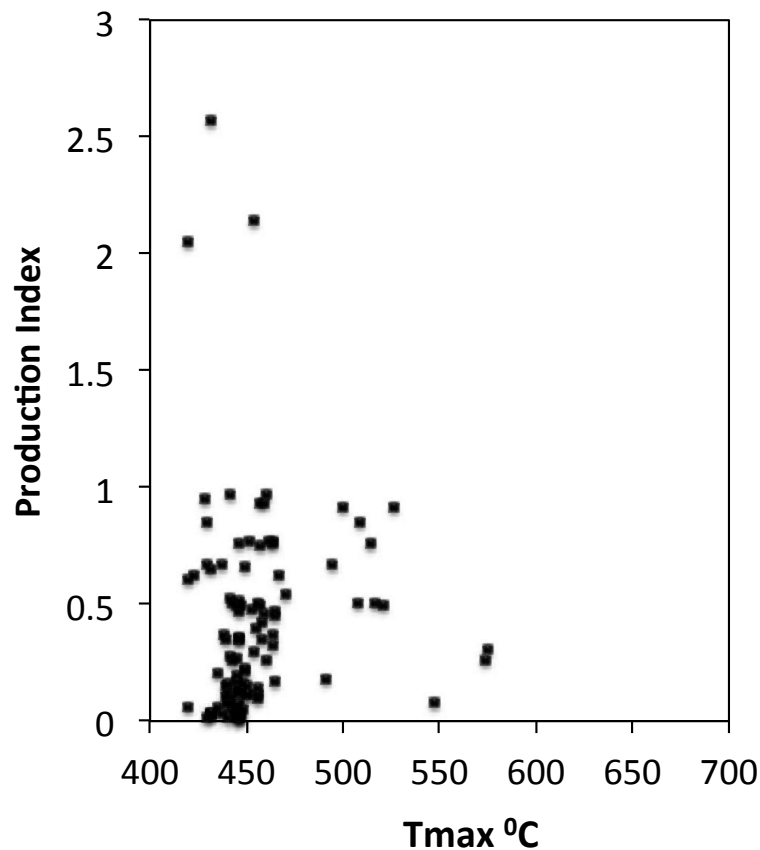


Figure 3.15. Shows that the Montney Formation kerogen is thermally matured, and extensively charged with gas.

Interpretation

The production index (PI) is also a parameter that is used in conjunction with other thermal maturity parameters to indicate type of hydrocarbon generated (Peters and Cassa, 1994), and was interpreted based on the geochemical parameters describing thermal maturation (Table 3.5). The PI values in this study indicate that the Montney Formation sediment is mostly matured and post matured (Table 3.5 and Fig. 3.15).

Table 3.5. Geochemical parameters describing the level of thermal maturation (Peters and Cassa, 1994).

Stage of Thermal Maturity	Maturation		
	R _o (%)	T _{max} (°C)	PI [S ₁ /(S ₁ + S ₂)]
Immature	0.2–0.6	<435	<0.10
Mature			
Early	0.6–0.65	435–455	0.10–0.15
Peak	0.65–0.9	455–450	0.25–0.40
Late	0.9–1.35	450–470	>0.40
Postmature	>1.35	>470	-

Reservoir Characteristics of the Montney Formation.

Porosity Data – Description

Approximately thirty data point from the Montney Formation samples were analyzed for porosity (porosity of bulk volume and gas filled porosity) in relation to depth (Fig. 3.16). The data show a side-by-side porosity value that nearly mimic bulk volume porosity and gas filled porosity (Fig. 3.16). The highest value of porosity (Table 3.6) from well 16-17-82-25W6 is 5.67% and lowest value is 1.22%. Some cores of the Montney Formation have porosity greater than 5.6% (Fig. 3. 17). Visual observation of porosity from thin-section petrographic analysis revealed vuggy porosity (Fig. 3.18)

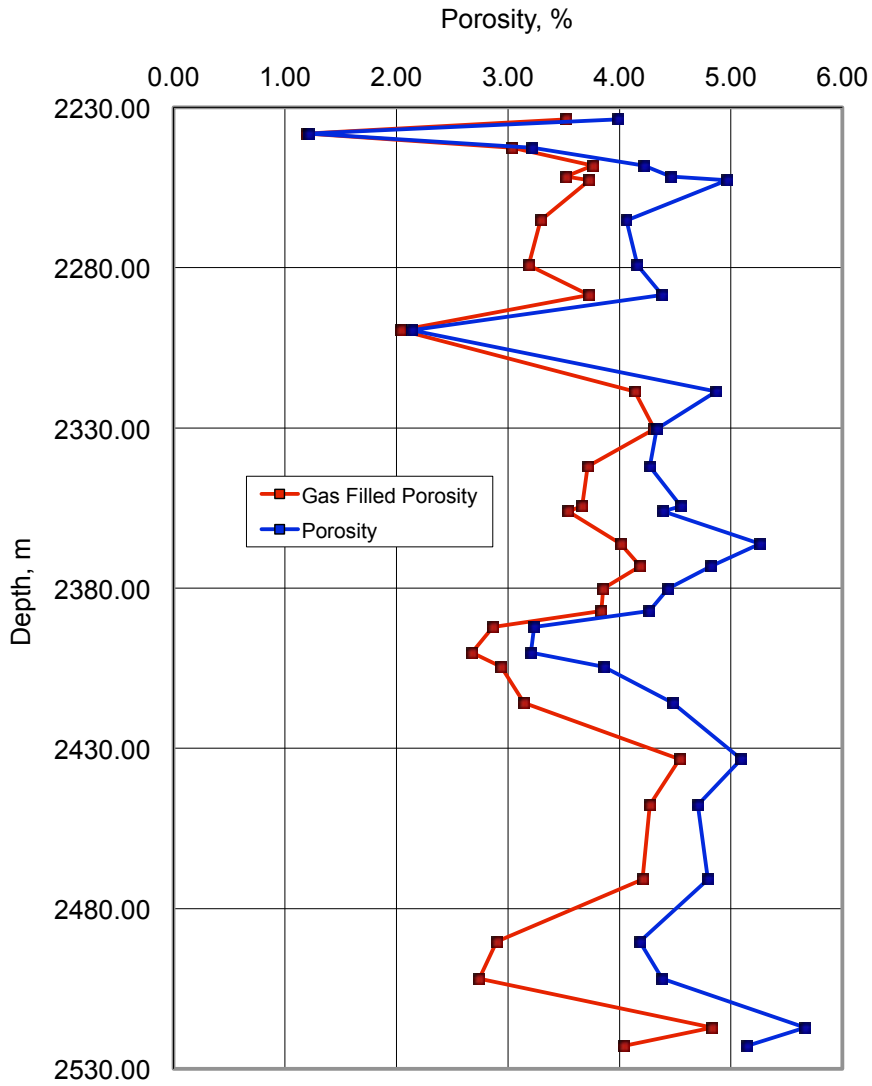


Figure 3.16. Shows porosity and gas filled porosity of the Montney Formation (well 16-17-82-25W6). The graph shows very excellent correlation between porosity and gas filled porosity. (Data source: B.C. Oil and Gas Commission).

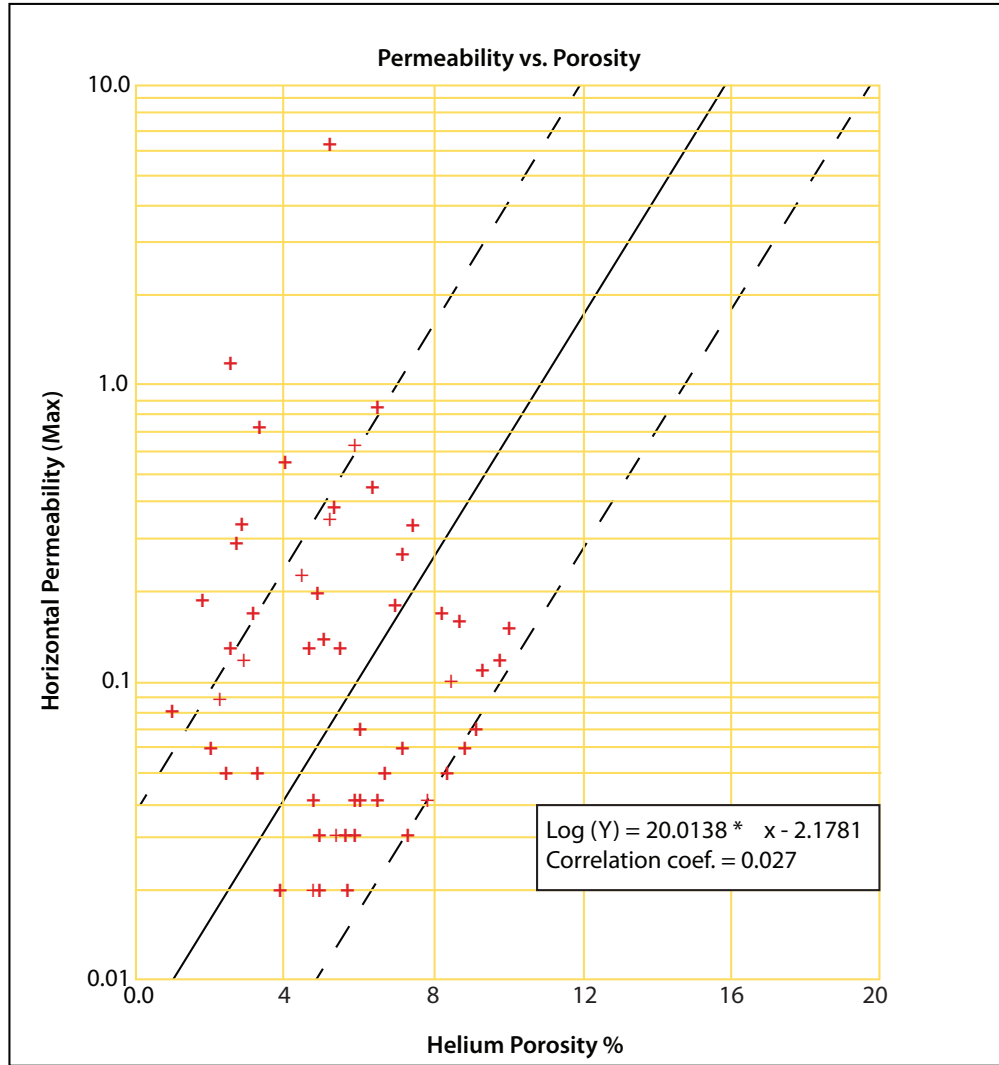


Figure 3.17. Porosity vs. permeability crossplot for the Montney Formation, well: 2-19-79-14W6 (depth 2037.40 - 2091.90 m). Data source: B.C. Oil and Gas Commission.

Interpretation

Porosity is dependent on grain texture, which is determined largely by grain shape, roundness, grain size, sorting, grain orientation, packing, and chemical composition (cement precipitation and diagenetic modification). Distribution of pore structure, or pore-throat controls the porosity in tight rock matrix. The low values of measured porosity as observed in thin-section petrography are evidence

of a combination of textural heterogeneity, mineral alteration, and transformation produced by diagenesis in the Montney Formation.

The petrographic analysis show evidence of uniformity of grain size, and sorting of the Montney Formation sediments, which is dominantly siltstone with matrix of clay admixed very fine-grained sandstone and dolomite, precludes the effective inter-particle (inter-void communication), thus, porosity is considerably reduced as evident by the measured porosity values (Table 3.6).

Observed vuggy porosity in some interval in the Montney Formation is associated with biogenic modification of textural fabric (Fig. 3.18). The observed porosity in thin-section is partly associated with organic matter dissolution and replacement by pyrite, and biogenically produced secondary porosity. Also, relatively higher porosity in the Montney Formation is associated with bedding plane fractures.

Bedding plane porosity observed in the Montney Formation results from varieties of concentrated parallel lamination to bedding planes. The larger geometry of many petroleum reservoirs are controlled by such bedding planes primarily formed by the differences of sediments calibre or particle sizes and arrangements influenced by the depositional environment (Tiab and Donaldson, 2004).

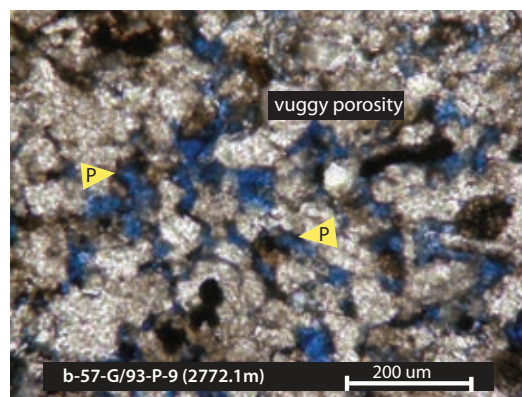


Figure 3.18. Microphotograph showing dolomitic siltstone facies and the associated vuggy porosity resulting from dissolution of material. Yellow arrow labeled 'P' is pointing to vuggy porosity.

Table 3.6. Petrophysical characterization of the Montney Formation in well 16-17-82-25W6 (Data source: B.C Oil and Gas Commission).

No. of Samples	Depth (m)	As Received Bulk Density (ρ_{bc})	As Received Grain Density (ρ_{gc})	Dry Grain Density (ρ_{gcd})	Porosity (% of BV)	Water Saturation (% of PV)	Gas Saturation (% of PV)	Mobile Oil Saturation (% of PV)	Gas Filled Porosity (% of BV)	Bound Hydrocarbon Saturation (% of BV)	Bound Clay Water (% of BV)	Pressure-Decay Permeability (mD)
1	2233.82	2.607	2.702	2.711	3.98	7.25	88.40	4.35	3.52	0.00	2.21	0.000216
2	2238.12	2.684	2.716	2.717	1.22	0.81	98.37	0.81	1.20	0.17	0.19	0.000114
3	2242.62	2.585	2.666	2.669	3.22	0.30	94.36	5.35	3.04	0.07	1.33	0.000194
4	2248.22	2.481	2.578	2.586	4.22	8.92	89.12	1.96	3.76	0.15	2.30	0.000297
5	2251.62	2.462	2.552	2.568	4.46	17.52	78.81	3.67	3.52	0.06	2.55	0.000254
6	2252.72	2.445	2.539	2.560	4.97	21.63	75.10	3.27	3.73	0.06	2.80	0.000227
7	2265.32	2.582	2.670	2.684	4.06	14.76	81.02	4.22	3.29	0.00	1.81	0.000132
8	2279.32	2.554	2.638	2.655	4.16	19.30	76.62	4.09	3.19	0.07	2.64	0.000172
9	2288.52	2.579	2.679	2.691	4.38	11.08	85.01	3.91	3.73	0.00	2.38	0.000140
10	2299.52	2.757	2.814	2.817	2.14	0.48	95.23	4.30	2.04	0.00	0.30	0.000110
11	2318.62	2.569	2.680	2.694	4.87	10.14	84.98	4.88	4.14	0.00	2.37	0.000118
12	2330.42	2.570	2.686	2.686	4.33	0.22	99.56	0.22	4.31	0.16	0.94	0.000151
13	2342.02	2.608	2.709	2.720	4.27	7.45	86.91	5.64	3.71	0.00	2.03	0.000118
14	2354.42	2.599	2.698	2.714	4.55	14.13	80.60	5.27	3.67	0.00	3.36	0.000166
15	2356.06	2.600	2.695	2.711	4.39	17.48	80.55	1.97	3.54	0.00	3.07	0.000133
16	2366.12	2.532	2.637	2.660	5.26	19.34	76.23	4.44	4.01	0.00	3.08	0.000221
17	2373.12	2.549	2.661	2.673	4.82	8.38	86.75	4.87	4.18	0.00	2.44	0.000137
18	2380.12	2.540	2.642	2.652	4.44	11.22	86.87	1.91	3.85	0.08	2.54	0.000151
19	2387.12	2.610	2.715	2.723	4.27	4.51	89.85	5.64	3.84	0.00	2.31	0.000134
20	2392.12	2.658	2.737	2.744	3.24	3.93	88.52	7.55	2.86	0.00	1.17	0.000110
21	2400.12	2.651	2.724	2.734	3.20	8.87	83.49	7.64	2.68	0.00	2.16	0.000131
22	2404.57	2.649	2.730	2.747	3.86	17.49	76.17	6.34	2.94	0.00	3.33	0.000162
23	2415.82	2.654	2.741	2.766	4.48	24.28	70.25	5.47	3.15	0.00	3.43	0.000161
24	2433.42	2.575	2.697	2.708	5.09	7.47	89.17	3.36	4.54	0.07	2.66	0.000145
25	2447.64	2.586	2.701	2.710	4.70	4.06	90.86	5.08	4.27	0.00	4.20	0.000237
26	2470.92	2.598	2.712	2.724	4.79	7.20	87.79	5.00	4.21	0.00	4.12	0.000207
27	2490.32	2.642	2.721	2.744	4.18	26.55	69.26	4.19	2.90	0.07	4.38	0.000214
28	2501.82	2.611	2.685	2.714	4.38	31.91	62.59	5.50	2.74	0.00	5.50	0.000222
29	2517.12	2.566	2.697	2.713	5.67	10.53	85.29	4.18	4.83	0.00	4.07	0.000337
30	2522.82	2.570	2.678	2.699	5.15	18.08	78.59	3.32	4.04	0.07	4.84	0.000312

Interpretation

Apart from the porosity of a reservoir, the ability of the rock to allow the flow of fluid through the interconnected pores, which is permeability, is a crucial reservoir parameter in the evaluation of any hydrocarbon play. The permeability of a rock depends on its effective porosity; which is controlled by grain size distribution, degree of sorting, grain shape, packing, and degree of cementation (Tiab and Donaldson, 2004; Chehrazi and Rezaee, 2012). The evaluation of permeability of heterogeneous clastic rocks from core or downhole is one of the most important goals of reservoir geoscience (Ahmed, et al., 1991).

The results from permeability analyses in this study are related to the overall textural heterogeneity, porosity, and in part, related to ichnofabric modification. The Montney Formation is composed of dolomitic, silt-size grains and subordinate very fine-grained sandstone. The implication of the grains-size in-terms of permeability is in relation to the fact that smaller grain-sizes have smaller permeabilities than those with larger grain-sizes because smaller grain-sizes will produce smaller pores and smaller pore throats, which can constrain the fluid flow in a manner lower than flows in larger grains, which produce larger pore throats (Chehrazi and Rezaee, 2012). Furthermore, the smaller the grain-size, the larger the exposed surface area to the flowing fluid, which leads to larger friction between the fluid and the rock, and hence lower permeability (Chehrazi and Rezaee, 2012). Ehrlich et al. (1997) have shown that there is strong correlation between permeability and grain-size of unconsolidated sands and gravels, with permeability increasing exponentially with increasing grain-size (Ehrlich et al., 1997).

Intervals were bedding plane fractures and ichnofabric modification occurs shows relatively higher values in permeability. The observed porosity in thin-section (micron scale), shows that the porosity is associated with: 1) dissolution of organic matter or dolomitic material caused by diagenesis 2); bioturbation-

enhanced porosity resulting from burrows by organisms; and 3) fracture porosity along bedding planes. Pemberton and Gingras (2005) and Gordon, et al. (2010) have shown that reservoir enhancement in unconventional thinly bedded, silty to muddy lithologies of unconventional reservoir with low permeability can be enhanced by the activity of burrows.

In general, permeability fabrics and the distribution of porosity in flow media primarily reflect the lithofacies heterogeneities such as laminae, ichnofabric perturbation, the arrangement and packing of grains, or local alteration of grains, random pore-throat distribution, or diagenetic modification of rock fabric (Gingras, et al., 2005). The important role of bioturbation in reservoir enhancement lies in the fact that: 1) trace fossils (animal burrows, tracks, trails, excavation, etc.) possess chemical characteristics that differ from the surrounding sedimentary media; 2) trace fossils modifies pore-throat distribution; 3) trace fossils act as loci of cementation; and/or dissolution during early diagenesis; 4) trace fossils serves as permeability conduit pipes interlinking burrows that consequently increases both vertical and horizontal permeability ($k_v = k_h$) thereby influencing the distribution of porosity and permeability within a permeable sedimentary media (Gingras, 2005).

Fluid Saturation – Data Description

Data analyzed for fluid saturation (gas saturation, mobile oil saturation, water saturation, and bound hydrocarbon saturation) indicates that water saturation is the second highest fluid, next to gas saturation; while, mobile oil saturation and bound hydrocarbon saturation (Fig. 3.20) are negligible in comparison with gas saturation or water saturation. By far, gas saturation is very high through out the interval of measurement, yielding as high as 99.56% at the depth of 2330.42m and the lowest value of gas saturation is 70.25% at the depth of 2415.82m (Fig. 3.4).

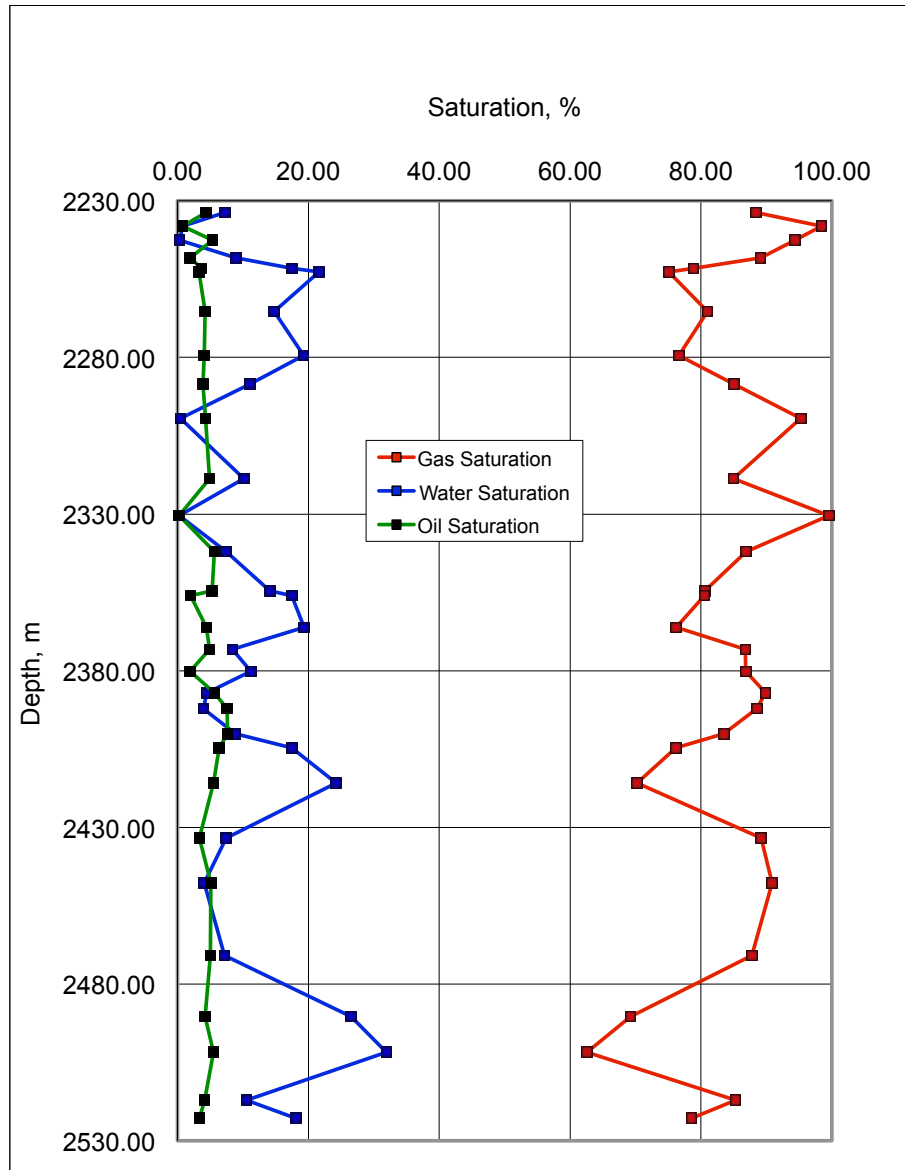


Figure 3.20. Illustrates fluid saturation (gas, oil, and water) of the Montney Formation from well 16-17-82-25W6, northeastern British Columbia (Data source: B.C. Oil and Gas Commission).

Interpretation

The amount of fluid in pore volume of a rock occupied by formation fluid (oil, gas, and water) refers to fluid saturation. (Asquith and Krygowski, 2004).

Results from this study shows that gas saturation is the most dominant fluid in the interstitial pores of the Montney Formation sediment (Fig. 3.20) varying from 99.64% to 62.59% through the depth profile. The oil saturation shows a near consistency graph level, particularly indicating a very low (0.81% to 7.64%) oil saturation through the depth profile. The implication of high gas saturation confirms that the Montney Formation in northeastern British Columbia is charged with gas. Water saturation varies significantly in an inversely proportional correlative pattern with gas saturation. The relationship of water saturation with gas saturation is interpreted in relation to the proportion of the ratio of gas to water in the pore volume. The relative low water saturation is crucial because water in pore space of low-permeability occupies critical pore-throat volume and can greatly diminish hydrocarbon permeability, even in rocks at irreducible water saturation (Castles and Brynes, 2005). Because of small pore-throat size, low-permeability, gas-producing sandstones are typically characterized by high water saturation and high capillary pressure (Thomas and Ward, 1972; Dutton et al., 1993).

DISCUSSION

Source-rock quality

For source-rock to have economic potential or exploration prospect, sufficient organic matter (OM) must have generated hydrocarbons. The measure of the quality of source-rock is the total organic carbon content (TOC) and the guidelines for ranking source rock quality were proposed by Peters (1986): 1) poor TOC richness range from 0.00 -0.50 wt % in shale; while in carbonates TOC range from 0.00 – 0.12 wt %; 2) fair TOC range from 0.50 – 1.00 wt % in shale; while in carbonates TOC range from 0.25 – 0.50 wt %; 3) good TOC range from 1.00 – 2.00 wt % in shale; while in carbonates TOC range from 0.25 – 0.50; 4) very good

TOC range from 2.00 – 4.00 wt % in shale; while in carbonates TOC range from 0.5 – 1.00 wt %; and 5) excellent TOC starts at values >4.00 wt % in shale; while in carbonates TOC must be >1.00 wt %.

Using the premise above as proposed by Peters (1986), the Montney Formation in the study area, has TOC content that is variably and statistically distributed in the order of highest percentile into low TOC (<1.5wt%), medium (1.5 – 3.5wt%), and high (>3.5wt%). Based on these results, the Montney Formation in the study area has good total organic carbon (TOC) richness (Fig. 3.16). In addition to the TOC content, The Montney Formation Kerogen has been interpreted and classified into: 1) Type III kerogen, which is primarily a gas prone kerogen (Waples, 1945; Peters, 1986; Dembicki, 2009); 2) Type IV kerogen, which is inertinite (gas prone), composed of hydrogen poor constituent, difficult to distinguish from type III kerogen by using only Rock-Eval pyrolysis; and 3) mixed Type II/II kerogen, which is oil prone (Waples, 1945; Peters, 1986), relatively rich in hydrogen and characterized by materials such as spores and pollen grains of land plants, marine phytoplankton cysts, some leaf and stem cuticles (Waples, 1945; Jacobson, 1991).

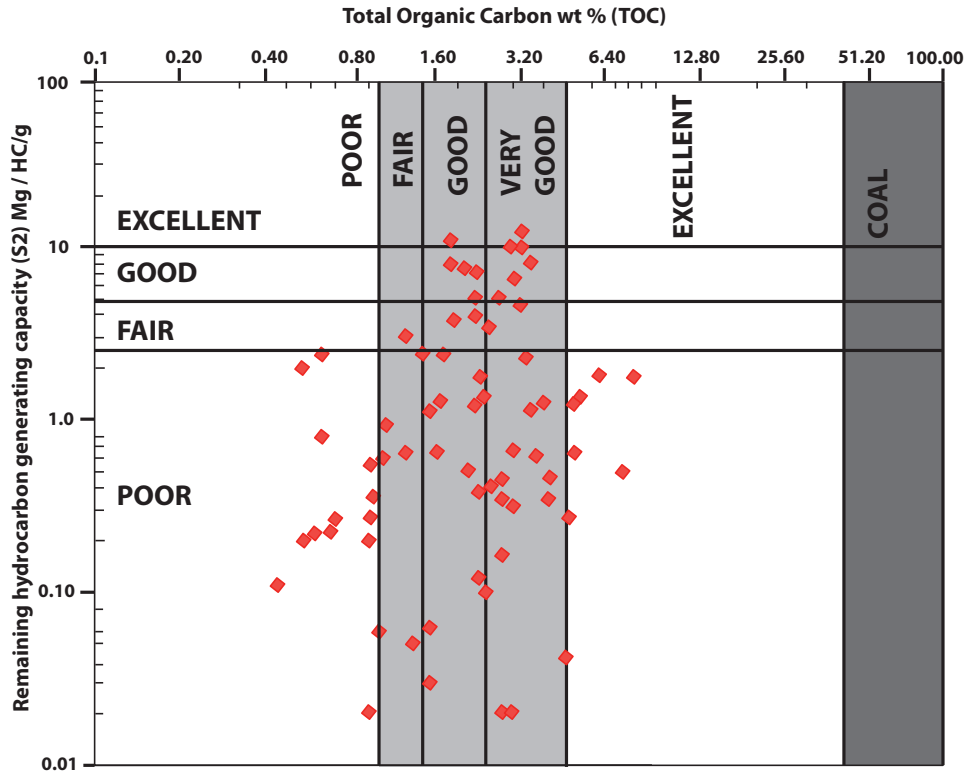


Figure 3.21. A cross plot showing total organic carbon (TOC wt%) values and S2 values (the amount of hydrocarbon formed during thermal decomposition of the kerogen). The higher S2 values indicate greater hydrocarbon generating potential. In general, the S2 and TOC values show that the Montney Formation in the study area, northeastern British Columbia has good source rock quality.

Thermal Maturity

The Montney Formation exhibits different thermal maturities (immature, mature, and post-mature). However, statistical distribution of the T_{max} values in the Montney Formation within the study area shows that > 95% of the reported T_{max} values are within 430 and 528 T_{max} , which is within the gas window (Senfle and Landis (1991). Some of the sediments are thermally over-matured (Fig. 3.12). Likewise, the vitrinite reflectance (R_o) results in this study shows that the Montney Formation in the study area is thermally matured, and it is composed mainly of gas with some oil (Fig. 3.14). A comparison of the T_{max} data, vitrinite reflectance data, and production index (PI) with show strong agreement and match very well in

terms of using multiple maturity parameters as argued by Waples (1945) as a better method of assessing the accuracy of thermal maturity index. The agreement of the T_{max} , R_o and PI (Figs. 3.12, 3.14 and 3.15) data boost the credibility of the thermal maturity synthesized and reported for the Montney Formation herein.

Future Exploration Prospect

The prospect and potential of any hydrocarbon exploration is driven and dependent upon economics. Primary factors of significant importance used as a yardstick for prospect evaluation are: resource estimates (volume), reservoir thickness, porosity and permeability, source-rock characteristics, hydrocarbon type (oil prone, or gas prone, or mixture of both), and logistics.

Hydrocarbon in-place estimated for the Montney Formation in northeastern British Columbia is 187 TCF of natural gas (Walsh et al., 2006). A break down of this volume split almost in a ratio 5:1 for free gas and absorbed gas respectively. The volume of free gas is 155 TCF and that of the absorbed gas is 32 TCF (Walsh, et al., 2006). This volume of gas in the Montney Formation in British Columbia is enormously significant as a resource with strong economic potential.

Reservoir thickness is crucial in prospect evaluation. Isopach map for the Montney Formation in the study area around Fort St. John, northeastern British Columbia shows a maximum thickness of 320 meters along the NNW – SE (Fig. 3.22). The lateral extend of this thickness varies from 320 meters in the west, and thin to about 200 meters in the eastern portion of British Columbia along the Alberta boundary border due to erosional removal (Edwards, et al., 1994). With this hectometers thickness, unconventional resource development method that incorporates hydraulic fracturing and well stimulation will enhance gas production from the Montney Formation.

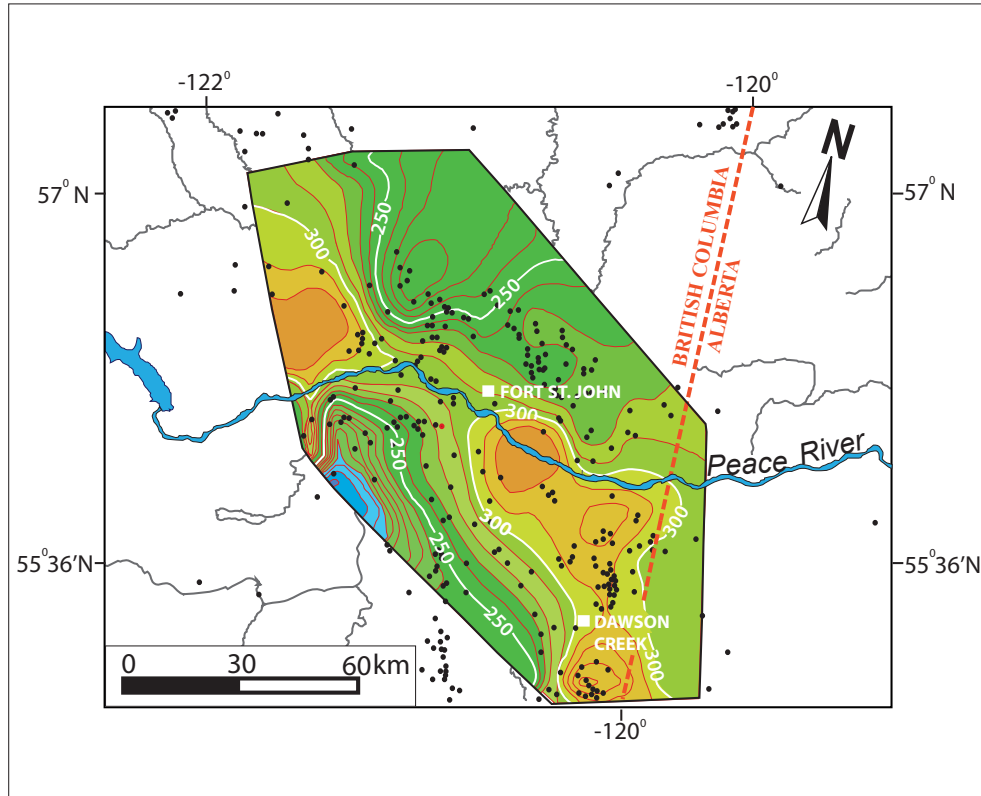


Figure 3.22. Isopach map of the Montney Formation showing the trends of thickness in the study area, northeastern British Columbia.

Porosity is a useful predictor of permeability, however, the major control on permeability is pore-throat size, which is related to grain size distribution, sorting, packing, and degree of cementation (Tiab and Donaldson, 2004; Castle and Brynes, 2005). The porosity of the Montney Formation is mostly very tight (2 – 10% porosity) tight gas reservoir classification standard of Haines (2006). However, relatively higher porosity of >10% was observed in thin-section as vuggy porosity (secondary porosity) due to dissolution of dolomitic materials. Because the Montney Formation in the study area is unconventional reservoir, porosity ranging from 10 – 12% or greater is considered modest for tight gas reservoir.

Evidently, the Montney Formation has very good source rock that is thermally matured, mainly a gas prone reservoir that lies within the ‘peak gas

window' with some oil because of the mixed Type II/III and Type IV kerogen in the study area. Based on the source-rock characteristic of the Montney Formation in the study area, future exploration prospect tight gas reservoir has economic promise in northeastern British Columbia.

Hydrocarbon in-place estimated for the Montney Formation in northeastern British Columbia is 187 TCF (Fig. 3.23) of natural gas (Walsh et al., 2006). A break down of this volume split almost in a ratio 5:1 for free gas and absorbed gas respectively. The volume of free gas is 155 TCF and that of the absorbed gas is 32 TCF (Walsh, et al., 2006). This volume of gas in the Montney Formation in northeastern British Columbia is enormously significant as a resource with strong economic potential.

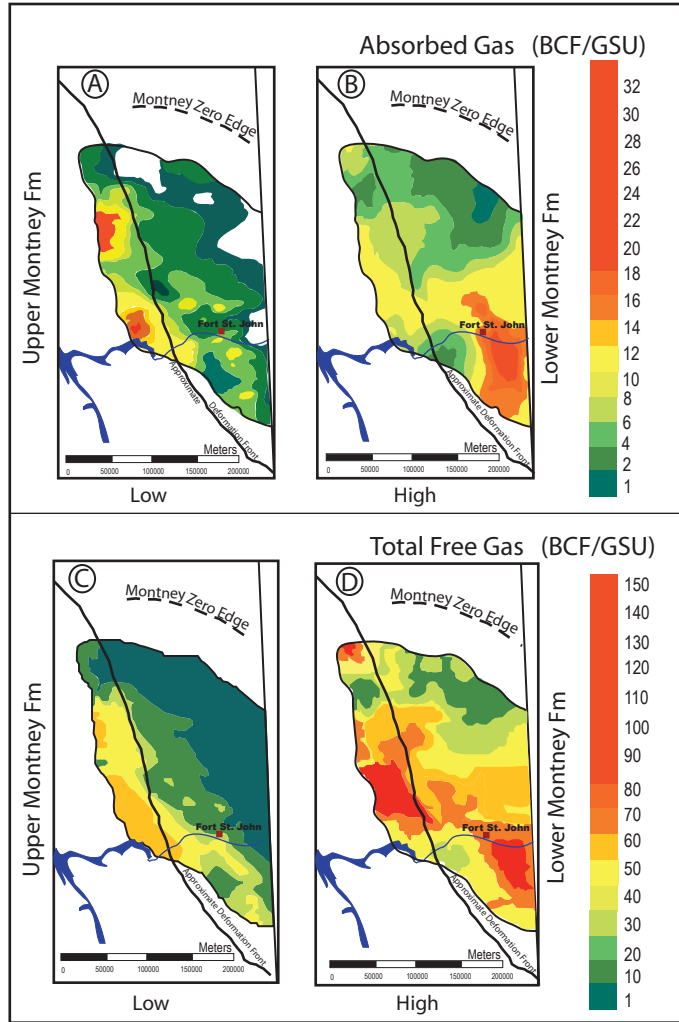


Figure 3.23. The Montney Formation gas in-place estimates (Walsh, et al., 2006).

CONCLUSIONS

Source-rock geochemistry is a pivotal step in the assessment of hydrocarbon reservoir. The Montney Formation source-rock characteristics presented in this study shows that TOC is statistically distributed into low (<1.5wt%), medium (1.5 – 3.5wt%), and high (>3.5wt%). The analysis and interpretation in this study shows that the Montney Formation in the study area is rich in TOC, and thermally matured. The type of hydrocarbon associated with the Montney Formation is mainly thermogenic gas, derived from kerogens of Type III/IV and mixed Type II/III kerogen. Thermal maturity Geographical distribution of the thermal maturity in the study area shows that the kerogen is vastly matured.

The prospect and potential of any hydrocarbon exploration is driven and dependent upon economics. Primary factors of significant importance used as a yardstick for prospect evaluation are: resource estimates (volume), reservoir thickness, porosity and permeability, source-rock characteristics, hydrocarbon type (oil prone, or gas prone, or mixture of both), and logistics. Fundamental properties affecting reservoir quality are rock texture and composition, gas in place (interstitial and adsorbed), permeability, organic content and degree of maturation, and pore pressure (Schlumberger, 2009). Other relevant parameters such as pore fluid saturation, clay type, and clay-bound water, are indirectly reflected by the above. Thus, most prolific gas-bearing units are identified based on measurements of total gas—canister desorption and a combination of adsorption isotherms and Tight Rock Analysis (TRA) to show gas-filled porosity, pore fluid saturations (water, gas, and mobile oil), clay-bound water, and bound.

Reservoir thickness is crucial in prospect evaluation. Isopach map for the Montney Formation in the study area around Fort St. John, northeastern British Columbia shows a maximum thickness of 320 meters along the NNW – SE (Fig.

3.22). The lateral extend of this thickness varies from 320 meters in the west, and thin to about 200 meters in the eastern portion of British Columbia along the Alberta boundary border due to erosional removal (Edwards, et al., 1994). With this hectometres thickness, unconventional resource development method that incorporates hydraulic fracturing and well stimulation will enhance gas production and success in the Montney Formation.

REFERENCES

- Alixant, J.L., W. Looyestijn, J. Hofman, 1998, Unusual logs in an unusual formation: NMR in Athel silicilyte, submitted for presentation at European, October 20 – 22. The Hague, Netherlands.
- Angling, F.M, and A.E. Beck, 1965, Regional heat flow in Western Canada. *Canadian Journal of Earth Sciences*, vol. 2, p. 176 – 182.
- Arnold, K.J., 1994, Origin and distribution of eolian sandstones in the Triassic Charlie Lake Formation, northeastern British Columbia. Unpublished M.Sc. Thesis, University of Alberta, Edmonton, 1 –320.
- Bachu, S., 1985, Influence of lithology and fluid flow on the temperature distribution in a sedimentary basin: A case study from the Cold Lake area, Alberta, Canada. *Tectonophysics*, vol. 120, p. 257 – 284.
- Bachu, S., 1988, Analysis of heat transfer processes and geothermal pattern in the Alberta Basin, Canada. *Journal of Geophysical Research*, vol. 93 (B7), p. 7767 – 7781.
- Bachu, S., 1990, On the effective thermal and hydraulic conductivity of binary heterogeneous sediments. *Tectonophysics*, vol. 190, p. 299 – 314.
- Bachu, S., 1992, Basement heat flow in the western Canada sedimentary basin. *Tectonophysics*, no. 222, Elsevier Science Publishers, Amsterdam, p. 119 – 133.
- Bachu, S. and R.A. Burwash, 1991, Regional-scale analysis of the geothermal regime in the Western Canada Sedimentary Basin. *Geothermics*, vol. 20 (5/6), p. 387 – 407.
- Bachu, S., and S. Cao, 1992, Present and past geothermal regimes and source rock maturation, Peace River Arch area, Canada. *American Association of Petroleum Geologists*, vol. 76, no. 10, p. 1533 – 1549.
- Barclay, J.E., Krause, F.F., Campbell, R.I., and Utting, J., 1990, Dynamic casting and growth faulting: Dawson Creek Graben Complex, Carboniferous-Permian Peace River Embayment, Western Canada, In: *Geology of the Peace River Arch*, S.C. O'Connell and J.S. Bell (eds.), *Bulletin of Canadian Petroleum Geology*, vol. 38A, p.115-145.
- Barker, C. E., 1974, Pyrolysis techniques for source rock evaluation. *American Association of Petroleum Geologists Bulletin*, vol. 58, 2349-2361.

- Barker, C.E., 1988, Geothermics of petroleum systems: implications of the stabilization of kerogen thermal maturation after a geologically brief heating duration at peak temperature. *In*: L.B. Magoon (ed.) Petroleum Systems of the United States. United States Geological Survey Bulletin, vol. 1870, p. 26 – 29.
- Barker, C.E., 1991. Implications to organic maturation studies of evidence for a geologically rapid increase and stabilization of vitrinite reflectance at peak temperature: Cerro Prieto geothermal system, Mexico. American Association of Petroleum Geologists Bulletin, vol. 75, p. 1852 – 1863.
- Berger, Z., M. Boast, and M. Mushayandebvu, 2009, The contribution of integrated HRAM studies to exploration and Exploitation of unconventional plays in North America. Part 2: Basement structures control on the development of the Peace River Arch's Montney / Doig resource plays. Reservoir, vol. 36, Issue 2, p. 40 – 44.
- Behar, F., Beaumont, V., and Penteado, H. L. De B., 2001, Rock-Eval 6 Technology: performances and Developments. Oil and gas Science and Technology -- Revue de l'Institut Francais du Petrole, vol. 56, p. 111-134.
- Cant, D.J., 1984, Possible syn-sedimentary tectonic controls on Triassic reservoirs, Halfway and Doig, Charlie Lake formations, west-central, Canadian Society of Petroleum Geologists, Calgary, p.45.
- Burnham, A.K., and J.J., Sweeney, 1989, A chemical kinetic model of vitrinite reflectance maturation. Geochimica et Cosmochimica Acta, vol. 53, p. 2649 – 2657.
- Cant, D.J., 1986, Hydrocarbon trapping in the Halfway Formation (Triassic), Wembly Field, Alberta, Bulletin of Canadian Petroleum Geology, vol. 34, p. 329-338.
- Claypool, G.E. and P.R. Reed, 1976, Thermal analysis technique for source rock evaluation: Quantitative estimate of organic richness and effects of lithologic variation. American Association of Petroleum Geologists Bulletin, vol. 60, p. 608-626.
- Corcoran, D.V. and G. Clayton, 2001, Interpretation of vitrinite reflectance profiles in sedimentary basins, onshore and offshore Ireland. *In*: The petroleum exploration of Ireland's offshore basins (P.M. Shannon, P.D.W. Haughton, and D.V. Corcoran, eds.). Geological Society, London, Special Publications, 188, p. 61 – 90.

- Core Lab, 2009, Reservoir characterization and production properties of gas shales. American Association of petroleum Geologists Bulletin, Short Course no. 10, Denver, Colorado.
- Clementz, D.M., G.J. Demaison, and A.R. Daly, 1979, Well site geochemistry by programmed pyrolysis. Proceedings of the 11th Annual Offshore Technology Conference, Houston, OTC 3410, vol.1, p. 465-470.
- Dembicki, H., Jr., 1984, An interlaboratory comparison of source rock data. *Geochemica et Cosmochimica Acta*, vol. 48, p. 2641 – 2649.
- Dembicki, H., Jr., 2009, Three common source rock evaluation errors made by geologists during prospect or play appraisals. *American Association of Petroleum Geologists bulletin*, vol. 93, no. 3, p. 341 – 356.
- Demaison, G.J., and G.T. Moor, 1980, Anoxic environments and oil source rock bed genesis. *American Association of Petroleum Geologists Bulletin*, vol. 64, p. 1179 – 1209.
- Demaison, G.J., A.J.J. Holck, R.W. Jones, and G.T. Moore, 1983, Predictive source bed stratigraphy; a guide to regional petroleum occurrence: *Proceedings of the 11th World Petroleum Congress, London*, vol. 2, p. 17 – 29.
- Dow, W., 1977, Kerogen studies and geological interpretations: *Journal of Geochemical Exploration*, vol. 7, p. 79–99.
- Edwards, D.E., Barclay, J.E., Gibson, D.W., Kvill, G.E., and Halton, E. 1994, Triassic strata of the Western Canada Sedimentary Basin. In: *Geological Atlas of the Western Canada Sedimentary Basin*. G.D. Mossop and I. Shetson (compilers). Canadian Society of Petroleum Geologists, p. 257–275.
- Eggbowaye, E.I., M.K. Gingras, and J-P., Zonneveld, 2011, The geochemistry of the Montney and Lower Doig tight gas reservoir, northeastern British Columbia. *American Association of Petroleum Geologists Abstract*, no. 90124. Accessed online on March 16, 2012: <http://sdsearch.datapages.com/data/search.do?selectedGroups=41&fullDoc=MONTNEY+FORMAT ION&Search.x=45&Search.y=12&Search=Search>
- Eggbowaye, E.I., J-P. Zonneveld, and M.K., Gingras, 2010, Tight gas reservoir evaluation in Montney and Lower Doig formations, northeastern British Columbia, western Canada. *American Association of Petroleum Geologists Abstract*, vol. 19, p. 66-67.

- Eggboway, E.I., Kravchinsky, V.A, Zonneveld, J-P, and Gingras, M.K, 2011, Magnetostratigraphy Dating and Correlation of the Lower Doig and Upper Montney Formations (Lower Triassic), Northeastern British Columbia, Western Canada. Canadian society of Petroleum Geologists, CSPG, CSEG, CWLS Convention Abstract, Calgary, Alberta, Canada, p. 1 – 5. Accessed online on February 22, 2012: <http://www.geoconvention.com/conference/technicalprogram/tuesday/pm-2/montney-i.html>
- Einsele, G., 2000, Sedimentary basins: evolution, facies, and sediment budget. Springer Verlag, Berlin, Heidelberg, 791p.
- Espitalié, J., F. Marquis, and I. Barsony, 1984, Geochemical logging: *In*: Analytical pyrolysis – Techniques and Applications (K.J. Voorhees ed.), Boston, Butterworth, p. 276-304.
- Espitalié, J., J. L. Laporte, M. Madec, F. Marquis, P. LePlat, J. Paulet, and A. Boutefeu, 1977, Methode rapide de caracterisation des roches meres de leur potentiel petrolier et de leur degre d'evolution: l'Institut Français du Pétrole, vol. 32, p. 23–42.
- Espitalié, J., G. Deroo, and F. Marquis, 1985, Rock-Eval pyrolysis and its applications: Revue de l'Institut Français du Pétrole, Rueil, France.
- Faraj, B., H. Williams, G. Addison, B. McKinstry, R. Donaleshen, G. Sloan, J. Lee, T. Anderson, R. Leal, C. Anderson, C. Lafleur, and J Ahlstrom, 2002, Shale potential of selected upper Cretaceous, Jurassic, Triassic and Devonian shale formations, in the WCSB of Western Canada: Implications for shale gas production. A report for Gas Technology Institute (GTI), Des Plaines, Illinois, USA.
- Gibson, D.W and J.E., Barclay, 1989, Middle Absaroka Sequence, the Triassic stable craton. In: Western Canada Sedimentary Basin: A Case History, B.D. Ricketts (ed.). Canadian Society of Petroleum Geologists, p. 219–231.
- Gibson, D.W. 1975, Triassic rocks of the Rocky Mountain Foothills and Front Ranges of northeastern British Columbia and west-central Alberta, Geological Survey of Canada, Bulletin 247, 61p.
- Gibson, D.W. 1993, Triassic. In: Sedimentary Cover in the Craton of Canada. D.F. Stottand J.D. Aitken (eds.). Geological Survey of Canada, Geology of Canada no. 5, p. 294–320.

- Gibson, D.W and Barclay, J.E. 1989, Middle Absaroka Sequence, the Triassic stable craton. In: *Western Canada Sedimentary Basin: A Case History*. B.D. Ricketts (ed.). Canadian Society of Petroleum Geologists, p. 219–231.
- Gibson, D.W and Edwards, D.E. 1990, An overview of Triassic stratigraphy and depositional environments in the Rocky Mountain Foothills and Western Interior Plains, Peace River Arch area. *Bulletin of Canadian Petroleum Geology*, vol. 38A, p. 146–158.
- Garland, G.D. and D.H. Lennox, 1962, Heat flow in western Canada. *Geophysical Journal*, vol. 6, p. 245 – 262.
- Garland, G.D and R.A. Burwash, 1959, Geophysical and petrological study of Precambrian of central Alberta. *American Association of Petroleum Geologists Bulletin*, vol. 43, p.790.
- Gehman, H. M. Jr., 1962, Organic matter in limestones; *Geochimica et Cosmochimica Acta*, vol. 26, p. 885-897.
- Habicht, J.K.A., 1979, Paleoclimate, paleomagnetism, and continental drift. *American Association of Petroleum Geologists Studies in Geology* 9, 1 – 29.
- Haines, L., N. Darbonne, M. A. Barbee, P. Williams, G.Clouser, D.Wagman, M. Conly, and J. Grant, 2006, Tight gas. A supplement to Oil and Gas Investor. Hart Energy Publishing, Houston, Texas, 14p.
- Héroux, Y.A., A. Chagnon, and R. Bertrand, 1976, Compilation and correlation of major thermal maturation indicators. *American Association of Petroleum Geologists Bulletin*, vol. 63, p. 2128 – 2144.
- Hitchon, B., 1984, Geothermal gradients, hydrodynamics and hydrocarbon occurrences, Alberta, Canada. *American Association of Petroleum Geologists Bulletin*, vol. 68, p. 713 – 743.
- Hood, A., C.C.M., Gutjahr., and R.L. Heacock, 1975, Organic metamorphism and generation of petroleum. *American Association of Petroleum Geologists Bulletin*, vol. 59, p. 986 – 996.
- Horsfield, B. 1985, Pyrolysis studies in petroleum exploration. *In: Advances in Petroleum Geochemistry* (edited by J. Brooks and D. Welte), Academic Press, New York, vol. 1, p. 247-298,
- Hunt, J.M., 1979, Source rock. *In: Petroleum geochemistry and geology* (2nd Ed.), New York, p. 323 – 380.

- Jacobson, S.R., 1991, Petroleum source rocks and organic facies. *In*: Source and migration processes and evaluation techniques edited by R.K. Merrill, 1991. American Association of Petroleum Geologists Treatise of Petroleum Geology, Handbook of Petroleum Geology, p. 3 – 11.
- Jarvie, D.M., 1991, Hydrocarbon generation modeling of naturally and artificially matured Barnett Shale, Forth Worth Basin, Texas: Southwest Regional Geochemistry meeting, September 8 – 9, 1991, The Woodlands, Texas.
- Jarvie, D.M., R.J. Hill, T.E. Rubble, and R.M. Pollastro, 2007, Unconventional shale-gas systems: Mississippian Barnett Shale of north-central Texas as one model for thermogenic shale-gas assessment: American Association of Petroleum Geologists Bulletin, vol. 19, p. 475 – 499.
- Jones, F.W., H.L. Lam, J.A. Majorowicz, 1985a. Temperature distributions at the Paleozoic and Precambrian surfaces and their implications for geothermal and energy recovery in Alberta. Canadian Journal of Earth Science, vol. 22, p. 1774 – 1780.
- Jones, F.W., J.A. Majorowicz, and H.L. Lam, 1985b, The variation of heat flow density with depth in the prairies basin of Western Canada. Tectonophysics, vol. 121, p. 35 – 44.
- Killops, S. and V. Killops, 2005, Introduction to Organic Geochemistry (ed.). Blackwell Science, Oxford, UK, 393p.
- Larter, S.R., and A.G. Douglas, 1982, Pyrolysis methods in organic geochemistry: An overview. Journal of Analytical Applied Pyrolysis, vol. 4, p. 1 -19.
- Lafargue, E., J. Espitalié, F. Marquis, and D. Pillot, 1998, Rock-Eval 6 applications in hydrocarbon exploration, production and in soil contamination studies. Institut Français du Pétrole, France, p. 1 – 23.
- Majorowicz, J.A. and A.M. Jessop, 1981, Regional heat flow patterns in the Western Canada Sedimentary Basin. Tectonophysics, vol. 74, p. 209 – 238.
- Majorowicz, J.A., F.W. Jones, H.L. Lam, and A.M. Jessop, 1984, The Variability of heat flow both regional and with depth in southern Alberta, Canada: effect of groundwater flow? Tectonophysics, vol. 106, p. 1 – 29.
- Majorowicz, J.A., F.W. Jones, H.L. Lam, and A.M. Jessop, 1985, Regional variations of heat flow differences with depth in Alberta, Canada. Geophysical Journal of the Royal Astronomical Society, vol. 81, p. 479 – 487.

- Majorowicz, J.A., Jones, F.W. and Jessop, A.M., 1986. Geothermics of the Williston basin in Canada in relation to hydrodynamics and hydrogen occurrences. *Geophysics*, vol. 51, no. 3, p. 767 – 779.
- Monger, J.W.H. and Price, R.A. 1979, Geodynamic evolution of the Canadian Cordillera- progress and problems. *Canadian Journal of Earth Sciences*, vol. 16, p. 770-791.
- Orchard, M.J. and J-P Zonneveld, 2009, The Lower Triassic Sulphur Mountain Formation in the Wapiti Lake area: Lithostratigraphy, conodont biostratigraphy, and a new biozonation for the lower Olenekian (Smithian): *Canadian Journal of Earth Sciences*, v. 46, p. 757–790.
- Peters, K.E., 1986, Guidelines for evaluating petroleum source rocks using programmed pyrolysis. *American Association of Petroleum Geologists Bulletin*, vol. 70, p. 318 – 329.
- Peters, K.E. and M.R. Cassa, 1994, Applied source rock geochemistry. In: *The petroleum system – from source to trap* edited by L.B Magoon and W.G Dow, 1984. *American Association of Petroleum Geologists Memoir*, no. 60, p. 93 – 111.
- Peters, K.E. and B.R.T. Simoneit, 1982, Rock-Eval pyrolysis of Quaternary sediments from Leg 64, sites 479 and 480, Gulf of California. *Initial Report of the Deep Sea Drilling Project*, vol. 64, p. 925-931.
- Porter, J. W., R. A. Price and R. G. McCrossan, 1982, The Western Canada Sedimentary Basin. *Philosophical Transaction Royal Society, London*, vol. 305, p. 169 – 192.
- Price, L.C., 1983, Geologic time as a parameter in organic metamorphism and vitrinite Reflectance as an absolute palaeogeothermometer. *Journal of Petroleum Geology*, vol. 6, p. 5 – 38.
- Price, R.A., 1994, Cordilleran Tectonics and the Evolution of the Western Canada Sedimentary Basin. *In: Geological Atlas of the Western Canada Sedimentary Basin*. G.D. Mossop and I. Shetson (compilers). *Canadian Society of Petroleum Geologists*, p. 257–275.
- Renov, A.B., 1985, Organic carbon in sedimentary rocks (in relation to the presence of Petroleum): *Geochemistry*, vol. 5, p. 497 – 509.
- Reineck, H.E. and Singh, I.B, 1972, Genesis of laminated sand and graded rhythmites in storm-sand layers of shelf mud. *Sedimentology*, vol. 18, p.123 – 128.

- Reinson, G.E., 1994, Barrier-island and associated strand-plain systems. In: R.G Walker (Ed) Facies Model, 2nd Edition, Geoscience Canada, Reprinted Series 1, Geological Association of Canada, Geotext 1, p. 179 – 194.
- Rybach, L., 1981, Geothermal systems, conductive heat flow, geothermal anomalies. *In*: Geothermal Systems: Principles and Case Histories (edited by L. Rybach and L.J.P. Muffler), Wiley, New York, NY, p. 3 – 76.
- Schmoker, J. W., 1995, Method for assessing continuous-type (unconventional) hydrocarbon accumulations *In*: D. L. Gautier, G. L. Dolton, K. I. Takahashi, and K. L. Varnes, eds., 1995 National assessment of United States oil and gas resources—Results, methodology, and supporting data: U.S. Geological Survey Digital Data Series 30, CD-ROM.
- Senftle, J. T., and C. R. Landis, 1991, Vitrinite reflectance as a tool to assess thermal maturity, in R. K. Merrill, ed., Source and migration processes and evaluation techniques: AAPG Treatise of Petroleum Geology, Handbook of Petroleum Geology, p. 119–125.
- Stach, E., D. Chandra, M. Mackowsky, G. Taylor, M. Teichmüller, and R. Teichmüller, 1982, Coal petrology (ed.). Geruder Borntraeger, Berlin, 535p.
- Sweeney, J.J. and A.K. Burnham, 1990, Evaluation of a simple model of vitrinite reflectance based on chemical kinetics. American Association of Petroleum Geologists Bulletin, vol. 74, p. 1559 – 1570.
- Teichmüller, M., 1982, Application of coal petrological methods in geology Including oil and natural gas prospecting. *In*: E. Stach, M.-Th. Mackowsky, M. Teichmüller, G. H. Taylor, D. Chandra, and R. Teichmüller, eds., Stach's textbook of coal petrology. Berlin, Gebrüder Borntraeger, p. 381–413.
- Teichmüller, M., 1989, The genesis of coal from the viewpoint of coal petrology: International Journal of Coal Geology, vol. 12, p. 1–87.
- Tissot, B.P., B. Durand, J. Espitalié, and A. Combaz, 1974, Influence of nature and diagenesis of organic matter in formation of petroleum. American Association of Petroleum Geologists Bulletin, vol. 58, p. 499 – 506.
- Tissot, B. P., and D. H. Welte, 1978, Petroleum formation and occurrence; Springer-Verlag, Berlin, 538 p.
- Tissot, B. P., and D. H. Welte, 1984, Petroleum Formation and Occurrence. A new approach to oil and gas exploration Berlin: Springer – Verlag, Berlin, 538p.

- Tozer, E.T., 1982, Marine Triassic faunas of North America: their significance for assessing plate and terrane movements. *Geologische Rundschau* 71, 1077–1104.
- Van Krevelan, D.W., 1961, *Coal*. Amsterdam, Elsevier, 514p.
- Walsh, W., Adams, A., Kerr, B. and Korol, J, 2006, “Regional Shale Gas” Potential of The Triassic Doig and Montney Formations, northeastern British Columbia. Ministry of Energy, Mines and Petroleum Resources, Oil and Gas Division, Resource Development and Geoscience Branch, British Columbia, Petroleum geology open file 2006-02, 19p.
- Waples, W. Douglas, 1945, *Geochemistry in Petroleum Exploration*. International Human Resources Development Corporation, Boston, 232p.
- Willis, A. J, 1992, *Sedimentology and Stratigraphic Framework of the Middle Triassic Halfway Formation, Wembly Oil field, Alberta*. Unpublished master’s degree thesis, University of Alberta, 412p.
- Wilson, K.M., Pollard, D., Hay, W.W., Thompson, S.L., Wold, C.N., 1994, General circulation model simulations of Triassic climates: preliminary results. *In*: G.D. Klein, (ed.), *Pangea: Paleoclimate, Tectonics, and Sedimentation during Accretion, Zenith, and Breakup of a Supercontinent*. Geological Society of America, Special Paper 288, 91–116.

CHAPTER 4: ISOTOPE GEOCHEMISTRY OF THE MONTNEY FORMATION (LOWER TRIASSIC), NORTHEASTERN BRITISH COLUMBIA, WESTERN CANADA

INTRODUCTION

The application of stable isotope geochemistry in the study of sedimentary rocks have increasingly become an integral part of sedimentary geology. In particular, isotopic composition of sediments are important in interpreting diagenesis resulting from dolomitization, and differentiating sources of organic matter (Sackett and Thompson, 1963; Hedges and Parker, 1976; Sturmer et al., 1978), classification of kerogen types (Lewan, 1986), and correlating crude oils with source rocks (Williams, 1974; Stahl, 1978; Galimov and Frick, 1985).

Urey (1947) first originated and formulated the idea of using thermometer to measure the variations with temperature of fractionation factors in isotopic exchange equilibria, particularly, in relation to the oxygen isotopes in the system. Subsequently, Epstein, et al. (1951) showcase that oxygen isotopes ($\delta^{18}\text{O}$) in sedimentary carbonates can serve as a paleothermometer, and can be used to estimate the temperature at which carbonate was formed. The concept of using oxygen isotope as paleothermometer was developed on the premise that calcium carbonates precipitated by organisms is in isotopic equilibrium with the seawater in which the organisms grow (Urey, 1947; Epstein, et al., 1951; Burdige, 2006).

This study of the Montney Formation in the Fort St. John area (T86N, R23W and T74N, R13W), northeastern British Columbia (Fig. 4.1) utilized stable isotope (^{13}C and ^{18}O) composition to interpret dolomitization of the Montney Formation because it is an established method for studying dolomitization and diagenesis in carbonates (Kasting, et al., 2006).

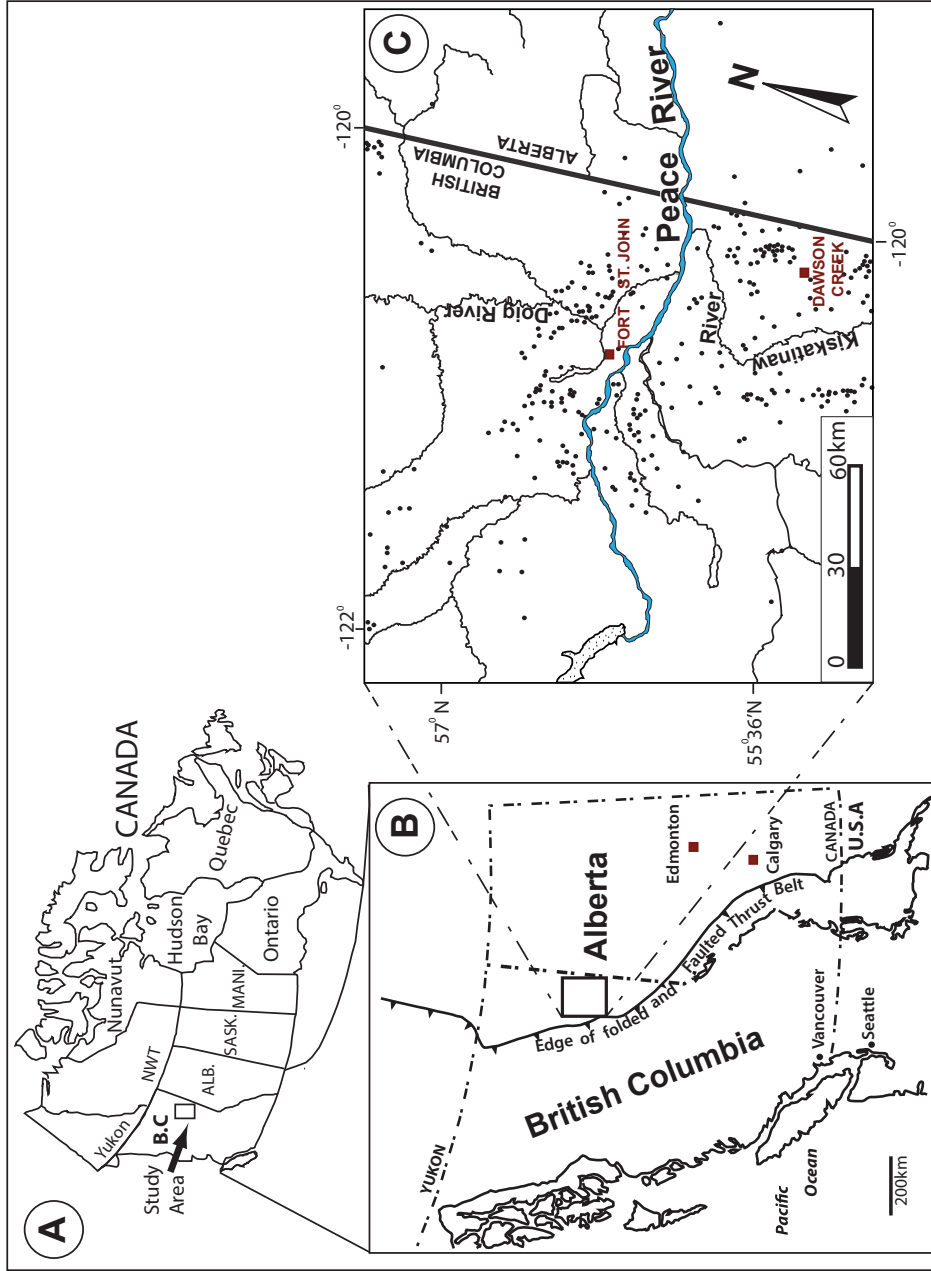


Figure 4.1. (A) Map of Canada showing provinces. (B) Shows tectonic deformation and structure in Western Canada Sedimentary Basin (Modified from Porter et al., 1982). (C) Shows location map of study area in northeastern British Columbia. The black dots represent drilled wells.

This chapter evaluates the Montney Formation isotope geochemistry in relation to paleotemperature, dolomitization and diagenesis.

GEOLOGICAL SETTING

The Triassic succession in the Western Canada Sedimentary Basin (WCSB) comprises six petroleum systems and hydrocarbons are produced from all Triassic lithostratigraphic units (Fig. 4.2). The sedimentary record in the WCSB indicates a westward thickening, which extend into the Cordilleran deformation front (Edwards, 1994).

The paleogeographic location of the Western Canada Sedimentary Basin (WCSB) during the Triassic time was situated at approximately 30° N paleolatitude based on analyses of paleomagnetic data, paleolatitude and paleoclimatic zonation (Habicht, 1979), and fauna record (Tozer, 1982). The paleoclimate reconstruction suggests that the paleoclimate may have ranged from sub-tropical to temperate (Habicht, 1979; Tozer, 1982; Gibson and Barclay, 1989; Barclay, et al., 1990). The region has been interpreted

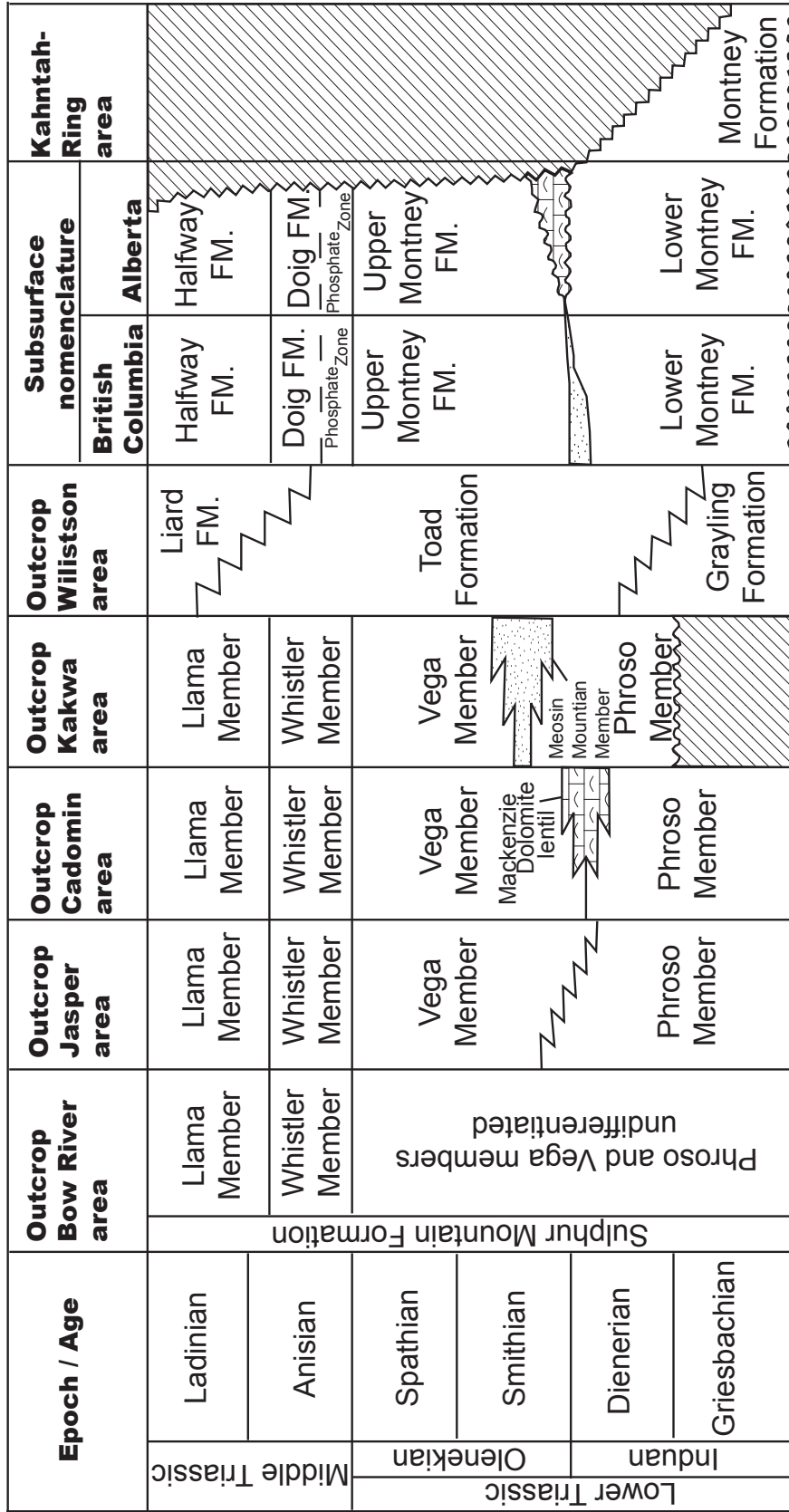


Figure 4.2. Stratigraphic chart showing Lower and Middle Triassic deposits and a correlation of outcrop with coeval subsurface strata in the western Canada Sedimentary Basin (Modified from Orchard and Zonneveld, 2009).

to be arid during the Triassic, and was dominated by winds from the west (Habicht, 1979; Arnold, 1994; Edwards, et al., 1994).

The WCSB forms a northeasterly tapering wedge of sedimentary rocks with thickness of more than 6,000 meters, which extends southwest from the Canadian Shield into the Cordilleran foreland thrust belt (Porter et al., 1982; Gibson and Barclay, 1989). The Cordilleran of the WCSB provides the evidence that the origin and development of the basin was associated with tectonic activity (Price, 1994; Gibson and Barclay, 1989). Later epeirogenic events resulted in subsidence that created the basin for sediment accumulation, which were attributed to the effects of contemporaneous episodes of orogenic deformation in the Cordillera (Porter, et al., 1982; Monger and Price, 1979); this is interpreted to be post Triassic, especially due to mountain influences (Gibson and Barclay, 1989). Wittenberg and Moslow (1991) and Cant (1994; 1986) interpreted sediment loading, evidenced by the deformed bed, slump structures and small-scale faults as indicators of tectonic influences on the deposition of Triassic successions. Within the Foothills and Rocky Mountain Front Ranges, Triassic rocks were subjected to Jurassic – Cretaceous Columbian and Upper Cretaceous – Lower Tertiary Laramide orogenies, which caused a series of imbricate thrust faults and folds in the region (Edwards et al., 1994; Berger, et al., 2009).

Stratigraphically (Fig. 4.2), the Triassic Montney Formation is Griesbachian to Spathian in age (Orchard and 2009). The Triassic isopach (Fig. 4.3) shows that the succession thickened westward (Edwards, et al., 1994), and rests unconformably in most areas, upon the Belloy Formation in outcrop of northeastern British Columbia; Carboniferous in parts of northeastern British Columbia and Alberta; and Fantasque Formation in outcrop at Williston (Orchard and Zonneveld, 2009). The thickness of Triassic deposits is about 1200 meters in the western-most outcrop in the Rocky Mountain Foothills (Willis, 1992). The thickness of the Montney For-

mation within the Fort St. John study area (T86N, R23W and T74N, R13W), varies in the east along British Columbia / Alberta boarder boundary and to the western portion of British Columbia as evidenced by isopach map (Fig. 4.3). The Montney Formation structure map (Fig. 4.4) indicates higher paleostructure in the east and low in the western portion of the study area. The structural tilt shows a depositional thinning to the east and north due to erosional removal (Edwards, et al., 1994). Isopach map of the Montney Formation indicates a maximum thickness of approximately 320 meters in the study area of northeastern British Columbia.

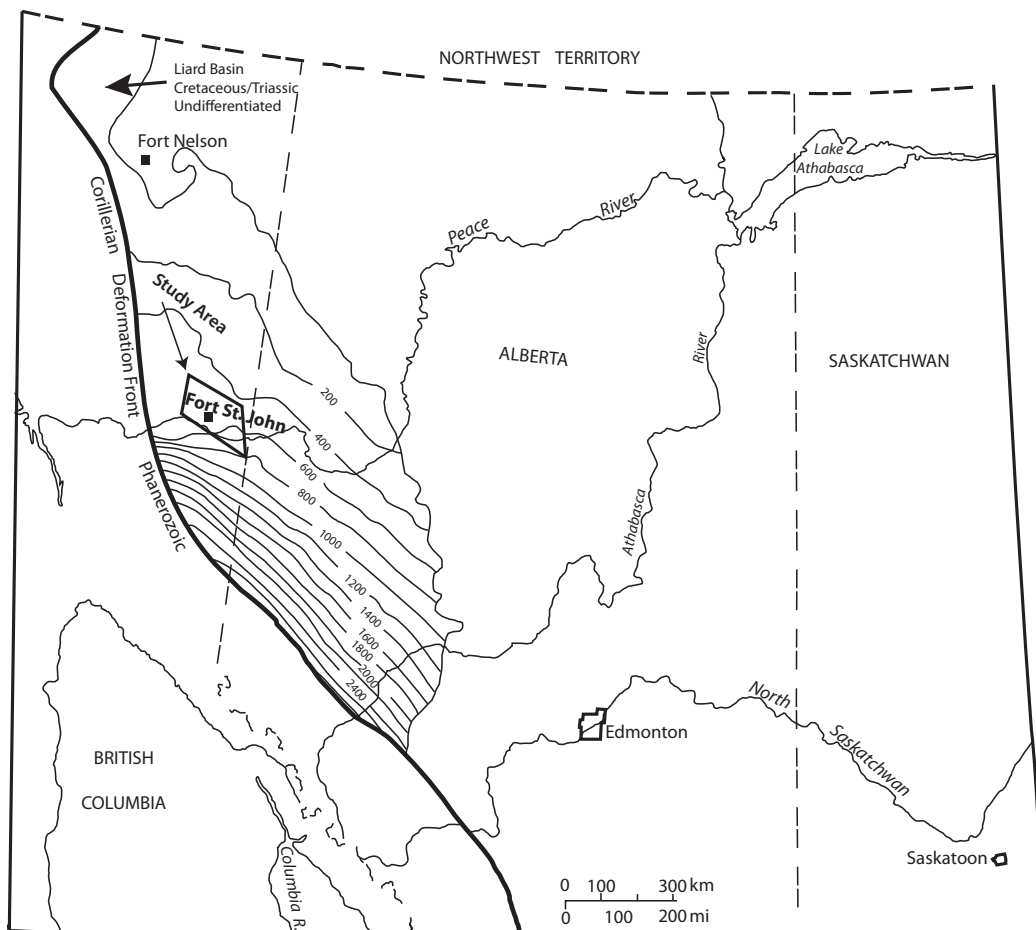


Figure 4.3. Shows the isopach of Triassic succession in the Western Canada Sedimentary Basin. The Succession thickened to the west from Alberta to British Columbia, towards the Cordilleran deformation front (Edwards and Gibson, 1994).

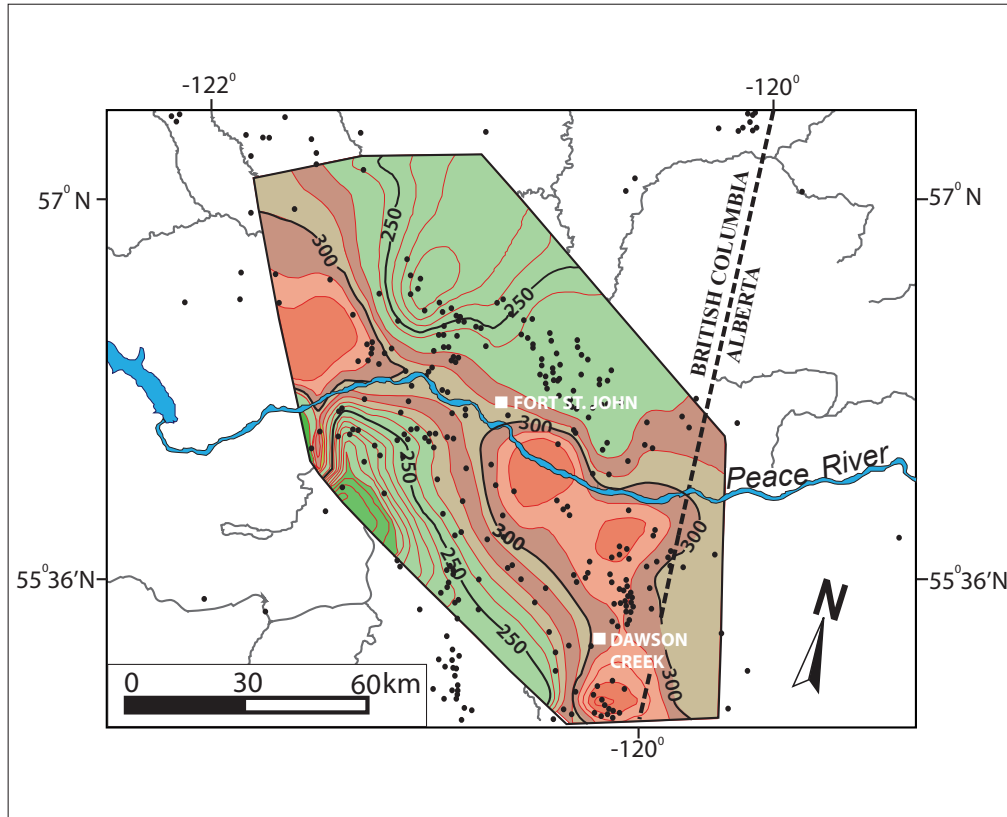


Figure 4.4. Isopach map of the Montney Formation showing the trends of thickness in the study area, northeastern British Columbia.

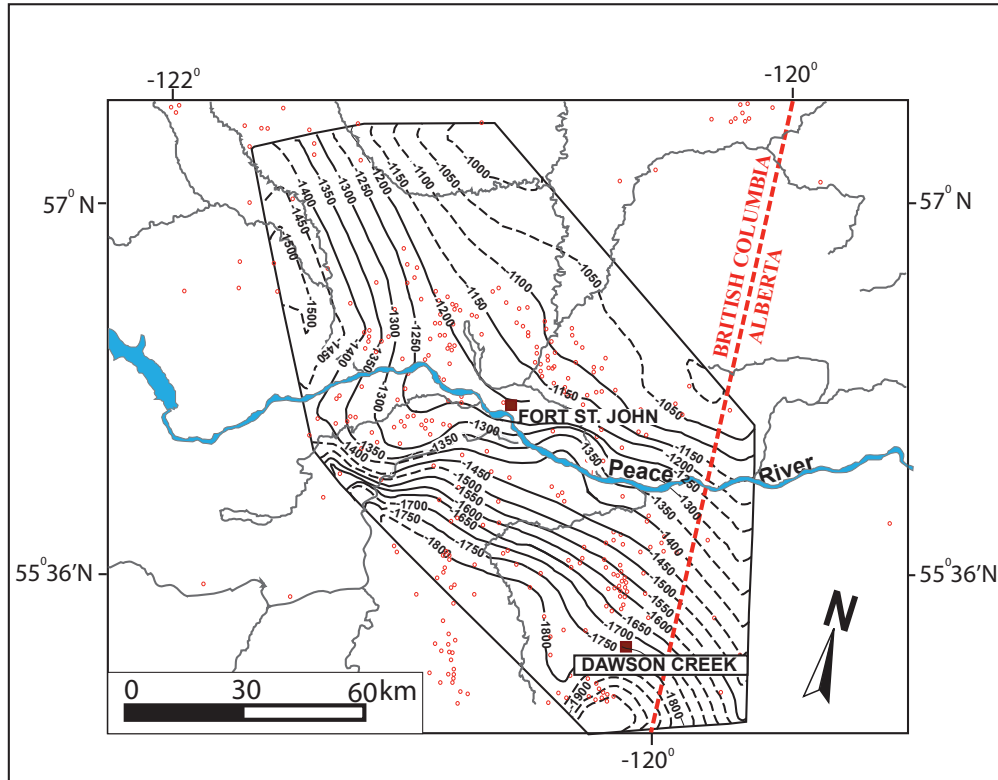


Figure 4.5. Structure contour map of the Montney Formation in the study area, northeastern British Columbia. Dash contour lines indicate no data point for well control. The structure map decreases in elevation westward, which indicates that sediment source area was from east, and prograded westward.

METHOD OF STUDY

The laboratory experiment and procedure for isotopic analysis in this study was performed in the isotope laboratory of Prof. Karlis Muehlenbachs in the Department of Earth and Atmospheric Sciences, University of Alberta. The extracted isotopic composition was analyzed in the Finnigan-MAT 252 Mass Spectrometer in the Stable isotope laboratory at the University of Alberta.

Stable isotope analysis for calcite and dolomite ($^{13}\text{C}/^{12}\text{C}$ and $^{18}\text{O}/^{16}\text{O}$) involves arrays of mechanics: 1) samples were grinded into uniform grains (powder

form) using the pulverizing shatter box-machine for homogeneity of samples in order to provide a uniform surface area for acid reaction with samples following the method of Walters et al. (1972), and samples were allowed to dry in air; 2) samples were measured ~ 40 – 50mg per sample and 3 ml of anhydrous phosphoric acid (H₃PO₄) were measured into each glass reaction vessel and evacuated overnight on a vacuum line to remove atmospheric components (gas) from the samples; 3) the samples were reacted with anhydrous phosphoric acid (H₃PO₄) at 25°C for one hour. The reaction is expressed chemically:



4) Following the method of Epstein, et al. (1963), CO₂ was evolved after one-hour time from the reaction of acid with calcite in the sample; 5) this CO₂ was purified by distillation through a dry ice trap, condensed in a sample collection tube immersed in liquid nitrogen, and analyzed for calcite δ¹³C and δ¹⁸O values; 6) the CO₂ gas formed between the first and the fourth hour from the time of reaction was pumped out into a collection vessel as CO₂ for calcite to avoid contamination; 7) the vessel was then placed in a hot water bath at 25°C and the reaction was left in that condition for 72 hours; 8) the CO₂ that formed during the remainder reaction was extracted in a similar process and analyzed for δ¹³C and δ¹⁸O of the dolomite component.

All analysis follows the standard method of McCrea (1950). The δ value is conventionally defined by Friedman and O'Neil (1977) using the following expression:

$$\delta = \left(\frac{R_{\text{sample}}}{R_{\text{standard}}} - 1 \right) \times 1000$$

Where $R = {}^{13}\text{C}/{}^{12}\text{C}$ or ${}^{18}\text{O}/{}^{16}\text{O}$. The standard for carbonate is PDB (Craig, 1957), and that for water is SMOW (Craig, 1961). The results derived from the analysis are shown in Table 4.1. Detailed results of isotopic analyses from Mass Spectrometer are shown in Appendix 3-A.

Table 4.1. Carbon and oxygen isotope data for bulk calcite cement and bulk dolomite of the Montney Formation, northeastern British Columbia.

Formation	Sample Location	Depth (m)	Bulk Calcite and Dolomite		
			$\delta^{13}\text{C}$	$\delta^{18}\text{O}$	$\delta^{18}\text{O}$
			‰ PDB	‰ PDB	‰ SMOW
Montney	9-29-79-14W6	1987	-5.07	-5.86	24.87
Montney	9-29-79-14W6	1989	-4.19	-16.15	24.66
Montney	9-29-79-14W6	2059	-5.08	-13.50	27.42
Montney	9-29-79-14W6	1981	-5.07	-5.86	24.87
Montney	9-29-79-14W6	1989.4	-3.70	-5.82	24.91
Montney	9-29-79-14W6	1983	-2.71	-5.51	25.33
Montney	9-29-79-14W6	1960	-2.87	-4.70	26.06
Montney	9-29-79-14W6	1987	-4.22	-7.19	23.58
Montney	9-29-79-14W6	1963	-4.22	-7.19	23.58
Montney	9-29-79-14W6	1987	-3.17	-5.39	25.35
Montney	11-04-79-14W6	2068	-3.83	-5.34	25.41
Montney	11-04-79-14W6	2074	-6.31	-3.66	27.14
Montney	11-04-79-14W6	1989	-4.10	-5.94	24.79
Montney	11-04-79-14W6	2068	-3.83	-5.34	25.41
Montney	11-04-79-14W6	2088.9	-8.46	-6.79	23.99
Montney	11-04-79-14W6	2059	-4.78	-3.54	27.67
Montney	11-04-79-14W6	1989.4	-2.78	-14.10	26.79
Montney	11-04-79-14W6	2091.2	-2.18	-3.66	27.14
Montney	d-39-F/93-P-9	2671.7	-2.18	-3.66	27.14
Montney	d-39-F/93-P-9	2668	-4.37	-8.17	22.48
Montney	7-13-79-15-W6	2055.3	-6.10	-5.84	24.90

Stable Isotope Geochemistry – Description of Data

Carbon and oxygen isotopes ($\delta^{13}\text{C}_{\text{PDB}}$ and $\delta^{18}\text{O}_{\text{PDB}}$) were analyzed in order to determine the bulk calcite and bulk dolomite ($\delta^{13}\text{C}$ and $\delta^{18}\text{O}$) isotopic signature of the Montney Formation (Table 4.1). The data show in general, depletion in isotopic composition ($\delta^{13}\text{C}_{\text{PDB}}$ and $\delta^{18}\text{O}_{\text{PDB}}$) of both calcite cement and dolomite in the host lithology (very fine-grained silty-sandstone).

The bulk calcite isotopic compositions of the Montney sediments range from ($\delta^{13}\text{C}_{\text{PDB}}$ -2.8 to -6.10‰ , and $\delta^{18}\text{O}_{\text{PDB}}$ -3.66 to -16.15‰), and bulk dolomite isotopic composition values range from ($\delta^{13}\text{C}_{\text{PDB}}$ -2.71 to -8.46‰ , and $\delta^{18}\text{O}_{\text{PDB}}$ -3.66 to -7.19‰) (Fig. 4.6). High values (-13.50‰ to -16.15‰) occur in intervals that probably have higher organic matter content or the presence of hydrocarbon. Craig (1957) shows that high negative $\delta^{13}\text{C}_{\text{PDB}}$ depleted values greater than -10 are associated with methane gas in the Formation. The oil and gas production map (Fig. 3.14) for the Montney Formation shows approximately 12,121,240 MCF of gas production from the Montney Formation as of January 12, 2013. The high methane (gas) is probably the cause of high negative isotopic values (-13.50‰ to -16.15‰) seen in some of the analyzed samples of the Montney Formation.

The calculation of the temperature of fractionation of calcite and dolomite are shown in Appendix 4-A.

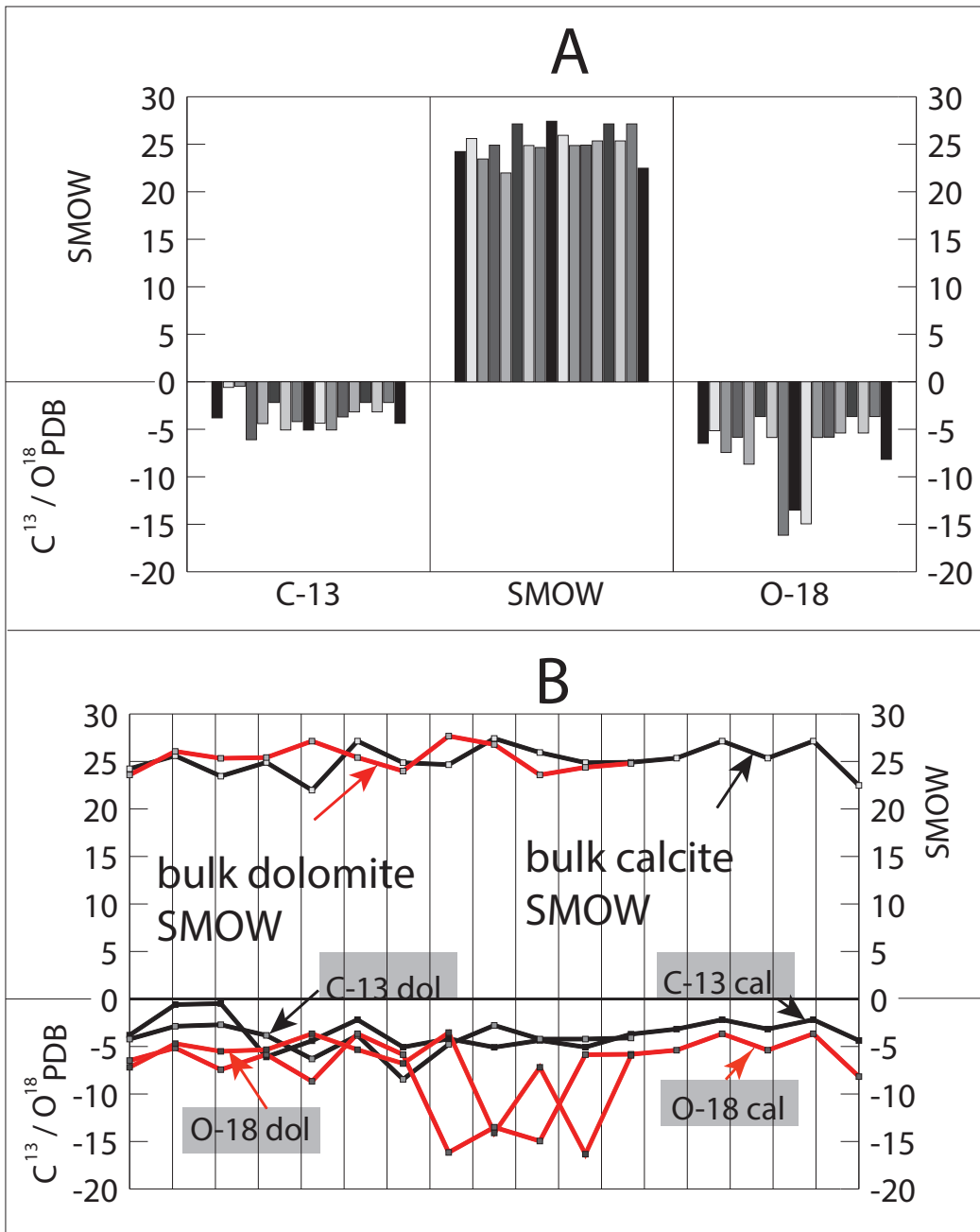


Figure 4.6. Isotopic data plot for the Montney Formation. **(A)** Bar graph showing calculated $\delta^{13}\text{C}$, and $\delta^{18}\text{O}$ and SMOW. **(B)** Displays the $\delta^{13}\text{C}$ and $\delta^{18}\text{O}$ (PDB) fields. **(C)** Crossplot of bulk calcite and bulk dolomite. **(D)** Shows linear graph of oxygen and carbon isotopes showing the bulk dolomite and bulk calcite (SMOW) of the isotopic composition. The lower linear graph shows the PDB of bulk calcite and bulk dolomite isotopic composition.

Interpretation of Isotopic Signature

The values of the result from $\delta^{13}\text{C}_{\text{PDB}}$ bulk calcite show depletion in the isotopic composition ($\delta^{13}\text{C}_{\text{PDB}}$ -2.1 to -8.46‰). The negative $\delta^{13}\text{C}_{\text{PDB}}$ values are indicative of pore-water derived from seawater and dissolution of metastable carbonate in conjunction with organic matter decomposition by bacteria in sulfate reducing environment. The organic carbon content of the Montney lithofacies is a result of high nutrient rich sediment source, rapid sedimentation, and preservation of organic matter (Muller and Suess, 1979) in oxygen-depleted, anoxic depositional environment (Demaison and Moore, 1980; Ekdale and Mason, 1988; Wishner, et al., 1990; Tyson and Pearson, 1991; Wignall and Hallam, 1991; Bentley and Nittrouer, 1999). This phenomenon explains the biasing of carbon isotope towards a very low (negative $\delta^{13}\text{C}_{\text{PDB}}$) discerned from the Montney Formation. The anoxic conditions generate high alkalinity, which increases the total dissolved carbon that causes calcite to precipitate from pore-water, thereby biased towards light $\delta^{13}\text{C}_{\text{PDB}}$ values during early diagenesis (Larsen and Chilingar, 1967).

The depleted $\delta^{18}\text{O}_{\text{PDB}}$ of bulk calcite values range from ($\delta^{18}\text{O}_{\text{PDB}}$ -3.54 to -16.15‰) and the $\delta^{18}\text{O}_{\text{SMOW}}$ range between 22.48 and 27.42‰ (which is within the fresh water range) reported by Taylor (1967) as indication of mixing of marine pore-water and meteoric groundwater during authigenic calcite precipitation. Applying the $\delta^{18}\text{O}_{\text{PDB}}$ range of the bulk calcite ($\delta^{18}\text{O}_{\text{PDB}}$ -3.54 to -16.15‰), the calcite fractionation equation $10^3 \ln \alpha_{\text{calcite-water}} = 2.78 \times 10^6 T^{-2} - 2.89$ (Friedman and O'Neil, 1977) and assuming that the $\delta^{18}\text{O}_{\text{SMOW}}$ values of pore-water is between -2 to -7.19, the paleotemperature under which the calcite have precipitated is interpreted to have occurred between approximately 13°C to 32°C. This interpretation is consistent with a warm paleotemperature reported for the Triassic period of western Canada (e.g. Habieth, 1979; Tozer, 1982; Arnold, 1994).

The bulk dolomite isotopic values ($\delta^{13}\text{C}_{\text{PDB}}$ -2.71 to -8.46‰) provide infor-

mation on the origin and the precipitation of the dolomite. The very low (negative) values of $\delta^{13}\text{C}_{\text{PDB}}$ from the Montney sediment indicate depleted $\delta^{13}\text{C}_{\text{PDB}}$ (–2.71 to –8.46). The interpretation for the negative values (light bulk-dolomite $\delta^{13}\text{C}_{\text{PDB}}$) indicates that biogenic CO_2 significantly contributed to the total dissolved inorganic carbon (Freidman and Murata, 1979). The evidence of biogenic CO_2 contribution from isotopic signature is supported by the total organic carbon (TOC) content based on Rock-Eval pyrolysis (Table 4.2 and Appendix 3-A) from the Montney Formation. The organic carbon content coupled with the depleted bulk dolomite ($\delta^{13}\text{C}_{\text{PDB}}$ –3.66 to –16.15‰) of the Montney Formation jointly indicate an anoxic, extremely poor oxidation environment where anaerobic sulfate reduction characteristic of early stage zone of methanogenesis occurs. The $\delta^{13}\text{C}_{\text{PDB}}$ has been used as a proxy of upwelling intensity because upwelling waters are ^{13}C depleted (Killingley and Berger, 1979). Bemis and Geary (1996) assert that the upwelling isotopic effect might be compensated by the effect of planktonic blooms induced by the nutrient enrichment of upwelled water. The present of apatite mineral (Table 4.3) in the Montney Formation indicate upwelling of nutrient rich waters, which implies the presence of dissolved carbon in anaerobic condition.

The biasing towards light (warm) bulk dolomite $\delta^{18}\text{O}_{\text{PDB}}$ results depleted in isotopic composition ($\delta^{18}\text{O}_{\text{PDB}}$ –2.71 to –8.46‰) indicates the present of meteoric water in the pore-water during precipitation of dolomite (Muehlebachs, 2011, personal communication). Further interpretation for the light, depleted isotopic values ($\delta^{18}\text{O}_{\text{PDB}}$ –2.71 to –8.46‰) suggest the formation within, or modification by meteoric water, or under elevated temperatures (Land, 1983). Applying the bulk calcite dolomite values of $\delta^{18}\text{O}_{\text{PDB}}$ –5.51 to –6.97‰, the dolomite-water fractionation equation $10^3 \ln \alpha_{\text{dolomite-water}} = 3.2 \times 10^6 \text{ T}^{-2} - 3.3$ (Land, 1983), assuming the pore-water $\delta^{18}\text{O}_{\text{smow}}$ of –5.51 to –6.97‰, the dolomite was precipitated in temperatures $\sim 33^\circ\text{C}$. According to Emilliani (1954), oxygen isotopic analysis of marine

carbonates gives at best, the estimate of temperatures at which the carbonate was deposited. The paleotemperature suggest that the Montney Formation has only encounter eodiagenetic realm of diagenetic stage.

On a geological time frame, the oxygen isotope composition of seawater is controlled by exchange of oxygen with silicate rocks (Muehlebachs and Clayton, 1976; Muehlebachs, 1998; Perry, et al., 1978; Kasting, et al., 2006). Unaltered silicate rocks are enriched in $\delta^{18}\text{O}$ relative to seawater by $\sim 5.7\text{‰}$ (Kasting, et al., 2006). The isotopic composition of seawater is controlled by kinetic steady-states, reflecting major influxes of continental input, principally the dissolved load of rivers; oceanic crust / seawater exchange at mid-oceanic ridges (Qing and Veizer, 1994); and removal of chemical species via sedimentation (Holland, 1984).

High temperature interactions between seawater and rocks that occur during hydrothermal circulation are at axial mid-ocean ridges drive the isotopic composition of seawater towards increasing $\delta^{18}\text{O}$ that of the rock (Muehlebachs, 1998). Low temperature interactions such as those that occur in off axis vent systems and during continental weathering, drive seawater isotopic composition towards low $\delta^{18}\text{O}$ (Muehlebachs, 1998) as found in the Montney Formation.

DISCUSSIONS

Carbon and Oxygen Isotope Geochemistry

Important observation from isotopic studies of the Montney Formation sediments (very fine-grained, dolomitic silty-shale) shows that paleotemperatures of dolomitization is $\sim 33^\circ\text{C}$. Such low temperature is characteristic of shallow burial, thus, suggests that the Montney Formation has only undergone eogenetic (early)

phase of diagenesis and diagenetic process. The drive for warm temperature during the Triassic period have been reported to be associated with increase in CO₂ content in the atmosphere, which led to a global temperature increase that heralded most of the Permian–Triassic period (Wignall, and Hallam, 1991; 1992; Wignall and Twitchett, 2002a, 2002b).

The extraction of CO₂ during isotopic lab analyses for bulk calcite and bulk dolomite reveal that although the sediments are believed to be dolomitized, some of the analyzed samples show no evidence of calcite and in some cases, dolomite where not found (and therefore, not extracted). This observation was confirmed by utilizing X-ray diffraction (XRD) analyses, which explicitly confirms that dolomite and calcite where both found in most samples, but, in other samples, calcite was not present with dolomite and vice versa. Interpretation for this important discovery in the Montney Formation samples can be surmise in relation to the mode of substitution of Mg and Ca in carbonate rocks.

Thermodynamically, dolomite is stable in most natural solutions at earth surface conditions, and a thermodynamic drive exists for the conversion of calcite to dolomite (Morrow, 1990). Characteristically, most natural dolomite exhibits some degree of mixing of calcium and magnesium between cation layers (Goldsmith and Graf, 1958; Carpenter, 1980). The phenomenon of the present/absent of calcite/dolomite in the Montney Formation proves that dolomites commonly depart from stoichiometric composition of an excess of calcium, which is accommodated in the magnesium layers (Goldsmith and Graf, 1958; Lumsden and Chimahusky, 1980). Other explanations for the absent of calcite in some of the Montney Formation samples may be due to the fact that several cations, principally, Fe, Sr, Na, and Mn, substitute for calcite in many dolomites (Veizer, et al., 1978). Significant amount of Fe, Sr, Na, and Mn in this study (Table 4.1; Fig. 4.7) support such possibility of substitution for calcite (Veizer, et al., 1978).

Overall, the stable isotope geochemistry and results of this study leads to two important conclusions: 1) isotopic composition ($\delta^{13}\text{C}$ and $\delta^{18}\text{O}$) of the Montney Formation in the study area serves as a paleothermometer and used to constrain the temperature at which the carbonate (dolomite and calcite) associated with the Montney Formation was formed at seawater temperature 33°C . Mineral precipitation at low temperatures are enriched in ^{18}O while minerals formed at high temperatures show less ^{18}O enrichment (Kasting, et al., 2006); and 2) dolomitized Montney Formation has mainly undergone eogenetic stage of diagenesis. The $\delta^{18}\text{O}_{\text{SMOW}_{\text{calcite}}}$ values of (-3.66 to -16.15‰), and that of $\delta^{18}\text{O}_{\text{dolomite}}$ range from -2.71 to -8.46‰ indicate some oxidation of organic matter during diagenesis. This interpretation conforms with isotopic signature of depleted $\delta^{18}\text{O}_{\text{SMOW}}$ of Friedman and O'Neil (1977) with respect to calcite-water fractionation equation, and dolomite-water fractionation of Land (1983).

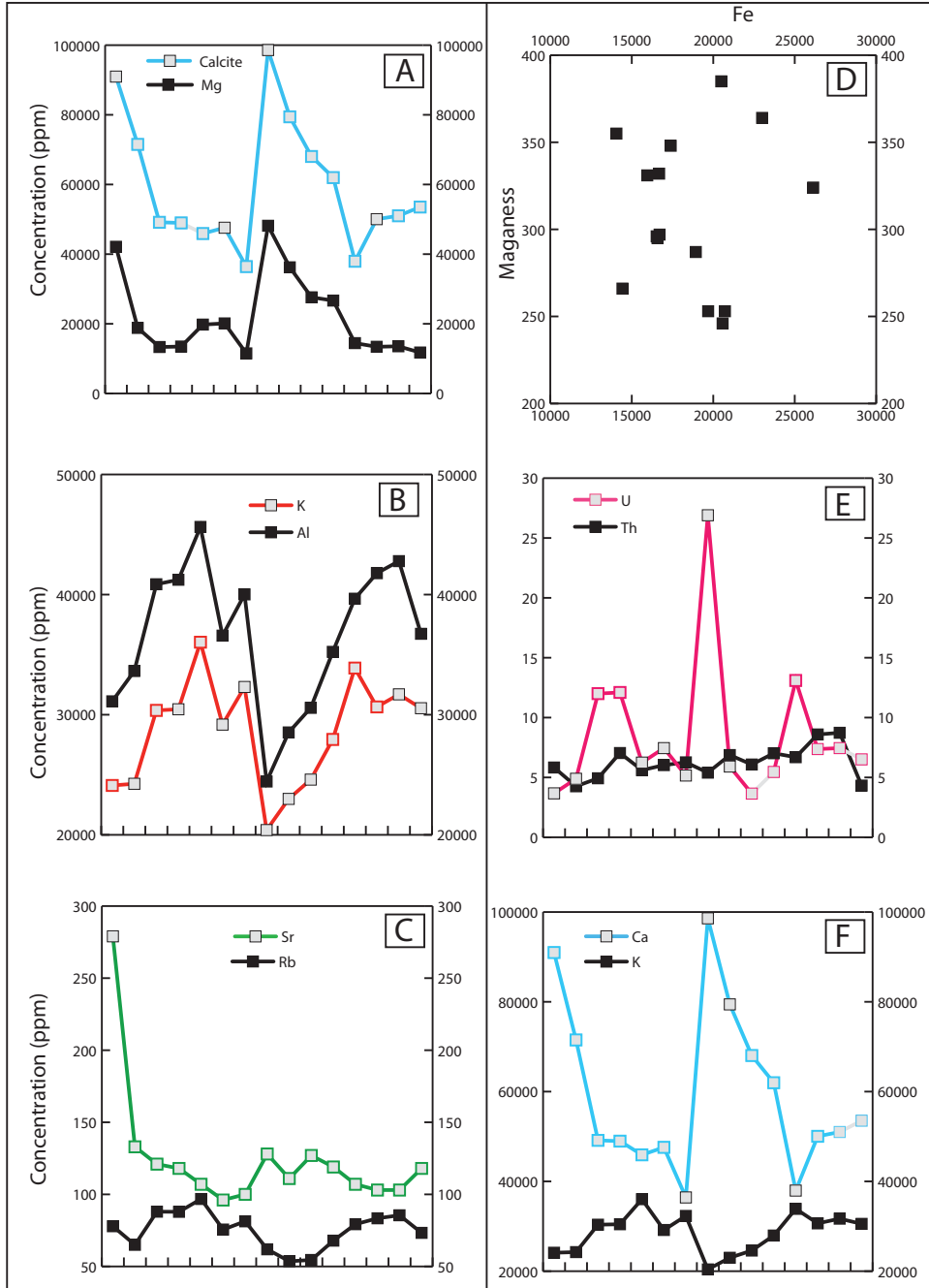


Figure 4.7. Shows the variation pattern of concentration of trace elements. **(A)** Illustrates the composition of dolomite, in which there is higher concentration of magnesium (Mg) relative to the calcite (Ca) component. The graph pattern shows good correlation between Mg and Ca. **(B)** Shows major elements, potassium (K) and aluminum (Al). The concentration of K is very high because of the clay mineral and the organic richness of the Montney Formation sediments. The A concentration is related to the clay mineralogy and partly has affinity to organic matter. The graph pattern of K and Al correlates very well. **(C)** Shows alkaline earth metals – Strontium (Sr) and Rubidium (Rb) concentration. **(D)** Illustrates the concentration of Iron (Fe) and Manganese (Mn). Fe and Mn are both related to diagenesis. The concentration of Fe is very high compared to the concentration of Mn. This indicates that Fe has more dominating diagenetic influence in the Montney Formation. Evidence from thin-section petrography **(Fig. 4.15-D)** shows replacement of organic matter by pyrite. **(E)** Shows the relationship between radioactive elements – Uranium (U) and Thorium (Th). These elements are particularly related to the clay mineralogy and organic components of the Montney Formation sediments. **(F)** Shows the relationship between calcite (Ca) and Potassium (K). Evidently, Ca has enormously high concentration due to the stoichiometric co-existence with dolomite.

Dolomitization of the Montney Formation

Ever since Dolomieu (1791) first introduced the term ‘*Dolomite*’ into the geological literature to describe a calcareous rock in the mountain range of north-western Italy where the rock ‘*dolomite*’ was first identified, the calcium magnesium carbonate $\text{CaMg}(\text{CO}_3)_2$ rock continue to be a subject of vast interest in geology owing to: 1) mode of formation of the mineral dolomite; 2) diagenesis, or diagenetic relationship and implications of dolomitization in reservoir rocks; and 3) its usefulness for paleotemperature interpretation, or as paleothermometer.

Dolomite is a rhombohedral carbonate with the ideal formula $\text{CaMg}(\text{CO}_3)_2$, in which calcium and magnesium occupy preferred sites (Land, 1983). Graf and Goldsmith (1956); Goldsmith and Heard (1961) used hydrothermal experiments extrapolated to low temperatures to demonstrate that calcite and dolomite are essentially ideal in composition at 25°C. Thus, any double carbonate crystal of Ca and

Mg at 25°C is not essentially pure dolomite, and is either metastable or unstable with respect to calcite (Land, 1982). This relationship is evident in XRD analysis (Table 4.3), which supports the co-existence of dolomite and calcite.

Isotopic signature obtained from bulk calcite and dolomite results from this study indicates depleted ($\delta^{13}\text{C}_{\text{PDB}}$ -2.71 to -8.46‰) and ($\delta^{18}\text{O}_{\text{PDB}}$ -2.71 to -8.46‰), which is interpreted in relation to the oxidation of organic matter during diagenesis. Diagenetic modification of the very fine-grained, silty-sandstone of the Montney Formation may have occurred in stages of progressive oxidation and reduction reactions involving chemical element such as Fe, which manifest in mineral form as pyrite, particularly, during early burial diagenesis (Dapples, 1967), or late stage diagenesis (Degens, 1967). Mineralogical changes in the form of cementation and mineral replacement involving calcite and dolomite are typical of diagenesis (Dapples, 1967), and are evident in the Montney Formation based on petrographic study and SEM.

Oxidation and reduction reaction mechanisms explains the modification of sediments, shortly after burial, prior to lithification or compaction during which fluids are ejected into the depositional interface (Weller, 1959; Von Engelhardt and Gaida, 1963). This drives the oxidation and reduction processes involving Fe, sulfur, and carbon (Dapples, 1967). The significant amounts of organic matter (TOC) in the Montney Formation essentially make these elements principal reactants. The carbon compound of the organic matter content is the most rapidly oxidized and consequently contributing energy to drive the Fe into the ferrous state, thereby causing fixation of sulfur as pyrite (Dapples, 1967). Because of the present of organic matter in the Montney sediments, pyrite occurs as scattered 'clots' throughout the rock, and this phenomenon is evident in thin-section petrography (Fig. 4.8). Pyrite is related to post-depositional emplacement (England, et al., 2002) caused by the dissolution of organic Matter Due To Diagenesis.

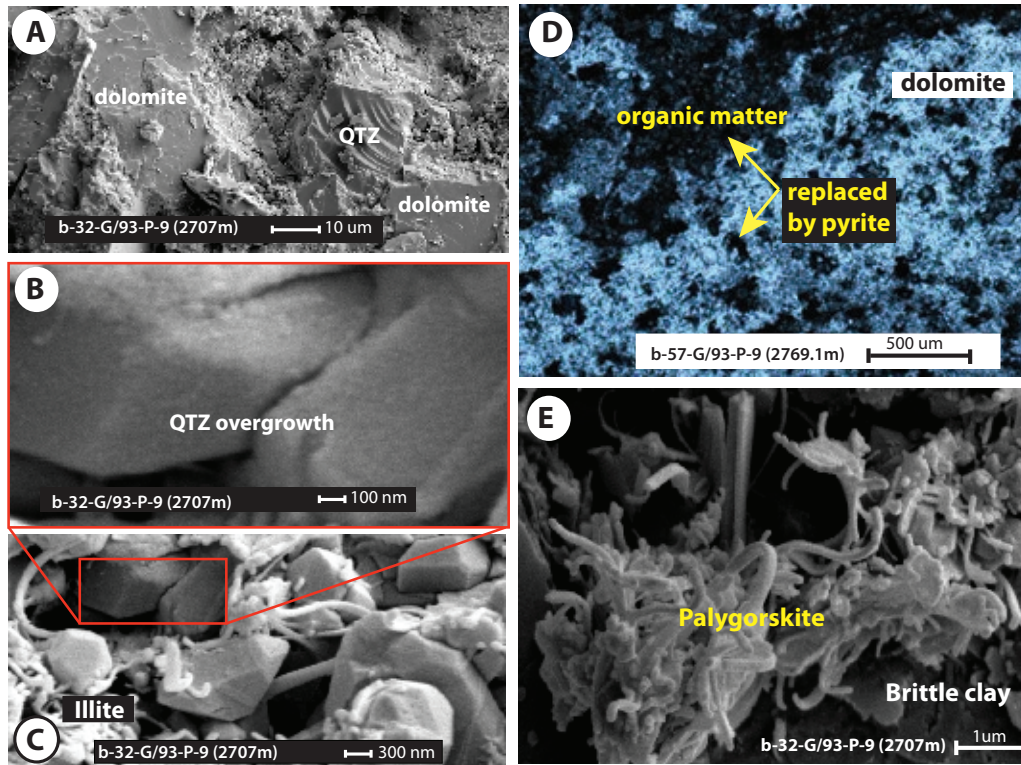


Figure 4.8. Microphotographs showing SEM and thin-section petrography of the Montney Formation illustrating the mineralogical composition. **(A)** Dolomite and quartz matrix. The quartz exhibits conchoidal fracture. **(B)** Shows magnification of plate C. Authigenic quartz overgrowth is illustrated in plate-B as evidence of grain dissolution due to diagenesis, and subsequent mineral precipitation (calcite) in the form of calcite cement that welded the grains together. **(C)** Shows quartz and illite with the authigenic quartz overgrowth. **(D)** Illustrates pyritized, dolomitized, organic carbon rich siltstone. Pyrite replaces organic matter in plate-D during decomposition of organic matter due to diagenesis. **(E)** Illustration of a very well formed palygorskite clay; a form of clay mineral growth, formed from the transformation of dickite to illite, and further transformation of illite to palygorskite due to severe temperature and pressure in a diagenetic regime.

High concentration of chemical elements in the Montney Formation, particularly, Ca and Mg show indicate dolomitization. It is interpreted herein, that calcite may have been precipitated into the interstitial pore space of the intergranular matrix of the very fine-grained silty-sandstone of the Montney Formation as cement by a complex mechanism resulting in the interlocking of grains, welded together by

calcite cement (Waldschmidt, 1941; Taylor, 1950; Dapples, 1967). Evidence of grain interlocking is revealed by SEM image showing authigenic quartz overgrowth (Fig. 4.8).

It is established through mineralogical composition in this study (Tables 4.3) that the Montney Formation is quartz rich and contains substantial clay minerals as well, including unstable mineral such as feldspar (Tables 4.3). This sort of compositional mixture of quartz, clay and feldspar minerals may have resulted in the decomposition of feldspar along the clay–quartz boundary due to processes involving hydrolysis in the course of diagenesis (Dapples, 1967).

The depositional environment interpreted for the Montney Formation is proximal to distal offshore marine setting (Zonneveld, et al., 2010; Egbobawaye, et al., 2010; 2011). In the marine environment, several weathering and transformation are prevalent. As a result, there exist an exchange of cations, in which the positions of clay minerals are changed, thereby resulting in the substitution of Mg for Ca (Goldsmith and Heard, 1961; Müller, 1967; Land, 1982). In the marine environment chlorite and illite minerals are formed by fixation of Mg and K in montmorillonite or degraded illite delivered into distal settings due to continental denudation resulting from fluvial processes (Müller, 1967). The present of illite and palygorskite clay mineral (Fig. 4.8) support the evidence of diagenesis in the Montney Formation formed from ionic solutions in extreme conditions of temperature and pressure (Müller, 1967). Weaver (1954) noted that the transformation of clay minerals into illite involves several factors such as preferential flocculation, current sorting of floods (hyperpycnal or hypopycnal) intensities, and variations in the composition and concentration of detritus during sedimentation and subsequently enhance clay transformation.

Table 4.3. X-ray diffraction (XRD) analyses showing mineralogy of the Montney Formation, well: 16-17-83-25 W6, northeastern British Columbia, Western Canada Sedimentary Basin. Data source: B.C. Oil and Gas Commission.

Depth (meters)	Formation	Quartz	K Feldspar	Plagioclase	Calcite	Dolomite	Pyrite	Marcasite	Apatite	Kerogen	Total Clay
2,233.70	Montney	21.2	4.5	6.0	32.9	20.7	1.8	0.0	0.0	5.4	7.6
2,236.40	Montney	15.2	5.2	2.1	52.9	9.8	1.1	0.0	2.8	8.1	2.9
2,238.00	Montney	19.8	5.3	5.0	50.0	15.8	1.1	0.0	0.0	1.2	1.8
2,240.80	Montney	19.0	4.8	3.4	25.0	20.3	2.5	0.0	0.0	17.6	7.3
2,242.50	Montney	16.6	2.9	3.5	43.5	5.9	1.1	0.0	18.6	6.9	1.0
2,245.60	Montney	23.0	4.5	5.2	36.1	8.2	2.0	0.0	6.5	8.7	5.8
2,248.10	Montney	30.9	9.1	7.2	14.4	8.9	2.4	0.0	3.9	15.9	7.3
2,251.50	Montney	24.4	5.5	5.4	31.9	7.7	2.2	0.0	2.0	11.3	9.6
2,252.60	Montney	24.0	6.9	5.1	28.8	8.7	1.8	0.3	2.2	13.2	8.9
2,259.50	Montney	33.6	13.0	9.0	10.7	14.7	1.2	0.6	2.5	11.7	3.1
2,260.60	Montney	20.7	3.8	9.1	39.5	18.7	0.9	0.0	0.0	3.9	3.3
2,262.00	Montney	22.9	6.7	9.5	43.0	10.0	1.2	0.6	0.0	1.5	4.7
2,262.70	Montney	49.0	7.9	12.1	9.7	9.5	1.5	0.6	0.0	0.0	9.7
2,265.20	Montney	20.6	4.7	7.3	53.1	6.2	1.2	0.3	0.0	2.4	4.4
2,273.00	Montney	41.3	7.9	9.7	8.8	15.9	2.0	0.7	0.9	3.6	9.4
2,279.20	Montney	34.6	9.0	10.9	9.9	17.4	1.6	0.5	0.0	6.3	9.8
2,281.20	Montney	37.5	7.4	10.1	11.8	12.9	1.5	0.5	0.0	8.1	10.2
2,282.40	Montney	39.9	7.8	9.9	10.4	9.8	1.8	0.4	1.0	9.1	10.0
2,288.40	Montney	38.7	8.5	10.7	10.4	13.5	1.5	0.4	0.0	5.8	10.4
2,294.60	Montney	44.9	7.9	13.6	9.0	12.6	1.4	0.4	0.0	0.1	10.2
2,299.40	Montney	31.9	6.3	11.4	25.4	10.5	0.9	1.0	0.0	4.6	7.9
2,317.80	Montney	33.3	7.1	9.9	2.9	33.1	1.1	0.7	0.0	2.6	9.4
2,318.50	Montney	38.3	8.4	12.5	3.0	20.3	1.3	0.4	0.0	3.5	12.1
2,323.90	Montney	37.8	7.8	12.5	3.4	21.4	1.2	0.4	0.0	4.5	11.0
2,330.30	Montney	40.8	7.8	13.4	4.8	15.7	2.2	0.8	0.0	0.1	14.5
2,332.80	Montney	31.0	6.5	8.6	4.7	31.7	1.5	0.0	0.0	6.8	9.2
2,341.90	Montney	43.2	6.8	12.3	6.2	14.2	1.1	0.5	0.0	4.8	10.9

The dolomite in the Montney Formation appears as detrital in thin-section petrography (Fig. 4.8). Such allogenic (non *in-situ*) dolomite and calcite may have only played a role (minimal) in the Montney Formation diagenesis, compared to sediments that are mainly composed of biogenic carbonate formed completely from aragonite and calcite (Müller, 1967). Thus, authigenic calcite may have played dominant role in the vast diagenetic phenomenon in the Montney Formation.

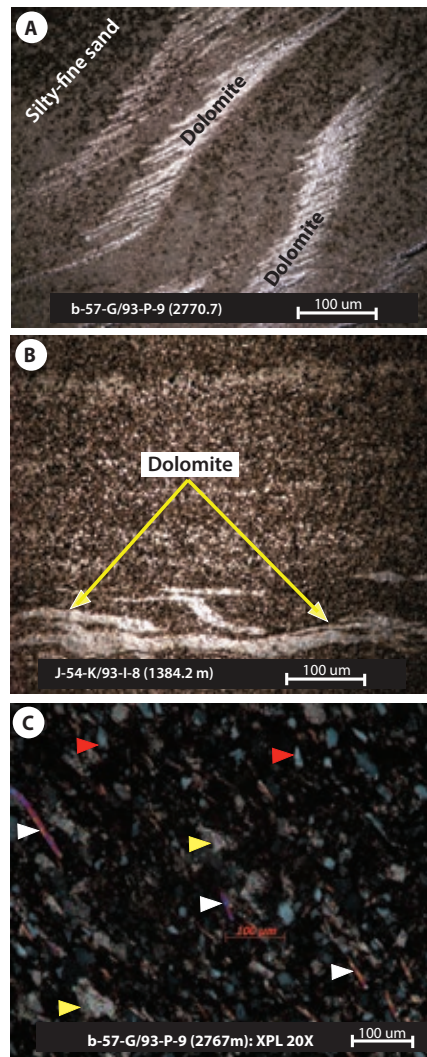


Figure 4.9. Photomicrographs showing Dolomitic silty-sandstone. **(A)** Shows detrital dolomite resembles ripple. **(B)** shows detrital dolomite admixed siltstone. **(C)** Crossed polarized light showing detrital dolomite (yellow – arrow), quartz (red – arrow), and mica (white – arrow).

CONCLUSIONS

Isotopic results from this study indicate depleted $\delta^{13}\text{C}_{\text{PDB}}$ (-2.71 to -8.46%) and interpreted as oxidation of organic matter during diagenesis. Diagenetic modification of the Montney Formation (very fine-grained, silty-sandstone) may have occurred in stages of progressive oxidation and reduction reactions involving chemical element such as Fe, which manifest in mineral form as pyrite, particular, during early burial diagenesis (Dapples, 1967), or late stage diagenesis (Degens, 1967). Mineralogical changes in the form of cementation and mineral replacement involving calcite and dolomite are typical of diagenesis. Based on isotopic signature and paleotemperature calculations, the calcite and dolomite of the Montney Formation may have formed at temperatures $\sim \pm 32^\circ\text{C}$, which is consistent with a warm, arid paleoclimate reported for the Triassic time (Habicht, 1979; Tozer, 1982; Gibson and Barclay, 1989; Barclay, et al., 1990)

REFERENCES

- Arnold, K.J., 1994, Origin and distribution of eolian sandstones in the Triassic Charlie Lake Formation, northeastern British Columbia. Unpublished M.Sc. thesis, University of Alberta, Edmonton, 320p.
- Barclay, J.E., Krause, F.F., Campbell, R.I., and Utting, J., 1990, Dynamic casting and growth faulting: Dawson Creek Graben Complex, Carboniferous Permian Peace River Embayment, Western Canada, In: Geology of the Peace River Arch, S.C. O'Connell and J.S. Bell (eds.), Bulletin of Canadian Petroleum Geology, vol. 38A, p.115-145.
- Bemis, B.E., and Geary, D.H., 1996, The Usefulness of Bivalve Stable Isotope Profiles as Environmental Indicators: Data from the Eastern Pacific Ocean and the Southern Caribbean Sea. *Palaios*, vol. 11, no. 4 p. 328 – 339.
- Berger, Z., M. Boast, and Mushayandebvu, M., 2009, The contribution of integrated HRAM studies to exploration and Exploitation of unconventional plays in North America. Part 2: Basement structures control on the development of the Peace River Arch's Montney / Doig resource plays. *Reservoir*, vol. 36, Issue 2, p. 40 – 44.
- Burdige, D.J., 2006, *Geochemistry of marine sediments* (ed.), Princeton University Press, New Jersey, 609p.
- Cant, D.J., 1984, Possible syn-sedimentary tectonic controls on Triassic reservoirs, Halfway and Doig, Charlie Lake formations, west-central, Canadian Society of Petroleum Geologists, Calgary, p.45.
- Cant, D.J., 1986, Hydrocarbon trapping in the Halfway Formation (Triassic), Wembly Field, Alberta, *Bulletin of Canadian Petroleum Geology*, vol. 34, p. 329-338.
- Carpenter, A.B., 1980, The chemistry of dolomite formation 1: the stability of dolomite. In: Zenger, D.H., Dunham, J.B. and Ethington, R.L., Eds., *Con-*

- cepts and Models of Dolomitization. Society of Economic Paleontologists and Mineralogists, Special Publication 28, p. 111 – 121.
- Craig, H., 1957, Isotopic standards for carbon and oxygen and correlation factors for mass-spectrometric analysis of carbon dioxide. *Geochim. Cosmochim. Acta*, vol. 12, p. 2347 – 2349.
- Craig, H., 1961, standard for reporting concentrations of deuterium and oxygen-18 in natural waters. *Science*, vol. 133, no. 3467, p. 1833 – 1834.
- Degens, E.T., 1967, Diagenesis of organic matter. In: *Diagenesis of sediments* edited by G. Larsen and G.V. Chilingar (eds.). Elsevier Publishing Co., New York, p. 343 – 390.
- Dolomieu, D. G. de, 1791, Sur un de pierres très-peu effervescentes avec les acides of phosphorescentes par la collision. *Jour. Physique*, vol. 39, p. 3 – 10.
- Dapples, E.C., 1967, Diagenesis in sandstones. In: *Diagenesis of sediments* edited by G. Larsen and G.V. Chilingar (eds.). Elsevier Publishing Co., New York, p. 91 – 125.
- Edwards, D.E., Barclay, J.E., Gibson, D.W., Kvill, G.E., and Halton, E. 1994, Triassic strata of the Western Canada Sedimentary Basin. In: *Geological Atlas of the Western Canada Sedimentary Basin*. G.D. Mossop and I. Shetson (compilers). Canadian Society of Petroleum Geologists, p. 257–275.
- Egbobawaye, E.I., M.K. Gingras, and J-P., Zonneveld, 2011, The geochemistry of the Montney and Lower Doig tight gas reservoir, northeastern British Columbia. *American Association of Petroleum Geologists Abstract*, no. 90124. Accessed online on March 16, 2012: <http://sdsearch.datapages.com/data/search.do?selectedGroups=41&fullDoc=MONTNEY+FORMATION&Search.x=45&Search.y=12&Search=Search>
- Egbobawaye, E.I., J-P. Zonneveld, and M.K., Gingras, 2010, Tight gas reservoir

- evaluation in Montney and Lower Doig formations, northeastern British Columbia, western Canada. *American Association of Petroleum Geologists Abstract*, vol. 19, p. 66-67.
- England, G.L., B. Rasmussen, B. Krapez, and D.I. Groves, 2002, Palaeoenvironmental significance of rounded pyrite in siliciclastic sequences of the Late Archean Witwatersrand Basin: oxygen-deficient atmosphere or hydrothermal alteration?. *International Association of Sedimentologists*, vol. 49, p. 1133 – 1156.
- Emiliani, C.M, 1954, Temperatures of Pacific bottom waters and polar superficial waters during the Tertiary. *Science*, vol. 119, p. 853 – 855.
- Epstein, S., Buchsbaum, R., Lowenstam, H., and Urey, H.C., 1951, Carbonate water isotopic temperature scale : *Geological Society of America Bulletin*, vol. 62, p. 417 – 425.
- Epstein, S., Graf, D.L., and Degens, E.T., 1963, Oxygen isotope studies on the origin of dolomites. *In* : H. Craig, S.L. Miller, and Wasserburg, G.J (eds.), *Isotopic and Cosmogenic chemistry*. North-Holland Publication Co., Amsterdam, p. 169 – 180.
- Friedman, I., and J.R. O'Neil, 1977 *Compilation of stable isotope fractionation factors of geochemical interest*. U.S. Geol. Surv. Prof. Paper 440 – KK, *Data of Geochemistry*, sixth ed., Chapter KK, p. KK1 – KK12.
- Friedman, I., and Murata, K.J., 1979, Origin of dolomite in Miocene Monterey Shale and related formations in the Temblor Range, California. *Geochim. Cosmochim. Acta*, vol. 43, no. 8, p. 1357 1365.
- Froelich, P.N., G.P. Klinkhammer, G.R. Bender, N.A. Luedtke, G.R. Heath, D. Cullen, P. Dauphine, D. Hammond, B. Hartman, 1979, Early oxidation of organic matter in pelagic sediments of the eastern equatorial Atlantic: suboxic diagenesis. *Geochim. Cosmochim. Acta*, 43, p. 1075 -1090.

- Gibson, D.W and J.E., Barclay, 1989, Middle Absaroka Sequence, the Triassic stable craton. In: Western Canada Sedimentary Basin: A Case History, B.D. Ricketts (ed.). Canadian Society of Petroleum Geologists, p. 219–231.
- Gibson, D.W and Barclay, J.E. 1989, Middle Absaroka Sequence, the Triassic stable craton. In: Western Canada Sedimentary Basin: A Case History. B.D. Ricketts (ed.). Canadian Society of Petroleum Geologists, p. 219–231.
- Galimov E. M. and Frick, M.G., 1985, Isotopic method of source-rocks diagnostic. *Geochemistry*, vol. 10, p. 1474 – 1486.
- Graf, D.L. and J.R. Goldsmith, 1956, Some hydrothermal syntheses of dolomite and protodolomite. *Journal of Geology*, vol. 64, p. 173 – 186.
- Goldsmith, J.R. and C.D Heard, 1961, Subsolvus phase relations in the system $\text{CaCO}_3\text{-MgCO}_3$. *Journal of Geology*, vol. 69, p. 45 – 74.
- Goldsmith, J.R. and Graf, D.G., 1958, Structural and compositional variations in some natural dolomites. *Journal of Geology*, vol. 66, p. 678 – 693.
- Habicht, J.K.A., 1979, Paleoclimate, paleomagnetism, and continental drift. *American Association of Petroleum Geologists Studies in Geology* 9, p. 1 – 29.
- Holland, H.D., 1984, *The chemical Evolution of the Atmosphere and Oceans*. Princeton's Series in Geochemistry, Princeton University Press, Princeton. 582p.
- Kasting, J.F., M. T. Howard, K. Wallman, J. Veizer, G. Shields, J. Jafres, 2006, Paleoclimates, ocean depth, and the oxygen isotopic composition of seawater. *Earth and Planetary Science Letters*, vol. 252, p. 82 – 93.
- Killingley, J.S. and Berger, W.H., 1979, Stable isotopes in a mollusk shell: detection of upwelling events. *Science*, vol. 205, p. 186 – 188.
- Larsen, G., and Chilingar, G.V., 1967, *Diagenesis in sediments*. Elsevier Publish-

ing Co., New York, 551p..

- Land, L.S., 1983, The application of stable isotopes to studies of the origin of dolomite and problems of diagenesis of clastic sediments. In: *Stable Isotope in Sedimentary Geology* (ed. M.A. Arthur, et al.) SEPM Short Course 10, p. 4.1 – 4.22.
- Lumsden, D.N. and Chimahusky, J.S., 1980, Relationship between dolomite non-stoichiometry and carbonate facies parameters. In: Zenger, D.H., Dunham, J.B. and Ethington, R.L., Eds., *Concepts and Models of Dolomitization*. Society of Economic Paleontologists and Mineralogists, Special Publication 28, p. 123 – 137.
- Lewan M. D., 1986, Stable carbon isotopes of amorphous kerogens from Phanerozoic sedimentary rocks. *Geochim. Cosmochim. Acta*, vol. 50, 1583--1593.
- McCrea, J.M., 1950, On the isotopic chemistry of carbonates and paleotemperature scale. *Journal of chemical Physics*, vol. 18, p. 849 – 857.
- Morrow, D.W., 1990, Dolomite part 1: The geochemistry of Dolomitization and Dolomite Precipitation. In: McIlreath, I.A and Morrow, D.W, 1990, *Diagenesis*. Geoscience Canada Reprint 4, p. 113 – 121.
- Monger, J.W.H., and Price, R.A., 1979. Geodynamic evolution of the Canadian Cordillera- progress and problems. *Canadian Journal of Earth Sciences*, vol. 16, p. 770-791.
- Muehlenbacks, K. and R.N. Clayton, 1976, Oxygen isotope composition of the oceanic crust and its bearing on seawater. *Journal of Geophysical Research*, vol. 81, p. 4365 – 4369.
- Muehlenbacks, K., 1998, The Oxygen isotopic composition of the oceans, sediments, and the sea floor. *Chemical Geology*, vol. 86, p. 263 – 273. Müller, G., 1967, Diagenesis in argillaceous sediments. In: *Diagenesis of sediments* edited by G. Larsen and G.V. Chilingar (eds.). Elsevier Publishing

- Co., New York, p. 128 – 177.
- Nesbitt, H.W., Young, G.M., 1982, Early Proterozoic climate and plate motions inferred from major element chemistry of lutites. *Nature*, vol. 299, p. 715 – 717.
- Orchard, M. J., and Zonneveld, J-P., 2009, The Lower Triassic Sulphur Mountain Formation in the Wapiti Lake area: lithostratigraphy, conodont biostratigraphy, and a new biozonation for the lower Olenekian (Smithian). *Canadian Journal of Earth Sciences*, vol. 46, no. 10, p. 757 – 790.
- Perry, E.C., S.N. Ahmad., and T.M. Swulius, 1978, The oxygen isotope composition of 2800 m.y. old metamorphosed chert and iron formation from Isukasia, West Greenland. *Journal of Geology*, vol. 86, p. 223 – 239.
- Porter, J.W., Price, R.A., and McCrossan, R.G. 1982. The Western Canada Sedimentary Basin. *Philosophical Transactions of the Royal Society of London*, v. A305, p. 169-182.
- Price, R.A., 1994, Cordilleran Tectonics and the Evolution of the Western Canada Sedimentary Basin. In: *Geological Atlas of the Western Canada Sedimentary Basin*. G.D. Mossop and I. Shetson (compilers). Canadian Society of Petroleum Geologists, p. 257–275.
- Quin, H. and J. Veizer, 1994, Oxygen and carbon isotopic composition of Ordovician brachiopods: implications for coeval seawater. *Geochim. Cosmochim. Acta* 58, 4429 – 4442.
- Sackett, W.M., and Thompson, R.R., 1963, Isotopic organic carbon composition of recent continental derived clastic sediments of Eastern Gulf Coast, Gulf of Mexico. *American Association of Petroleum Geologists Bulletin*, vol. 47, p. 525.
- Sturmer, D. H., Peters K. E., and Kaplan I. R., 1978, Source indicators of humic substances and proto-kerogen: Stable isotope ratios, elemental composi-

- tion, and electron spin resonance spectra. *Geochimica et Cosmochimica Acta*, vol. 42, p. 989 – 997.
- Stahl, W. J., 1978, Source rock-crude oil correlation by isotope type-curves. *Geochimica et Cosmochimica Acta*, vol 43, p. 1573 – 1577.
- Taylor, H.P.JR., 1967, Oxygen isotope studies of hydrothermal mineral deposits. *In*: Barnes, H.L. (eds.), *Geochemistry of hydrothermal Ore Deposits*: Holt, Rinehart and Winston, New York, p. 109 – 142.
- Tozer, E.T., 1982, Marine Triassic faunas of North America: their significance for assessing plate and terrane movements. *Geologische Rundschau* 71, 1077–1104.
- Tyson, R.V., and Pearson, T.H., 1991, Modern and ancient continental shelf anoxia: An overview: in Tyson, R.V., and Pearson T.H., eds., *Modern and Ancient Continental Shelf Anoxia*: Geological Society of London Special Publication 58, p. 1 – 24.
- Urey, H.C., 1974, The thermodynamic properties of isotopic substances: *Journal of Chemical Society*, p. 323 – 329.
- Von Engelhardt, W., and Gaida, K.H., 1963, Concentration changes of pore solutions during the compaction of clay sediments. *Journal of sedimentary petrography*, vol. 33, p. 919 – 930.
- Veizer, J., Lemieux, J., Jones, B., Gilling, J.R., and Savelle, J., 1978, Paleosalinity and dolomitization of a Lower Paleozoic carbonate sequence, Somerset and Prince of Wales Island, Arctic Canada. *Canadian Journal of Earth Sciences*, vol. 15, p. 1448 1461.
- Waldschmidt, W.A., 1941, Cementing materials in sandstones and their probable influence on the migration and accumulation of oil and gas. *American Association of Petroleum Geologists Bulletin*, vol. 25, p. 1839 – 1879.
- Weaver, C.E., 1954, Possible uses of clay minerals in the search for oil. *AAPG*

- bulletin, vol. 44, p.1505-1518.
- Weise, B.R., 1980, Wave-dominated Delta Systems of the Upper Cretaceous San Miguel Formation, Maverick Basin, South Texas. Bureau of Economic Geology, Report of investigations, 107, Austin, Texas, 33p.
- Weller, J.M., 1959, Compaction, of sediments. American Association of Petroleum Geologists, vol. 43, p. 273 – 310.
- Wittenberg, J., and Moslow, T.F., 1991, Origin and variability of overthickened sandstone in the Doig Formation, west-central Alberta, Canadian Society of Petroleum Geologists, Calgary, p. 146.
- Willis, A. J, 1992, Sedimentology and Stratigraphic Framework of the Middle Triassic Halfway Formation, Wembly Oil field, Alberta. Unpublished master's degree thesis, University of Alberta, 412p.
- Walters, L.J., Claypool, G.E. and Choquette, P.W., 1972. Reaction rates and $\delta^{18}\text{O}$ variation for the carbonate-phosphoric acid preparation method. *Geochimica et Cosmochimica Acta*, vol. 36, p. 129-140.
- Wignall, P.B., and Hallam, A., 1992, Anoxia as a cause of the Permian/Triassic mass extinction: Facies evidence from northern Italy and the western United States. *Palaeogeography, Palaeoclimatology, Palaeoecology*, vol. 93, p. 21 – 46.
- Wignall, P.B., and Twitchett, R.J., 2002a, Oceanic anoxia and the end Permian mass extinction: *Science*, v. 272, p. 1155–1158.
- Wignall, P.B., and Twitchett, R.J., 2002b, Extent, duration, and nature of the Permian-Triassic superanoxic event, in Koeberl, C., and MacLeod, K.C., eds., *Catastrophic Events and Mass Extinctions: Impacts and Beyond*: Geological Society of America Special Paper 356, p. 393–413.
- Zonneveld, J.P., MacNaughton, R.B, Utting, J, Beatty, T.W, Pemberton, S.G, and Henderson, C.M., 2010, Sedimentology and ichnology of the Lower

Triassic Montney Formation in the Pedigree-Ring/Border-Kahntah River area, northwestern Alberta and northeastern British Columbia. *Bulletin of Canadian Society of Petroleum Geology*, vol. 57, No. 2, p. 115-140.

CHAPTER 5: MAGNETOSTRATIGRAPHY DATING AND CORRELATION OF THE UPPER MONTNEY AND LOWER DOIG FORMATIONS, NORTHEASTERN BRITISH COLUMBIA, WESTERN CANADA SEDIMENTARY BASIN

INTRODUCTION

Paleomagnetism studies the magnetic properties of rocks and sediments, providing a record of past configurations of the geomagnetic field, which aids refinement of stratigraphic correlations and geochronologic calibrations of both marine and non-marine sedimentary successions (Butler, 1998). Creer (1958, 1959) pioneered geomagnetic concept integrated with stratigraphy in the Triassic succession of the United Kingdom, in which a set of paleomagnetic samples were placed into stratigraphic order to construct a simple magnetostratigraphy, i.e. identification of a sequence of the normal and reverse polarity intervals in geological section.

The research field of magnetostratigraphy has been established based upon the well-known evidence that the Earth reverses the polarity of its magnetic field (Hailwood, 1989). David (1904) and Brunhes (1906) studied the rocks baked by the lava flows and discovered that such rocks were magnetized in a direction opposite to the present day geomagnetic field. Subsequently, Matuyama (1929) was the first to discover that volcanic rocks recorded magnetization directions similar to the orientation of the present day Earth's magnetic field so that the north seeking lines of magnetic force are alternately directed toward the north or the south geographic poles. Marcanton (1926) was first to figure out that the rocks with the reversal magnetizations proved that the Earth's magnetic field had opposite to the present day polarity. Matuyama (1929) discovered that some volcanic rocks recorded older

magnetization directions that were in the opposite direction to the present day Earth's magnetic field. Heirtzler, et al. (1968) constructed the first geomagnetic polarity time scale built on the basis of the marine magnetic anomalies.

The present day geomagnetic polarity, which is the mean magnetic north corresponds to geographic north, generally referred to as the normal (N) polarity state, and the opposite to geomagnetic polarity, is known as the reverse (R) polarity state. Long intervals of stable normal or reversed polarity, polarity chrons, last on average from 50 kyr to 5 Myr and more (Kravchinsky, 2012, personal communication). The polarity chrons are interrupted by shorter polarity subchrons lasting for 20–50 kyr (Merrill et al., 1996). These changes in polarities are imprinted on a wide range of rock types (igneous and sedimentary) at the time of their formation or deposition respectively. These natural records of sequences of the polarity intervals makes the study and application of paleomagnetism a useful tool in interpretation of successive layers of sedimentary sequences, thus, it is possible to reconstruct the polarity changes during the deposition of sedimentary strata. Furthermore, geomagnetic polarity reversals are synchronous on a worldwide scale occurrence; hence, they provide important sets of time-correlative datum within sedimentary and igneous successions as boundary marker, and can play a very important role in worldwide geological correlations (Hailwood, 1989).

Naturally, sediments acquire a depositional remnant magnetization shortly after fine-grained magnetic minerals settle down through the water column and are deposited. These mineral grains orient themselves along the acting earth's magnetic field as detrital remnant magnetization (Butler, 1992). The magnetization, which is acquired after the magnetic minerals are deposited, is a depositional remnant magnetization. And, if the magnetization is acquired soon after deposition; it is a post-depositional remnant magnetization. Upon burial, the orientation of the magnetization is preserved, the minerals in effect, behaves like tiny compasses.

Both the remnant magnetization and post depositional remnant magnetization are applicable in stratigraphic correlation.

The global nature of geomagnetic polarity reversals has made magnetostratigraphy an essential tool for precise correlation between widely distributed sections of rocks of different lithological characteristics (Kent, et al., 1989). One of the major objectives of geochronology is the “calibration” of chronostratigraphic boundaries (Kent, et al., 1989).

This chapter used paleomagnetic data to correlate the Triassic Upper Montney and Lower Doig formations in northeastern British Columbia, Western Canada Sedimentary Basin (WCSB).

STUDY OBJECTIVES

In the course of the stratigraphic correlation of the Upper Montney Formation and Lower Doig Formation (along the stratigraphic boundary) using drill cores in the Fort St. John study area (T86N, R23W and T74N, R13W) of northeastern British Columbia (Fig. 5.1), paleomagnetic technique was utilized. In this study of the Upper Montney Formation and Lower Doig Formation, magnetostratigraphic technique was applied for dating and correlating sedimentary sequences along the Montney / Doig boundary. The samples were measured to determine their characteristic remnant magnetization (ChRM) and to evaluate the polarity of the Earth’s magnetic field at the time the sediments were deposited.

Magnetostratigraphy was employed in this study because accurate correlation within non-fossiliferous, fine-grained clastic successions such as the Upper Montney and Lower Doig formations is commonly problematical, and available wire-line log correlations are subjective, and unambiguously synchronous marker horizons are not common, therefore, this study delve into the application of magnetostratigraphy to address the anecdotal ‘diachronous boundary hypothesis’ along the Upper Montney and Lower Doig formations.

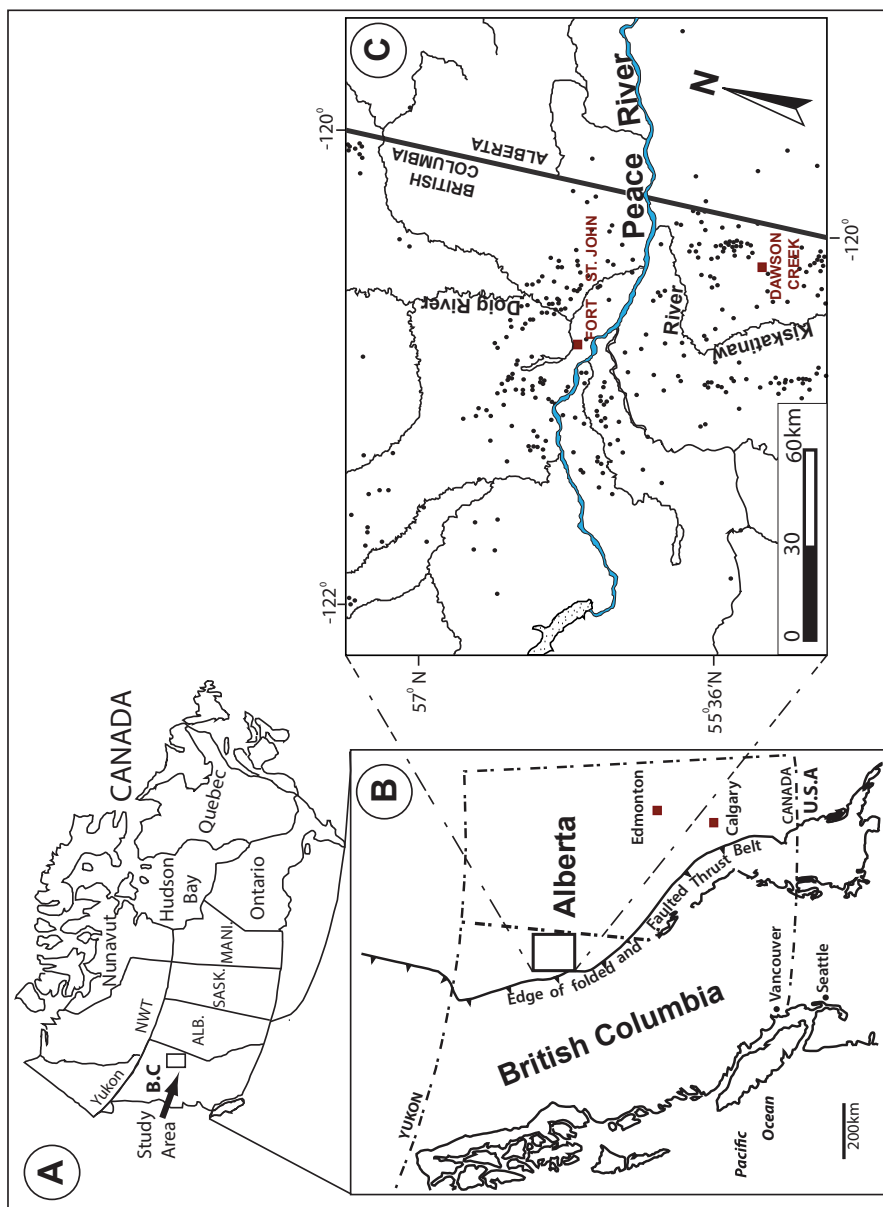


Figure 5.1. (A) Map of Canada showing provinces. (B) Shows tectonic deformation and structure in Western Canada Sedimentary Basin (Modified from Porter et al., 1982). (C) Shows location map of study area in northeastern British Columbia. The black dots represent drilled wells.

Lithologically, the Triassic Montney and Lower Doig formations successions consist of very fine-grained sandstone interbedded with siltstone and mudstone. These units have previously been correlated primarily using conventional geophysical well logs (e.g. Dixon 2000; 2005). Remnant magnetization data were used to obtain the polarity record of the geomagnetic field in order to provide geochronological constrains and to augment local and regional correlations along the Montney and Lower Doig formation stratigraphic boundary.

LABORATORY METHODS AND PROCEDURES

Oriented samples from six cores from the Upper Montney and Lower Doig formations were collected for paleomagnetic study. Only two of the cores show normal and reverse polarity. The other four cores have been remagnetized, and therefore show only normal polarity. The large plugs were cut into cubic samples with size of 0.8 cm by 2.2 cm for measurement with the cryogenic magnetometer facility (Fig. 5.2).

Magnetic measurements were performed in a magnetically shielded room of the paleomagnetic laboratory in the Department of Physics, University of Alberta (Fig. 5.3). Remnant magnetization measurements were carried out using a 2G Enterprises superconducting horizontal magnetometer, and the magnetic susceptibility was measured with a Barrington susceptibility meter system. The demagnetization procedure using the alternating field (AF) was conducted on 128 samples over 14 incremental steps up to 100 mT. The details on the measured samples, and their characteristics are shown in Table 5.1.

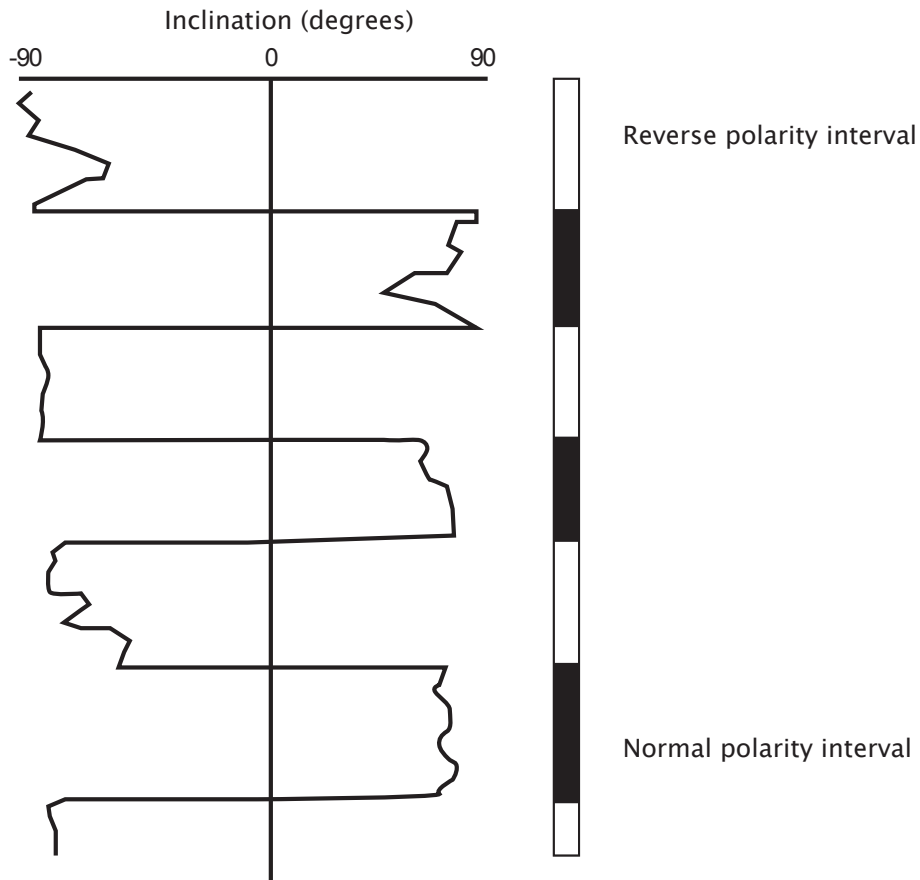


Figure 5.2. Synthetic example of magnetostratigraphic dating in the drilled core where alternating polarity intervals are registered. Normal polarity (black color intervals), coincides with present day geomagnetic field direction and is observed in the studied Montney and Lower Doig formations cores. Reverse polarity (white color intervals) corresponds to the geomagnetic field direction which is opposite to the present day geomagnetic field and is observed in the Montney Formation.

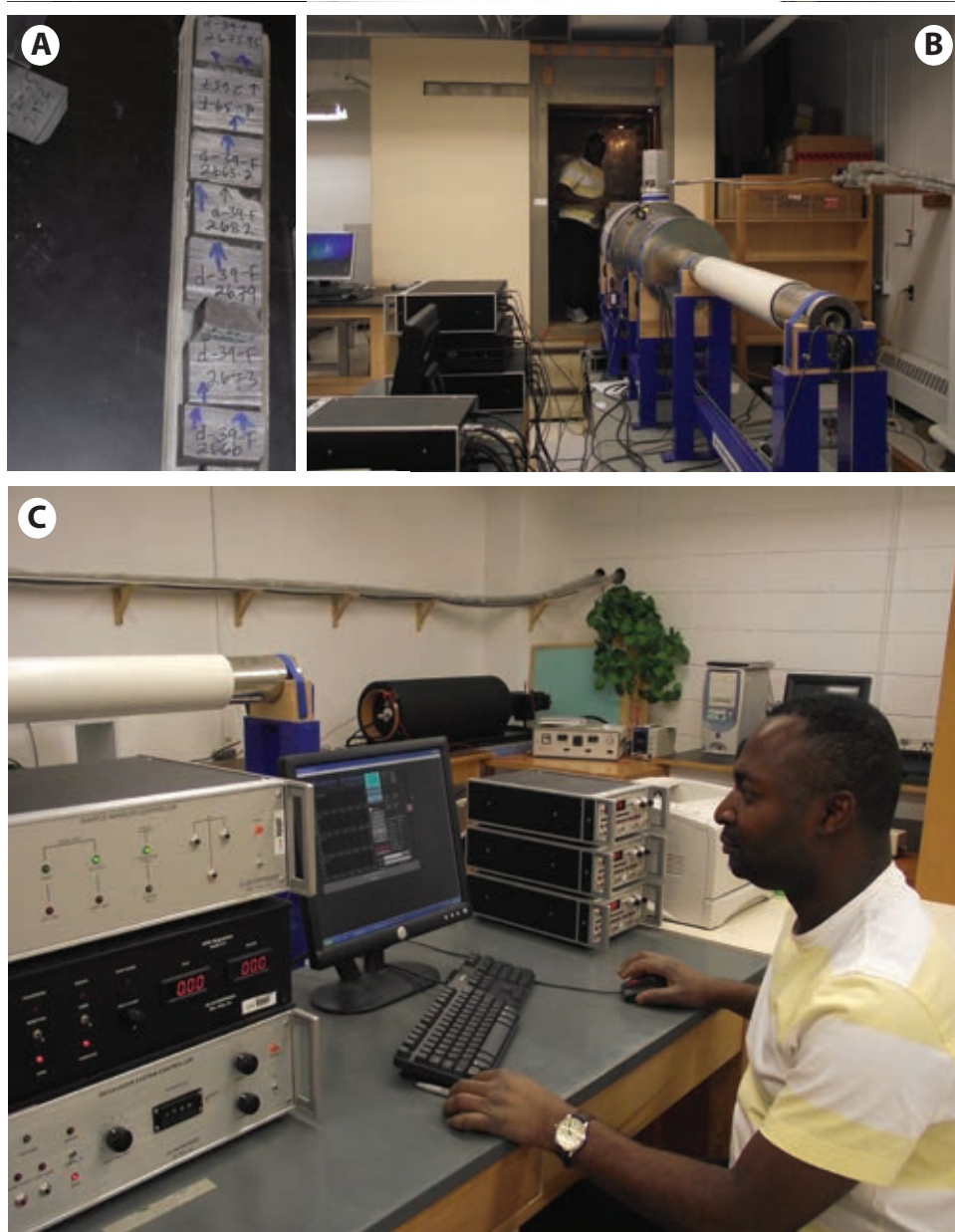


Figure 5.3. (A) Shows sample preparation for demagnetization measurement. Samples size and precise orientation indicating magnetic north is crucial. The top (magnetic north) of samples are distinguished from the bottom (south orientation) by marking an arrow on samples to indicate top. (B) Shows the cryogenic machine and samples were being loaded into the machine for demagnetization experiment. (C) Illustrates sample measurement in progress and rendering of samples in incremental steps to demagnetize remnant magnetization in the Paleomagnetic Lab, Department of Physics, University of Alberta.

Table 5.1. Data showing well location, sample depth and analyses from Cryogenic machine.

Sample depth (m)	Well Location	Number of steps in analysis	Declination (degrees)	Inclination (degrees)	Intensity (A/m)	Sample depth (m)
2018	12-35-14-W6	0-450	1.5	335.5	79.2	2.28E-03
2021	12-35-14-W6	50-400	1.3	263.7	82.5	4.72E-03
2023.9	12-35-14-W6	50-350	2.7	65.1	-82.6	2.01E-03
2027	12-35-14-W6	80-500	0.5	319.1	74.1	3.13E-03
2030	12-35-14-W6	60-400	1.4	23.8	74.1	1.59E-03
2030.5	12-35-14-W6	80-500	1.5	335.2	68.6	8.70E-04
2033.5	12-35-14-W6	60-400	2.6	174.8	74.2	9.54E-04
2036.5	12-35-14-W6	60-600	3.3	325.8	78.8	1.25E-03

DirOPCA = Characteristic direction forced through the origin evaluated using Principal Component Analysis

STEP RANGE = Incremental steps in demagnetization process

N = North

The demagnetization experiments demonstrated the presence of characteristic remnant magnetization of normal and reverse polarity in all samples from cores from wells 12-35-14W6. and 9-29-79-14W6 (Figs. 5.4 and 5.5). Demagnetization results were plotted as orthogonal vectors diagrams and as equal-area projections (Fig. 5.6). The paleomagnetic directions were determined using principal component analysis (Kirshvink, 1980). All interpretations and data processing were carried out using the PaleoMac software (Cogné, 2003) and Enkin's PC software (Enkin, 1996).

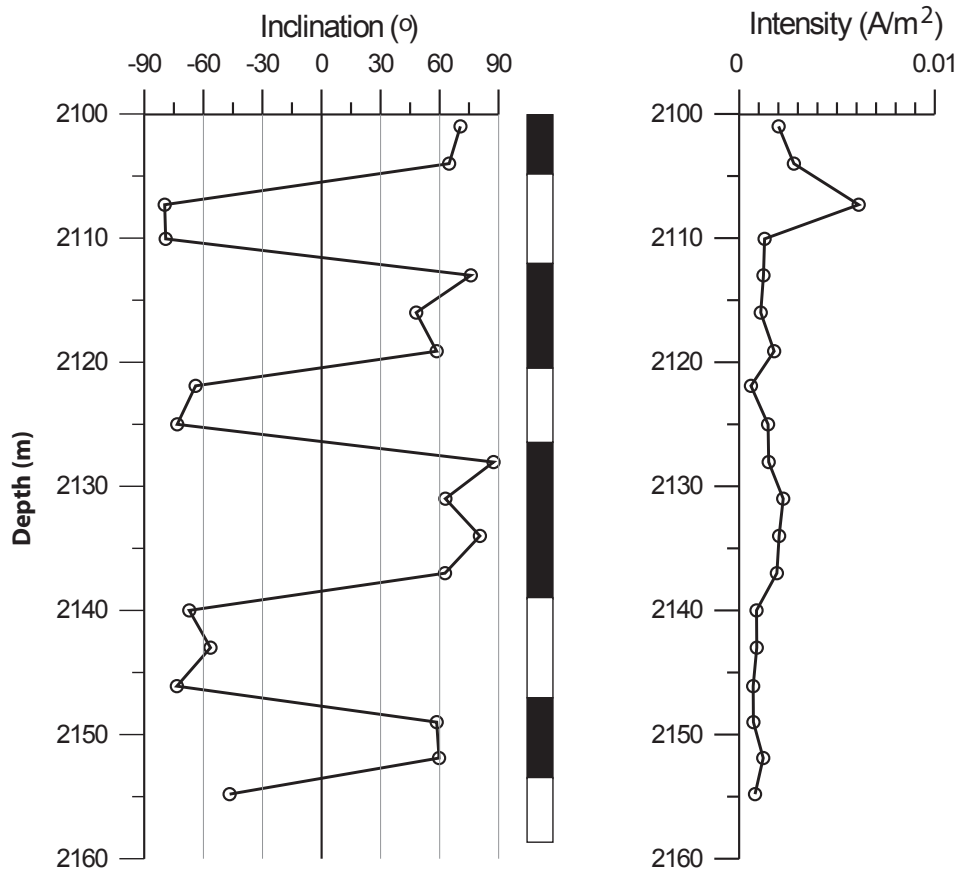
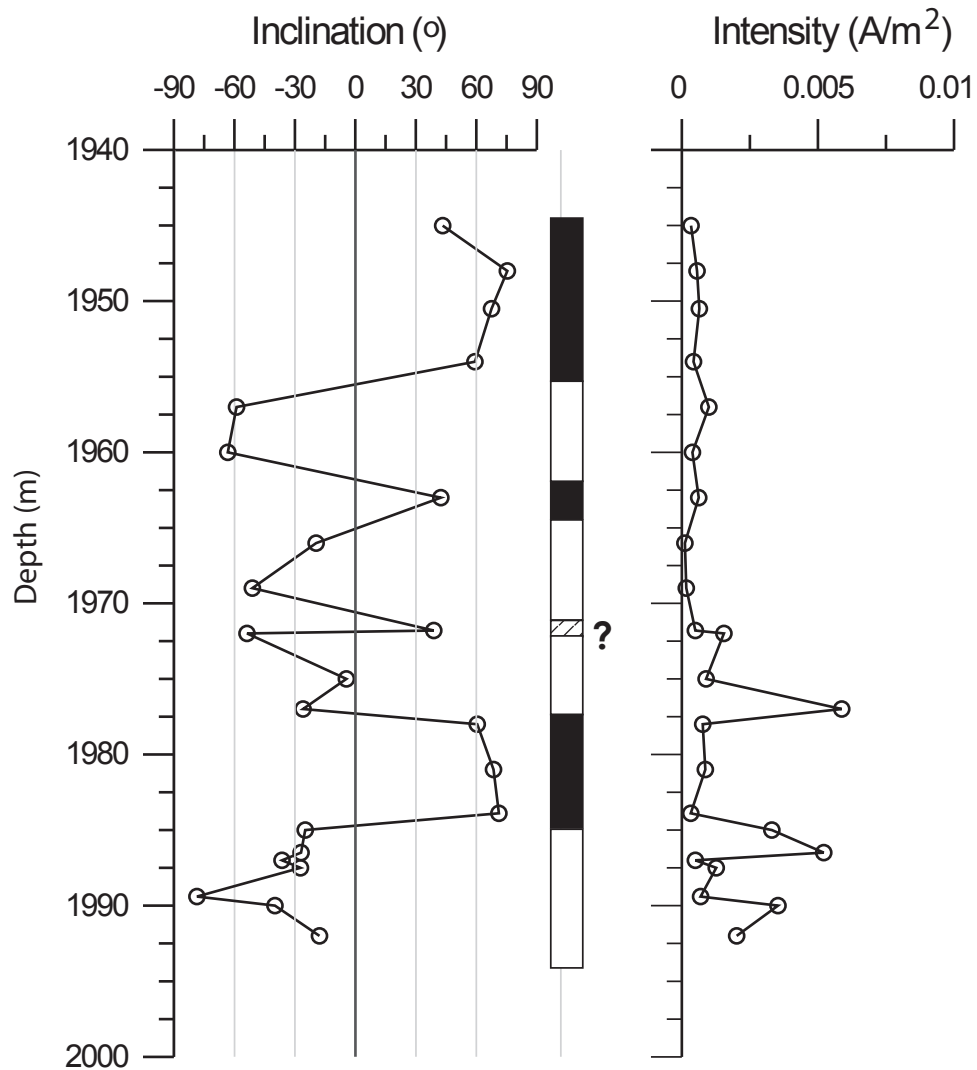


Figure 5.4. Shows normal and reverse polarity of measured samples from well: 12-35-14W6. The expected normal polarity inclination for the Early-Middle Triassic deposits range from 30 to 60 degrees. The expected reverse polarity inclination for the Early-Middle Triassic deposits range from -60 to -30 degrees. The observed inclination match the expected inclination for the Early-Middle Triassic.



- Normal polarity interval
- Reverse polarity interval
- Undefined polarity interval (only one sample)

Figure 5.5. Shows normal and reverse polarity of measured samples from well: 9-29-79-14W6. The expected normal polarity inclination for the Early – Middle Triassic deposits range from 30 to 60 degrees. The expected reverse polarity inclination for the Early – Middle Triassic deposits range from -30 to -60 degrees. The observed inclination presented in this figure match the expected inclination for the Early – Middle Triassic.

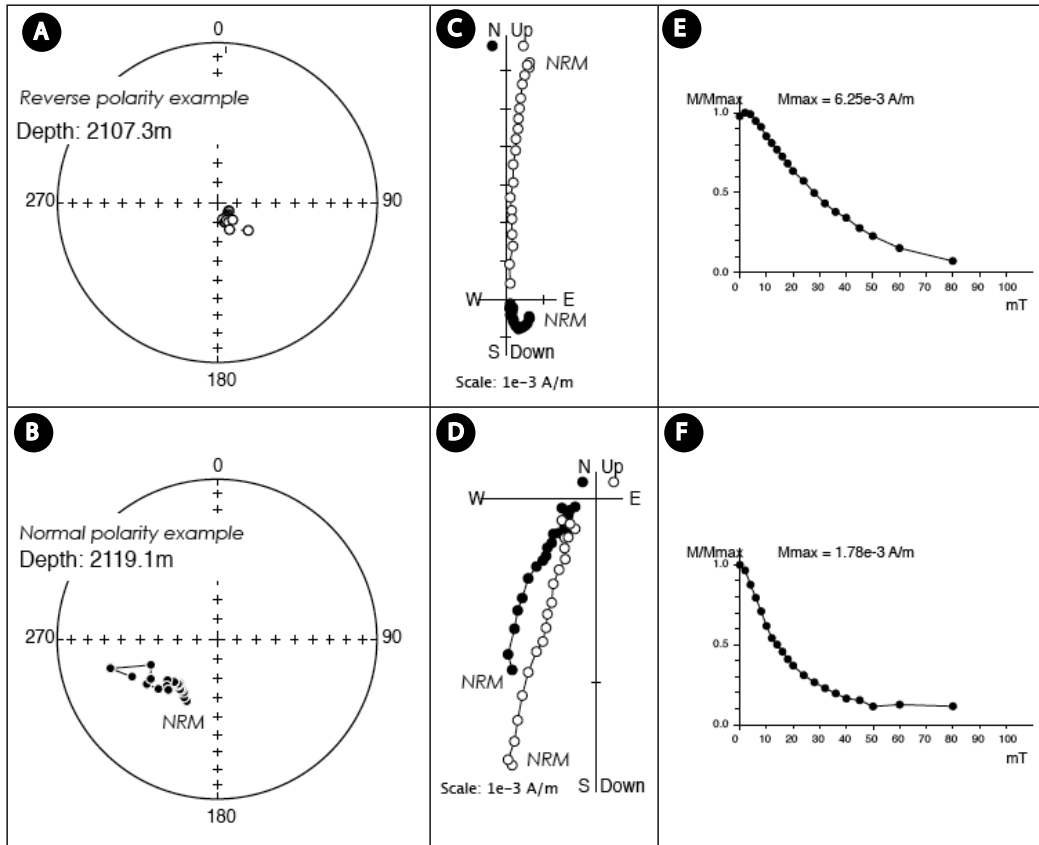


Figure 5.6. Results of alternating field demagnetization for the reverse and normal polarity for samples obtained from core (well: 12-35-79-17-W6). **(A and B)** Illustrates typical equal-area projections showing demagnetization paths during experiments. **(C and D)** Shows demagnetization orthogonal vector plots indicating strong normal remnant magnetization. **(E and F)** Illustrates normalized intensity of magnetization versus applied laboratory field in mT. Closed (open) symbols in orthogonal plots: projections onto the horizontal (vertical) plane. The core was not oriented azimuthally therefore declination is arbitrary.

RESULTS

A total of 128 samples of the Montney and Lower Doig formations from the Fort St. John study area (T86N, R23W and T74N, R13W) northeastern British Columbia were analyzed. Two of the studied wells (09-29-79-14W6 and 12-35-79-14W6) reveal both normal and reverse polarity intervals. Representative samples with the characteristic component of the reverse and normal are shown in (Figs. 5.4 and 5.5). A correlation of the geomagnetic polarity from this study matches a known portion of the Triassic geomagnetic polarity time scale (GPTS) at 245 Ma (Houselow, , 2008b)

DISCUSSIONS

The normal and reverse polarity intervals have been identified across the Upper Montney and lower Doig formations boundary. The position of the intervals with similar characteristics along the different core depths can be determined even where interpretations based on the well-log signature (gamma-ray, resistivity, seismic velocity) correlation is ambiguous. The geomagnetic polarity correlation from this study can be matched with known intervals of the Triassic GPTS (Houselow and Muttoni, 2010) at 245 Ma (Fig. 5.7). The results suggest that throughout the study area the lowermost Doig phosphatic zone (Montney / Doig boundary) may occur within a single magnetostratigraphic interval. Correlation of magnetostratigraphic data with as yet unpublished biostratigraphic data indicates that the base of the Doig phosphate coincides approximately with the Olenekian-Anisian boundary (=Lower-Middle Triassic boundary).

The results from this study suggest that the lowermost Doig phosphate zone may have identical paleomagnetic characteristics across the Montney and Doig boundary in different areas. This boundary is a coplanar *Trypanites – Glossifungites* demarcated discontinuity surface in all wells analyzed in this study and is herein interpreted to be a regionally correlatable surface (Eggbowaye, et al., 2011).

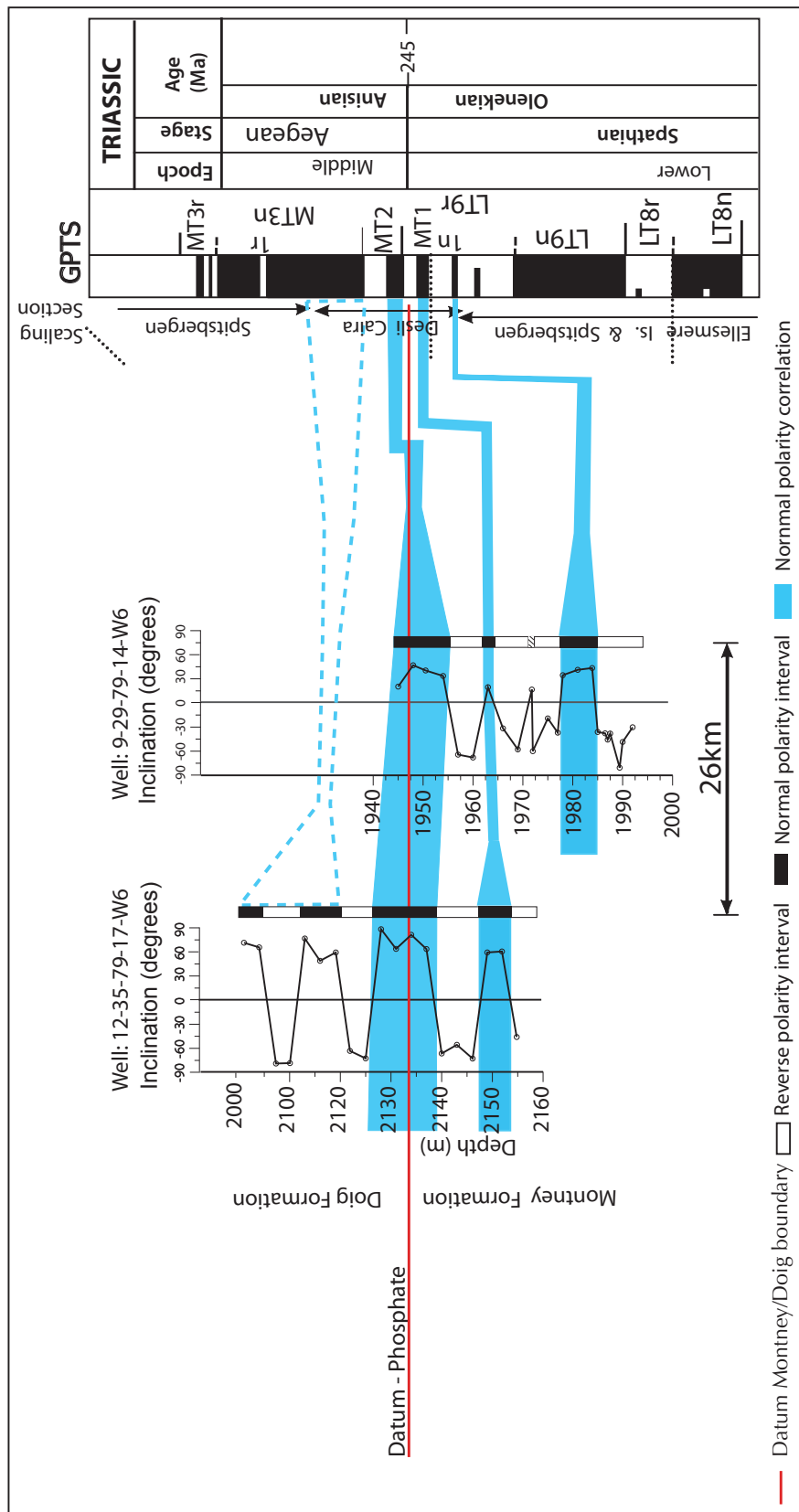


Figure 5.7. Paleomagnetic correlation of Lower Triassic (Lower Doig and Upper Montney formations) with known Triassic paleomagnetic data for Triassic. Ellesmere Island composite is from the Smith Creek and Creek of Embry sections of Ogg and Steiner (1991) and Orchard (2008). Upper Silesia composite (Nawrocki 1997; Nawrocki and Szulc, 2000); Spitsbergen composite (Hounslow et al., 2008a, b; Galfetti, et al., 2007b). The base Anisian used is the first occurrence of *Cs. timorensis* in the De_sli Cairra section (Gra_dinaru et al. 2007).

CONCLUSIONS

Accurate correlation within non-fossiliferous, fine-grained clastic successions such as the upper Montney and lower Doig formations is commonly problematic in the study area. Wire-line log correlations are often subjective and unambiguously synchronous marker horizons are not always common. A total of 128 samples from six well drill cores the Fort St. John study area (T86N, R23W and T74N, R13W) of northeastern British Columbia, were analyzed to evaluate the potential of applying magnetostratigraphic correlation techniques to the studied interval.

The results of these paleomagnetic measurements exhibit both normal and reverse polarities in the wells discussed herein (09-29-79-14W6 and 12-35-79-17W6). A correlation of the geomagnetic polarity from this study matches a known portion of the Triassic geomagnetic polarity time scale (GPTS) at 245 Ma (Fig. 5.7). The results suggest that the lowermost Doig phosphate zone may have identical paleomagnetic characteristics across the Montney and Doig formations boundary in different areas. This boundary is a coplanar *Trypanites* – *Glossifungites* demarcated discontinuity surface in all wells analyzed in this study and is herein interpreted to be a singular, regionally correlatable surface.

The boundary between Montney and Doig formations corresponds to the normal polarity interval MT2 in the bottom of the Anisian age that starts at ~ 245 Ma. This magnetostratigraphic record suggests that the Montney - Doig formation boundary may not be as diachronous as has previously been suggested.

The presence of the primary magnetization of normal and reverse polarity in the studied Triassic sedimentary cores suggests that magnetostratigraphy can be a useful chronostratigraphic tool in these strata. The geomagnetic polarity change, which is a global phenomenon, and provides an independent means of correlation that is not reliant upon well-log interpretations.

REFERENCES

- Butler, R.F., 1992, *Paleomagnetism: Magnetic Domains to Geologic Terranes*. Boston, Blackwell Scientific Publications, 238p.
- Brunhes, B., 1906, Recherches sur le direction d'aimantation des roches volcaniques. *Journal of Physics*, vol. 5, p. 705 – 724.
- Cogné, J.-P., 2003, PaleoMac: A Macintosh™ application for treating paleomagnetic data and making plate reconstructions. *Geochemistry Geophysics Geosystems*, vol. 4, no. 1, p.1007.
- Creer, K. M. 1959, AC demagnetisation of unstable Triassic Keuper Marls from SW England. *Geophysical Journal of the Royal Astronomical Society*, vol. 2, p. 261 – 275.
- Creer, K. M., IRVING, E. & RUNCORN, S. K. 1954. The direction of the geomagnetic field in remote epochs in Britain. *Philosophical Transactions of the Royal Society of London, Series A*, vol. 250, p. 144 – 156.
- Dixon, J., 2000, Regional lithostratigraphic units in the Triassic Montney Formation of Western Canada. *Bulletin of Canadian Petroleum Geology*, vol. 48, no. 1, p. 80 – 83.
- Dixon, J., 2005, A major unconformity at the base of the Upper Triassic Charlie Lake Formation in the Western Canada Sedimentary Basin. *Bulletin of Canadian Petroleum Geology*, vol. 53, no. 4, p. 432 – 453.
- Eggbowaye, E.I., Kravchinsky, V.A, Zonneveld, J-P, and Gingras, M.K, 2011, Magnetostratigraphy Dating and Correlation of the Lower Doig and Upper Montney Formations (Lower Triassic), Northeastern British Columbia, Western Canada. *Canadian society of Petroleum Geologists, CSPG, CSEG, CWLS Convention Abstract*, Calgary, Alberta, Canada, 5p. Accessed online on April 21, 2012.
- Enkin, R.J., 1996, A computer program package for analysis and presentation of paleomagnetic data, Pacific Geoscience Center, Geological Survey of Canada.
- Galfetti, T., Hochulu, P.A., Bucher, H., Wessert, H. and Vigran, J.O., 2007b, Smithian – Spathian boundary event: evidence from global climatic change in the wake of the end-Permian biotic crisis. *Geology*, vol. 35, p. 291– 294.
- Gradinaru, E., Orchard, M.J., et al., 2007, The Global Boundary Stratotype Section and Point (GSSP) for the base of the Anisian: Deșli Caira Hill, North Dobrogea, Romania. *Albertiana*, vol. 36, p. 54 – 71.

- Hailwood, E. A., 1989, The role of magnetostratigraphy in the development of geological time scales. *Paleoceanography*, vol. 4, no 1, p. 1 – 18.
- J. R. Heirtzler, G. O. Dickson, E. M. Herron, W. C. Pitman, III, and X. Le Pichon, Marine magnetic anomalies, geomagnetic field reversals, and motions of the ocean floor and continents, *J. Geophys. Res.*, v. 73, 2119–2136, 1968.
- Hillhouse, J. W., 1986, Magnetostratigraphy of the Koobi Fora Formation, Lake Turkana, Kenya. *Journal of Geophysical Research*, vol. 91, no. B11, p.11,581 – 11,595.
- Houselow, M.W., Peters, C., Mørk, A., Weitschat, W. and Vigran, J.O., 2008a, Biomagnetostratigraphy of the Vikinghøgda Formation, Svalbard (arctic Norway) and the geomagnetic polarity timescale for the Lower Triassic. *Geological Society of America Bulletin*, vol. 120, p. 1305 – 1325.
- Houselow, M.W., Hu, M., Mørk, A., Weitschat, W., Vigran, J.O., Karlouko-vski, V., and Orchard, M.J., 2008b, Intercalibration of Boreal and Tethyan timescales: the magneto-biostratigraphy of the Middle Triassic and the latest Early Triassic, central Spitsbergen (arctic Norway). *Polar Research*, vol. 27, p. 469 – 490.
- Houselow, M.W., Muttoni, G., 2010, The geomagnetic polarity timescale for the Triassic: linkage to stage boundary definitions. *Geological Society, London, Special Publications*, vol. 334, p. 61–102.
- Kent, D. V., Olsen, P.E., and Witte, W.K., 1995, Late Triassic-earliest Jurassic geomagnetic polarity sequence and paleolatitudes from drill cores in the Newark rift basin, eastern North America. *Journal of Geophysical Research*, vol. 100, no. B8, p.14,965 – 14,998.
- Kirschvink, J.L., 1980. The least-squares line and plane and the analysis of paleomagnetic data, *Geophysical Journal of Research and Astronomy Society*, vol. 62, p. 699 – 718.
- Matuyama, M., 1929, On the direction of magnetization in basalt in Japan, Tyosen and Manchuria. *Proceedings of the Imperial Academy of Japan*, vol. 5, p. 203 – 205.
- Merrill, R.T., M.W. McElhinny and P.L. McFadden, 1996. *The Magnetic Field of the Earth Paleomagnetism, the Core, and the Deep Mantle*, San Diego: Academic Press, 531 p. 1996.
- Nawrocki, J. 1997, Permian to early Triassic magnetostratigraphy from the central European basin in Poland: implications on regional and worldwide correlations. *Earth Planetary Science Letters*, vol. 152, p. 37 – 58.

- Nawrocki, J., and Szulc, J., 2000, The Middle Triassic magnetostratigraphy from the Peri-Tethys basin in Poland. *Earth and Planetary Science Letters*, vol. 182, p. 77 – 92.
- Ogg, J.G., and Steiner, M.B., 1991, Early Triassic polarity time-scale: integration of magnetostratigraphy, ammonite zonation and sequence stratigraphy from stratotype sections (Canadian Arctic Archipelago). *Earth and Planetary Science Letters*, vol. 107, p. 69 – 89.
- Orchard, M.J., 2008. Lower Triassic conodonts from the Canadian arctic, their intercalibration with ammonoid-based stages and a comparison with other North American Olenekian faunas. *Polar Research*, vol. 27, p. 393 – 412.

CHAPTER 6: SUMMARY AND CONCLUSIONS

This dissertation emerged at a time when unconventional (shale or tight) gas reservoir is the new focus for hydrocarbon exploration and production in the petroleum industry. This paradigm shift from conventional oil and gas exploration methods occurred because most conventional reservoir basins around the world have reached maturity, and are almost depleted. Thus, attention is shifting to alternative reservoir systems, such as shale gas or tight oil and gas reservoirs.

Methods used in this study comprises core logging, whole-rock and bulk mineralogical analysis, thin-section petrography, scanning electron microscopy (SEM), x-ray diffraction (XRD) analysis, tight rock analysis (TRA), Rock-Eval pyrolysis, whole-rock elemental geochemical analysis (using ICP-MS), and stable isotope geochemistry (Carbon and Oxygen).

The results presented in this study show a characterization of the Montney Formation with respect to all the elements that are crucial in unconventional gas reservoir exploration, such as integration of sedimentological, ichnological and depositional characteristics, including systematic and detailed facies heterogeneity analysis (discussed in chapter 2). Source-rock geochemical evaluation and interpretation of the Montney Formation is discussed in chapter 3. Analyses of isotope geochemistry in relation to paleotemperature, dolomitization and diagenesis is discussed in chapter 4. Chapter 5 discussed paleomagnetic technique, which was utilized in this study to correlate the Lower Doig Formation and the Upper Montney Formation because paleomagnetism provides a record of past configurations of the geomagnetic field, which aids refinement of stratigraphic correlations and geochronologic calibrations of both marine and non-marine sedimentary successions (Butler, 2004).

The Montney Formation is the basal stratigraphic unit of the Triassic suc-

cession in the subsurface of western Canada. It rests, unconformably in most areas, upon carbonate or mixed siliciclastic-carbonate strata of Carboniferous to Permian age (Edward et al., 1994; Pudruski, et al., 1988; Gibson and Edwards, 1990; Zonneveld, et al., 2010b). The succession was deposited in a west-facing, arcuate extensional basin on the western margin of Pangaea Supercontinent (Davies et al., 1997; Orchard and Tozar, 1997; Zonneveld, 1999; Zonneveld et al., 2001).

The Montney Formation consists of siltstone with subordinate interlaminated very fine-grained sandstone. Based on sedimentological and ichnological criteria, the Montney Formation in the Fort St. John area (T86N, R23W and T74N, R13W), northeastern British Columbia, five Facies Associations were identified in the study interval (Table 2.1): Lithofacies F-1 (organic rich, wavy to parallel laminated, organic rich, black colored siltstone); Lithofacies F-2 (very fine-grained sandstone interbedded with siltstone); Lithofacies F-3A (bioturbated silty-sandstone attributed to the *Skolithos* ichnofacies); Lithofacies F-3B (bioturbated siltstone composed of *Cruziana* ichnofacies); Lithofacies F-4 (dolomitic, very fine-grained sandstone); and Lithofacies F-5 (massive siltstone).

The depositional environments interpreted for the Montney Formation in the study area is lower shoreface through proximal offshore to distal offshore settings. The lower shoreface environment record trace fossils attributed to the *Skolithos* ichnofacies; the proximal offshore environment have sedimentary structures formed under quiescent depositional conditions typically found below the fair weather wave base such as lamination; and the distal offshore environment have trace fossils attributed to distal expression of the *Cruziana* ichnofacies, including sedimentary structures depicting sediment loading (convolute lamination /bedding) and infauna escape traces (fugichnia), which are evidence of storm events, or small scale episodic deposition due to local transport from lower shoreface or proximal offshore to distal setting. The ichnofauna of the Montney Formation in the study

area is less diverse, and ichnofauna abundance is mainly composed of mono-specific ichnogenera. The most commonly well-preserved trace fossils in cores are *Planolites*, indicating infauna behavior associated with feeding. The impoverished ichnofauna diversity and abundances probably suggests the effects of the aftermath recovery of the Permian-Triassic (P-T) extinction.

The Triassic Montney Formation in the Forth St. John study area is classified as unconventional hydrocarbon reservoir (Faraj, et al., 2002, Walsh, et al., 2006; Berger, et al., 2009; Core Lab, 2009; Egbobawaye, et al., 2010, 2011). In general, unconventional hydrocarbon reservoirs comprises tight gas, shale gas and coalbed methane (Haines, et al., 2006). Until recently, these reservoirs were previously considered non-economical, unproductive, and non-exploitable geological formations owing to lesser advancement in technology. The inherent petrophysical properties of unconventional reservoirs are low matrix porosity of $\leq 10\%$ and permeability of ≤ 0.1 millidarcy, exclusive of fracture permeability (Haines, et al., 2006). Typically, these reservoirs depend on stimulation for production, and in general, contain large amounts of hydrocarbons; although, gas recovery factors may be low (Schmoker, 1995).

The Montney Formation in the study area has the following reservoir characteristics: 1) it is a source rock rich in organic matter (Riediger, et al., 1990); 2) it has a thermal maturity that lies within the gas generating window, and it is primarily a gas prone mixed Type II/III kerogen (Riediger, et al., 1990); 3) the present study shows that the kerogen of the Montney Formation in the study area is mainly composed of Type III/IV and some mixed Type II/III kerogen with average TOC of 0.5 – 4%; and are upto 8.2% TOC (rare, but present); 4) it has a reservoir thickness upto 320 meters in the study area; 5) it hosts substantial volumes of unconventional gas, estimated to be 187 TCF (Walsh, et al., 2006); and 6) porosities range from 2 – 10%, and sporadically $>10\%$ in some intervals where ichnofabric or dolomite dis-

solution have resulted in the formation of secondary porosity. These criteria make the Montney Formation an unconventional resource play with high potential within the Fort St. John study area, northeastern British Columbia (Fig. 3.1).

The result from $\delta^{13}\text{C}_{\text{PDB}}$ bulk calcite in this study show depletion in the isotopic composition ($\delta^{13}\text{C}_{\text{PDB}}$ -2.8 to -6.10%). The negative $\delta^{13}\text{C}_{\text{PDB}}$ values are indicative of pore-water derived from seawater and dissolution of metastable carbonate in conjunction with organic matter decomposition by bacteria in sulfate reducing environment. The organic carbon content of the Montney lithofacies is a result of high nutrient rich sediment source, rapid sedimentation, and preservation of organic matter (Muller and Suess, 1979) in oxygen-depleted, anoxic depositional environment (Demaison and Moore, 1980; Ekdale and Mason, 1988; Wishner, et al., 1990; Tyson and Pearson, 1991; Wignall and Hallam, 1991; Bentley and Nittrouer, 1999). This phenomenon explains the biasing of carbon isotope towards a very low (negative $\delta^{13}\text{C}_{\text{PDB}}$) discerned from the Montney Formation. The anoxic condition generate high alkalinity, which increases the total dissolved carbon that causes calcite to precipitate from pore-water, thereby biased towards light $\delta^{13}\text{C}_{\text{PDB}}$ values during early diagenesis (Larsen and Chilingar, 1967).

The depleted $\delta^{18}\text{O}_{\text{PDB}}$ of bulk calcite values range from ($\delta^{18}\text{O}_{\text{PDB}}$ -3.66 to -16.15%) and the $\delta^{18}\text{O}_{\text{SMOW}}$ range between 22.48 and 27.42% (which is within the fresh water range) reported by Taylor (1967) as indication of mixing of marine pore-water and meteoric groundwater during authigenic calcite precipitation. The paleotemperature under which the calcite may have been precipitated is interpreted to have occurred between approximately 32°C to 33°C . This interpretation is consistent with a warm paleotemperature reported for the Triassic period of western Canada (e.g. Habieth, 1979; Tozer, 1982; Arnold, 1994).

The bulk dolomite isotopic values ($\delta^{13}\text{C}_{\text{PDB}}$ -2.71 to -8.46%) provide information on the origin and the precipitation of the dolomite. The very low (negative)

values of $\delta^{13}\text{C}_{\text{PDB}}$ of bulk dolomite from the Montney sediment indicate depletion ($\delta^{13}\text{C}_{\text{PDB}} -2.71$ to -8.46%). The interpretation for the negative values (light bulk-dolomite $\delta^{13}\text{C}_{\text{PDB}}$) indicates that biogenic CO_2 significantly contributed to the total dissolved inorganic carbon (Freidman and Murata, 1979).

The petrophysical properties of the Montney Formation show evidence that the porosity and permeability is controlled by grain texture, pore-throat structure, which is determined by grain shape, grain size, sorting, grain orientation, packing, and chemical composition (cementation and diagenetic modification). Porosity distribution within the study area is pervasively tight and they are in the range from 2% to 10%, and exceptionally few data point in some wells intervals, > 12% porosity is evident. Strikingly, there is no perfect correlation between porosity and permeability (as usually expected) in the wells where continuous porosity and permeability measurement is plotted in depth relationship. Although permeability is significantly variable in most intervals: extremely low ($K = 0.000040\text{mD}$), low permeability range ($K = 0.01$ to 0.56mD), and moderately low ($K = 0.1 - 5.8\text{mD}$). However, permeability values, shows that relatively higher permeability values were in intervals were trace fossils 'burrows' have occurred. Thus, suggesting that burrows may have been the intertwining link of intra-pore spaces, contributing to matrix / inter-particle interconnectivity of pores, thereby resulting in effective porosity that produces the permeability.

In the course of the stratigraphic correlation of the Upper Montney Formation and Lower Doig Formation (along the boundary) in the Fort St. John study area, paleomagnetic technique was utilized. The demagnetization experiments demonstrated the presence of primary magnetization of normal and reverse polarity in all samples (Figs. 5.4 and 5.5). Demagnetization results were plotted as orthogonal vectors diagrams and as equal-area projections (Fig. 5.6). The paleomagnetic directions were determined using principal component analysis (Kirshvink, 1980).

All interpretations and data processing were carried out using the PaleoMac software (Cogné, 2003) and Enkin's PC software (Enkin, 1996).

Two of the studied wells (09-29-79-14W6 and 12-35-79-14W6) reveal both normal and reverse polarity intervals. Representative samples with the characteristic component of the reverse and normal intervals are shown in (Figs. 5.4 and 5.5). A correlation of the geomagnetic polarity from this study matches a known portion of the Triassic geomagnetic polarity time scale (GPTS) at 245 Ma.

REFERENCES

- Arnold, K.J., 1994, Origin and distribution of eolian sandstones in the Triassic Charlie Lake Formation, northeastern British Columbia. Unpublished M.Sc. thesis, University of Alberta, Edmonton, 320p.
- Butler, R.F., 1992, Paleomagnetism: Magnetic Domains to Geologic Terranes. Boston, Blackwell Scientific Publications, 238p.
- Barclay, J.E., Krause, F.F., Campbell, R.I., and Utting, J., 1990, Dynamic casting and growth faulting: Dawson Creek Graben Complex, Carboniferous-Permian Peace River Embayment, Western Canada, In: Geology of the Peace River Arch, S.C. O'Connell and J.S. Bell (eds.), Bulletin of Canadian Petroleum Geology, vol. 38A, p.115-145.
- Bentley, S.J. and Nitouer, C.A., 1999, Physical and biological influences on the formation of sedimentary fabric in an oxygen-restricted depositional environment: Eckernförde bay, southwestern Baltic Sea. *Palaios*, vol. 14, p. 585 – 600.
- Berger, Z., M. Boast, and M. Mushayandebvu, 2009, The contribution of Integrated HRAM studies to exploration and Exploitation of unconventional plays in North America. Part 2: Basement structures control on the development of the Peace River Arch's Montney / Doig resource plays. *Reservoir*, vol. 36, Issue 2, p. 40 – 44.
- Cogné, J.-P., 2003, PaleoMac: A Macintosh™ application for treating paleomagnetic data and making plate reconstructions. *Geochemistry Geophysics Geosystems*, vol. 4, no. 1, p.1007.
- Demaison, G.J., and G.T. Moor, 1980, Anoxic environments and oil source rock bed genesis. *American Association of Petroleum Geologists Bulletin*, vol. 64, p. 1179 – 1209.

- Ekdale, A.A., and Mason, T.R., 1988, Characteristic trace-fossil associations in oxygen-poor sedimentary environments. *Geology*, vol. 16, p. 720 – 723.
- Eggbowaye, E.I., J.P., Zonneveld, and M.K., Gingras, 2010, Tight gas reservoir evaluation in Montney and Lower Doig formations, northeastern British Columbia, western Canada. *AAPG Abstract*, vol. 19, p. 66-67.
- Eggbowaye, E.I., Kravchinsky, V.A, Zonneveld, J-P, and Gingras, M.K, Magnetostratigraphy Dating and Correlation of the Lower Doig and Upper Montney Formations (Lower Triassic), Northeastern British Columbia, Western Canada. Canadian society of Petroleum Geologists, CSPG, CSEG, CWLS Convention Abstract, Calgary, Alberta, Canada, 5p. Accessed online on June 20, 2011: <http://www.geoconvention.com/conference/technicalprogram/tuesday/pm-2/montney-i.html>
- Enkin, R.J., 1996, A computer program package for analysis and presentation of paleomagnetic data, Pacific Geoscience Center, Geological Survey of Canada.
- Edwards, D.E., Barclay, J.E., Gibson, D.W., Kvill, G.E., and Halton, E. 1994, Triassic strata of the Western Canada Sedimentary Basin. In: *Geological Atlas of the Western Canada Sedimentary Basin*. G.D. Mossop and I. Shetso (compilers). Canadian Society of Petroleum Geologists, p. 257–275.
- Espitalie, J., Deroo, G. and Marquis, F., 1985, Rock Eval Pyrolysis and Its Faraj, B., H. Williams, G. Addison, B. McKinstry, R. Donaleshen, G. Sloan, J. Lee, T. Anderson, R. Leal, C. Anderson, C. Lafleur, and J Ahlstrom, 2002, Shale potential of selected upper Cretaceous, Jurassic, Triassic and Devonian shale formations, in the WCSB of Western Canada: Implications for shale gas production. A report for Gas Technology Institute (GTI), Des Plaines, Illinois, USA.
- Friedman, I., and Murata, K.J., 1979, Origin of dolomite in Miocene Monterey

- Shale and related formations in the Temblor Range, California. *Geochim Cosmochim. Acta*, vol. 43, no. 8, p. 1357-1365.
- Gibson, D.W. and Edwards, D.E. 1990, An overview of Triassic stratigraphy and depositional environments in the Rocky Mountain Foothills and Western Interior Plains, Peace River Arch area. *Bulletin of Canadian Petroleum Geology*, vol. 38A, p. 146-158.
- Haines, L., N. Darbonne, M. A. Barbee, P. Williams, G. Clouser, D. Wagman, M. Conly, and J. Grant, 2006, Tight gas. A supplement to Oil and Gas Investor. Hart Energy Publishing, Houston, Texas, 14p.
- Habicht, J.K.A., 1979, Paleoclimate, paleomagnetism, and continental drift. *American Association of Petroleum Geologists Studies in Geology* 9, 1 - 29.
- Kirschvink, J.L., 1980, The least-squares line and plane and the analysis of paleomagnetic data, *Geophysical Journal of Research and Astronomy Society*, vol. 62, p. 699 - 718.
- Larsen, G., and Chilingar, G.V., 1967, Diagenesis in sediments. Elsevier Publishing Co., New York, 551p.
- Orchard, M.J. and Tozer, E.T., 1997, Triassic conodont biochronology, its calibration with the ammonoid standard, and a biostratigraphic summary for Western Canada Sedimentary Basin. *Bulletin of Canadian Petroleum Geology*, vol. 45, 675-692p.
- Podruski, J.A., Barclay, J.E., Hamblin, A.P., Lee, P.J., Osadetz, K.G., Procter, R.M., and Taylor, G.C., 1988, Conventional Oil Resources of Western Canada.
- Reidiger, C.L., Fowler, M.G., Brooks, P.W. and Snowdon, L.R. 1990a, Triassic oils and potential Mesozoic source rocks, Peace River Arch area, Western Canada Basin. *Organic Geochemistry*, v. 16, p. 295-305.

- Schmoker, J. W., 1995, Method for assessing continuous-type (unconventional) hydrocarbon accumulations *In*: D. L. Gautier, G. L. Dolton, K. I. Takahashi, and K. L. Varnes, eds., 1995 National assessment of United States oil and gas resources—Results, methodology, and supporting data: U.S. Geological Survey Digital Data Series 30, CD-ROM.
- Taylor, H.P.JR., 1967, Oxygen isotope studies of hydrothermal mineral deposits. *In*: Barnes, H.L. (eds.), *Geochemistry of hydrothermal Ore Deposits*: Holt, Rinehart and Winston, New York, p. 109 – 142.
- Tozer, E.T., 1982, Marine Triassic faunas of North America: their significance for assessing plate and terrane movements. *Geologische Rundschau* 71, 1077–1104.
- Tyson, R.V., and Pearson, T.H., 1991, Modern and ancient continental shelf anoxia: An overview: in Tyson, R.V., and Pearson T.H., eds., *Modern and Ancient Continental Shelf Anoxia*: Geological Society of London Special Publication 58, p. 1 – 24.
- Walsh, W., Adams, A., Kerr, B. and Korol, J, 2006, “Regional Shale Gas” Potential of the Triassic Doig and Montney Formations, Northeastern British Columbia. Ministry of Energy, Mines and Petroleum Resources, Oil and Gas Division, Resource Development and Geoscience Branch, British Columbia, Petroleum geology open file 2006-02, 19p.
- Wishner, K., Levin, L., Gowing, M., And Mullineaux, L., 1990, Involvement of the oxygen minimum in benthic zonation on a deep seamount. *Nature*, vol. 346, p. 57–58.
- Wignall, P.B., and Hallam, A., 1991, Biofacies, stratigraphic distribution, and depositional models of British onshore Jurassic black shales: in Tyson, R.V., and Pearson, T.H., eds., *Modern and Ancient Continental Shelf Anoxia*:

Geological Society of London Special Publication 58, p. 291–309.

- Wignall, P.B., and Hallam, A., 1992, Anoxia as a cause of the Permian/Triassic mass extinction: Facies evidence from northern Italy and the western United States. *Palaeogeography, Palaeoclimatology, Palaeoecology*, vol. 93, p. 21 – 46.
- Zonneveld, J.P., Gingras, M.K., and Pemberton, S.G., 2001, Trace fossils assemblages in a Middle Triassic mixed siliciclastic-carbonate marginal marine depositional system, British Columbia. *Palaeogeography, Palaeoclimatology, Palaeoecology*, vol. 166 (3-4), p.249-276.
- Zonneveld, J.P., 1999, Sedimentology and sequence biostratigraphic framework of mixed siliciclastic-carbonate depositional system, Middle Triassic, north-eastern British Columbia. Unpublished Ph.D. Dissertation, University of Alberta, 287p.
- Zonneveld, J-P., Gingras, M.K., and Beatty, T.W., 2010b, Diverse Ichnofossil Assemblages Following The P-T mass extinction, Lower Triassic, Alberta and British Columbia, Canada: Evidence For Shallow Marine Refugia on the northwestern coast of Pangaea. *Palaios*, vol. 25, no. 6, p. 368 – 392.

APPENDIX – 1: Table below is showing compilation of all the wells in the study area that penetrated the Montney Formation in the subsurface of northeastern British Columbia. The Montney Formation tops and base were picked in all wells generate the isopach and structure maps of the Montney Formation.

Well Location	Well Name	Latitude	Longitude	Field
100010508821W600	BAYTEX ET AL W STODDART	56.5971	-121.29931	STODDART WEST
100011008223W600	ADU MONIAS 01-10-082-23	56.09043	-121.51667	MONIAS
100011408419W600	PENN WEST FT. ST. JOHN 08	56.27977	-120.87596	FORT ST JOHN
100011508619W600	PENN WEST STODDART 01-15-	56.45302	-120.90373	STODDART
100011708018W600	SHELL IMP SUNSET 01-17-08	55.92748	-120.77133	SUNSET PRAIRIE
100012308421W600	TERRA BEAR FLAT 09-23-084	56.29791	-121.19138	BOUDREAU
100012507918W600	ECA SUNRISE 01-25-079-18	55.87248	-120.66704	SUNRISE
100012508820W600	CNRL BUICK A01-25-088-20	56.65609	-121.03623	BUICK CREEK
100012608015W600	VINTAGE DOE 01-26-080-15	55.95965	-120.22359	DOE
100013008422W600	PENGROWTH ET AL ATTACHIE	56.30741	-121.45746	ATTACHIE
100013107914W600	ARC DAWSON 01-31-079-14	55.88401	-120.16855	REGIONAL HERITA
100013408223W600	ADU MONIAS 01-34-082-23	56.14669	-121.50112	MONIAS
100013408625W600	CNRL HALFWAY 01-34-086-25	56.49687	-121.85221	HALFWAY
100013607815W600	ARC KILKERRAN 01-36-078-1	55.79639	-120.1722	REGIONAL HERITA
100013607915W600	ARC DAWSON 01-36-079-15	55.884	-120.19298	REGIONAL HERITA
100013608122W600	ADU MONIAS 01-36-081-22	56.06064	-121.29238	MONIAS
100020508821W600	BAYTEX ET AL HZ W STODDAR	56.59126	-121.30903	STODDART WEST
100021708517W600	TALISMAN ET AL W FLATROCK	56.36531	-120.64198	FLATROCK WEST
100022708216W600	PROGRESS TWO RIVERS 02-27	56.13365	-120.4081	OTHER AREAS
100022907914W600	ARC DAWSON 02-29-079-14	55.86974	-120.14883	REGIONAL HERITA
100023008116W600	STORM EXP PARKLAND 02-30-	56.04549	-120.491	OTHER AREAS
100023008721W600	BAYTEX ET AL HZ W STODDAR	56.57183	-121.31608	STODDART WEST
100023208518W600	CNRES STODDART 02-32-085-	56.40926	-120.80359	STODDART
100030207815W600	ECAOG S DAWSON 03-02-078-	55.7242	-120.21094	OTHER AREAS
100030908516W600	CDN FOREST ET AL FLATROCK	56.35027	-120.4649	FLATROCK
100031408221W600	ECA ECOG MONIAS 03-14-082	56.10266	-121.17425	MONIAS
100031507919W600	SHELL ET AL SUNSET 03-15-	55.84269	-120.8883	REGIONAL HERITA
100031508019W600	ESSO CHEL HORSESHOE 03-15	55.93012	-120.88787	OTHER AREAS
100031508523W600	CEGO ET AL COPLIN 03-15-0	56.36607	-121.54839	OTHER AREAS
100031808222W600	ECA ECOG MONIAS 03-18-082-22	56.1029987	-121.4334071	
				GROUND BIRCH
100032907819W600	COPOL ET AL GROUND BIRCH 0	55.78242	-120.9121	
100033008014W600	SUNCOR SUNCOR DOE 03-30-0	55.95707	-120.18128	DOE
100041308415W600	SUNCOR PC BOUNDARY 04-13-	56.2781	-120.23714	BOUNDARY LAKE
100041507917W600	ECA HZ SUNRISE 03-21-079-17	55.85502095	-120.6016962	SUNRISE
100041707714W600	ECA BISSETTE 04-17-077-14	55.66799	-120.13993	REGIONAL HERITA
100042408423W600	CEGO ET AL ATTACHIE 04-24	56.29147	-121.49891	OTHER AREAS
100042508820W600	CNRL HZ BUICK 01-25-088-2	56.65609	-121.03432	BUICK CREEK
100042807914W600	ARC DAWSON 04-28-079-14	55.86975	-120.13294	REGIONAL HERITA
100042908318W600	PENN WEST ET AL FT ST JOH	56.22053	-120.81329	FORT ST JOHN
	INVERNESS SCEPTRE BDLKS			
100043208412W600	4-32-84-12	56.3223269	-119.8653343	BOUNDARY LAKE SOUTH
100043408321W600	TAQA NORTH ET AL MONIAS 0	56.23497	-121.23614	MONIAS
100050107816W600	ECA SUNRISE 05-01-078-16	55.72918	-120.3478	SUNRISE
100050308118W600	SHELL ET AL SUNSET 05-03-	55.99235	-120.73651	SUNSET PRAIRIE

100050708222W600	ADU HZ MONIAS 05-07-082-2	56.09313	-121.43707	MONIAS
100050908019W600	SHELL SATURN 05-09-080-19	55.91935	-120.91586	SATURN
100051108317W600	STARPOINT ET AL SE FORT ST JOHN	56.1816838	-120.5807614	
100051407811W600	AECOG (W) PCOUPES 5-14-78-11	55.7589041	-119.5959115	
100051808219W600	ESSO ET AL STEWART 14-07-	56.09872	-120.96658	OTHER AREAS
100052107914W600	ARC DAWSON 05-21-079-14	55.86047	-120.13414	REGIONAL HERITA
100052307819W600	SHELL GROUNDBIRCH 05-23-0	55.77226	-120.83983	GROUNDBIRCH
100052808721W600	BAYTEX ET AL HZ W STODDAR	56.56781	-121.30274	STODDART WEST
100052908013W600	HESS UPRI DOE 05-29-080-1	55.96048	-120.00717	DOE
100053208623W600	HUSKY INGA B06-32-086-23	56.49931	-121.6008	INGA
100053307819W600	SHELL GROUNDBIRCH 05-33-0	55.8018	-120.89317	GROUNDBIRCH
100060208223W600	CNRL SHELL MONIAS 06-02-0	56.07972	-121.48371	OTHER AREAS
100060508223W600	EXXONMOBIL BOUCHER 06-05-	56.07986	-121.56452	OTHER AREAS
100060707920W600	SHELL GROUNDBIRCH 06-07-0	55.83075	-121.12065	GROUNDBIRCH
100060708517W600	PENN WEST CECIL 06-07-085	56.35422	-120.6771	CECIL LAKE
100060808422W600	HOME ET AL ATTACHIE 06-08	56.26642	-121.44203	OTHER AREAS
100060908322W600	BA ET AL MOBERLY 06-09-08	56.18001	-121.41428	OTHER AREAS
100061007714W600	DOVE TOTAL TUPPER 06-10-0	55.65583	-120.08395	OTHER AREAS
100061008422W600	LADD ATTACHIE 06-10-084-2	56.26559	-121.39095	OTHER AREAS
100061008516W600	CDN FOREST ET AL FLATROCK	56.35373	-120.43854	FLATROCK
100061008525W600	DEVON ET AL FARRELL 06-10	56.35354	-121.86346	OTHER AREAS
100061207719W600	COPOL BRASSEY 06-12-077-1	55.65623	-120.80921	BRASSEY
100061207912W600	AECOG (W) GRDONDLE	55.83166	-119.7362431	
100061208517W600	COPOL ET AL W FLATROCK 06	56.35316	-120.54719	FLATROCK WEST
100061308316W600	GALLEON TWO RIVERS 06-13-	56.19377	-120.38816	TWO RIVERS
100061308421W600	TERRA BOUDREAU 06-13-084-	56.28037	-121.17716	BOUDREAU
100061308521W600	SCURRY ET AL RED CREEK 06	56.36841	-121.17878	RED CREEK
100061408417W600	ATLANTIS KEYSTONE FLATROC	56.28155	-120.57102	FLATROCK
100061408518W600	MURPHY N PINE 06-14-085-1	56.36784	-120.72984	PINE NORTH
100061508114W600	TAQA NORTH ET AL MICA 06-	56.02003	-120.1029	MICA
100061608520W600	PROGRESS W STODDART 06-16	56.36903	-121.09949	STODDART WEST
100061708222W600	CNRL SHELL MONIAS 06-17-0	56.10724	-121.41039	MONIAS
100061708519W600	SCURRY ET AL S STODDART 0	56.36831	-120.96783	STODDART SOUTH
100061708618W600	DOVE STODDART 06-17-086-1	56.45552	-120.81073	OWL
100061808013W600	GULF DOE 06-18-080-13	55.93387	-120.02656	DOE
100061808015W600	DEVON PEMBINA FARMINGTON	55.93261	-120.33796	DAWSON CREEK
100061808520W600	SCURRY ET AL RED CREEK 06	56.36829	-121.15217	RED CREEK
100062108417W600	PROGRESS ET AL CECIL 06-2	56.29605	-120.62434	CECIL LAKE
100062808518W600	KILO STODDART 06-28-085-1	56.3973	-120.78346	STODDART
100062808619W600	FOCUS ET AL STODDART 06-2	56.48414	-120.94034	STODDART
100062908422W600	DEVON ESSO ATTACHIE 06-29	56.31087	-121.44051	ATTACHIE
100063008316W600	PROGRESS ET AL AIRPORT 06	56.22313	-120.52274	AIRPORT
100063107813W600	ARC BRIAR RIDGE 06-31-078	55.80105	-120.00486	BRIAR RIDGE
100063108518W600	PENN WEST STODDART 06-31-	56.41182	-120.83603	STODDART
100063408420W600	NUMAC ET AL TEA 06-34-084	56.3246	-121.07422	OTHER AREAS
100070207819W600	SHELL GROUNDBIRCH 07-02-0	55.72978	-120.82669	OTHER AREAS
100070208014W600	AMOCO DOE 07-02-080-14	55.90311	-120.06951	DOE
100070208222W600	DEVON MONIAS 07-02-082-22	56.07813	-121.32322	MONIAS
100070508219W600	TERRA ET AL SEPTIMUS 07-0	56.07832	-120.93095	OTHER AREAS
100070608223W600	NUMAC GATES 07-06-082-23	56.07851	-121.58374	OTHER AREAS
100070608622W600	LADD BLUEJAY 07-06-086-22	56.4273	-121.4622	OTHER AREAS

100070807918W600	OEI ATAPCO SUNSET 07-08-0	55.82988	-120.77724	OTHER AREAS
100070808421W600	INVERNESS ET AL BOUDREAU	56.26554	-121.27591	OTHER AREAS
100071007919W600	SHELL IMP GROUNDBIRCH 07-	55.82901	-120.87998	GROUNDBIRCH
100071008315W600	GALLEON ET AL TWO RIVERS	56.17872	-120.27829	TWO RIVERS
100071307915W600	ARC DAWSON 07-13-079-15	55.84666	-120.20333	REGIONAL HERITA
100071607919W600	SHELL ET AL GROUNDBIRCH 0	55.84663	-120.90795	GROUNDBIRCH
100071708221W600	CNRL ET AL MONIAS 07-17-0	56.10625	-121.24383	MONIAS
100071908220W600	ITERATION MONIAS 07-19-08	56.12086	-121.11483	MONIAS
100072008422W600	DEVON ET AL ATTACHIE 07-2	56.29553	-121.43562	ATTACHIE
100072108221W600	CNRL ET AL MONIAS 07-21-0	56.12099	-121.21767	MONIAS
100072207719W600	BRC HTR BLUEGOOSE 07-22-0	55.68685	-120.8554	OTHER AREAS
100072208014W600	PENN WEST DOE 07-22-080-1	55.948	-120.09611	DOE
100072208416W600	GALLEON TALISMAN FLATROCK	56.29545	-120.43506	FLATROCK
100072208422W600	DEVON ET AL ATTACHIE 07-2	56.29556	-121.38295	OTHER AREAS
100072208516W600	SIEBENS ET AL GOPHER 07-2	56.3828	-120.43407	OTHER AREAS
100072408316W600	SUNCOR TWO RIVERS 07-24-0	56.20938	-120.38103	TWO RIVERS
100072508020W600	CNRL SATURN 07-25-080-20	55.96063	-120.98502	OTHER AREAS
100072608422W600	LADD ATTACHIE 07-26-084-2	56.31144	-121.35571	OTHER AREAS
100072708118W600	PENN WEST NUMAC SEPTIMUS	56.05068	-120.7203	OTHER AREAS
100072708221W600	CNRL ET AL MONIAS 07-27-0	56.13662	-121.19108	MONIAS
100073008220W600	DEVON MONIAS 07-30-082-20	56.13652	-121.11266	MONIAS
100073008314W600	CNRL ALCES 07-30-083-14	56.22412	-120.1955	ALCES
100073008415W600	PENN WEST FLATROCK 07-30-	56.31012	-120.35531	FLATROCK
100073108721W600	BAYTEX ET AL HZ W STODDAR	56.58166	-121.34275	STODDART WEST
100073208021W600	ESSO ET AL WINDY 07-32-08	55.97576	-121.24591	OTHER AREAS
100073408517W600	NUMAC ET AL PLUTO 07-34-0	56.4119	-120.59252	PLUTO
100073508319W600	KXL GRAND HAVEN 07-35-083	56.23859	-120.87957	FORT ST JOHN
100073608015W600	TALISMAN DOE 07-36-080-15	55.97645	-120.19972	DOE
100080108320W600	TERRA WILDER 11-01-083-20	56.16974	-121.01815	WILDER
100080108320W602	TERRA WILDER 11-01-083-20	56.16974	-121.01815	WILDER
100080607920W600	SHELL GROUNDBIRCH 08-06-0	55.81703	-121.10633	GROUNDBIRCH
100081308421W600	TERRA BOUDREAU 10-13-084-	56.28336	-121.1723	OTHER AREAS
100081408014W600	ARC ET AL DOE 08-14-080-1	55.93251	-120.06527	DOE
100083208417W600	TRI-STAR ET AL CECIL 08-3	56.32585	-120.64092	CECIL LAKE
100083308520W600	DEVON ET AL W STODDART 08	56.41186	-121.08659	STODDART WEST
100083608522W600	CNRL HZ N RED 04-06-086-2	56.42124	-121.31959	RED CREEK NORTH
100090208725W600	CNRL HALFWAY 09-02-087-25	56.51833	-121.85966	HALFWAY
100090507919W600	SHELL GROUNDBIRCH 08-05-0	55.81757	-120.92523	SUNSET PRAIRIE
100091707914W600	ARC ET AL DAWSON 09-17-07	55.8478	-120.14404	REGIONAL HERITA
100091708220W600	AMOCO WAINOCO E MONIAS 09	56.11169	-121.08039	OTHER AREAS
100092108516W600	ECA FLATROCK 08-21-085-16	56.38408	-120.45435	FLATROCK
100092508418W600	DEVON UNIT EAGLE 09-25-08	56.3151	-120.69299	EAGLE
100092608622W600	PROGRESS N RED 09-26-086-	56.48812	-121.35059	RED CREEK NORTH
100092907914W600	ARC DAWSON 09-29-079-14	55.87939	-120.14231	REGIONAL HERITA
100093107914W600	ARC DOE 09-31-079-14	55.89132	-120.16663	DOE
100093308320W600	SUNCOR PAC CHAMBERLAIN 09	56.24096	-121.08657	OTHER AREAS
100100408321W600	CNRL NUMAC MONIAS 10-04-0	56.16825	-121.25217	MONIAS
100100608014W600	PENN WEST IMP DOE 10-06-0	55.90798	-120.17398	DOE
100100608517W600	PENN WEST CECIL 10-06-085	56.34235	-120.67062	CECIL LAKE
100100608520W600	COP BRC RED CREEK 10-06-0	56.34262	-121.14534	RED CREEK

100100807914W600	ARC DAWSON 10-08-079-14	55.83306	-120.1485	REGIONAL HERITA
100101208320W600	TERRA ET AL WILDER 15-12-	56.18496	-121.01133	WILDER
100101208622W600	DEVON ET AL N RED 10-12-0	56.44448	-121.33029	RED CREEK NORTH
100101408320W600	WSOG HUSKY DOME WILDER 10	56.1974	-121.04038	OTHER AREAS
100101607914W600	ARC DAWSON 10-16-079-14	55.84801	-120.12237	REGIONAL HERITA
100101807914W600	ARC DOE 10-18-079-14	55.84898	-120.17646	DAWSON CREEK
100101808113W600	TALISMAN ET AL MICA 10-18	56.02224	-120.02074	MICA
100101808319W600	TERRA WILDER 10-18-083-19	56.19788	-120.98775	WILDER
100101908319W600	PENN WEST ET AL WILDER 10	56.21183	-120.98768	WILDER
100102208015W600	CNRL ET AL DOE 10-22-080-	55.95189	-120.25491	DOE
100102208425W600	TERRA ALTARES 10-22-084-2	56.30014	-121.85554	OTHER AREAS
100102308416W600	COPOL ET AL FLATROCK 10-2	56.30049	-120.40796	FLATROCK
100102508315W600	CNRL ALCES 10-25-083-15	56.2274	-120.22187	ALCES
100102608014W600	DEVON DOE 10-26-080-14	55.96491	-120.0704	DOE
100102608417W600	CNRL FLATROCK 10-26-084-1	56.31383	-120.56632	FLATROCK
100102608517W600	CNRL ET AL W FLATROCK 10-	56.39975	-120.56839	FLATROCK WEST
100102708220W600	DEVON NEC E MONIAS 10-27-	56.13935	-121.03897	OTHER AREAS
100102708223W600	ADU HB BOUCHER 10-27-082-	56.13981	-121.50563	OTHER AREAS
100102708725W600	PROGRESS ET AL HALFWAY 10	56.57415	-121.89281	OTHER AREAS
100103008621W600	DEVON RED 10-30-086-21	56.4881	-121.30382	RED CREEK NORTH
100103108721W600	BAYTEX ET AL HZ W STODDAR	56.58514	-121.34483	STODDART WEST
100103208525W600	WESTMIN ET AL FARRELL 10-	56.41422	-121.9082	OTHER AREAS
100103308420W600	PENN WEST BEAR FLAT 10-33	56.32677	-121.09409	BEAR FLAT
100103308521W600	PETROBANK RED 10-33-085-2	56.41561	-121.25154	RED CREEK
100103507915W600	ARC DAWSON 10-35-079-15	55.89232	-120.22909	REGIONAL HERITA
100103508115W600	PENN WEST ET AL HZ PARKLA	56.06704	-120.22718	PARKLAND
100110207820W600	BRC HTR ESSO RANGER 11-02	55.73207	-120.98793	OTHER AREAS
100110308617W600	NUMAC ET AL PLUTO 11-03-0	56.4301	-120.59916	OTHER AREAS
100110407914W600	ARC DAWSON 11-04-079-14	55.81862	-120.12699	REGIONAL HERITA
100110408516W600	TALISMAN FLATROCK 11-04-0	56.34286	-120.46486	FLATROCK
100110508520W600	PENN WEST BEAR FLAT 11-05	56.34243	-121.12389	BEAR FLAT
100110607718W600	SHELL BRASSEY 11-06-077-1	55.64614	-120.78001	BRASSEY
100110608015W600	CPEC DOE 11-06-080-15	55.90565	-120.33853	OTHER AREAS
100110708618W600	CALCO ET AL STODDART 11-0	56.4455	-120.83782	STODDART
100111108621W600	PZLCAN ET AL W STODDART 1	56.44449	-121.20503	OTHER AREAS
100111508321W600	CNRL MONIAS 11-15-083-21	56.19793	-121.23108	MONIAS
100111608416W600	ENERMARK CDN FOREST FLATR	56.28585	-120.46987	FLATROCK
100111707818W600	HUSKY ET AL SLOANE 11-17-	55.7623	-120.75466	OTHER AREAS
100111807916W600	CPEC ET AL SUNRISE 11-18-	55.84895	-120.49455	SUNRISE
100112007914W600	ARC DAWSON 11-20-079-14	55.86216	-120.15313	REGIONAL HERITA
100112008619W600	CNRL STODDART 11-20-086-1	56.47295	-120.9695	STODDART
100112208114W600	TAQA NORTH ET AL MICA 11-	56.03688	-120.10143	MICA
100112208120W600	OEI WESTCOAST WORTH 11-22	56.03633	-121.04302	OTHER AREAS
100112208122W600	CNRL ET AL MONIAS 11-22-0	56.03684	-121.35295	OTHER AREAS
100112608220W600	NUMAC MONIAS 11-26-082-20	56.13942	-121.01433	MONIAS
100112608221W600	NUMAC MONIAS 11-26-082-21	56.14055	-121.17468	MONIAS
100112707716W600	ECA ET AL BISSETTE 11-27-	55.70432	-120.3951	REGIONAL HERITA
100112908220W600	DEVON MONIAS 11-29-082-20	56.13974	-121.09543	MONIAS
100113008215W600	PROGRESS TWO RIVERS 11-30	56.13953	-120.33723	TWO RIVERS

100113108013W600	RIGEL UMC DOE 11-31-080-1	55.97986	-120.02435	DOE
100113208115W600	SUNCOR ET AL PARKLAND 11-	56.06704	-120.31248	PARKLAND
100113507916W600	ESSO ET AL URQUHART 11-35	55.89083	-120.3926	OTHER AREAS
100113508015W600	SEMC DOE 11-35-080-15	55.98004	-120.23203	DOE
100113508820W600	CNRL HZ BUICK 01-34-088-2	56.67078	-121.08686	BUICK CREEK
100113607815W600	FPC KILKERRAN 11-36-078-1	55.80499	-120.18728	OTHER AREAS
100113608518W600	RENAISSANCE ET AL N PINE	56.41546	-120.70386	PINE NORTH
100120108722W600	PROGRESS ET AL N RED 12-0	56.51978	-121.37635	RED CREEK NORTH
100120507714W600	ECA ECOG SWAN 12-05-077-1	55.64492	-120.14157	REGIONAL HERITA
100120708513W600	PROGRESS BOUNDARY 12-07-0	56.3584	-120.05252	BOUNDARY LAKE
100121108220W600	CREW HZ SEPTIMUS 03-12-08	56.08901	-120.99147	REGIONAL HERITA
100121208421W600	KMG BOUDREAU 12-12-084-21	56.26838	-121.18662	BOUDREAU
100121908220W600	DEVON MONIAS 12-19-082-20	56.12608	-121.12605	MONIAS
100122507916W600	GULF URQUHART 12-25-079-1	55.87919	-120.37214	OTHER AREAS
100122508117W600	TERRA PARKLAND 12-25-081-	56.05289	-120.52897	TOWER LAKE
100122708013W600	STAR POUCE COUPE 12-27-80-13	55.9667914	-119.9504689	POUCE COUPE
100122708420W600	PENN WEST ET AL BEAR FLAT	56.31273	-121.07833	BEAR FLAT
100122907818W600	ARC GROUNDBIRCH 12-29-078	55.78925	-120.76123	GROUNDBIRCH
100122908018W600	SHELL HZ SUNSET B14-21-08	55.95478	-120.75647	REGIONAL HERITA
100122908022W600	JUMBO WINDY 12-29-080-22	55.96592	-121.41516	OTHER AREAS
100122908721W602	BAYTEX ET AL HZ W STODDAR	56.5754	-121.31594	STODDART WEST
100123008417W600	SCURRY KOCH CECIL 12-30-0	56.31318	-120.68551	CECIL LAKE
100123308520W600	DEVON W STODART 12-33-085	56.41551	-121.10651	STODDART WEST
100123508820W600	CNRL HZ BUICK 11-34-088-2	56.67661	-121.10041	BUICK CREEK
100130107715W600	ECA BISSETTE 13-01-077-15	55.64727	-120.19079	REGIONAL HERITA
100130108725W600	CNRL HALFWAY 13-01-087-25	56.52161	-121.85372	HALFWAY
100130208015W600	PENN WEST ET AL DOE 13-02	55.91189	-120.24099	DOE
100130608113W600	TALISMAN MICA 13-06-081-1	55.99657	-120.0331	MICA
100131107716W600	CNRL PROGRESS 13-11-077-1	55.66227	-120.37549	OTHER AREAS
100131408018W600	IMP CHEL SCOTT 13-14-080-	55.94159	-120.71049	OTHER AREAS
100131507719W600	TALISMAN HZ BRASSEY 15-10	55.6642	-120.85318	REGIONAL HERITA
100131708013W600	IMP DOE 13-17-080-13	55.93996	-120.00718	DOE
100131908520W600	DEVON NEC W STODDART 13-1	56.39051	-121.15974	STODDART WEST
100132708722W602	BAYTEX HZ CACHE 12-27-087	56.57555	-121.42867	CACHE CREEK
100132807819W600	SHELL HZ GROUNDBIRCH B04-	55.78486	-120.86499	REGIONAL HERITA
100133007813W600	ARC BRIAR RIDGE 13-30-078	55.7943	-120.01362	BRIAR RIDGE
100133307819W600	SHELL IMP GROUNDBIRCH 16-	55.80887	-120.89716	GROUNDBIRCH
100133308320W600	TERRA BEAR FLAT 13-33-083	56.24374	-121.10692	BEAR FLAT
100133308417W600	DAYLIGHT ET AL W FLATROCK	56.33159	-120.63047	FLATROCK WEST
100133408121W600	LADD MONIAS 13-34-081-21	56.0703	-121.20343	OTHER AREAS
100133608521W600	DEVON NEC W STODDART 13-3	56.41951	-121.18366	STODDART WEST
100140408119W600	MOBIL SATURN 14-04-081-19	55.99974	-120.9132	SATURN
100140907711W600	NORCEN POUCE COUPES	55.6617349	-119.6460015	POUCE COUPE SOUTH
100140907914W600	ARC DAWSON 14-09-079-14	55.83635	-120.12856	REGIONAL HERITA
100140907919W600	SHELL GROUNDBIRCH 14-09-0	55.83702	-120.91221	GROUNDBIRCH
100141208219W600	HUSKY SEPTIMUS 14-12-082-	56.09965	-120.83217	OTHER AREAS
100141308421W600	TERRA BOUDREAU 14-13-084-	56.289	-121.17673	BOUDREAU
100141408417W600	PROGRESS FLATROCK A14-14-	56.28828	-120.57189	FLATROCK
100141508221W600	CNRL NUMAC MONIAS 14-15-0	56.11444	-121.19873	MONIAS
100141608520W600	DEVON ET AL W STODDART 14	56.3761	-121.09858	OTHER AREAS

100141808621W600	DEVON NEC N RED 14-18-086	56.46114	-121.31256	RED CREEK NORTH
100141908417W600	SCURRY ET AL CECIL 14-19-	56.30327	-120.67831	CECIL LAKE
100142208421W600	DEVON ARL GOOSE 13-22-084	56.30094	-121.2354	GOOSE
100142407814W600	ARC BRIAR RIDGE 14-24-078	55.78056	-120.03182	OTHER AREAS
100142508520W600	PEMBINA ET AL STODDART 14	56.40437	-121.02053	STODDART WEST
100143308520W600	DEVON ET AL STODDART 14-3	56.42007	-121.09759	STODDART WEST
100143507817W600	TRIDENT ET AL SUNRISE 14-	55.80812	-120.52149	SUNRISE
100150608113W600	CEQUENCE MICA 15-06-081-1	55.99689	-120.02075	MICA
100150608113W604	CEQUENCE MICA 15-06-081-1	55.99689	-120.02075	MICA
100150608620W600	CNRL W STODDART 15-06-086	56.43417	-121.14669	STODDART WEST
100150807816W600	ECA SUNRISE 15-08-078-16	55.74966	-120.43932	SUNRISE
100150808112W600	TALISMAN POUCE COUPE 15-8-	56.0112478	-119.8341563	POUCE COUPE
100151307914W600	ARC ET AL BRIAR RIDGE 15-	55.85177	-120.04674	BRIAR RIDGE
100151308421W600	TERRA BOUDREAU 15-13-084-	56.28716	-121.16902	BOUDREAU
100151408522W600	DEVON NEC NUMAC GOOSE 15-	56.37599	-121.35631	OTHER AREAS
100151708115W600	SUNCOR PC ET AL PARKLAND	56.02635	-120.30288	PARKLAND
100151708115W602	SUNCOR PC ET AL PARKLAND	56.02635	-120.30288	PARKLAND
100151708116W600	STORM EXP PARKLAND 15-17-	56.02564	-120.46407	PARKLAND
100151708422W600	DEVON ET AL ATTACHIE 15-1	56.28897	-121.43349	ATTACHIE
100151908517W600	SUNCOR N PINE 15-19-085-1	56.38956	-120.67151	PINE NORTH
100152107914W600	ARC DAWSON 15-21-079-14	55.8653	-120.12508	REGIONAL HERITA
100152108518W600	TALISMAN STODDART 15-21-0	56.38866	-120.77916	STODDART
100153007914W600	ARC DAWSON 15-30-079-14	55.88131	-120.17727	REGIONAL HERITA
100153007917W600	ECA SUNRISE 15-30-079-17	55.88044	-120.64694	OTHER AREAS
100153207814W600	SHELL ET AL KILKERRAN 15-	55.80778	-120.12609	OTHER AREAS
100160208618W600	PENGROWTH ET AL OAK 16-02	56.43381	-120.71801	OAK
100160407815W600	GULF S DAWSON 16-04-078-1	55.73595	-120.25215	OTHER AREAS
100160508416W600	AMOCO FLATROCK 16-05-084-	56.25772	-120.47859	FLATROCK
100161108417W600	DEVON NEC FLATROCK 16-11-	56.27419	-120.55861	OTHER AREAS
100161507819W600	SHELL GROUNDBIRCH 16-15-0	55.7642	-120.8489	GROUNDBIRCH
100161808117W600	STORM EXP TOWER 03-19-081	56.02945	-120.65328	OTHER AREAS
100162508520W600	PROGRESS STODDART 16-25-0	56.40407	-121.00755	STODDART
100162907819W600	SHELL ET AL GROUNDBIRCH 1	55.79434	-120.89716	GROUNDBIRCH
100163008118W600	DEVON SEPTIMUS 16-30-081-	56.05527	-120.7963	SEPTIMUS
100163508418W600	DEVON ET AL EAGLE 16-35-0	56.33122	-120.72047	EAGLE
100163608418W600	BAYTEX EAGLE 16-36-084-18	56.33127	-120.69037	OTHER AREAS
102011208423W600	PENGROWTH ATTACHIE A01-12	56.26213	-121.48037	OTHER AREAS
102023008721W600	BAYTEX ET AL HZ W STODDAR	56.56885	-121.3508	STODDART WEST
102053208417W600	CNRL CECIL A05-32-084-17	56.32572	-120.65881	CECIL LAKE
102060908322W600	NAL ACE MONIAS A06-09-083	56.17796	-121.41815	MONIAS
102062608414W600	CCS BOUNDARY A06-26-084-1	56.31098	-120.09559	BOUNDARY LAKE
102071108518W600	TERRA ET AL W EAGLE A07-1	56.35328	-120.72454	EAGLE
102072608422W600	DEVON ATTACHIE A07-26-084	56.31053	-121.35553	OTHER AREAS
102133307819W600	SHELL ET AL GROUNDBIRCH A	55.80726	-120.88983	GROUNDBIRCH
102152808420W600	PENN WEST BEAR FLAT A15-2	56.31762	-121.09102	BEAR FLAT
102161208417W600	CCS FLATROCK A16-12-084-1	56.27309	-120.53423	OTHER AREAS
102161308414W600	CCS BOUNDARY A16-13-084-1	56.28905	-120.05652	BOUNDARY LAKE
102163208520W600	DEVON NEC W STODDART A16-	56.41964	-121.11193	STODDART WEST
103132807819W600	SHELL HZ GROUNDBIRCH D04-	55.78483	-120.86499	REGIONAL HERITA
200A003G093P0900	ECA SWAN A-003-G/093-P-09	55.58726	-120.15003	SWAN LAKE

200A005G093P0900	ECA SWAN A-005-G/093-P-09	55.58351	-120.1806	SWAN LAKE
200A009H093P0900	NUMAC ET AL TUPPER A-009-	55.58354	-120.10607	OTHER AREAS
200A023A094A1400	CNRL ET AL HZ BUICK B-014	56.75934	-121.04723	BUICK CREEK
200A029H093P0900	ECA SWAN A-029-H/093-P-09	55.60015	-120.10613	REGIONAL HERITA
200A040H093P0900	ECA SWAN B-039-H/093-P-09	55.60851	-120.11154	SWAN LAKE
200A044A094A1400	CNRL ET AL HZ BUICK C-A04	56.79039	-121.05655	BUICK CREEK
200A046A094A1400	CNRL ET AL HZ BUICK A-056	56.79194	-121.06447	BUICK CREEK
200A047B094A1300	PENN WEST ET AL INGA A-04	56.78464	-121.70412	INGA
200A056A094B0900	SUNCOR PC KOBES C-A056-A/	56.54829	-122.07109	KOBES
200A067I094B0900	BRC HTR ET AL W BLUEBERRY	56.7186	-122.0772	OTHER AREAS
200A076A094A1402	CNRL ET AL HZ BUICK D-065	56.80658	-121.05149	BUICK CREEK
200B003A094A1400	CNRL HZ BUICK C-004-A/094	56.75784	-121.04398	BUICK CREEK
200B015A094A1400	CNRL ET AL HZ BUICK C-B00	56.75588	-121.0749	BUICK CREEK
200B029H093P0900	ECA ECOG SWAN B-029-H/093	55.60173	-120.11233	REGIONAL HERITA
200B029K094A1200	SUNCOR ET AL BLUEBERRY B-	56.68621	-121.85687	BLUEBERRY
200B030H093P0900	ECA SWAN B-030-H/093-P-09	55.60189	-120.12468	REGIONAL HERITA
200B032F093P1002	COPOL BRASSEY D-B033-F/09	55.61478	-120.78002	BRASSEY
200B032G093P0900	ECA SWAN B-032-G/093-P-09	55.60841	-120.14667	REGIONAL HERITA
200B033A094B1600	UCEL GUNDY B-033-A/094-B-	56.777	-122.03523	GUNDY CREEK
200B044C093P1000	BRC HTR BRASSEY B-044-C/0	55.53687	-120.7977	OTHER AREAS
200B046A094B0900	CREW ET AL KOBES B-046-A/	56.53713	-122.07312	KOBES
200B047F093P0900	ECA BISSETTE B-047-F/093-	55.61869	-120.33712	REGIONAL HERITA
200B057G093P0900	ECA SWAN B-057-G/093-P-09	55.62705	-120.20644	REGIONAL HERITA
200B059F093P1000	COPOL BRASSEY B-059-F/093	55.62582	-120.85965	DEEP BASIN
200B077A094A1300	PENN WEST ET AL HZ FIREWE	56.80459	-121.5767	FIREWEED
200B095C093P0900	ECA SWAN B-095-C/093-P-09	55.57835	-120.30717	SWAN LAKE
200B097I094A1102	CNRL ET AL HZ BUICK A-096	56.74382	-121.06757	BUICK CREEK
200C004A094A1400	CNRL ET AL HZ BUICK A-006	56.75144	-121.06381	BUICK CREEK
200C006K094A1200	SUNCOR ET AL BLUEBERRY C-	56.67392	-121.82128	BLUEBERRY
200C010H093P0900	ECA ECOG SWAN C-010-H/093	55.58884	-120.12181	REGIONAL HERITA
200C017I094A1100	CNRL HZ BUICK C-018-I/094	56.68285	-121.09807	BUICK CREEK
200C025G094A1400	CNRL BUICK C-025-G/094-A-	56.85665	-121.18288	BUICK CREEK
200C032J094A1200	ARC INGA C-032-J/094-A-12	56.69946	-121.64927	INGA
200C034F093P1000	COPOL BRASSEY C-034-F/093	55.61316	-120.79593	BRASSEY
200C042F093P0900	ECA BISSETTE C-042-F/093-	55.62354	-120.27478	REGIONAL HERITA
200C054A094A1400	CNRL ET AL HZ BUICK D-065	56.80658	-121.05149	BUICK CREEK
200C054J094B0900	BRC HTR N TOWNSEND C-054-	56.71328	-122.17343	OTHER AREAS
200C082C093P0900	ECA WESTROCK KNOP C-082-C	55.57151	-120.27303	SWAN LAKE
200C085I094A1100	CNRL ET AL HZ BUICK B-075	56.7269	-121.05766	BUICK CREEK
200C087I094A1100	CNRL ET AL HZ BUICK A-096	56.74382	-121.06757	BUICK CREEK
200C088I094A1102	CNRL ET AL HZ BUICK A-A08	56.73702	-121.08023	BUICK CREEK
200C091C093P1000	COPOL HZ BRASSEY C-091-C/	55.58125	-120.75938	BRASSEY
200D003A094A1400	CNRL HZ BUICK C-012-A/094	56.76509	-121.02391	BUICK CREEK
200D013F093P1000	COPOL BRASSEY D-013-F/093	55.59792	-120.77813	BRASSEY
200D017H093P0900	ECA BISSETTE D-017-H/093-	55.5992	-120.08021	REGIONAL HERITA
200D021G093P0900	ECA SWAN D-021-G/093-P-09	55.60457	-120.13095	REGIONAL HERITA
200D022F093P1000	COPOL BRASSEY D-022-F/093	55.60665	-120.76847	BRASSEY
200D027I094A1100	CNRL HZ BUICK C-028-I/094	56.69072	-121.09444	BUICK CREEK
200D033F093P1000	COPOL BRASSEY D-033-F/093	55.61458	-120.77814	BRASSEY
200D037F093P1000	COPOL BRASSEY D-037-F/093	55.61397	-120.82789	DEEP BASIN

200D039F093P0900	ECA BISSETTE D-039-F/093-	55.61572	-120.3519	REGIONAL HERITA
200D040G093P1000	COPOL BRASSEY A-A031-F/09	55.60861	-120.75241	BRASSEY
200D044G093P0900	ECA SWAN D-044-G/093-P-09	55.6223	-120.16326	REGIONAL HERITA
200D051C093P1000	COPOL BRASSEY D-051-C/093	55.54729	-120.75277	BRASSEY
200D054A094A1500	PROGRESS TORO RIGEL D-054	56.79716	-120.54022	RIGEL
200D055F093P1000	COPOL BRASSEY D-055-F/093	55.63137	-120.80323	BRASSEY
200D057B093P1000	SHELL SUNDOWN D-057-B/093	55.54959	-120.70068	SUNDOWN
200D059I094B0900	CREW ET AL BLUEBELL D-059	56.71569	-122.10002	OTHER AREAS
200D061C093P1000	COPOL BRASSEY D-061-C/093	55.55679	-120.75295	BRASSEY
200D069C093P1000	COPOL ESSO W BRASSEY D-06	55.55699	-120.85521	DEEP BASIN
200D073C093P1000	COPOL BRASSEY D-073-C/093	55.56401	-120.77768	BRASSEY
200D075H094B0800	CNRL ALTARES D-075-H/094-	56.39792	-122.05313	OTHER AREAS
200D083L094A1200	KXL BLUEBERRY D-083-L/094	56.7404	-121.90186	BLUEBERRY
202A001J094B0900	CREW ET AL N TOWNSEND A-A	56.66942	-122.12872	TOWNSEND
202B056I094A1100	CNRL ET AL HZ BUICK C-058	56.71308	-121.0951	BUICK CREEK
202B064I094A1100	CNRL HZ BUICK A-A063-I/09	56.72047	-121.02862	BUICK CREEK
202B077I094A1100	CNRL ET AL HZ BUICK A-A08	56.73702	-121.08023	BUICK CREEK
202C060K094A1200	SUNCOR ET AL BLUEBERRY C-	56.71408	-121.86893	BLUEBERRY
202D019K094A1200	SUNCOR ET AL BLUEBERRY D-	56.68043	-121.85176	BLUEBERRY
202D071C093P1000	COPOL BRASSEY D-A071-C/09	55.56494	-120.7533	BRASSEY
202D098I094A1100	CNRL HZ BUICK B-086-I/094	56.73717	-121.07337	BUICK CREEK
203D027I094A1100	CNRL HZ BUICK A-028-I/094	56.68401	-121.08872	BUICK CREEK

APPENDIX – 1 – B: Letter of authorization to publish core analysis data from British Columbia Ministry of Energy, B.C. Oil and Gas Commission.

EDWIN I. EGBOBAYE (egbobawa@ualberta.ca) – wrote email on

April-04-12 9:28 AM to B.C. Oil and Gas Commission:

Please I'm requesting for permission to use any of these data for journal publications along with my other research data. I would reference British Columbia Oil and Gas Commission as the source of the data. Please advise me if I can do this.

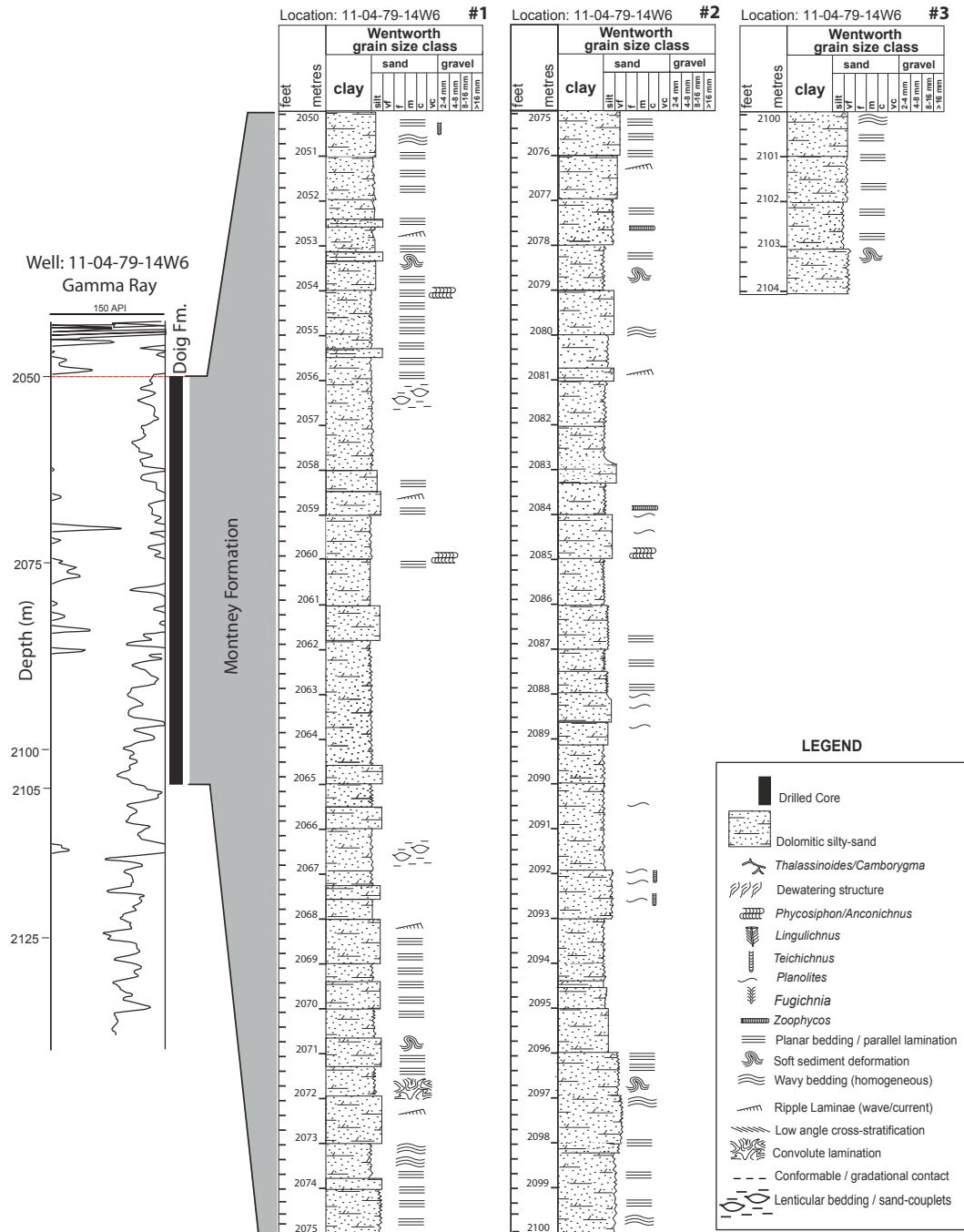
B.C. OIL AND GAS COMMISSION – replied via email on 5 April, 2012 3:39:41 PM MDT:

Hi Edwin:

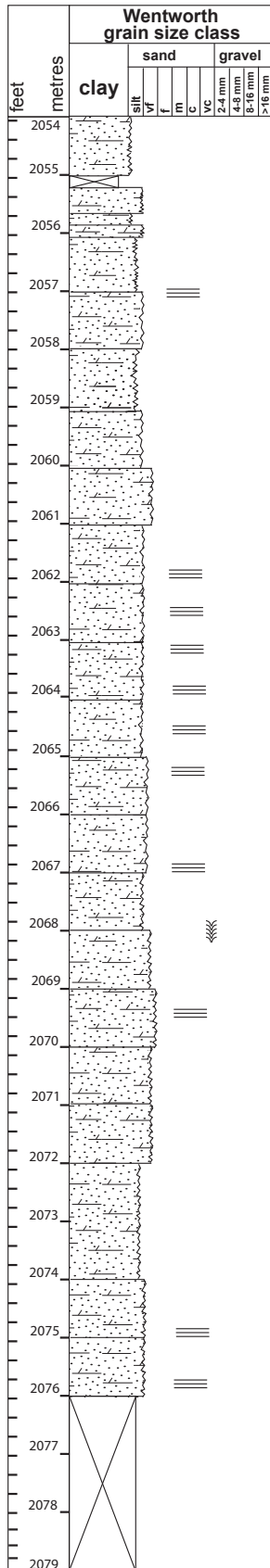
You have permission to use the data along with a reference.

*Thanks,
Hardy Friedrich
Manager, Communications
Hardy.Friedrich@bcogc.ca*

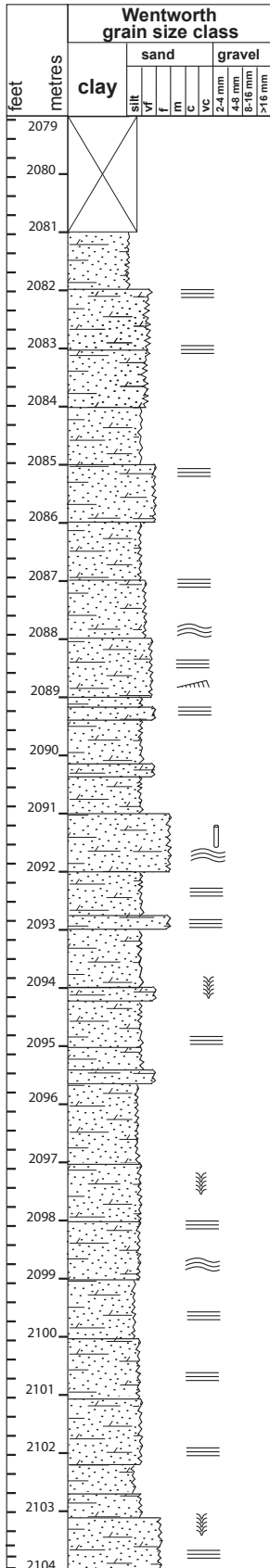
APPENDIX 2 – A: Logged core showing facies of the Montney Formation, north-eastern British Columbia, Western Canada



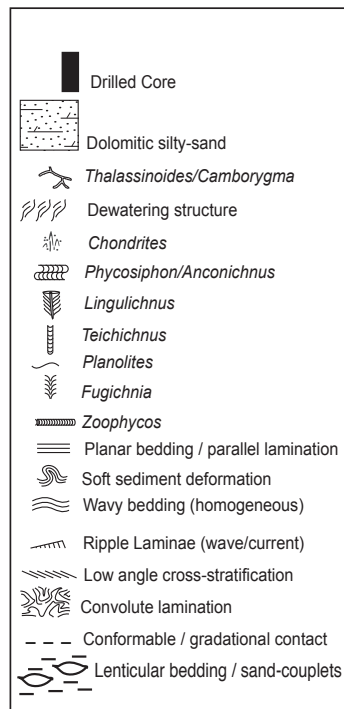
Location: 7-13-79-15W6 #1

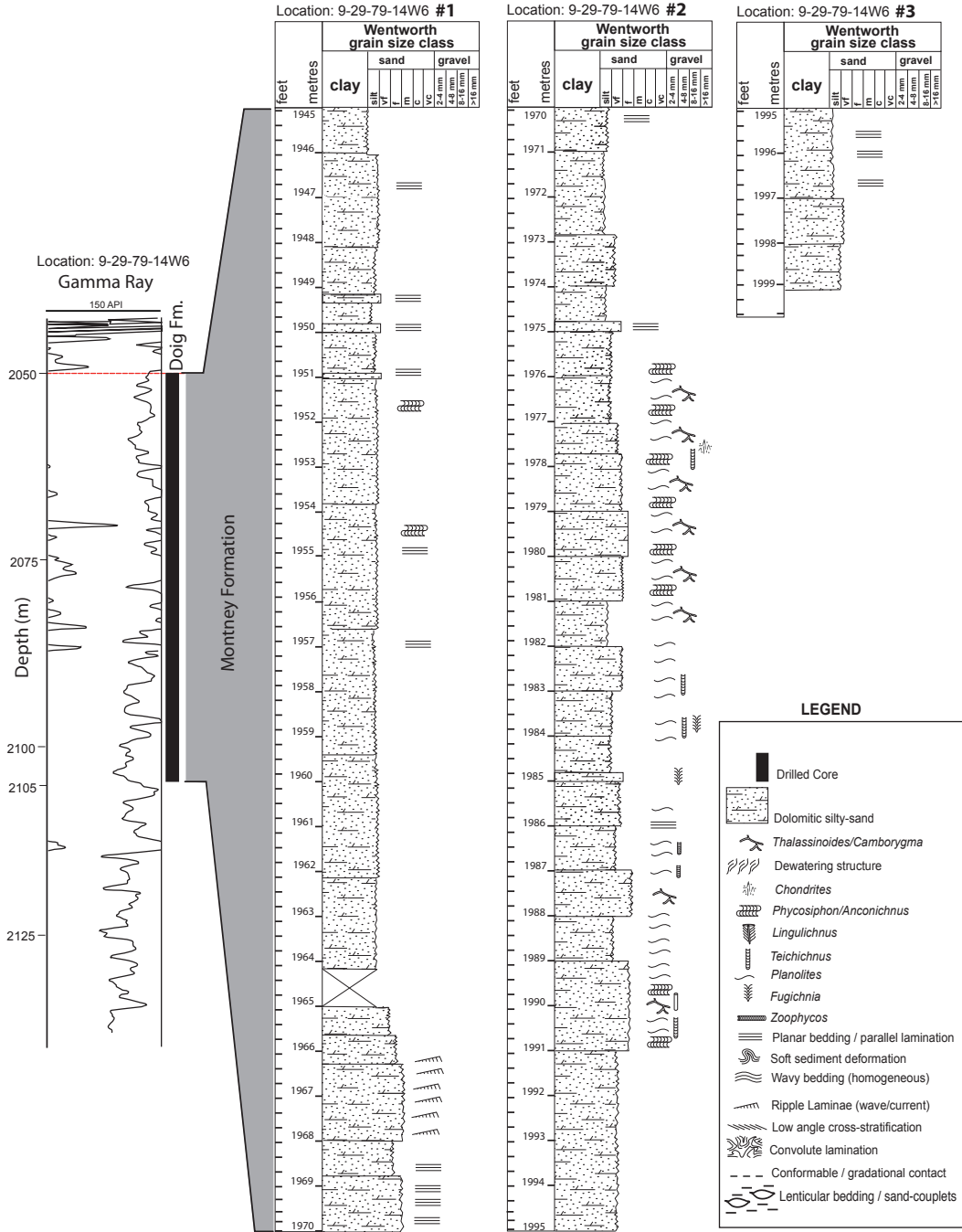


Location: 7-13-79-15W6 #2

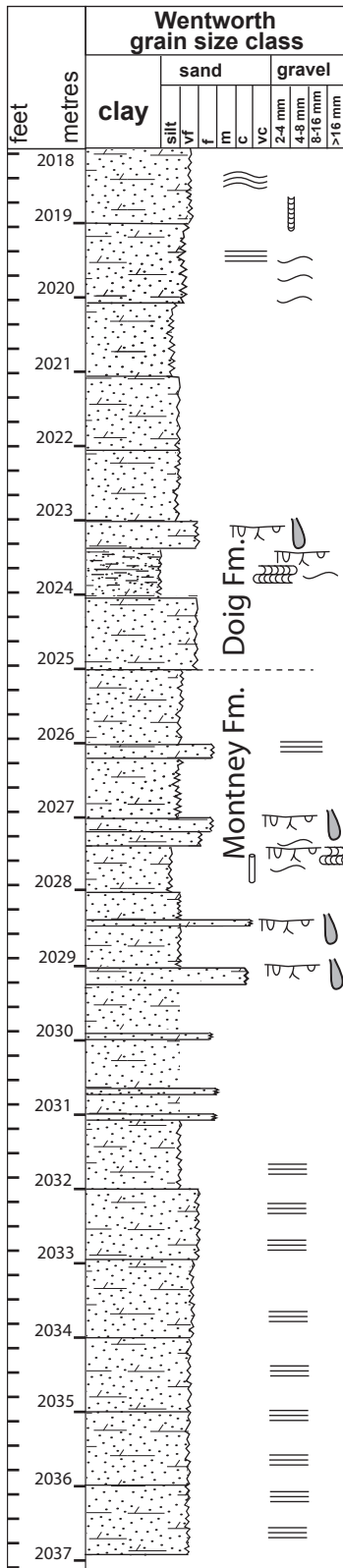


LEGEND

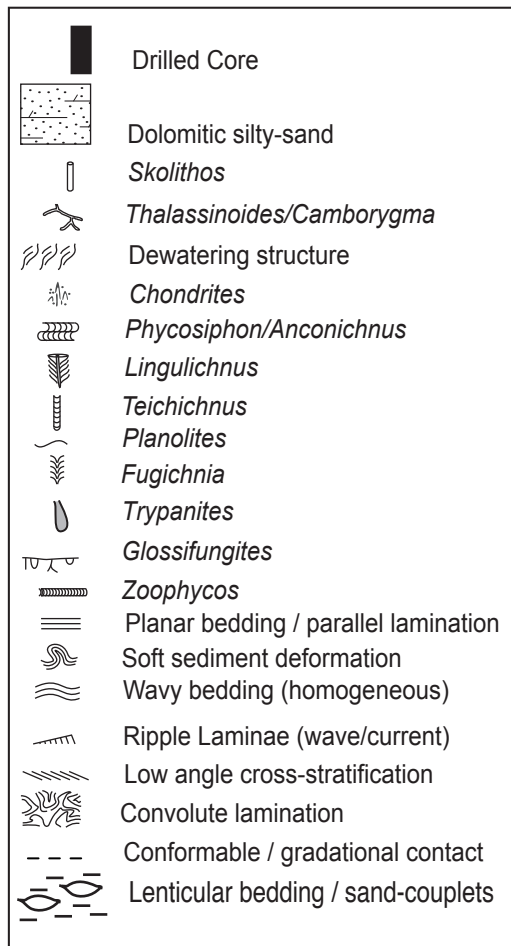




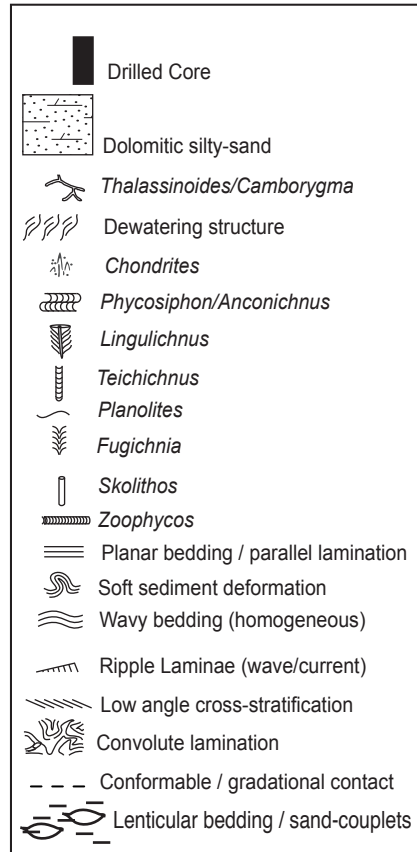
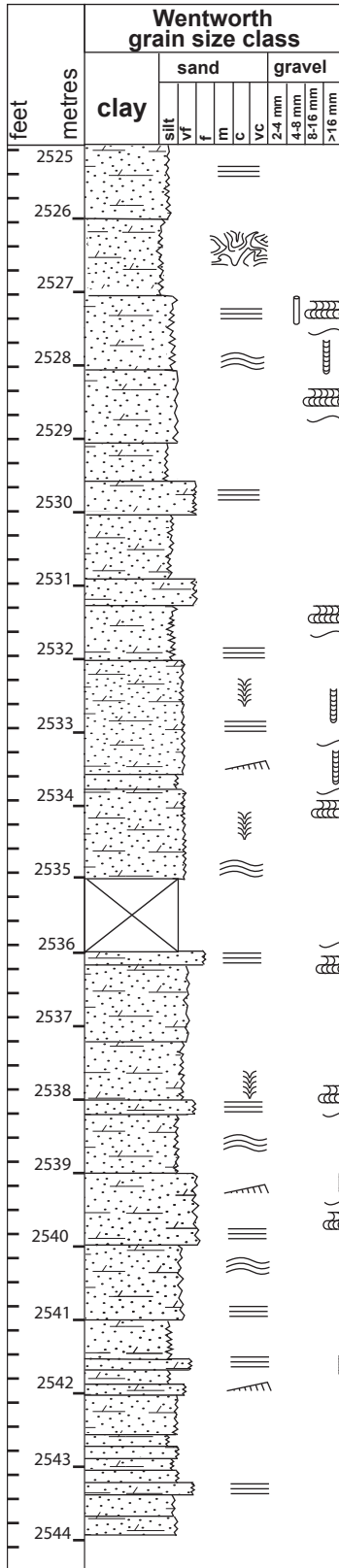
Location: 14-5-81-17W6 #1



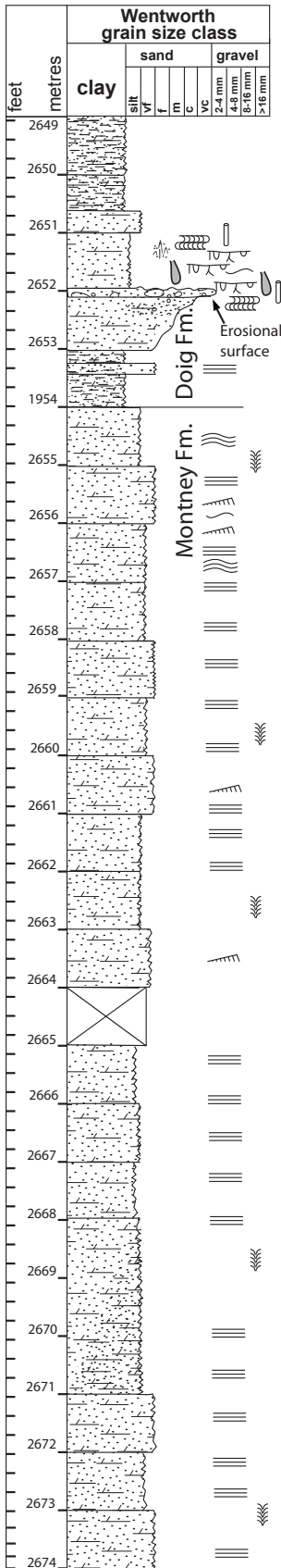
LEGEND



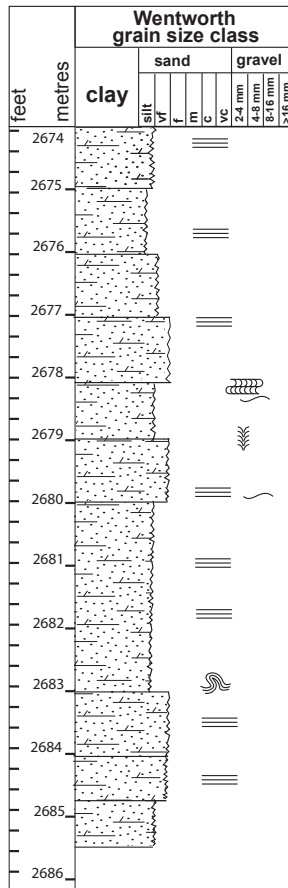
Location: d-21-G/93-P-9 #1



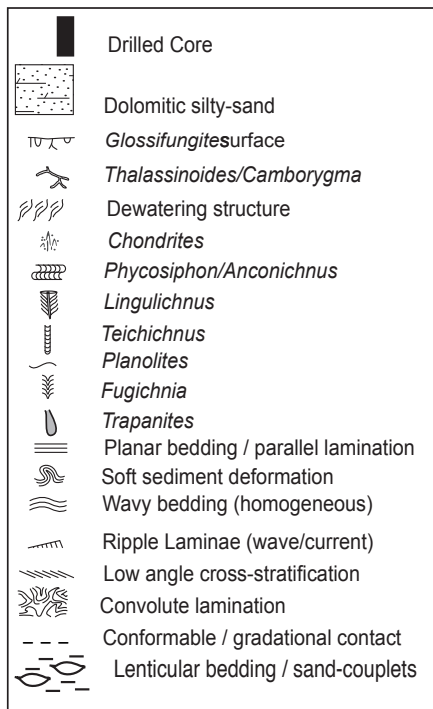
Location: d-39-F/93-P-9 #1



Location: d-39-F/93-P-9 #2



LEGEND



Appendix 2-B. List of thin-sections analyzed in this study.

Number of slides	Well Name	Sample Depth (m)	Formation	Age	Sample Analyses
1	d-054-K/93-P-09	1381.65m	Montney	Lower Triassic	Thin-Sections
2	d-054-K/93-P-09	1382.5m	Montney	Lower Triassic	Thin-Sections
3	d-054-K/93-P-09	1382.8m	Montney	Lower Triassic	Thin-Sections
4	d-054-K/93-P-09	1383.6m	Montney	Lower Triassic	Thin-Sections
5	d-054-K/93-P-09	1384.2m	Montney	Lower Triassic	Thin-Sections
6	d-054-K/93-P-09	1385.6m	Montney	Lower Triassic	Thin-Sections
7	d-054-K/93-P-09	1386.0m	Montney	Lower Triassic	Thin-Sections
8	d-054-K/93-P-09	1386.6m	Montney	Lower Triassic	Thin-Sections
9	d-021-G/93-P-09	2527m	Montney	Lower Triassic	Thin-Sections
10	d-021-G/93-P-09	2539m	Montney	Lower Triassic	Thin-Sections
11	d-021-G/93-P-09	2727m	Montney	Lower Triassic	Thin-Sections
12	d-021-G/93-P-09	2541.6m	Montney	Lower Triassic	Thin-Sections
13	d-021-G/93-P-09	2537.1m	Montney	Lower Triassic	Thin-Sections
14	d-021-G/93-P-09	2526m	Montney	Lower Triassic	Thin-Sections
15	d-021-G/93-P-09	2529.45m	Montney	Lower Triassic	Thin-Sections
16	d-021-G/93-P-09	2529.5m	Montney	Lower Triassic	Thin-Sections
17	d-021-G/93-P-09	2528m	Montney	Lower Triassic	Thin-Sections
18	d-021-G/93-P-09	2530.5m	Montney	Lower Triassic	Thin-Sections
19	d-021-G/93-P-09	2527.35m	Montney	Lower Triassic	Thin-Sections
20	d-021-G/93-P-09	2533.8m	Montney	Lower Triassic	Thin-Sections
21	d-021-G/93-P-09	2541.8m	Montney	Lower Triassic	Thin-Sections
22	d-021-G/93-P-09	2529.45m	Montney	Lower Triassic	Thin-Sections
23	b-032-G/93-P-09	2703.25m	Montney	Lower Triassic	Thin-Sections
24	b-032-G/93-P-09	2705.0m	Montney	Lower Triassic	Thin-Sections
25	b-032-G/93-P-09	2706.0m	Montney	Lower Triassic	Thin-Sections
26	b-032-G/93-P-09	2707.0m	Montney	Lower Triassic	Thin-Sections
27	b-032-G/93-P-09	2708.0m	Montney	Lower Triassic	Thin-Sections
28	b-032-G/93-P-09	2709.0m	Montney	Lower Triassic	Thin-Sections
29	b-032-G/93-P-09	2710.0m	Montney	Lower Triassic	Thin-Sections
30	b-032-G/93-P-09	2711.0m	Montney	Lower Triassic	Thin-Sections
31	b-032-G/93-P-09	2711.45m	Montney	Lower Triassic	Thin-Sections
32	b-032-G/93-P-09	2711.5m	Montney	Lower Triassic	Thin-Sections
33	b-032-G/93-P-09	2712.0m	Montney	Lower Triassic	Thin-Sections
34	b-032-G/93-P-09	2713.0m	Montney	Lower Triassic	Thin-Sections
35	b-032-G/93-P-09	2713.35m	Montney	Lower Triassic	Thin-Sections
36	b-032-G/93-P-09	2714.0m	Montney	Lower Triassic	Thin-Sections
37	b-032-G/93-P-09	2715.0m	Montney	Lower Triassic	Thin-Sections
38	b-032-G/93-P-09	2716.15m	Montney	Lower Triassic	Thin-Sections
39	b-032-G/93-P-09	2717.0m	Montney	Lower Triassic	Thin-Sections
40	b-032-G/93-P-09	2717.35m	Montney	Lower Triassic	Thin-Sections
41	b-032-G/93-P-09	2718.0m	Montney	Lower Triassic	Thin-Sections
42	b-032-G/93-P-09	2718.6m	Montney	Lower Triassic	Thin-Sections
43	b-032-G/93-P-09	2719.0m	Montney	Lower Triassic	Thin-Sections
44	b-057-G/93-P-09	2763.5m	Montney	Lower Triassic	Thin-Sections

Number of slides	Well Name	Sample Depth (m)	Formation	Age	Sample Analyses
45	b-057-G/093-P-09	2764.2m	Montney	Lower Triassic	Thin-Sections
46	b-057-G/093-P-09	2765.0m	Montney	Lower Triassic	Thin-Sections
47	b-057-G/093-P-09	2765.95m	Montney	Lower Triassic	Thin-Sections
48	b-057-G/093-P-09	2767.0m	Montney	Lower Triassic	Thin-Sections
49	b-057-G/093-P-09	2768.05m	Montney	Lower Triassic	Thin-Sections
50	b-057-G/093-P-09	2769.1	Montney	Lower Triassic	Thin-Sections
51	b-057-G/093-P-09	2769.9	Montney	Lower Triassic	Thin-Sections
52	b-057-G/093-P-09	2770.1m	Montney	Lower Triassic	Thin-Sections
53	b-057-G/093-P-09	2770.7m	Montney	Lower Triassic	Thin-Sections
54	b-057-G/093-P-09	2771.1m	Montney	Lower Triassic	Thin-Sections
55	b-057-G/093-P-09	2772.1m	Montney	Lower Triassic	Thin-Sections
56	b-057-G/093-P-09	2773.0m	Montney	Lower Triassic	Thin-Sections
57	b-057-G/093-P-09	2774.05m	Montney	Lower Triassic	Thin-Sections
58	b-057-G/093-P-09	2774.9m	Montney	Lower Triassic	Thin-Sections
59	b-057-G/093-P-09	2776.2m	Montney	Lower Triassic	Thin-Sections
60	b-057-G/093-P-09	2776.9m	Montney	Lower Triassic	Thin-Sections
61	b-057-G/093-P-09	2777.9m	Montney	Lower Triassic	Thin-Sections
62	b-057-G/093-P-09	2779.0m	Montney	Lower Triassic	Thin-Sections
63	b-057-G/093-P-09	2780.0m	Montney	Lower Triassic	Thin-Sections
64	b-057-G/093-P-09	2781.0m	Montney	Lower Triassic	Thin-Sections
65	b-057-G/093-P-09	2782.0m	Montney	Lower Triassic	Thin-Sections
66	J-54-K/93-I-8	1382.8m	Montney	Lower Triassic	Thin-Sections
67	J-54-K/93-I-8	1381.65m	Montney	Lower Triassic	Thin-Sections
68	J-54-K/93-I-8	1382.5m	Montney	Lower Triassic	Thin-Sections
69	J-54-K/93-I-8	1383.6m	Montney	Lower Triassic	Thin-Sections
70	J-54-K/93-I-8	1384.2m	Montney	Lower Triassic	Thin-Sections
71	J-54-K/93-I-8	1386.6m	Montney	Lower Triassic	Thin-Sections
72	J-54-K/93-I-8	2786m	Montney	Lower Triassic	Thin-Sections
73	J-54-K/93-I-8	1385.6m	Montney	Lower Triassic	Thin-Sections

APPENDIX 3 – A

Complete Rock-Eval data set used in this study for evaluation of hydrocarbon potential of the Montney Formation in northeastern British Columbia and part of Alberta. These data were also used to make TOC and Tmax maps presented in this study. Additional Rock-Eval data comes from Faraj, et al. (2002) and B.C. Oil and Gas Commission, Ministry of Energy and Mines, British Columbia.

Location	Long.	Lat.	Depth (m)	TOC	Ave. TOC	P1	Tmax	Ave. Tmax	S1	S2	S3	HI	OI
01-10-082-23W6	-121.513664	56.090519	2005.00	1.49		0.50	442		0.27	0.27	0.42	18	28
01-10-082-23W6	-121.513664	56.090519	2013.24	2.01		0.44	449		0.34	0.43	0.40	21	20
01-10-082-23W6	-121.513664	56.090519	1864.70	10.09		0.14	494		0.46	2.94	0.53	29	5
01-10-082-23W6	-121.513664	56.090519	1846.20	5.79		n/a	536.8		2.76	2.11	n/a	n/a	n/a
01-10-082-23W6	-121.513664	56.090519	1849.50	5.70		n/a	536.2		3.03	2.21	n/a	n/a	n/a
01-10-082-23W6	-121.513664	56.090519	1857.10	6.61		n/a	528.5		2.77	2.03	n/a	n/a	n/a
01-10-082-23W6	-121.513664	56.090519	1861.60	5.73		n/a	532.9		2.21	1.66	n/a	n/a	n/a
01-10-082-23W6	-121.513664	56.090519	1863.10	11.50		n/a	537.8		4.66	3.63	n/a	n/a	n/a
01-10-082-23W6	-121.513664	56.090519	1866.20	2.89	5.7	n/a	528.2	509.4	1.24	0.80	n/a	n/a	n/a
07-13-079-15W6	-120.203317	55.856596	2084.50	1.29		0.50	442		0.31	0.31	0.32	24	25
07-13-079-15W6	-120.203317	55.856596	2078.50	0.90		0.51	442		0.40	0.39	0.38	43	42
07-13-079-15W6	-120.203317	55.856596	2055.22	3.54	1.9	0.37	464	449.3	0.70	1.18	0.44	33	12
02-19-079-14W6	-120.177257	55.854919	2085.00	2.13		0.53	445		0.81	0.71	0.33	33	15
02-19-079-14W6	-120.177257	55.854919	2048.00	1.43		0.43	458		0.50	0.68	0.21	48	15
02-19-079-14W6	-120.177257	55.854919	2069.50	1.27	1.6	0.46	459	454	0.55	0.65	0.28	51	22
11-04-079-14W6	-120.126989	55.818622	2064.10	1.66		0.43	450		0.60	0.81	0.45	49	27
11-04-079-14W6	-120.126989	55.818622	2073.20	0.95	1.3	0.50	434	442	0.28	0.28	0.50	29	53
09-29-079-14W6	-120.142304	55.879387	1999.00	1.96	1.9	0.48	455	455	0.75	0.81	0.34	41	17
b-39-H/093-P-09	-120.108556	55.608377	2042.00	0.32	1.9	0.29	347	347	0.02	0.04	0.30	12	94
b-32-G/093-P-09	-120.146669	55.608417	2707.00	1.16	1.1	0.60	424	424	0.40	0.27	0.34	23	29

Location	Long.	Lat.	Depth (m)	TOC	Ave. TOC	P1	Tmax	Ave. Tmax	S1	S2	S3	HI	OI
13-16-79-14-W6	-120.133768	55.85108	2015.00	1.63	1.7	0.47	454	489.6	0.61	0.68	0.36	42	22
a-20-H-93-P-9	-120.118003	55.595608	2460.57	0.94		n/a	416			n/a	n/a	n/a	n/a
a-20-H-93-P-9	-120.118003	55.595608	2455	2.42		n/a	443		0.94	n/a	n/a	n/a	n/a
a-20-H-93-P-9	-120.118003	55.595608	2457	0.72	1.3	n/a	428	429	2.42	n/a	n/a	n/a	n/a
d-39-F/93-P-9	-120.351903	55.616303	2656.75	1.24		-	-	-	0.13	0.07	-	-	-
d-39-F/93-P-9	-120.351903	55.616303	2659	1.72		-	-	-	0.12	0.10	-	-	-
d-39-F/93-P-9	-120.351903	55.616303	2662.65	0.83		-	-	-	0.11	0.05	-	-	-
d-39-F/93-P-9	-120.351903	55.616303	2669.1	1.29	1.30	-	-	-	0.15	0.07	-	-	-
d-39-F/93-P-9	-120.351903	55.616303	2672.22	1.35		-	-	-	0.18	0.07	-	-	-
d-39-F/93-P-9	-120.351903	55.616303	2676.85	1.40		-	-	-	0.18	0.14	-	-	-
d-39-F/93-P-9	-120.351903	55.616303	2684.05	1.28		-	-	-	0.16	0.08	-	-	-
B-57-G/93-P-9	-	-	2761.5	1.82		-	468	-	0.25	0.27	0.06	-	-
B-57-G/93-P-9	-	-	2772.1	1.41	1.58	-	454	469	0.05	0.10	0.02	-	-
B-57-G/93-P-9	-	-	2778.7	1.52		-	485	-	0.09	0.12	0.03	-	-
7-13-79-15W6	-120.01563	55.485417	2090.6	1.72		-	-	-	0.37	0.34	-	-	-
7-13-79-15W6	-120.01563	55.485417	2095.5	2.0		-	-	-	0.64	0.67	-	-	-
7-13-79-15W6	-120.01563	55.485417	2098.4	1.18		-	-	-	0.41	0.27	-	-	-
7-13-79-15W6	-120.015632	55.485417	2102.7	1.53		-	-	-	0.51	0.40	-	-	-
7-13-79-15W6	-120.015632	55.485417	2107.7	2.17		-	-	-	0.65	0.56	-	-	-
11-04-79-14W6	-120.126989	55.818622	2063.7	1.33		0.26	450	-	0.05	0.14	0.15	11	11
11-04-79-14W6	-120.126989	55.818622	2068.5	0.64		0.26	481	-	0.06	0.17	0.12	27	19
11-04-79-14W6	-120.126989	55.818622	2069.5	1.25		0.22	447	-	0.07	0.25	0.03	20	2

Location	Long.	Lat.	Depth (m)	TOC	Ave. TOC	P1	Tmax	Ave. Tmax	S1	S2	S3	HI	OI
11-04-79-14W6	-120.126989	55.818622	2083.5	0.62		0.19	485		0.04	0.17	0.17	27	27
11-04-79-14W6	-120.126989	55.818622	2087	1.44		0.29	488		0.09	0.21	0.14	15	10
11-04-79-14W6	-120.126989	55.818622	2088.4	0.93		0.21	488		0.05	0.19	0.08	21	9
11-04-79-14W6	-120.126989	55.818622	2092.9	1.62	1.11	0.11	451		0.06	0.50	0.08	31	5
11-04-79-14W6	-120.126989	55.818622	2093.4	0.45		0.41	515	433	0.02	0.03	0.18	7	40
11-04-79-14W6	-120.126989	55.818622	2095.3	1.72		0.14	449		0.05	0.30	0.12	17	7
11-04-79-14W6	-120.126989	55.818622	2096.9	1.19		0.29	446		0.04	0.10	0.11	8	9
11-04-79-14W6	-120.126989	55.818622	2100.1	1.97		0.18	452		0.07	0.32	0.09	16	5
11-04-79-14W6	-120.126989	55.818622	2100.15	2.08		0.16	454		0.06	0.30	0.10	14	5
11-04-79-14W6	-120.126989	55.818622	2101.8	0.42		0.36	516		0.06	0.11	0.15	26	36

Location	Long.	Lat.	Depth (m)	TOC	Ave. TOC	P1	Tmax	Ave. Tmax	S1	S2	S3	HI	OI
15-11-79-12W6	119.745374	55.837185	1758.1	2.32		0.56	447		1.17	0.94	0.46	40	19
15-11-79-12W6	119.745374	55.837185	1758.6	1.52		0.57	445		1.47	1.12	0.44	73	28
15-11-79-12W6	119.745374	55.837185	1758.6	1.52		0.58	443		1.52	1.09	0.4	71	26
15-11-79-12W6	119.745374	55.837185	1759.2	1.49		0.65	449		1.57	0.86	0.38	57	25
15-11-79-12W6	119.745374	55.837185	1759.2	1.5		0.61	444		1.63	1.06	0.4	70	26
15-11-79-12W6	119.745374	55.837185	1761	1.71		0.48	450		1.28	1.39	0.47	81	27
15-11-79-12W6	119.745374	55.837185	1761	1.68	1.6	0.48	453	450.5	1.24	1.32	0.49	78	29
6-8-90-11W6	-119.719045	56.255455	1350	3.5		0.28	441		3.47	8.76	0.95	250	27
6-8-90-11W6	-119.719045	56.255455	1351.6	3.77		0.22	450		2.32	8.08	0.34	214	9
6-8-90-11W6	-119.719045	56.255455	1351.6	3.82		0.22	453		2.19	7.91	0.31	207	8
6-8-90-11W6	-119.719045	56.255455	1351.9	2.53		0.18	441		1.85	8.33	1.75	329	69
6-8-90-11W6	-119.719045	56.255455	1351.9	2.56		0.18	443		1.9	8.78	0.82	342	32
6-8-90-11W6	-119.719045	56.255455	1354.7	4.38		0.15	448		2.7	15.6	4.66	356	106

Location	Long.	Lat.	Depth (m)	TOC	Ave. TOC	P1	Tmax	Ave. Tmax	S1	S2	S3	HI	OI
8-16-74-10W6	-119.461438	55.41007	2260.9	3.93		0.49	453		1.81	1.85	0.25	47	6
8-16-74-10W6	-119.461438	55.41007	2261.4	3.54		0.47	454		1.65	1.86	0.26	52	7
8-16-74-10W6	-119.461438	55.41007	2261.4	3.02		0.45	449		1.72	2.13	0.25	70	8
8-16-74-10W6	-119.461438	55.41007	2262.3	4.4		0.45	455		1.69	2.06	0.25	46	5
8-16-74-10W6	-119.461438	55.41007	2262.3	3.36		0.43	453		1.8	2.4	0.22	71	6
8-16-74-10W6	-119.461438	55.41007	2264.1	1.58		0.67	444		2.27	1.14	0.37	72	23
8-16-74-10W6	-119.461438	55.41007	2264.1	1.55	3.1	0.67	437	449.7	2.27	1.13	0.4	72	25
10-15-76-4W6	-118.524507	55.587756	1480.1	1.31		0.17	444		0.68	3.29	0.88	251	59
10-15-76-4W6	-118.524507	55.587756	1480.1	1.3		0.16	443		0.66	3.35	0.83	257	57
10-15-76-4W6	-118.524507	55.587756	1482.5	4.33		0.11	441		1.64	13.03	0.93	300	20
10-15-76-4W6	-118.524507	55.587756	1482.5	4.21		0.11	439		1.75	13.59	0.84	322	18
10-15-76-4W6	-118.524507	55.587756	1484.1	2.23		0.13	443		0.95	6.55	0.82	293	34
10-15-76-4W6	-118.524507	55.587756	1484.1	2.28	2.6	0.12	441	441.8	1.01	7.18	0.73	314	31
14-11-77-10W6	-119.437951	55.661759	1942.1	2.79		0.14	447		1.05	6.37	0.59	230	21
14-11-77-10W6	-119.437951	55.661759	1942.1	2.84		0.13	443		1.07	6.83	0.6	243	21
14-11-77-10W6	-119.437951	55.661759	1947.6	5.97		0.12	447		2.05	14.6	0.61	246	10
14-11-77-10W6	-119.437951	55.661759	1947.6	5.87		0.12	445		1.95	14.58	0.63	249	10
14-11-77-10W6	-119.437951	55.661759	1951.7	3.69		0.19	448		1.93	8.29	0.49	227	13

Location	Long.	Lat.	Depth (m)	TOC	Ave. TOC	P1	Tmax	Ave. Tmax	S1	S2	S3	HI	OI
d-69-J/94-A-15	-120.728135	56.972919	1225.4	2.07		0.32	443		2.15	4.65	0.43	224	20
d-69-J/94-A-15	-120.728135	56.972919	1226.1	2.08		0.33	446		2.13	4.33	0.53	208	25
d-69-J/94-A-15	-120.728135	56.972919	1226.1	2.1		0.33	446		2.19	4.54	0.51	216	24
d-69-J/94-A-15	-120.728135	56.972919	1226.3	2.01		0.3	446		1.73	3.95	0.53	196	26
d-69-J/94-A-15	-120.728135	56.972919	1226.3	2.04		0.29	446		1.71	4.12	0.51	201	25
d-69-J/94-A-15	-120.728135	56.972919	1226.5	2.04		0.29	445		1.58	3.84	0.34	188	16
d-69-J/94-A-15	-120.728135	56.972919	1226.5	2.03		0.29	448		1.51	3.7	1.45	182	71
d-69-J/94-A-15	-120.728135	56.972919	1227.9	2.46		0.25	444		1.51	4.47	0.39	181	15
d-69-J/94-A-15	-120.728135	56.972919	1227.9	2.44		0.25	449		1.42	4.27	0.33	175	13
d-69-J/94-A-15	-120.728135	56.972919	1228.2	2.97		0.23	448		1.59	5.25	0.48	176	16
d-69-J/94-A-15	-120.728135	56.972919	1228.2	2.92		0.23	451		1.54	5.2	0.29	178	9
d-69-J/94-A-15	-120.728135	56.972919	1230.8	2.3		0.26	446		1.57	4.53	0.29	196	12
d-69-J/94-A-15	-120.728135	56.972919	1231	2.57		0.23	447		1.44	4.84	0.53	188	20
d-69-J/94-A-15	-120.728135	56.972919	1231	2.59		0.23	446		1.47	4.9	0.32	189	12
d-69-J/94-A-15	-120.728135	56.972919	1237.3	3.28		0.28	454		2.03	5.3	0.38	161	11
d-69-J/94-A-15	-120.728135	56.972919	1237.3	3.23	2.2	0.29	454	446.9	2.02	4.98	0.62	154	19
a-59-G/94-A-16	-120.227563	56.877093	1150.2	2.63		0.15	443		2.26	12.43	0.44	472	16
a-59-G/94-A-16	-120.227563	56.877093	1150.2	2.64		0.15	444		2.22	12.61	0.48	477	18
a-59-G/94-A-16	-120.227563	56.877093	1153.2	2.71		0.15	441		2.13	12.43	0.51	458	18

Location	Long.	Lat.	Depth (m)	TOC	Ave. TOC	P1	Tmax	Ave. Tmax	S1	S2	S3	HI	OI
a-59-G/94-A-16	-120.227563	56.877093	1156.4	2.37		0.13	442		1.74	11.52	0.5	486	21
a-59-G/94-A-16	-120.227563	56.877093	1156.4	2.44		0.13	443		1.73	11.46	0.86	469	35
a-59-G/94-A-16	-120.227563	56.877093	1159.2	3.05		0.15	441		2.27	13.13	0.47	430	15
a-59-G/94-A-16	-120.227563	56.877093	1159.2	3.23	2.7	0.15	439	442	2.26	13.08	0.47	404	14
d-81-E/94-H-1	-120.378113	57.15624	1068.3	2.11		0.1	454		0.83	7.52	0.18	356	8
d-81-E/94-H-1	-120.378113	57.15624	1068.3	2.07	2.0	0.09	456	455	0.78	7.63	0.33	368	15
8-14-86-20W6	-121.034934	56.456122	1613.5	2.54		0.48	450		3.39	3.64	1.21	143	47
8-14-86-20W6	-121.034934	56.456122	1613.5	2.52	2.5	0.49	447	448.5	3.49	3.7	1.29	146	51
b-10-C/94-H-1	-120.371829	57.002063	1123.18	1.87		0.21	452		0.98	3.76	0.83	201	44
b-10-C/94-H-1	-120.371829	57.002063	1123.18	1.88	1.8	0.22	449	450.5	1.09	3.95	0.74	210	39
d-25-D/94-H-1	-120.42815	57.022934	1120.14	3.06		0.15	451		1.19	6.91	0.92	225	30
b-10-C/94-H-1	-120.371829	57.002063	1123.18	1.87		0.21	452		0.98	3.76	0.83	201	44
b-10-C/94-H-1	-120.371829	57.002063	1123.18	1.88	1.8	0.22	449	450.5	1.09	3.95	0.74	210	39
d-25-D/94-H-1	-120.42815	57.022934	1120.14	3.06		0.15	451		1.19	6.91	0.92	225	30
b-10-C/94-H-1	-120.371829	57.002063	1123.18	1.87		0.21	452		0.98	3.76	0.83	201	44
b-10-C/94-H-1	-120.371829	57.002063	1123.18	1.88	1.8	0.22	449	450.5	1.09	3.95	0.74	210	39
d-25-D/94-H-1	-120.42815	57.022934	1120.14	3.15	3.1	0.15	450	450.5	1.2	6.83	0.92	216	29
d-4-B/94-H-2	-120.665601	57.006234	1178.9	2.82		0.2	452		1.43	5.63	0.98	199	34
d-4-B/94-H-2	-120.665601	57.006234	1178.9	2.75	2.7	0.21	449	450.5	1.5	5.56	0.9	202	32

Location	Long.	Lat.	Depth (m)	TOC	Ave. TOC	P1	Tmax	Ave. Tmax	S1	S2	S3	HI	OI
b-64-I/94-A-12	-121.546866	56.71876	1712	1.74	1.7	0.36	446	446.5	1.37	2.45	1.18	140	67
10-18-67-23W5	-117.491943	54.801731	1864.9	0.52		0.19	433		0.47	1.97	0.32	378	61
10-18-67-23W5	-117.491943	54.801731	1864.9	0.54	0.5	0.2	435	434	0.51	2.05	0.34	379	62
6-30-67-23W5	-117.501253	54.827962	1840.8	0.92		0.45	431		1.65	2.05	0.17	222	18
6-30-67-23W5	-117.501253	54.827962	1849.3	0.67		0.21	438		0.67	2.51	0.19	374	28
6-30-67-23W5	-117.501253	54.827962	1849.3	0.65	0.7	0.19	445	434.5	0.6	2.52	0.21	387	32
6-4-72-3W6	-118.400407	55.206503	1755.1	1.84		0.06	436		0.57	8.35	0.51	453	27
6-4-72-3W6	-118.400407	55.206503	1755.1	1.84	1.8	0.06	435	435.5	0.56	8.51	0.54	462	29
7-29-73-1W6	-118.109542	55.349671	1481.1	1.86		0.06	446		0.7	11.95	0.47	642	25
7-29-73-1W6	-118.109542	55.349671	1481.1	1.86	1.8	0.06	445	445.5	0.7	11.69	0.47	628	25
4-8-74-5W6	-118.739222	55.390577	2075.8	1.13		0.68	430		1.86	0.89	0.49	78	41
4-8-74-5W6	-118.739222	55.390577	2075.8	1.11	1.1	0.67	429	429.5	1.98	0.97	0.55	87	45
15-34-77-1W6	-118.060662	55.72121	1123.5	1.57		0.36	438		1.5	2.67	0.58	170	36
15-34-77-1W6	-118.060662	55.72121	1123.5	1.48	1.5	0.37	438	438	1.46	2.5	0.64	168	43
14-9-77-11W6	-119.646138	55.661656	2270	0.86		0.73	445		1.41	0.54	0.31	62	36
14-9-77-11W6	-119.646138	55.661656	2270	0.89		0.73	445		1.39	0.52	0.27	58	30
14-9-77-11W6	-119.646138	55.661656	2274.1	0.85		0.76	438		2.13	0.67	0.35	78	41
14-9-77-11W6	-119.646138	55.661656	2274.1	0.85		0.75	442		2.04	0.69	0.36	81	42
14-9-77-11W6	-119.646138	55.661656	2278	1.48		0.7	454		1.31	0.57	0.33	38	22

Location	Long.	Lat.	Depth (m)	TOC	Ave. TOC	P1	Tmax	Ave. Tmax	S1	S2	S3	HI	OI
14-9-77-11W6	-119.646138	55.661656	2279.9	0.91		0.73	443		1.65	0.61	0.42	67	46
14-9-77-11W6	-119.646138	55.661656	2279.9	0.94		0.78	444		1.6	0.44	0.43	46	45
14-9-77-11W6	-119.646138	55.661656	2280.4	0.97		0.67	450		0.66	0.32	0.22	32	22
14-9-77-11W6	-119.646138	55.661656	2280.4	0.97	0.9	0.66	449	446.4	0.67	0.35	0.25	36	25
3-22-78-10W6	-119.463783	55.770423	1843.6	2.85		0.18	445		2.06	9.66	0.72	338	25
3-22-78-10W6	-119.463783	55.770423	1843.6	2.88		0.18	444		2.11	9.93	0.68	344	23
3-22-78-10W6	-119.463783	55.770423	1846.3	1.26		0.27	445		1.13	3.01	0.74	238	58
3-22-78-10W6	-119.463783	55.770423	1846.3	1.26	2.0	0.26	443	444.2	1.16	3.24	0.74	257	58
8-10-84-18W6	-120.742816	56.2671	1868.9	1.27		0.76	463		0.61	0.2	0.15	15	11
8-10-84-18W6	-120.742816	56.2671	1868.9	1.26		0.68	463		0.64	0.31	0.08	24	6
8-10-84-18W6	-120.742816	56.2671	1873.1	0.59	1.0	0.62	423	449.6	0.35	0.21	0.04	35	6
14-26-84-18W6	-120.733685	56.317123	1804.4	0.58		0.6	424		0.3	0.2	0.09	34	15
14-26-84-18W6	-120.733685	56.317123	1804.4	0.56	0.5	0.6	420	422	0.3	0.2	0.16	35	28
1-12-84-23W6	-121.480545	56.262129	1899.9	1.24		0.68	451		0.78	0.36	0.37	29	29
1-12-84-23W6	-121.480545	56.262129	1901.5	1.24		0.7	450		1.11	0.47	0.5	37	40
1-12-84-23W6	-121.480545	56.262129	1901.5	1.26		0.69	450		1.13	0.51	0.63	40	50
1-12-84-23W6	-121.480545	56.262129	1902.4	1.05		0.62	450		0.8	0.49	0.22	46	20
1-12-84-23W6	-121.480545	56.262129	1902.4	1.06		0.62	451		0.81	0.49	0.39	46	36
1-12-84-23W6	-121.480545	56.262129	1904.5	0.95		0.71	448		0.85	0.35	0.42	36	44

Location	Long.	Lat.	Depth (m)	TOC	Ave. TOC	P1	Tmax	Ave. Tmax	S1	S2	S3	HI	OI
1-12-84-23W6	-121.480545	56.262129	1905.1	0.71		0.73	453		0.95	0.36	0.44	50	61
1-12-84-23W6	-121.480545	56.262129	1905.1	0.71	1.0	0.77	452	450.4	0.88	0.26	0.28	36	39
6-17-86-19W6	-121.967968	56.455749	1827.6	0.6		0.52	442		0.64	0.6	0.44	100	73
6-17-86-19W6	-121.967968	56.455749	1827.6	0.66		0.52	442		0.66	0.6	0.4	90	60
6-17-86-19W6	-121.967968	56.455749	1831.3	0.88		0.52	449		0.67	0.61	0.11	69	12
6-17-86-19W6	-121.967968	56.455749	1831.3	0.88		0.51	446		0.68	0.66	0.08	75	9
6-17-86-19W6	-121.967968	56.455749	1832.5	0.69		0.52	442		0.49	0.45	0.07	65	10
6-17-86-19W6	-121.967968	56.455749	1832.5	0.68		0.54	438		0.49	0.42	0.08	61	11
6-17-86-19W6	-121.967968	56.455749	1834.5	0.64		0.53	449		0.38	0.34	0.07	53	10
6-17-86-19W6	-121.967968	56.455749	1834.5	0.63		0.5	448		0.38	0.38	0.06	60	9
6-17-86-19W6	-121.967968	56.455749	1835.7	0.87		0.52	456		0.49	0.46	0.05	52	5
6-17-86-19W6	-121.967968	56.455749	1835.7	0.87		0.49	453		0.5	0.53	0.05	60	5
6-17-86-19W6	-121.967968	56.455749	1836.1	0.95		0.28	440		0.22	0.57	0.02	60	2
6-17-86-19W6	-121.967968	56.455749	1836.1	0.96	0.7	0.28	442	445.5	0.22	0.57	0.03	59	3
16-8-86-20W6	-121.111972	56.4487	1896.1	0.54		0.6	423		0.67	0.45	0.04	83	7
16-8-86-20W6	-121.111972	56.4487	1897.8	0.91		0.51	450		1.01	0.97	0.03	106	3
16-8-86-20W6	-121.111972	56.4487	1897.8	0.93		0.51	446		1.03	0.97	0.11	104	11
16-8-86-20W6	-121.111972	56.4487	1901	1.52		0.53	452		1.72	1.5	0	98	0
16-8-86-20W6	-121.111972	56.4487	1901	1.5		0.53	452		1.72	1.55	0	103	0

Location	Long.	Lat.	Depth (m)	TOC	Ave. TOC	P1	Tmax	Ave. Tmax	S1	S2	S3	HI	OI
16-8-86-20W6	-121.111972	56.4487	1901.9	0.96		0.68	438		1.21	0.58	0.57	60	59
16-8-86-20W6	-121.111972	56.4487	1905.2	0.66		0.51	441		0.88	0.85	0.52	128	78
16-8-86-20W6	-121.111972	56.4487	1905.2	0.65	0.9	0.52	442	441.8	0.88	0.81	0.24	124	36
10-24-86-21W6	-121.172125	56.473571	1964.1	1.57		0.55	455		1.33	1.07	0.17	68	10
10-24-86-21W6	-121.172125	56.473571	1970.8	1.06		0.48	467		0.53	0.58	0	54	0
10-24-86-21W6	-121.172125	56.473571	1970.8	1.05	1.3	0.47	465	461.2	0.52	0.59	0	56	0
7-5-87-20W6	-121.148678	56.513766	1941.7	1.69		0.43	461		1	1.32	0.45	78	26
7-5-87-20W6	-121.148678	56.513766	1941.7	1.69		0.43	463		1.01	1.35	0.23	79	13
7-5-87-20W6	-121.148678	56.513766	1944.6	1.63		0.48	461		1.05	1.13	0.17	69	10
7-5-87-20W6	-121.148678	56.513766	1944.6	1.58		0.5	460		1.06	1.07	0.31	67	19
7-5-87-20W6	-121.148678	56.513766	1946	1.2		0.52	453		0.99	0.93	0.63	77	52
7-5-87-20W6	-121.148678	56.513766	1946	1.18		0.53	451		0.99	0.88	0.2	74	16
7-5-87-20W6	-121.148678	56.513766	1947.4	1.64		0.55	458		0.72	0.61	0.21	37	12
7-5-87-20W6	-121.148678	56.513766	1947.4	1.63		0.55	458		0.72	0.59	0.53	36	32
7-5-87-20W6	-121.148678	56.513766	1948.1	2.78		0.44	458		0.34	0.45	0.23	16	8
7-5-87-20W6	-121.148678	56.513766	1948.1	2.77	1.7	0.42	458	458.1	0.33	0.45	0.25	16	9
8-11-87-25W6	-121.856206	56.53041	1564.2	1.25		0.5	457		1.02	1.04	0.2	83	16
8-11-87-25W6	-121.856206	56.53041	1564.2	1.28		0.52	458		1	0.92	0.28	71	21
8-11-87-25W6	-121.856206	56.53041	1951.4	1.38		0.53	454		0.7	0.63	0.13	45	9
8-11-87-25W6	-121.856206	56.53041	1951.4	1.33		0.61	449		0.63	0.42	0.22	31	16

Location	Long.	Lat.	Depth (m)	TOC	Ave. TOC	P1	Tmax	Ave. Tmax	S1	S2	S3	HI	OI
8-11-87-25W6	-121.856206	56.53041	1952.9	1.32		0.69	463		0.66	0.3	0.13	22	9
8-11-87-25W6	-121.856206	56.53041	1953.3	0.89		0.48	460		0.44	0.48	0.01	53	1
8-11-87-25W6	-121.856206	56.53041	1953.3	0.88		0.49	461		0.41	0.44	0	50	0
8-11-87-25W6	-121.856206	56.53041	1954.1	1.04		0.62	458		0.64	0.41	0.27	39	25
8-11-87-25W6	-121.856206	56.53041	1954.1	1.06		0.61	459		0.63	0.42	0.1	39	9
8-11-87-25W6	-121.856206	56.53041	1954.5	1.28		0.49	458		0.66	0.71	0	55	0
8-11-87-25W6	-121.856206	56.53041	1954.5	1.27	1.1	0.5	456	457.8	0.68	0.68	0	53	0
4-27-88-17W6	-120.6296	56.655466	1369.2	1.53		0.57	453		1.25	0.94	0.28	61	18
4-27-88-17W6	-120.6296	56.655466	1369.2	1.53		0.55	449		1.23	1.01	0.31	66	20
4-27-88-17W6	-120.6296	56.655466	1371	2.27		0.48	454		1.26	1.36	0.3	59	13
4-27-88-17W6	-120.6296	56.655466	1371	2.33	1.9	0.49	457	453.2	1.26	1.3	0.33	55	14
6-8-90-11W6	-119.719045	56.789921	1361.8	2.38		0.12	451		1.19	8.99	0.37	377	15
6-21-56-8W5	-119.719045	56.789921	1515.2	5.49		0.11	439		2.32	19.66	0.65	358	11
6-21-56-8W5	-119.719045	56.789921	1515.2	5.38		0.1	440		2.2	19.12	1.17	355	21
6-21-56-8W5	-119.719045	56.789921	1516.1	2.26		0.13	444		0.96	6.23	0.49	275	21
7-5-87-20W6	-121.148678	56.513766	1947.4	1.64		0.55	458		0.72	0.61	0.21	37	12
7-5-87-20W6	-121.148678	56.513766	1947.4	1.63		0.55	458		0.72	0.59	0.53	36	32
7-5-87-20W6	-121.148678	56.513766	1948.1	2.78		0.44	458		0.34	0.45	0.23	16	8
7-5-87-20W6	-121.148678	56.513766	1948.1	2.77	1.7	0.42	458	458.1	0.33	0.45	0.25	16	9
8-11-87-25W6	-121.856206	56.53041	1564.2	1.25		0.5	457		1.02	1.04	0.2	83	16

Location	Long.	Lat.	Depth (m)	TOC	Ave. TOC	P1	Tmax	Ave. Tmax	S1	S2	S3	HI	OI
10-26-56-23W5	-117.305187	53.87137	3089.2	11.19		0.19	506		0.72	3.02	0.24	26	2
10-26-56-23W5	-117.305187	53.87137	3089.5	10.16		0.15	484		0.58	3.31	0.21	32	2
10-26-56-23W5	-117.305187	53.87137	3089.5	10.3		0.15	484		0.58	3.25	0.19	31	1
10-26-56-23W5	-117.305187	53.87137	3090	11.7		0.19	490		0.77	3.4	0.29	29	2
10-26-56-23W5	-117.305187	53.87137	3090	10.39	10.7	0.18	491	493.5	0.79	3.51	0.29	33	2
5-16-56-4W6	-118.541595	53.838415	3606.6	0.82		0	537		0	0.44	0.09	53	10
5-16-56-4W6	-118.541595	53.838415	3606.6	0.77		0	544		0	0.36	0.09	46	11
5-16-56-4W6	-118.541595	53.838415	3805.3	2.97		0.19	564		0.07	0.3	0	10	0
5-16-56-4W6	-118.541595	53.838415	3805.3	2.89		0.19	563		0.08	0.35	0	12	0
5-16-56-4W6	-118.541595	53.838415	3808.6	6.14		0.29	573		0.08	0.2	0.18	3	2
5-16-56-4W6	-118.541595	53.838415	3811	7.48		0.22	569		0.09	0.32	0.19	4	2
5-16-56-4W6	-118.541595	53.838415	3811	7.9		0.18	574		0.07	0.31	0	3	0
5-16-56-4W6	-118.541595	53.838415	3811.5	5.03		0.25	575		0.07	0.21	0.1	4	1
5-16-56-4W6	-118.541595	53.838415	3811.5	5	4.3	0.3	575	563.7	0.09	0.22	0	4	0
16-23-57-6W6	-118.77054	53.947044	2377.1	7.07		0.1	544		0.09	0.79	0.54	11	7
16-23-57-6W6	-118.77054	53.947044	2377.1	5.88		0.1	537		0.1	0.88	0.48	14	8
16-23-57-6W6	-118.77054	53.947044	2377.8	3.44		0.08	535		0.04	0.46	0.39	13	11
16-23-57-6W6	-118.77054	53.947044	2377.8	3.51		0.05	536		0.02	0.39	0.37	11	10
16-23-57-6W6	-118.77054	53.947044	2382.2	4.96		0.13	548		0.05	0.34	0.47	6	9
16-23-57-6W6	-118.77054	53.947044	2382.2	5.58		0.14	547		0.06	0.37	0.52	6	9
16-23-57-6W6	-118.77054	53.947044	2384.1	2.81		0.17	550		0.05	0.26	0.36	9	12

Location	Long.	Lat.	Depth (m)	TOC	Ave. TOC	P1	Tmax	Ave. Tmax	S1	S2	S3	HI	OI
16-23-57-6W6	-118.77054	53.947044	2384.1	2.77		0.18	551		0.07	0.31	0.43	11	15
16-23-57-6W6	-118.77054	53.947044	2386	6.42		0.11	557		0.08	0.65	0.27	10	4
16-23-57-6W6	-118.77054	53.947044	2386	6.16		0.12	553		0.1	0.75	0.26	12	4
10-6-60-20W5	-116.984503	54.162338	2451.6	6.97		0.45	462		7.46	9.14	0.93	131	13
10-6-60-20W5	-116.984503	54.162338	2451.6	6.9		0.46	461		7.59	9.03	0.96	130	13
10-6-60-20W5	-116.984503	54.162338	2453.7	4.89		0.44	458		5.94	7.55	0.76	154	15
10-6-60-20W5	-116.984503	54.162338	2453.7	4.91		0.43	456		5.91	7.73	0.8	157	16
10-6-60-20W5	-116.984503	54.162338	2454.9	3.09		0.39	468		3.46	5.34	0.92	172	29
10-6-60-20W5	-116.984503	54.162338	2454.9	3.15		0.4	466		3.52	5.33	0.83	169	26
10-6-60-20W5	-116.984503	54.162338	2458.2	5.29		0.37	461		3.44	5.85	0.79	110	14
10-6-60-20W5	-116.984503	54.162338	2458.2	5.43		0.36	462		3.28	5.9	0.96	108	17
10-6-60-20W5	-116.984503	54.162338	2459.6	5.88		0.36	467		4.09	7.17	0.88	121	14
10-6-60-20W5	-116.984503	54.162338	2459.6	6.08		0.36	467		4.09	7.31	0.81	120	13
10-6-60-20W5	-116.984503	54.162338	2462.6	3.09		0.36	467		2.32	4.08	0.63	132	20
10-6-60-20W5	-116.984503	54.162338	2462.6	3.15		0.36	467		2.28	4.09	0.55	129	17
10-6-60-20W5	-116.984503	54.162338	2462.7	1.29		0.76	456		1.2	0.39	0.41	30	31
10-6-60-20W5	-116.984503	54.162338	2462.7	1.11		0.68	464		1.17	0.55	0.37	49	33
10-6-60-20W5	-116.984503	54.162338	2463.4	3.24		0.52	430		5	4.54	1.05	140	32
10-6-60-20W5	-116.984503	54.162338	2463.4	3.3		0.52	430		5.22	4.81	0.77	145	23

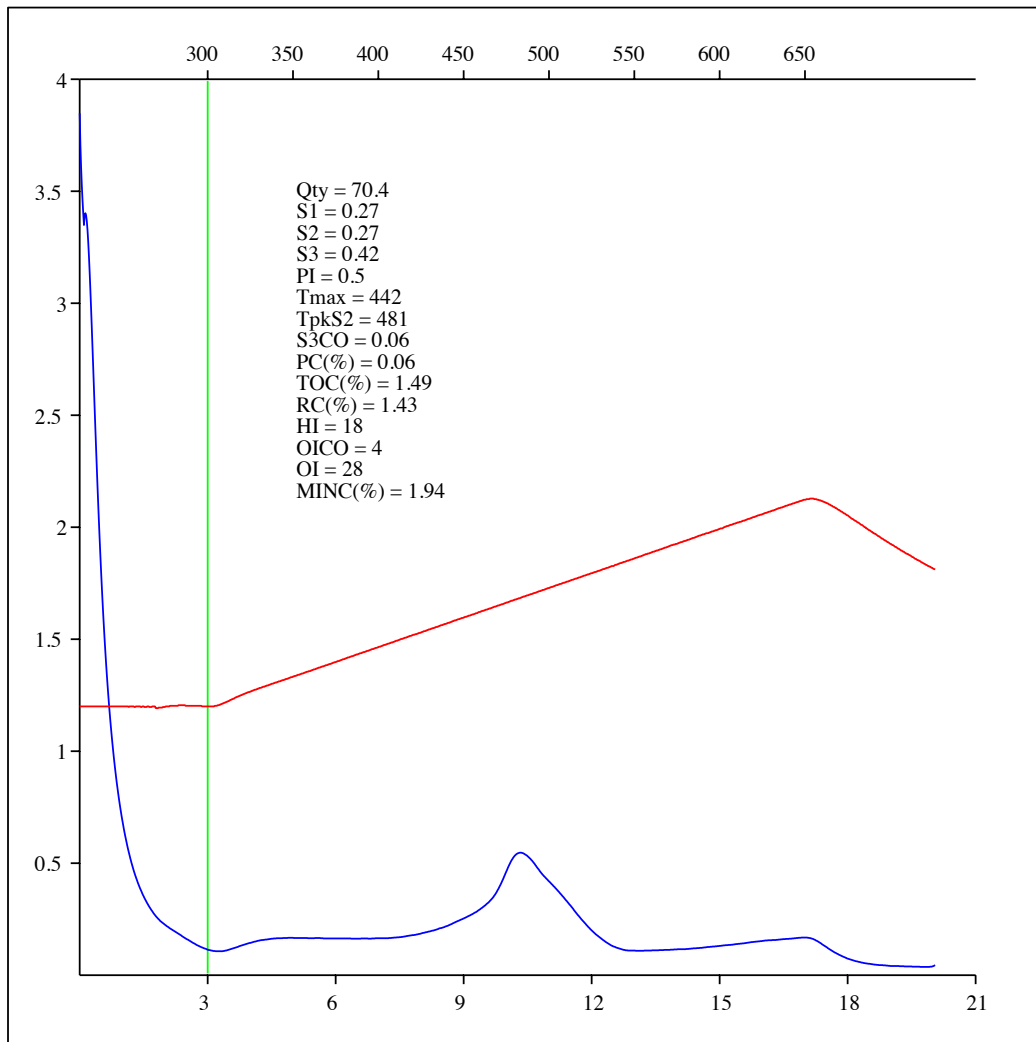
Location	Long.	Lat.	Depth (m)	TOC	Ave. TOC	P1	Tmax	Ave. Tmax	S1	S2	S3	HI	OI
2-27-82-16W6	120.40809	56.133665	1211.6	2.84		0.4	457		1.42	2.12	0	74	0
2-27-82-16W6	120.40809	56.133665	1211.6	2.75		0.38	460		1.36	2.18	0.08	79	2
2-27-82-16W6	120.40809	56.133665	1212.8	7.26		0.33	465		5.71	11.84	0.02	163	0
2-27-82-16W6	120.40809	56.133665	1212.8	6.94		0.33	466		5.64	11.62	0.44	167	6
2-27-82-16W6	120.40809	56.133665	1213.7	6.48		0.33	464		5	10.32	0.2	159	3
2-27-82-16W6	120.40809	56.133665	1214.9	3		0.3	467		1.27	3.01	0.26	100	8
2-27-82-16W6	120.40809	56.133665	1214.9	2.81		0.28	467		1.23	3.09	0.46	109	16
2-27-82-16W6	120.40809	56.133665	1215.2	3.42	4.5	0.32	464	463.9	1.12	2.4	0.84	70	24
4-9-83-17W6	-120.632702	56.174582	1167.4	7.07		0.3	457		3.51	8.13	0.07	114	0
4-9-83-17W6	-120.632702	56.174582	1167.4	6.53		0.29	460		3.51	8.68	0	132	0
4-9-83-17W6	-120.632702	56.174582	1167.8	5.93		0.18	459		1.8	8.47	0.7	142	11
4-9-83-17W6	-120.632702	56.174582	1167.8	7.03		0.18	461		1.86	8.71	0.72	123	10
4-9-83-17W6	-120.632702	56.174582	1168.5	2.44		0.28	460		0.55	1.4	0.33	57	13
4-9-83-17W6	-120.632702	56.174582	1168.5	2.44	5.2	0.26	460	459.5	0.5	1.41	0.54	57	22
1-12-84-23W6	-121.480545	56.262119	1132.5	1.1		0.45	470		0.6	0.75	0.33	68	30
1-12-84-23W6	-121.480545	56.262119	1132.6	0.8		0.46	469		0.42	0.5	0.21	62	26
1-12-84-23W6	-121.480545	56.262119	1132.6	0.81		0.47	471		0.41	0.47	0.17	58	20
1-12-84-23W6	-121.480545	56.262119	1133.2	1.96		0.4	476		0.84	1.26	0.51	64	26
1-12-84-23W6	-121.480545	56.262119	1133.2	2.07		0.4	473		0.85	1.29	0.29	62	14
1-12-84-23W6	-121.480545	56.262119	1134.7	0.71		0.72	431		0.76	0.3	0.18	42	25
1-12-84-23W6	-121.480545	56.262119	1134.7	0.7	1.1	0.75	457	464.6	0.69	0.23	0.3	32	42

Location	Long.	Lat.	Depth (m)	TOC	Ave. TOC	P1	Tmax	Ave. Tmax	S1	S2	S3	HI	OI
6-28-61-15W5	-116.191339	57.18976	1926.3	1.2		0.47	440		2.9	3.31	0.54	275	45
6-28-61-15W5	-116.191339	57.18976	1926.3	1.47		0.49	436		2.91	2.99	0.75	203	51
6-28-61-15W5	-116.191339	57.18976	1929.4	4.48	3.5	0.09	442		1.27	12.88	0.55	287	12
6-28-61-15W5	-116.191339	57.18976	1929.4	4.67		0.09	440		1.34	12.96	0.53	277	11
6-28-61-15W5	-116.191339	57.18976	1935.2	5.76		0.1	442		1.94	16.61	0.49	288	8

APPENDIX 3 – B: Graphs showing Rock-Eval pyrolysis for samples analyzed and used in this study.

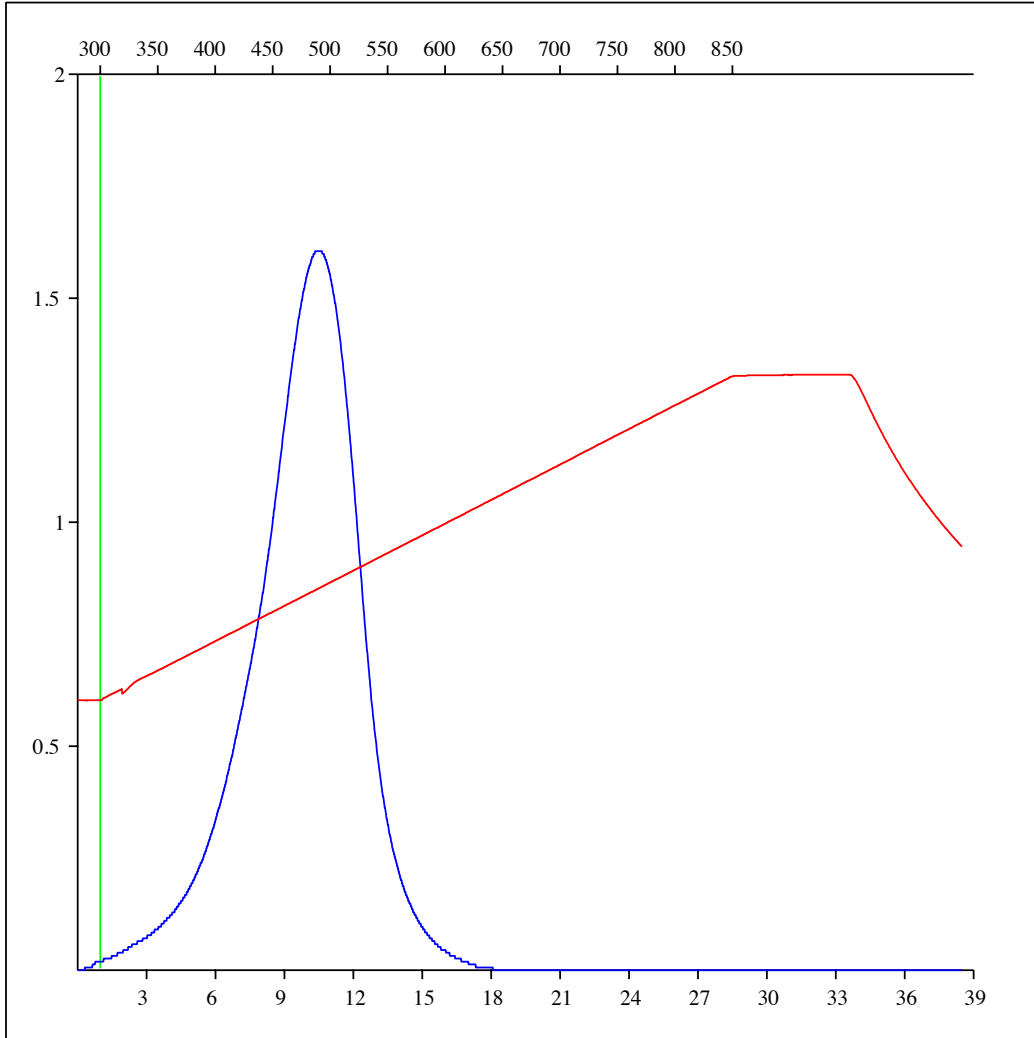
Sample: C-492833
Acquisition Date: 08-FEB-2012
Location: ADU MONIAS 01-10-082-23
Depth: 2005 m
Analysis
Instrument: RockEval 6
Data Processing Software: Vinci

FID hydrocarbons



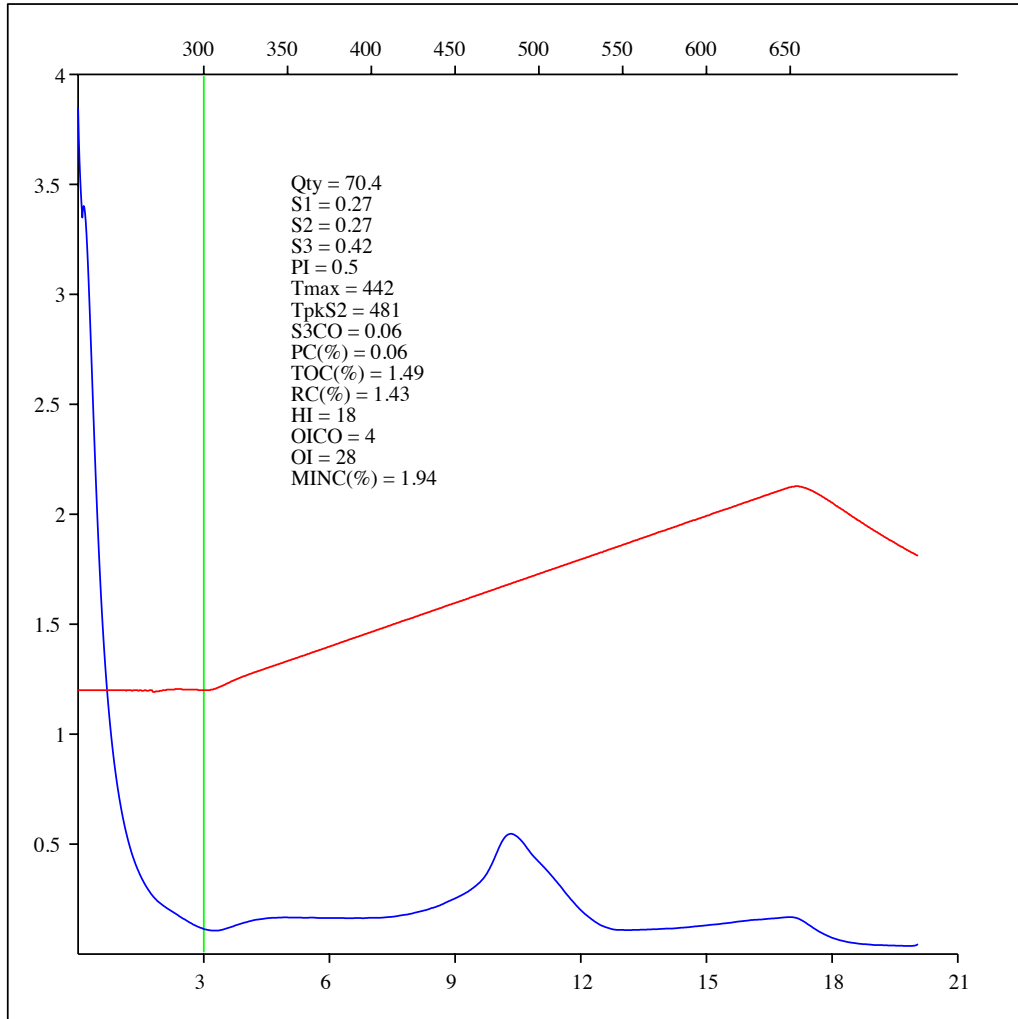
Sample: C-492833
Acquisition Date: 08-FEB-2012
Location: ADU MONIAS 01-10-082-23
Depth: 2005 m
Analysis
Instrument: RockEval 6
Data Processing Software: Vinci

Oxidation carbon monoxide



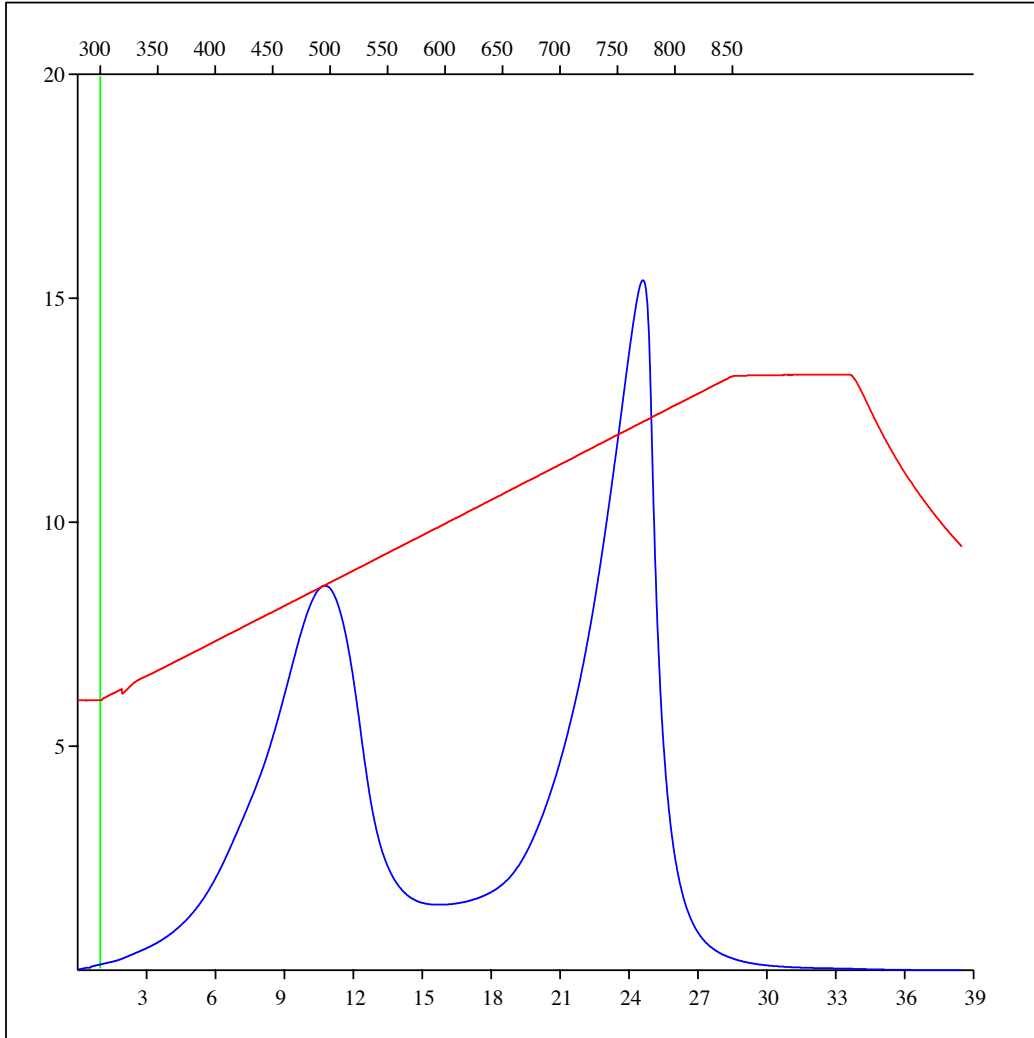
Sample: C-492833
Acquisition Date: 08-FEB-2012
Location: ADU MONIAS 01-10-082-23
Depth: 2005 m
Analysis
Instrument: RockEval 6
Data Processing Software: Vinci

FID hydrocarbons



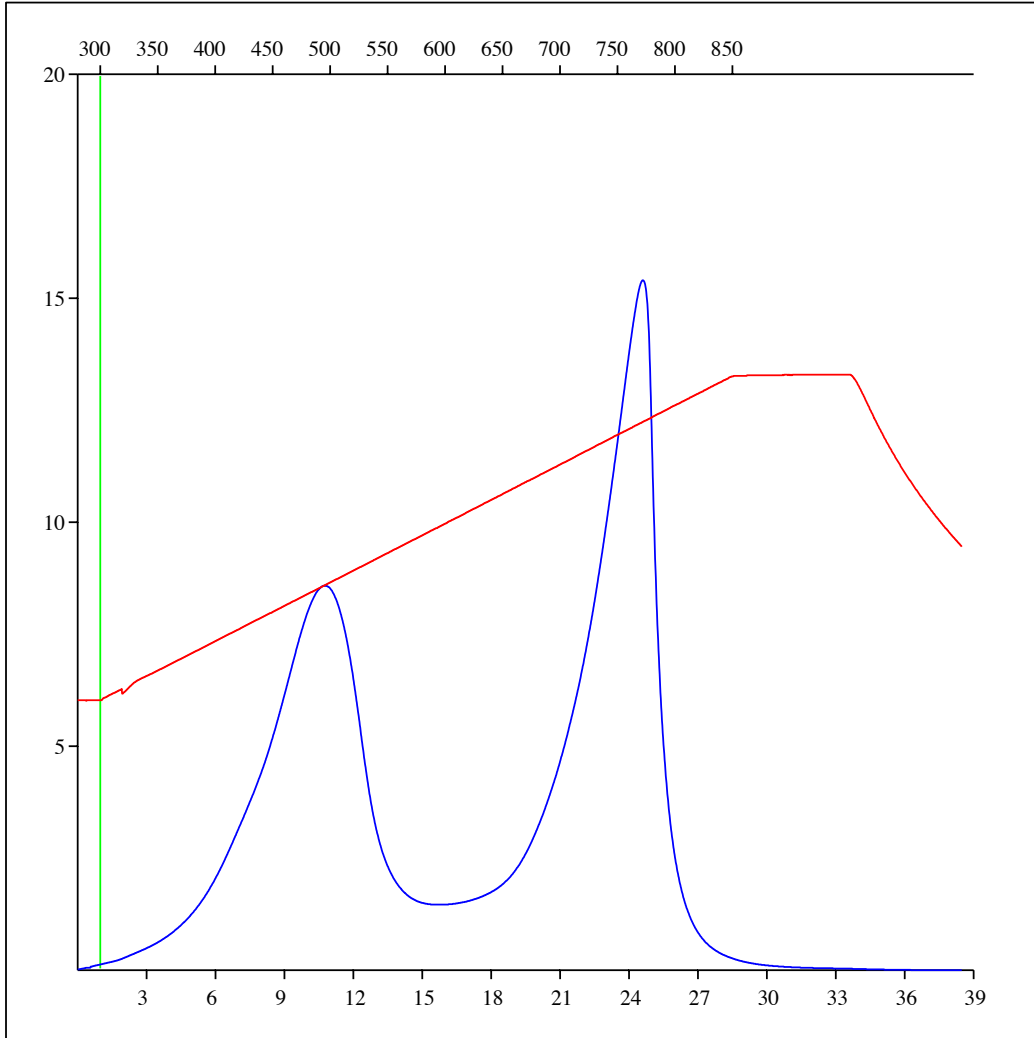
Sample: C-492833
Acquisition Date: 08-FEB-2012
Location: ADU MONIAS 01-10-082-23
Depth: 2005 m
Analysis
Instrument: RockEval 6
Data Processing Software: Vinci

Oxidation carbon dioxide



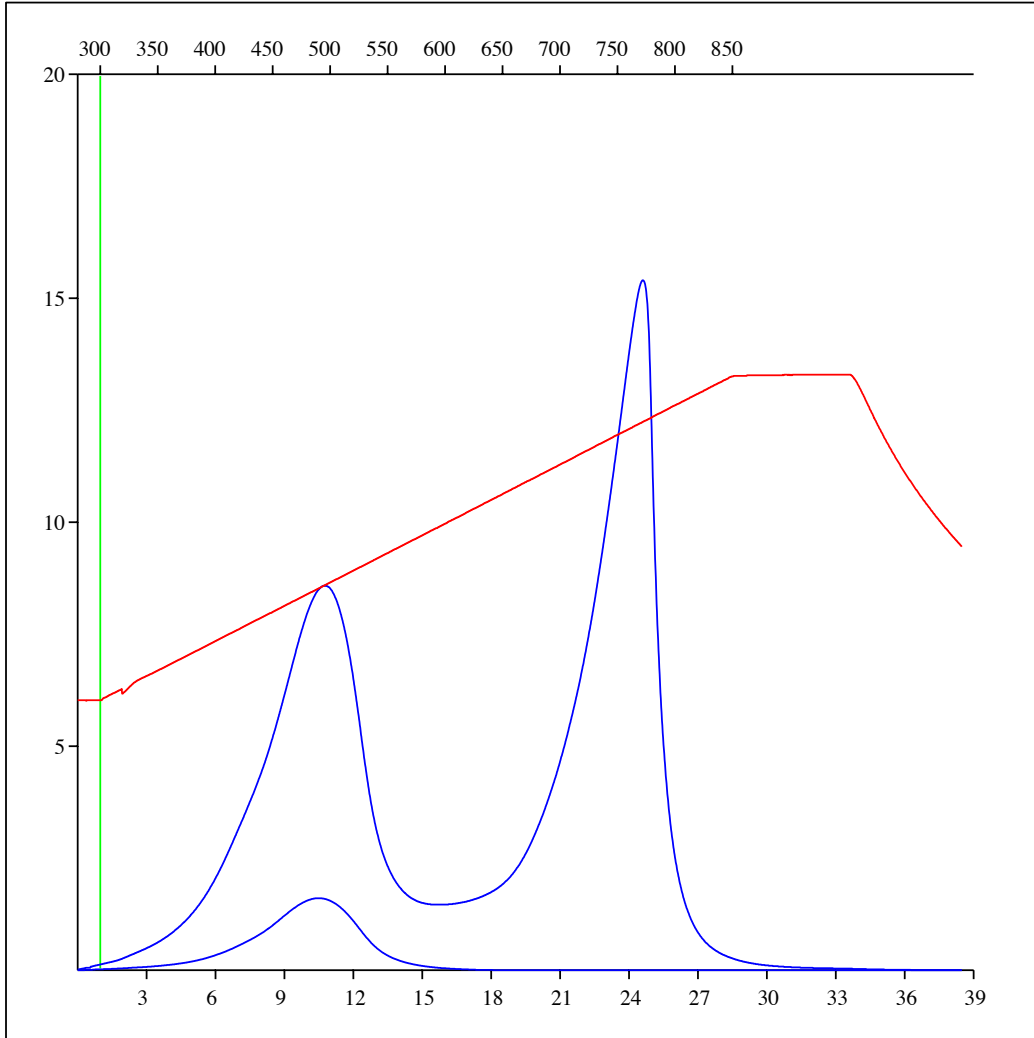
Sample: C-492833
Acquisition Date: 08-FEB-2012
Location: ADU MONIAS 01-10-082-23
Depth: 2005 m
Analysis
Instrument: RockEval 6
Data Processing Software: Vinci

Oxidation carbon dioxide



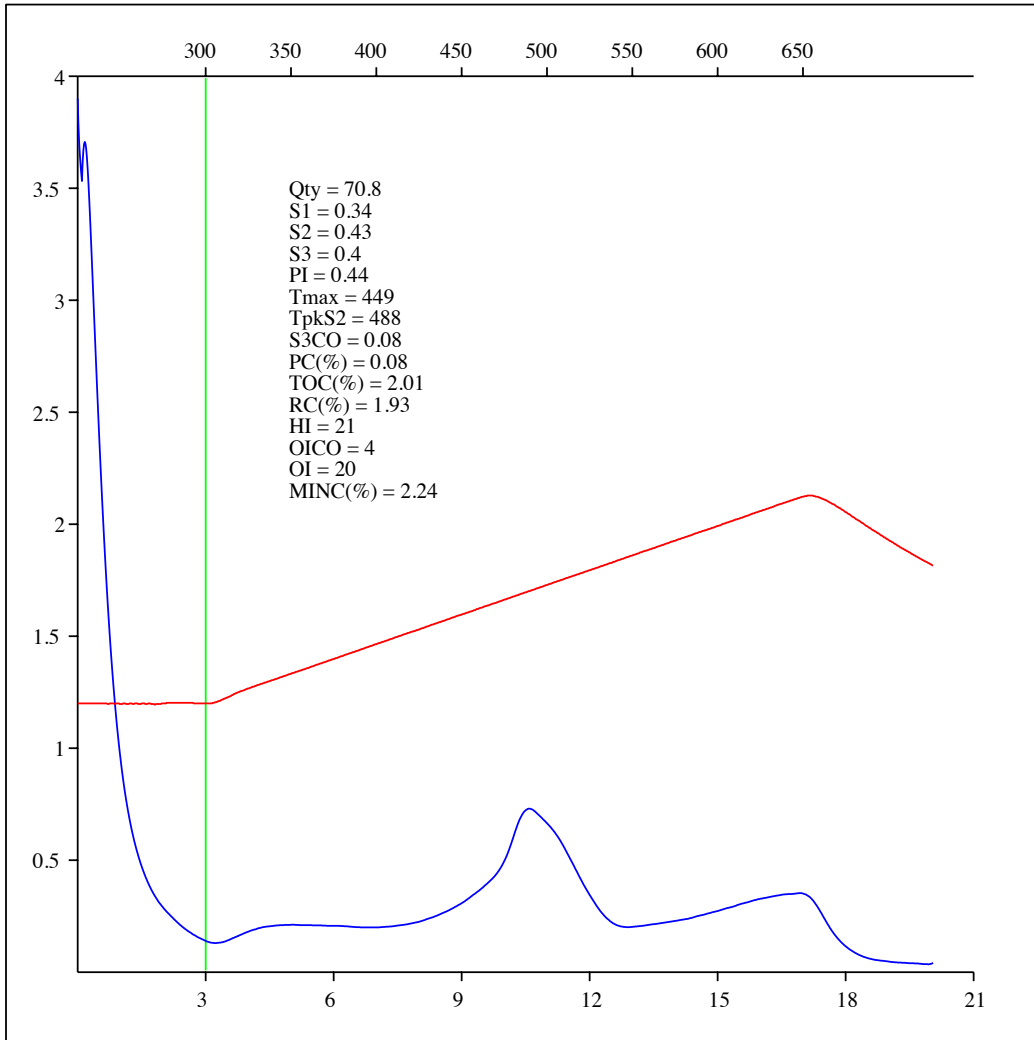
Sample: C-492833
Acquisition Date: 08-FEB-2012
Location: ADU MONIAS 01-10-082-23
Depth: 2005 m
Analysis
Instrument: RockEval 6
Data Processing Software: Vinci

Oxidation carbon monoxide & carbon dioxide



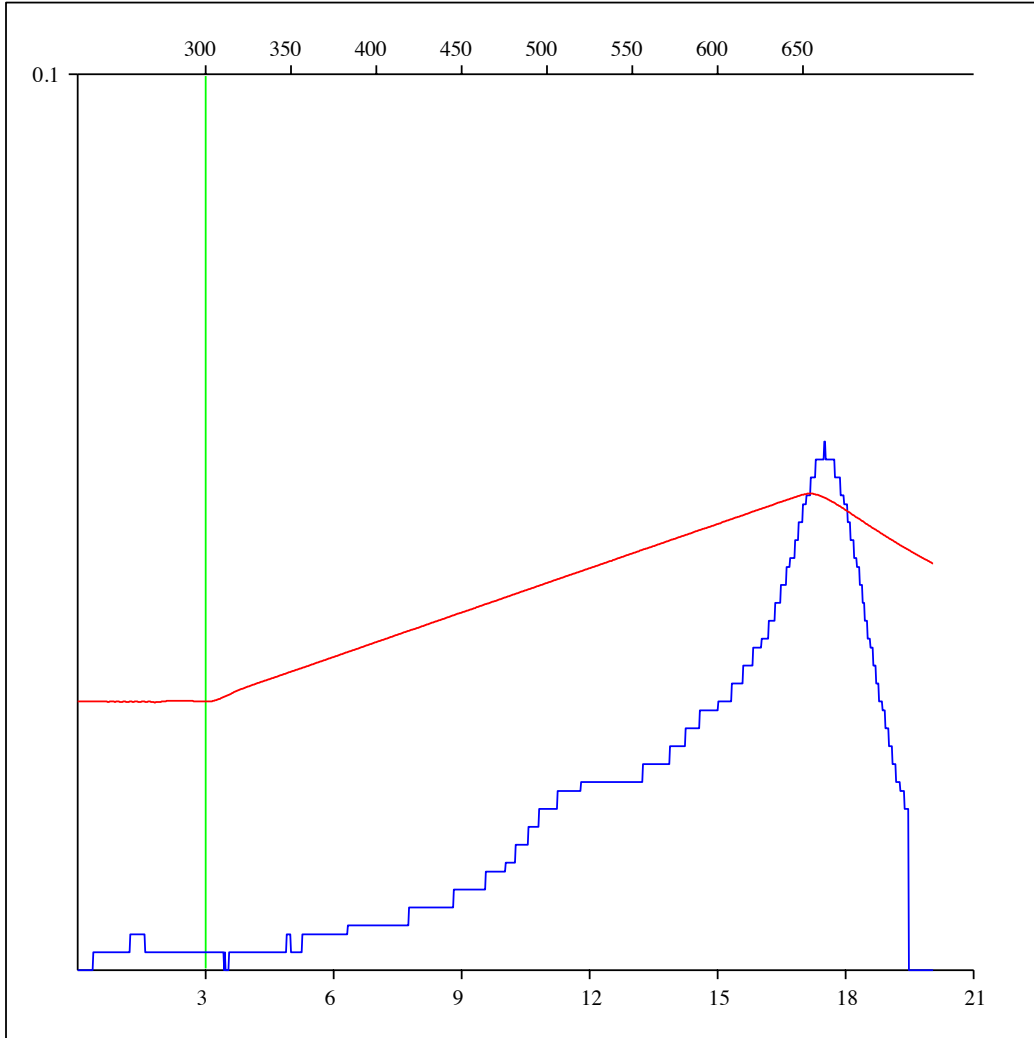
Sample: C-492834
Acquisition Date: 08-FEB-2012
Location: ADU MONIAS 01-10-082-23
Depth: 2013.24 m
Analysis
Instrument: RockEval 6
Data Processing Software: Vinci

FID hydrocarbons



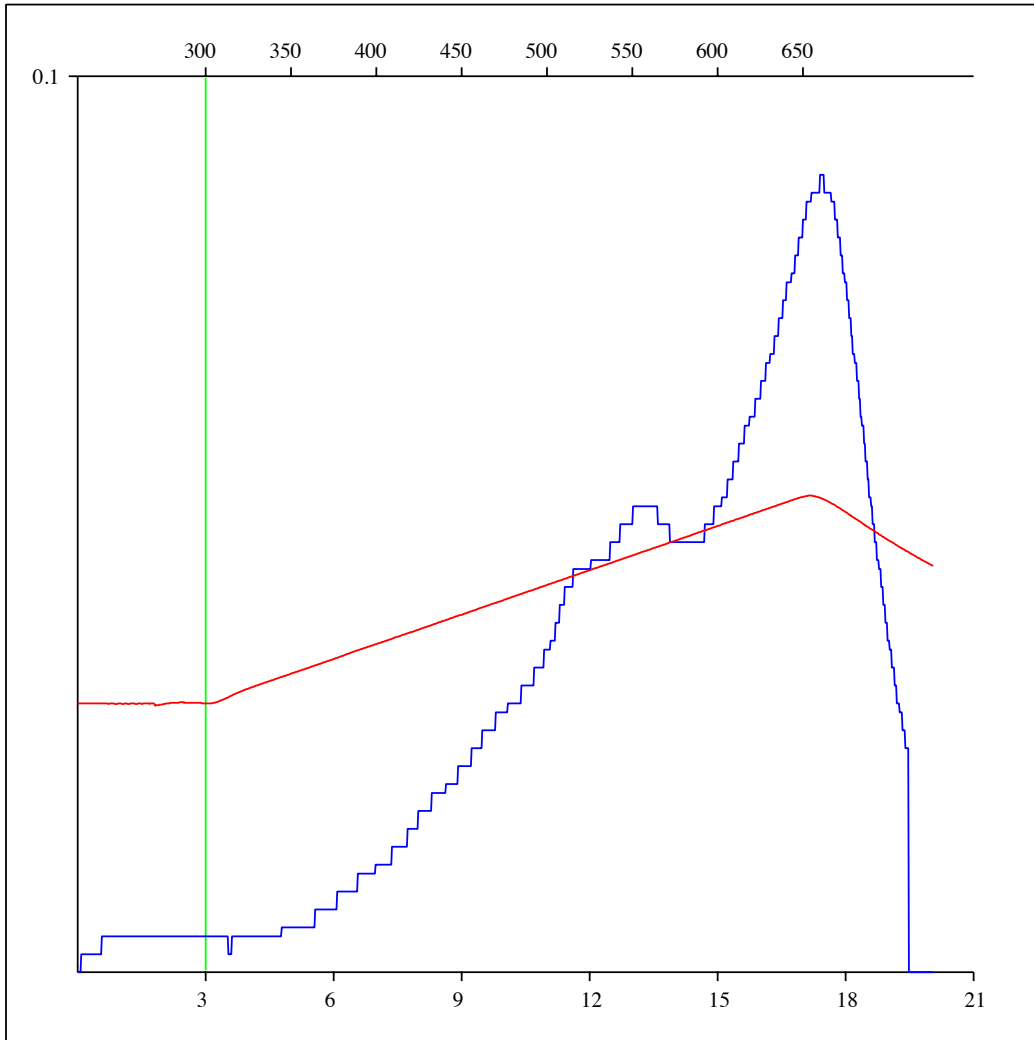
Sample: C-492834
Acquisition Date: 08-FEB-2012
Location: ADU MONIAS 01-10-082-23
Depth: 2013.24 m
Analysis
Instrument: RockEval 6
Data Processing Software: Vinci

Pyrolysis carbon monoxide



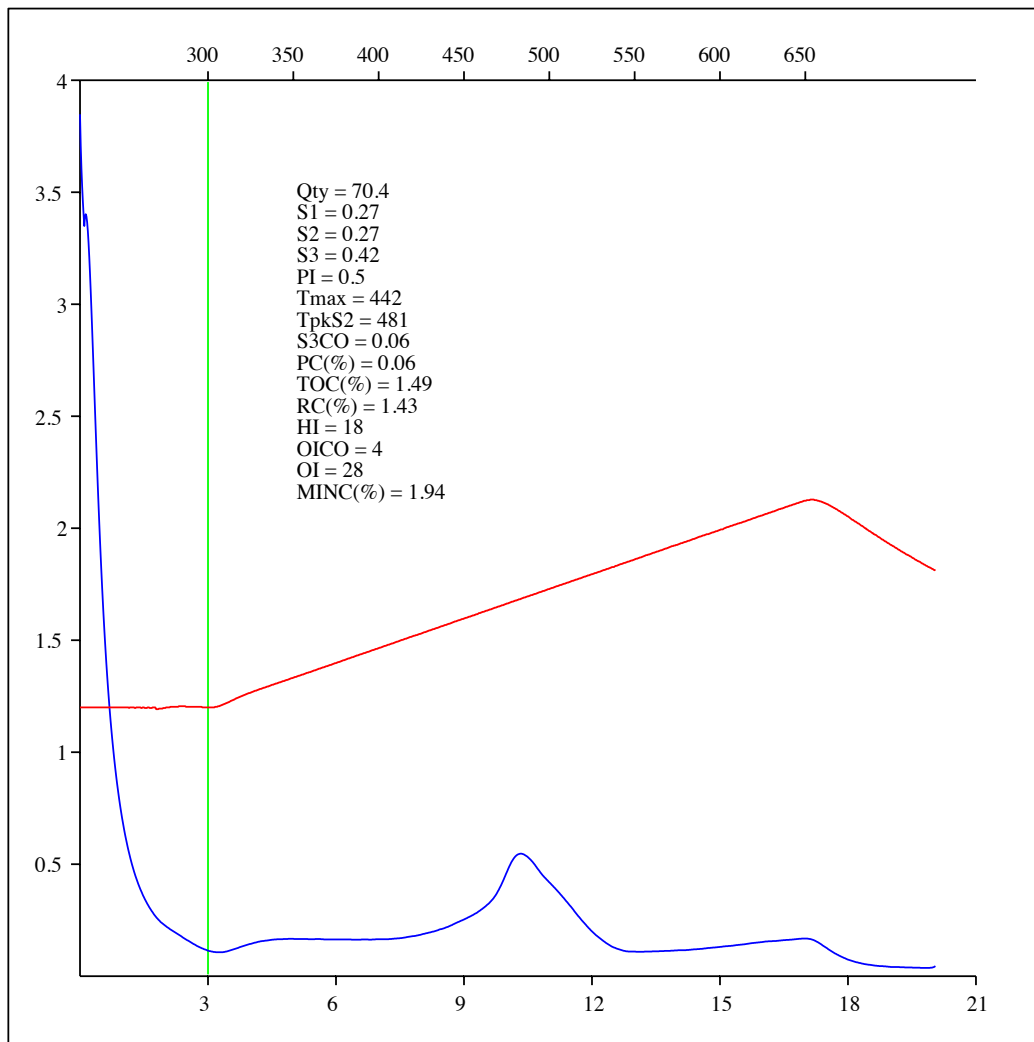
Sample: C-492844
Acquisition Date: 08-FEB-2012
Location: ARC DAWSON 07-13-079-15
Depth: 2055.22 m
Analysis
Instrument: RockEval 6
Data Processing Software: Vinci

Pyrolysis carbon monoxide



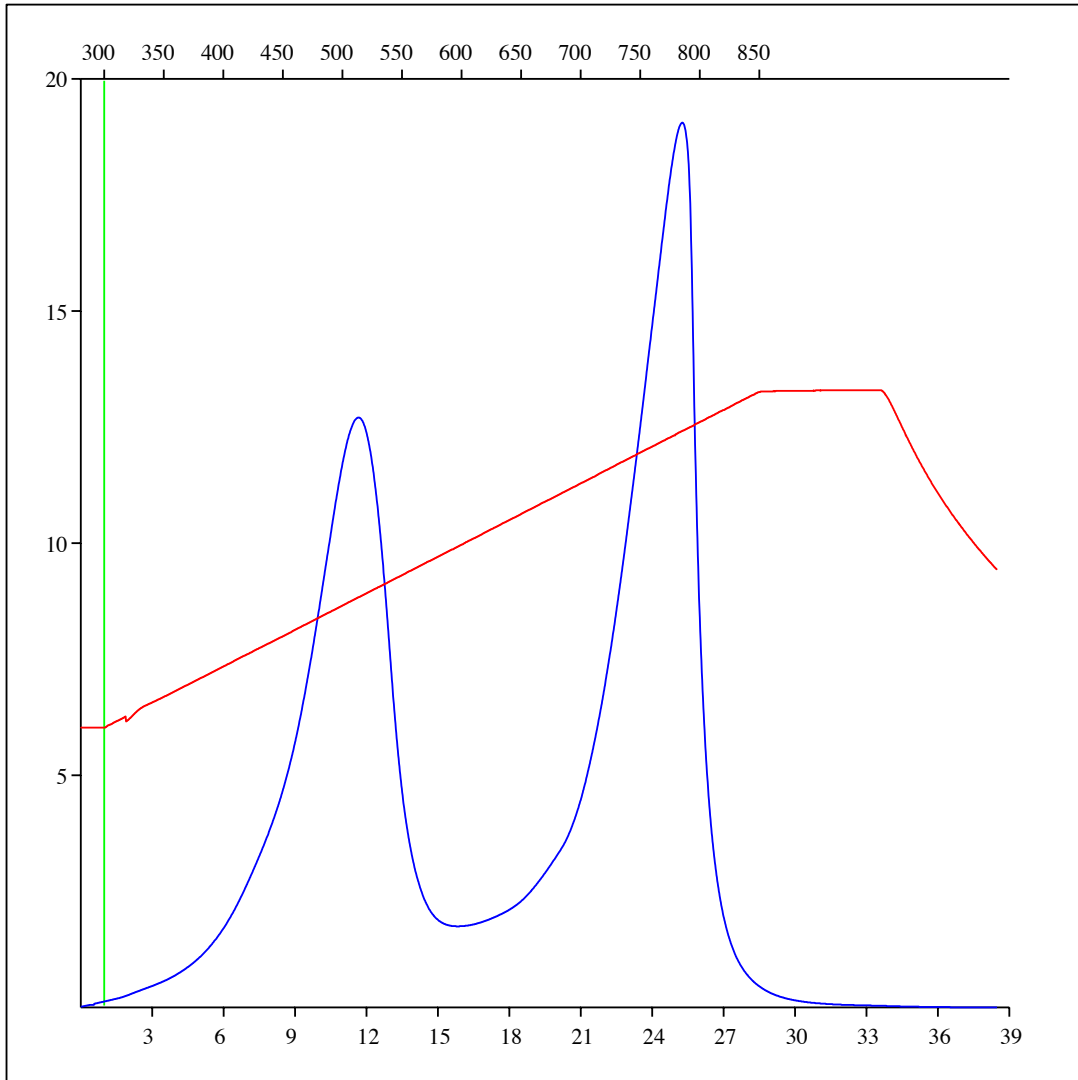
Sample: C-492833
Acquisition Date: 08-FEB-2012
Location: ADU MONIAS 01-10-082-23
Depth: 2005 m
Analysis
Instrument: RockEval 6
Data Processing Software: Vinci

FID hydrocarbons



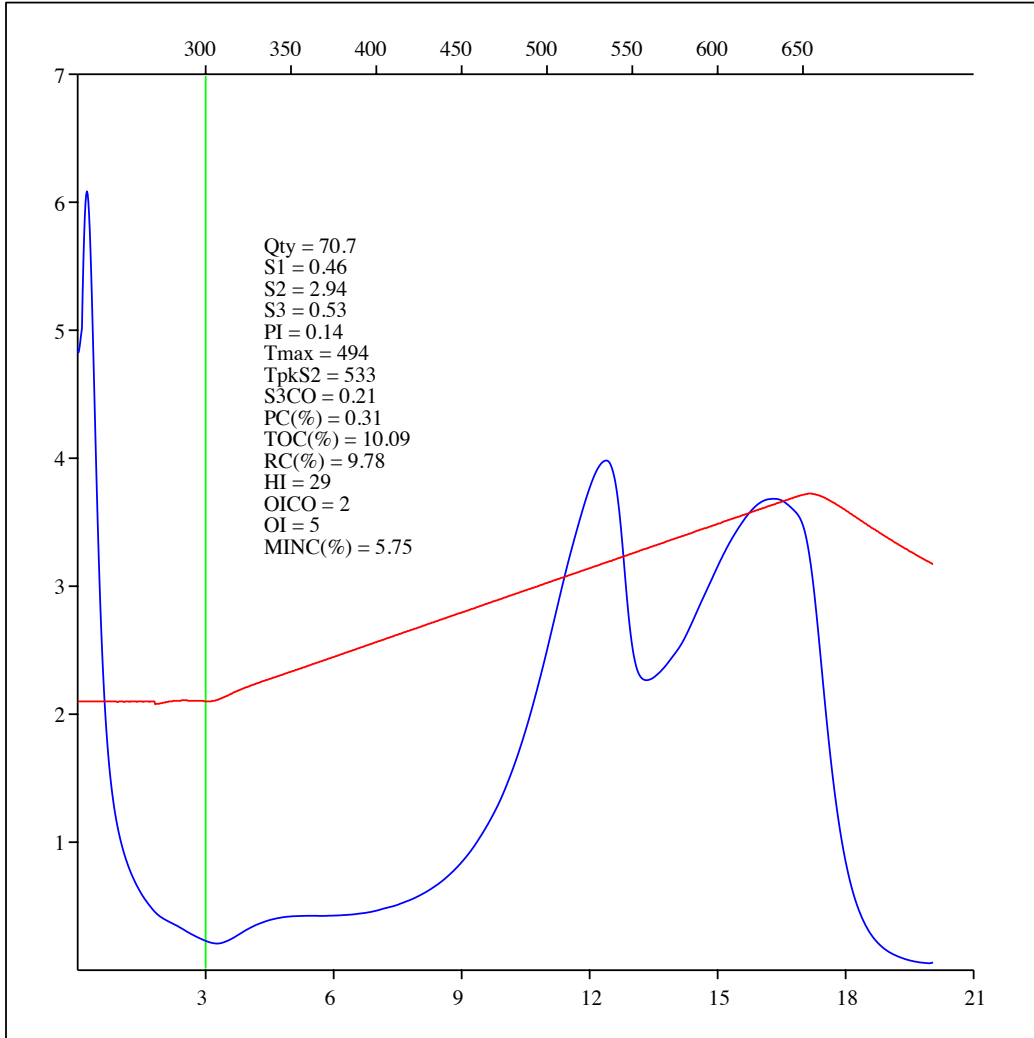
Sample: C-492834
Acquisition Date: 08-FEB-2012
Location: ADU MONIAS 01-10-082-23
Depth: 2013.24 m
Analysis
Instrument: RockEval 6
Data Processing Software: Vinci

Oxidation carbon dioxide



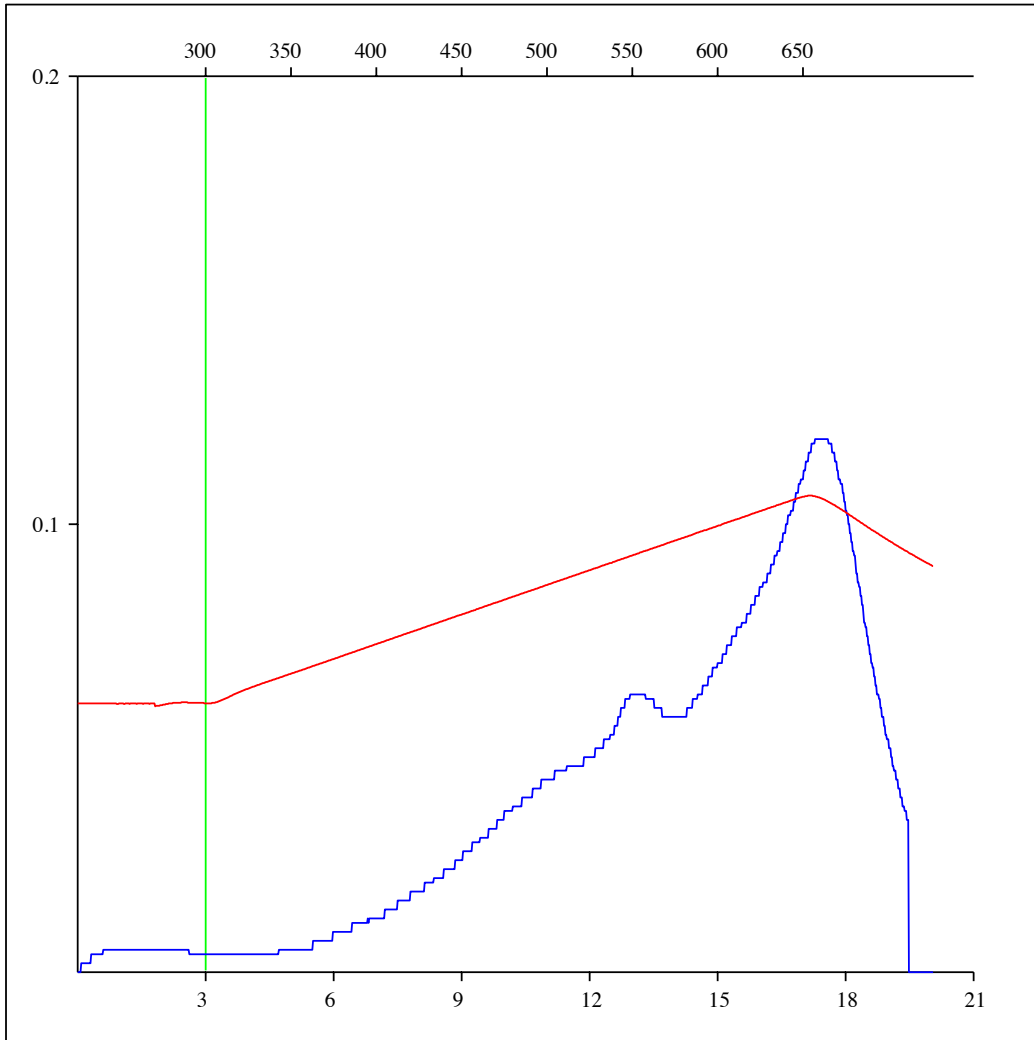
Sample: C-492835
Acquisition Date: 08-FEB-2012
Location: ADU MONIAS 01-10-082-23
Depth: 1864.7 m
Analysis
Instrument: RockEval 6
Data Processing Software: Vinci

FID hydrocarbons



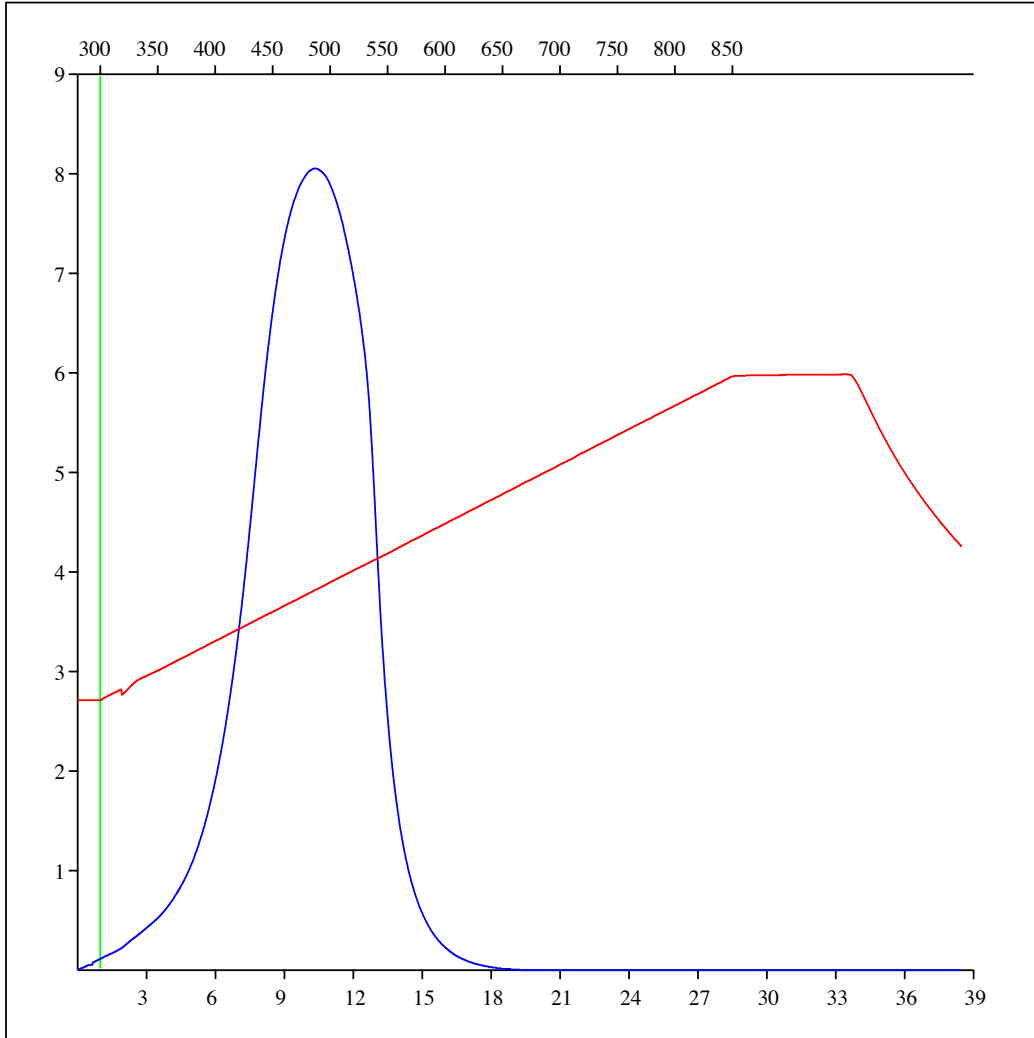
Sample: C-492835
Acquisition Date: 08-FEB-2012
Location: ADU MONIAS 01-10-082-23
Depth: 1864.7 m
Analysis
Instrument: RockEval 6
Data Processing Software: Vinci

Pyrolysis carbon monoxide



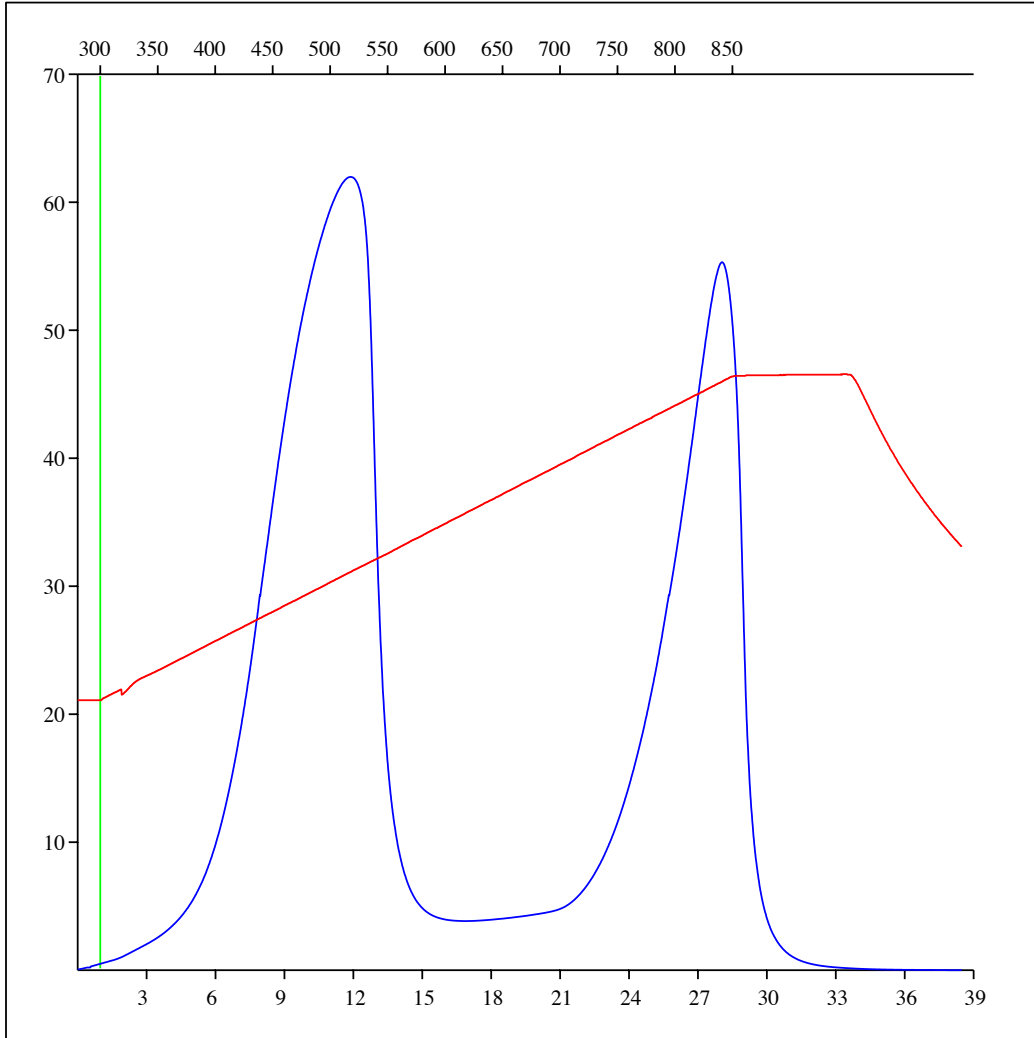
Sample: C-492835
Acquisition Date: 08-FEB-2012
Location: ADU MONIAS 01-10-082-23
Depth: 1864.7 m
Analysis
Instrument: RockEval 6
Data Processing Software: Vinci

Oxidation carbon monoxide



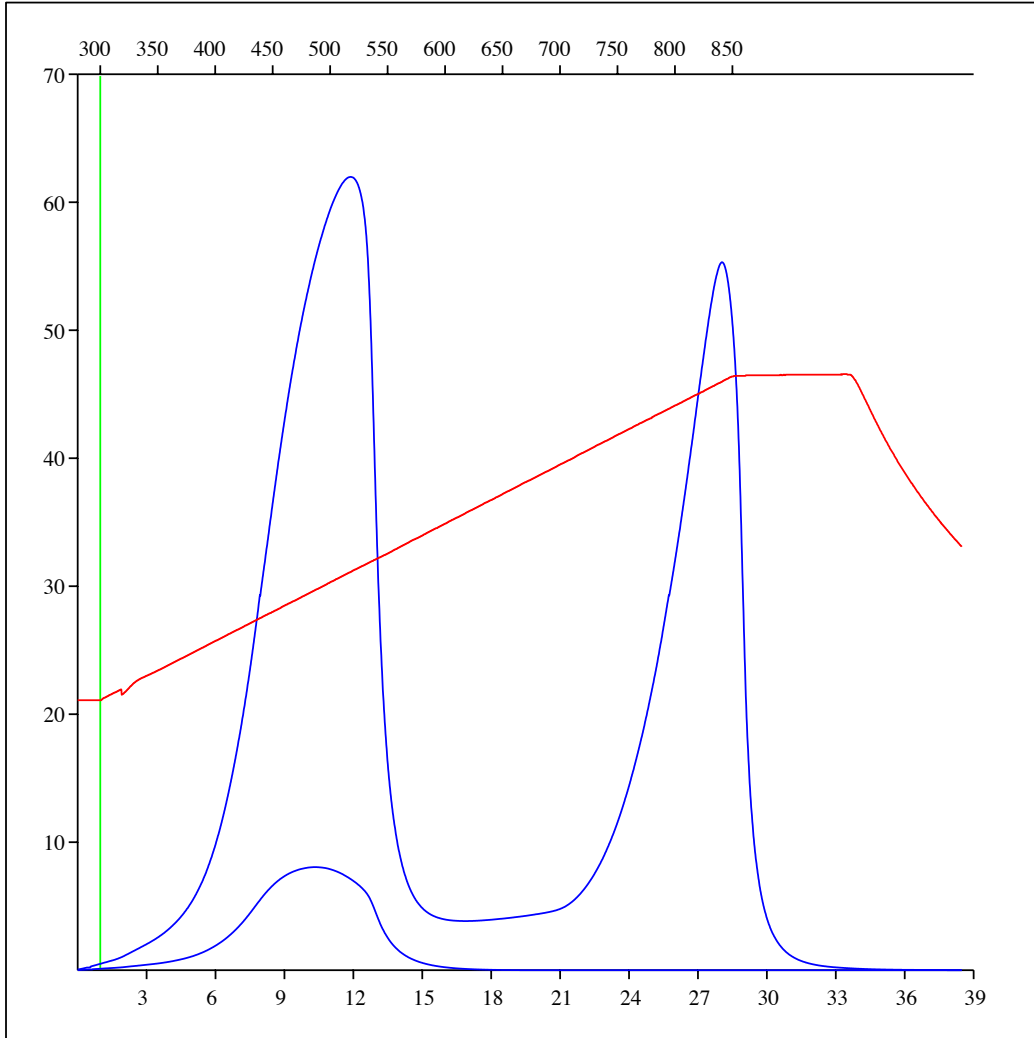
Sample: C-492835
Acquisition Date: 08-FEB-2012
Location: ADU MONIAS 01-10-082-23
Depth: 1864.7 m
Analysis
Instrument: RockEval 6
Data Processing Software: Vinci

Oxidation carbon dioxide



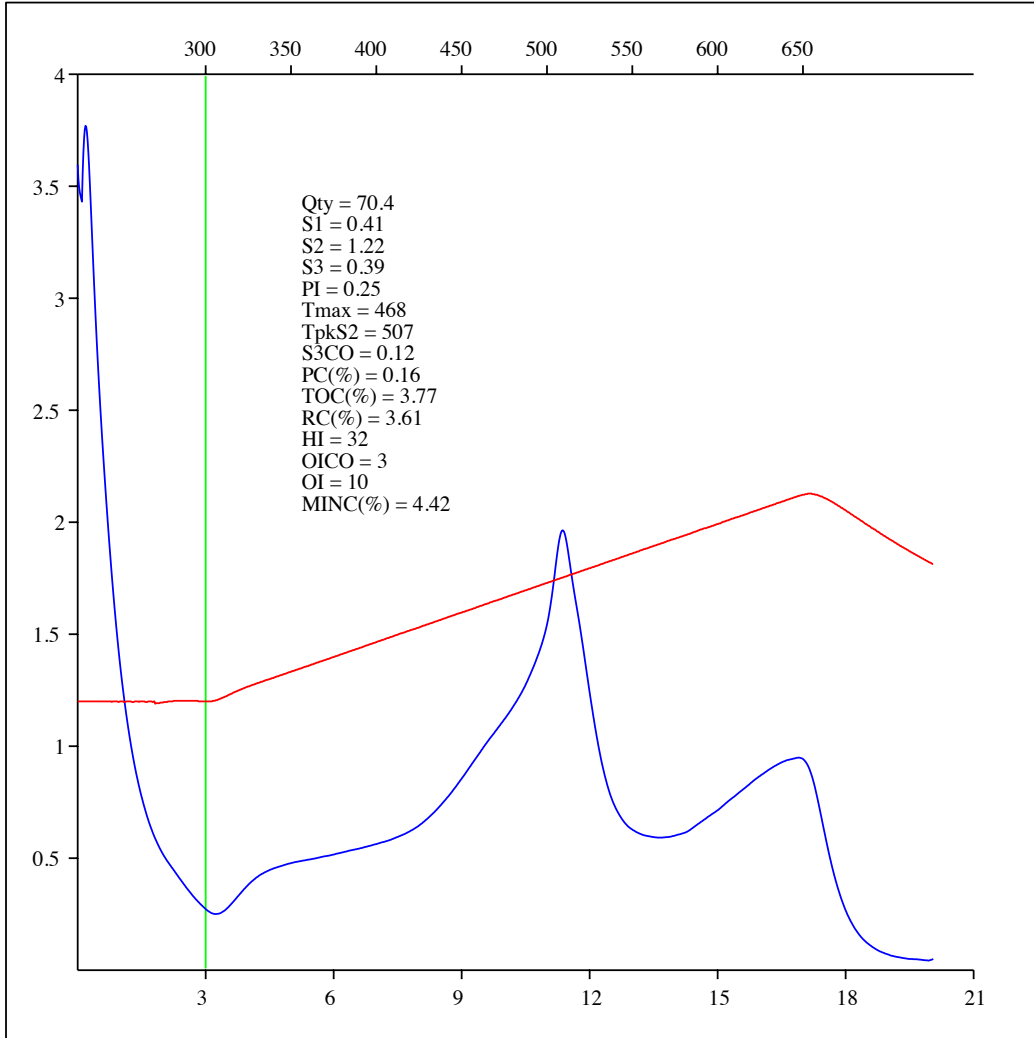
Sample: C-492835
Acquisition Date: 08-FEB-2012
Location: ADU MONIAS 01-10-082-23
Depth: 1864.7 m
Analysis
Instrument: RockEval 6
Data Processing Software: Vinci

Oxidation carbon monoxide & carbon dioxide



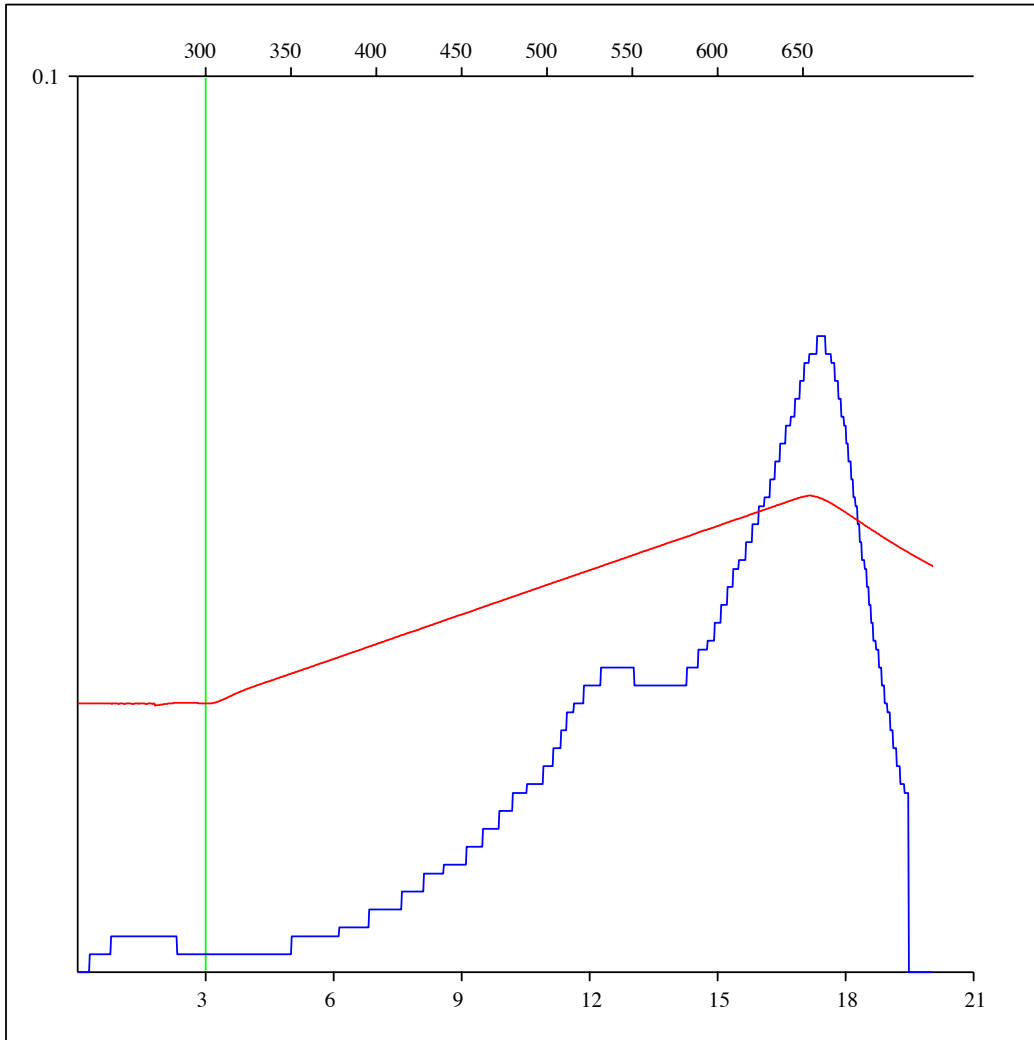
Sample: C-492836
Acquisition Date: 08-FEB-2012
Location: ADU MONIAS 01-10-082-23
Depth: 1855.58 m
Analysis
Instrument: RockEval 6
Data Processing Software: Vinci

FID hydrocarbons



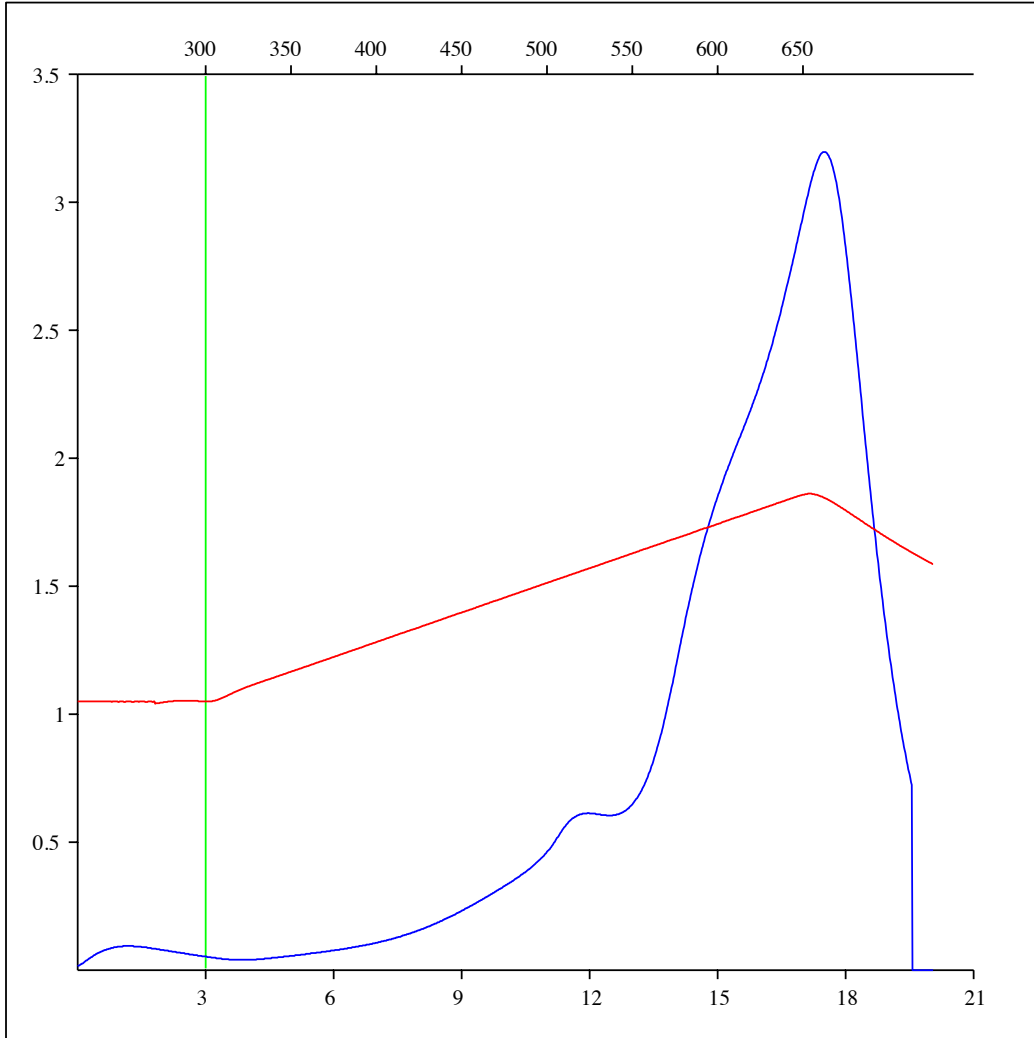
Sample: C-492836
Acquisition Date: 08-FEB-2012
Location: ADU MONIAS 01-10-082-23
Depth: 1855.58 m
Analysis
Instrument: RockEval 6
Data Processing Software: Vinci

Pyrolysis carbon monoxide



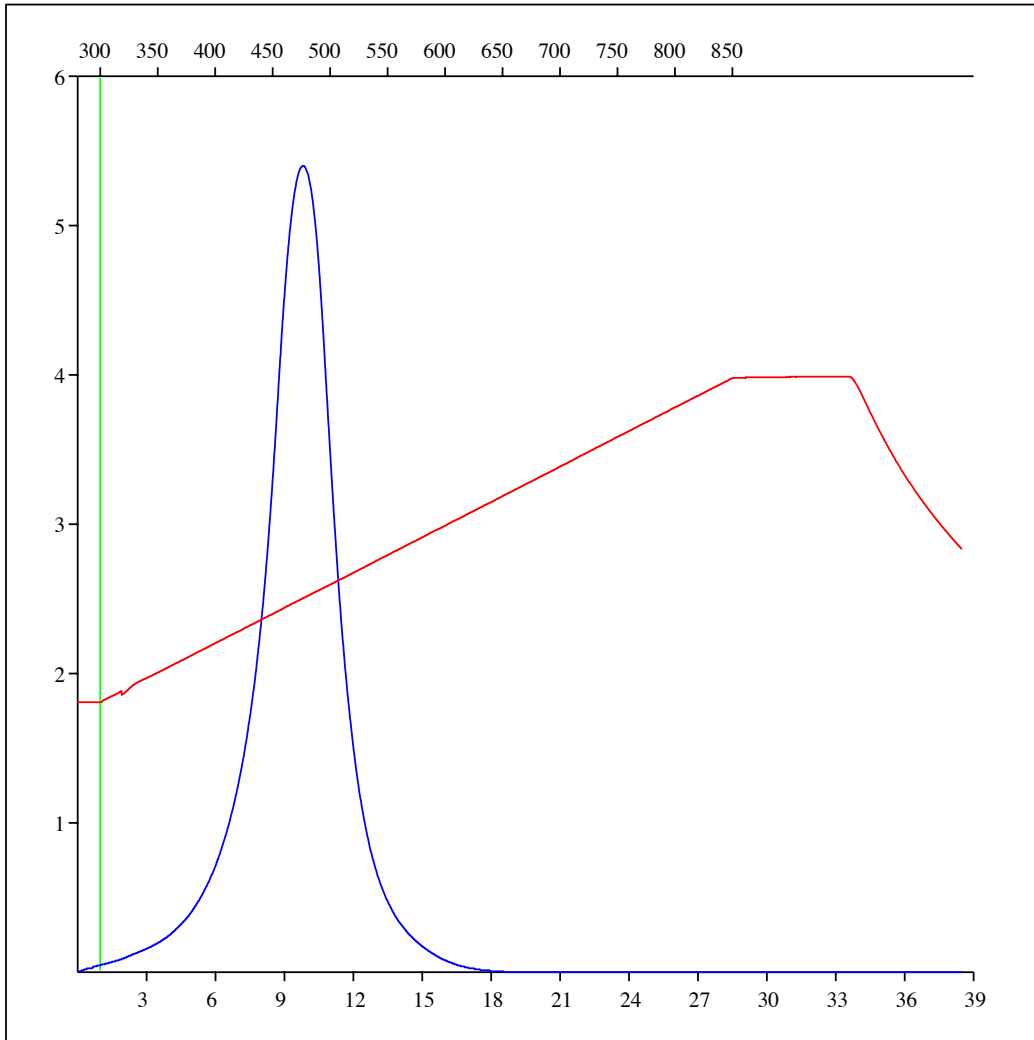
Sample: C-492836
Acquisition Date: 08-FEB-2012
Location: ADU MONIAS 01-10-082-23
Depth: 1855.58 m
Analysis
Instrument: RockEval 6
Data Processing Software: Vinci

Pyrolysis carbon dioxide



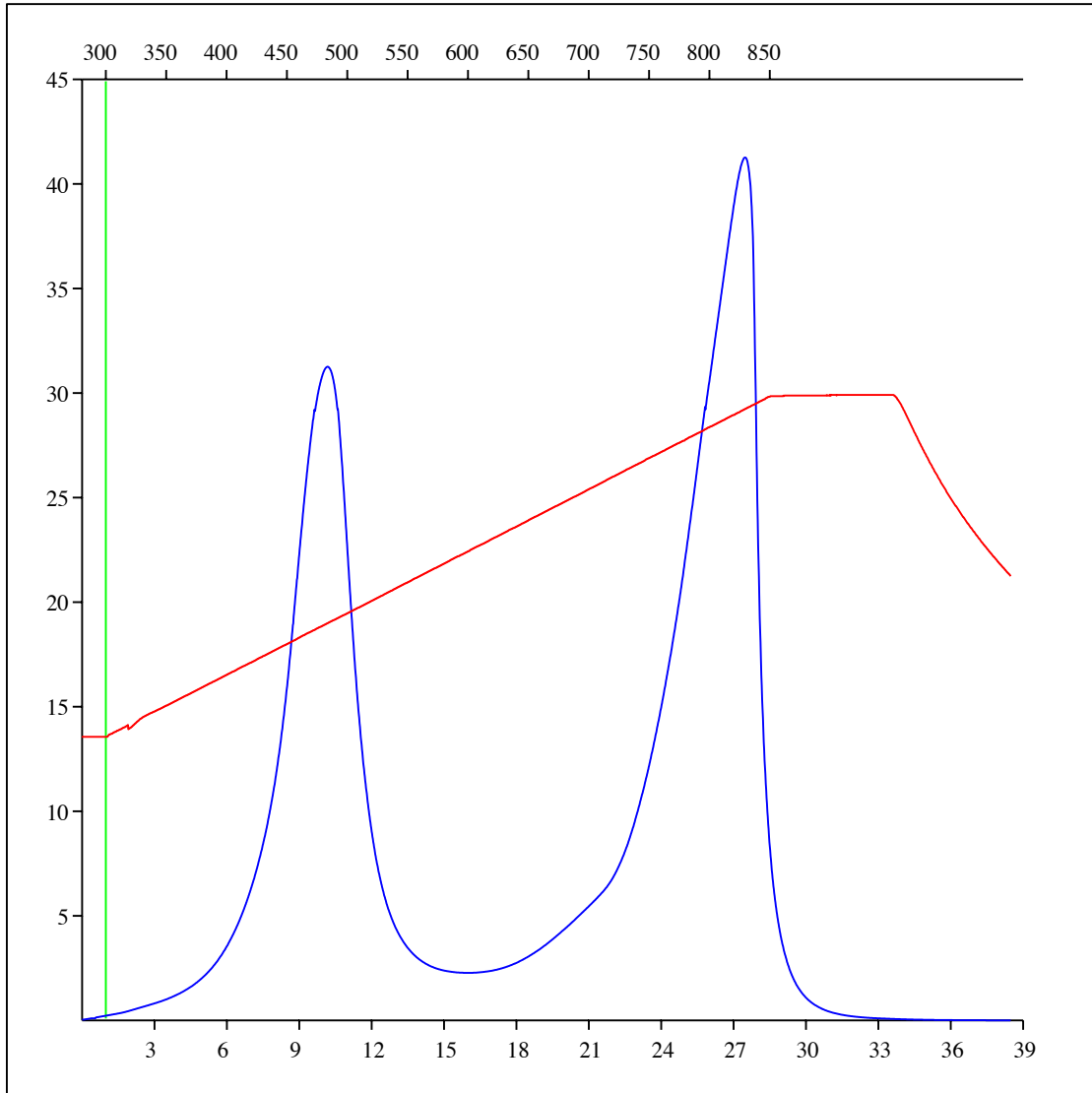
Sample: C-492836
Acquisition Date: 08-FEB-2012
Location: ADU MONIAS 01-10-082-23
Depth: 1855.58 m
Analysis
Instrument: RockEval 6
Data Processing Software: Vinci

Oxidation carbon monoxide



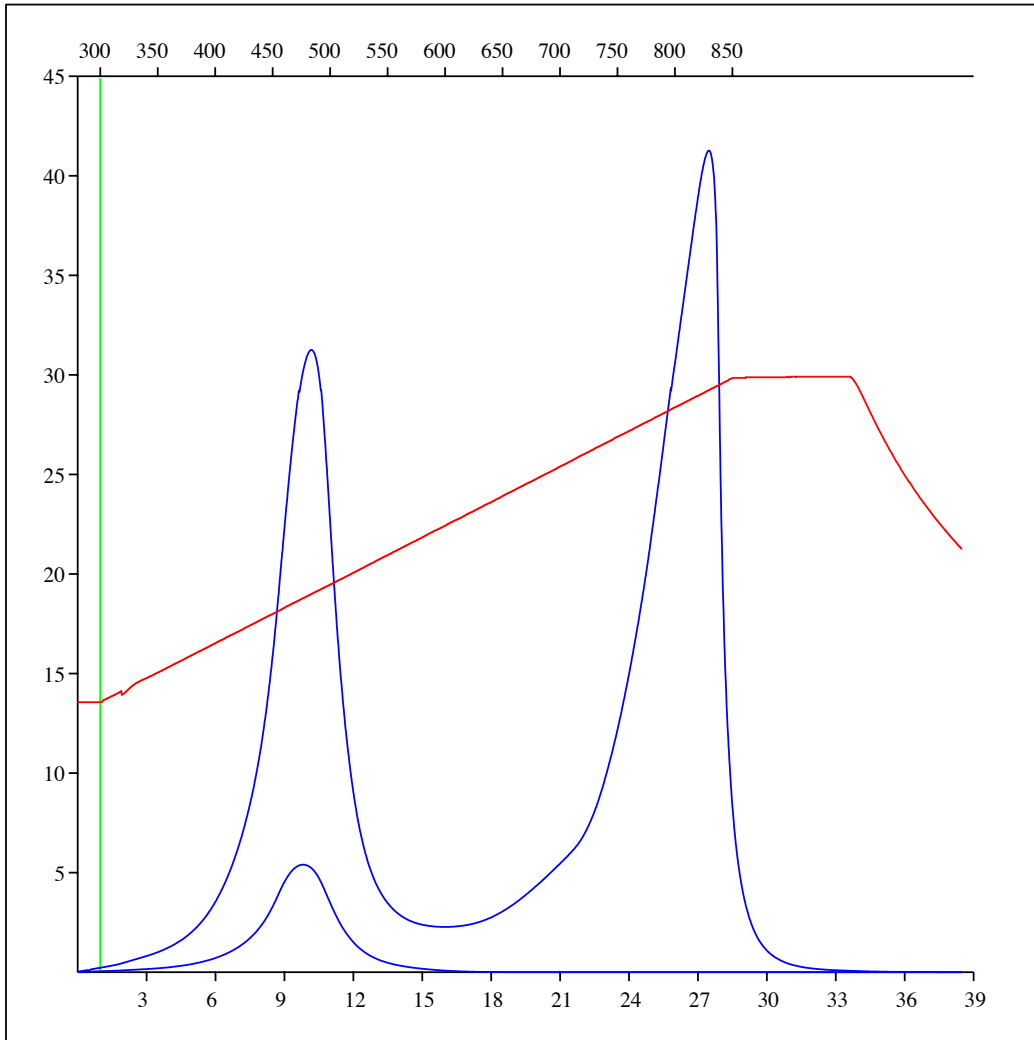
Sample: C-492836
Acquisition Date: 08-FEB-2012
Location: ADU MONIAS 01-10-082-23
Depth: 1855.58 m
Analysis
Instrument: RockEval 6
Data Processing Software: Vinci

Oxidation carbon dioxide



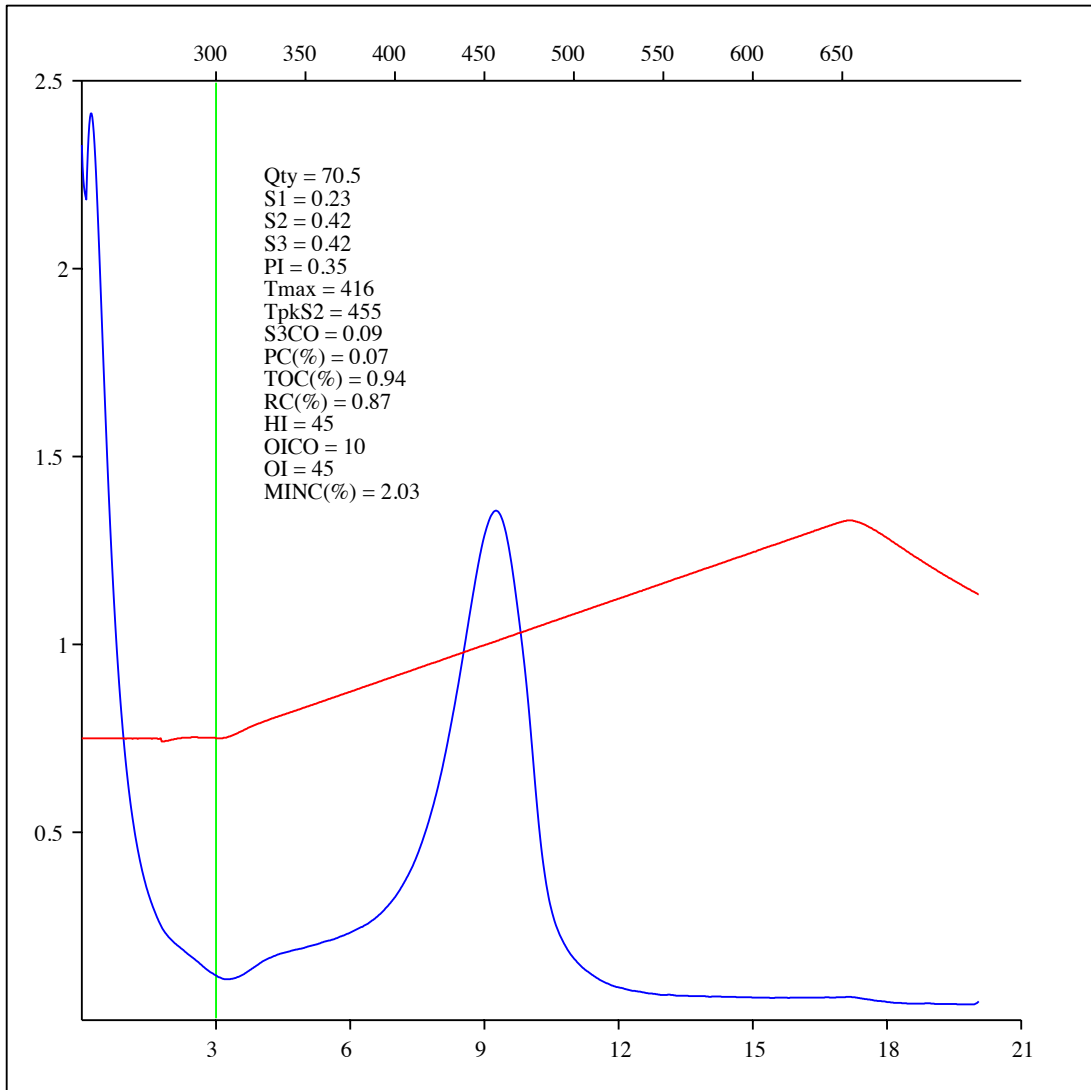
Sample: C-492836
Acquisition Date: 08-FEB-2012
Location: ADU MONIAS 01-10-082-23
Depth: 1855.58 m
Analysis
Instrument: RockEval 6
Data Processing Software: Vinci

Oxidation carbon monoxide & carbon dioxide



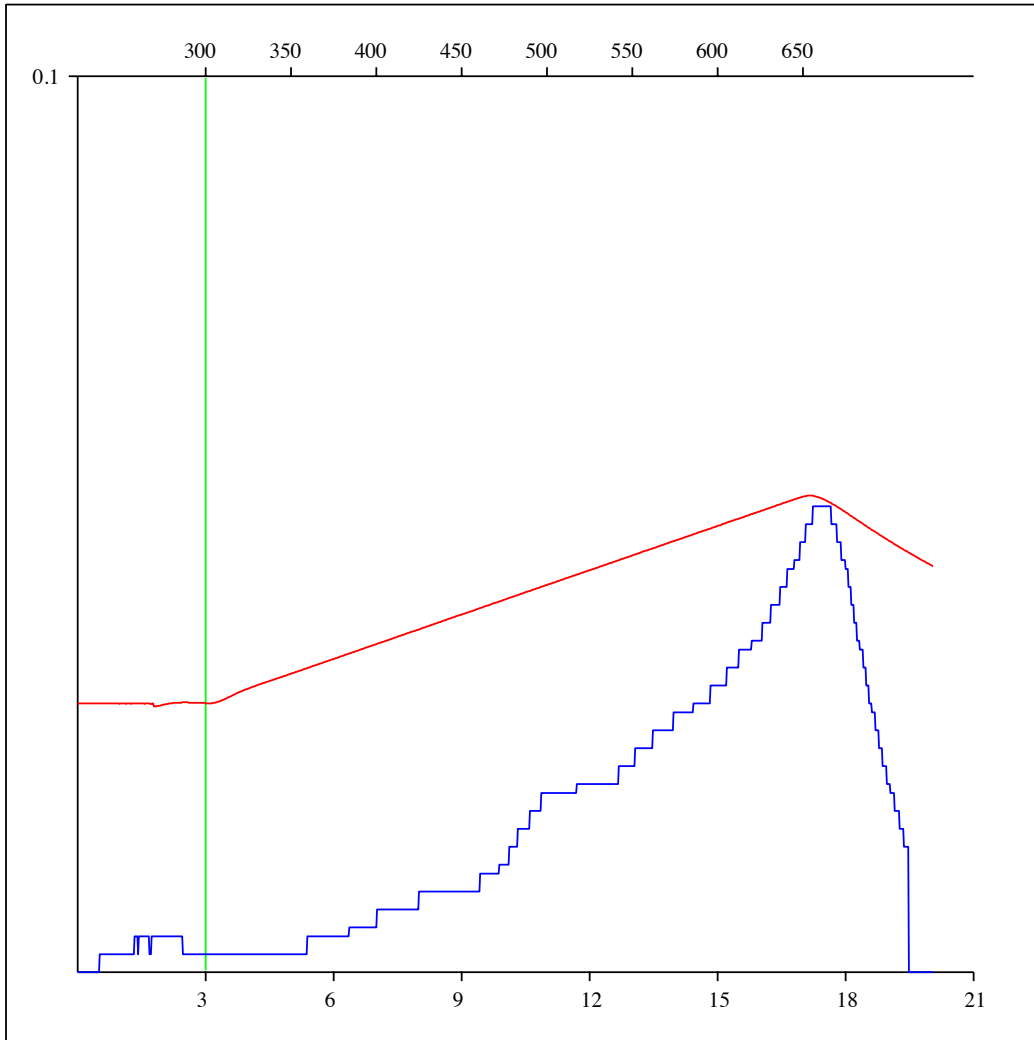
Sample: C-492837
Acquisition Date: 08-FEB-2012
Location: ECA SWAN A- 020-H/093-P-09
Depth: 2460.57 m
Analysis
Instrument: RockEval 6
Data Processing Software: Vinci

FID hydrocarbons



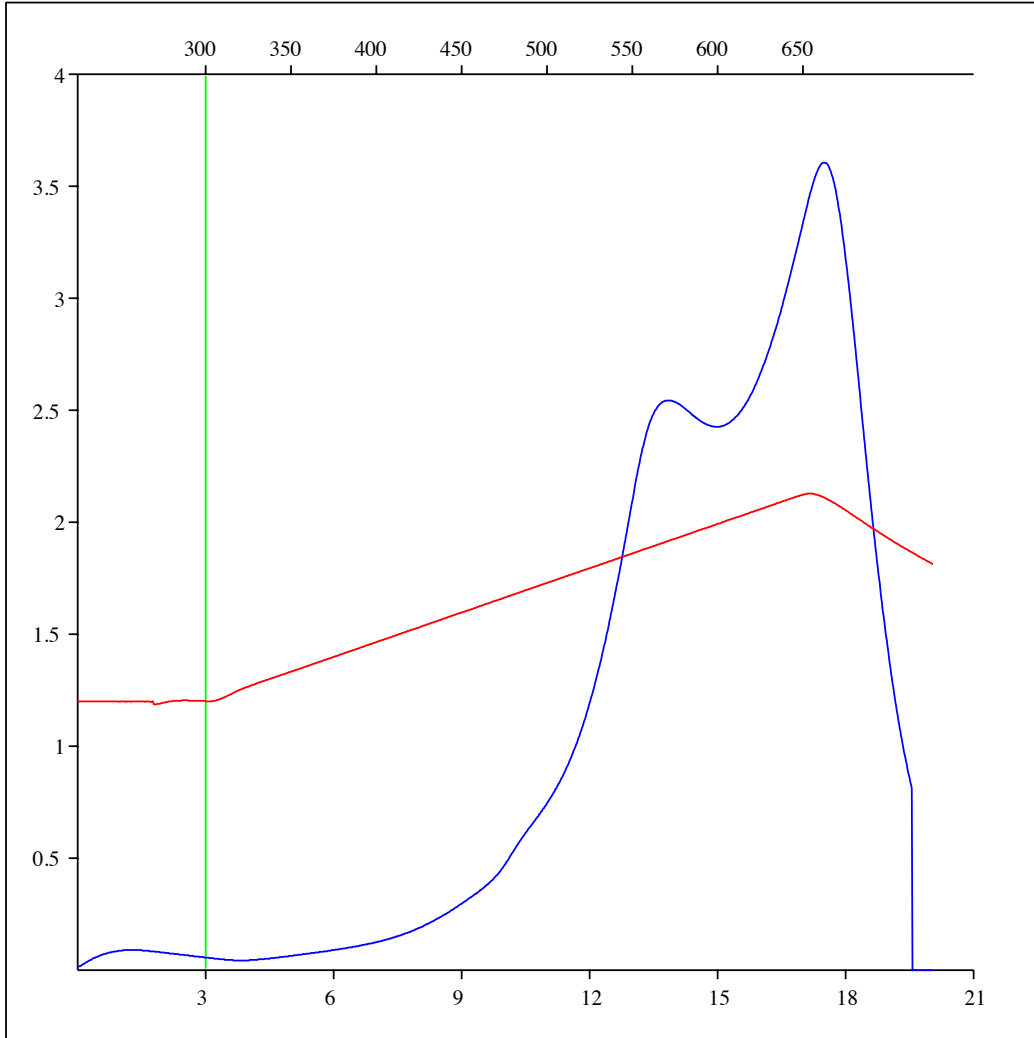
Sample: C-492837
Acquisition Date: 08-FEB-2012
Location: ECA SWAN A- 020-H/093-P-09
Depth: 2460.57 m
Analysis
Instrument: RockEval 6
Data Processing Software: Vinci

Pyrolysis carbon monoxide



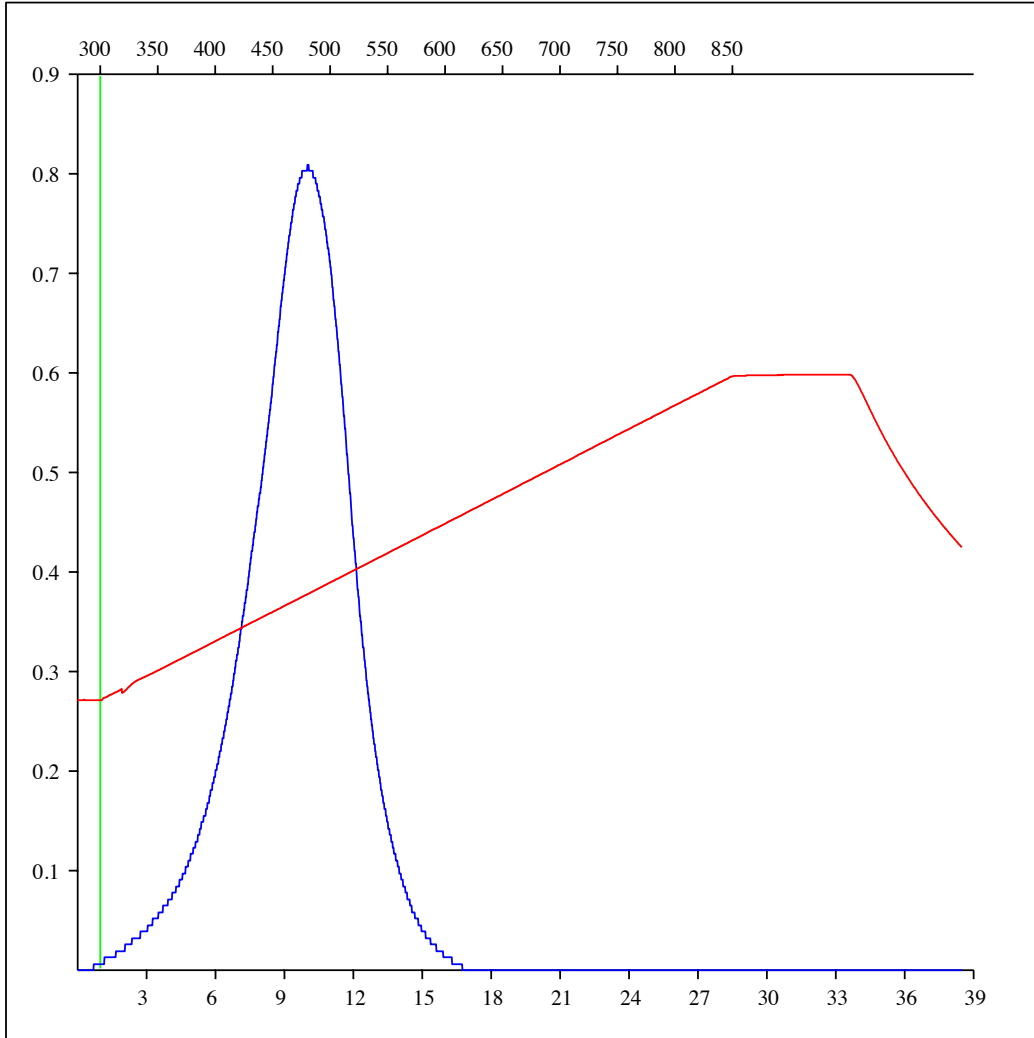
Sample: C-492837
Acquisition Date: 08-FEB-2012
Location: ECA SWAN A- 020-H/093-P-09
Depth: 2460.57 m
Analysis
Instrument: RockEval 6
Data Processing Software: Vinci

Pyrolysis carbon dioxide



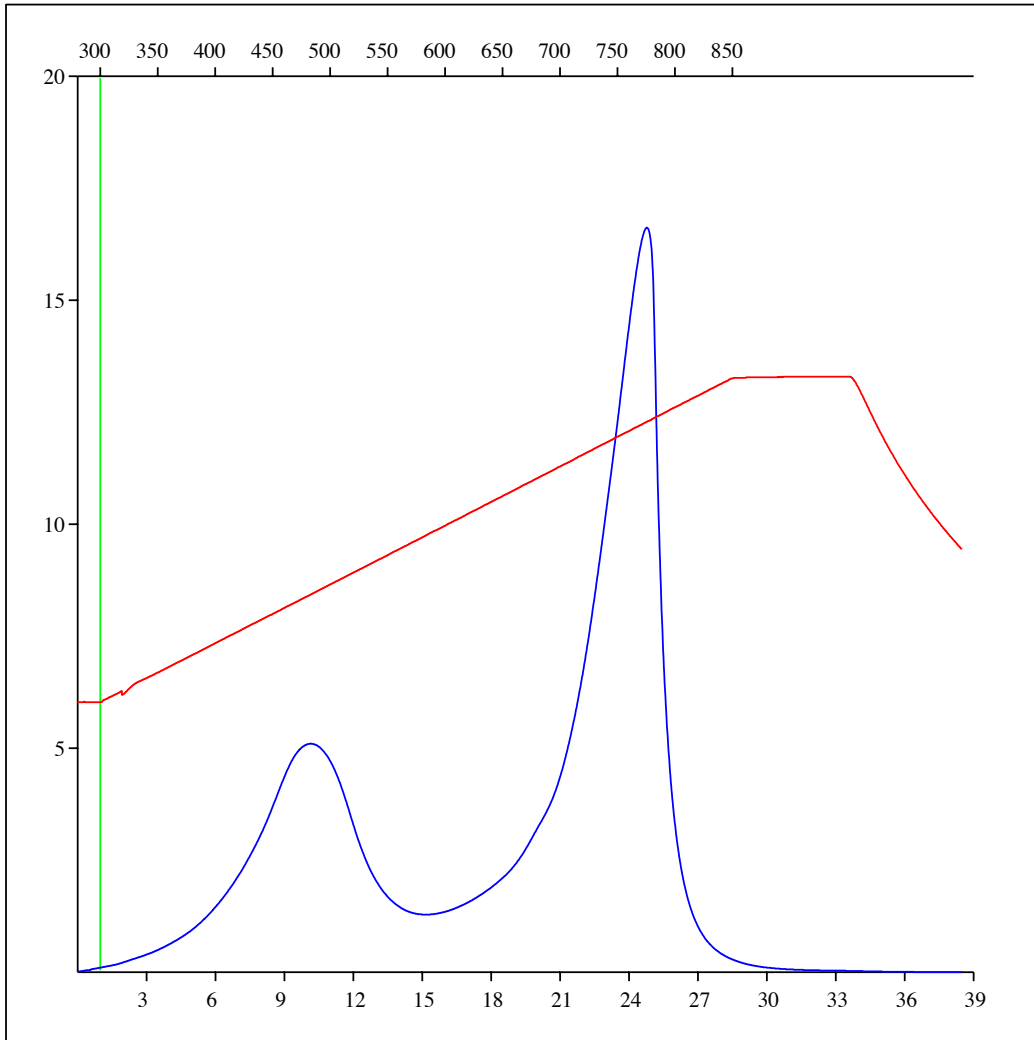
Sample: C-492837
Acquisition Date: 08-FEB-2012
Location: ECA SWAN A- 020-H/093-P-09
Depth: 2460.57 m
Analysis
Instrument: RockEval 6
Data Processing Software: Vinci

Oxidation carbon monoxide



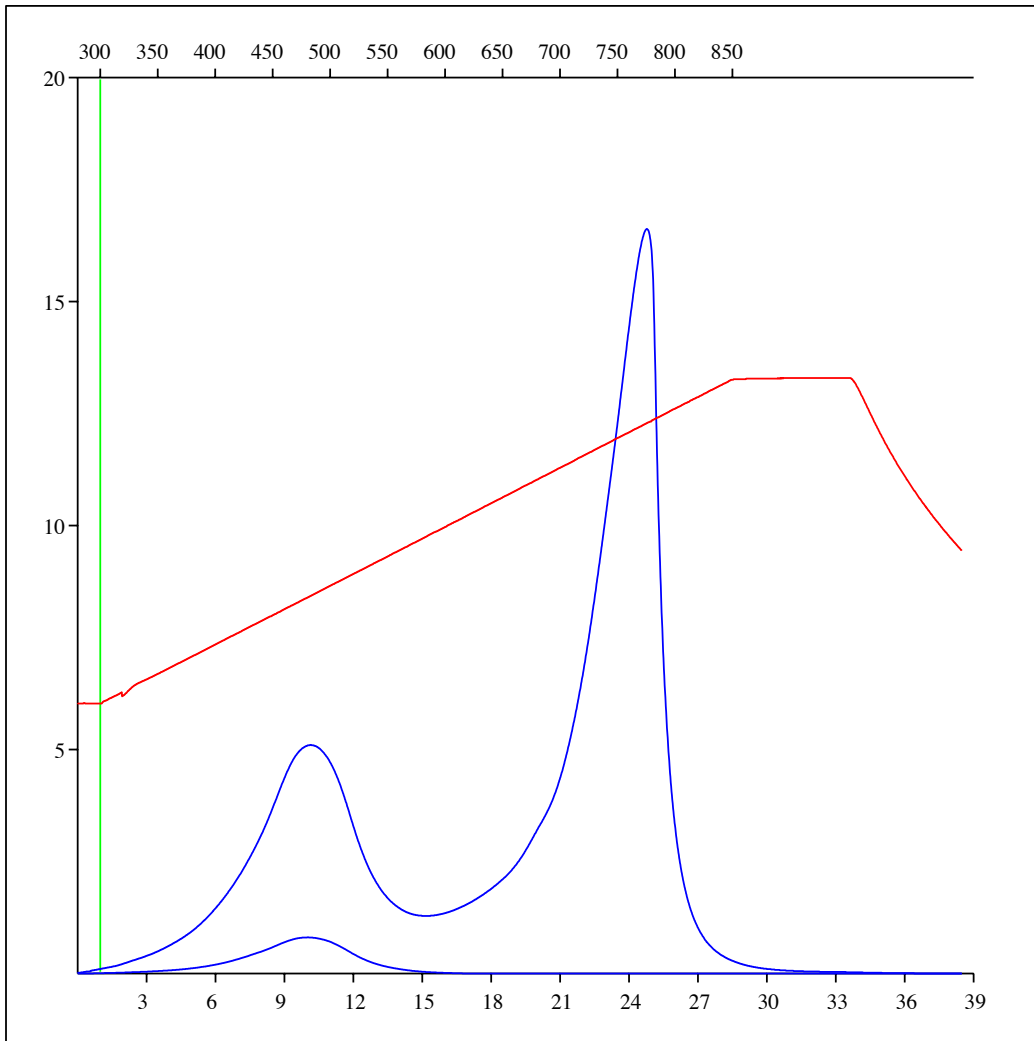
Sample: C-492837
Acquisition Date: 08-FEB-2012
Location: ECA SWAN A- 020-H/093-P-09
Depth: 2460.57 m
Analysis
Instrument: RockEval 6
Data Processing Software: Vinci

Oxidation carbon dioxide



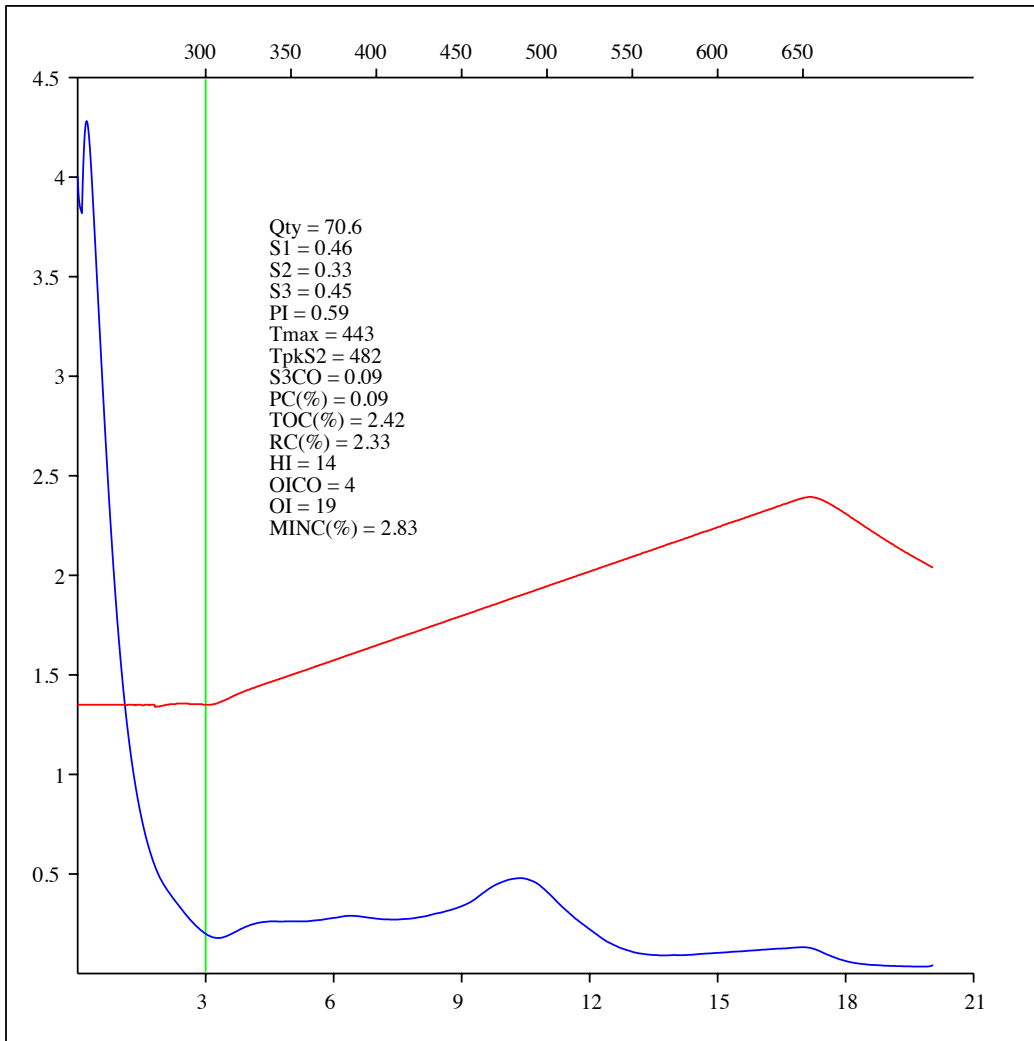
Sample: C-492837
Acquisition Date: 08-FEB-2012
Location: ECA SWAN A- 020-H/093-P-09
Depth: 2460.57 m
Analysis
Instrument: RockEval 6
Data Processing Software: Vinci

Oxidation carbon monoxide & carbon dioxide



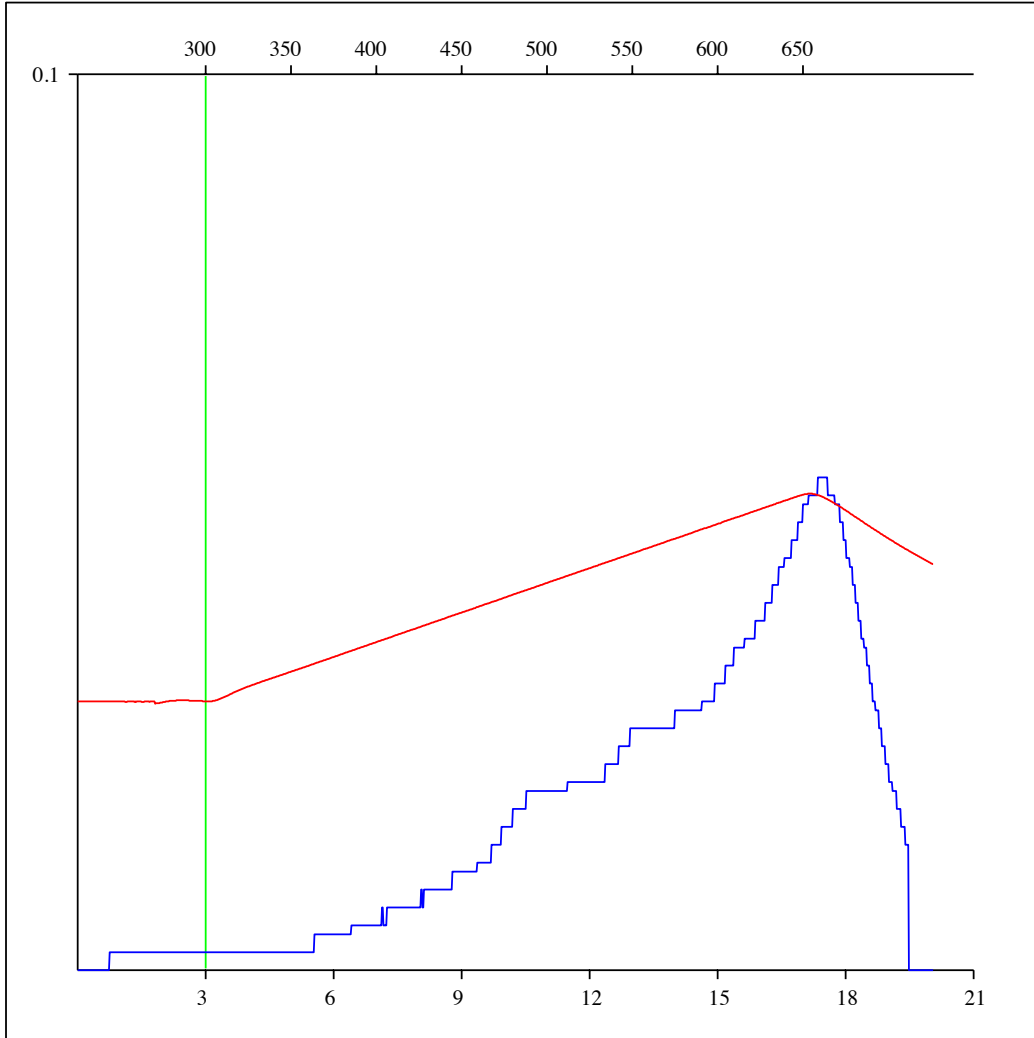
Sample: C-492838
Acquisition Date: 08-FEB-2012
Location: ECA SWAN A- 020-H/093-P-09
Depth: 2455 m
Analysis
Instrument: RockEval 6
Data Processing Software: Vinci

FID hydrocarbons



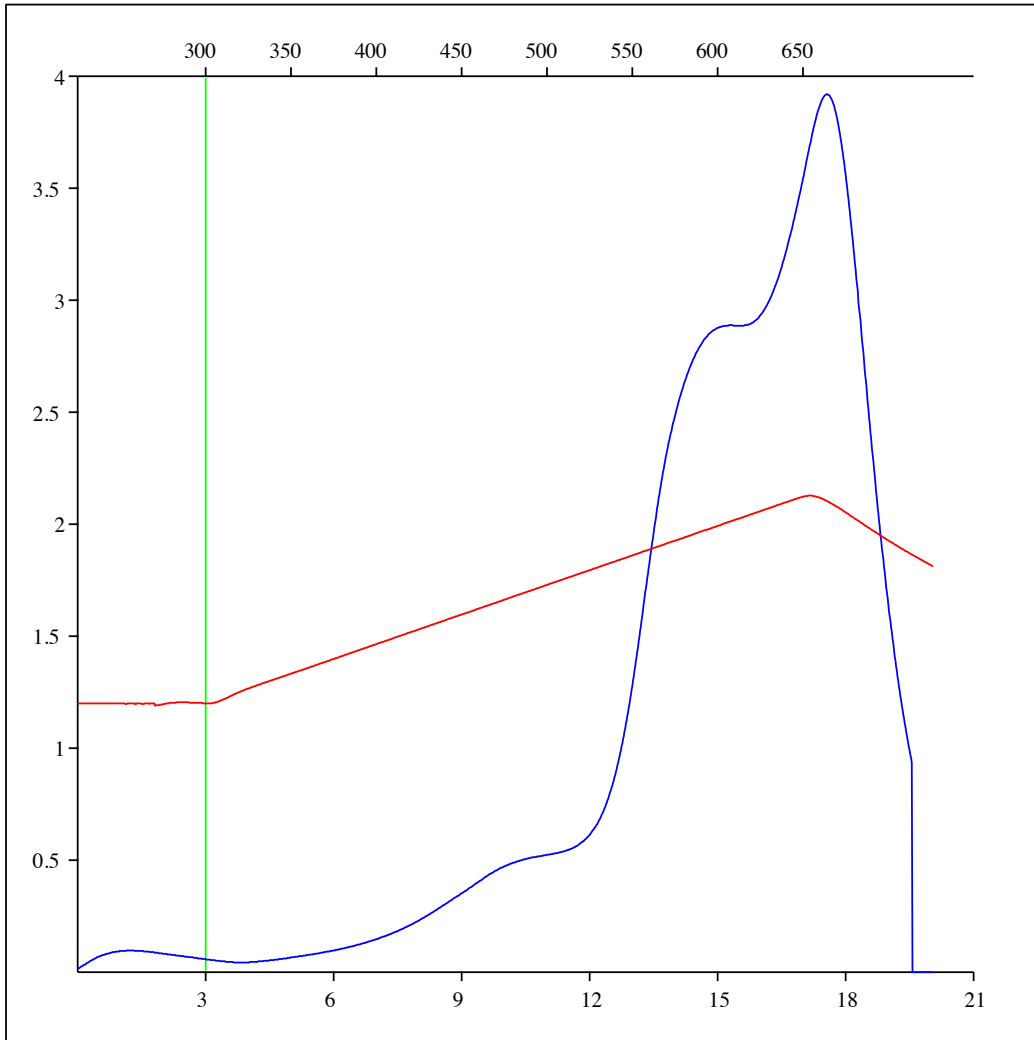
Sample: C-492838
Acquisition Date: 08-FEB-2012
Location: ECA SWAN A- 020-H/093-P-09
Depth: 2455 m
Analysis
Instrument: RockEval 6
Data Processing Software: Vinci

Pyrolysis carbon monoxide



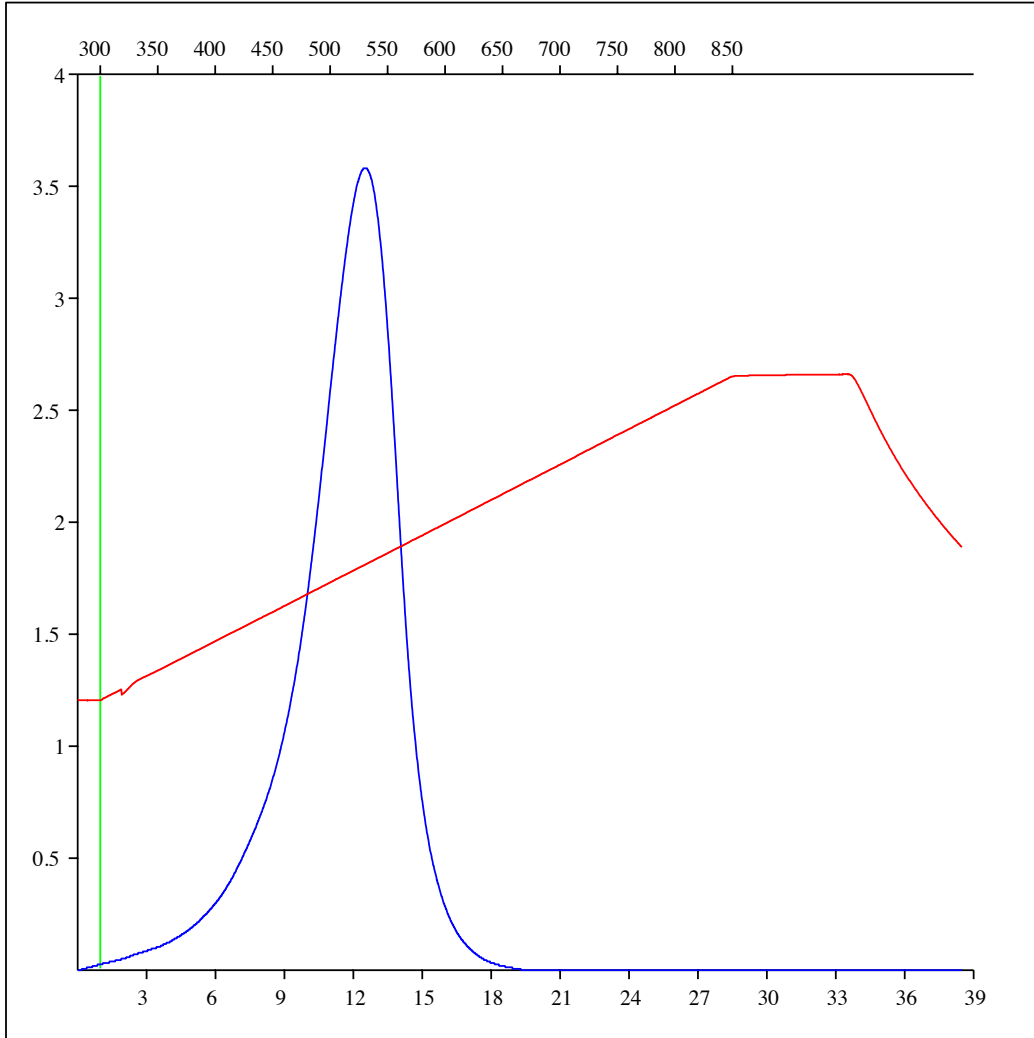
Sample: C-492838
Acquisition Date: 08-FEB-2012
Location: ECA SWAN A- 020-H/093-P-09
Depth: 2455 m
Analysis
Instrument: RockEval 6
Data Processing Software: Vinci

Pyrolysis carbon dioxide



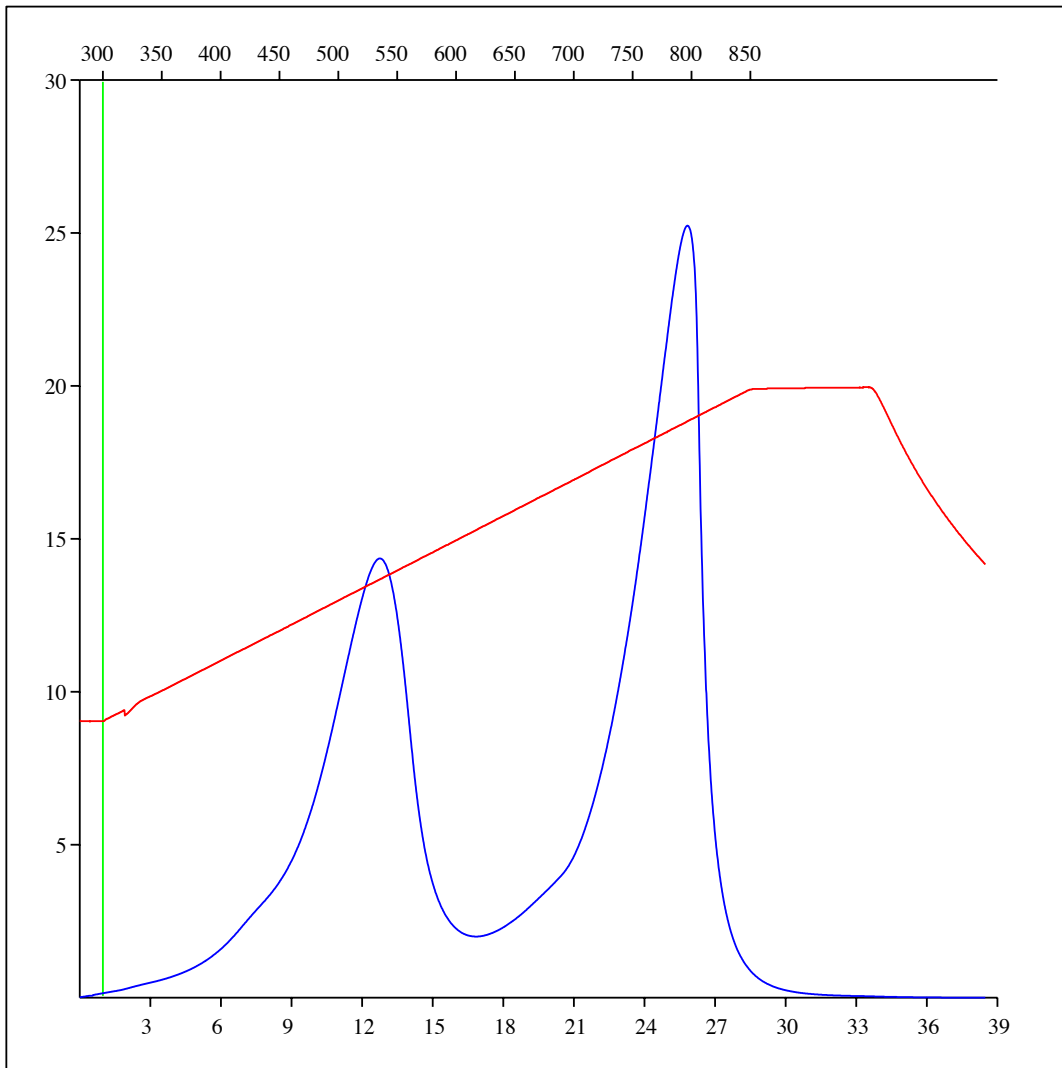
Sample: C-492838
Acquisition Date: 08-FEB-2012
Location: ECA SWAN A- 020-H/093-P-09
Depth: 2455 m
Analysis
Instrument: RockEval 6
Data Processing Software: Vinci

Oxidation carbon monoxide



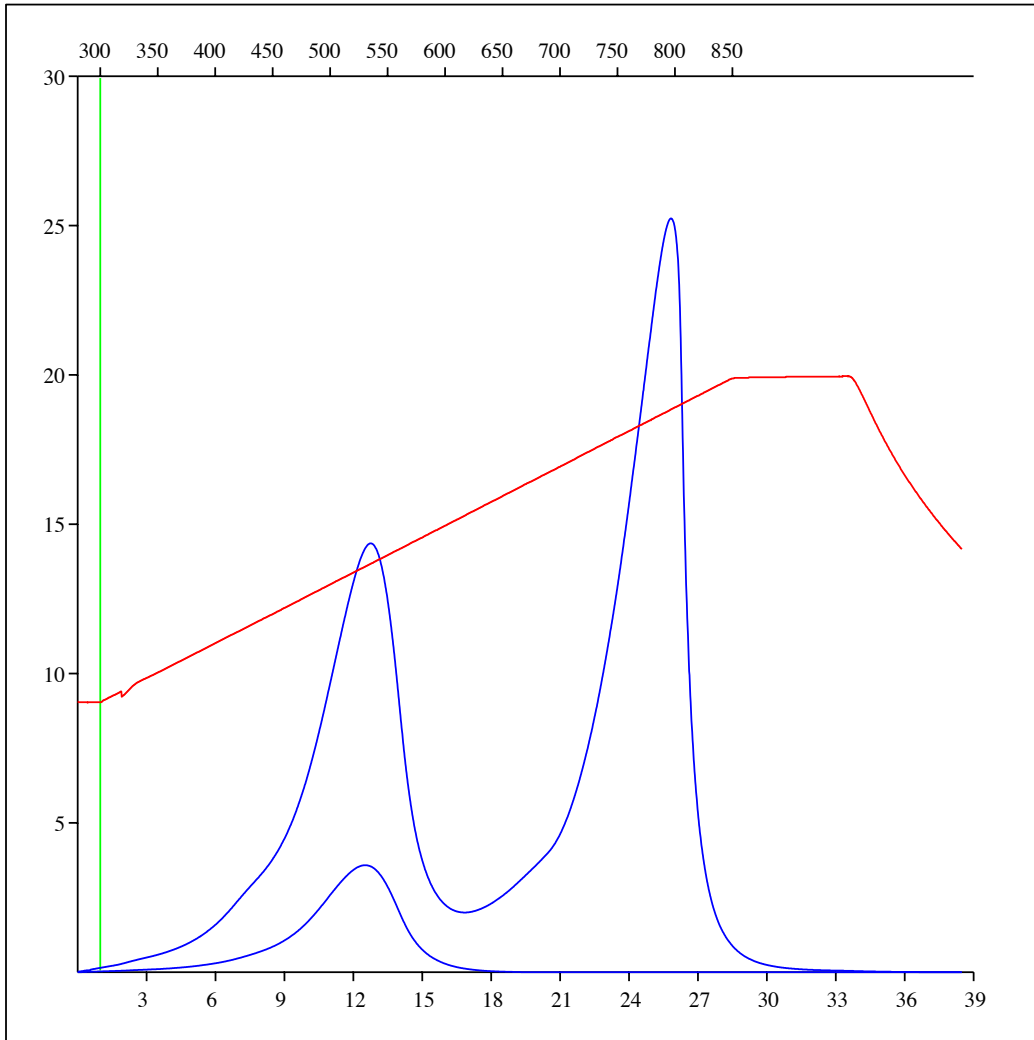
Sample: C-492838
Acquisition Date: 08-FEB-2012
Location: ECA SWAN A- 020-H/093-P-09
Depth: 2455 m
Analysis
Instrument: RockEval 6
Data Processing Software: Vinci

Oxidation carbon dioxide



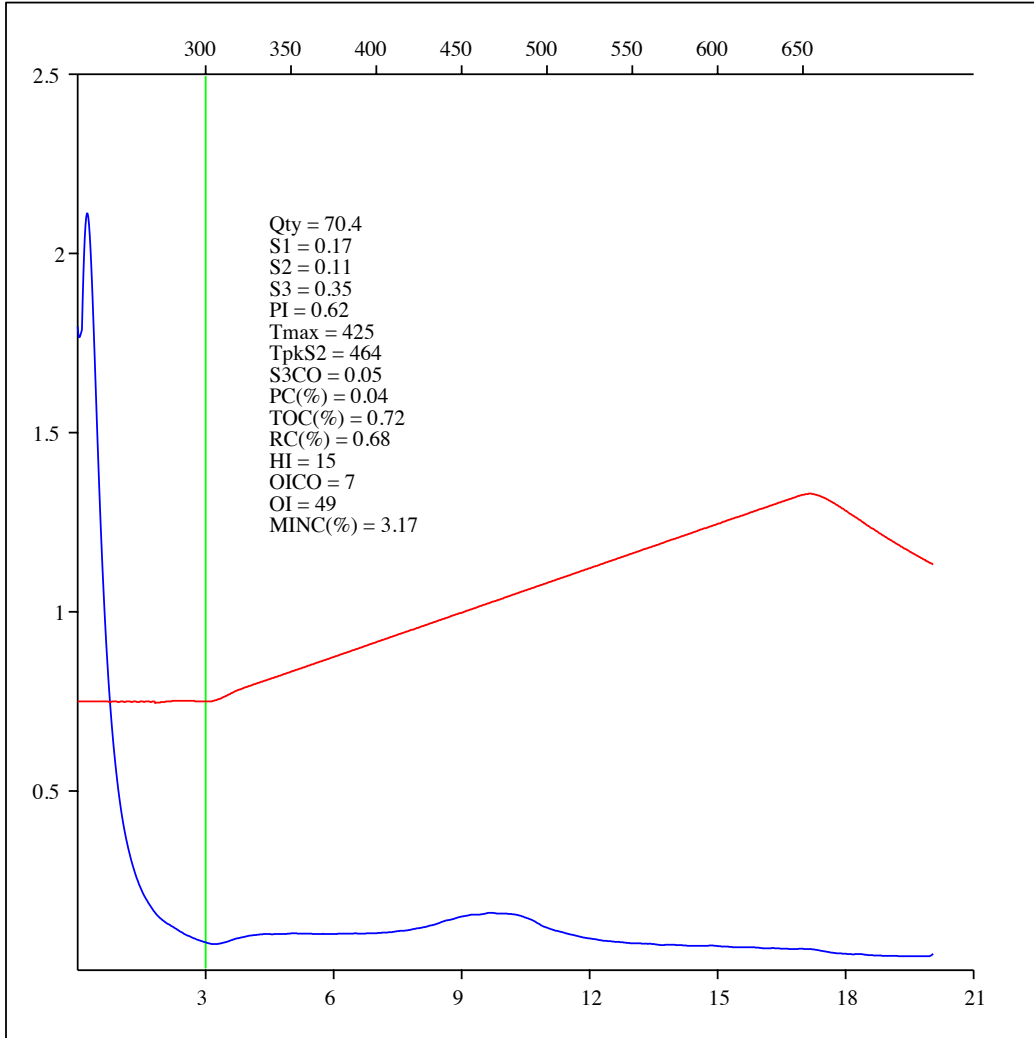
Sample: C-492838
Acquisition Date: 08-FEB-2012
Location: ECA SWAN A- 020-H/093-P-09
Depth: 2455 m
Analysis
Instrument: RockEval 6
Data Processing Software: Vinci

Oxidation carbon monoxide & carbon dioxide



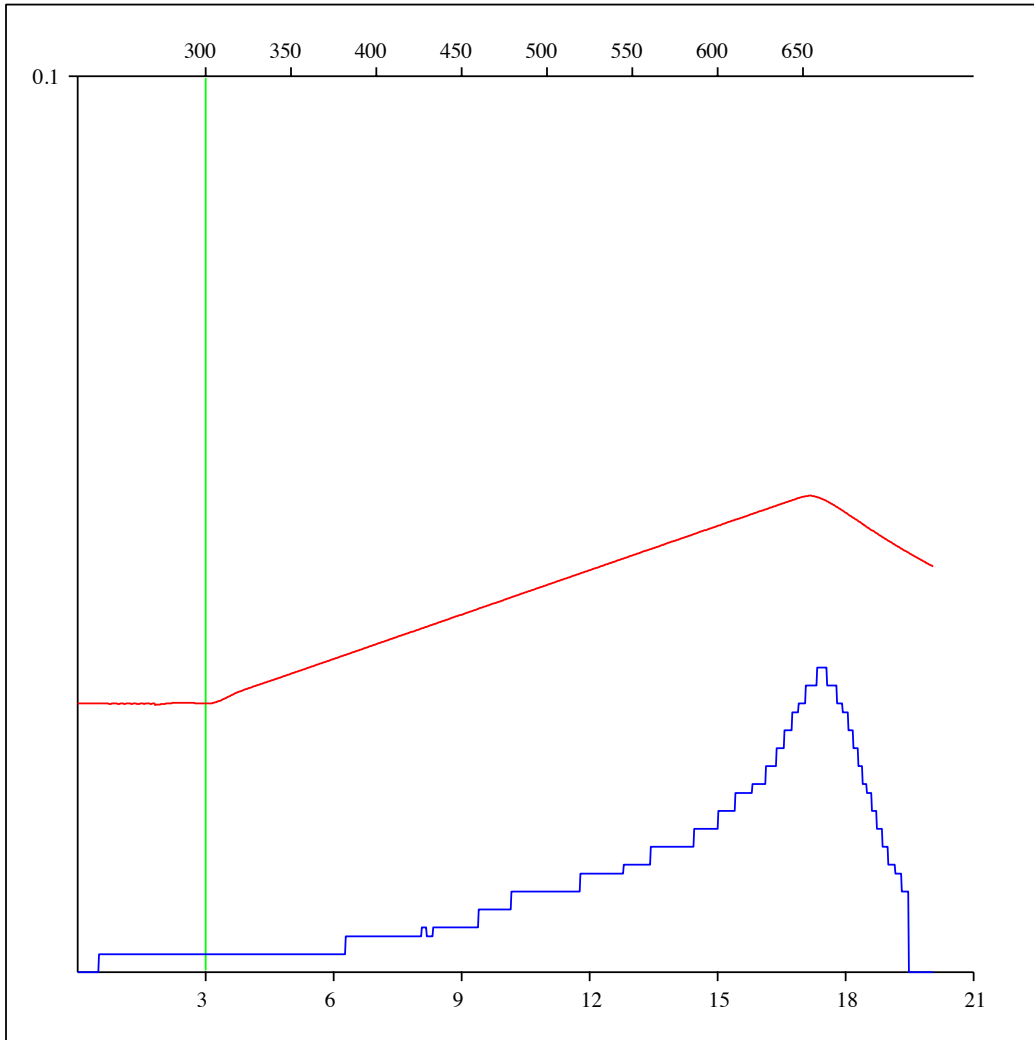
Sample: C-492839
Acquisition Date: 08-FEB-2012
Location: ECA SWAN A- 020-H/093-P-09
Depth: 2457 m
Analysis
Instrument: RockEval 6
Data Processing Software: Vinci

FID hydrocarbons



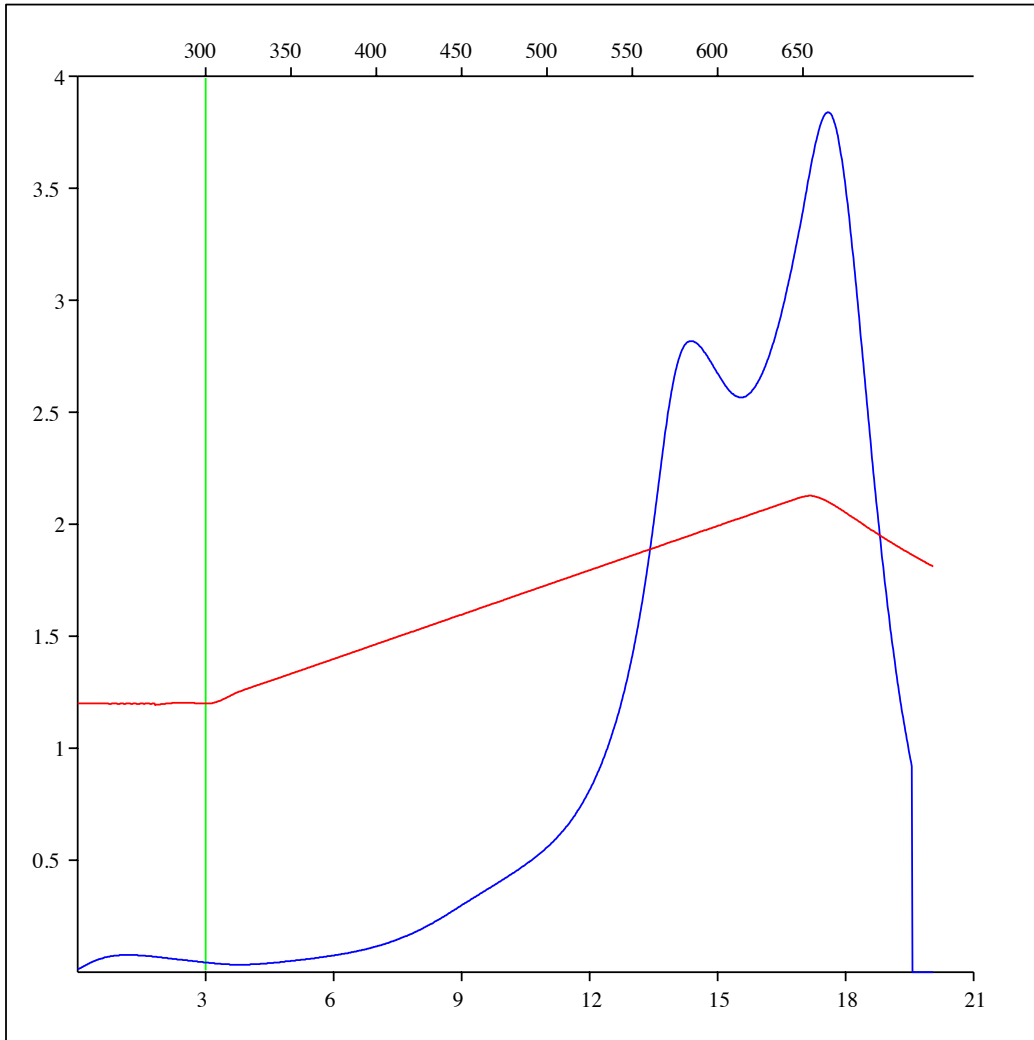
Sample: C-492839
Acquisition Date: 08-FEB-2012
Location: ECA SWAN A- 020-H/093-P-09
Depth: 2457 m
Analysis
Instrument: RockEval 6
Data Processing Software: Vinci

Pyrolysis carbon monoxide



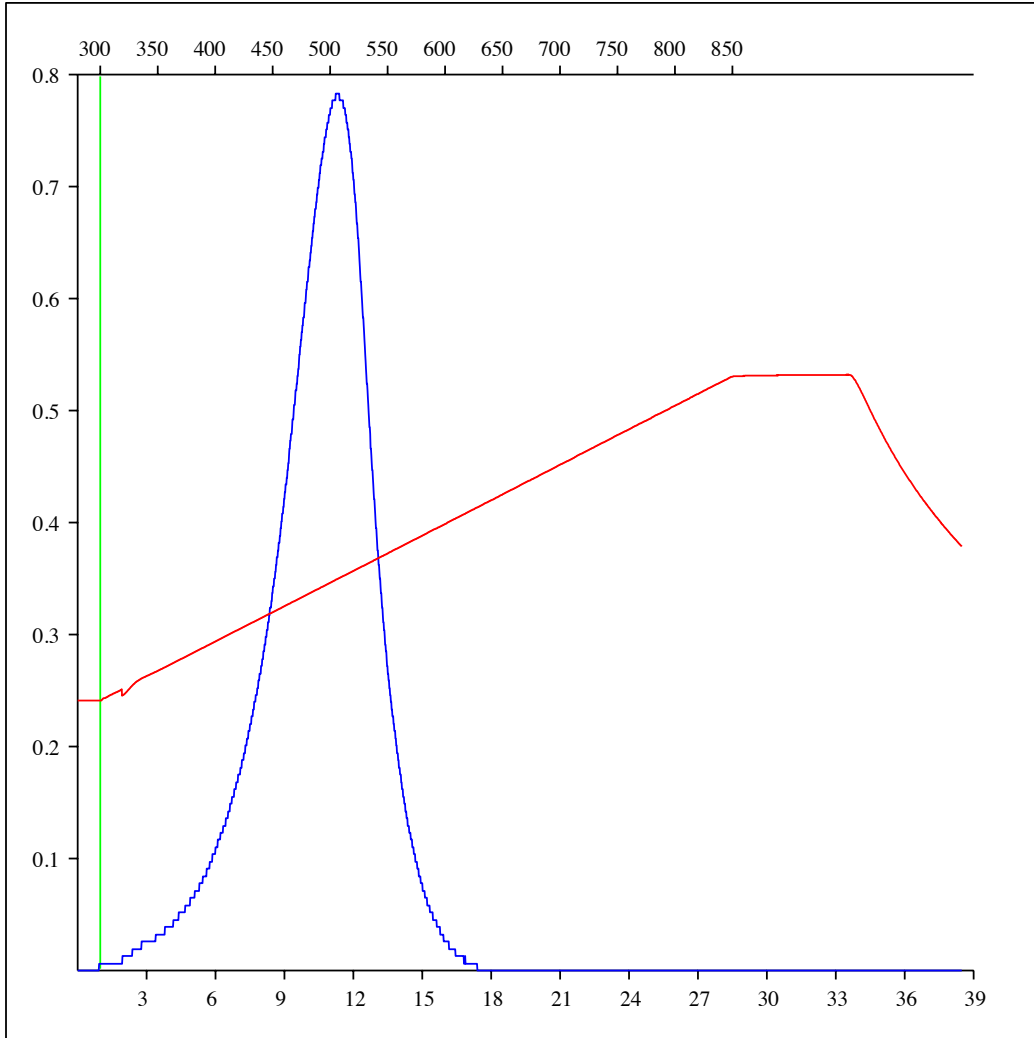
Sample: C-492839
Acquisition Date: 08-FEB-2012
Location: ECA SWAN A- 020-H/093-P-09
Depth: 2457 m
Analysis
Instrument: RockEval 6
Data Processing Software: Vinci

Pyrolysis carbon dioxide



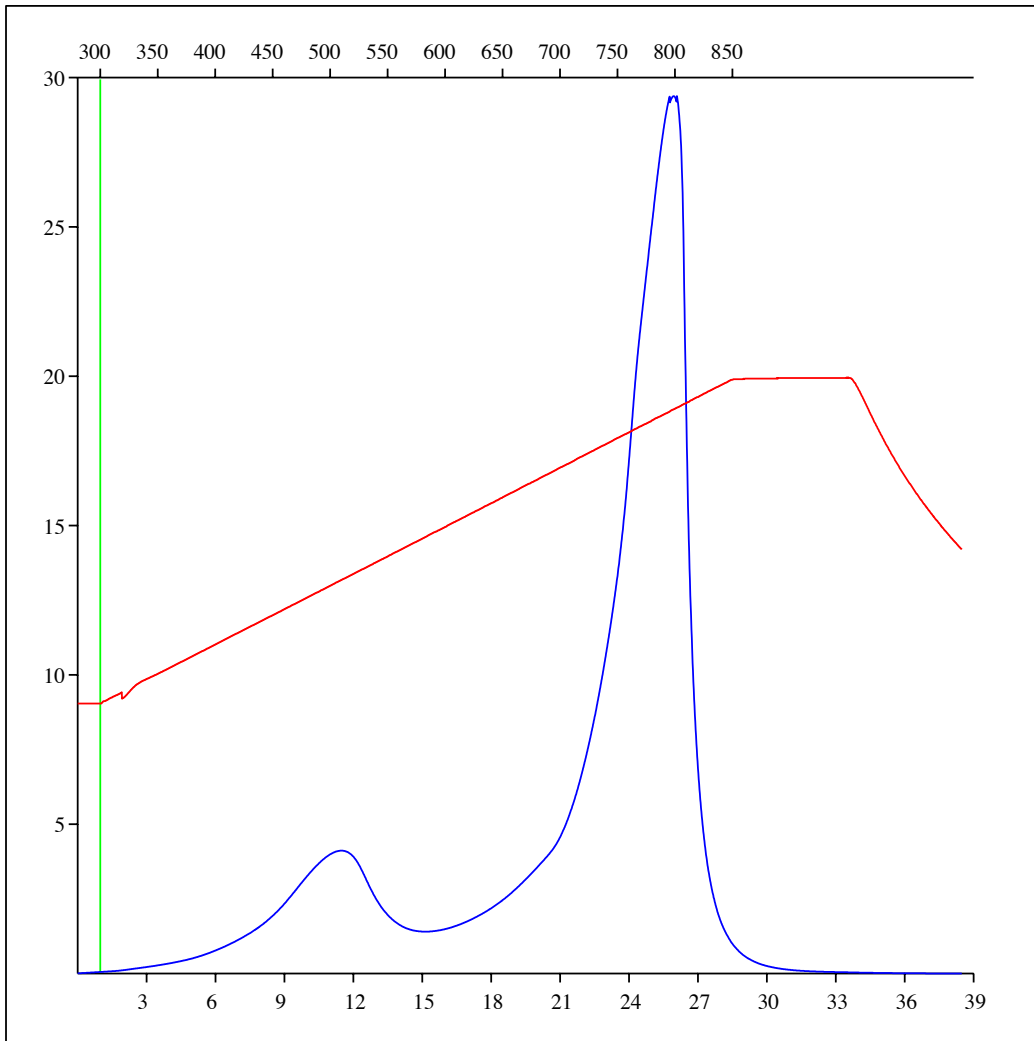
Sample: C-492839
Acquisition Date: 08-FEB-2012
Location: ECA SWAN A- 020-H/093-P-09
Depth: 2457 m
Analysis
Instrument: RockEval 6
Data Processing Software: Vinci

Oxidation carbon monoxide



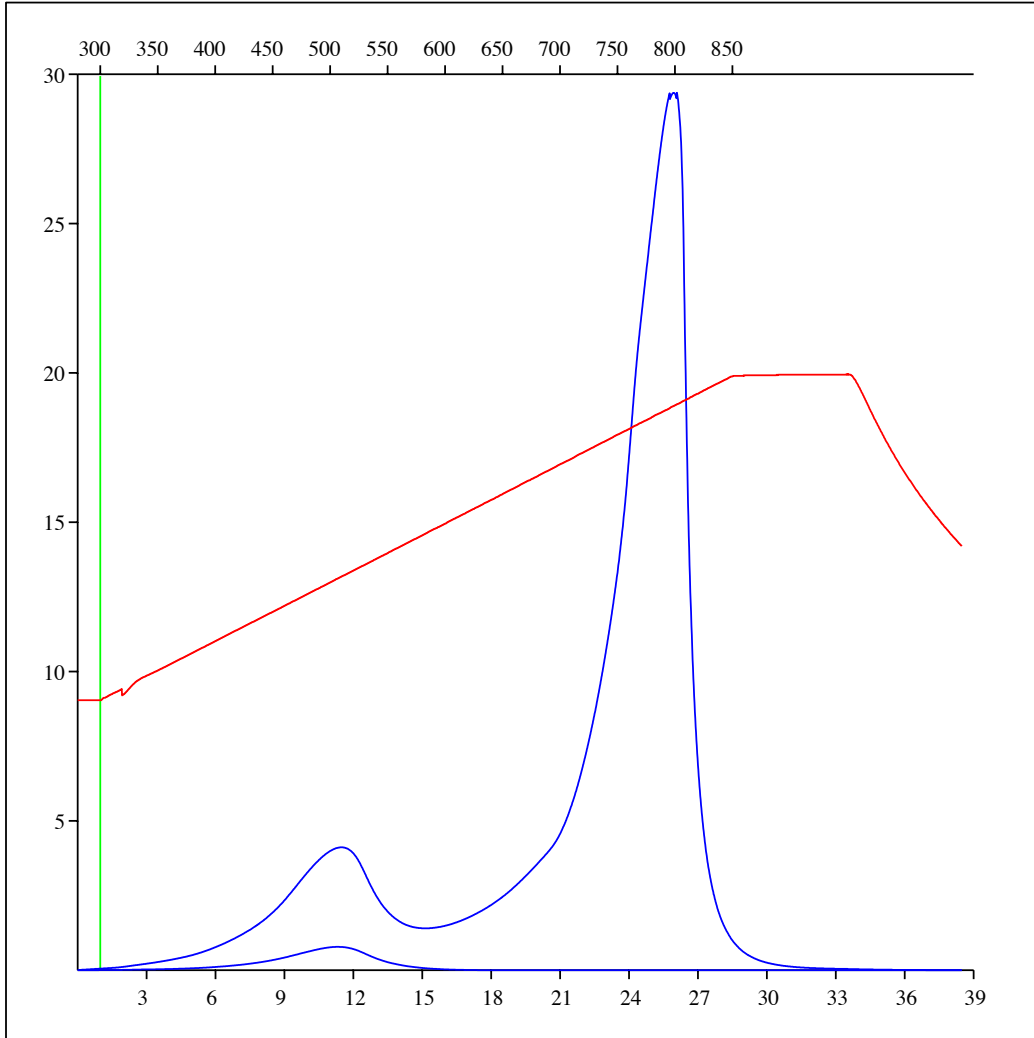
Sample: C-492839
Acquisition Date: 08-FEB-2012
Location: ECA SWAN A- 020-H/093-P-09
Depth: 2457 m
Analysis
Instrument: RockEval 6
Data Processing Software: Vinci

Oxidation carbon dioxide



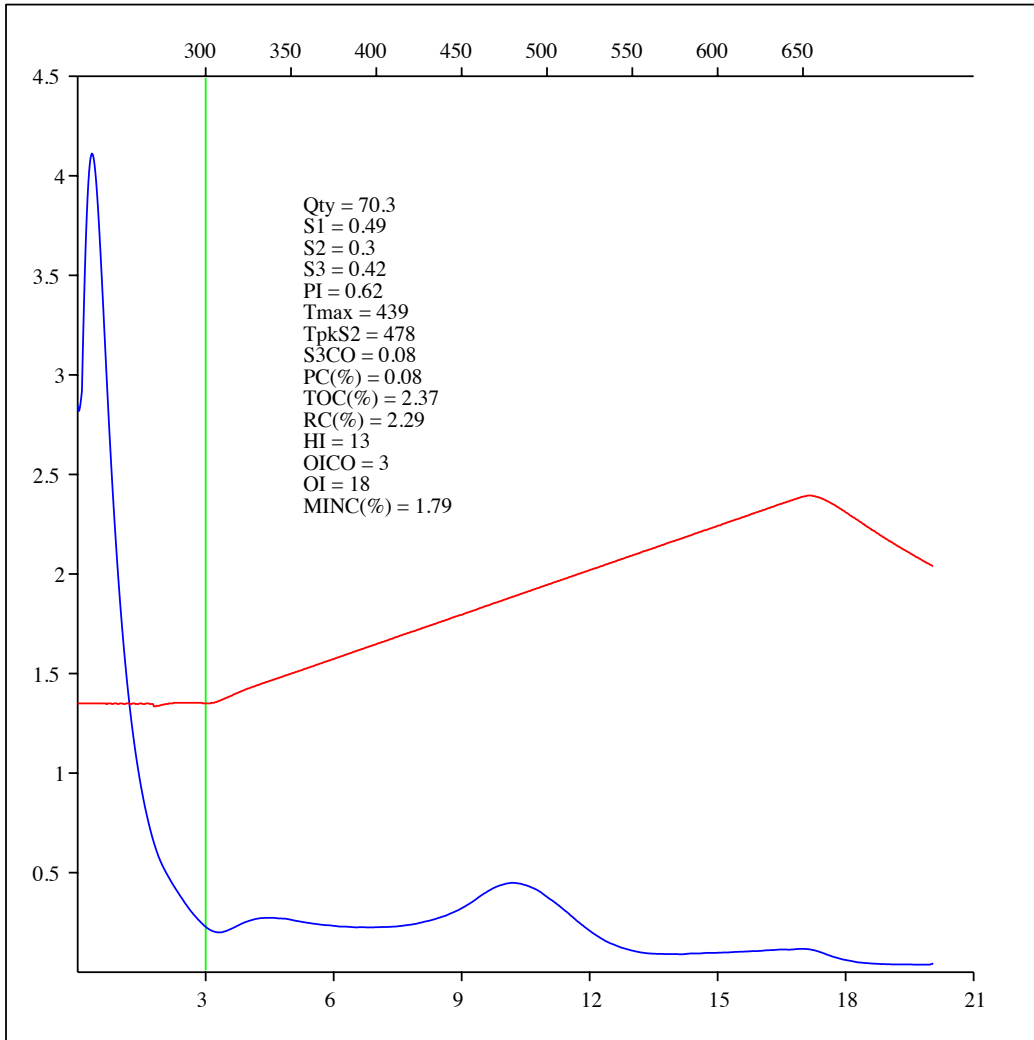
Sample: C-492839
Acquisition Date: 08-FEB-2012
Location: ECA SWAN A- 020-H/093-P-09
Depth: 2457 m
Analysis
Instrument: RockEval 6
Data Processing Software: Vinci

Oxidation carbon monoxide & carbon dioxide



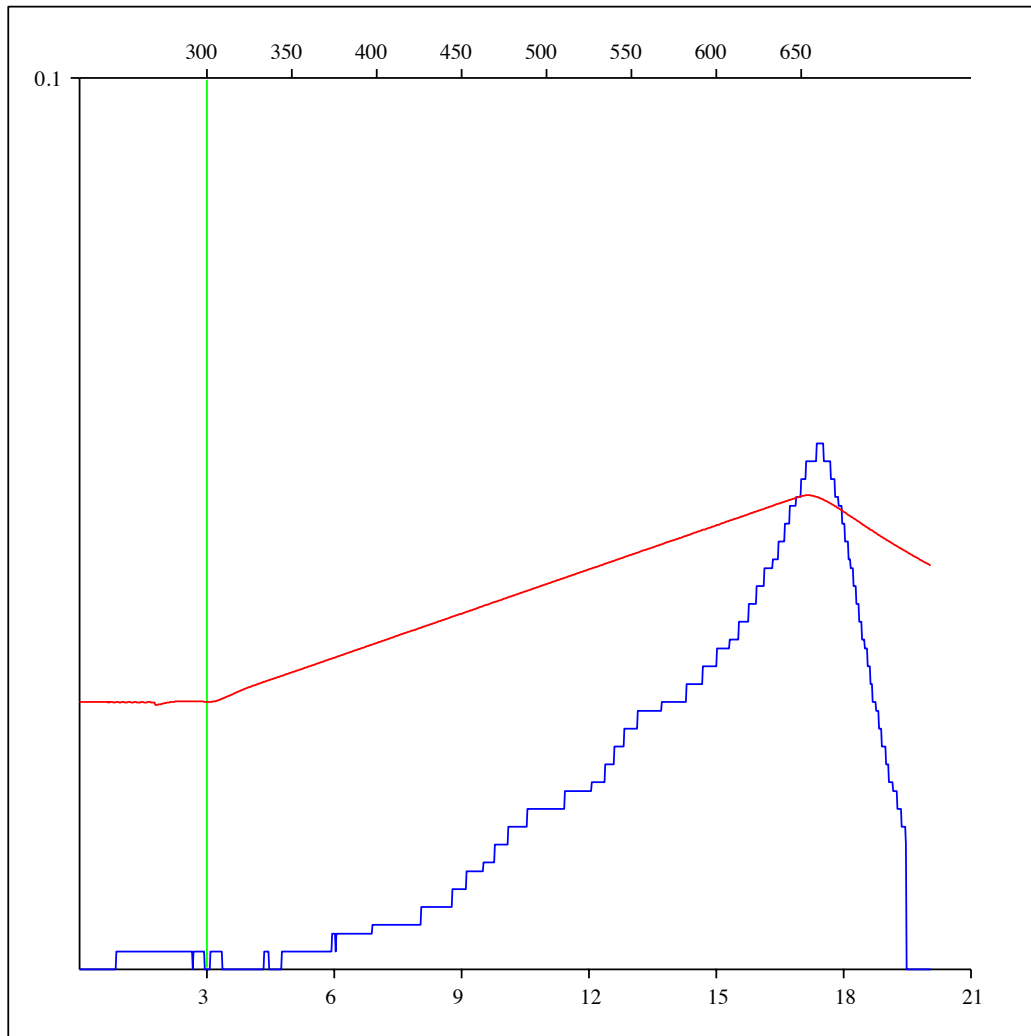
Sample: C-492840
Acquisition Date: 08-FEB-2012
Location: ECA BISSETTE D- 039-F/093-P-09
Depth: 2685.4 m
Analysis
Instrument: RockEval 6
Data Processing Software: Vinci

FID hydrocarbons



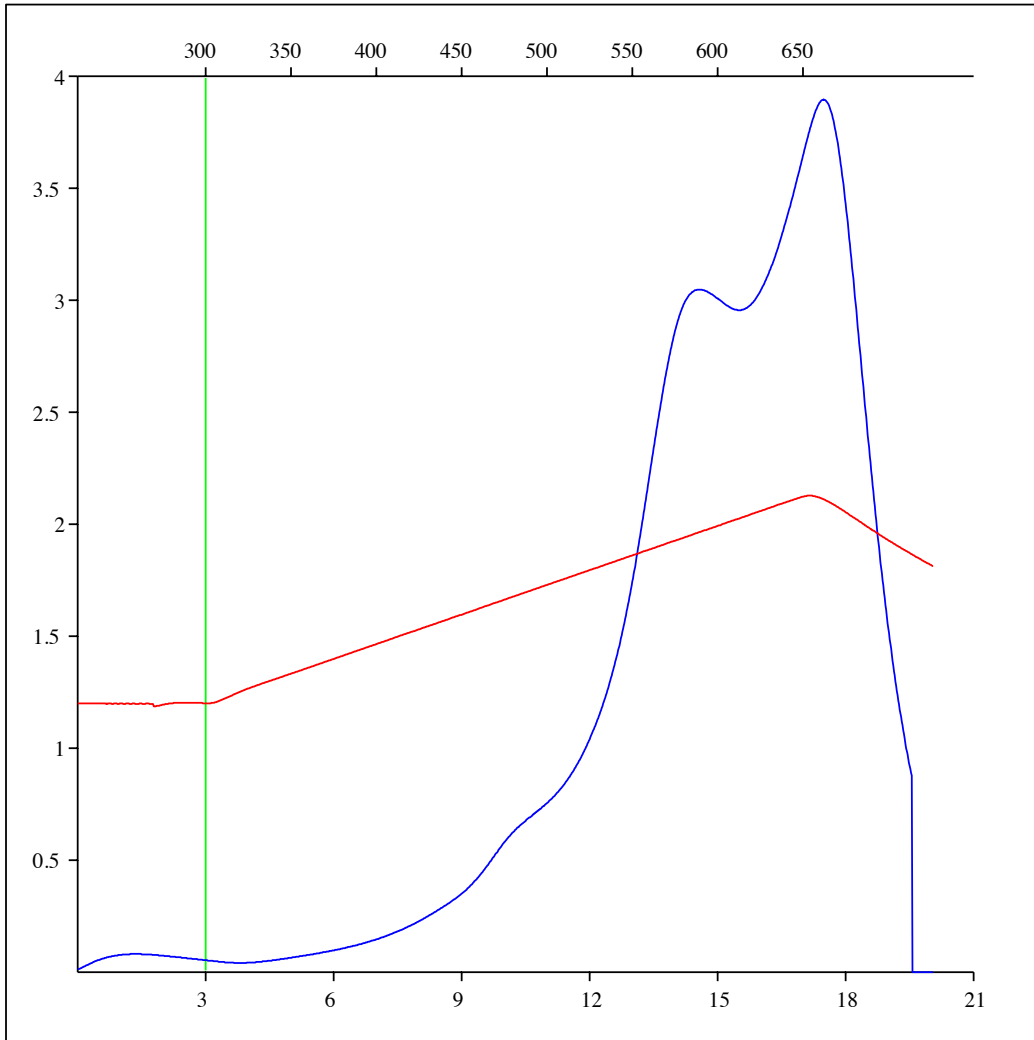
Sample: C-492840
Acquisition Date: 08-FEB-2012
Location: ECA BISSETTE D- 039-F/093-P-09
Depth: 2685.4 m
Analysis
Instrument: RockEval 6
Data Processing Software: Vinci

Pyrolysis carbon monoxide



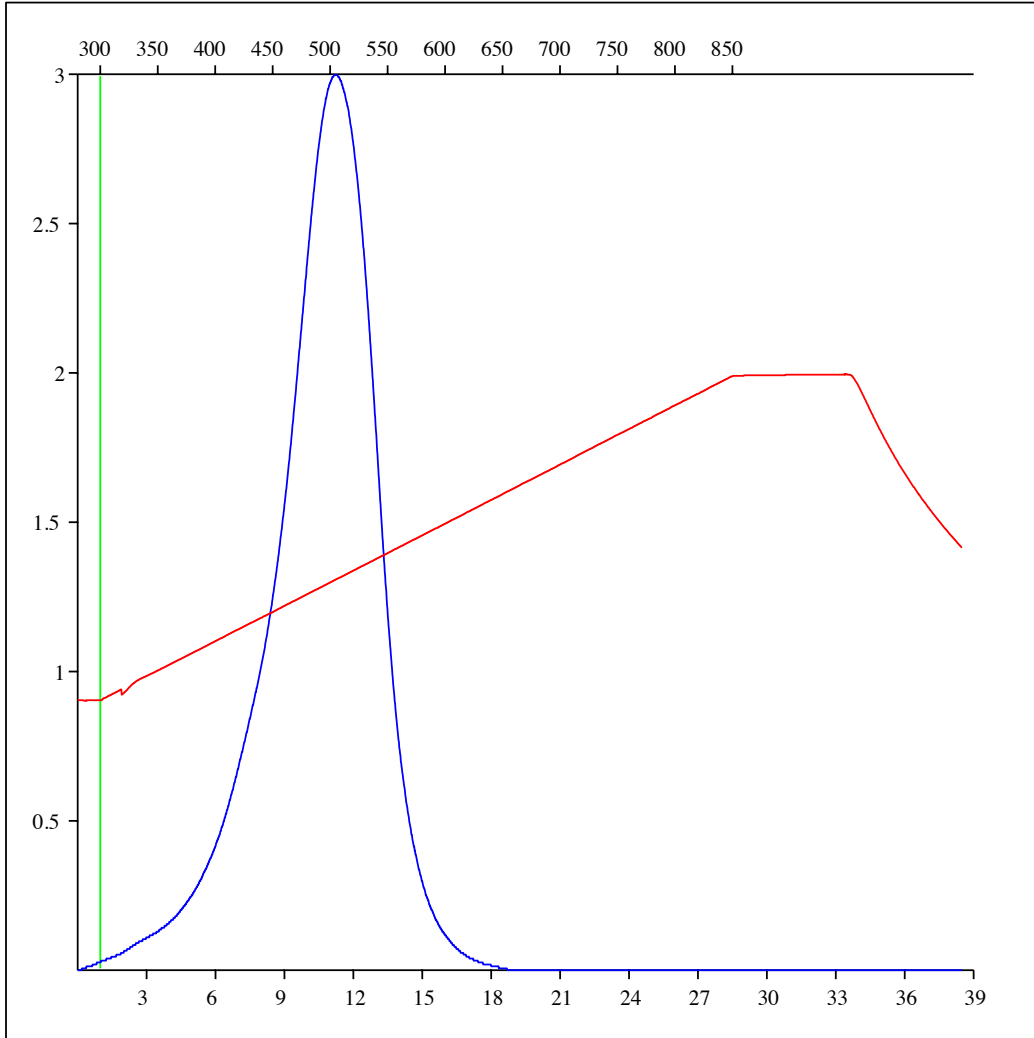
Sample: C-492840
Acquisition Date: 08-FEB-2012
Location: ECA BISSETTE D- 039-F/093-P-09
Depth: 2685.4 m
Analysis
Instrument: RockEval 6
Data Processing Software: Vinci

Pyrolysis carbon dioxide



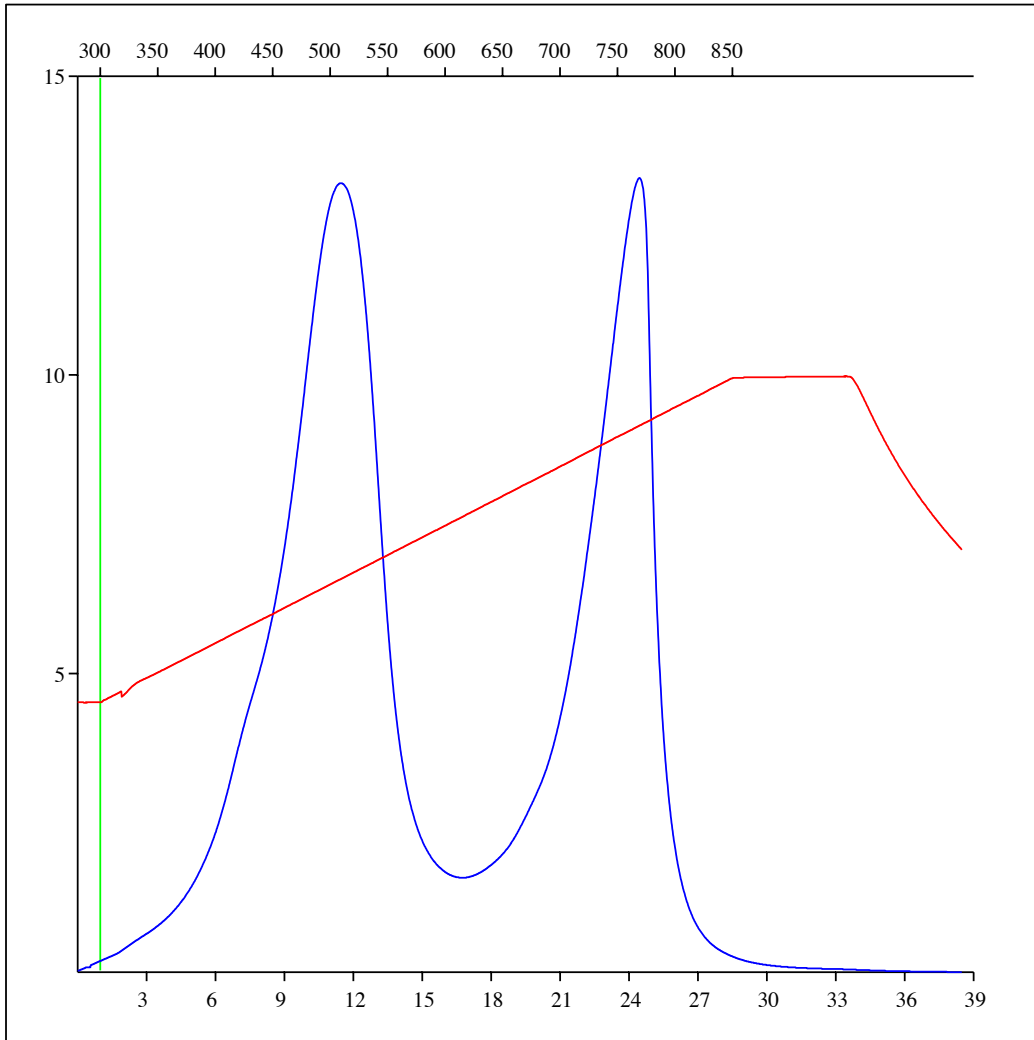
Sample: C-492840
Acquisition Date: 08-FEB-2012
Location: ECA BISSETTE D- 039-F/093-P-09
Depth: 2685.4 m
Analysis
Instrument: RockEval 6
Data Processing Software: Vinci

Oxidation carbon monoxide



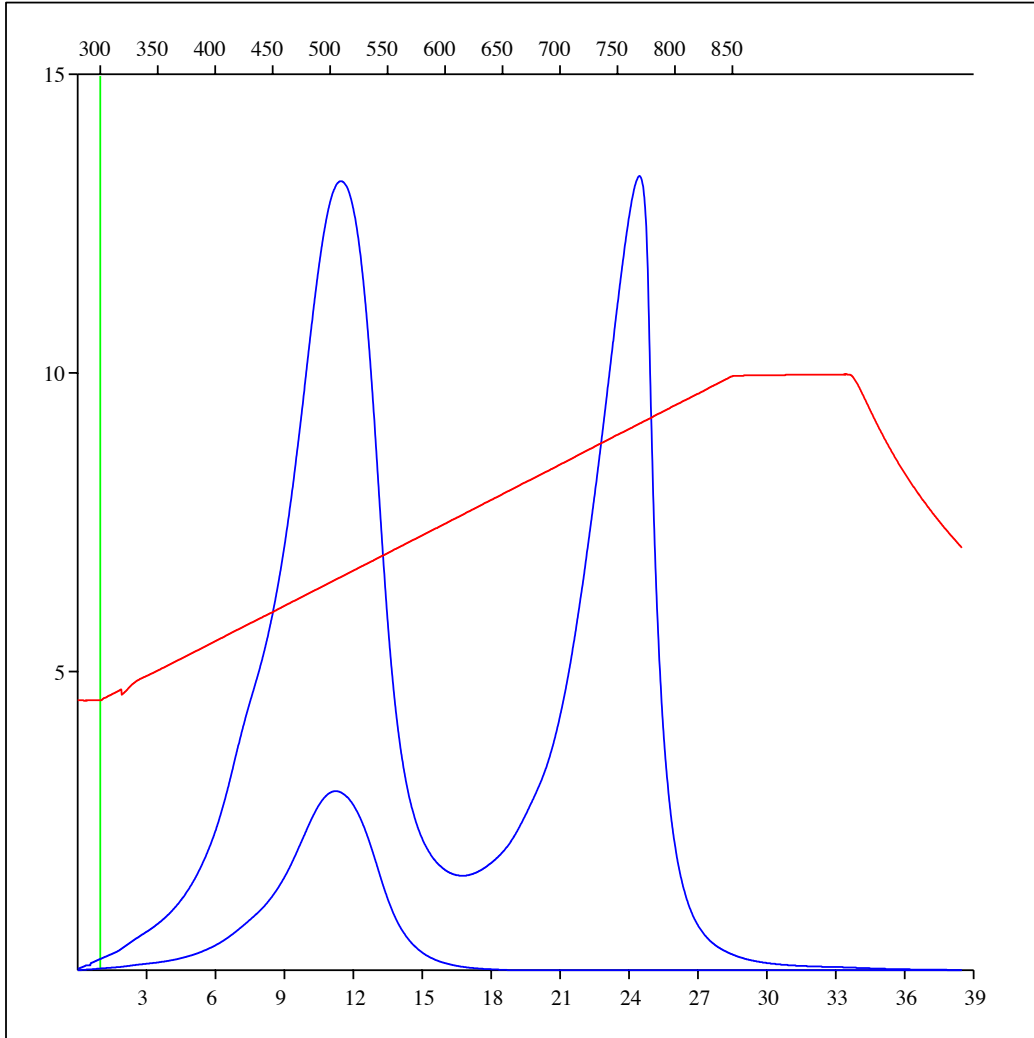
Sample: C-492840
Acquisition Date: 08-FEB-2012
Location: ECA BISSETTE D- 039-F/093-P-09
Depth: 2685.4 m
Analysis
Instrument: RockEval 6
Data Processing Software: Vinci

Oxidation carbon dioxide



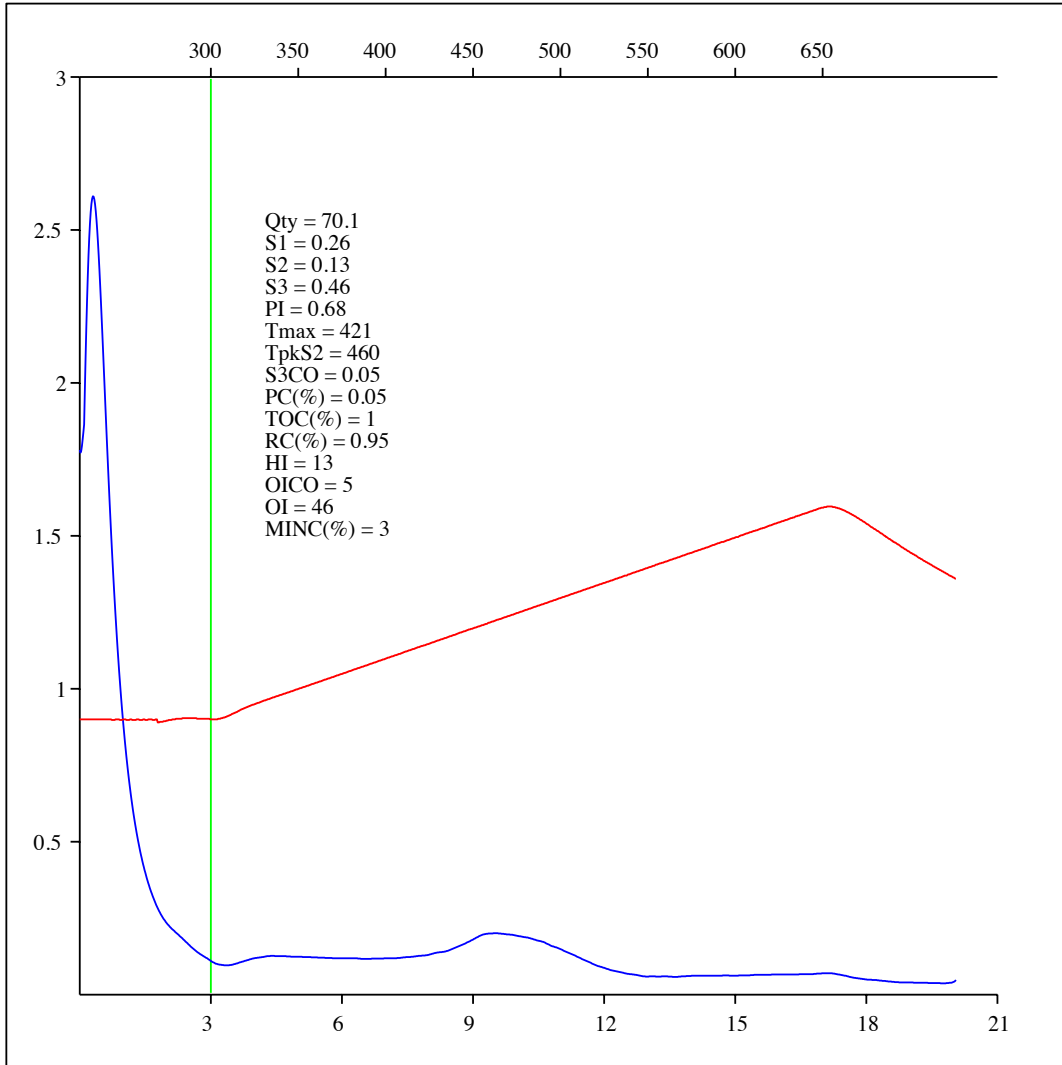
Sample: C-492840
Acquisition Date: 08-FEB-2012
Location: ECA BISSETTE D- 039-F/093-P-09
Depth: 2685.4 m
Analysis
Instrument: RockEval 6
Data Processing Software: Vinci

Oxidation carbon monoxide & carbon dioxide



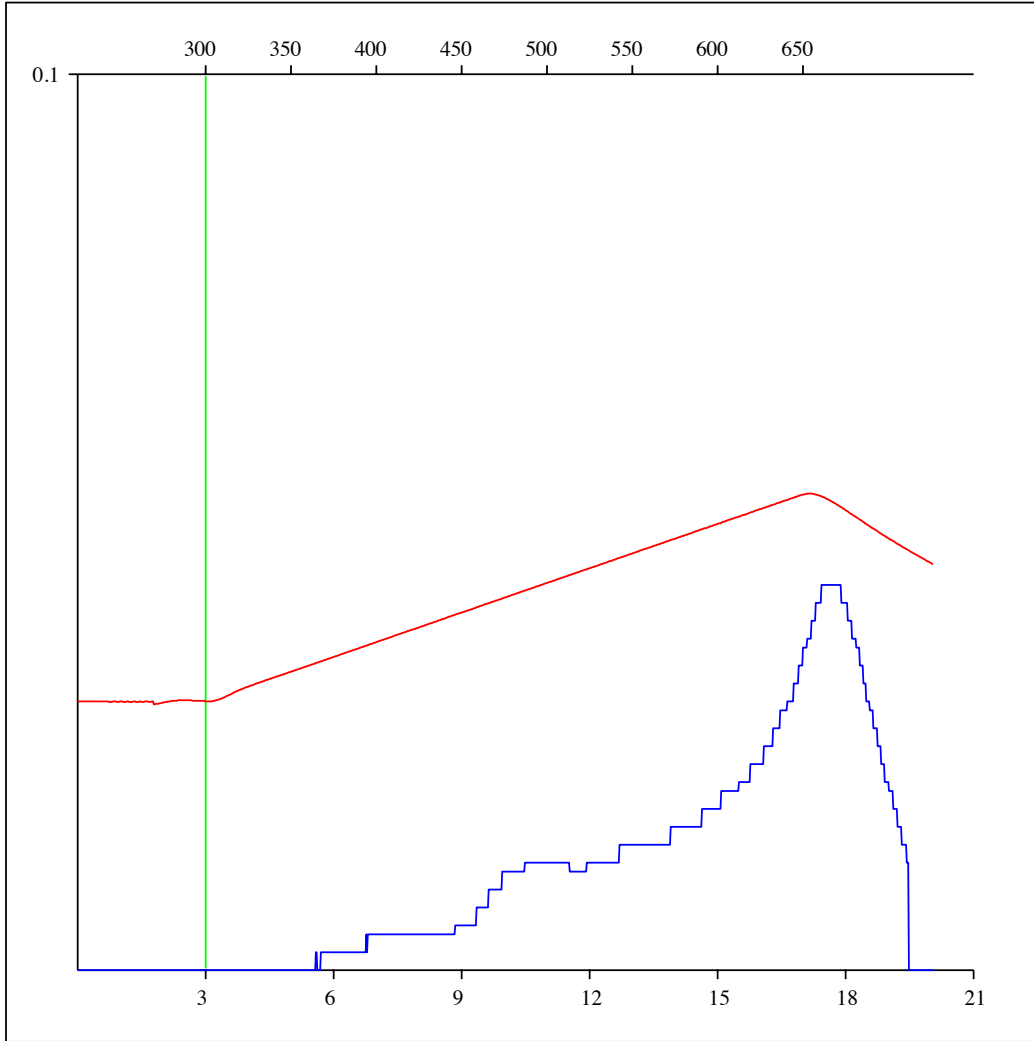
Sample: C-492841
Acquisition Date: 08-FEB-2012
Location: ECA BISSETTE D- 039-F/093-P-09
Depth: 2668.88 m
Analysis
Instrument: RockEval 6
Data Processing Software: Vinci

FID hydrocarbons



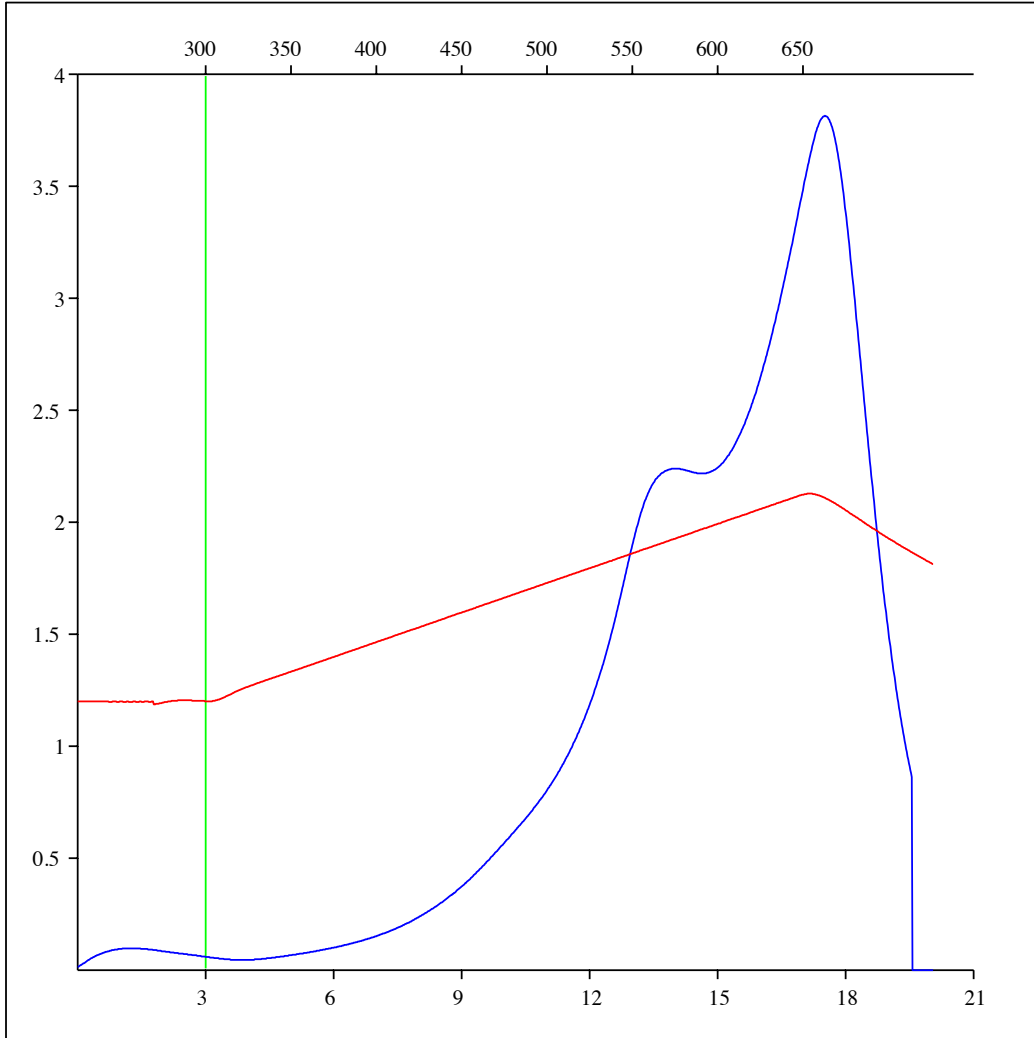
Sample: C-492841
Acquisition Date: 08-FEB-2012
Location: ECA BISSETTE D- 039-F/093-P-09
Depth: 2668.88 m
Analysis
Instrument: RockEval 6
Data Processing Software: Vinci

Pyrolysis carbon monoxide



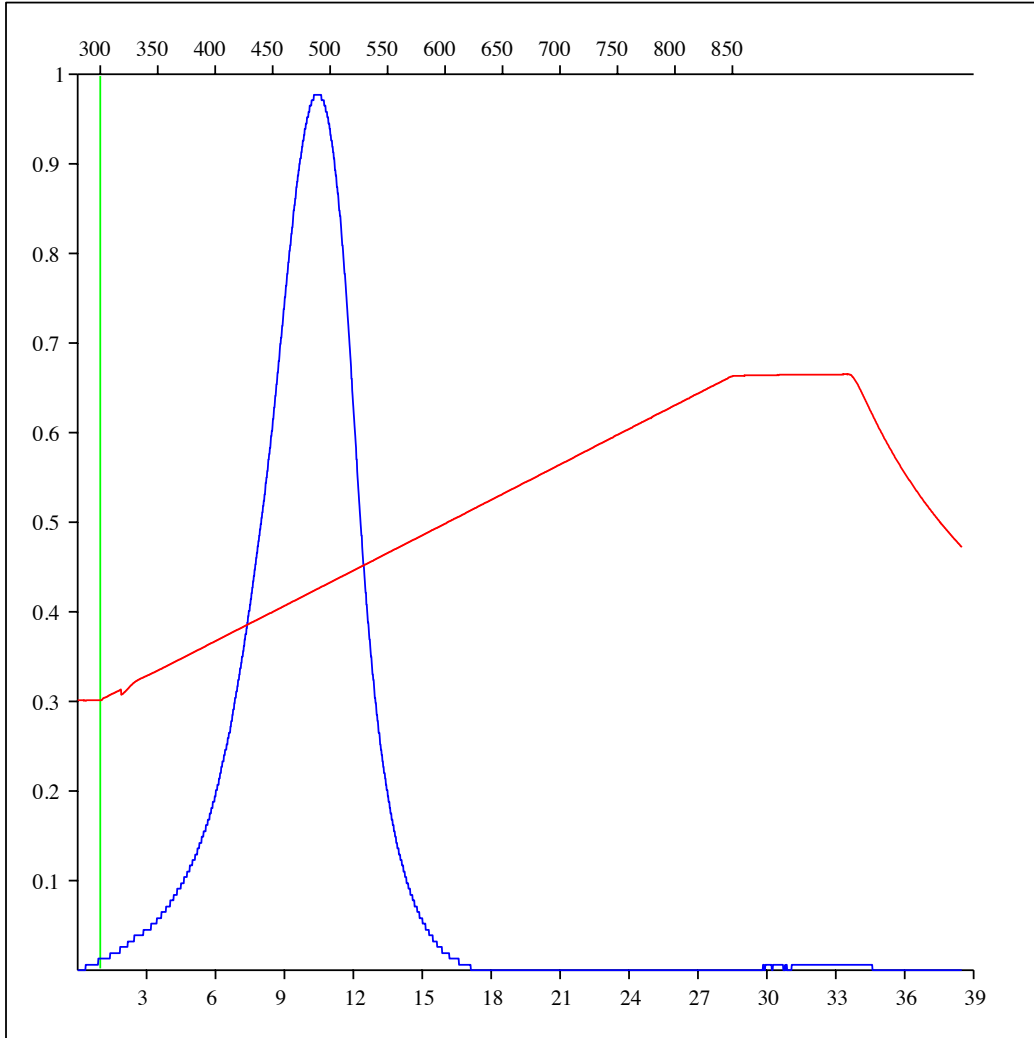
Sample: C-492841
Acquisition Date: 08-FEB-2012
Location: ECA BISSETTE D- 039-F/093-P-09
Depth: 2668.88 m
Analysis
Instrument: RockEval 6
Data Processing Software: Vinci

Pyrolysis carbon dioxide



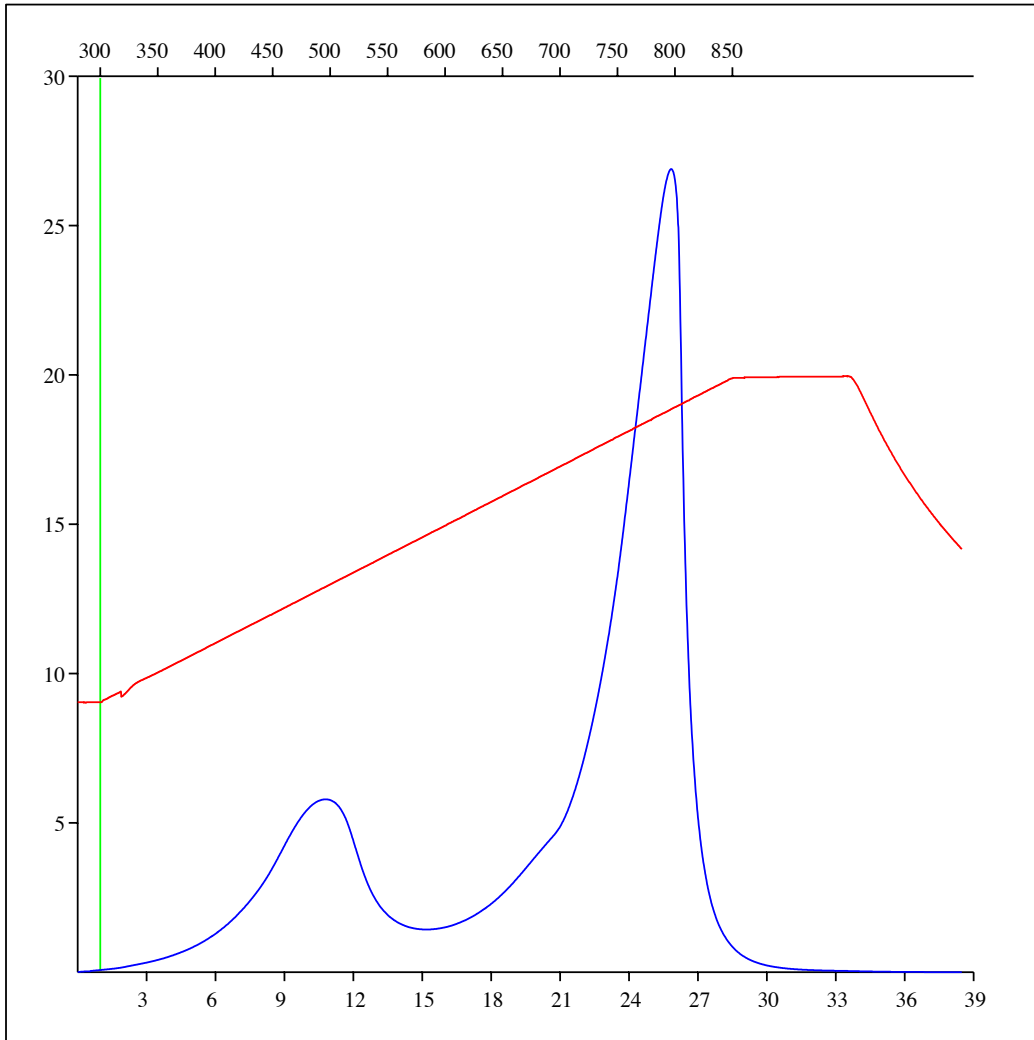
Sample: C-492841
Acquisition Date: 08-FEB-2012
Location: ECA BISSETTE D- 039-F/093-P-09
Depth: 2668.88 m
Analysis
Instrument: RockEval 6
Data Processing Software: Vinci

Oxidation carbon monoxide



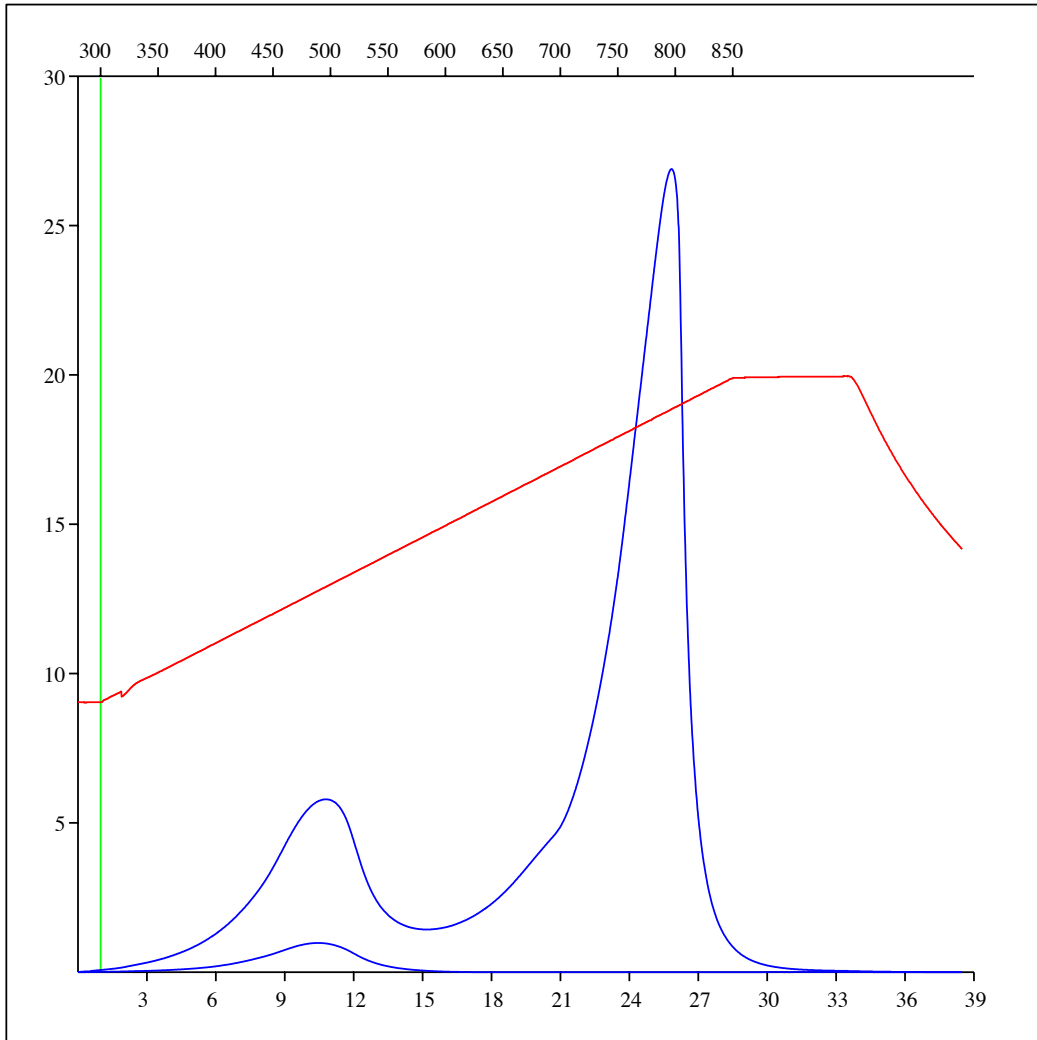
Sample: C-492841
Acquisition Date: 08-FEB-2012
Location: ECA BISSETTE D- 039-F/093-P-09
Depth: 2668.88 m
Analysis
Instrument: RockEval 6
Data Processing Software: Vinci

Oxidation carbon dioxide



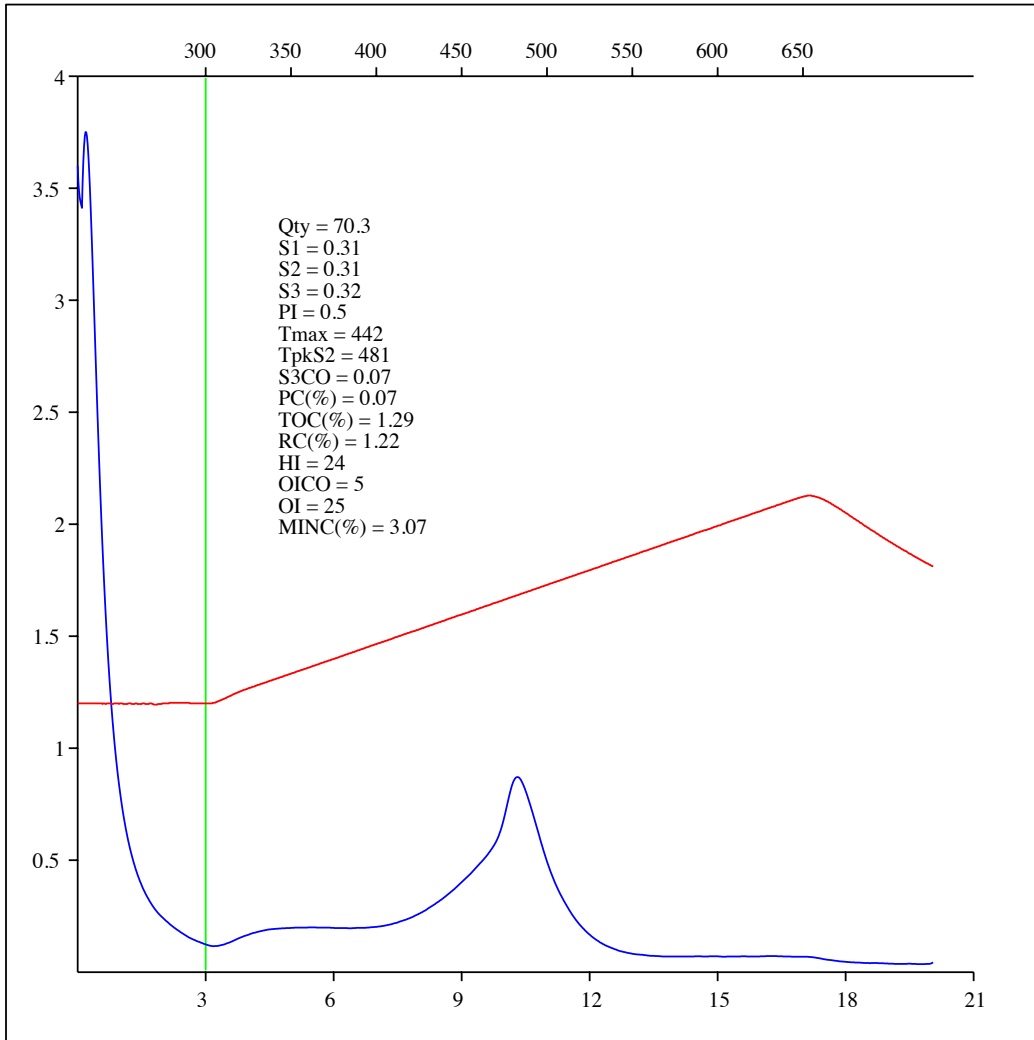
Sample: C-492841
Acquisition Date: 08-FEB-2012
Location: ECA BISSETTE D- 039-F/093-P-09
Depth: 2668.88 m
Analysis
Instrument: RockEval 6
Data Processing Software: Vinci

Oxidation carbon monoxide & carbon dioxide



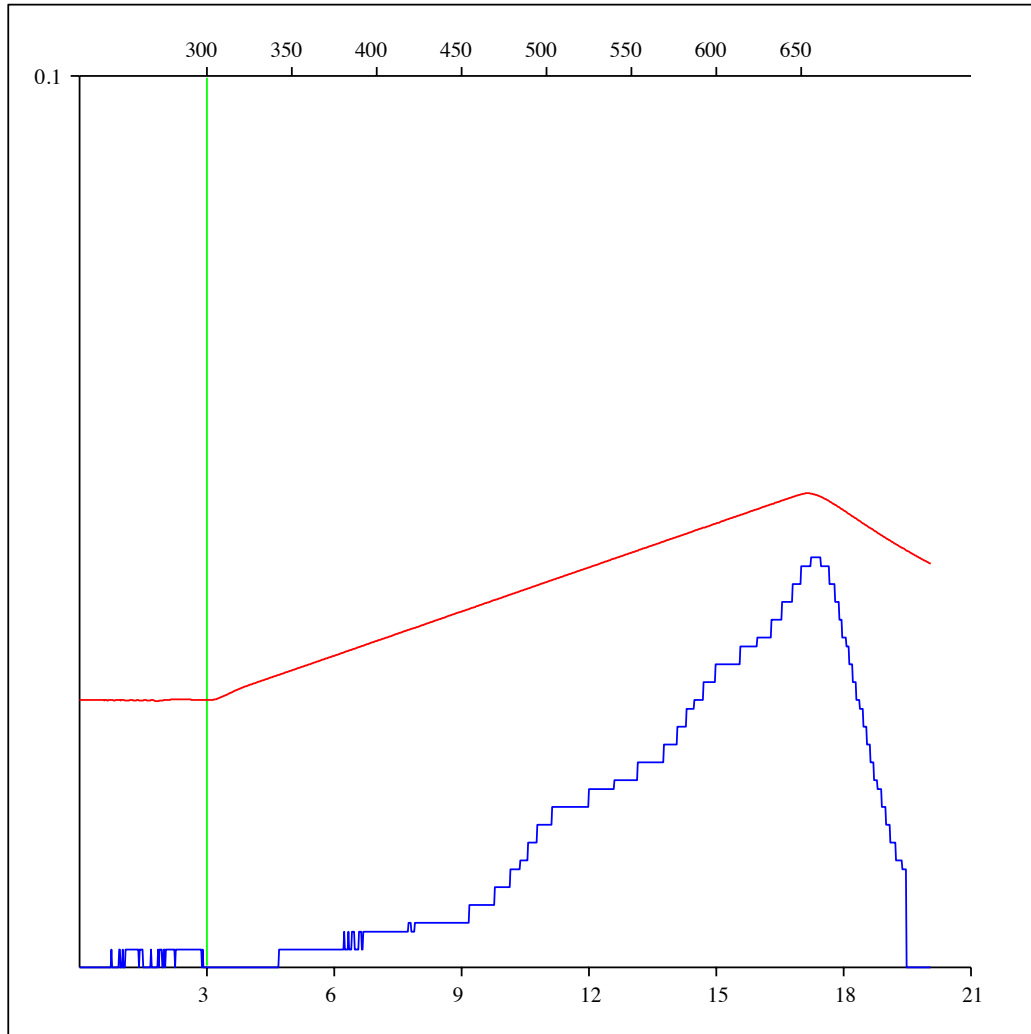
Sample: C-492842
Acquisition Date: 08-FEB-2012
Location: ARC DAWSON 07-13-079-15
Depth: 2084.5 m
Analysis
Instrument: RockEval 6
Data Processing Software: Vinci

FID hydrocarbons



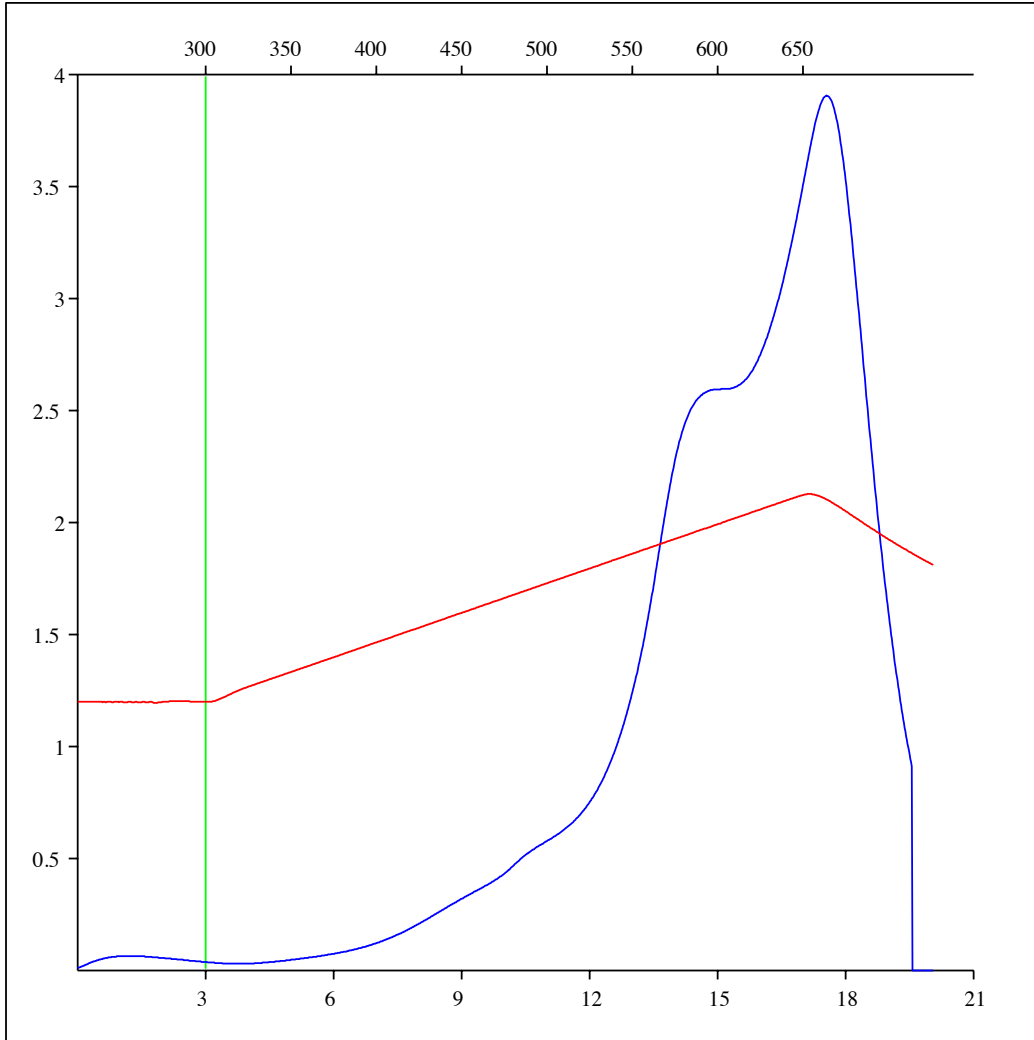
Sample: C-492842
Acquisition Date: 08-FEB-2012
Location: ARC DAWSON 07-13-079-15
Depth: 2084.5 m
Analysis
Instrument: RockEval 6
Data Processing Software: Vinci

Pyrolysis carbon monoxide



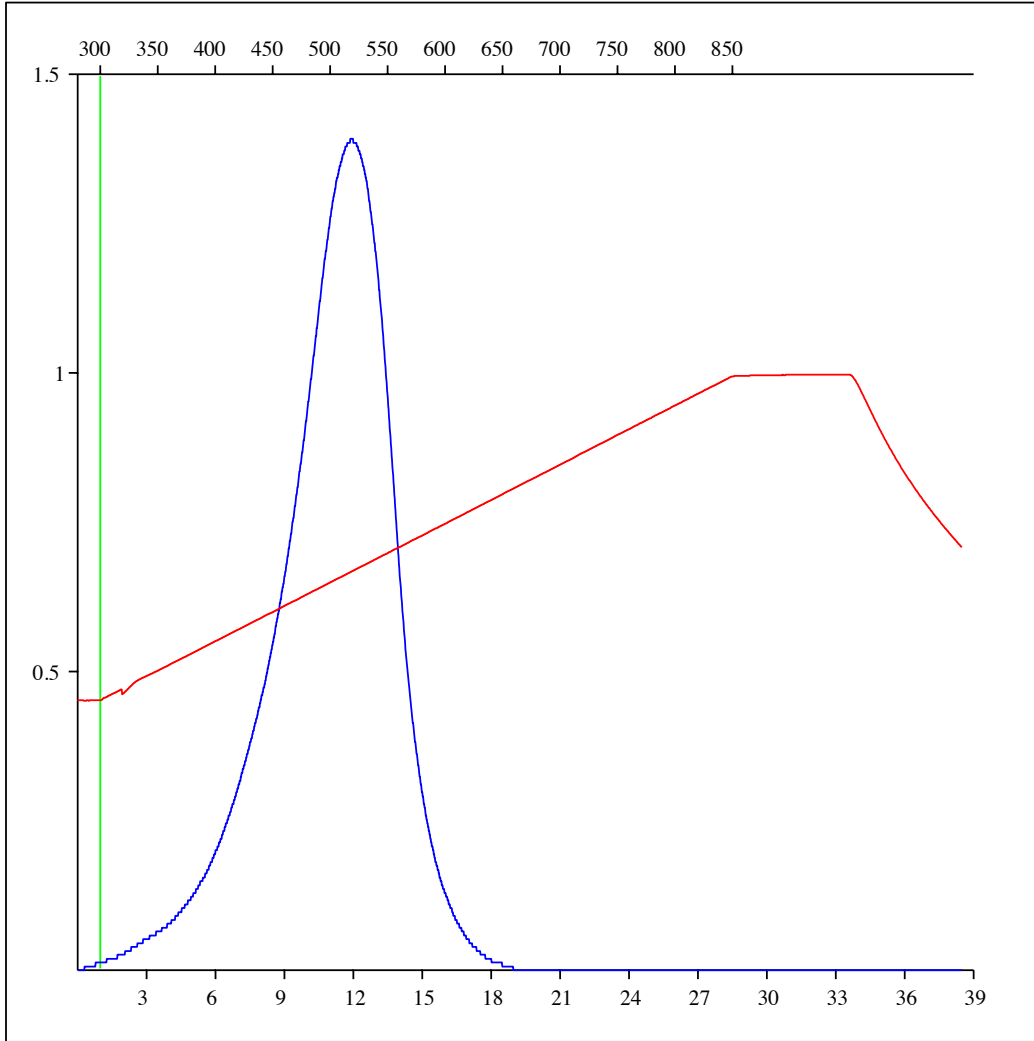
Sample: C-492842
Acquisition Date: 08-FEB-2012
Location: ARC DAWSON 07-13-079-15
Depth: 2084.5 m
Analysis
Instrument: RockEval 6
Data Processing Software: Vinci

Pyrolysis carbon dioxide



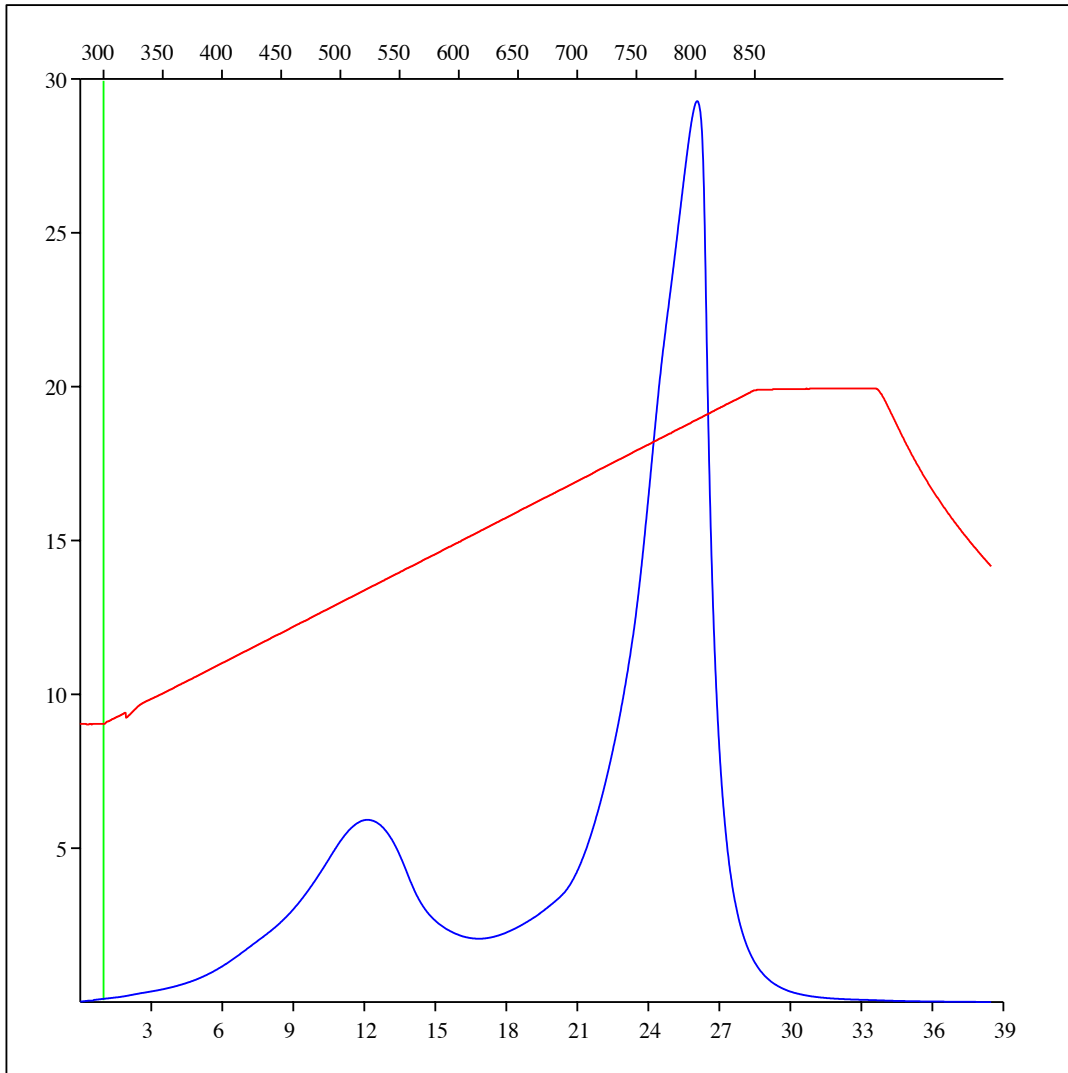
Sample: C-492842
Acquisition Date: 08-FEB-2012
Location: ARC DAWSON 07-13-079-15
Depth: 2084.5 m
Analysis
Instrument: RockEval 6
Data Processing Software: Vinci

Oxidation carbon monoxide



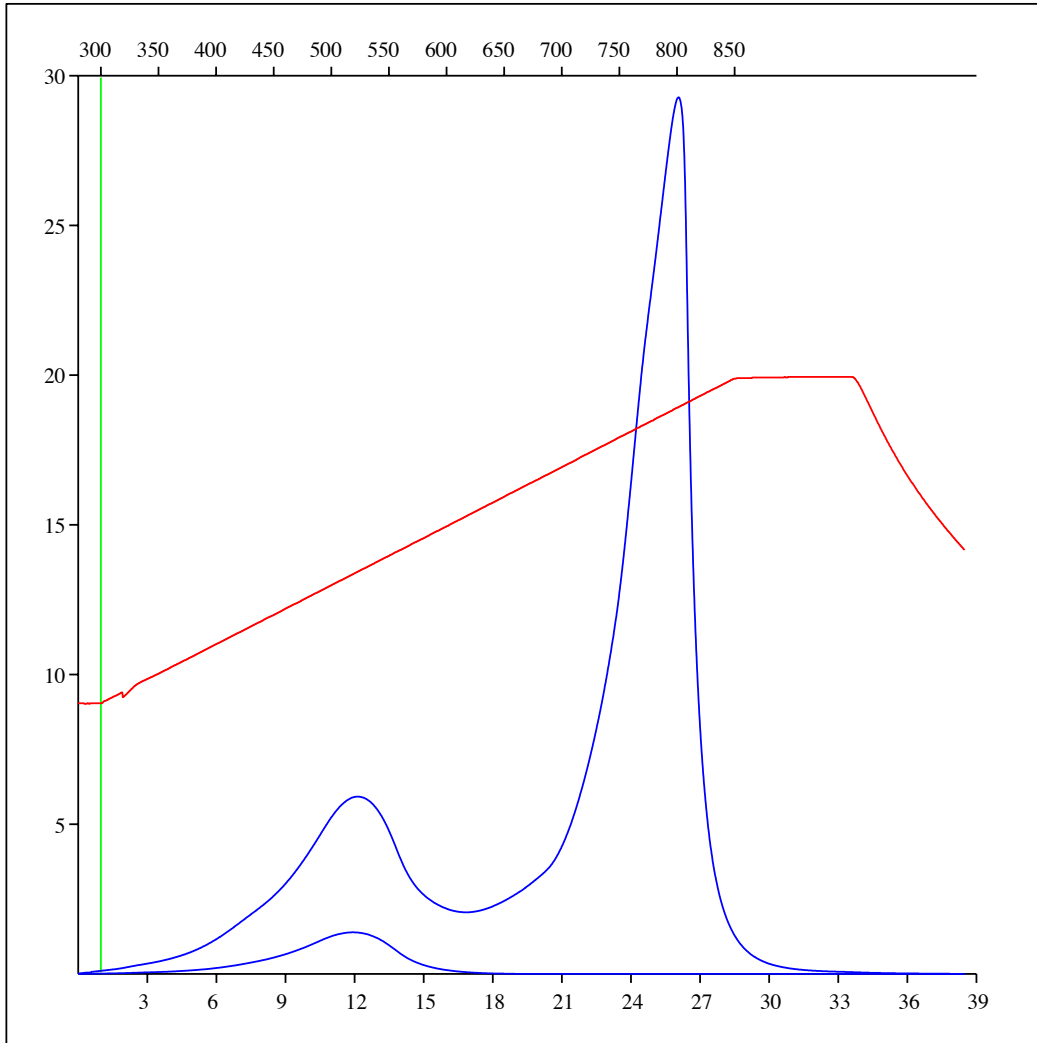
Sample: C-492842
Acquisition Date: 08-FEB-2012
Location: ARC DAWSON 07-13-079-15
Depth: 2084.5 m
Analysis
Instrument: RockEval 6
Data Processing Software: Vinci

Oxidation carbon dioxide



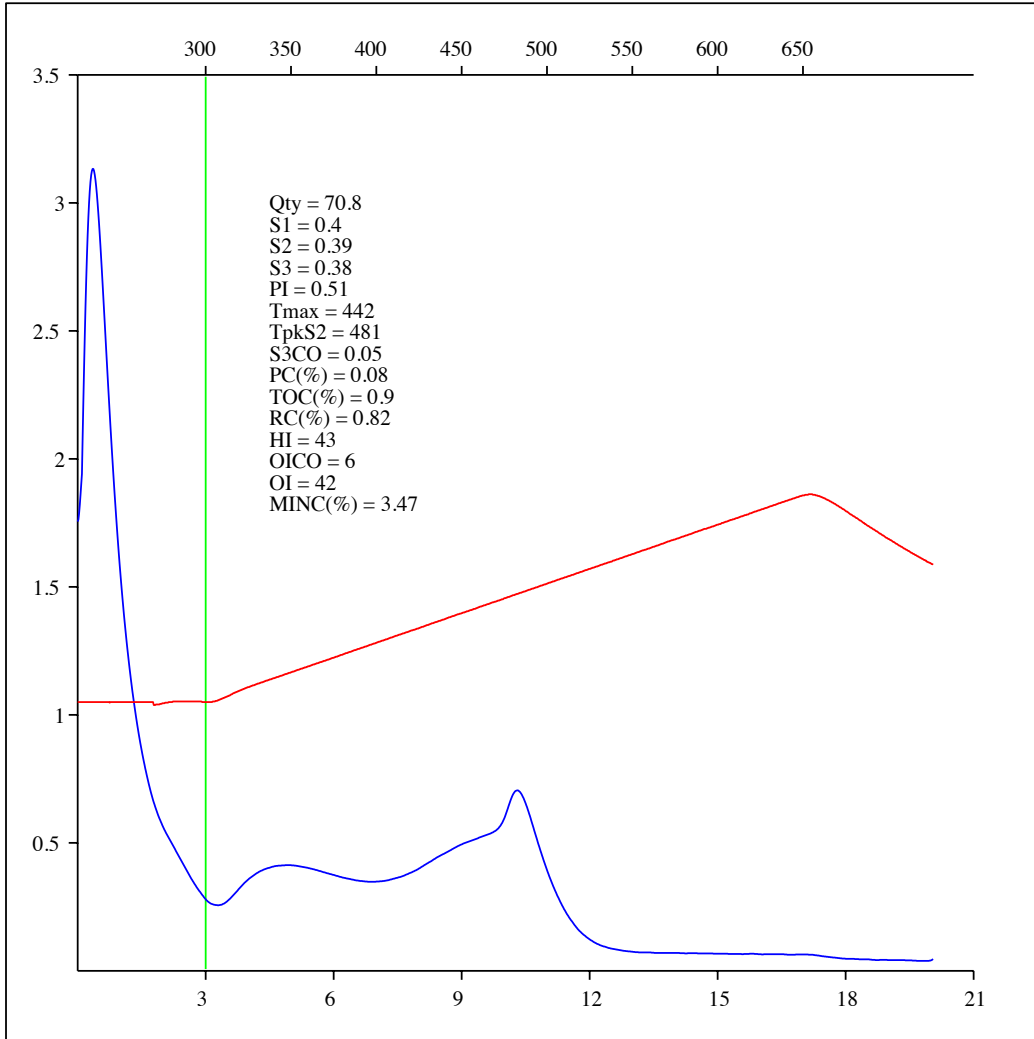
Sample: C-492842
Acquisition Date: 08-FEB-2012
Location: ARC DAWSON 07-13-079-15
Depth: 2084.5 m
Analysis
Instrument: RockEval 6
Data Processing Software: Vinci

Oxidation carbon monoxide & carbon dioxide



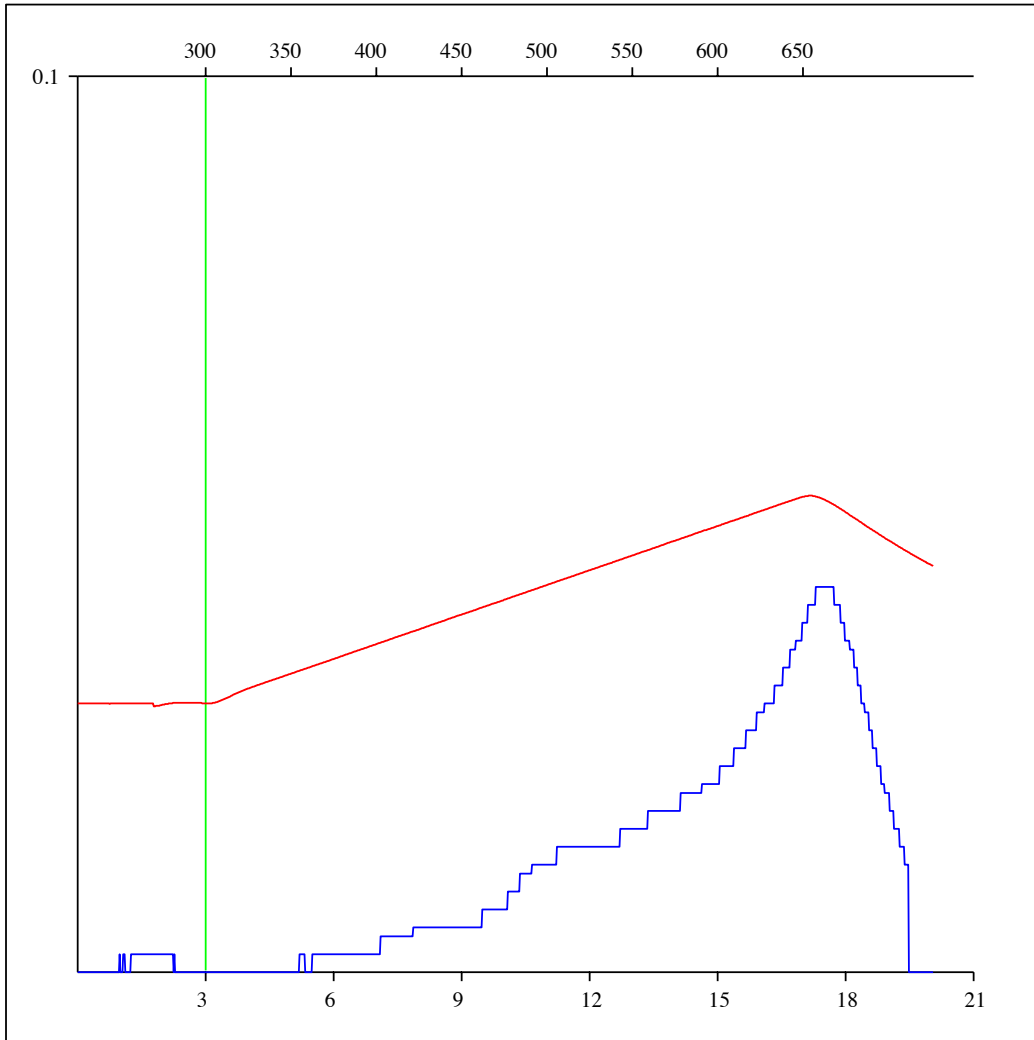
Sample: C-492843
Acquisition Date: 08-FEB-2012
Location: ARC DAWSON 07-13-079-15
Depth: 2078.5 m
Analysis
Instrument: RockEval 6
Data Processing Software: Vinci

FID hydrocarbons



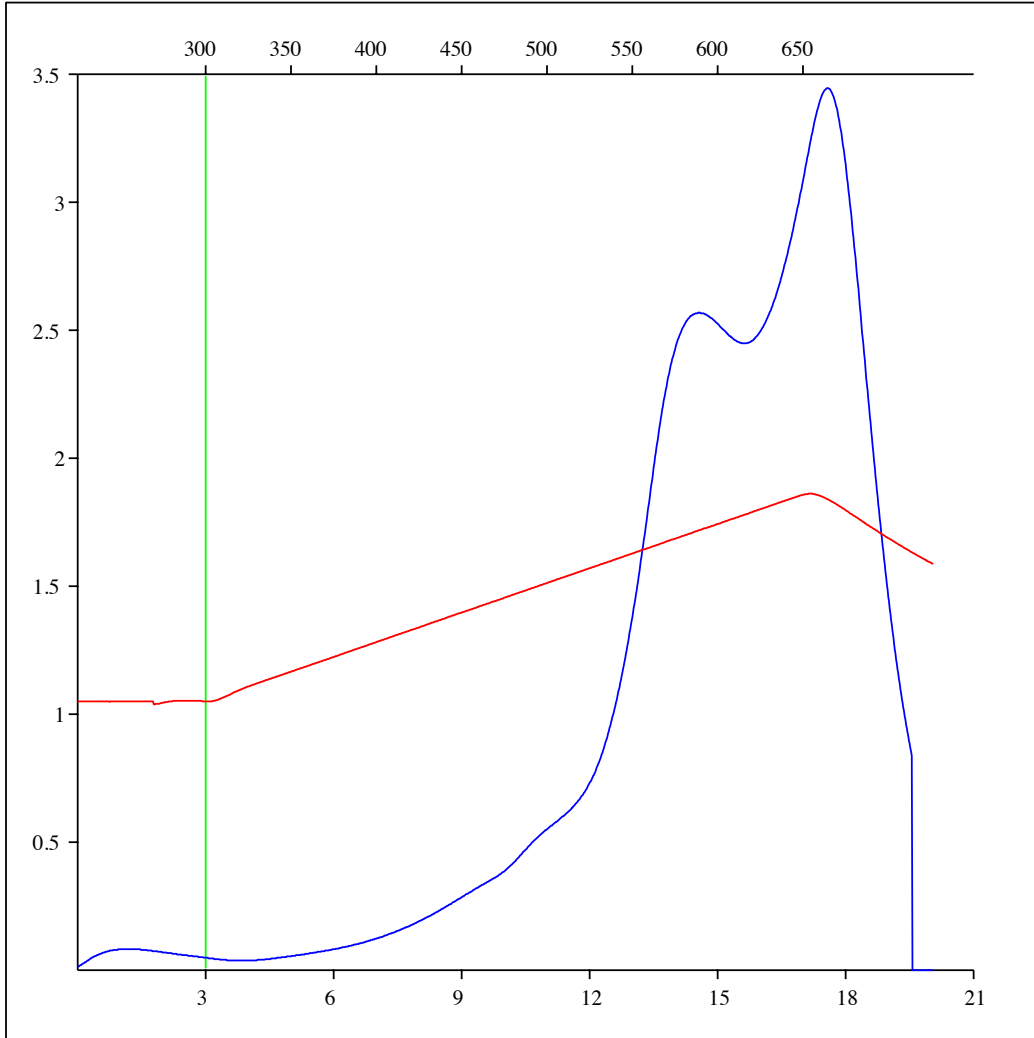
Sample: C-492843
Acquisition Date: 08-FEB-2012
Location: ARC DAWSON 07-13-079-15
Depth: 2078.5 m
Analysis
Instrument: RockEval 6
Data Processing Software: Vinci

Pyrolysis carbon monoxide



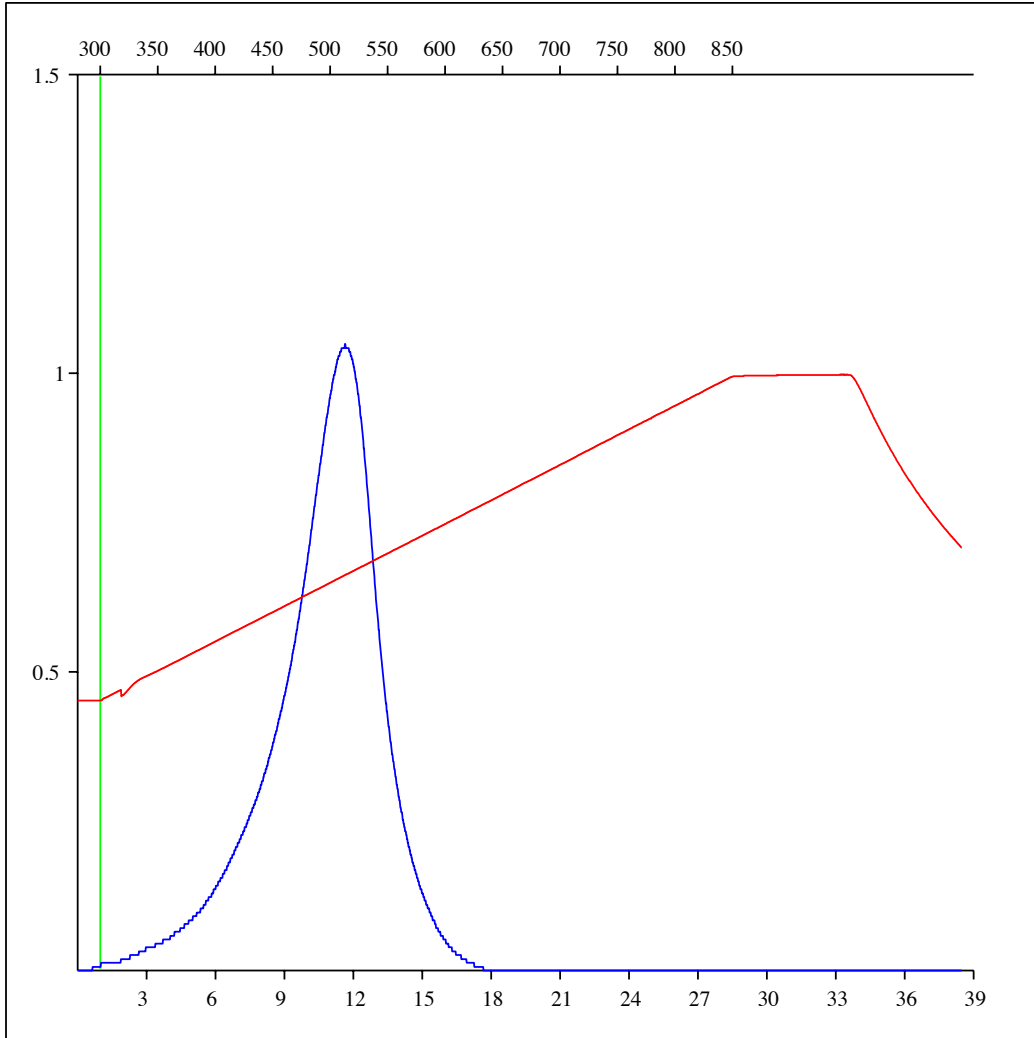
Sample: C-492843
Acquisition Date: 08-FEB-2012
Location: ARC DAWSON 07-13-079-15
Depth: 2078.5 m
Analysis
Instrument: RockEval 6
Data Processing Software: Vinci

Pyrolysis carbon dioxide



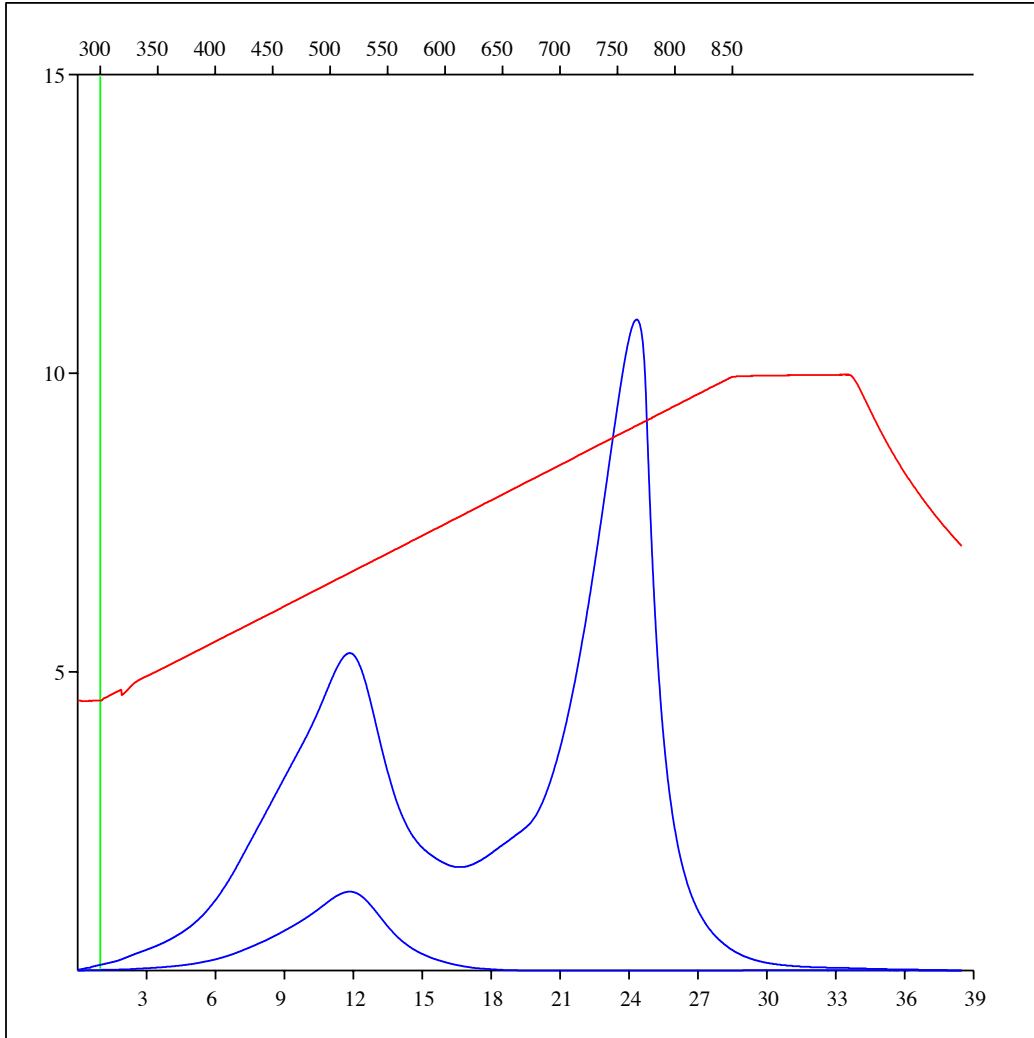
Sample: C-492843
Acquisition Date: 08-FEB-2012
Location: ARC DAWSON 07-13-079-15
Depth: 2078.5 m
Analysis
Instrument: RockEval 6
Data Processing Software: Vinci

Oxidation carbon monoxide



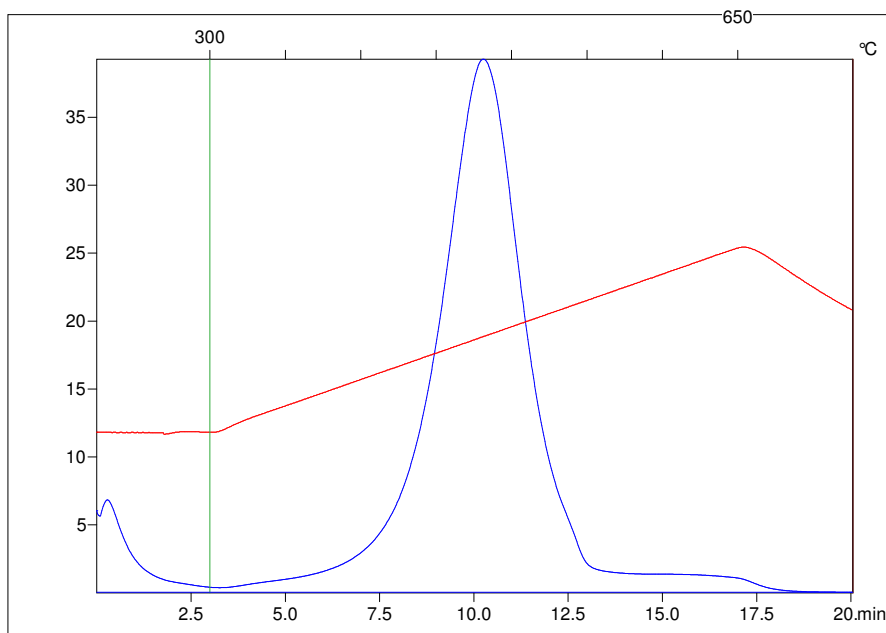
Sample: C-492854
Acquisition Date: 08-FEB-2012
Location: ECA SWAN B- 032-G/093-P-09
Depth: 2707 m
Analysis
Instrument: RockEval 6
Data Processing Software: Vinci

Oxidation carbon monoxide & carbon dioxide



Customer :	Customer part :
<input type="text" value="customer"/>	<input type="text" value="customer part"/>
Comment :	
<input type="text" value="Comment"/>	

S1(mg/g)=0.76	Sample =9107
S2(mg/g)=12.52	Method =Bulk Rock
Tmax(°C)=441	Cycle=Basic
TpkS2(°C)=480.0	KFID(10 ⁹)=1290
PI=0.06	Qty(mg)=70.9
HI=247	TOC(%)=5.07

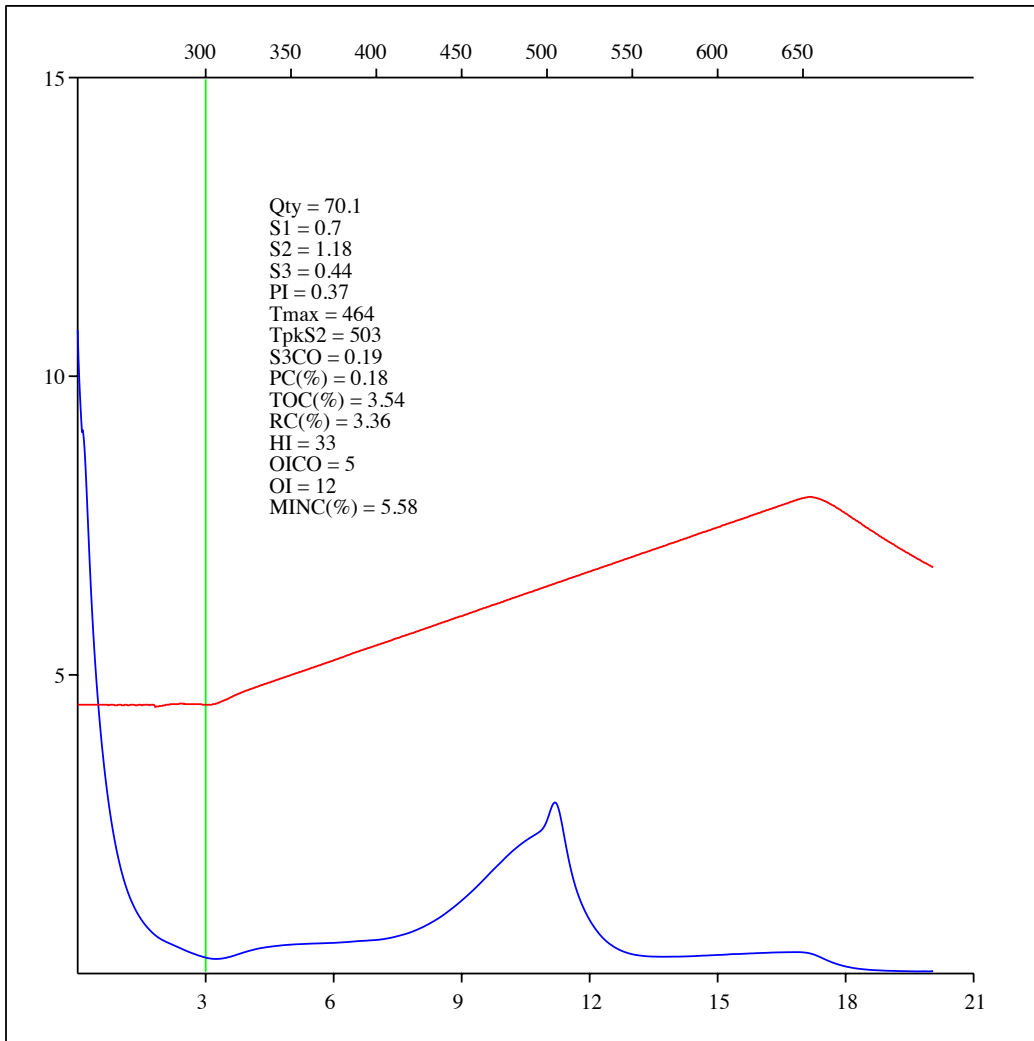


C:\VINCI\UOFA_101\UA002.R00 : FID pyrolysis graphic

State	<input type="text" value="Ok"/>
Pyro Status	<input type="text" value="No blank subtraction"/>
Oxi Status	<input type="text" value="No blank subtraction"/>

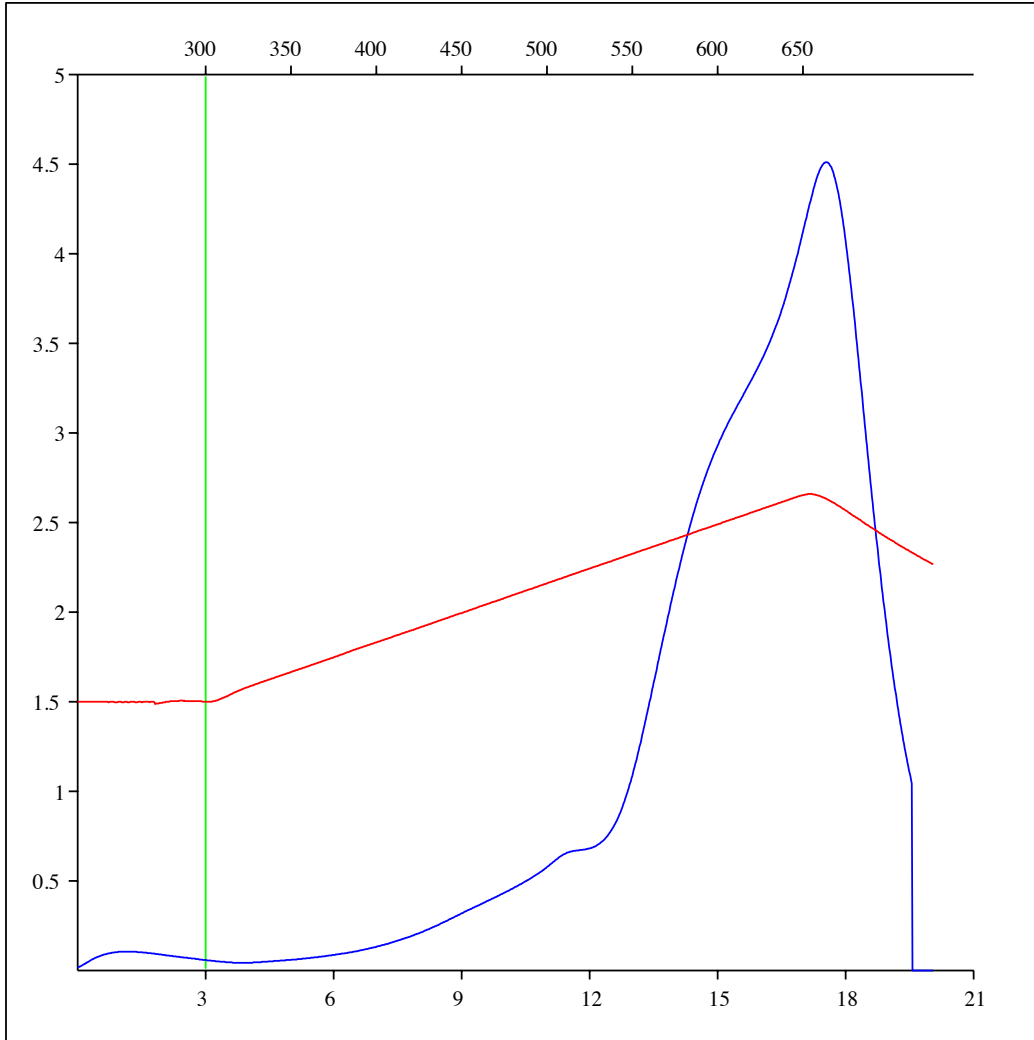
Sample: C-492844
Acquisition Date: 08-FEB-2012
Location: ARC DAWSON 07-13-079-15
Depth: 2055.22 m
Analysis
Instrument: RockEval 6
Data Processing Software: Vinci

FID hydrocarbons



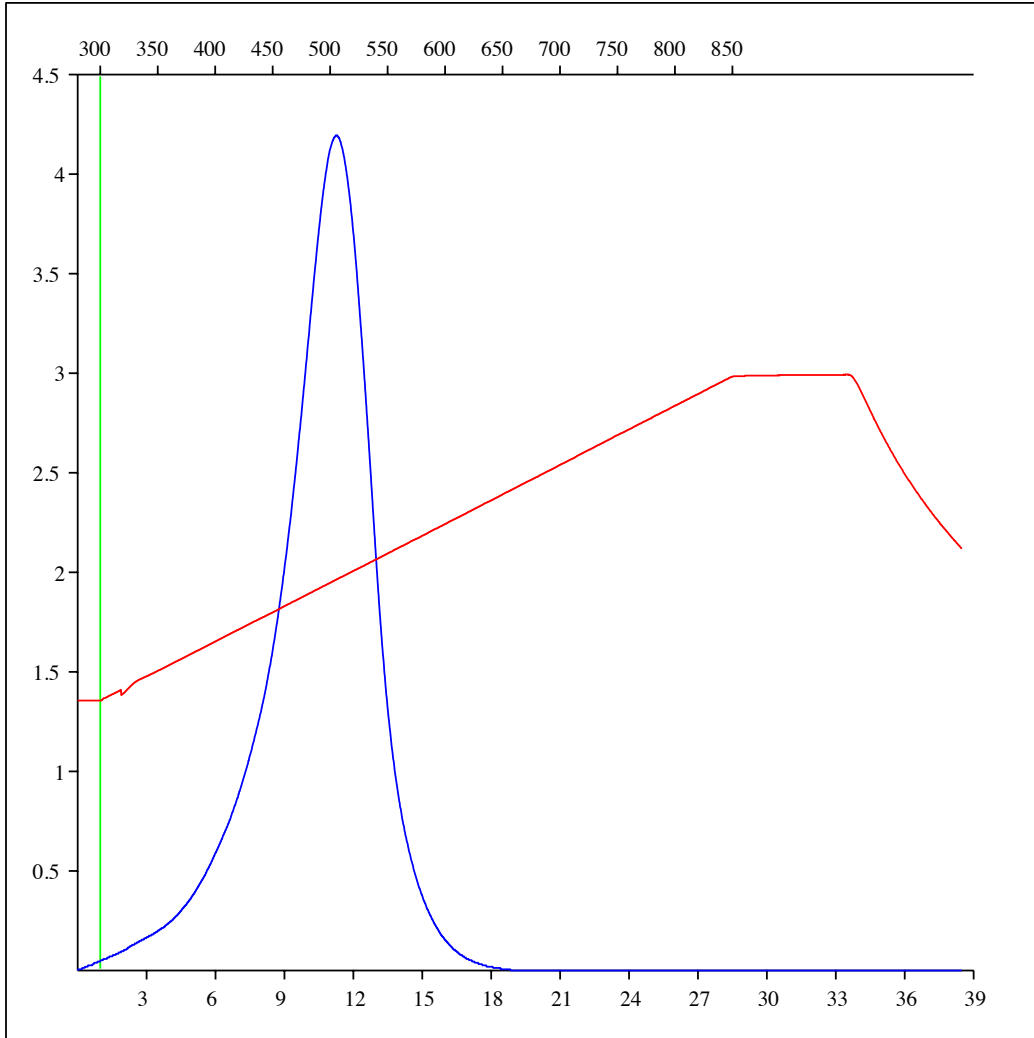
Sample: C-492844
Acquisition Date: 08-FEB-2012
Location: ARC DAWSON 07-13-079-15
Depth: 2055.22 m
Analysis
Instrument: RockEval 6
Data Processing Software: Vinci

Pyrolysis carbon dioxide



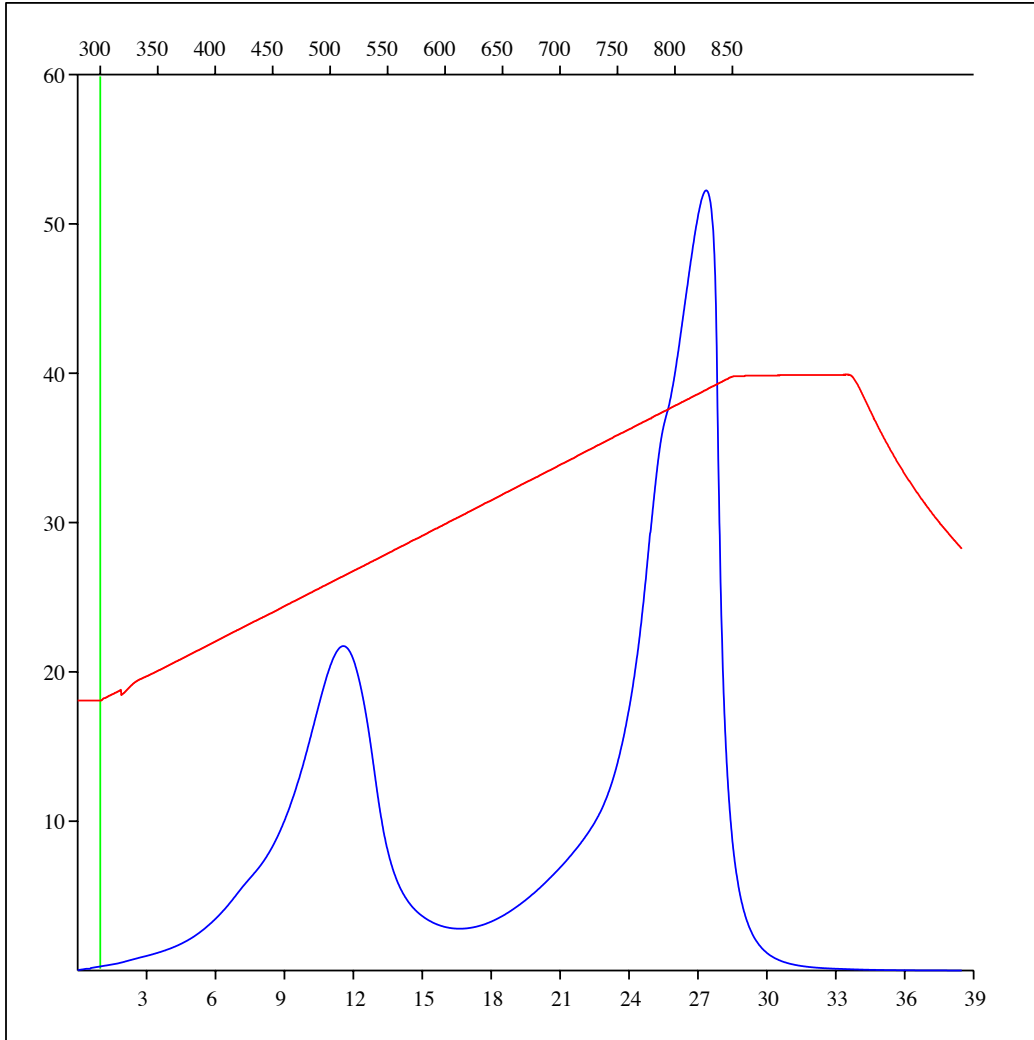
Sample: C-492844
Acquisition Date: 08-FEB-2012
Location: ARC DAWSON 07-13-079-15
Depth: 2055.22 m
Analysis
Instrument: RockEval 6
Data Processing Software: Vinci

Oxidation carbon monoxide



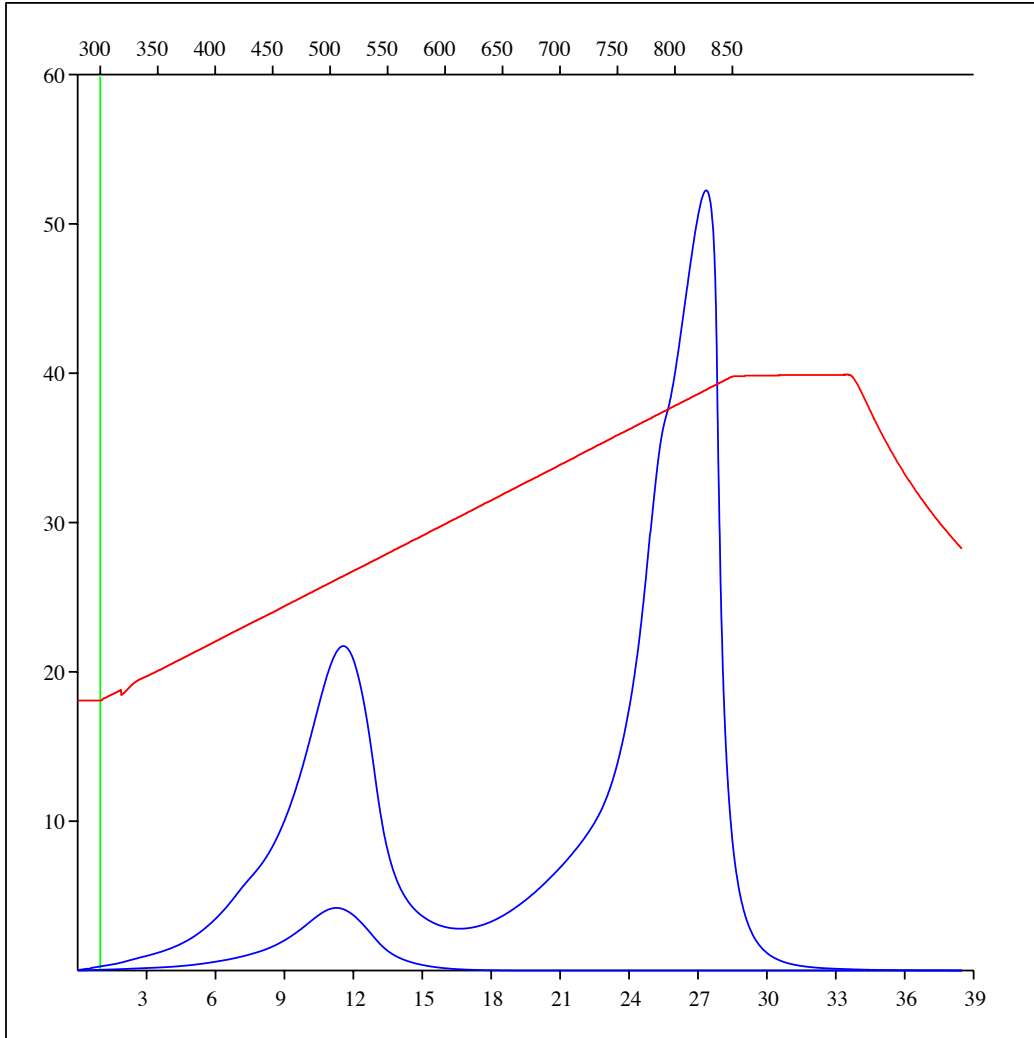
Sample: C-492844
Acquisition Date: 08-FEB-2012
Location: ARC DAWSON 07-13-079-15
Depth: 2055.22 m
Analysis
Instrument: RockEval 6
Data Processing Software: Vinci

Oxidation carbon dioxide



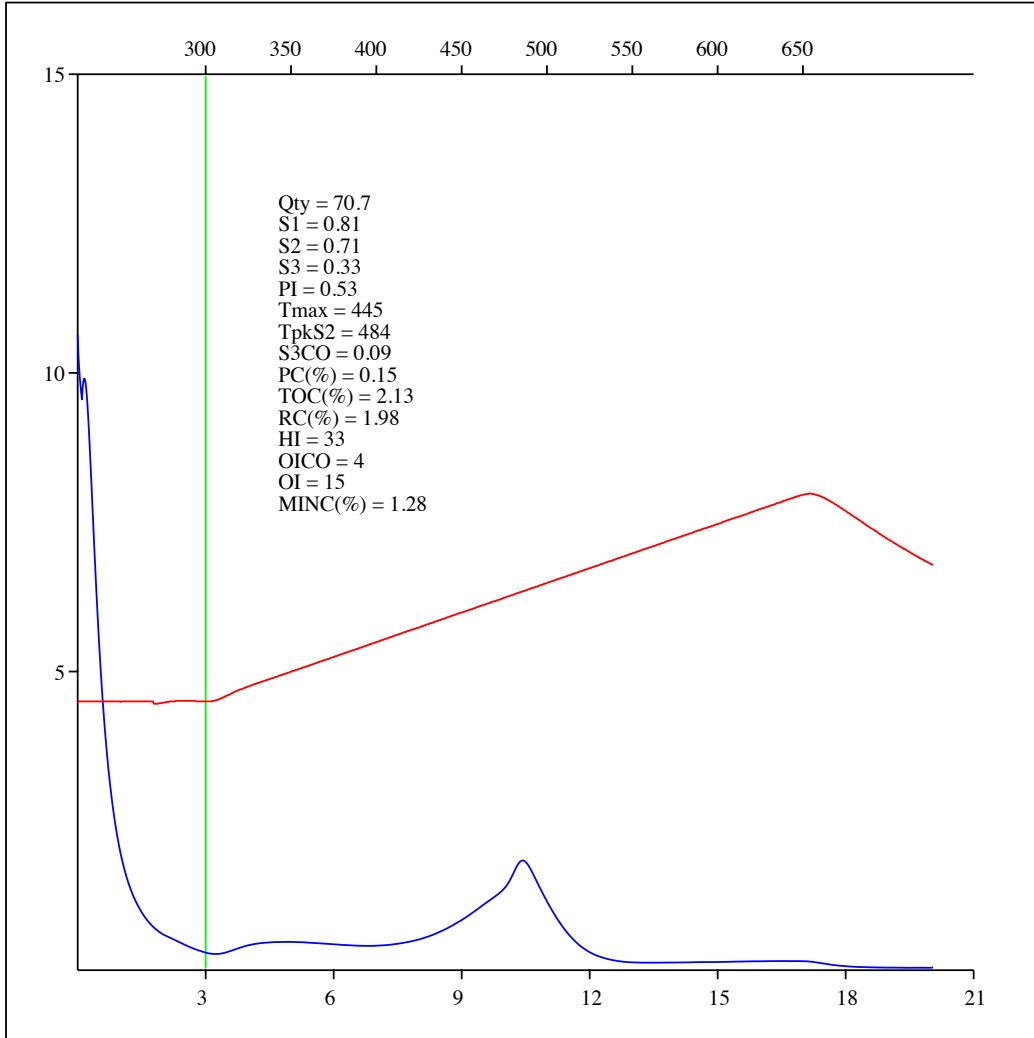
Sample: C-492844
Acquisition Date: 08-FEB-2012
Location: ARC DAWSON 07-13-079-15
Depth: 2055.22 m
Analysis
Instrument: RockEval 6
Data Processing Software: Vinci

Oxidation carbon monoxide & carbon dioxide



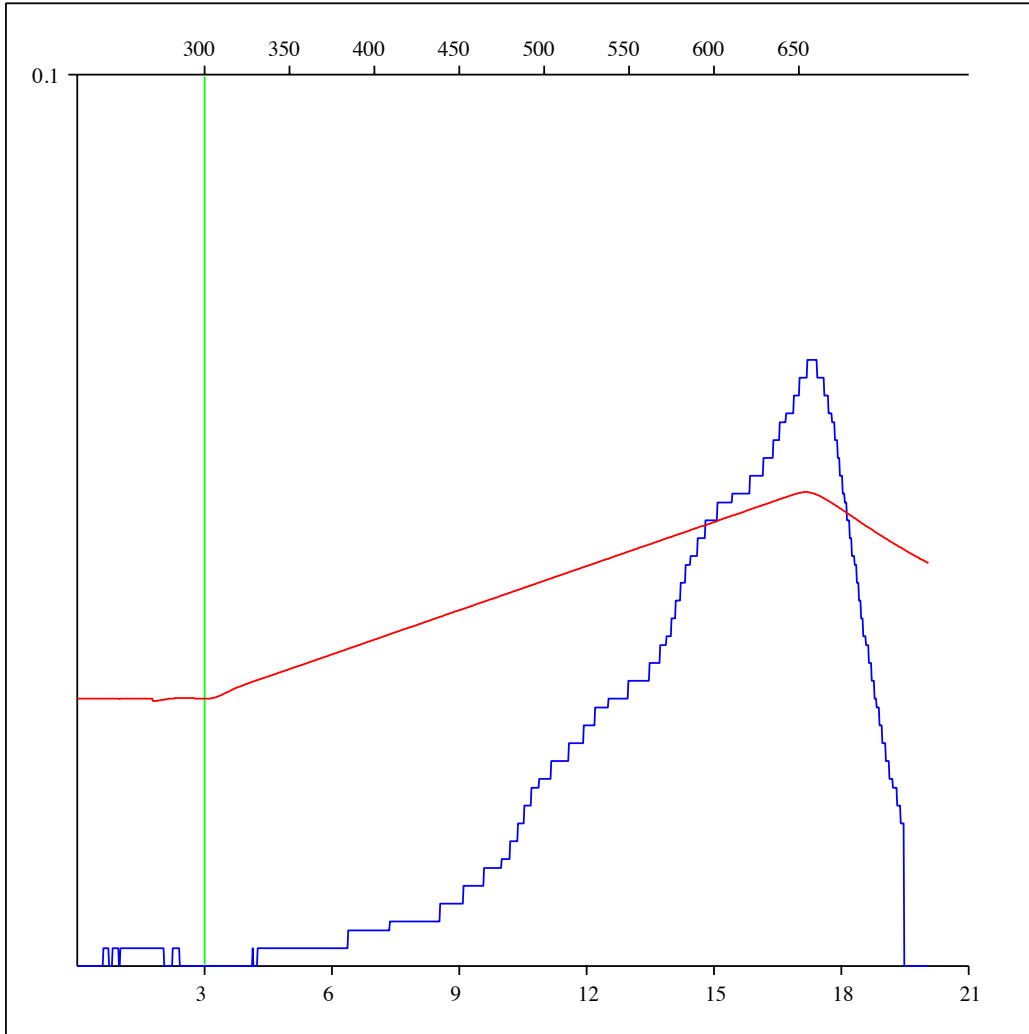
Sample: C-492845
Acquisition Date: 08-FEB-2012
Location: ARC DAWSON 02-19-079-14
Depth: 2085 m
Analysis
Instrument: RockEval 6
Data Processing Software: Vinci

FID hydrocarbons



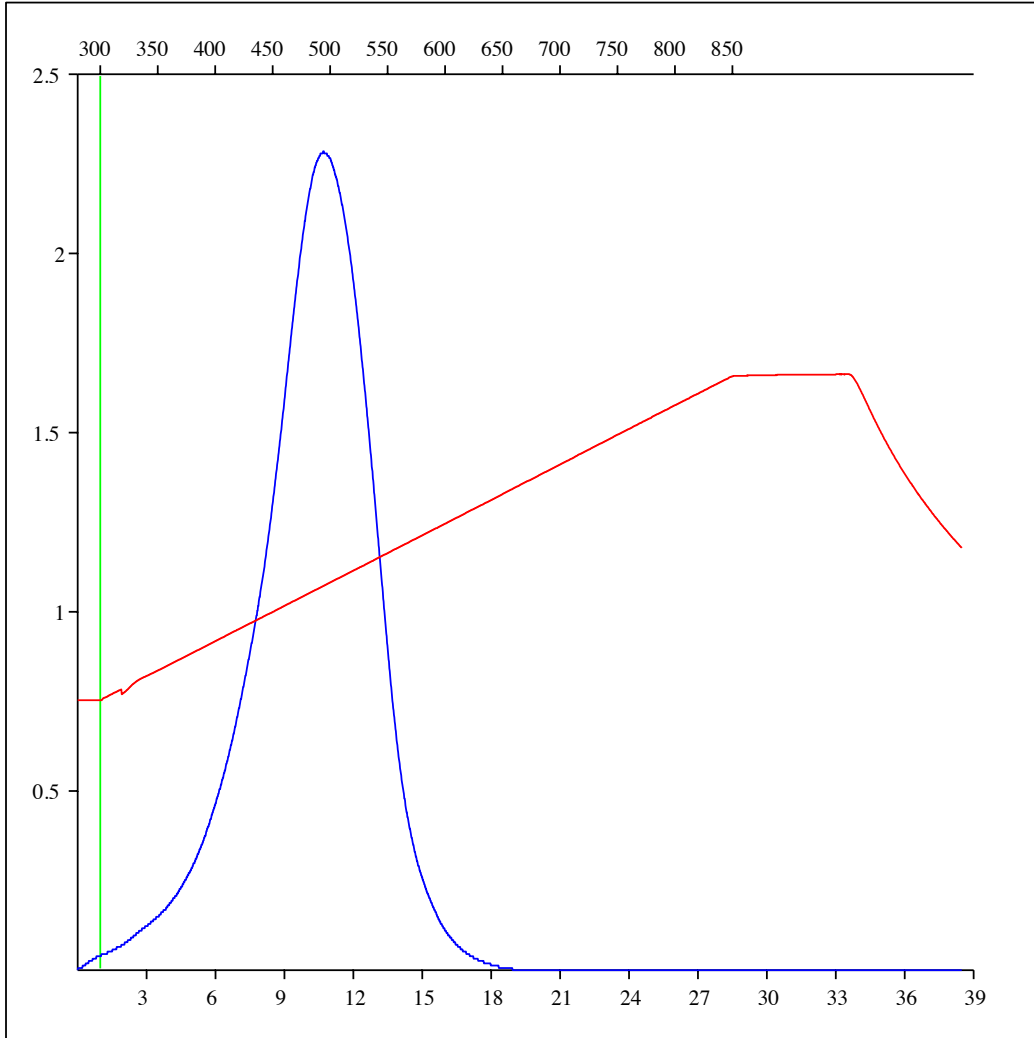
Sample: C-492845
Acquisition Date: 08-FEB-2012
Location: ARC DAWSON 02-19-079-14
Depth: 2085 m
Analysis
Instrument: RockEval 6
Data Processing Software: Vinci

Pyrolysis carbon monoxide



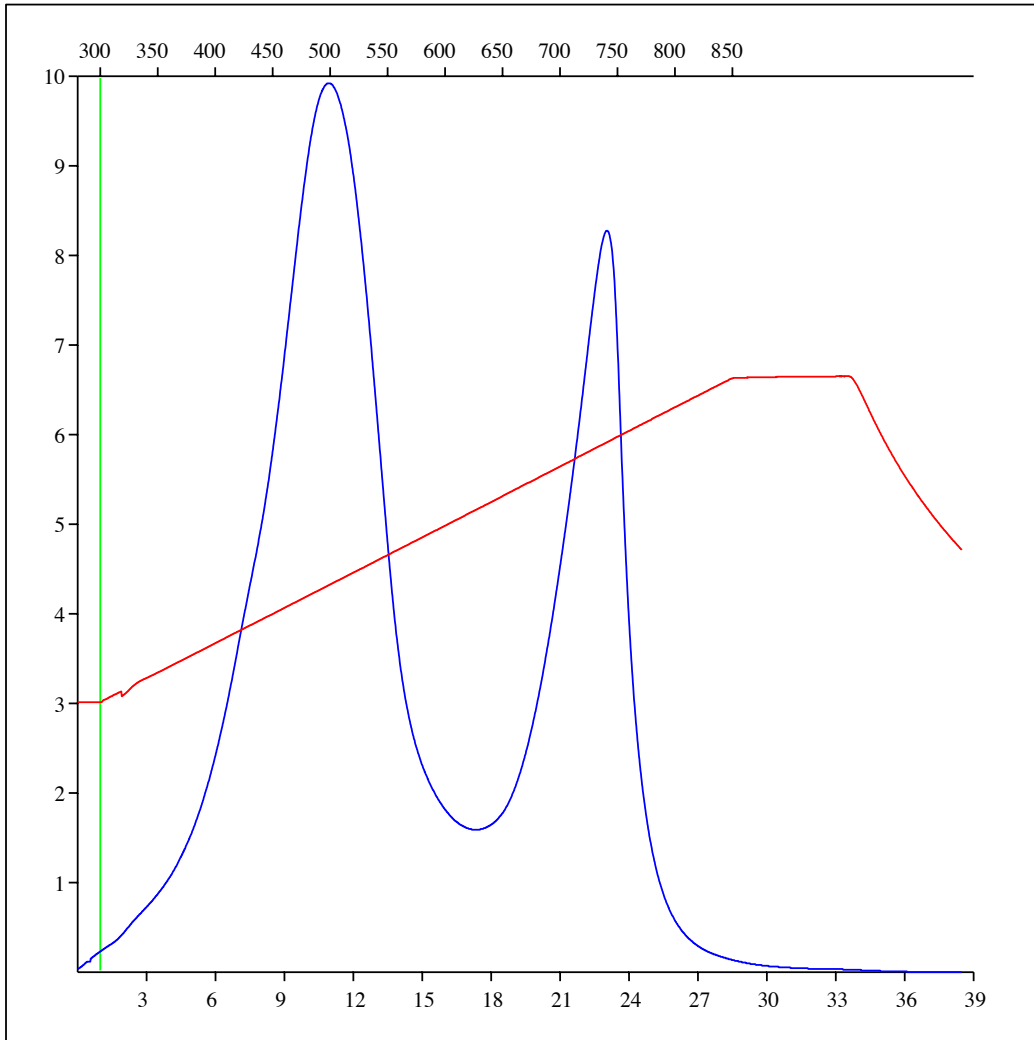
Sample: C-492845
Acquisition Date: 08-FEB-2012
Location: ARC DAWSON 02-19-079-14
Depth: 2085 m
Analysis
Instrument: RockEval 6
Data Processing Software: Vinci

Oxidation carbon monoxide



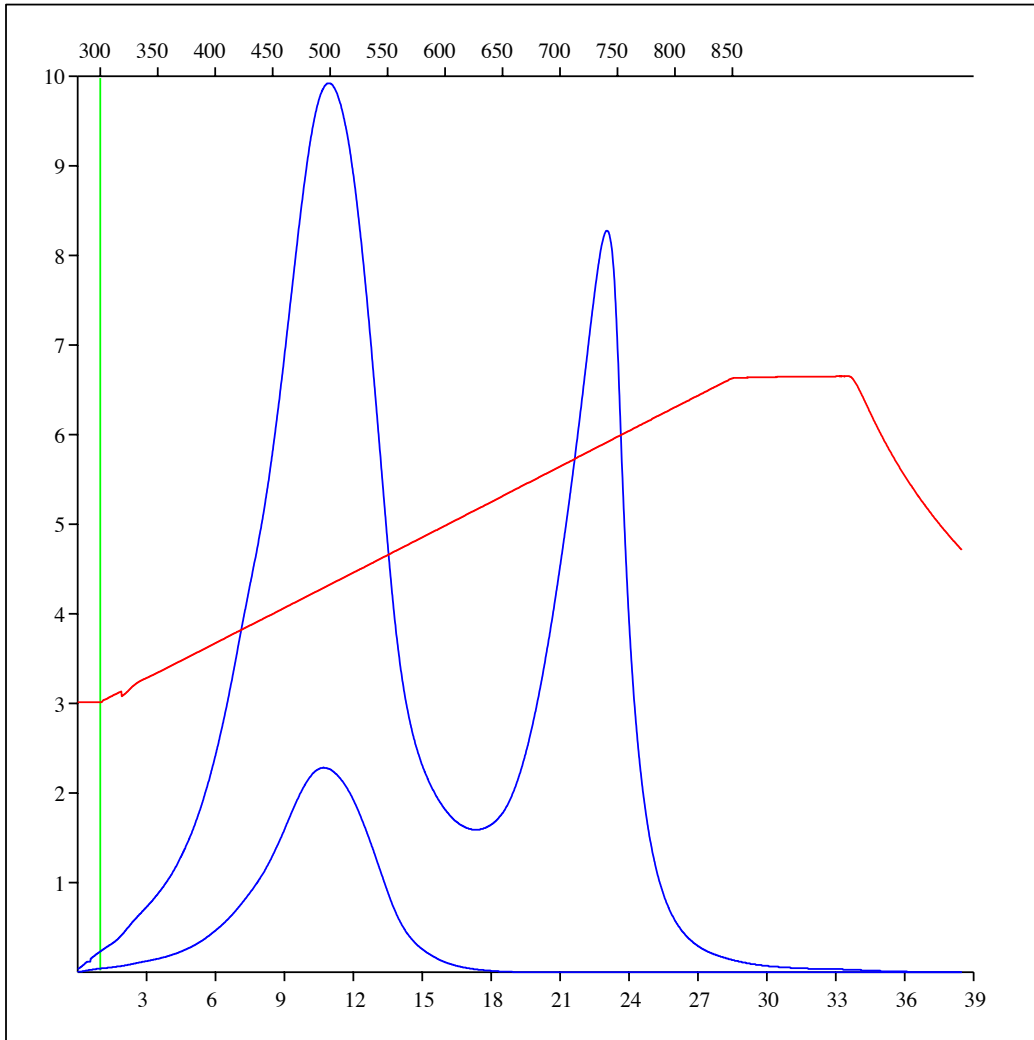
Sample: C-492845
Acquisition Date: 08-FEB-2012
Location: ARC DAWSON 02-19-079-14
Depth: 2085 m
Analysis
Instrument: RockEval 6
Data Processing Software: Vinci

Oxidation carbon dioxide



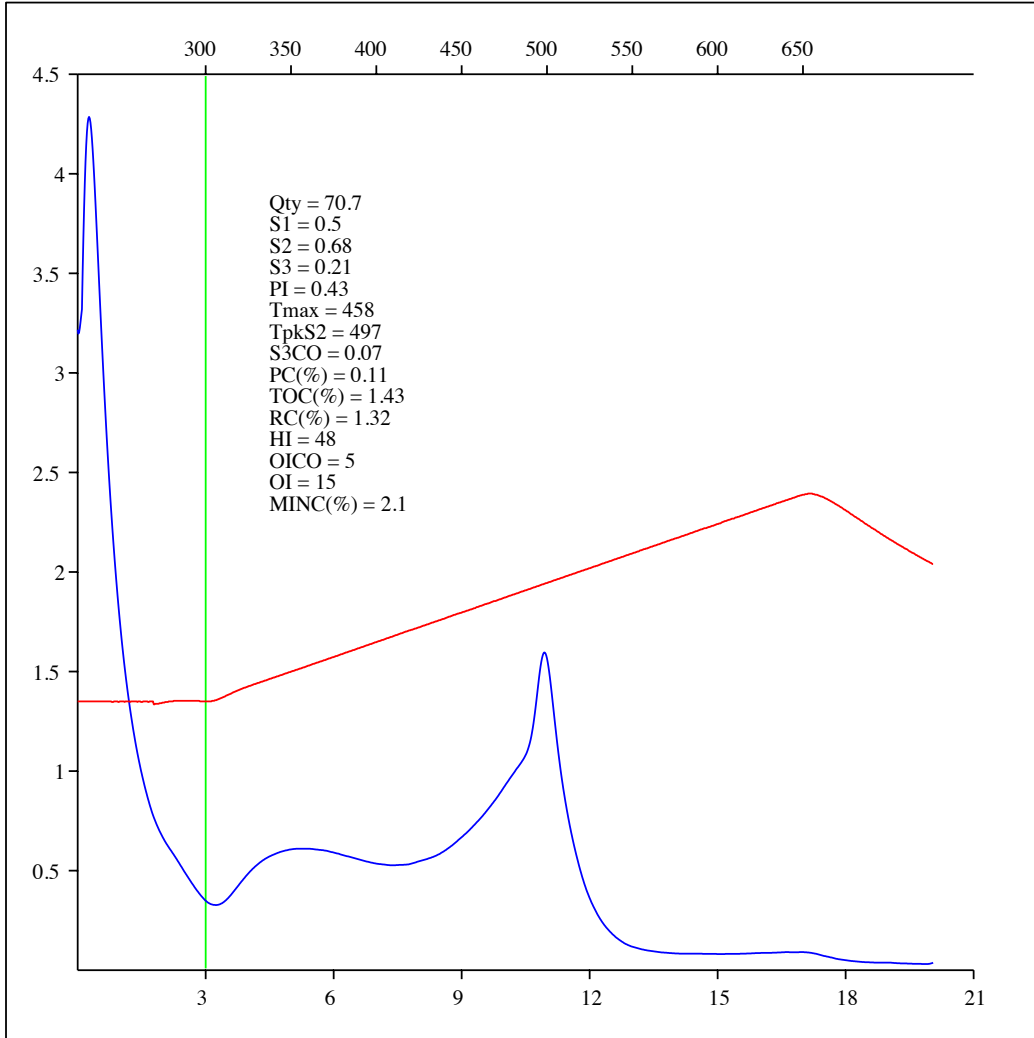
Sample: C-492845
Acquisition Date: 08-FEB-2012
Location: ARC DAWSON 02-19-079-14
Depth: 2085 m
Analysis
Instrument: RockEval 6
Data Processing Software: Vinci

Oxidation carbon monoxide & carbon dioxide



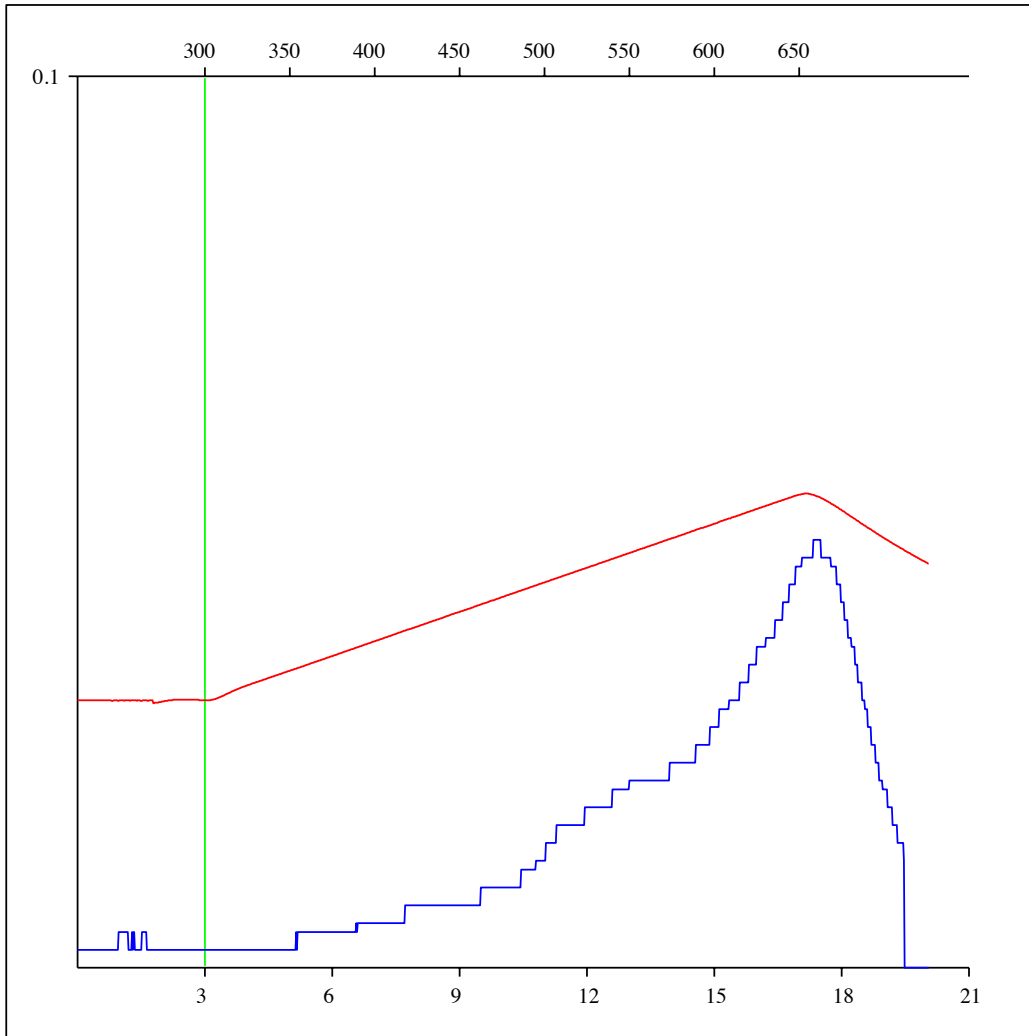
Sample: C-492846
Acquisition Date: 08-FEB-2012
Location: ARC DAWSON 02-19-079-14
Depth: 2048 m
Analysis
Instrument: RockEval 6
Data Processing Software: Vinci

FID hydrocarbons



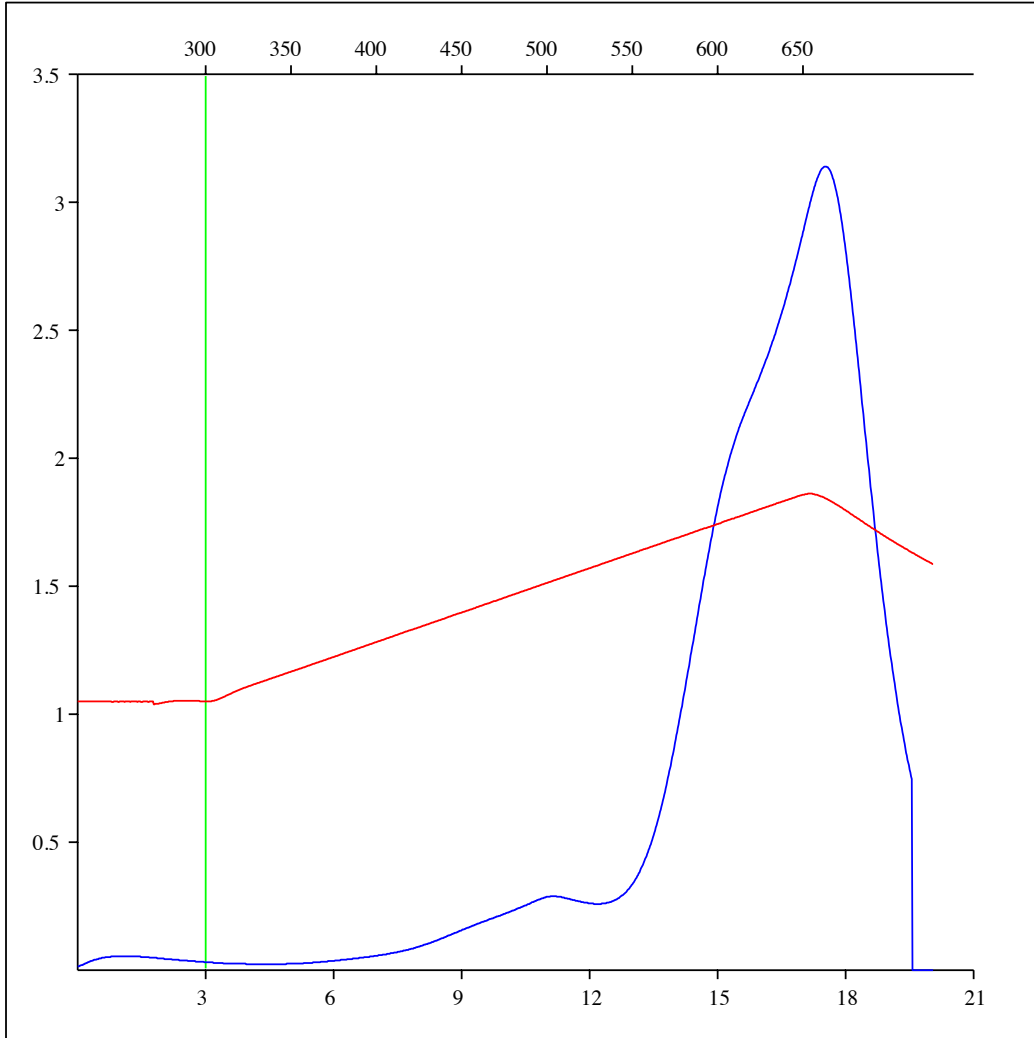
Sample: C-492846
Acquisition Date: 08-FEB-2012
Location: ARC DAWSON 02-19-079-14
Depth: 2048 m
Analysis
Instrument: RockEval 6
Data Processing Software: Vinci

Pyrolysis carbon monoxide



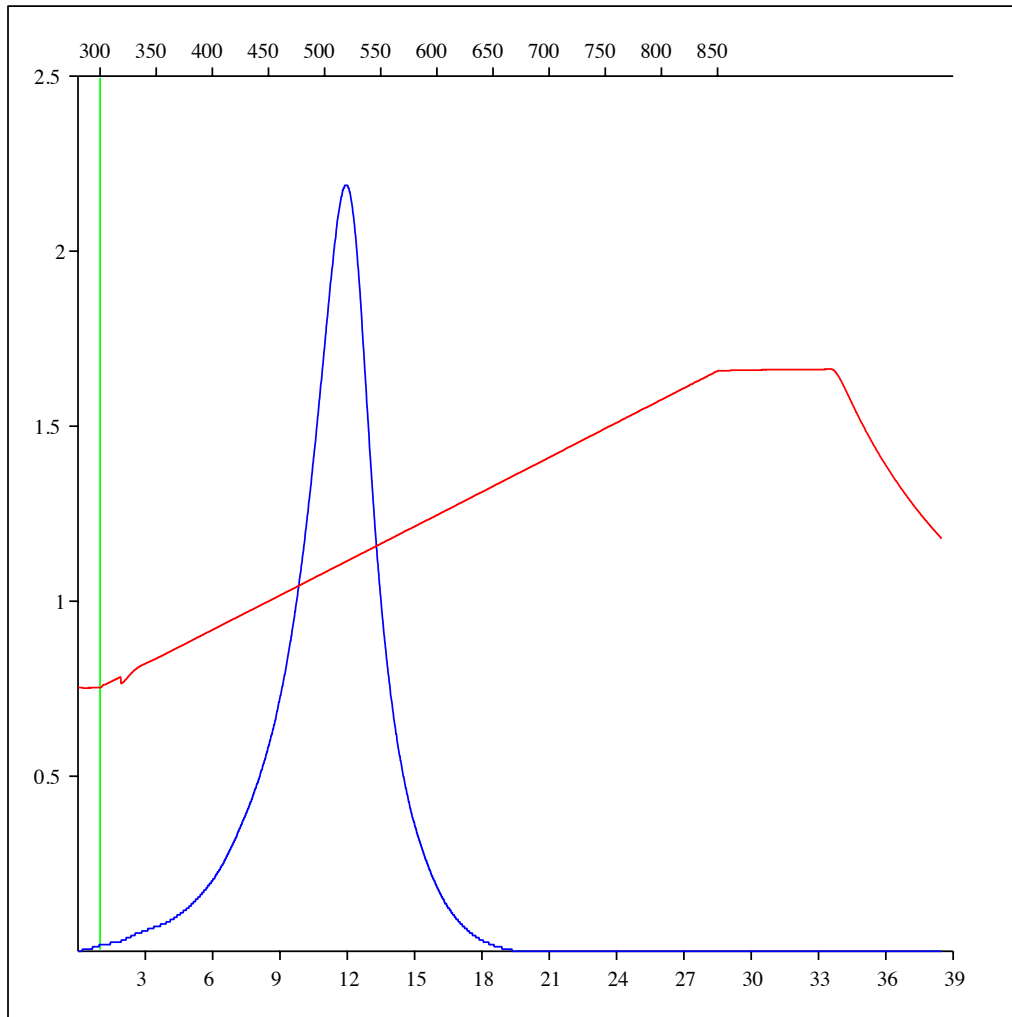
Sample: C-492846
Acquisition Date: 08-FEB-2012
Location: ARC DAWSON 02-19-079-14
Depth: 2048 m
Analysis
Instrument: RockEval 6
Data Processing Software: Vinci

Pyrolysis carbon dioxide



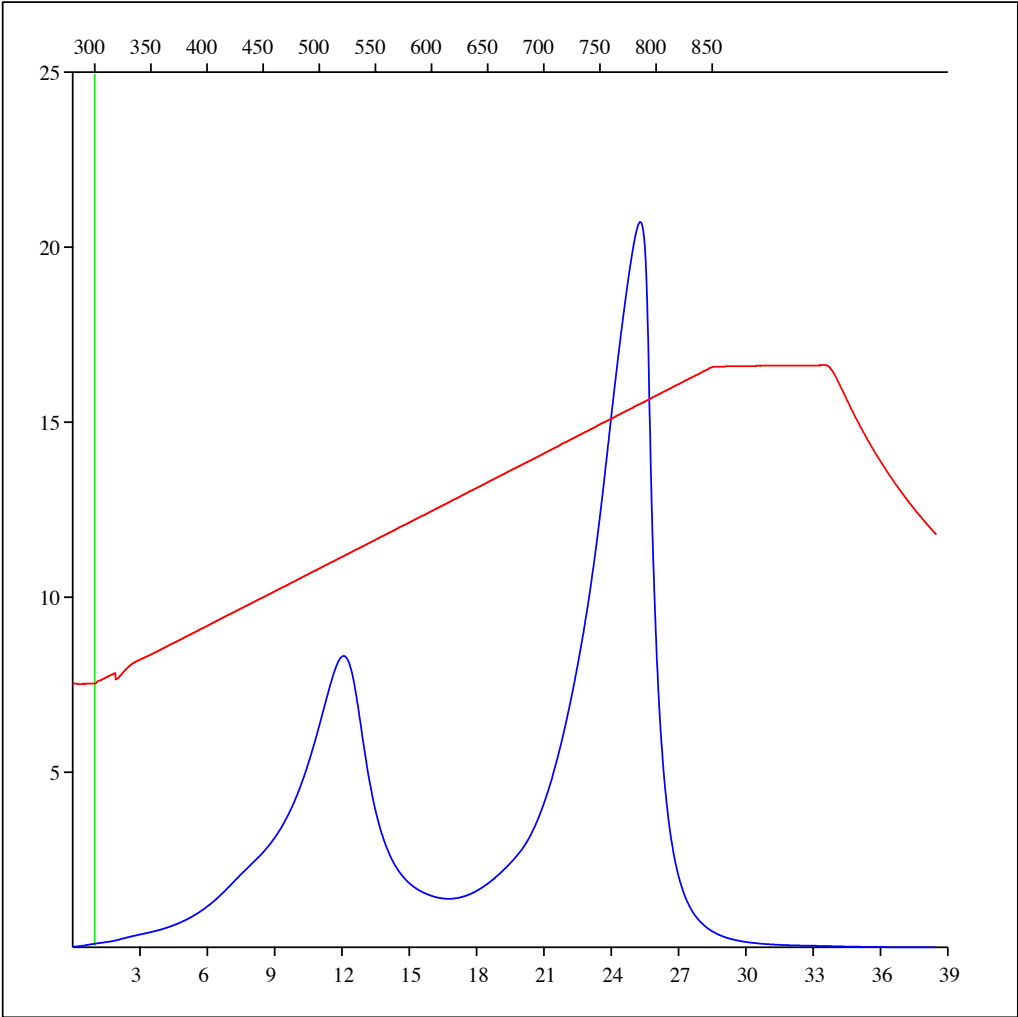
Sample: C-492846
Acquisition Date: 08-FEB-2012
Location: ARC DAWSON 02-19-079-14
Depth: 2048 m
Analysis
Instrument: RockEval 6
Data Processing Software: Vinci

Oxidation carbon monoxide



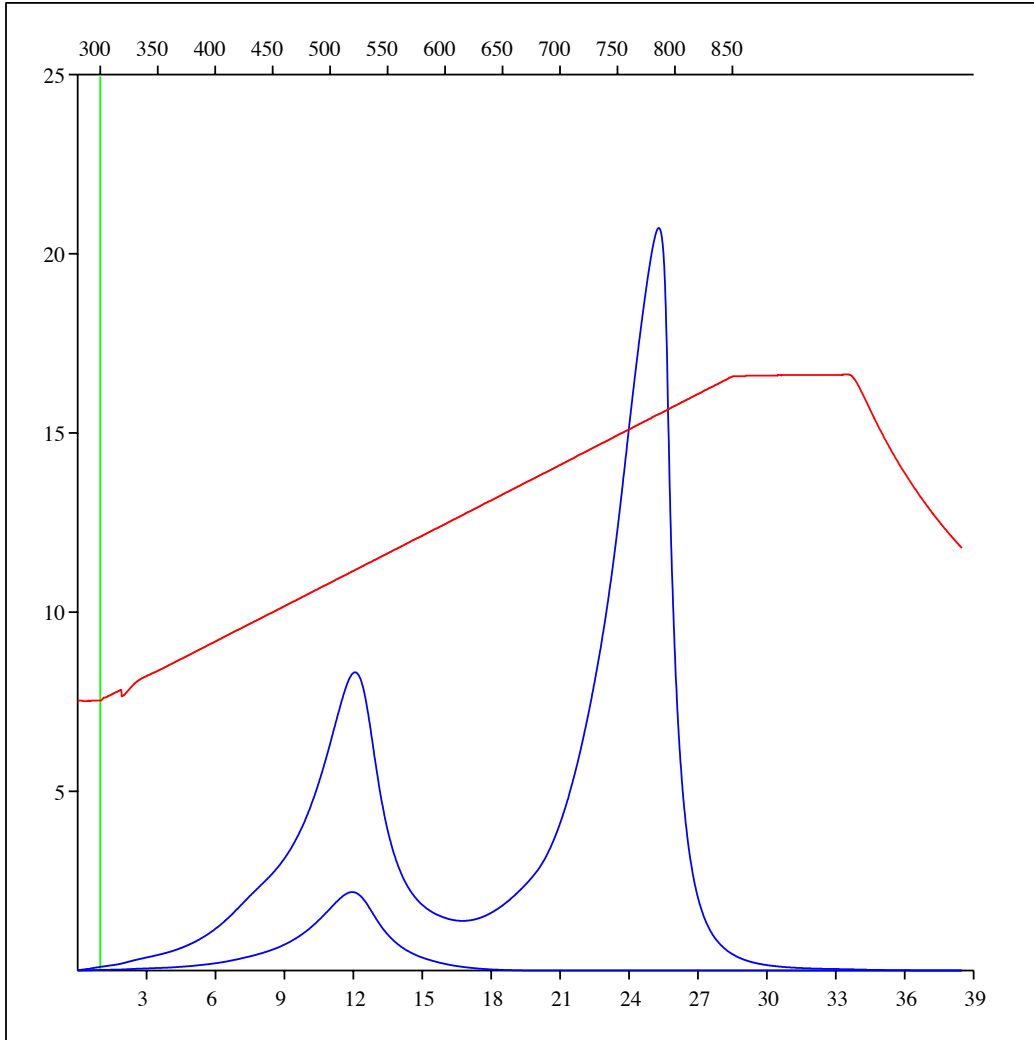
Sample: C-492846
Acquisition Date: 08-FEB-2012
Location: ARC DAWSON 02-19-079-14
Depth: 2048 m
Analysis
Instrument: RockEval 6
Data Processing Software: Vinci

Oxidation carbon dioxide



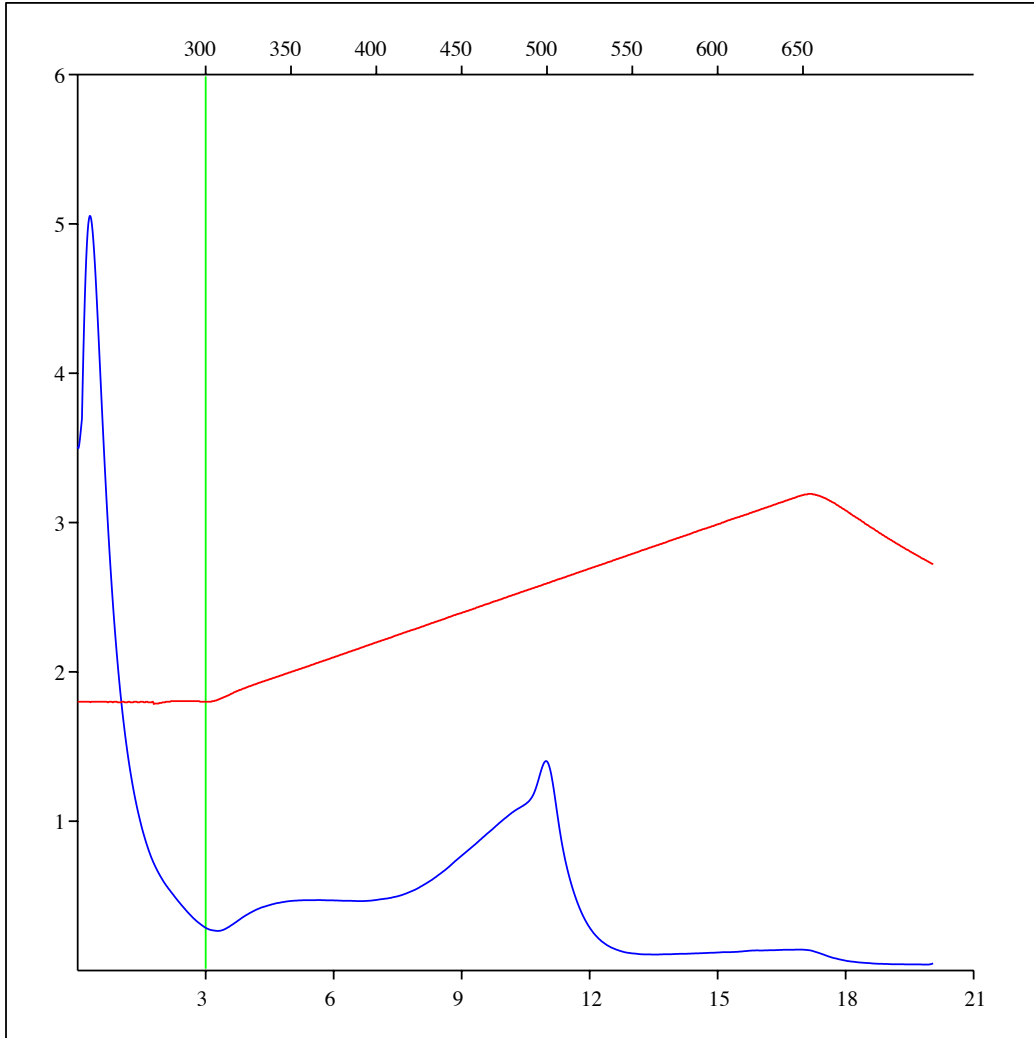
Sample: C-492846
Acquisition Date: 08-FEB-2012
Location: ARC DAWSON 02-19-079-14
Depth: 2048 m
Analysis
Instrument: RockEval 6
Data Processing Software: Vinci

Oxidation carbon monoxide & carbon dioxide



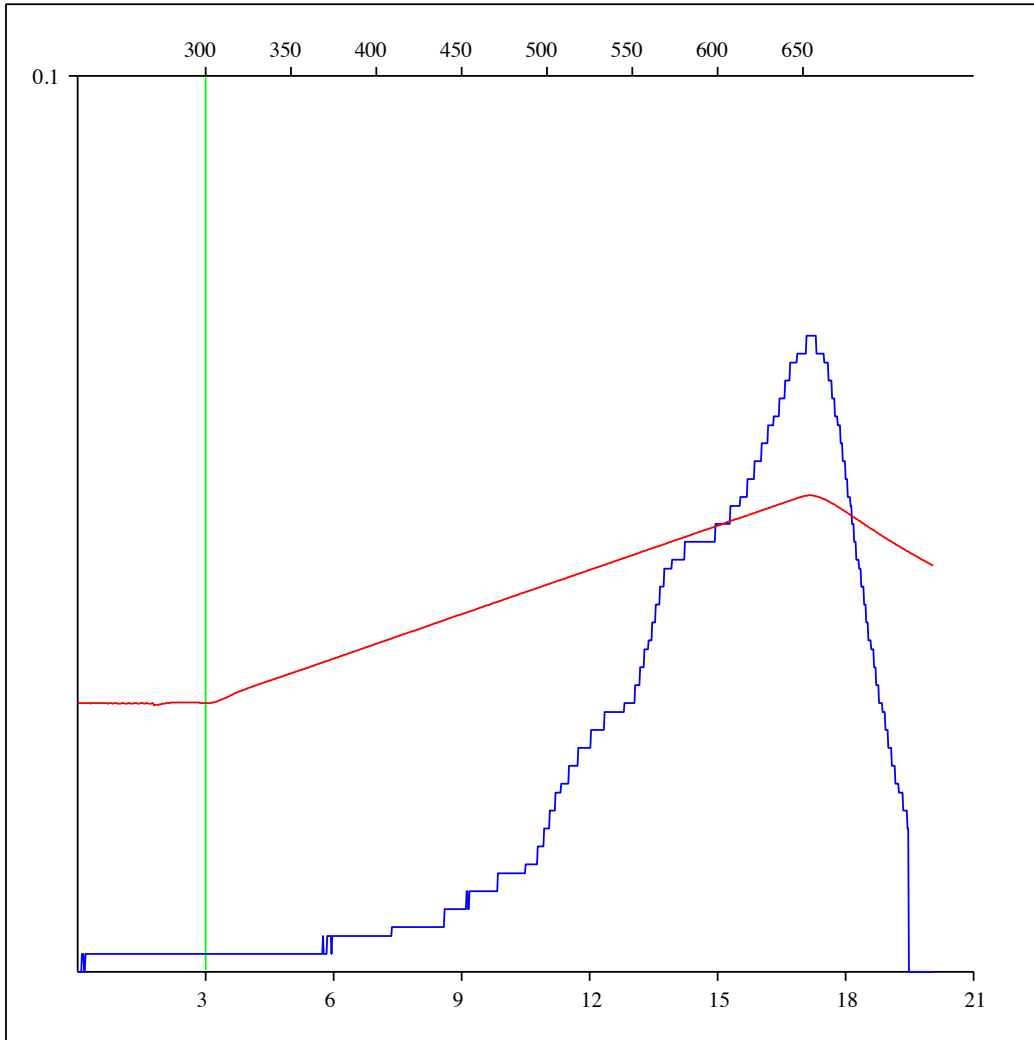
Sample: C-492847
Acquisition Date: 08-FEB-2012
Location: ARC DAWSON 02-19-079-14
Depth: 2069.5 m
Analysis
Instrument: RockEval 6
Data Processing Software: Vinci

FID hydrocarbons



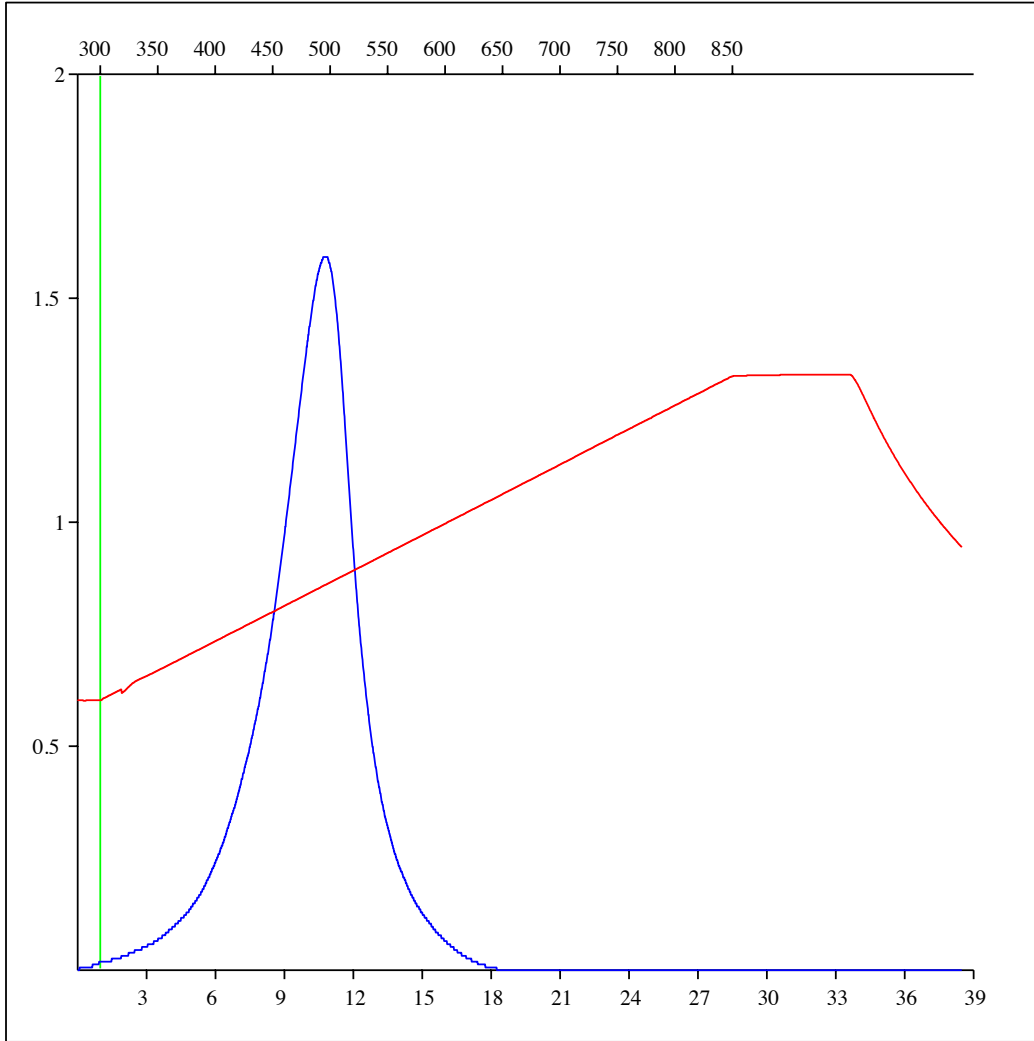
Sample: C-492847
Acquisition Date: 08-FEB-2012
Location: ARC DAWSON 02-19-079-14
Depth: 2069.5 m
Analysis
Instrument: RockEval 6
Data Processing Software: Vinci

Pyrolysis carbon monoxide



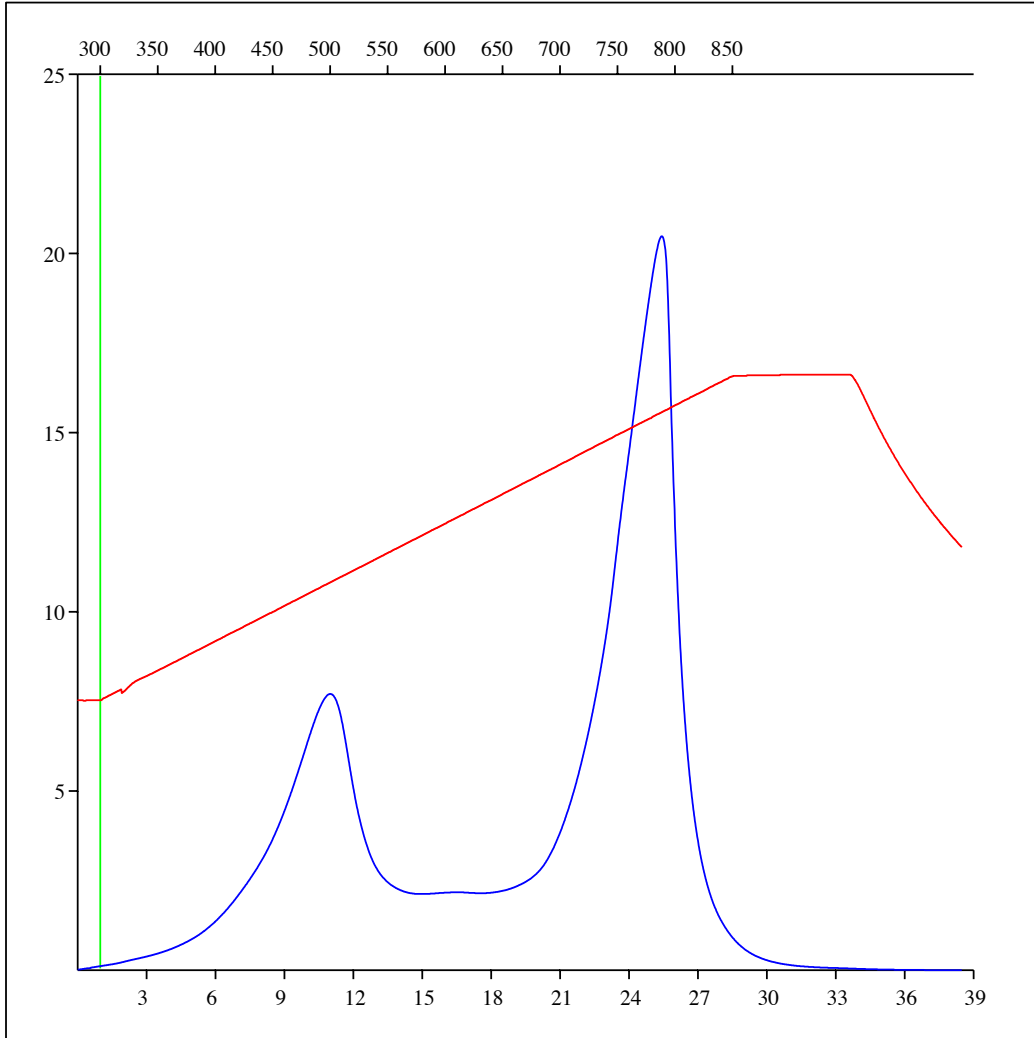
Sample: C-492847
Acquisition Date: 08-FEB-2012
Location: ARC DAWSON 02-19-079-14
Depth: 2069.5 m
Analysis
Instrument: RockEval 6
Data Processing Software: Vinci

Oxidation carbon monoxide



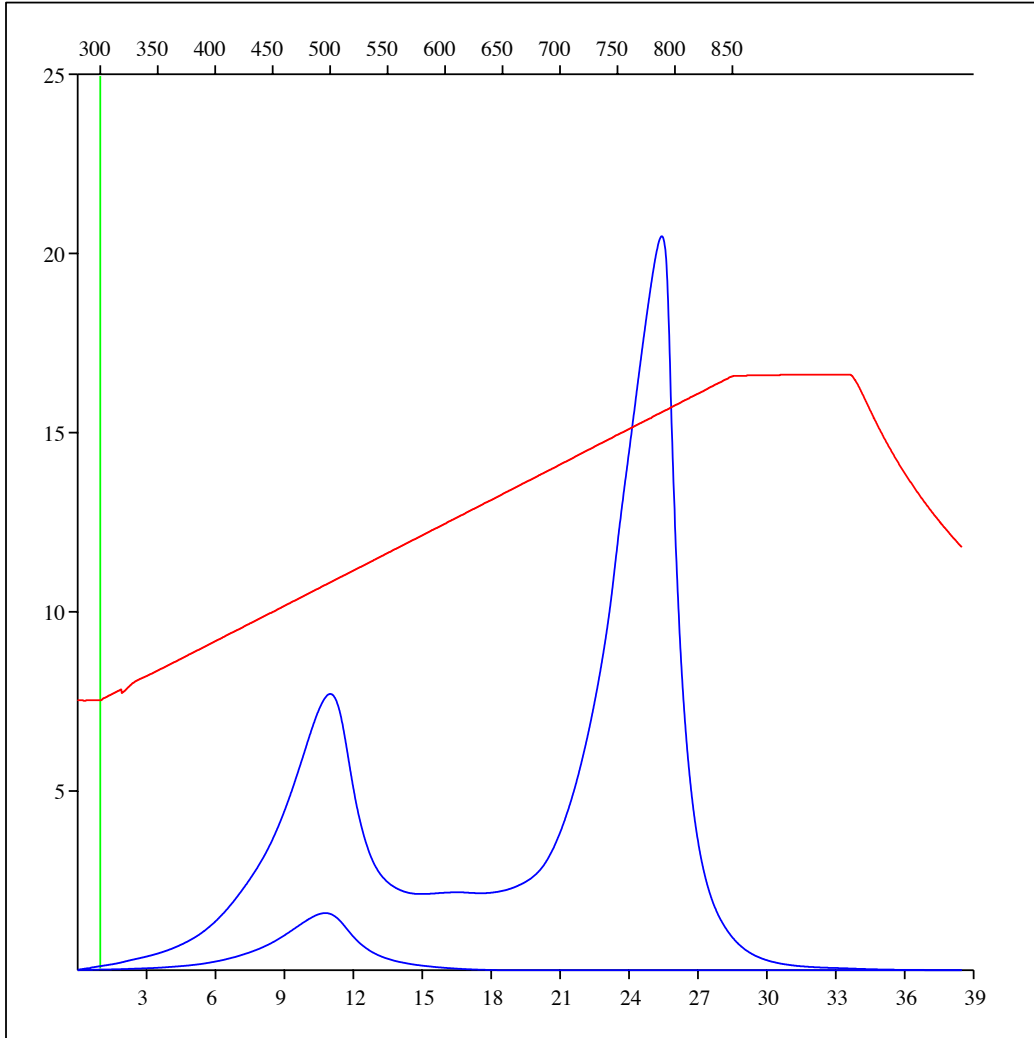
Sample: C-492847
Acquisition Date: 08-FEB-2012
Location: ARC DAWSON 02-19-079-14
Depth: 2069.5 m
Analysis
Instrument: RockEval 6
Data Processing Software: Vinci

Oxidation carbon dioxide



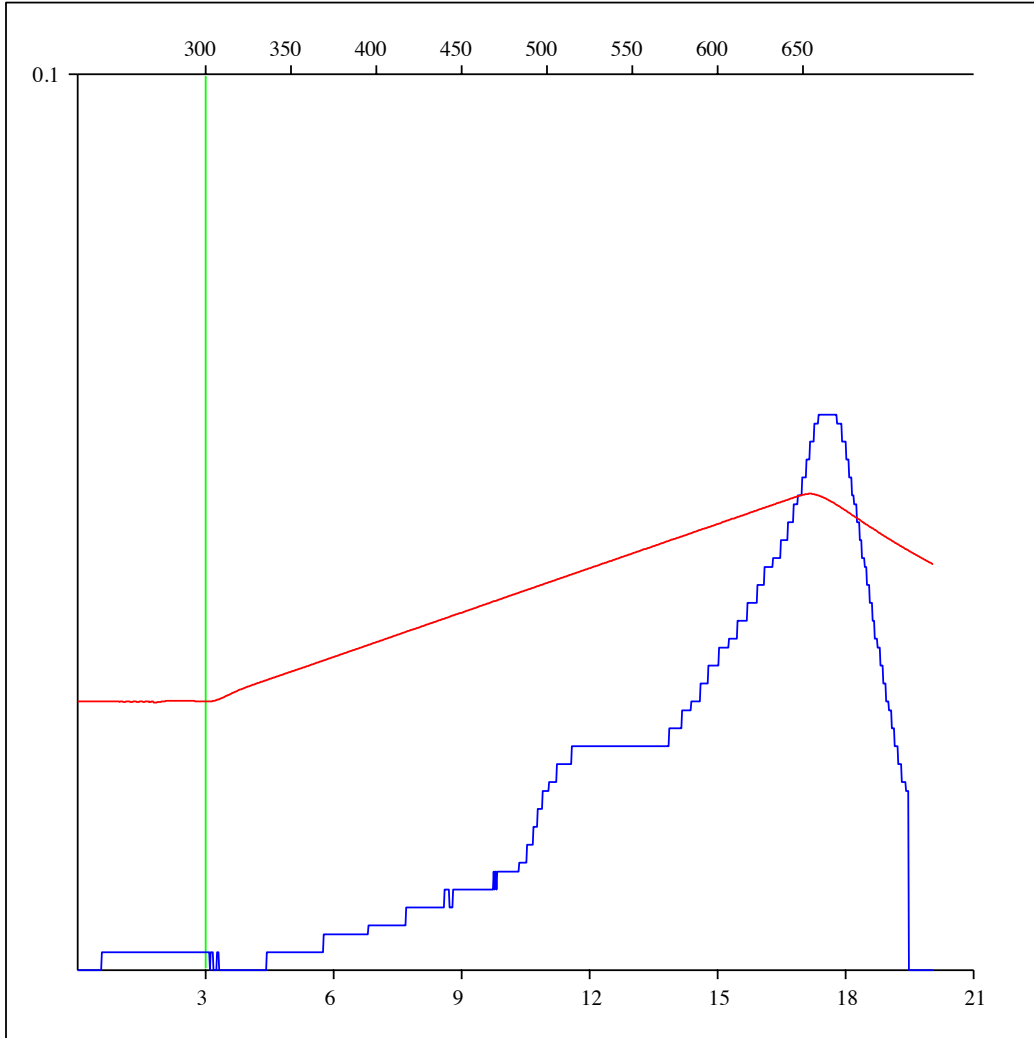
Sample: C-492847
Acquisition Date: 08-FEB-2012
Location: ARC DAWSON 02-19-079-14
Depth: 2069.5 m
Analysis
Instrument: RockEval 6
Data Processing Software: Vinci

Oxidation carbon monoxide & carbon dioxide



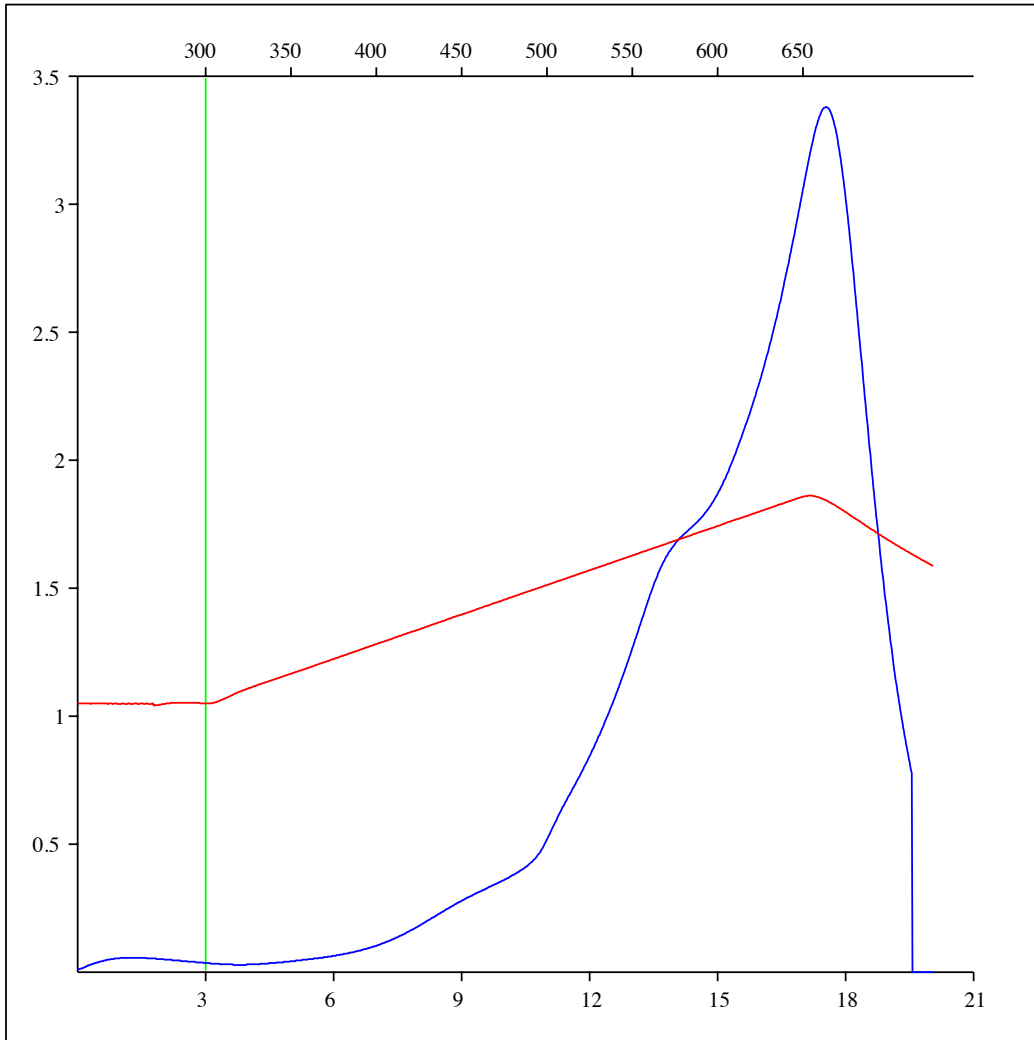
Sample: C-492848
Acquisition Date: 08-FEB-2012
Location: ARC DAWSON 11-04-079-14
Depth: 2064.1 m
Analysis
Instrument: RockEval 6
Data Processing Software: Vinci

Pyrolysis carbon monoxide



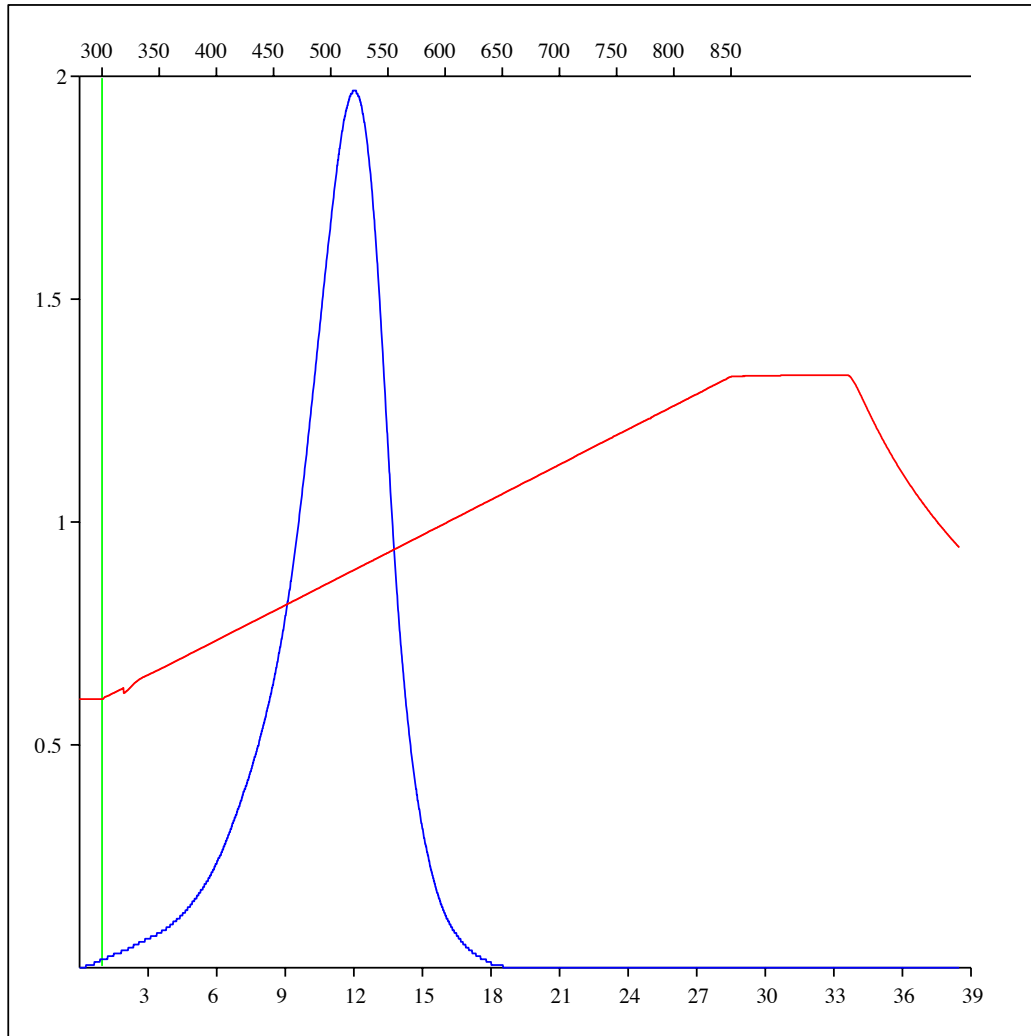
Sample: C-492847
Acquisition Date: 08-FEB-2012
Location: ARC DAWSON 02-19-079-14
Depth: 2069.5 m
Analysis
Instrument: RockEval 6
Data Processing Software: Vinci

Pyrolysis carbon dioxide



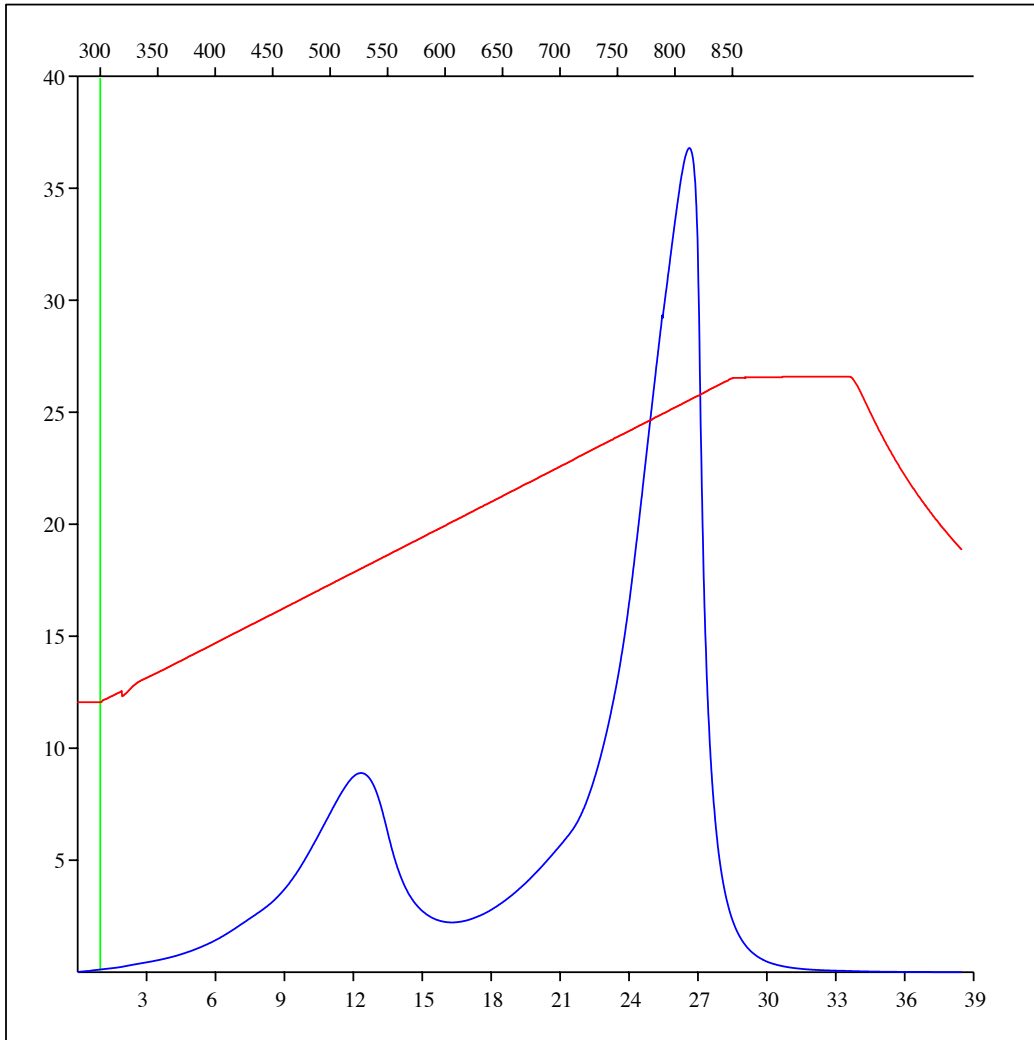
Sample: C-492848
Acquisition Date: 08-FEB-2012
Location: ARC DAWSON 11-04-079-14
Depth: 2064.1 m
Analysis
Instrument: RockEval 6
Data Processing Software: Vinci

Oxidation carbon monoxide



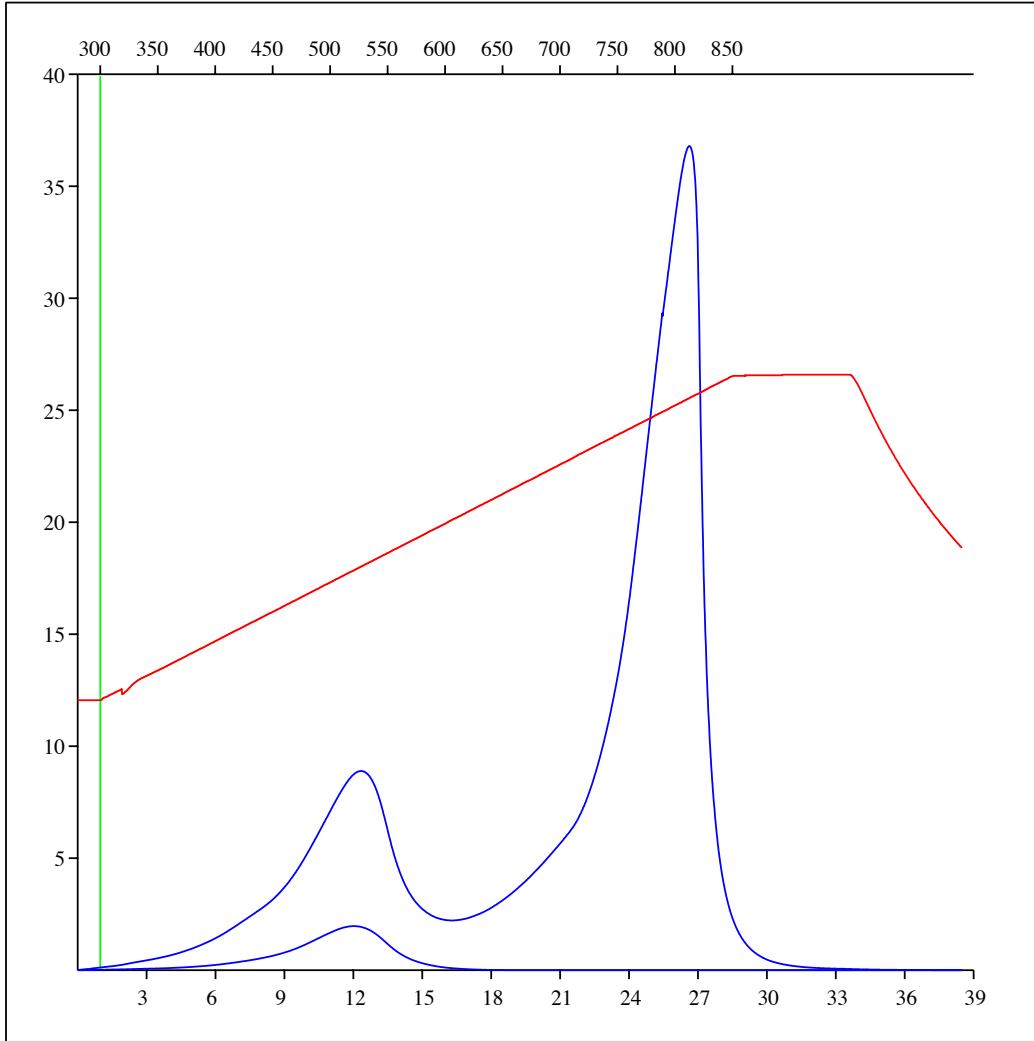
Sample: C-492848
Acquisition Date: 08-FEB-2012
Location: ARC DAWSON 11-04-079-14
Depth: 2064.1 m
Analysis
Instrument: RockEval 6
Data Processing Software: Vinci

Oxidation carbon dioxide



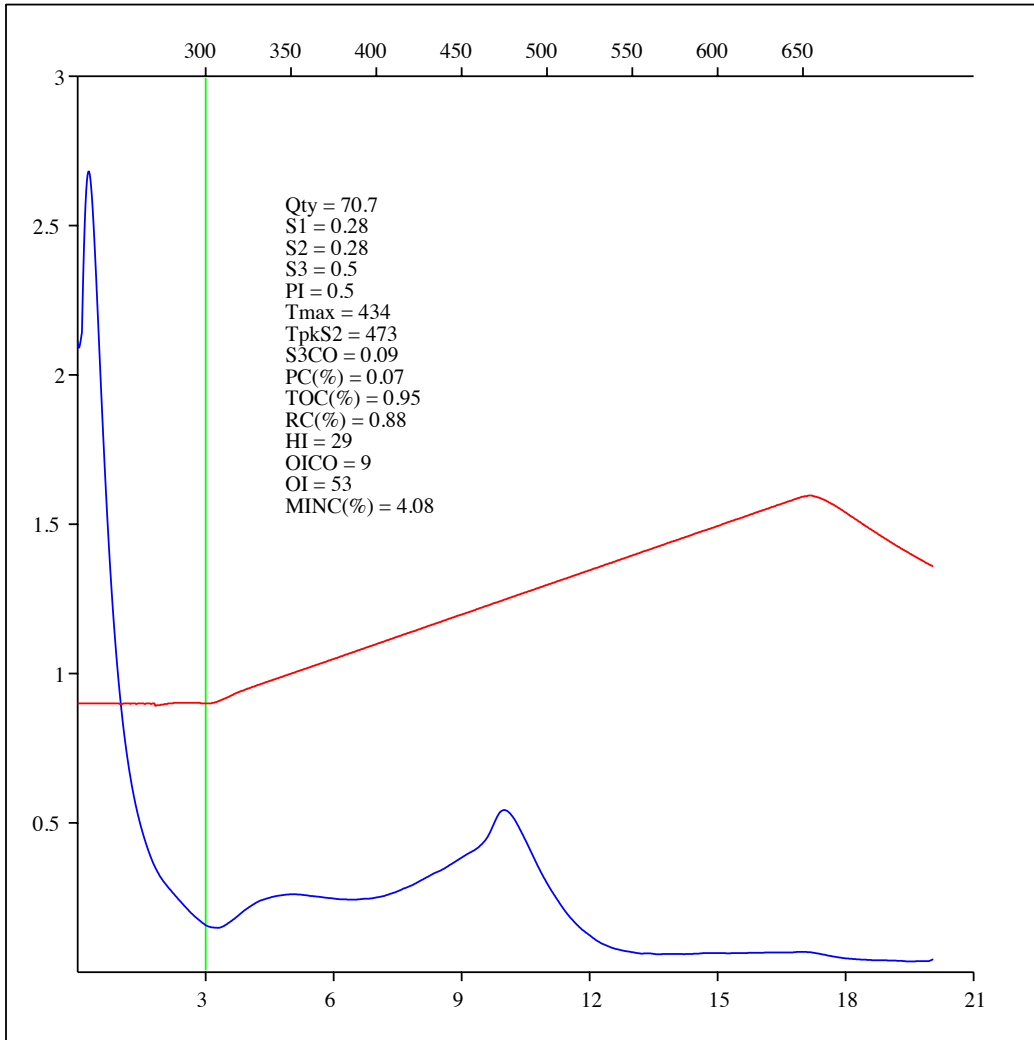
Sample: C-492848
Acquisition Date: 08-FEB-2012
Location: ARC DAWSON 11-04-079-14
Depth: 2064.1 m
Analysis
Instrument: RockEval 6
Data Processing Software: Vinci

Oxidation carbon monoxide & carbon dioxide



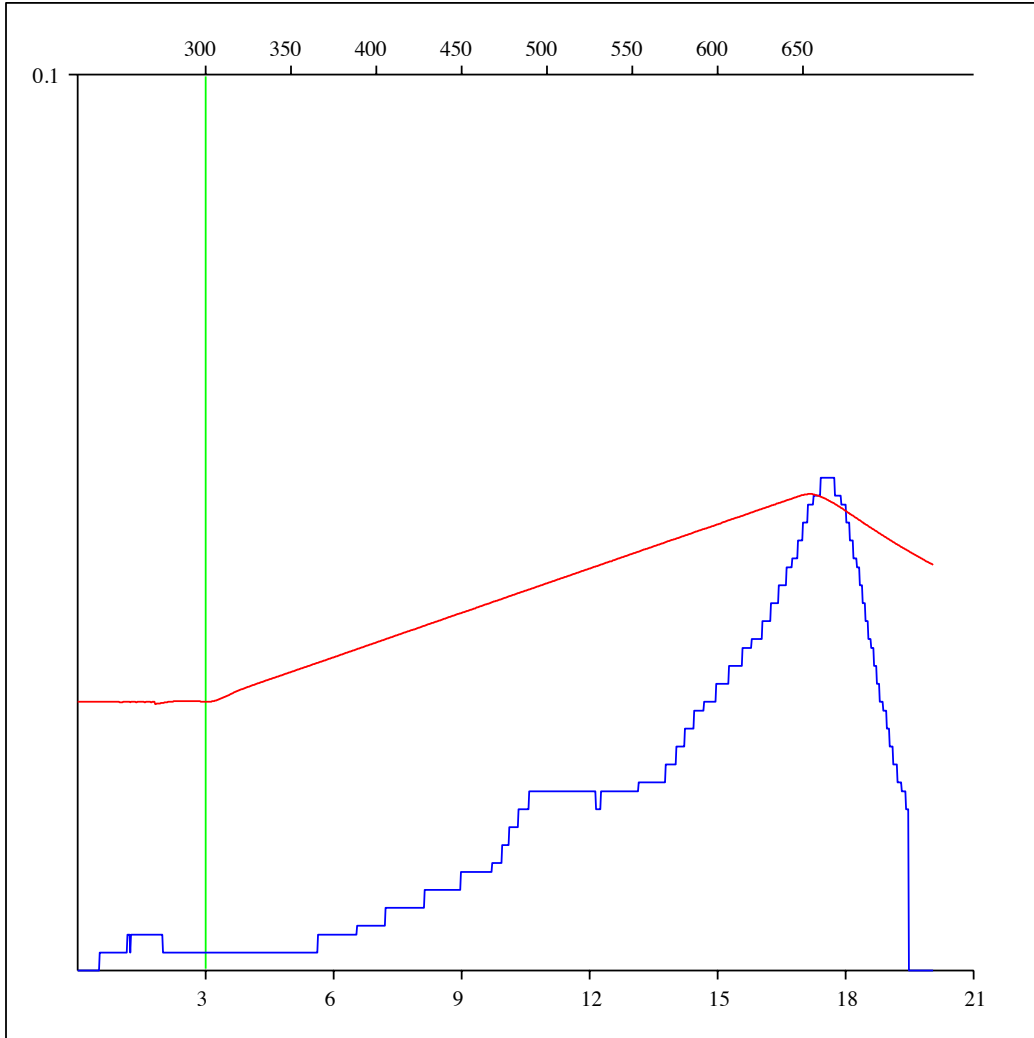
Sample: C-492849
Acquisition Date: 08-FEB-2012
Location: ARC DAWSON 11-04-079-14
Depth: 2073.2 m
Analysis
Instrument: RockEval 6
Data Processing Software: Vinci

FID hydrocarbons



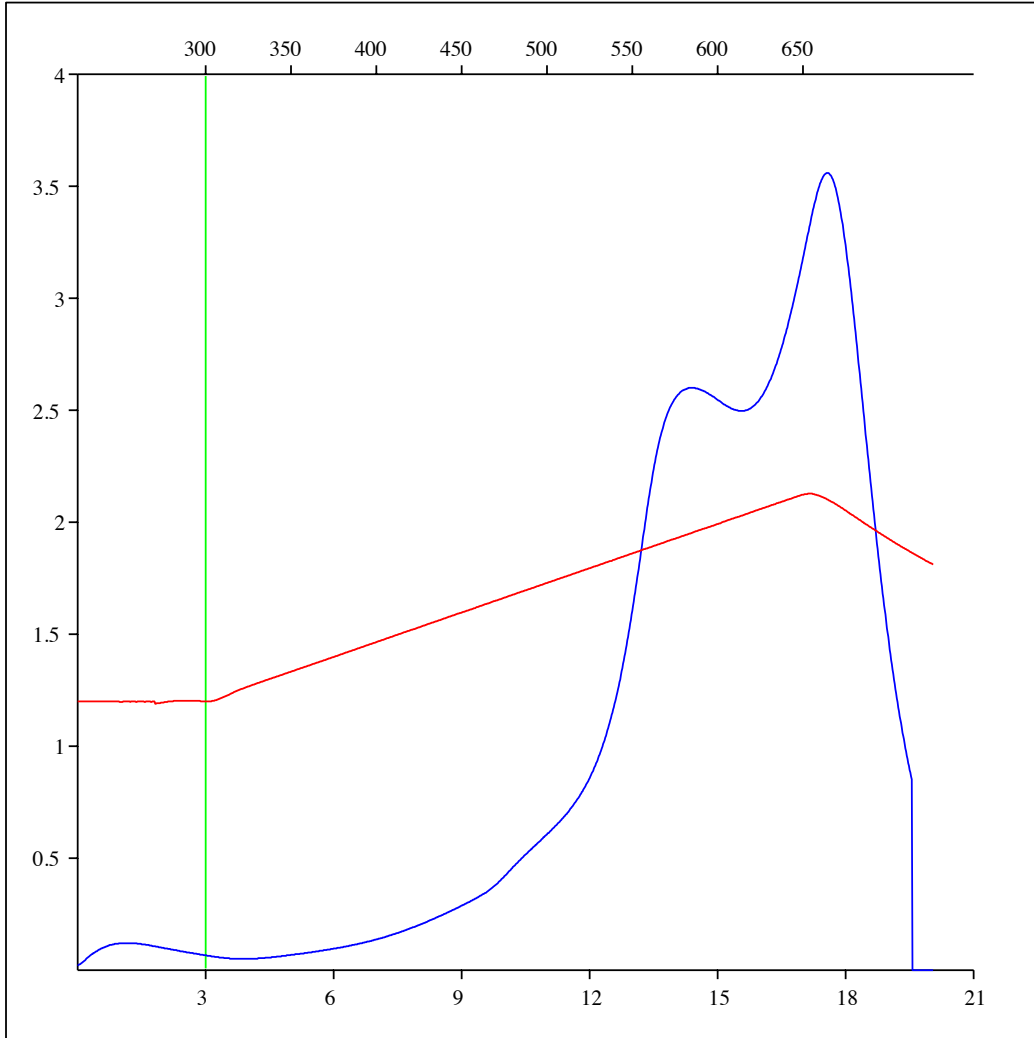
Sample: C-492849
Acquisition Date: 08-FEB-2012
Location: ARC DAWSON 11-04-079-14
Depth: 2073.2 m
Analysis
Instrument: RockEval 6
Data Processing Software: Vinci

Pyrolysis carbon monoxide



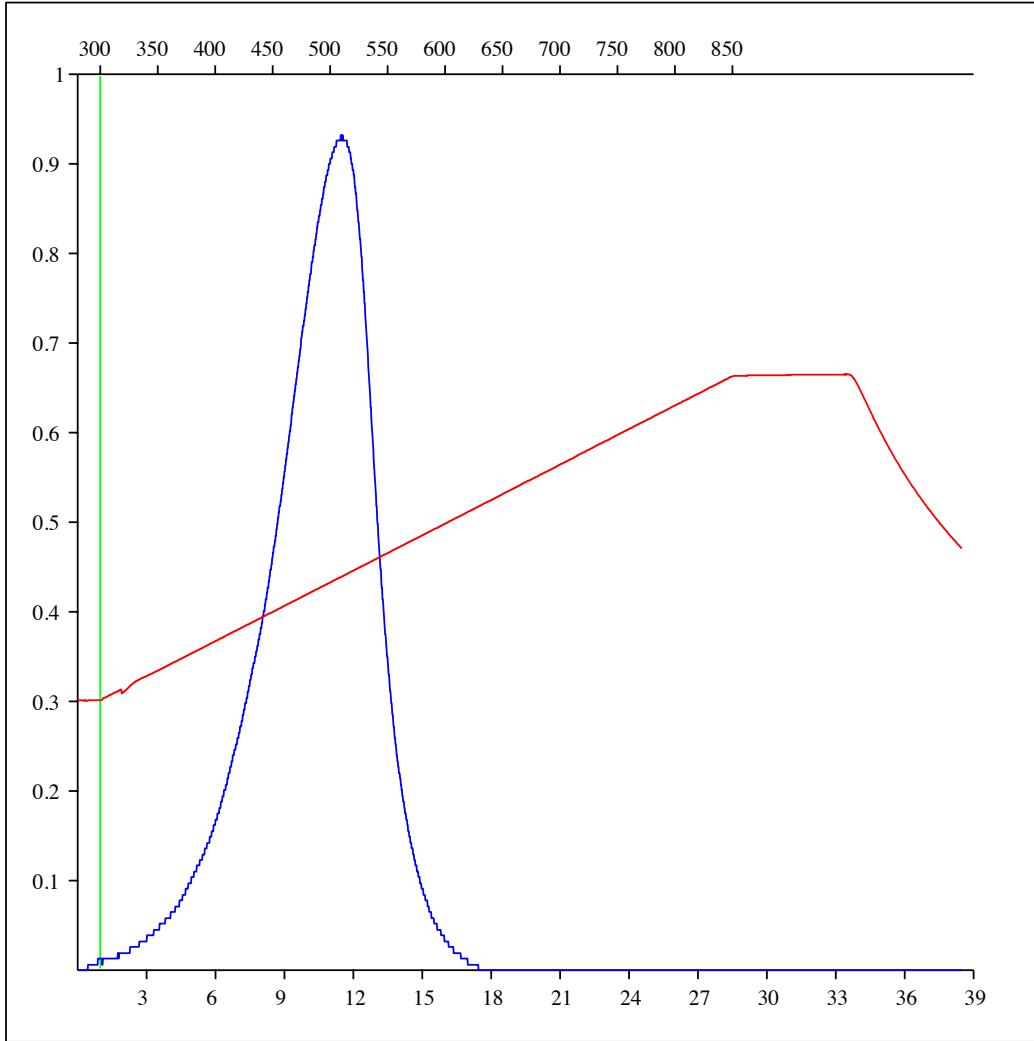
Sample: C-492849
Acquisition Date: 08-FEB-2012
Location: ARC DAWSON 11-04-079-14
Depth: 2073.2 m
Analysis
Instrument: RockEval 6
Data Processing Software: Vinci

Pyrolysis carbon dioxide



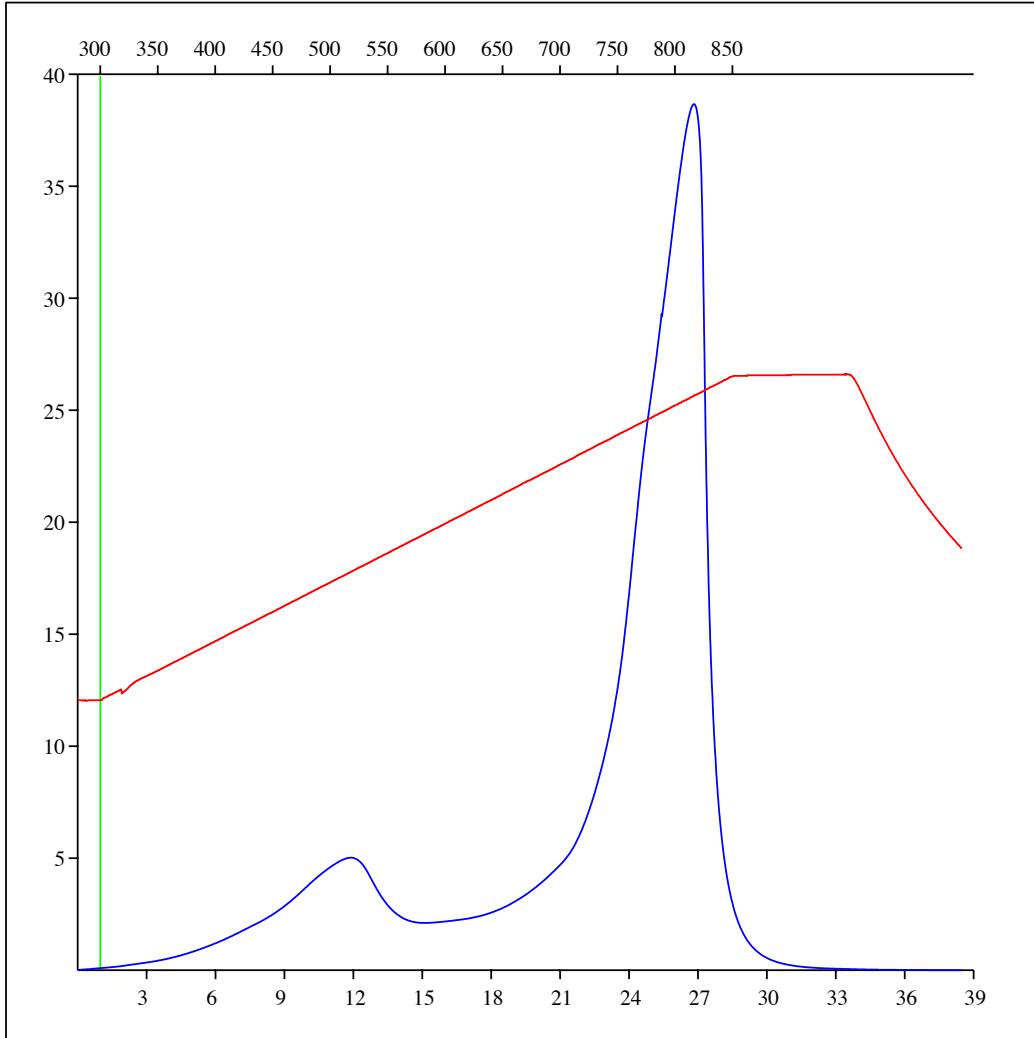
Sample: C-492849
Acquisition Date: 08-FEB-2012
Location: ARC DAWSON 11-04-079-14
Depth: 2073.2 m
Analysis
Instrument: RockEval 6
Data Processing Software: Vinci

Oxidation carbon monoxide



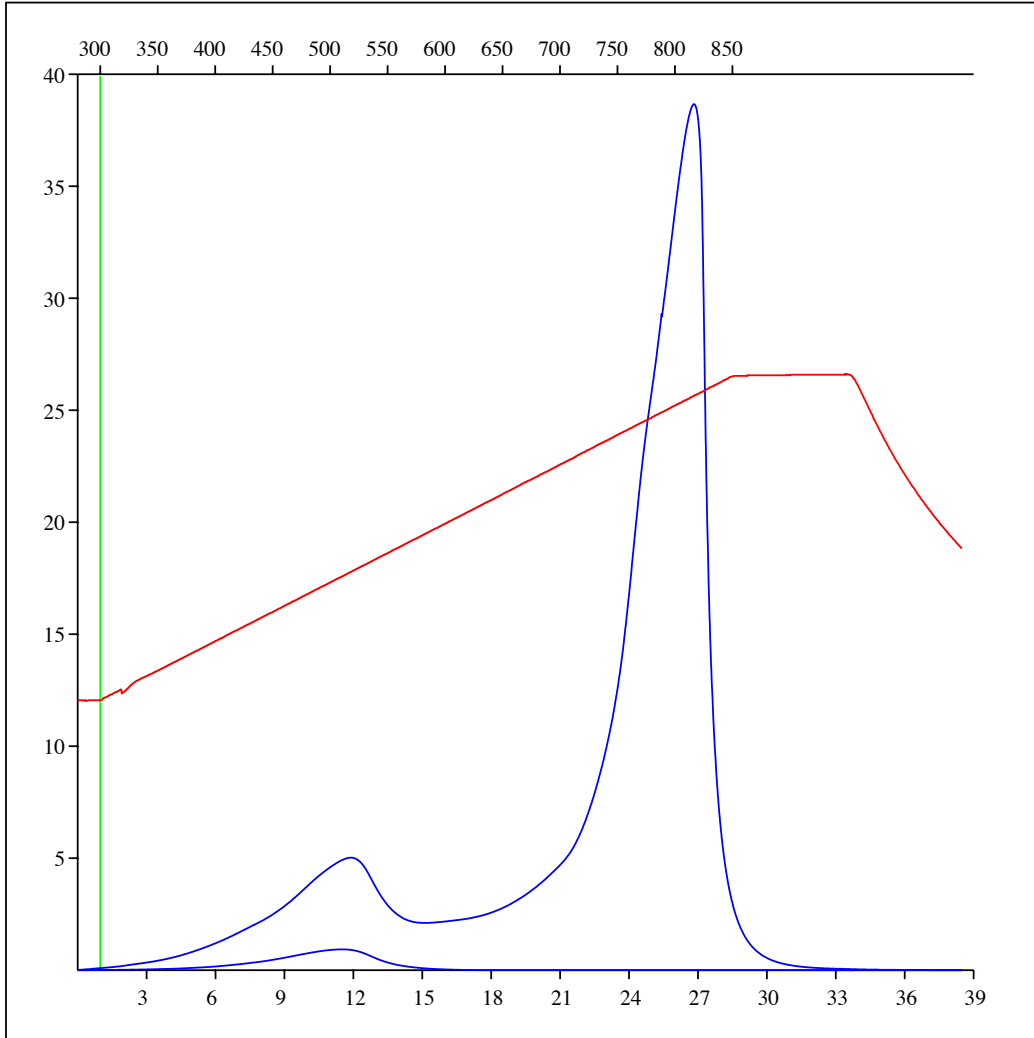
Sample: C-492849
Acquisition Date: 08-FEB-2012
Location: ARC DAWSON 11-04-079-14
Depth: 2073.2 m
Analysis
Instrument: RockEval 6
Data Processing Software: Vinci

Oxidation carbon dioxide



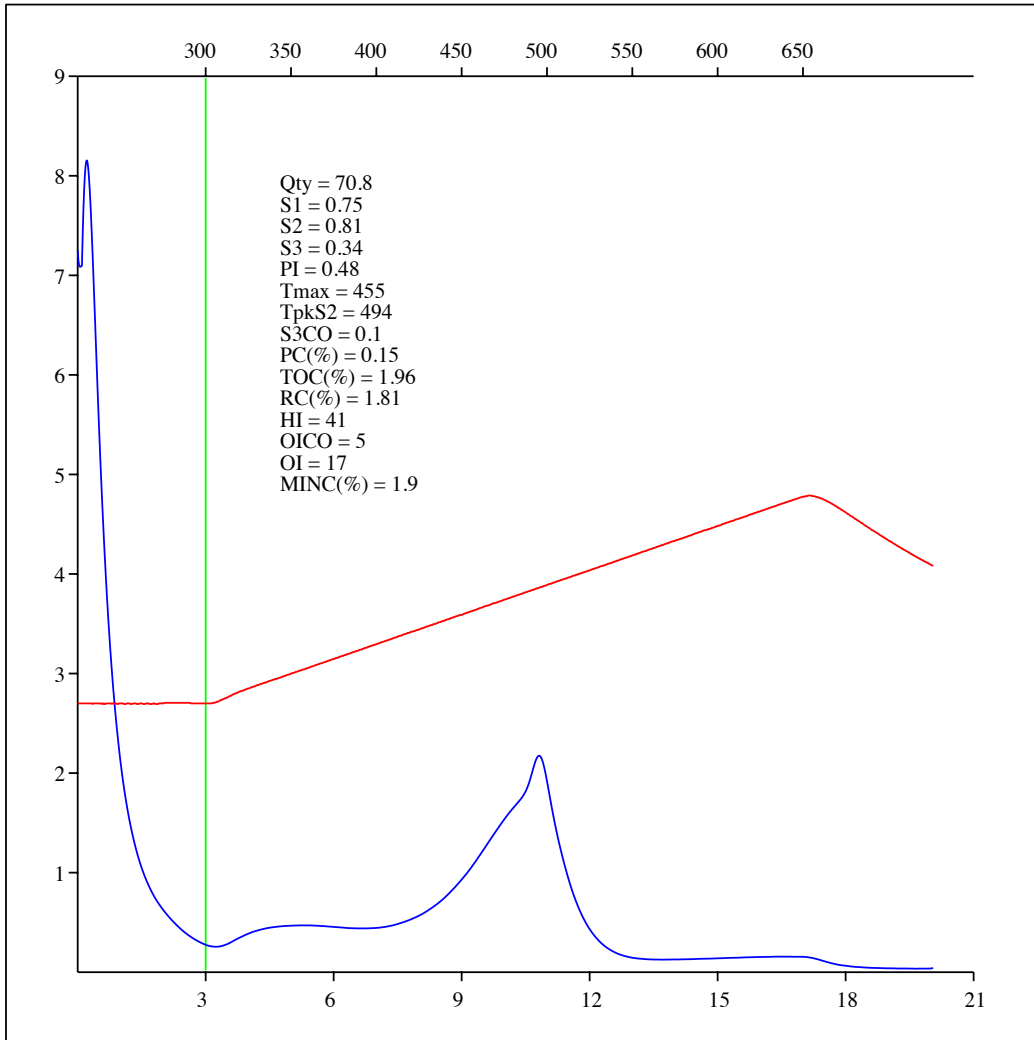
Sample: C-492849
Acquisition Date: 08-FEB-2012
Location: ARC DAWSON 11-04-079-14
Depth: 2073.2 m
Analysis
Instrument: RockEval 6
Data Processing Software: Vinci

Oxidation carbon monoxide & carbon dioxide



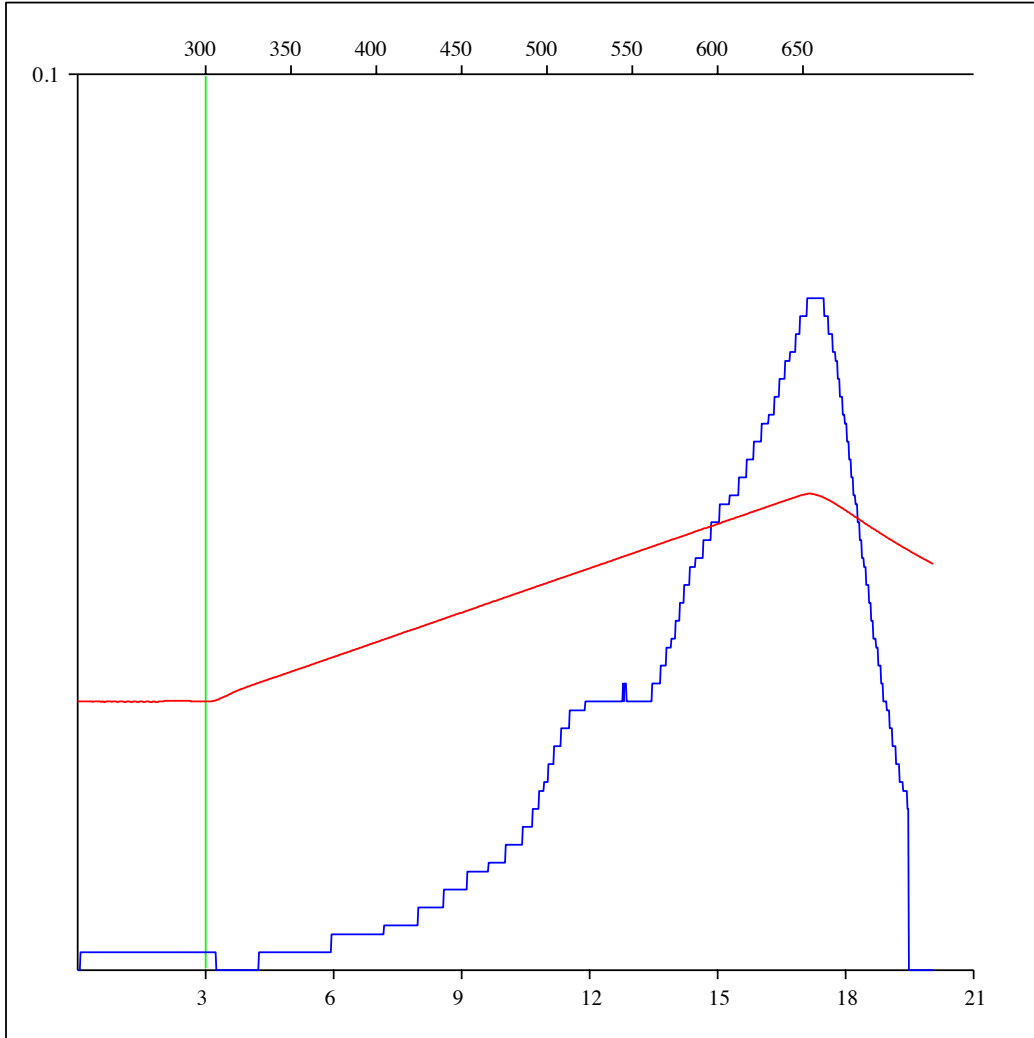
Sample: C-492850
Acquisition Date: 08-FEB-2012
Location: ARC DAWSON 09-29-079-14
Depth: 1999 m
Analysis
Instrument: RockEval 6
Data Processing Software: Vinci

FID hydrocarbons



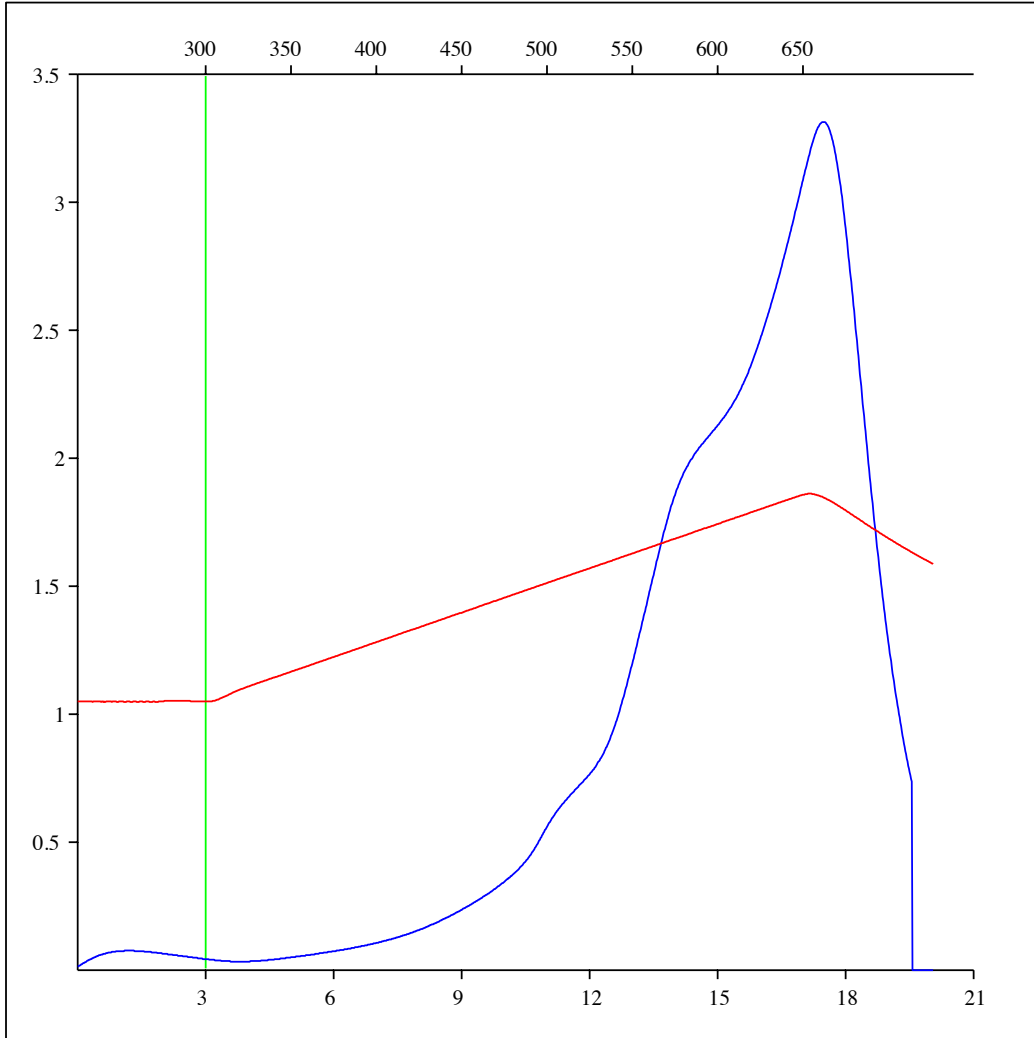
Sample: C-492850
Acquisition Date: 08-FEB-2012
Location: ARC DAWSON 09-29-079-14
Depth: 1999 m
Analysis
Instrument: RockEval 6
Data Processing Software: Vinci

Pyrolysis carbon monoxide



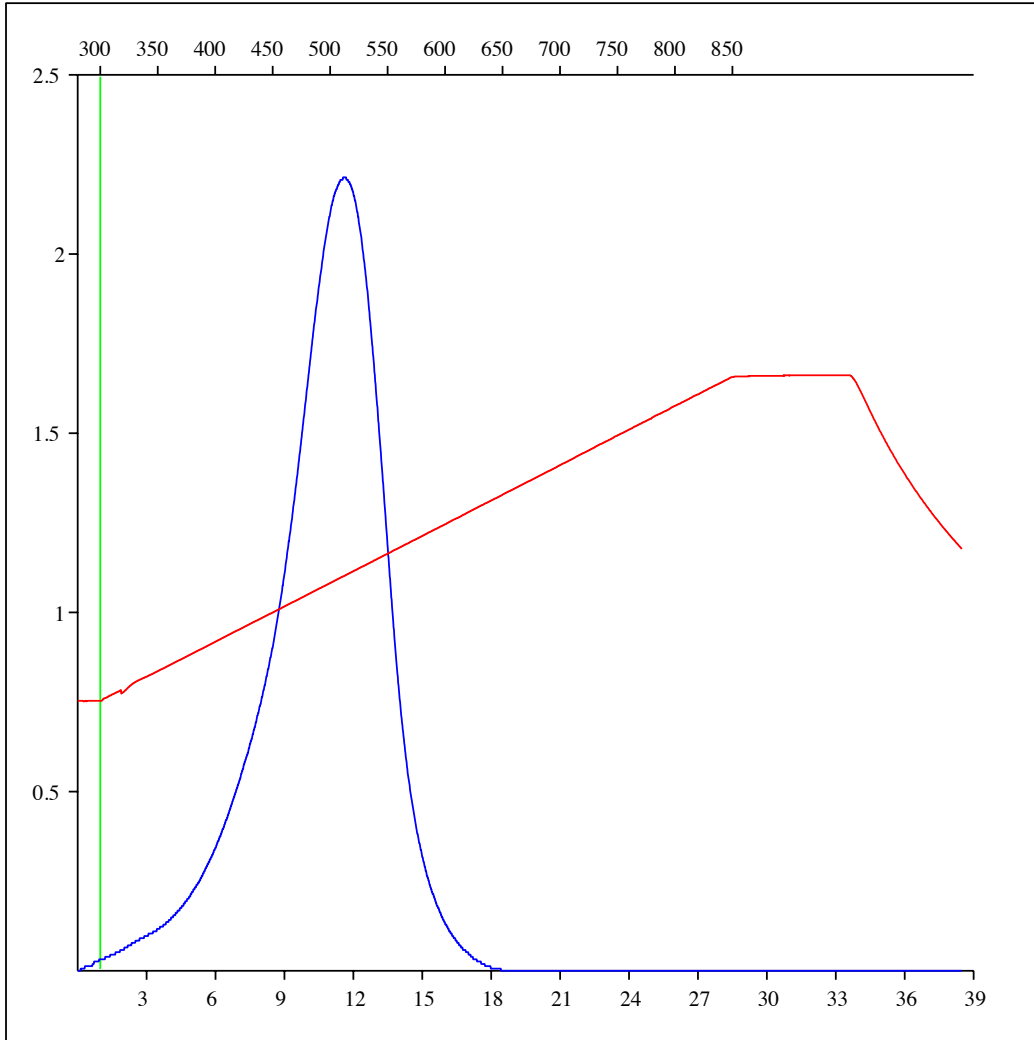
Sample: C-492850
Acquisition Date: 08-FEB-2012
Location: ARC DAWSON 09-29-079-14
Depth: 1999 m
Analysis
Instrument: RockEval 6
Data Processing Software: Vinci

Pyrolysis carbon dioxide



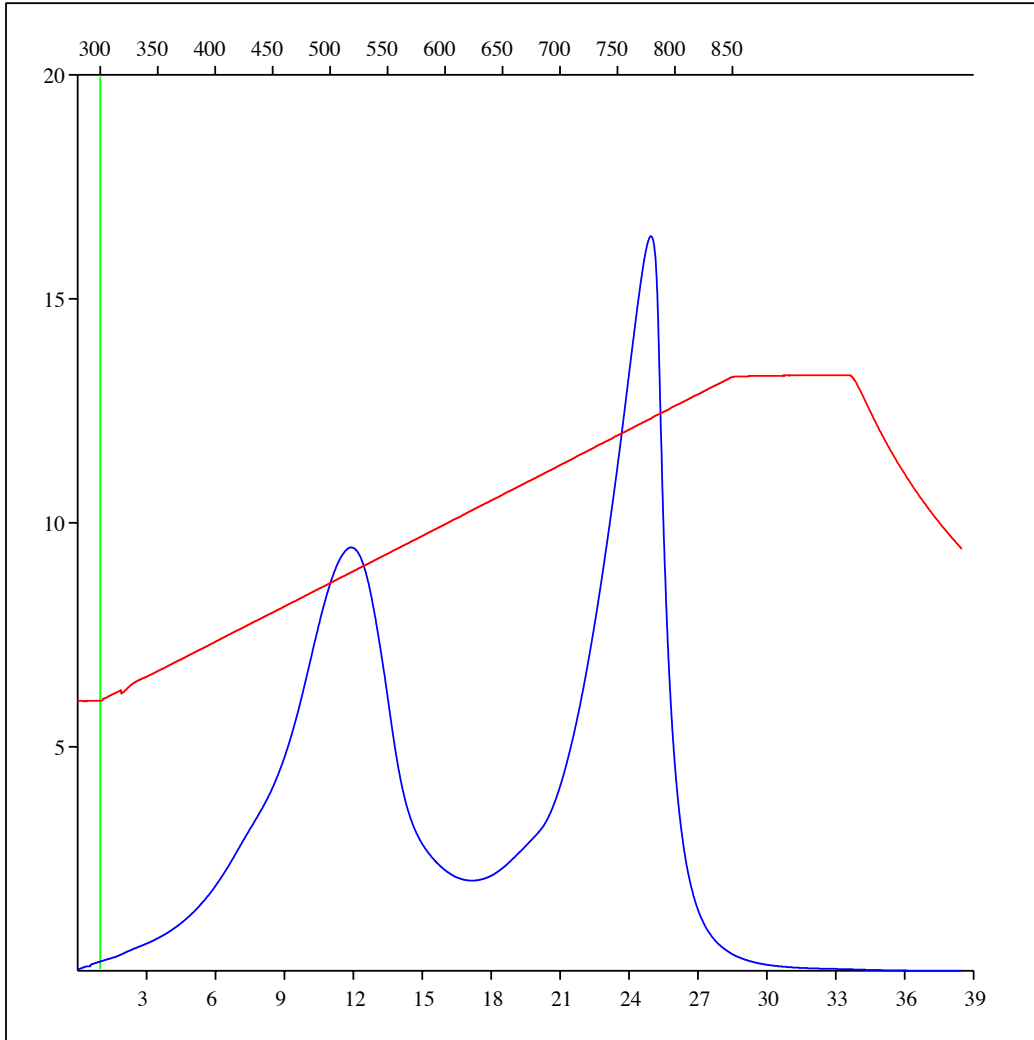
Sample: C-492850
Acquisition Date: 08-FEB-2012
Location: ARC DAWSON 09-29-079-14
Depth: 1999 m
Analysis
Instrument: RockEval 6
Data Processing Software: Vinci

Oxidation carbon monoxide



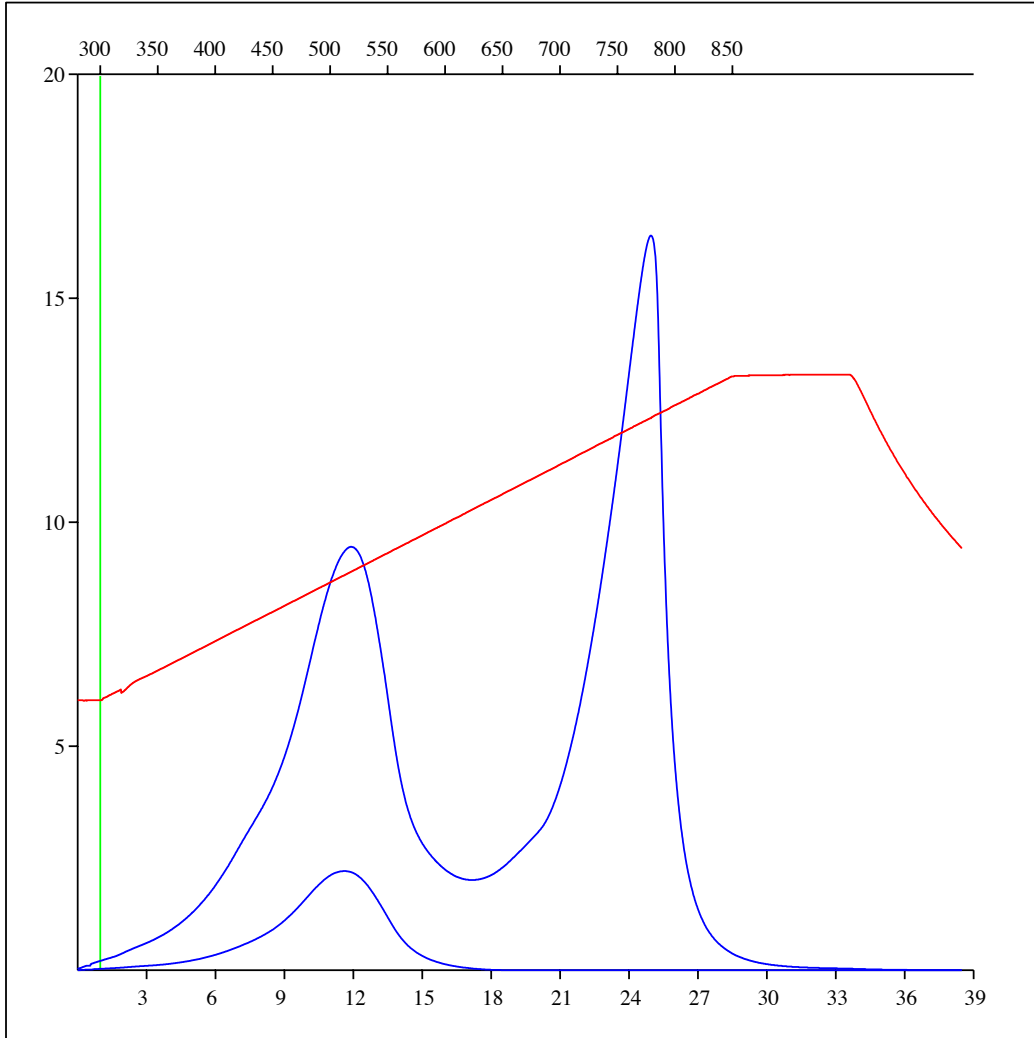
Sample: C-492850
Acquisition Date: 08-FEB-2012
Location: ARC DAWSON 09-29-079-14
Depth: 1999 m
Analysis
Instrument: RockEval 6
Data Processing Software: Vinci

Oxidation carbon dioxide



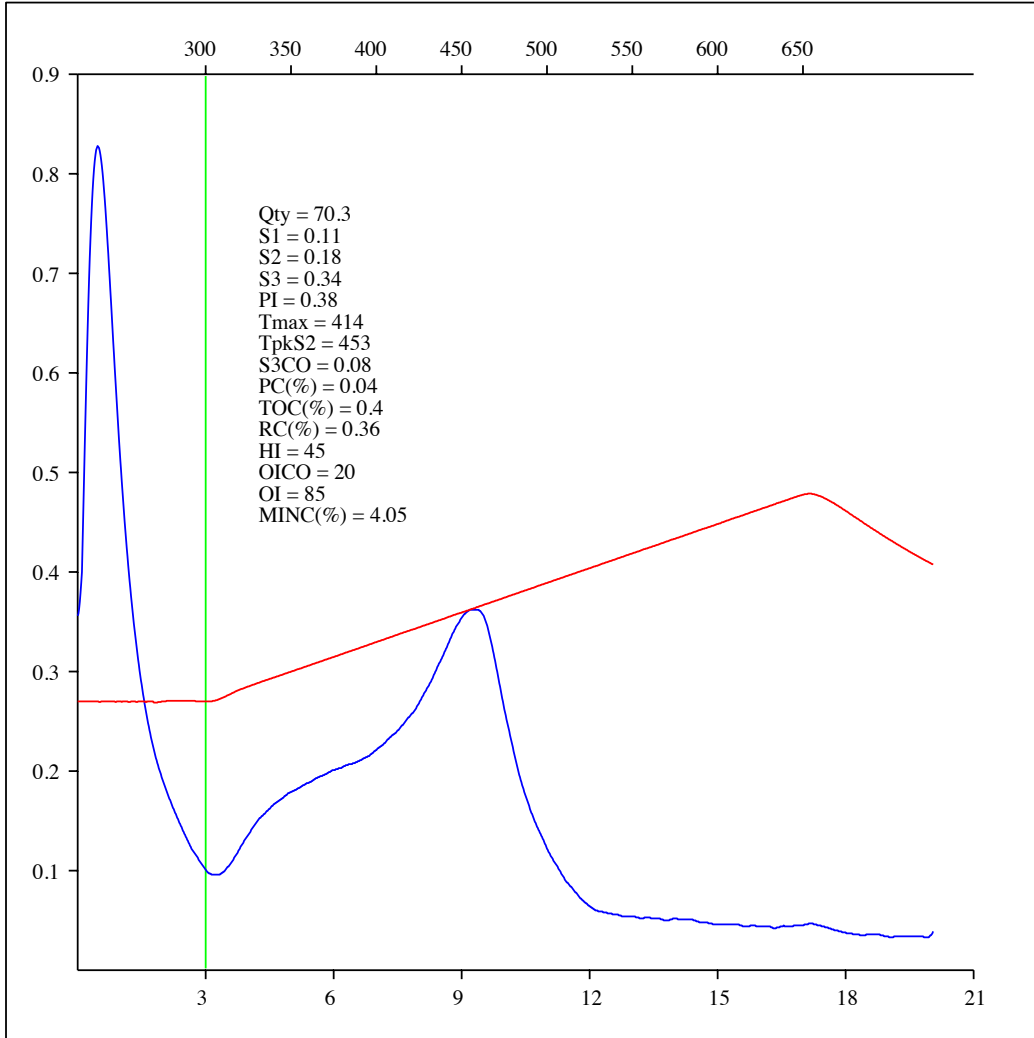
Sample: C-492850
Acquisition Date: 08-FEB-2012
Location: ARC DAWSON 09-29-079-14
Depth: 1999 m
Analysis
Instrument: RockEval 6
Data Processing Software: Vinci

Oxidation carbon monoxide & carbon dioxide



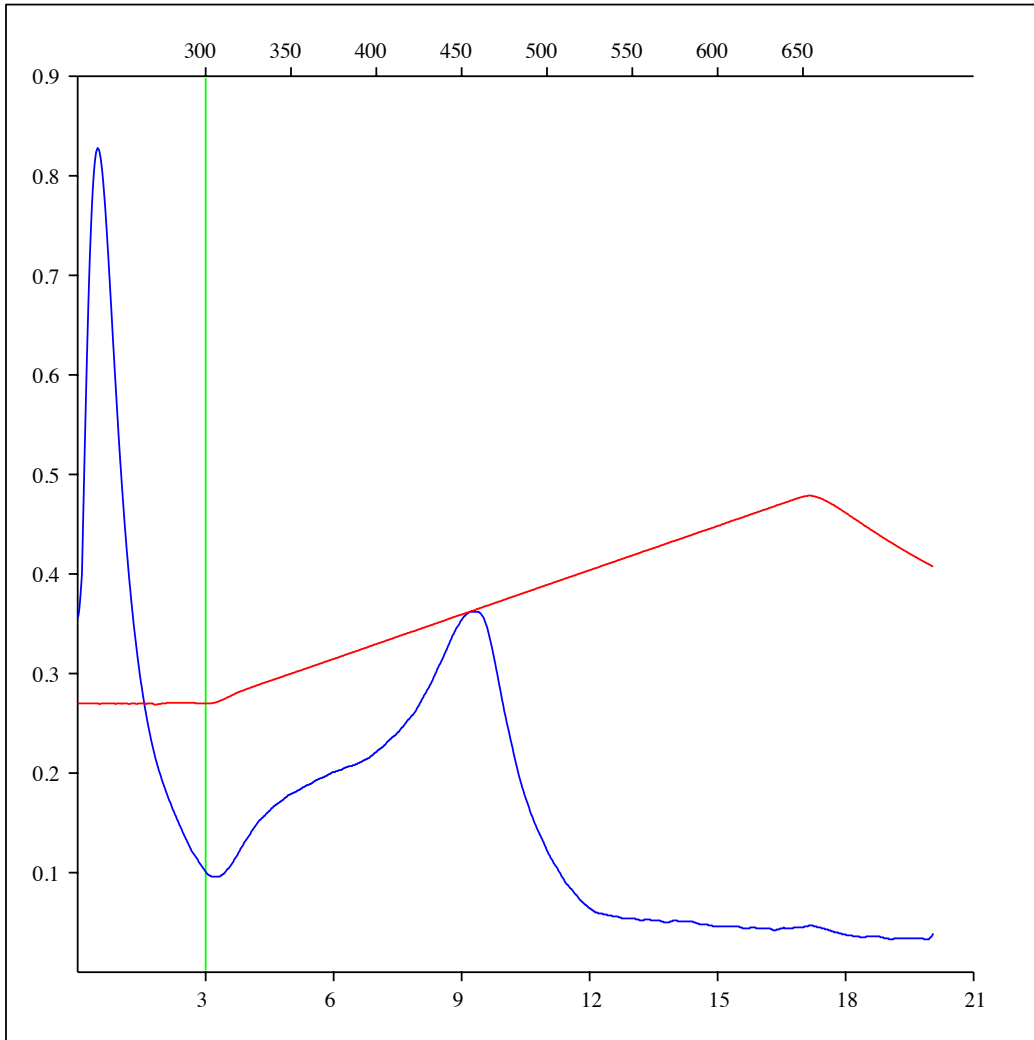
Sample: C-492851
Acquisition Date: 08-FEB-2012
Location: DEVON MONIAS 15-23-082-21
Depth: 1448.1 m
Analysis
Instrument: RockEval 6
Data Processing Software: Vinci

FID hydrocarbons



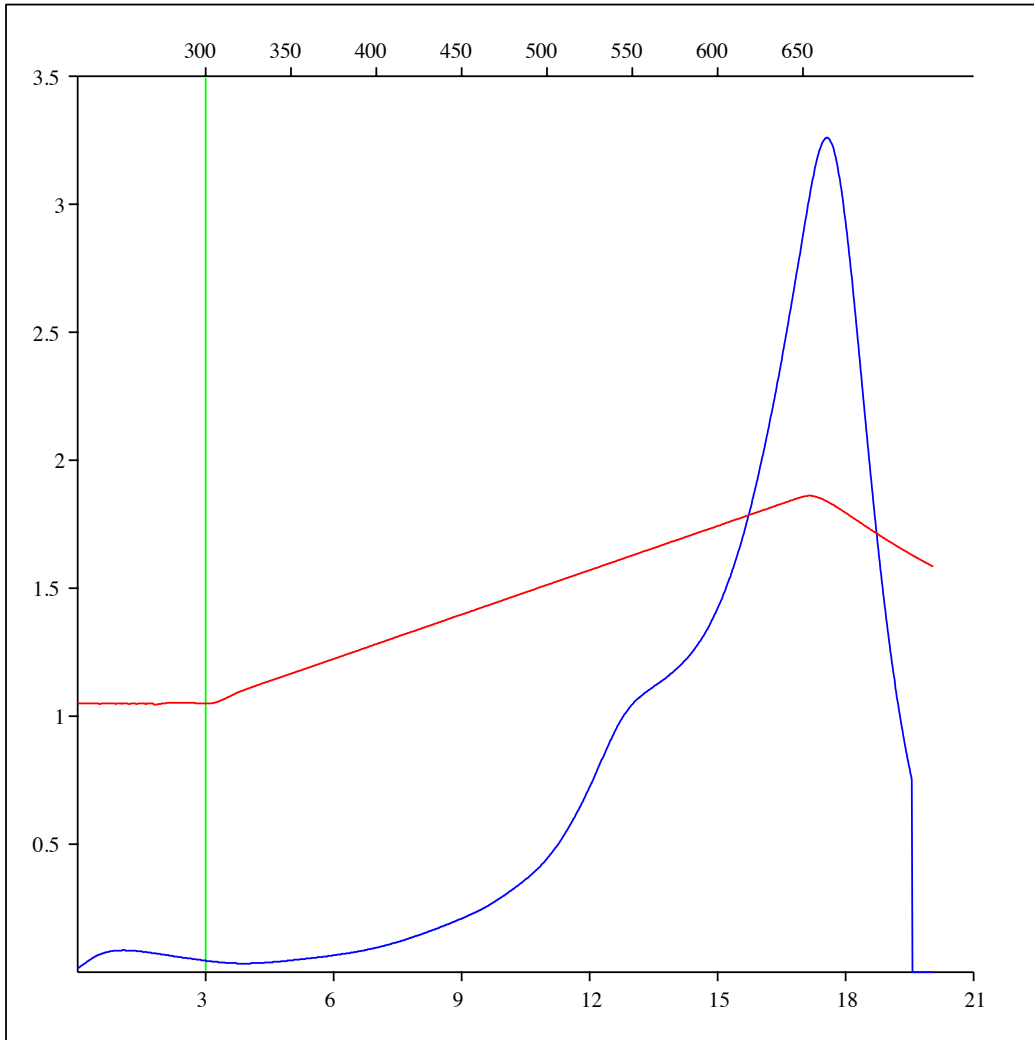
Sample: C-492851
Acquisition Date: 08-FEB-2012
Location: DEVON MONIAS 15-23-082-21
Depth: 1448.1 m
Analysis
Instrument: RockEval 6
Data Processing Software: Vinci

FID hydrocarbons



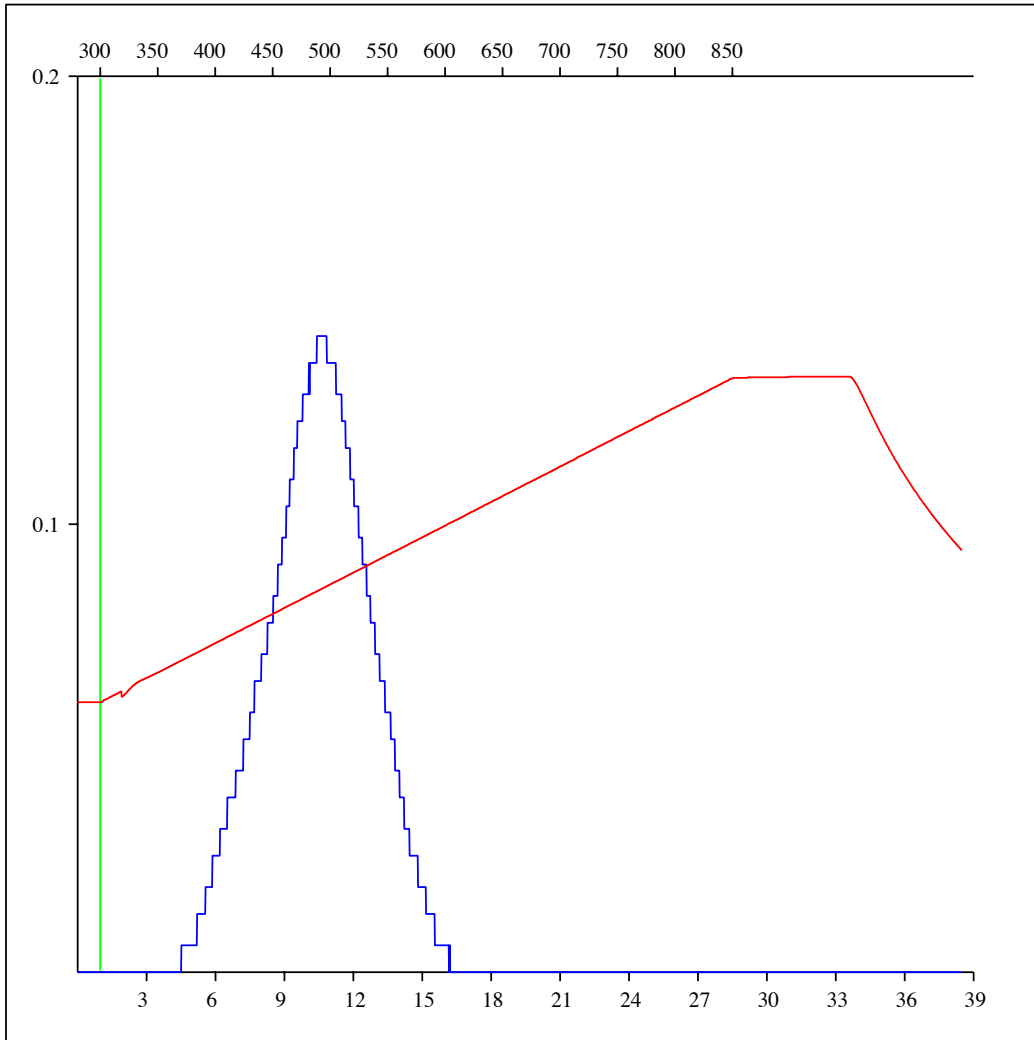
Sample: C-492851
Acquisition Date: 08-FEB-2012
Location: DEVON MONIAS 15-23-082-21
Depth: 1448.1 m
Analysis
Instrument: RockEval 6
Data Processing Software: Vinci

Pyrolysis carbon dioxide



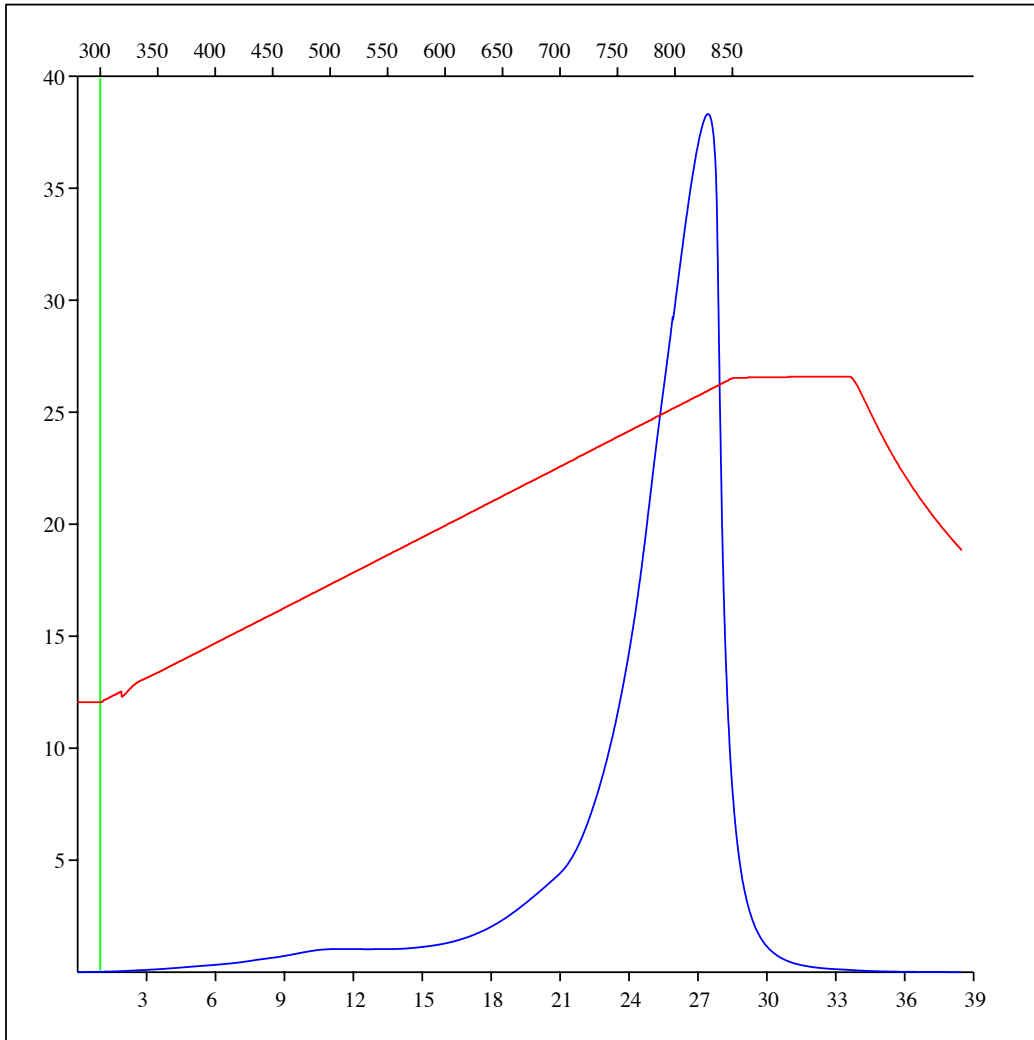
Sample: C-492851
Acquisition Date: 08-FEB-2012
Location: DEVON MONIAS 15-23-082-21
Depth: 1448.1 m
Analysis
Instrument: RockEval 6
Data Processing Software: Vinci

Oxidation carbon monoxide



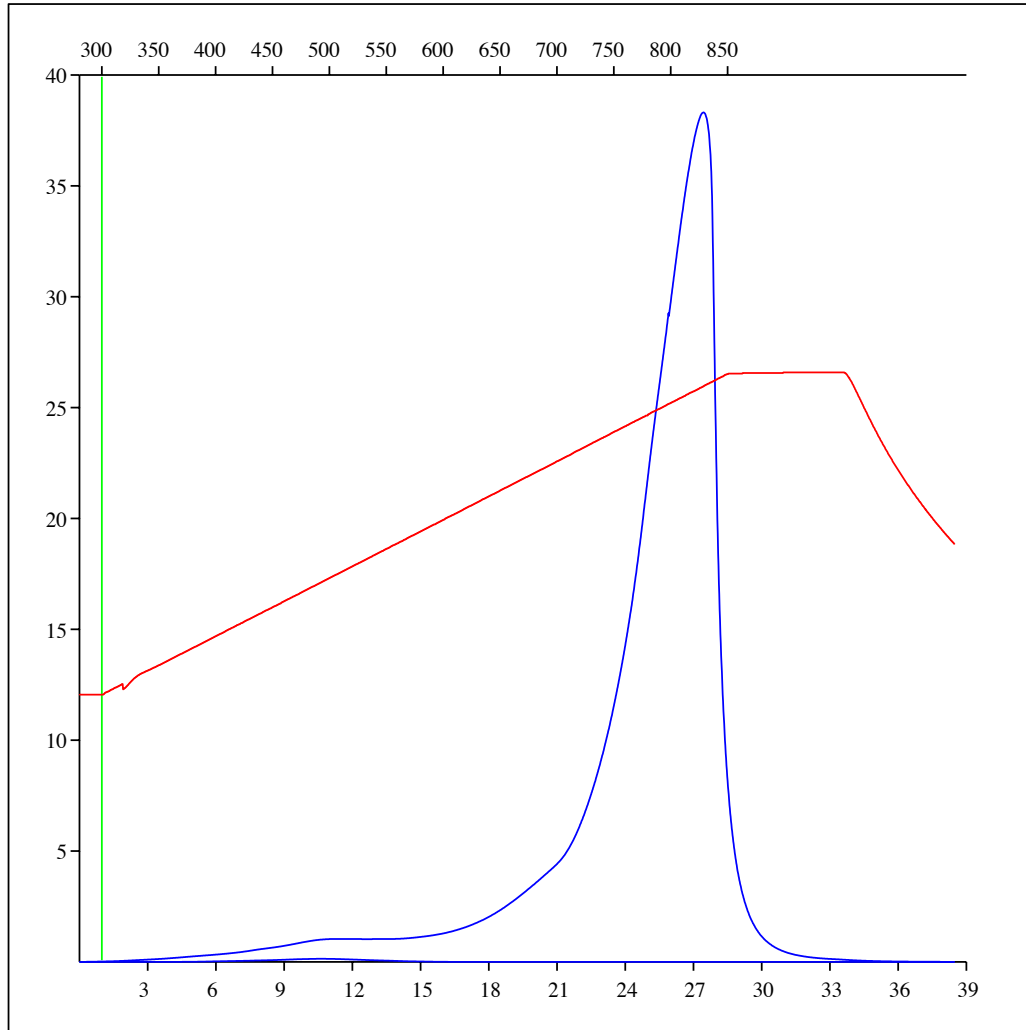
Sample: C-492851
Acquisition Date: 08-FEB-2012
Location: DEVON MONIAS 15-23-082-21
Depth: 1448.1 m
Analysis
Instrument: RockEval 6
Data Processing Software: Vinci

Oxidation carbon dioxide



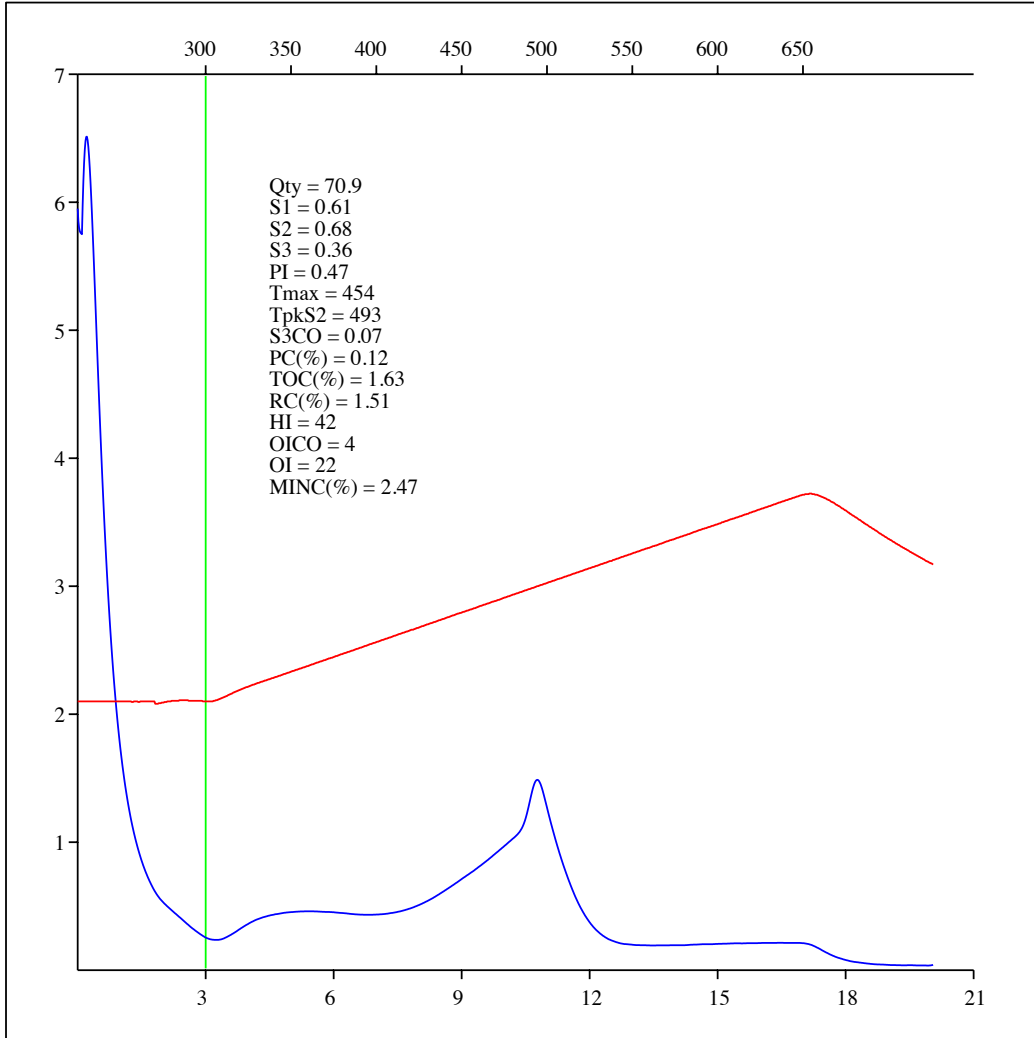
Sample: C-492851
Acquisition Date: 08-FEB-2012
Location: DEVON MONIAS 15-23-082-21
Depth: 1448.1 m
Analysis
Instrument: RockEval 6
Data Processing Software: Vinci

Oxidation carbon monoxide & carbon dioxide



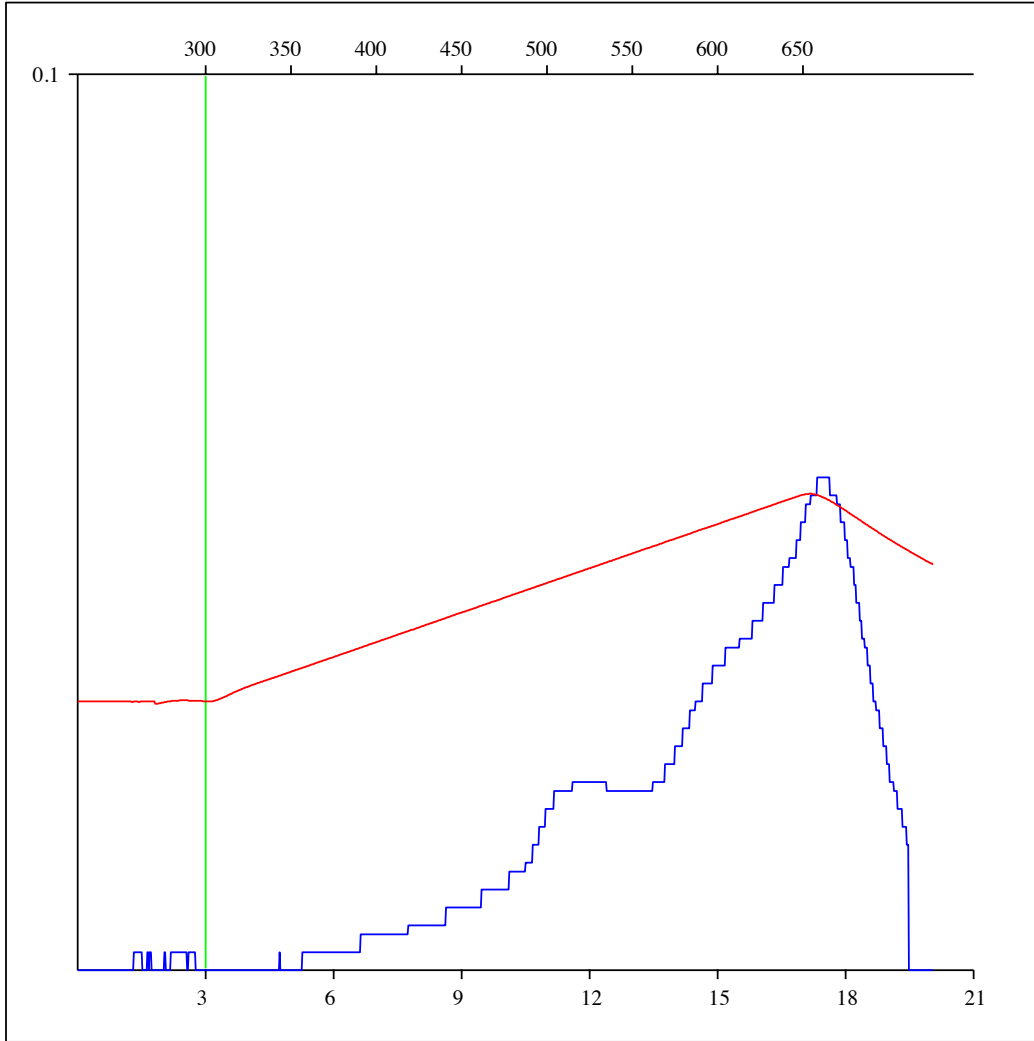
Sample: C-492852
Acquisition Date: 08-FEB-2012
Location: ARC DAWSON 13-16-079-14
Depth: 2015 m
Analysis
Instrument: RockEval 6
Data Processing Software: Vinci

FID hydrocarbons



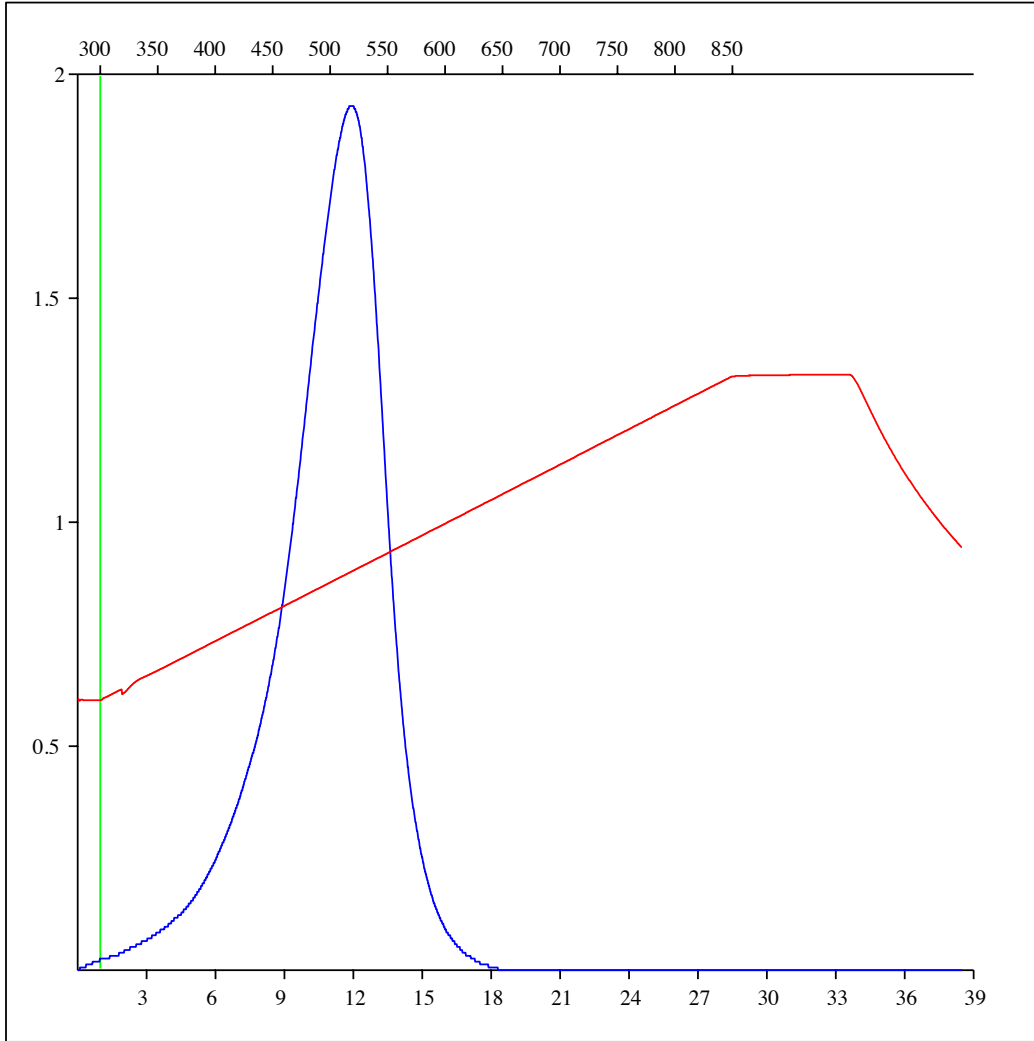
Sample: C-492852
Acquisition Date: 08-FEB-2012
Location: ARC DAWSON 13-16-079-14
Depth: 2015 m
Analysis
Instrument: RockEval 6
Data Processing Software: Vinci

Pyrolysis carbon monoxide



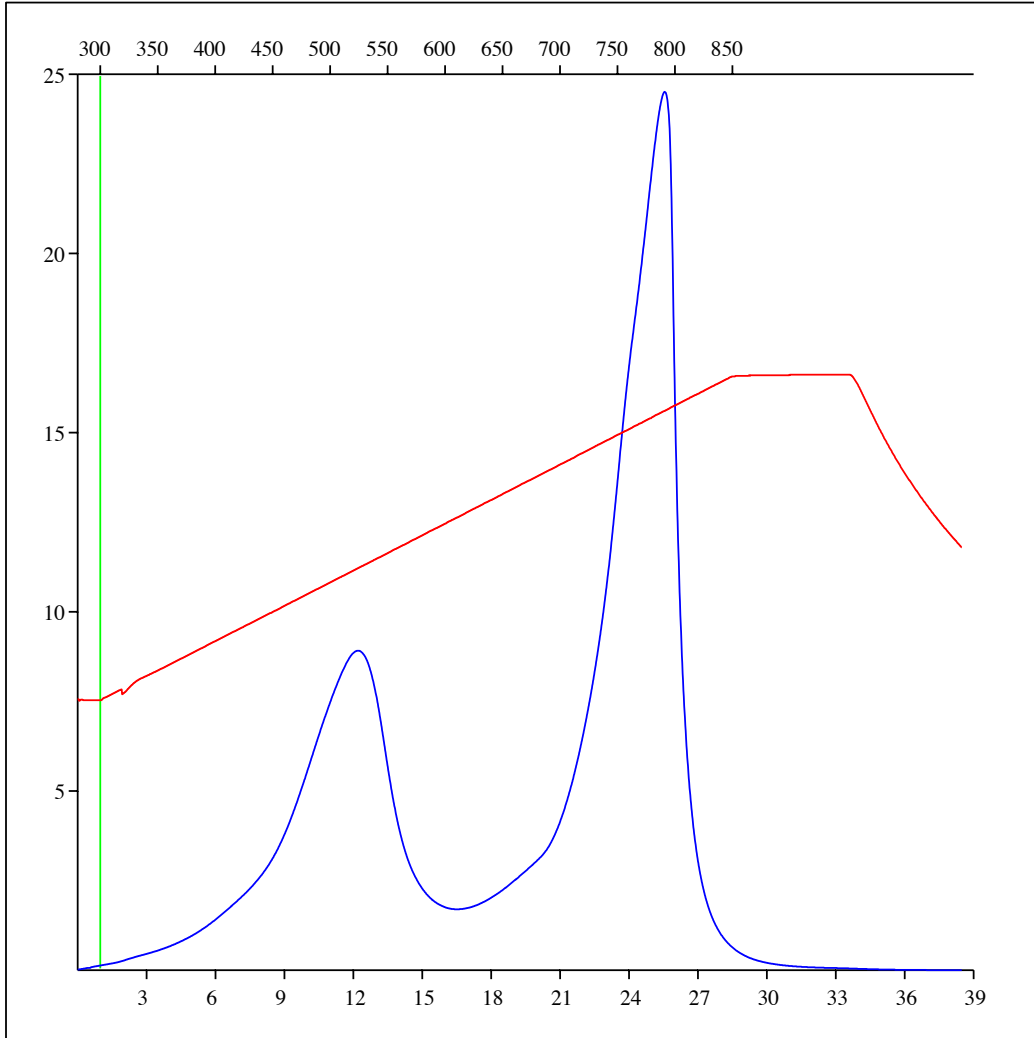
Sample: C-492852
Acquisition Date: 08-FEB-2012
Location: ARC DAWSON 13-16-079-14
Depth: 2015 m
Analysis
Instrument: RockEval 6
Data Processing Software: Vinci

Oxidation carbon monoxide



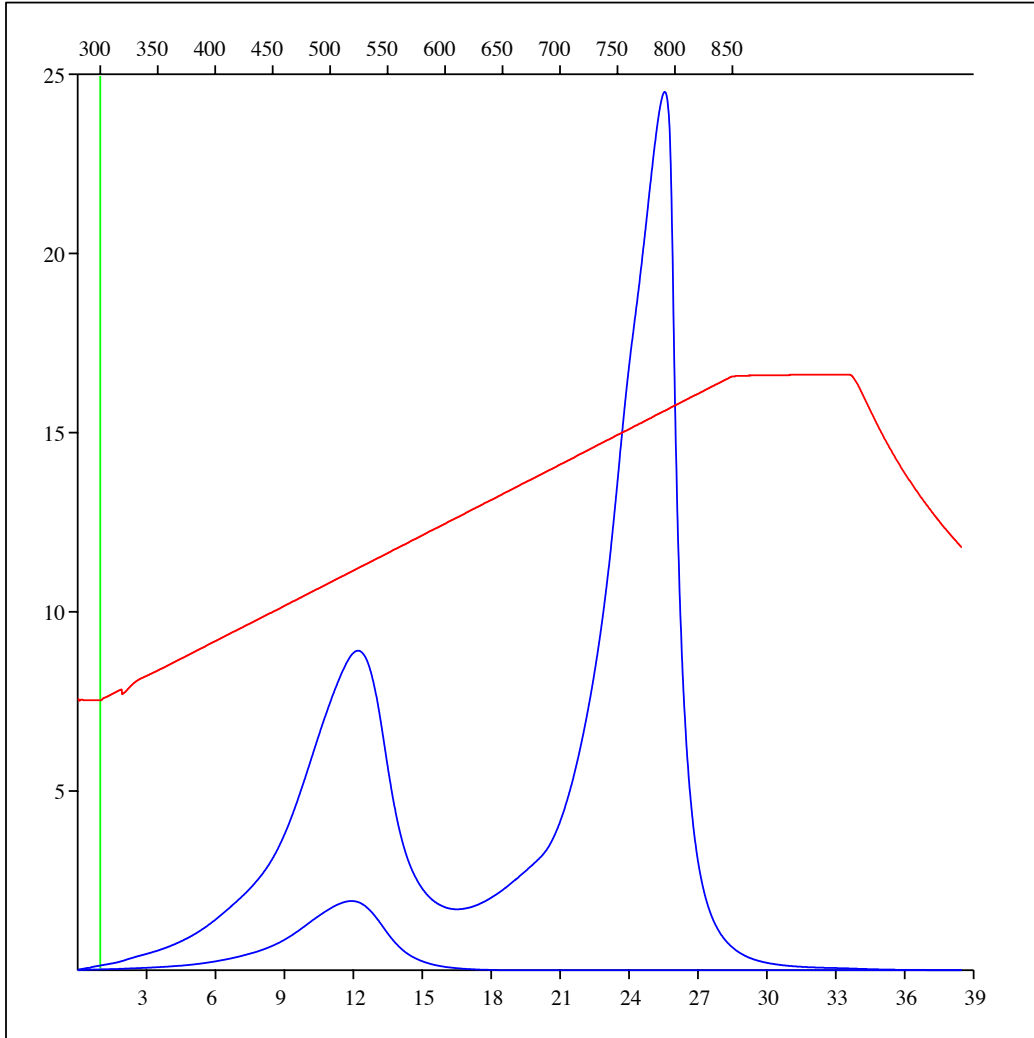
Sample: C-492852
Acquisition Date: 08-FEB-2012
Location: ARC DAWSON 13-16-079-14
Depth: 2015 m
Analysis
Instrument: RockEval 6
Data Processing Software: Vinci

Oxidation carbon dioxide



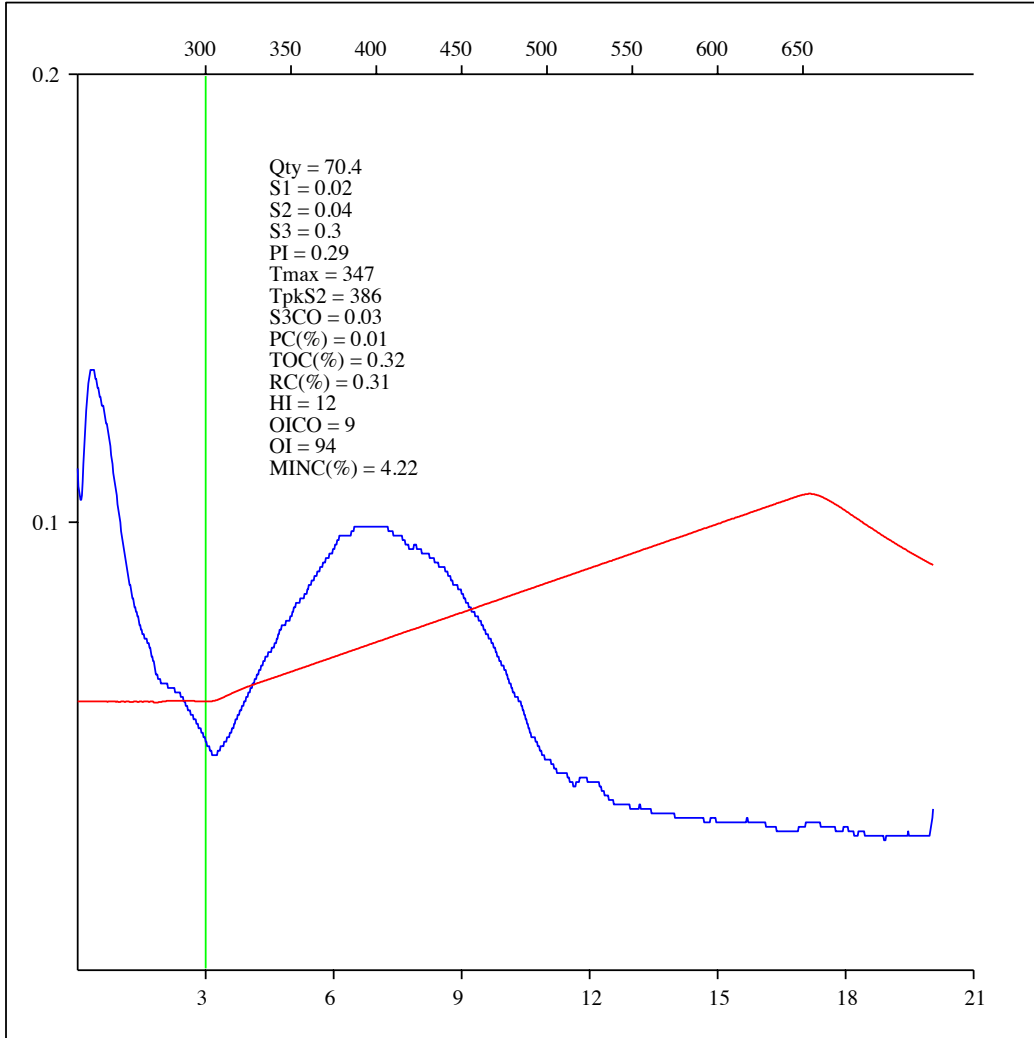
Sample: C-492852
Acquisition Date: 08-FEB-2012
Location: ARC DAWSON 13-16-079-14
Depth: 2015 m
Analysis
Instrument: RockEval 6
Data Processing Software: Vinci

Oxidation carbon monoxide & carbon dioxide



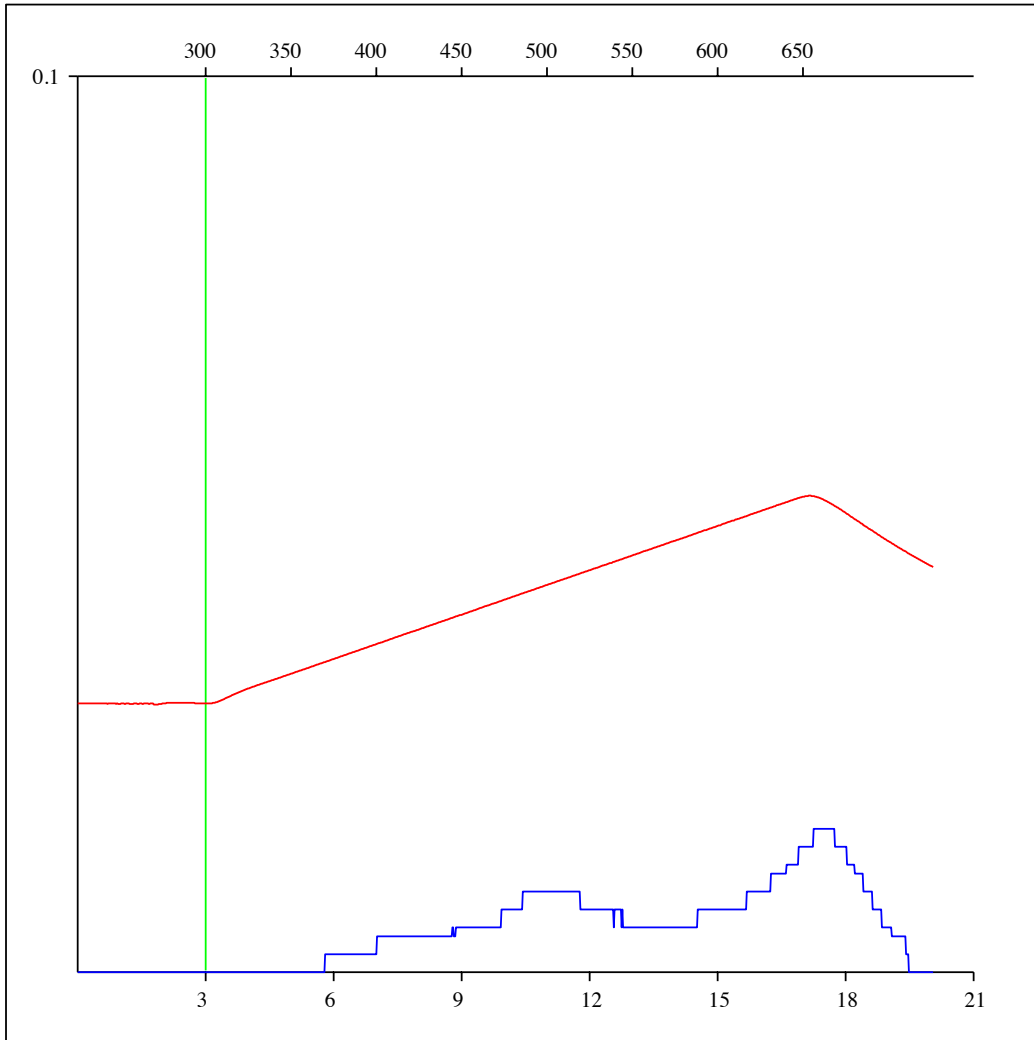
Sample: C-492853
Acquisition Date: 08-FEB-2012
Location: ECA SWAN B- 039-H/093-P-09
Depth: 2042 m
Analysis
Instrument: RockEval 6
Data Processing Software: Vinci

FID hydrocarbons



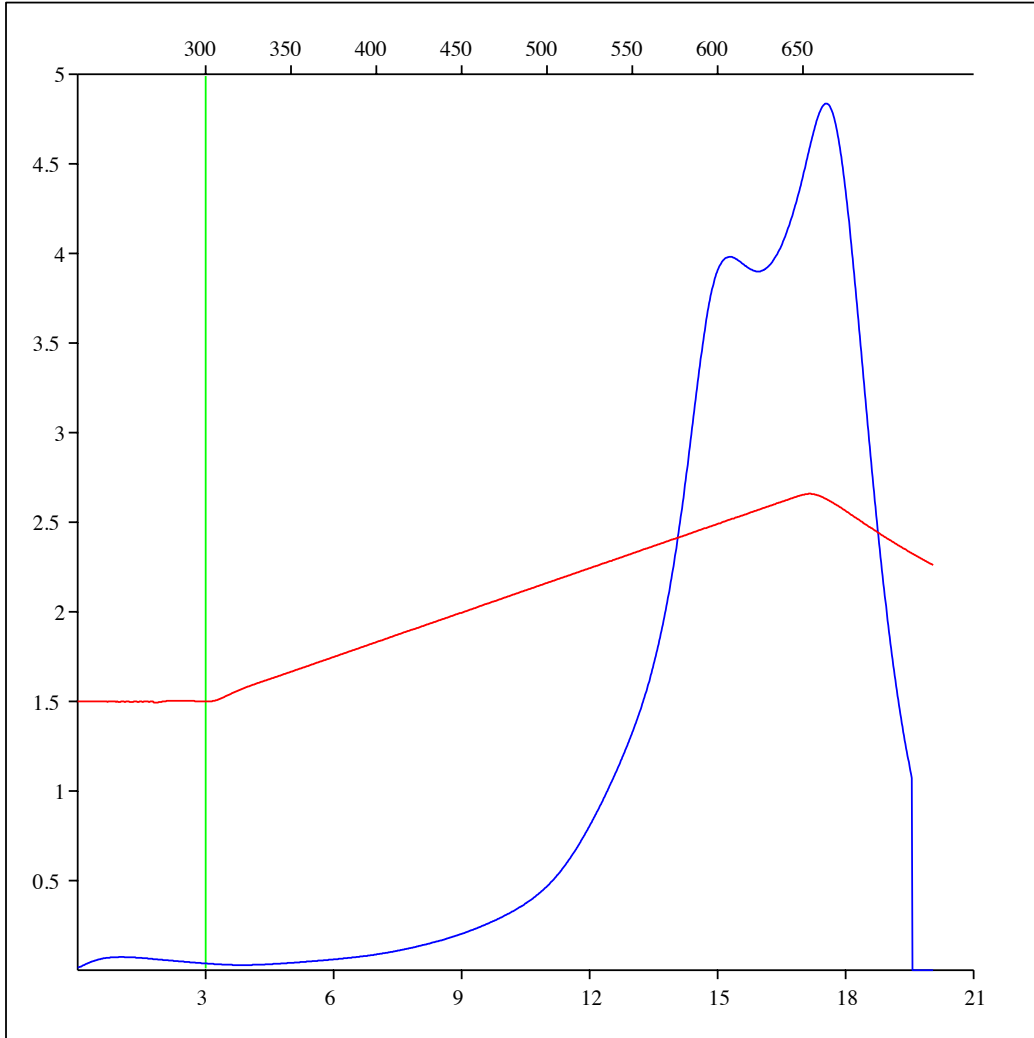
Sample: C-492853
Acquisition Date: 08-FEB-2012
Location: ECA SWAN B- 039-H/093-P-09
Depth: 2042 m
Analysis
Instrument: RockEval 6
Data Processing Software: Vinci

Pyrolysis carbon monoxide



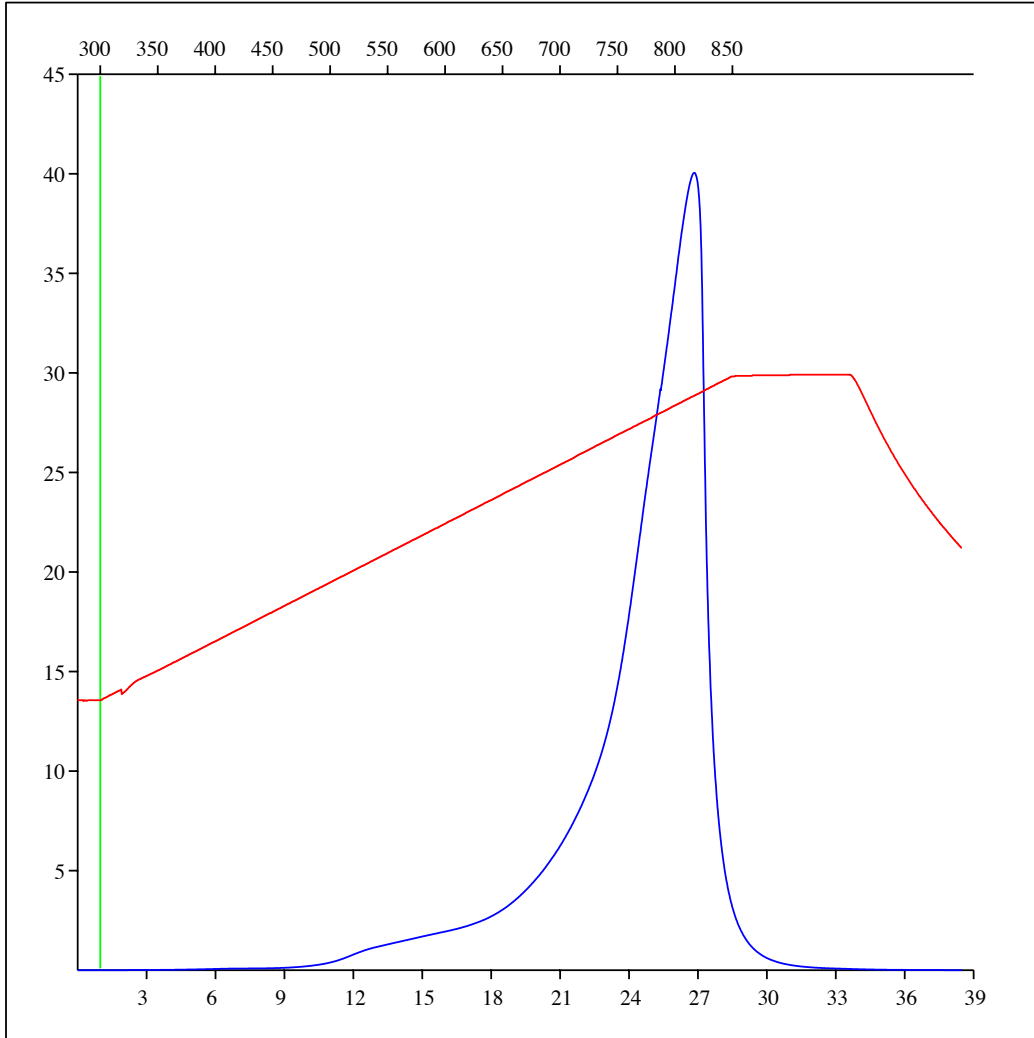
Sample: C-492853
Acquisition Date: 08-FEB-2012
Location: ECA SWAN B- 039-H/093-P-09
Depth: 2042 m
Analysis
Instrument: RockEval 6
Data Processing Software: Vinci

Pyrolysis carbon dioxide



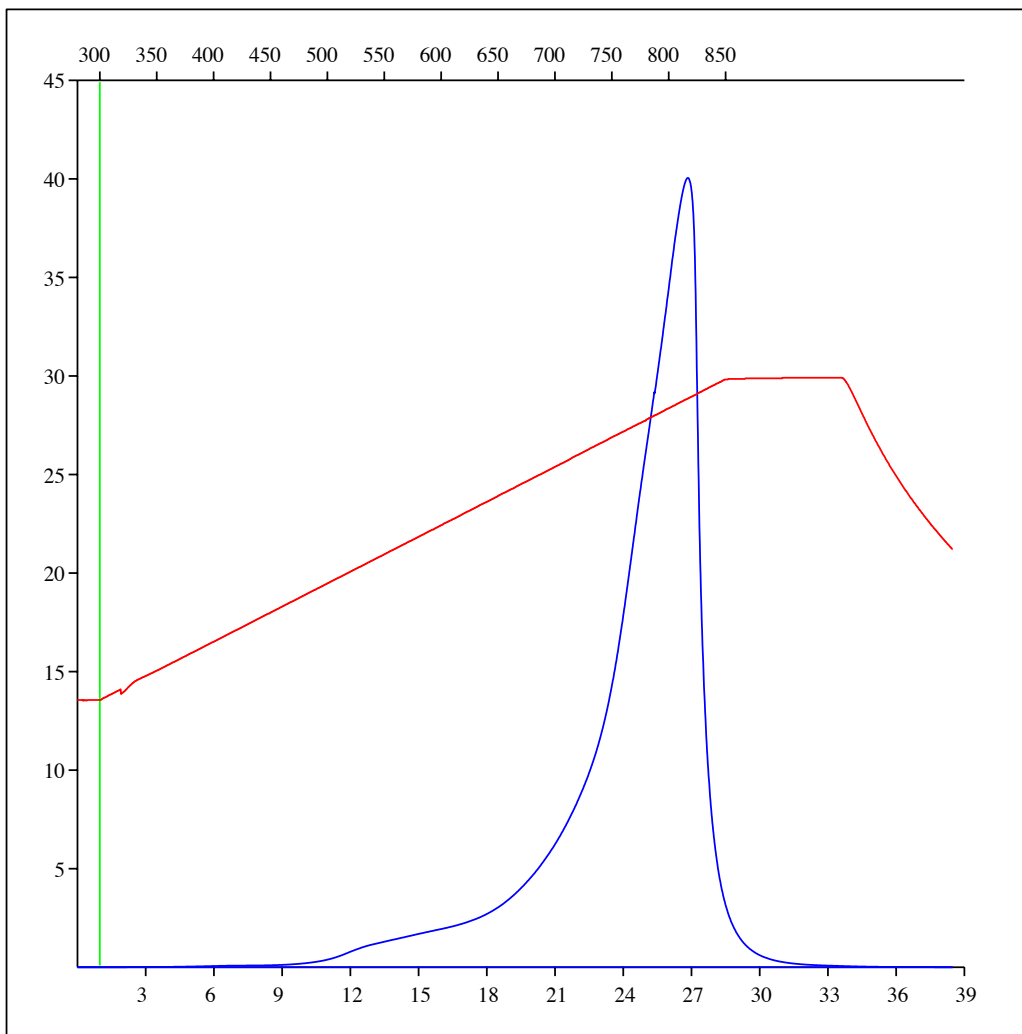
Sample: C-492853
Acquisition Date: 08-FEB-2012
Location: ECA SWAN B- 039-H/093-P-09
Depth: 2042 m
Analysis
Instrument: RockEval 6
Data Processing Software: Vinci

Oxidation carbon dioxide



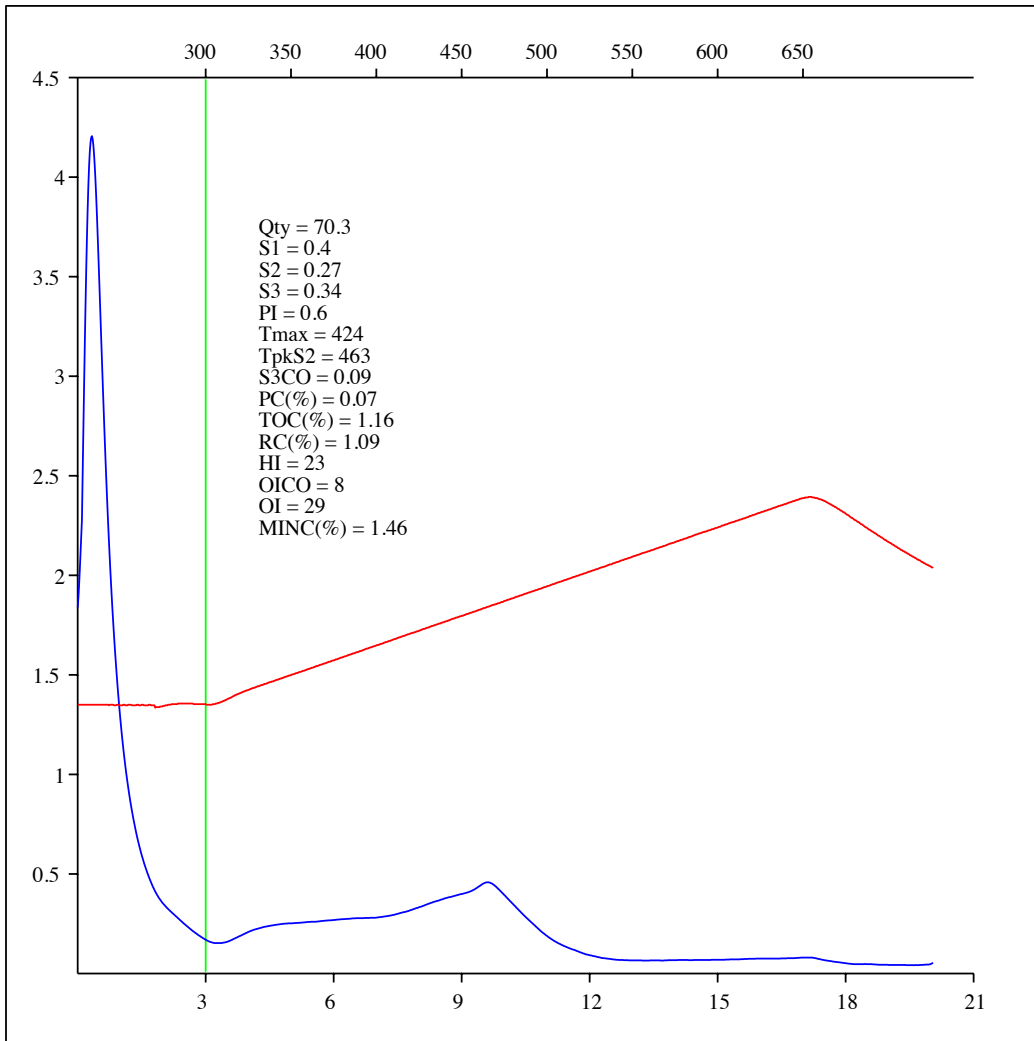
Sample: C-492853
Acquisition Date: 08-FEB-2012
Location: ECA SWAN B- 039-H/093-P-09
Depth: 2042 m
Analysis
Instrument: RockEval 6
Data Processing Software: Vinci

Oxidation carbon monoxide & carbon dioxide



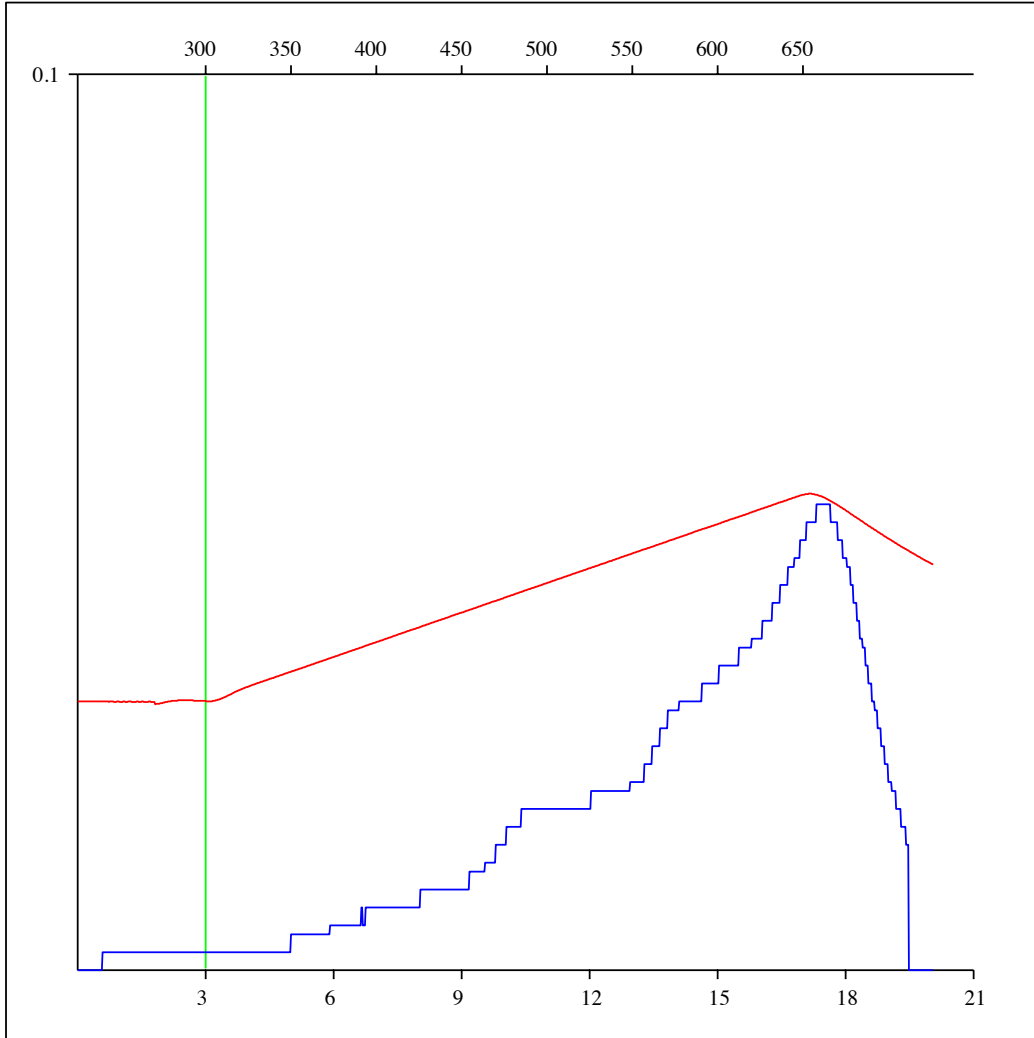
Sample: C-492854
Acquisition Date: 08-FEB-2012
Location: ECA SWAN B- 032-G/093-P-09
Depth: 2707 m
Analysis
Instrument: RockEval 6
Data Processing Software: Vinci

FID hydrocarbons



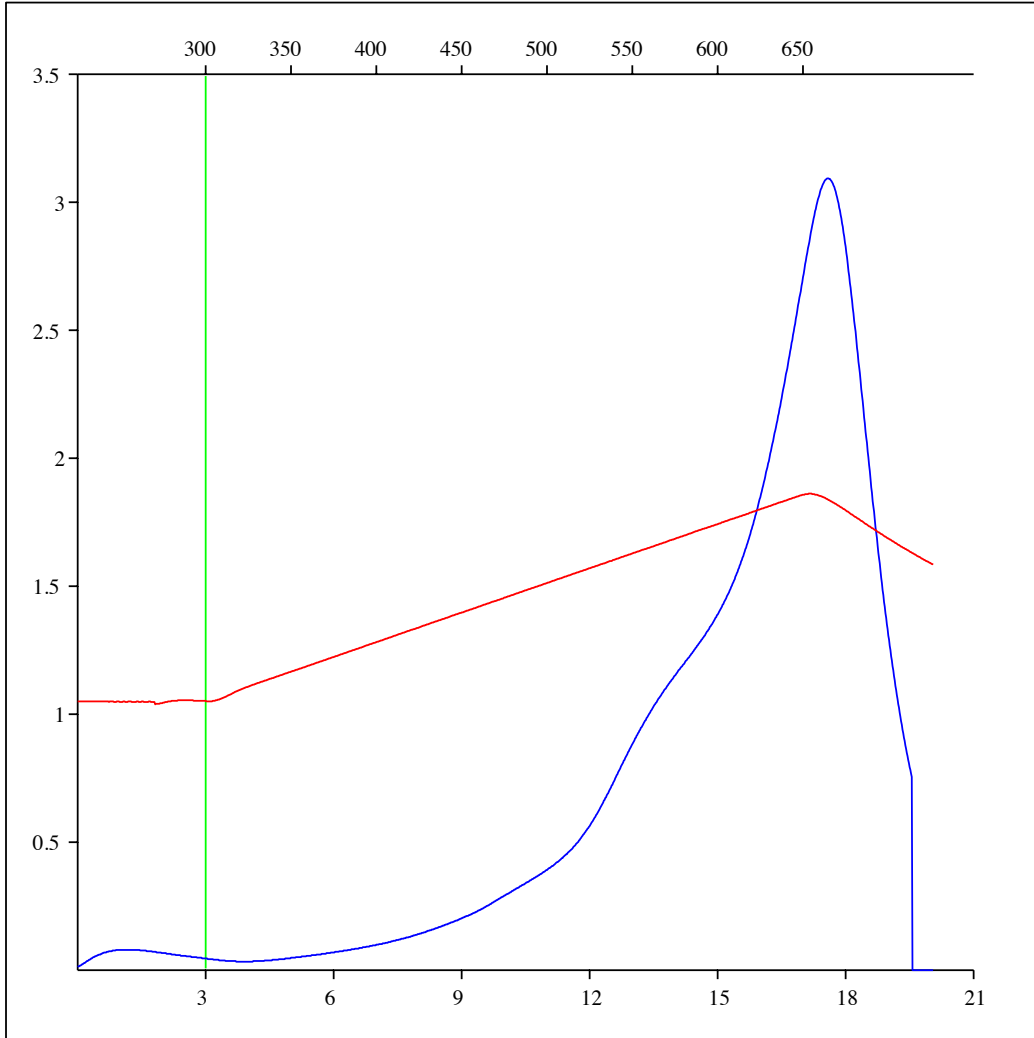
Sample: C-492854
Acquisition Date: 08-FEB-2012
Location: ECA SWAN B- 032-G/093-P-09
Depth: 2707 m
Analysis
Instrument: RockEval 6
Data Processing Software: Vinci

Pyrolysis carbon monoxide



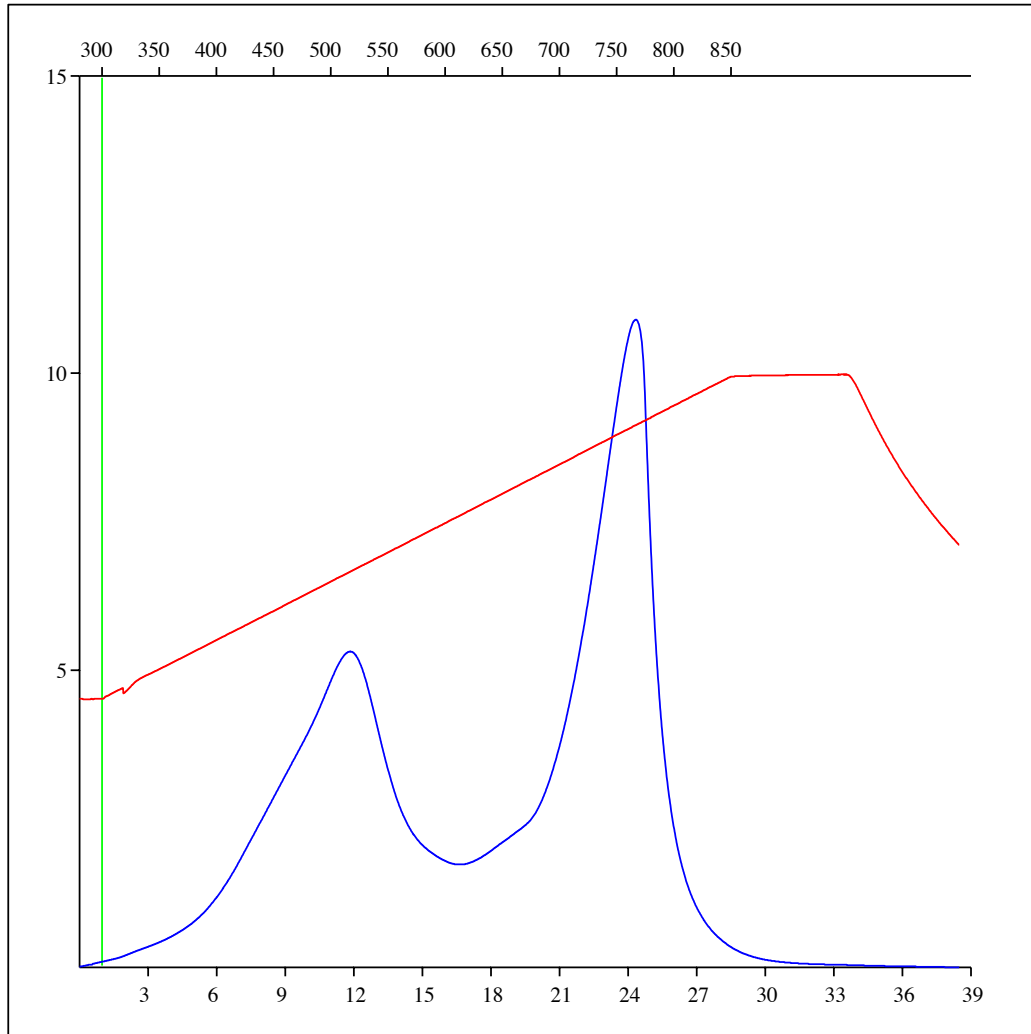
Sample: C-492854
Acquisition Date: 08-FEB-2012
Location: ECA SWAN B- 032-G/093-P-09
Depth: 2707 m
Analysis
Instrument: RockEval 6
Data Processing Software: Vinci

Pyrolysis carbon dioxide



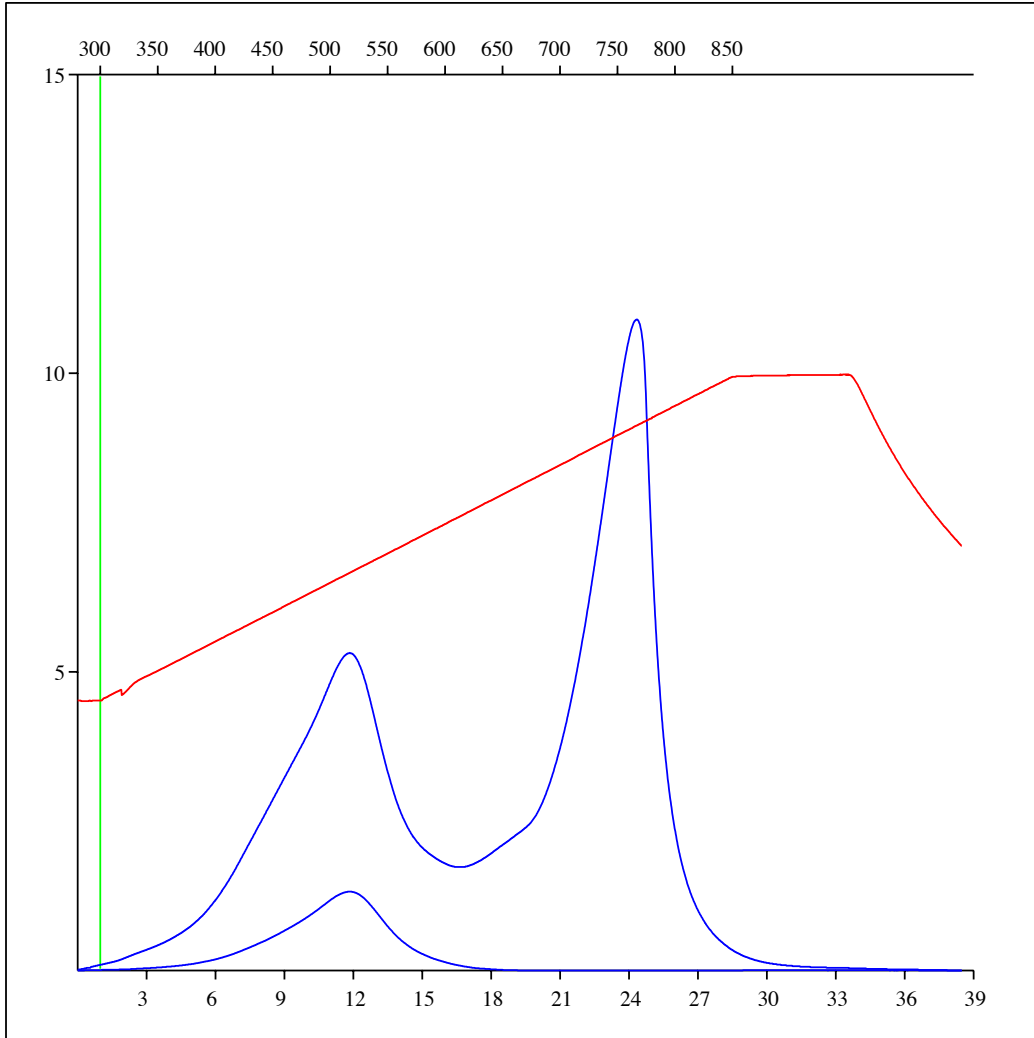
Sample: C-492854
Acquisition Date: 08-FEB-2012
Location: ECA SWAN B- 032-G/093-P-09
Depth: 2707 m
Analysis
Instrument: RockEval 6
Data Processing Software: Vinci

Oxidation carbon dioxide



Sample: C-492854
Acquisition Date: 08-FEB-2012
Location: ECA SWAN B- 032-G/093-P-09
Depth: 2707 m
Analysis
Instrument: RockEval 6
Data Processing Software: Vinci

Oxidation carbon monoxide & carbon dioxide



APPENDIX – 4A: Calculation of the temperature of fractionation using isotopic data from the Montney Formation, northeastern British Columbia, Western Canada.

The calculation of the temperature of fractionation of calcite was rendered using the equation below:

$$10^3 \ln \alpha_{\text{calcite-water}} = 2.78 \times 10^6 T^{-2} - 2.89 \quad \text{eqn. (1)}$$

(Friedman and O'Neil, 1977).

There is a relationship: $10^3 \ln \alpha_{\text{calcite-water}} \approx \delta^{18}\text{O}_{\text{calcite}} - \delta^{18}\text{O}_{\text{water}}$ eqn. (2)

Therefore: $\delta^{18}\text{O}_{\text{calcite}} - \delta^{18}\text{O}_{\text{water}} = 2.78 \times 10^6 T^{-2} - 2.89$ eqn. (3)

Using the $\delta^{18}\text{O}_{\text{PDB}}$ range of bulk calcite (-2 to -7.19) assuming the $\delta^{18}\text{O}_{\text{SMOW}}$ value of pore water is between -2 and -7‰ (based on laboratory experiment which show a depleted $\delta^{18}\text{O}$ values).

The resultant expression by substituting into eqn. (3) gives the following:

$$24.91(\text{SMOW})_{\text{calcite}} - (-2) \delta^{18}\text{O}_{\text{water}} = 2.78 \times 10^6 T^{-2} - 2.89$$

$$24.91 + 2 = 2.78 \times 10^6 T^{-2} - 2.89$$

$$26.91 = \frac{2.78 \times 10^6}{T^2} - 2.89$$

$$26.91 T^2 = 2.78 \times 10^6 - 2.89 T^2$$

$$26.91 T^2 + 2.89 T^2 = 2.78 \times 10^6$$

$$29.8 T^2 = 2.78 \times 10^6$$

$$T^2 = \frac{2.78 \times 10^6}{29.8}$$

$$T = \sqrt{\frac{2.78 \times 10^6}{29.8}}$$

$$T = 305.43 \text{ Kelvin (K)}$$

The temperature is required in degrees Celsius. To convert temp (K) to Temp (°C),

$$T \text{ } ^\circ\text{C} = 305.43 \text{ (K)} - 273.15$$

Therefore: T = 32.42°C (paleotemperature of precipitation of calcite) during the Lower Triassic Period in the study area is ~32 °C.

For the calculation of the temperature of fractionation of dolomite, the equation below is used:

$$10^3 \ln \alpha_{\text{dolomite-water}} = 3.2 \times 10^6 T^{-2} - 3.3 \text{ ----- eqn. (4) (Land, 1983).}$$

$$\text{Therefore: } \delta^{18}\text{O (SMOW)}_{\text{dolomite}} - \delta^{18}\text{O}_{\text{water}} = 3.2 \times 10^6 T^{-2} - 3.3 \text{ eqn. (5)}$$

Using the $\delta^{18}\text{O}_{\text{PDB}}$ range of bulk dolomite (-5 to -6.79) assuming the $\delta^{18}\text{O}_{\text{SMOW}}$ value of pore water is between -5 and -7‰ (based on laboratory experiment which show a depleted $\delta^{18}\text{O}$ values).

By substituting into eqn. (5), the following is derived:

$$23.99_{\text{SMOW}} - (-6.79) \delta^{18}\text{O}_{\text{water}} = 3.2 \times 10^6 T^{-2} - 3.3$$

$$23.99 + 6.79 = 3.2 \times 10^6 T^{-2} - 3.3$$

$$30.78 = \frac{3.2 \times 10^6}{T^2} - 3.3$$

$$30.78T^2 = 3.2 \times 10^6 T^{-2} - 3.3T^2$$

$$30.78T^2 + 3.3T^2 = 3.2 \times 10^6$$

$$34.08T^2 = 3.2 \times 10^6$$

$$T^2 = \frac{3.2 \times 10^6}{34.08}$$

$$T = \sqrt{\frac{3.2 \times 10^6}{34.08}}$$

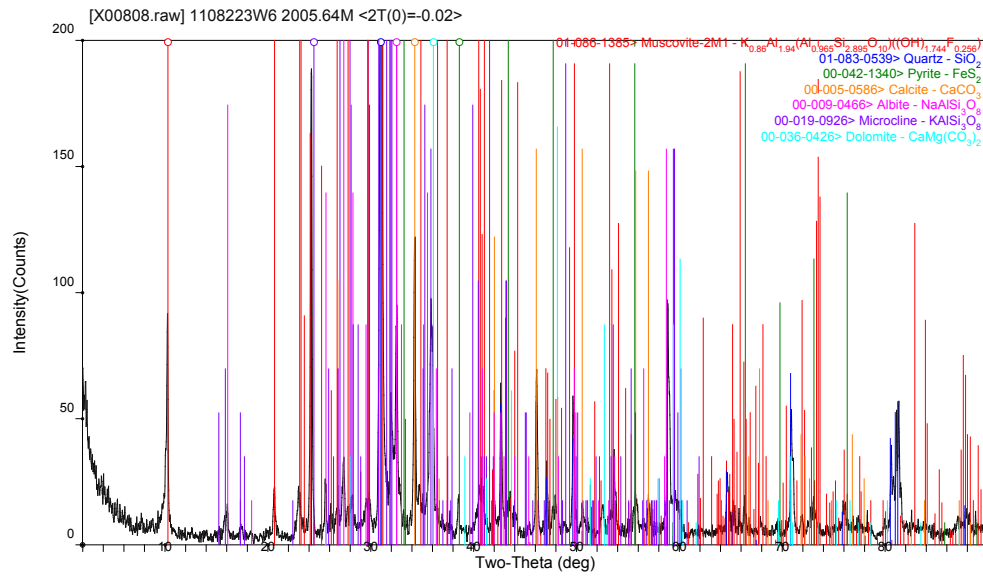
$$T = 306.4 \text{ Kelvin (K)}$$

To report the temperature in degrees Celsius, conversion of temp (K) to Temp (°C) is calculated:

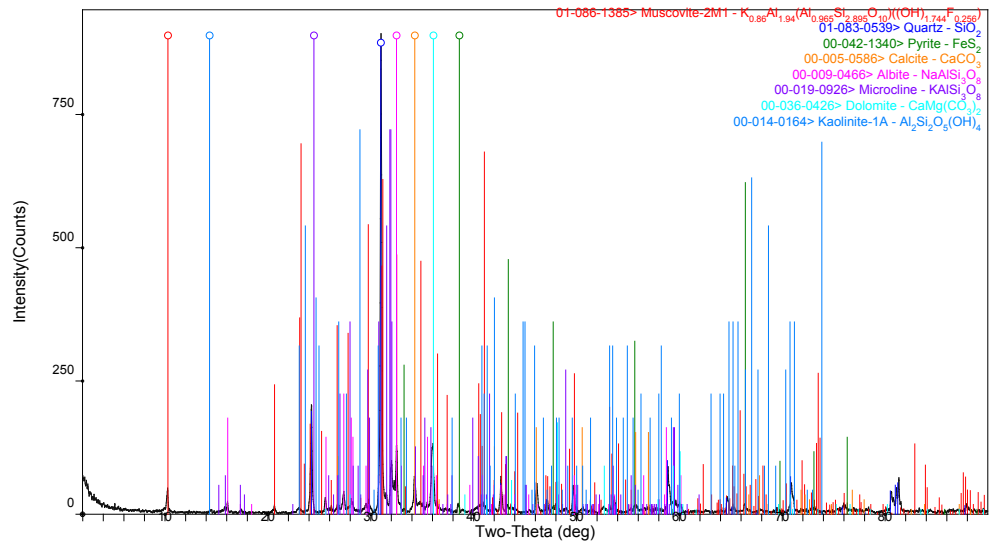
$$T \text{ } ^\circ\text{C} = 306.4 \text{ (K)} - 273.15$$

Therefore, $T = 33.3 \text{ } ^\circ\text{C}$ (paleotemperature of precipitation of dolomite) during the Lower Triassic Period in the study area is $\sim 33 \text{ } ^\circ\text{C}$.

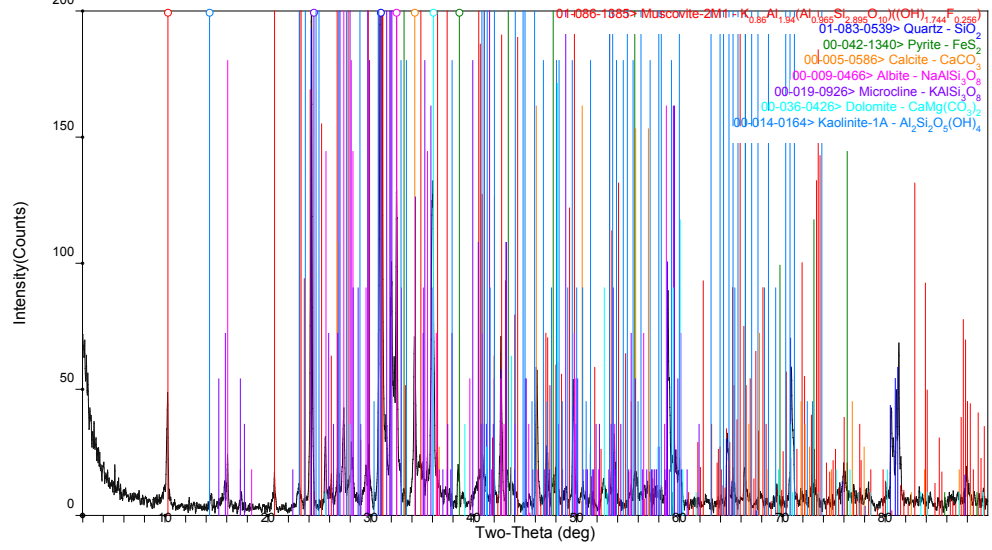
APPENDIX – 4 B: X-ray Diffraction Analyses (XRD) results of the Montney Formation, showing mineralogical composition of each sample from the study area, northeastern British Columbia, Western Canada.

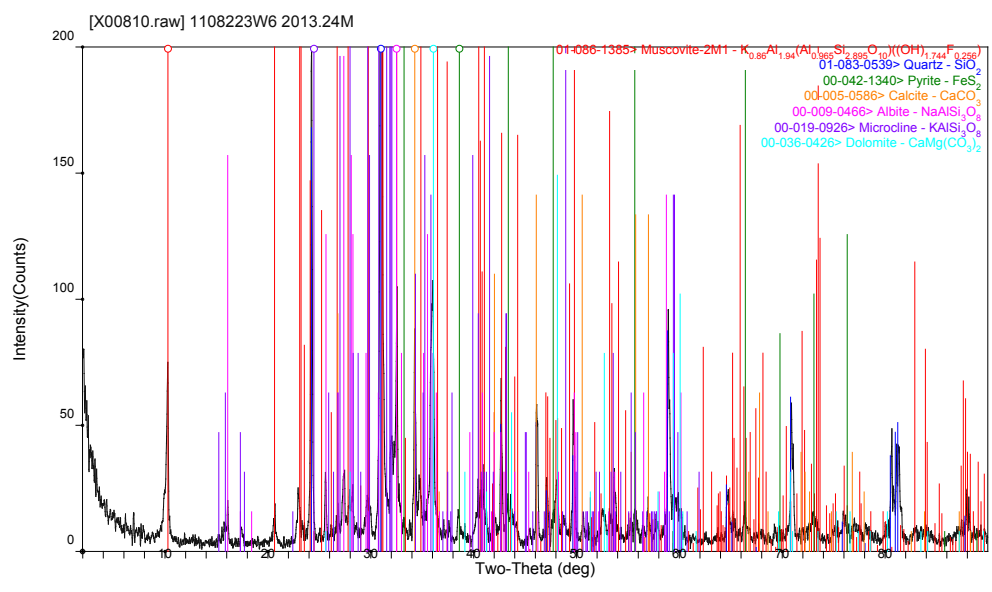
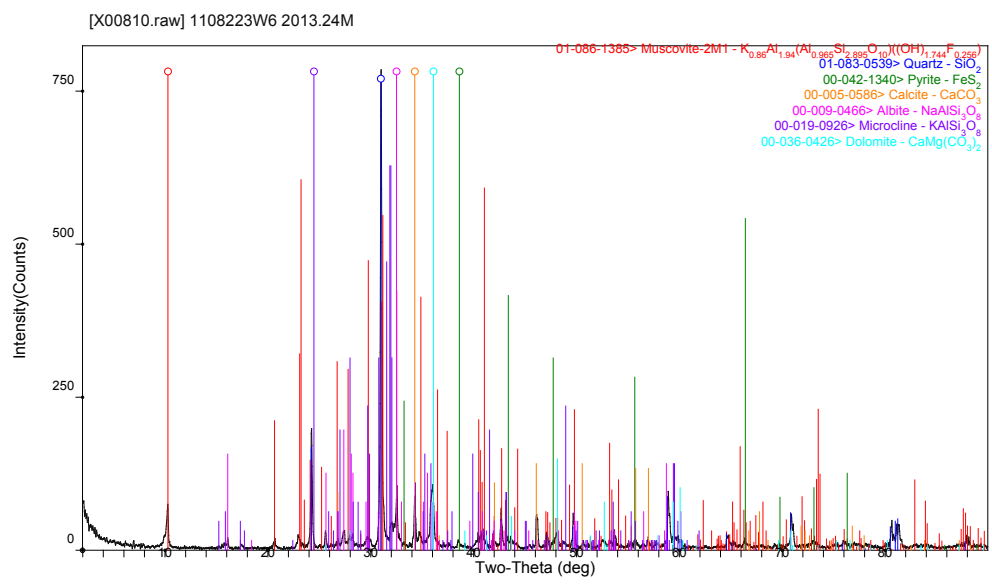


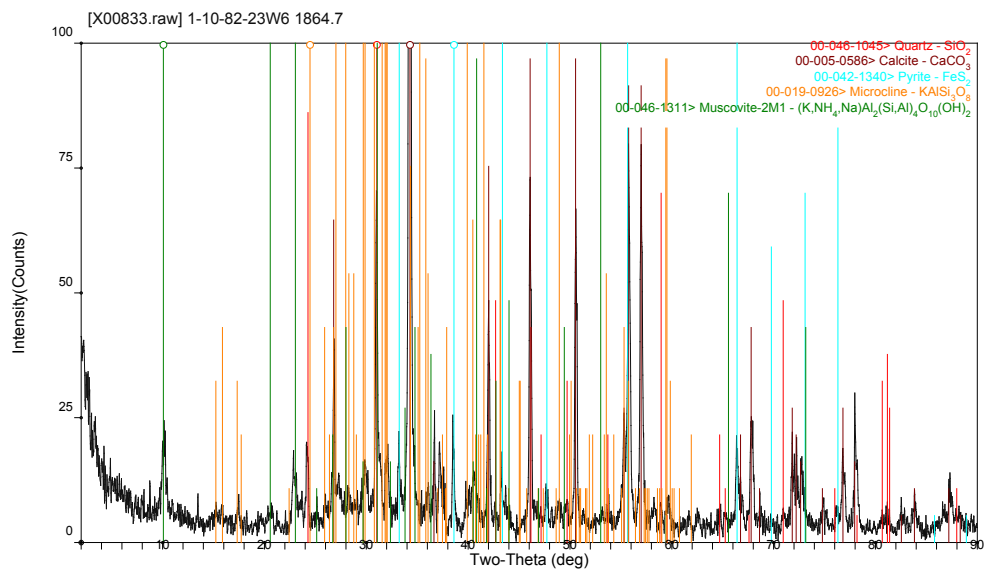
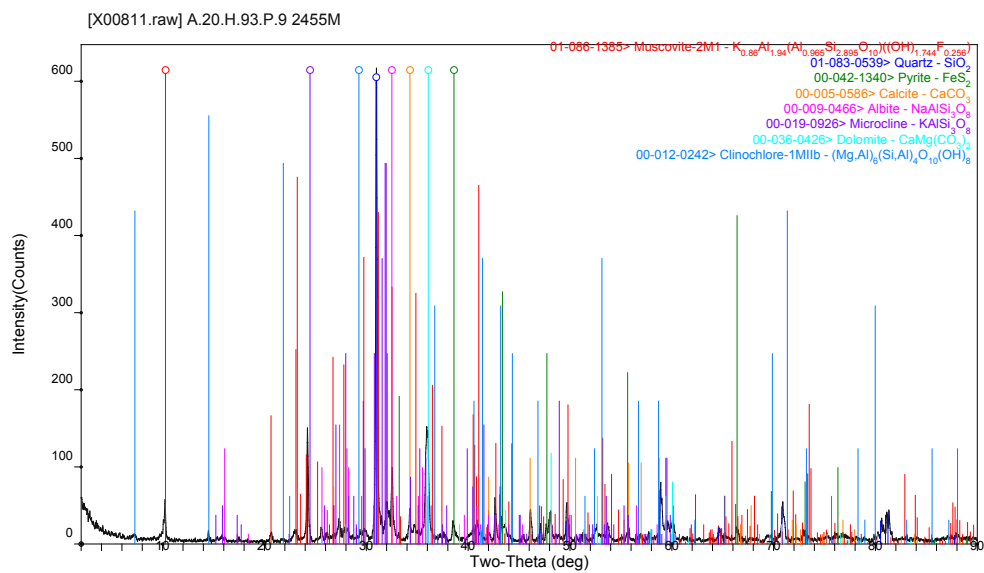
[X00809.raw] A.20.H.93.P.9 2460.57M <2T(0)=-0.02>

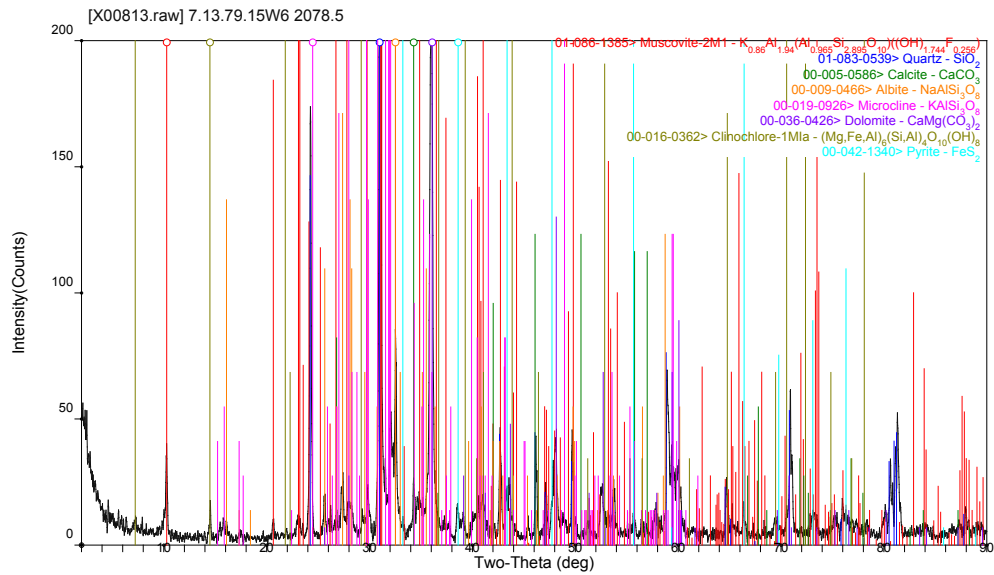
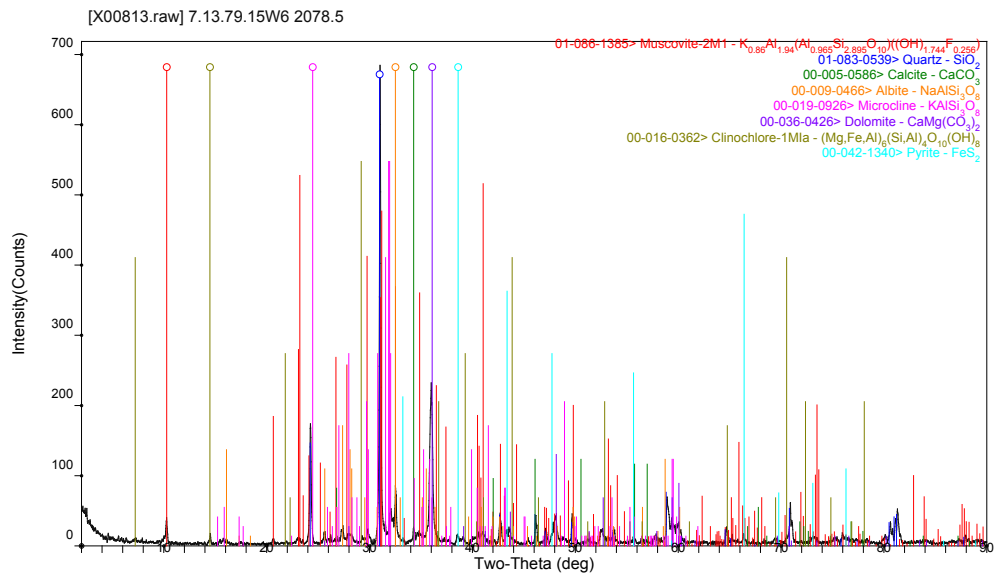


[X00809.raw] A.20.H.93.P.9 2460.57M <2T(0)=-0.02>

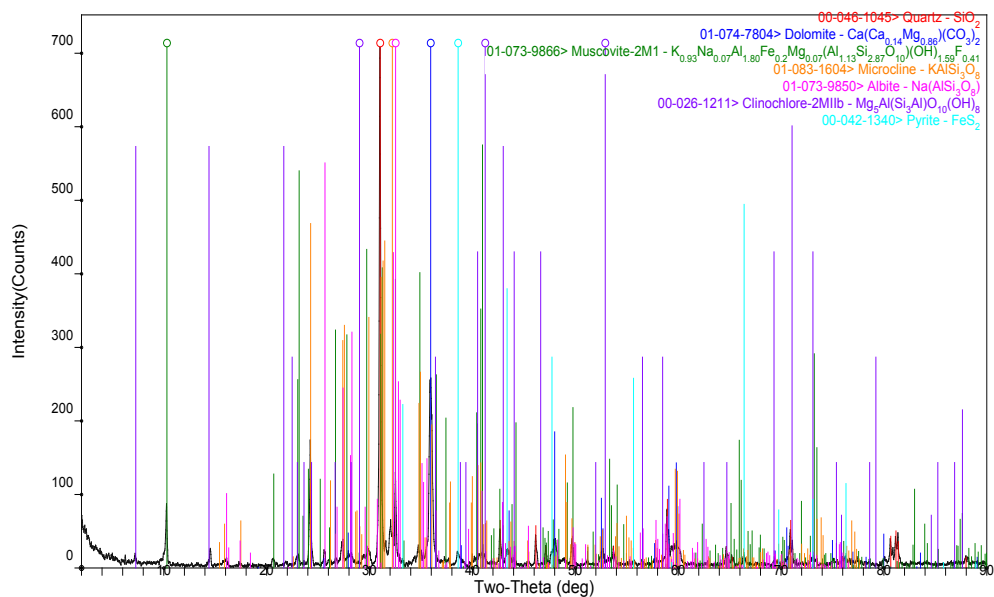




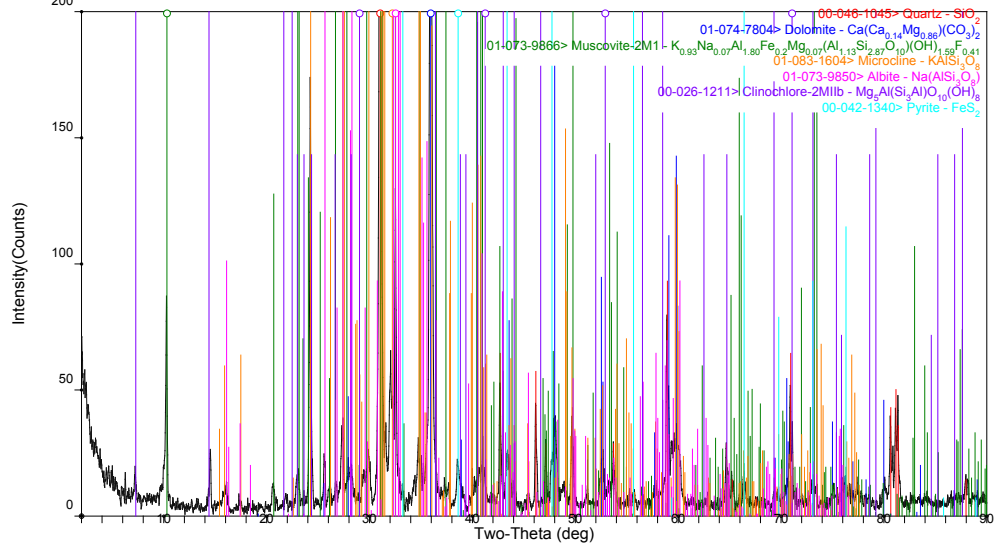




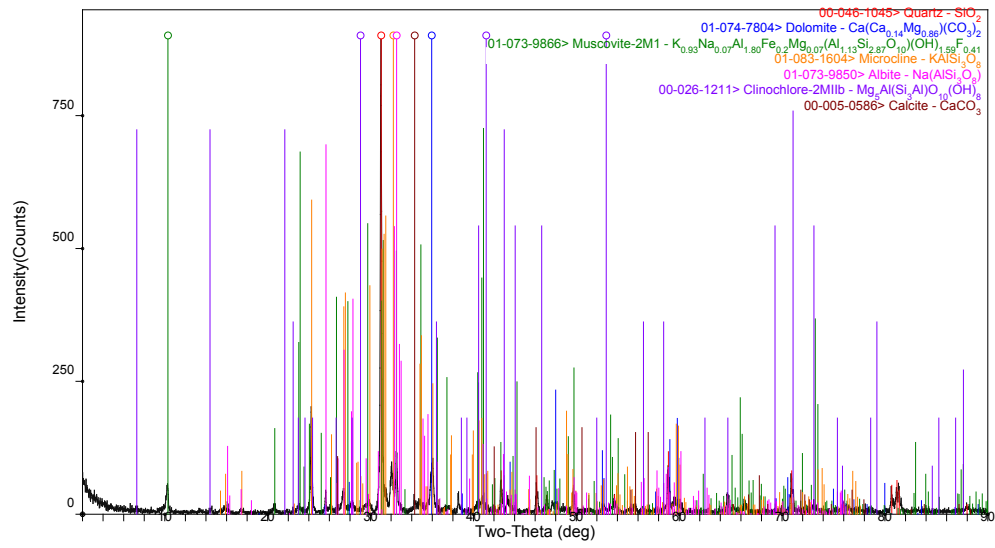
[X00814.Raw] 7.13.79.15W6 2084.5



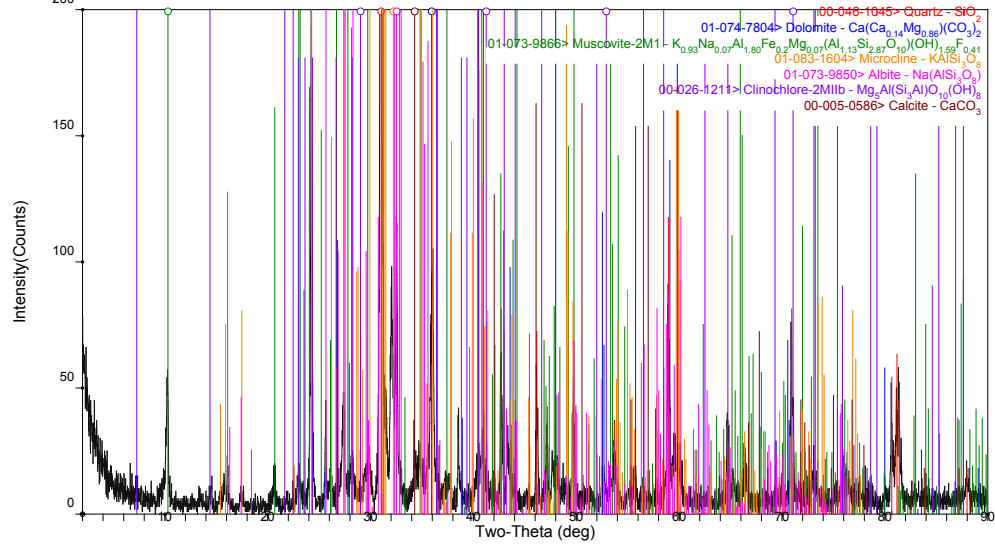
[X00814.Raw] 7.13.79.15W6 2084.5

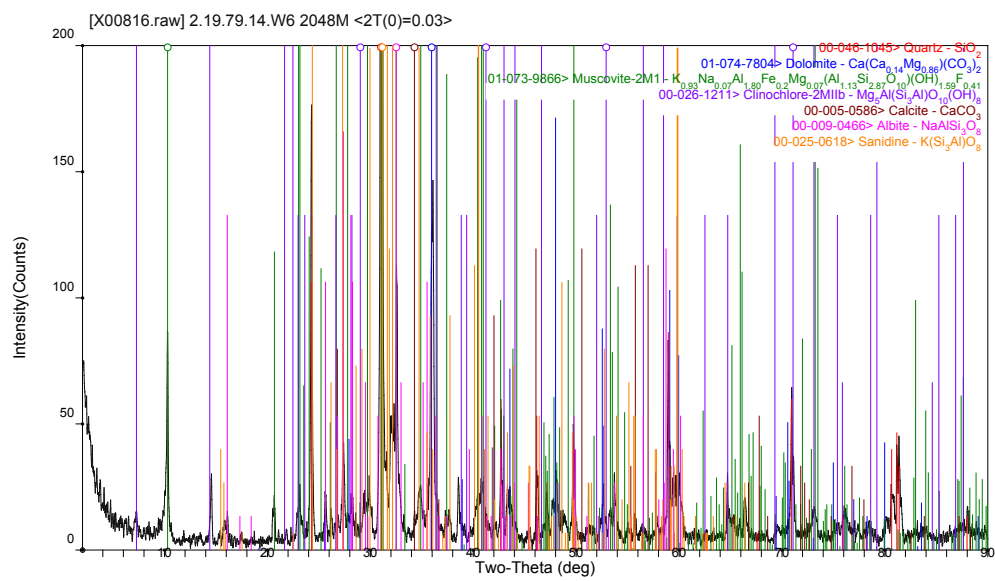
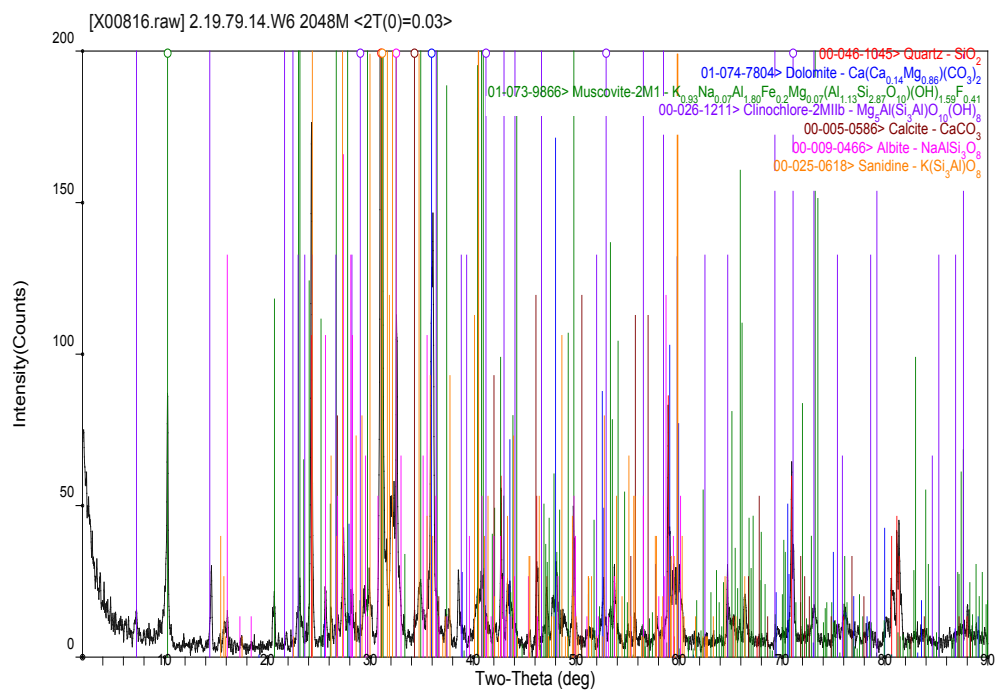


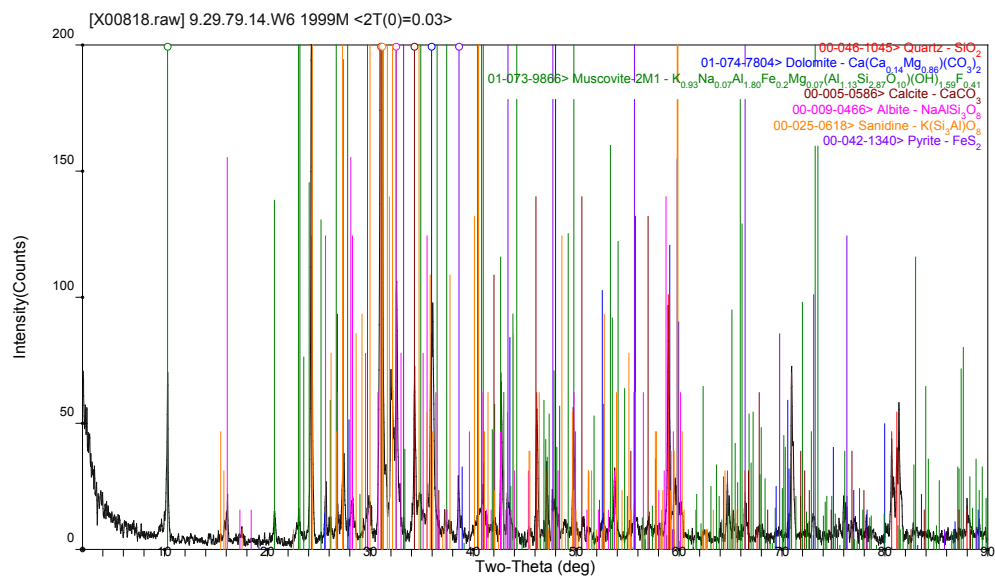
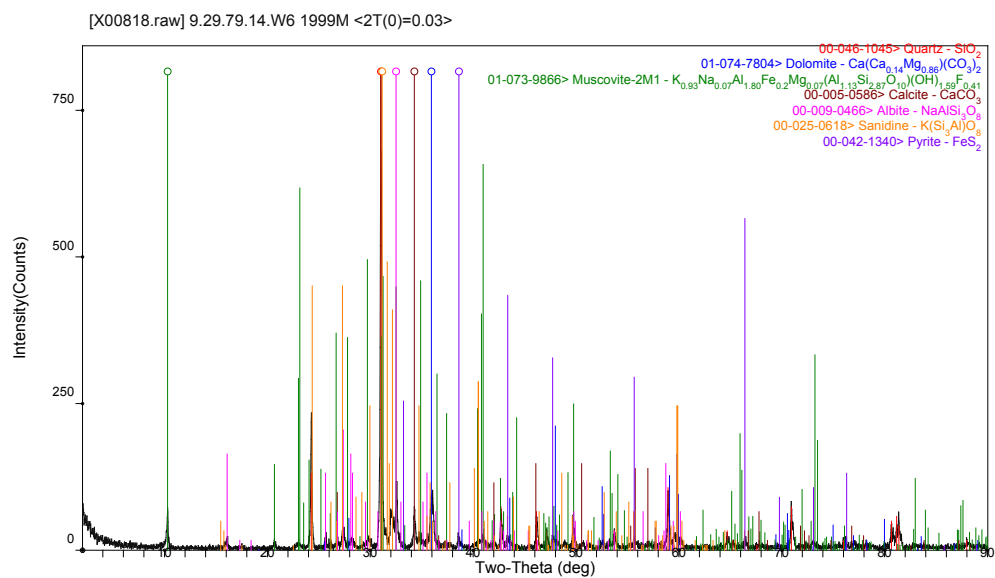
[X00815.raw] 2.19.79.14.W6 2085M

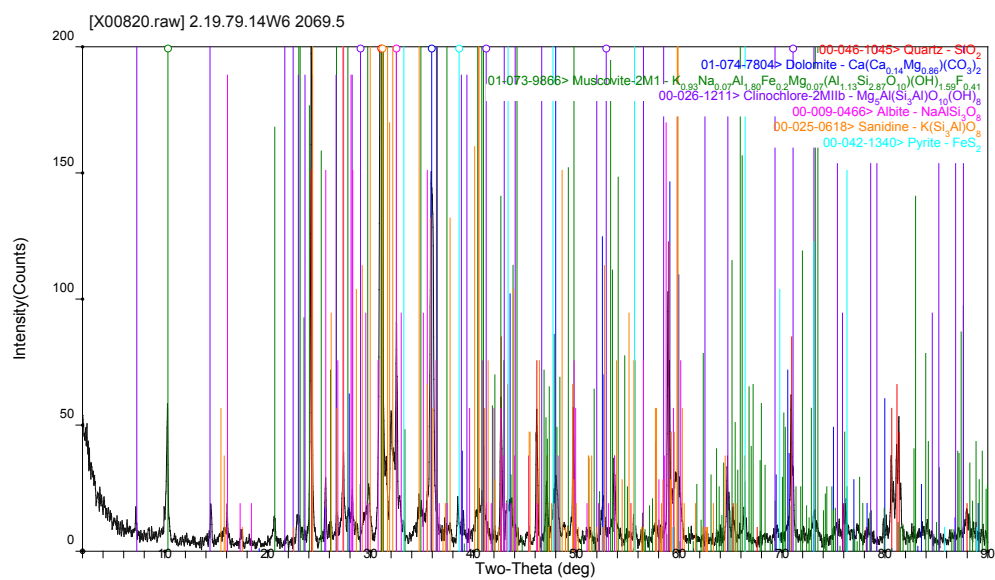
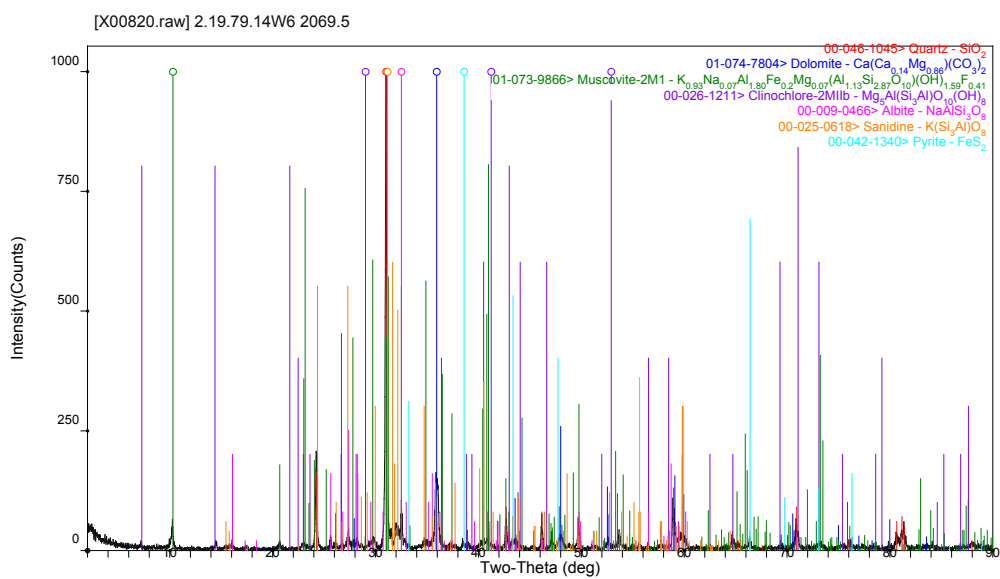


[X00815.raw] 2.19.79.14.W6 2085M

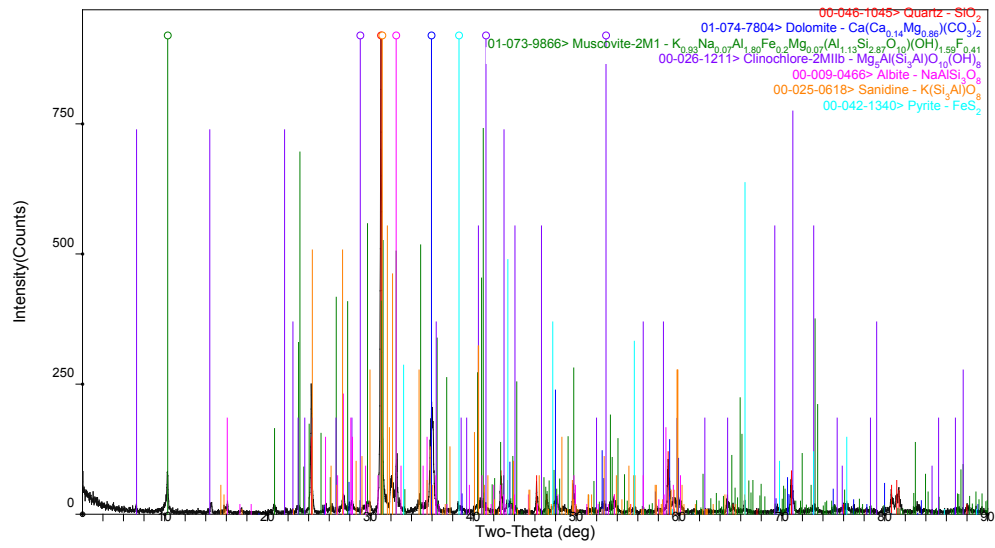




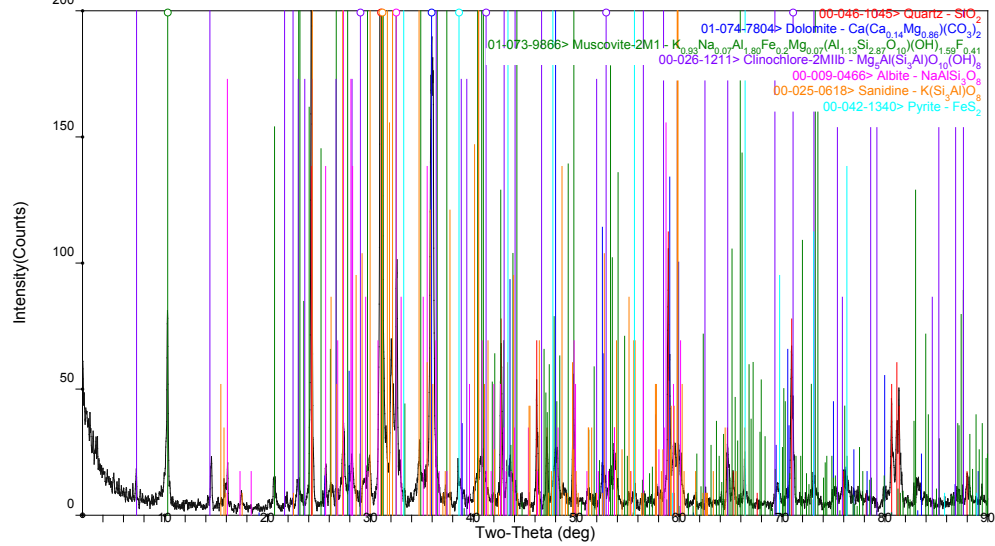




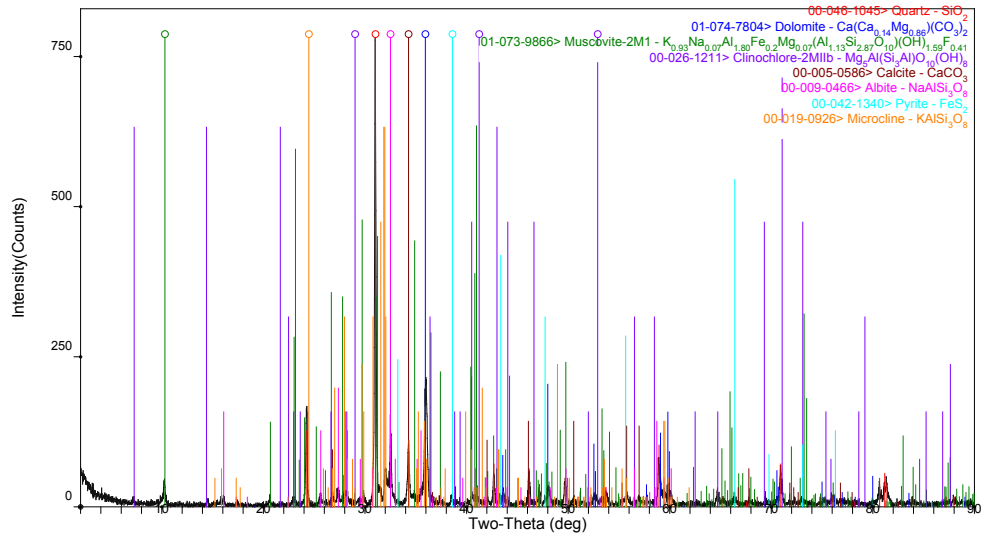
[X00821.raw] 2.19.79.14W6 2069.5 <2T(0)=0.02>



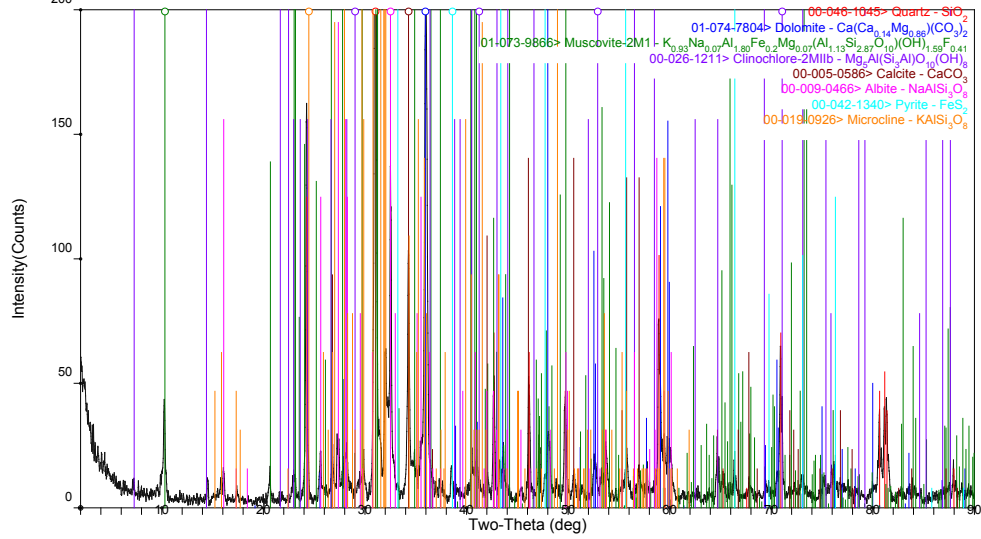
[X00821.raw] 2.19.79.14W6 2069.5 <2T(0)=0.02>

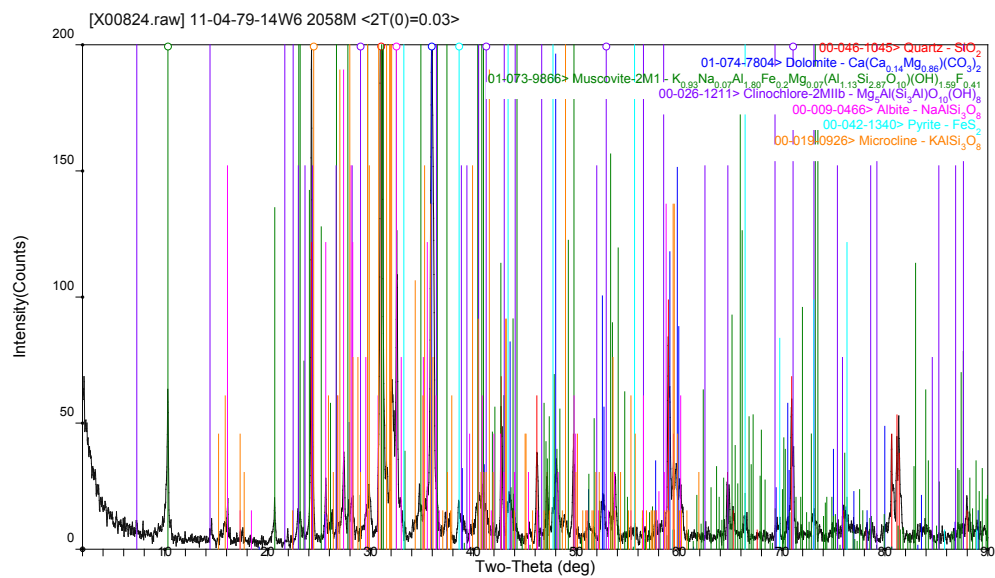
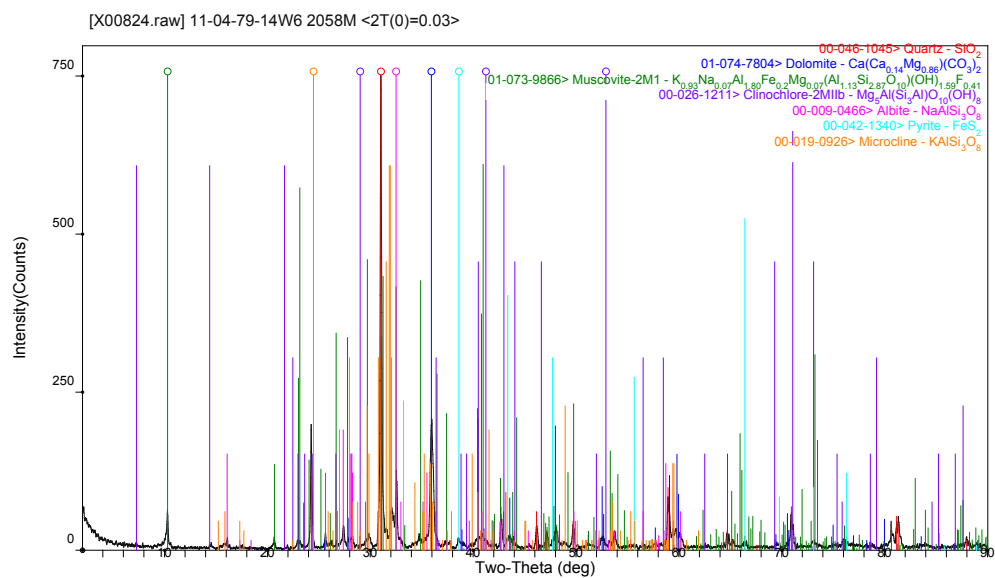


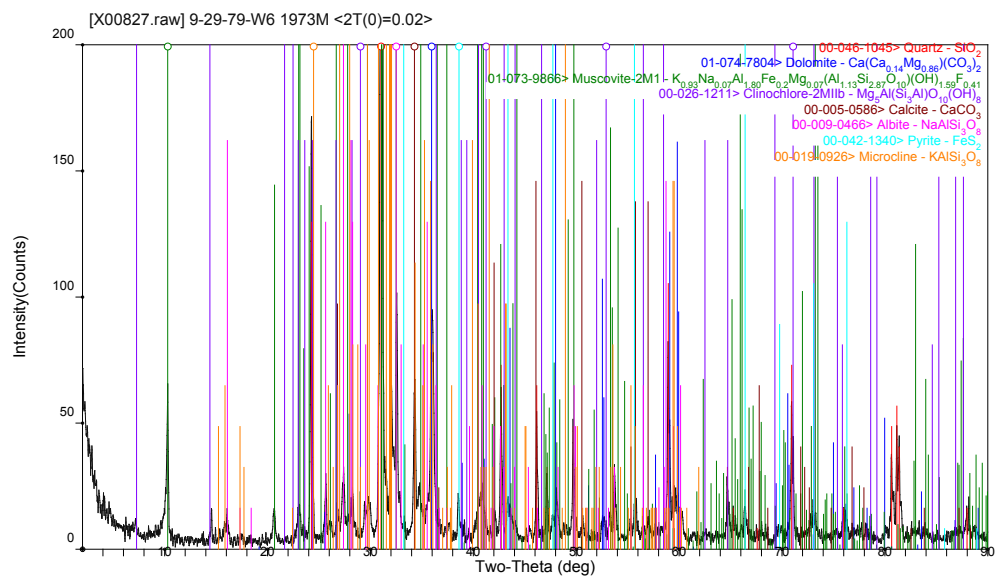
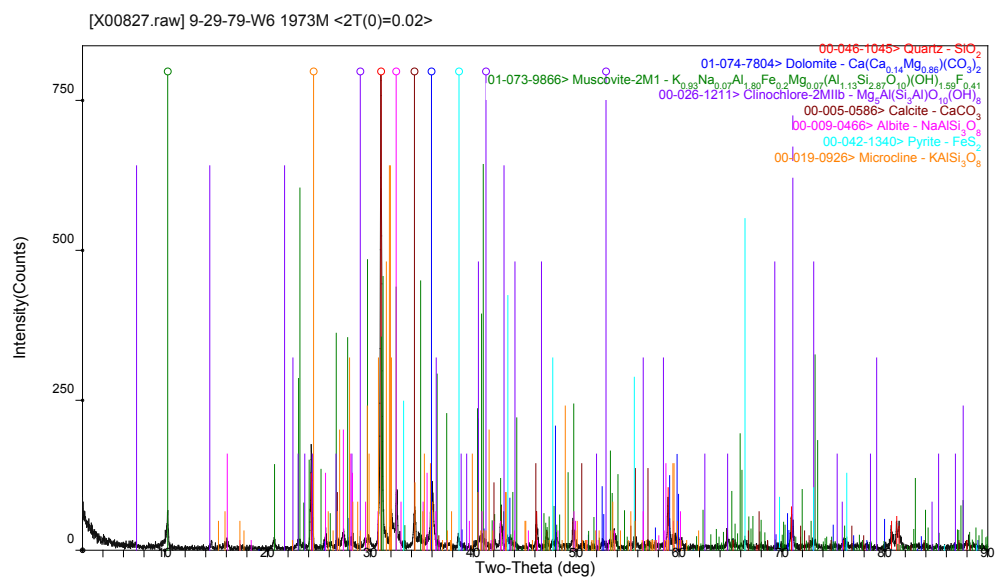
[X00823.raw] d39-F-93-P9 266.88M

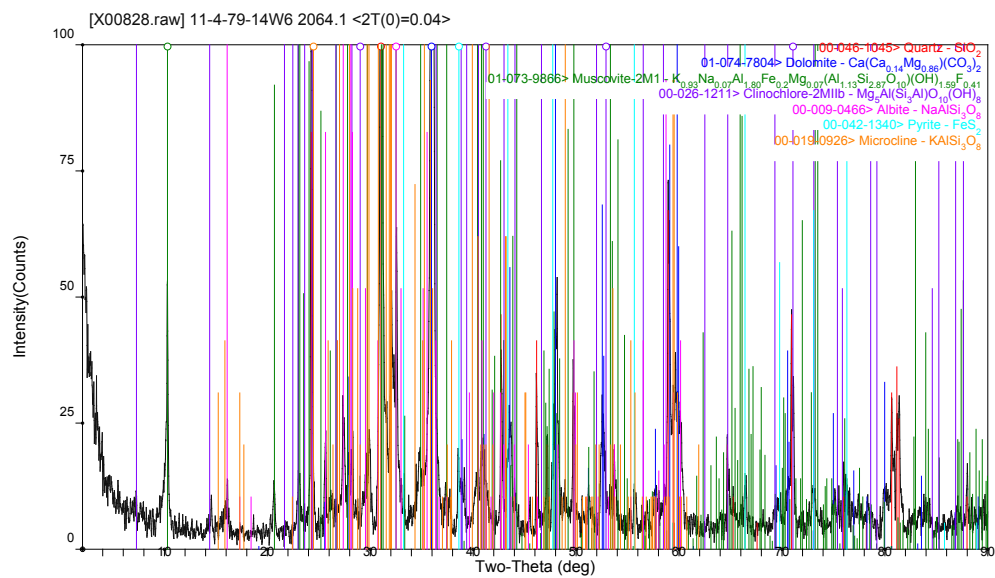
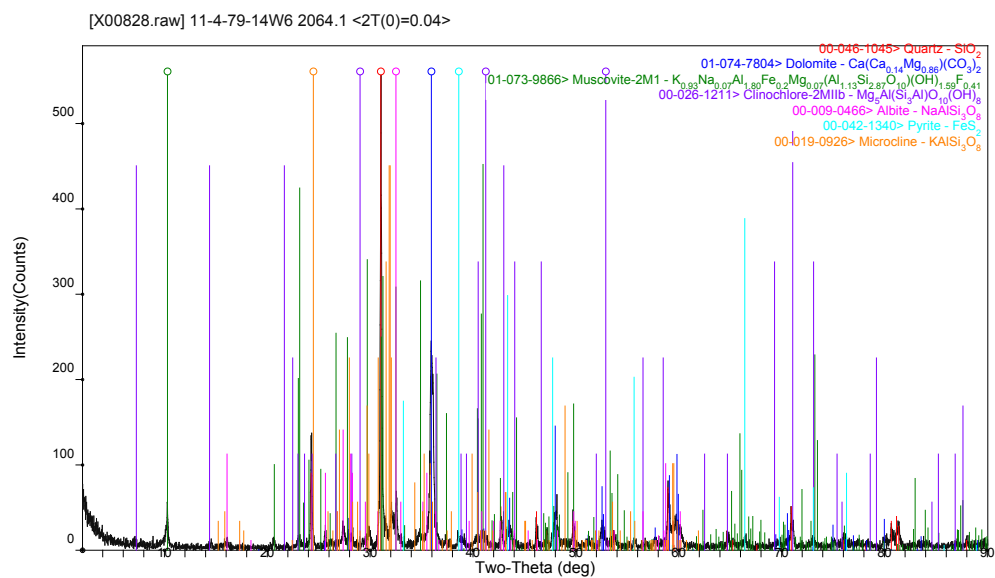


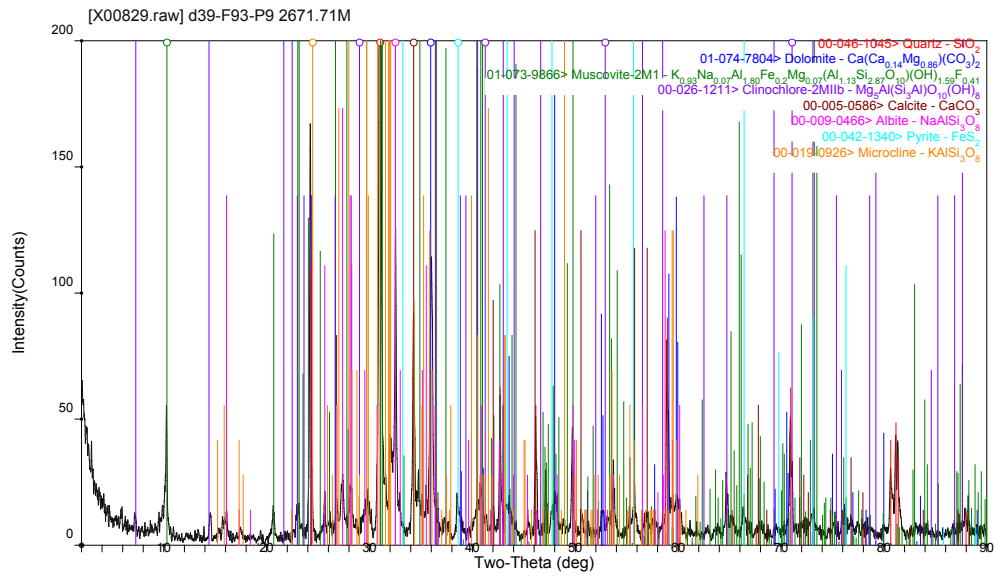
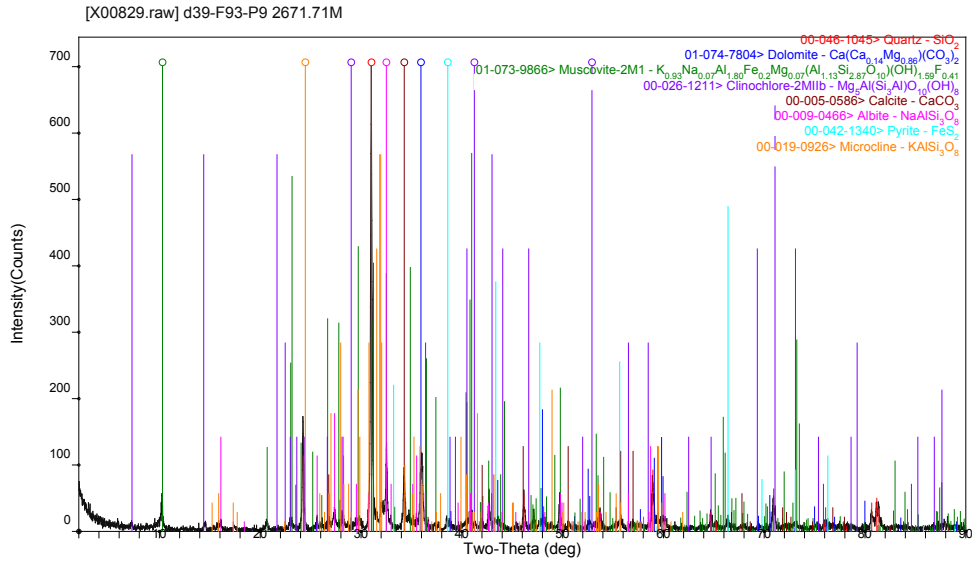
[X00823.raw] d39-F-93-P9 266.88M

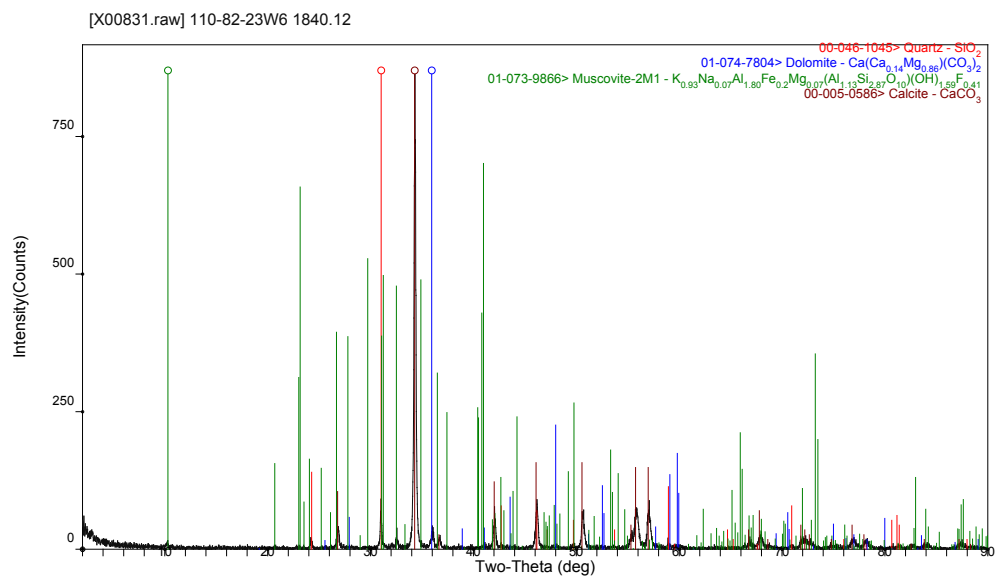
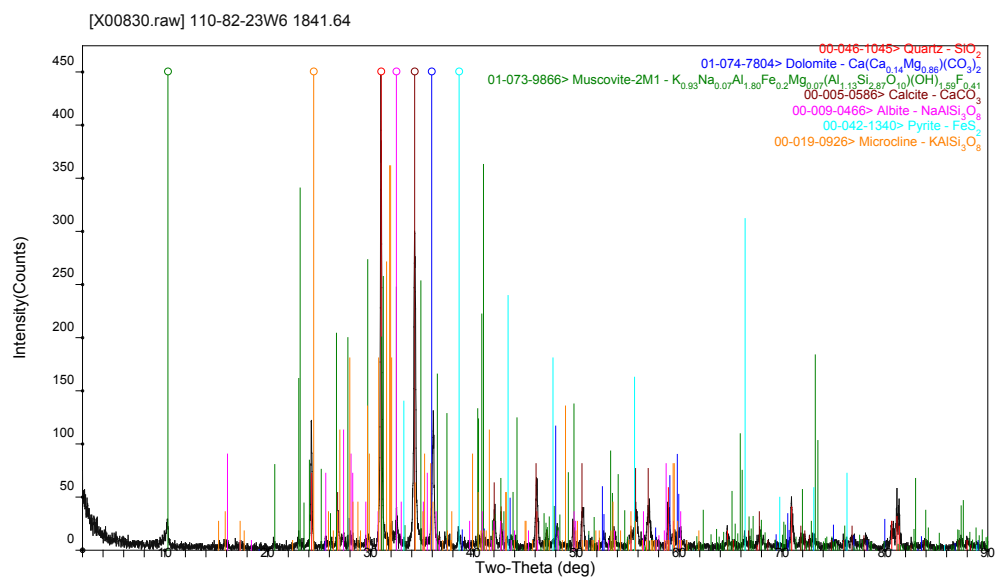


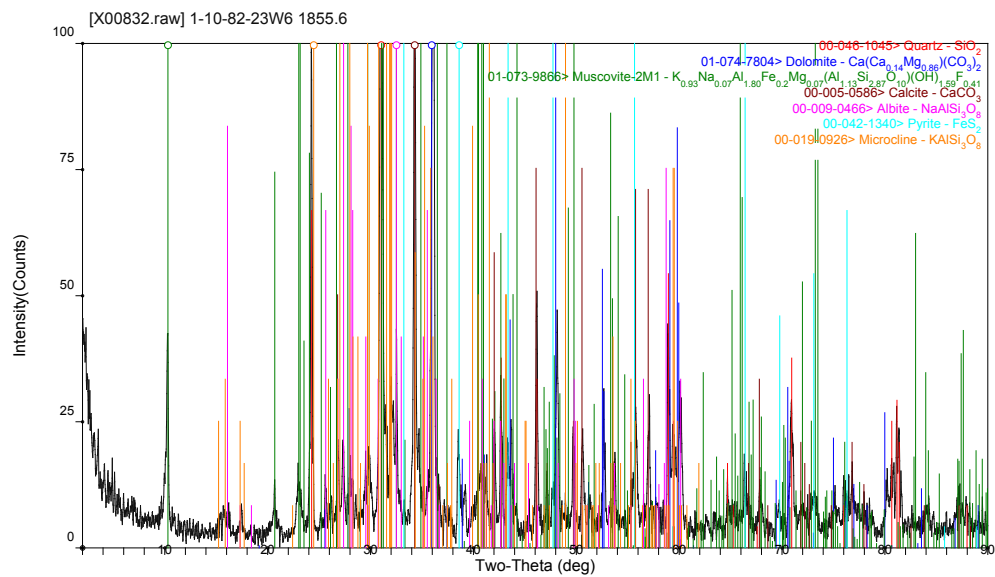
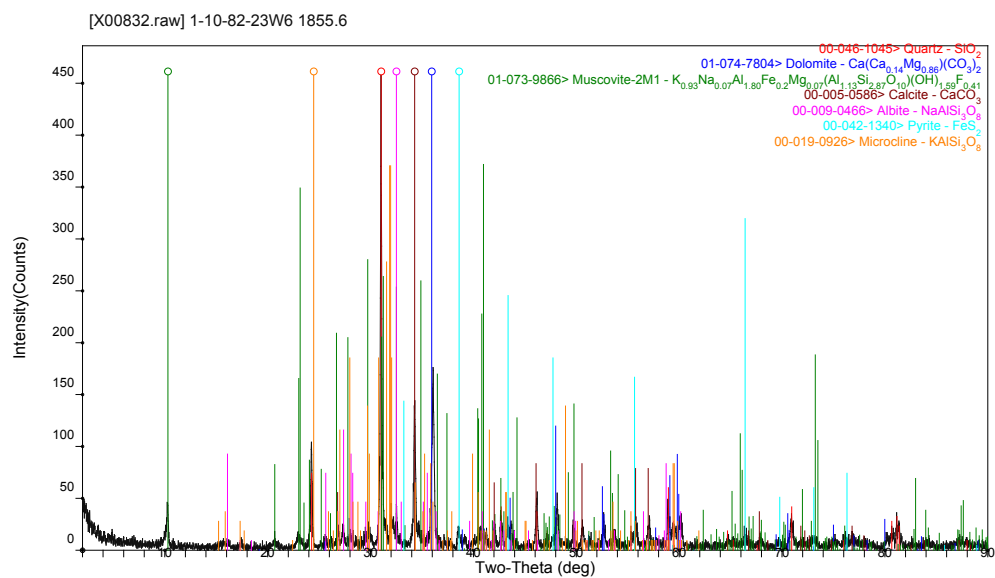




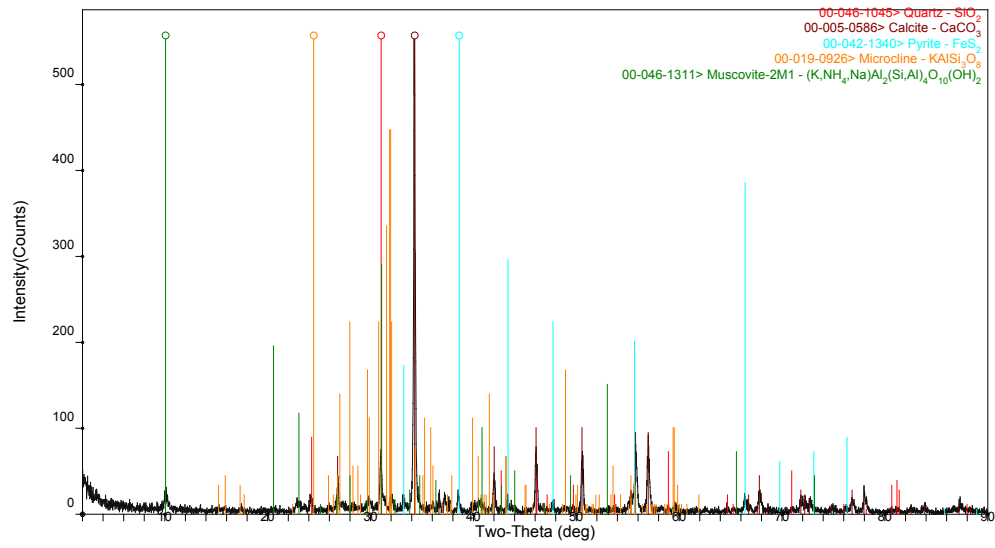








[X00833.raw] 1-10-82-23W6 1864.7



[X00834.raw] 7-13-79-15W6 2061.3

